

Volume 7

Atomic and Electron Physics

Atomic Interactions

PART B

Edited by

BENJAMIN BEDESON

*Department of Physics
New York University
Bronx, New York*

WADE L. FITE

*Department of Physics
University of Pittsburgh
Pittsburgh, Pennsylvania*



ACADEMIC PRESS

A Subsidiary of Harcourt Brace Jovanovich, Publishers

New York London Toronto Sydney San Francisco

COPYRIGHT © 1968, BY ACADEMIC PRESS, INC.
ALL RIGHTS RESERVED.
NO PART OF THIS BOOK MAY BE REPRODUCED IN ANY FORM,
BY PHOTOSTAT, MICROFILM, OR ANY OTHER MEANS, WITHOUT
WRITTEN PERMISSION FROM THE PUBLISHERS.

ACADEMIC PRESS, INC.
111 Fifth Avenue, New York, New York 10003

United Kingdom Edition published by
ACADEMIC PRESS, INC. (LONDON) LTD.
24/28 Oval Road, London NW1

LIBRARY OF CONGRESS CATALOG CARD NUMBER: 68-56970

PRINTED IN THE UNITED STATES OF AMERICA
80 81 82 9 8 7 6 5 4 3 2

CONTRIBUTORS TO VOLUME 7, PART B

Numbers in parentheses indicate the pages on which the authors' contributions begin.

- MANFRED A. BIONDI, *Atomic and Plasma Physics Laboratory, Physics Department, University of Pittsburgh, Pittsburgh, Pennsylvania* (78)
- H. P. BROIDA, *Department of Physics, University of California, Santa Barbara, California* (189)
- S. DATZ, *Oak Ridge National Laboratory, Oak Ridge, Tennessee* (231)
- L. H. FISHER, *Lockheed Missiles and Space Company, Palo Alto, California* (29)
- WADE L. FITE, *Department of Physics, University of Pittsburgh, Pittsburgh, Pennsylvania* (124)
- R. A. HARTUNIAN, *Aerospace Corporation, Los Angeles, California* (141)
- H. O. LUTZ, *Oak Ridge National Laboratory, Oak Ridge, Tennessee* (231)
- F. G. MAJOR,* *Physikalisches Institut, Universität Bonn, Bonn, Germany* (1)
- C. J. POWELL, *Electron Physics Section, National Bureau of Standards, Washington, D.C.* (275)
- K. SCHOFIELD,** *University of California, Santa Barbara, California* (189)
- R. VARNEY, *Lockheed Missiles and Space Company, Palo Alto, California* (29)
- W. L. WIESE, *Plasma Spectroscopy Section, National Bureau of Standards, Washington, D.C.* (307)

* Present address: NASA Goddard Space Flight Center, Greenbelt, Maryland.

** Present address: Cornell Aeronautical Laboratory, Incorporated, Buffalo, New York.

FOREWORD

In the foreword to Volume 4, I explained the reasons for the Atomic and Electron Physics volumes having grown from two into four volumes. This "mushrooming" of text reflects more than the predilections of the editor; in good conscience we could not compress this wealth of material into fewer pages and meet the needs of the scientific community. Yet, some of the chapters may have been condensed to a greater degree than some of our readers may desire; we hope the result proves to be a reasonable compromise between the somewhat conflicting requirements of clear and at the same time economical presentation.

Our readers may also wonder why various aspects of plasma physics are neglected. Upon advice of many of our friends it was decided to extend the framework of "Methods of Experimental Physics" by adding another volume on the methods used by the plasma physicist. I am happy to report that this volume is now being organized by Professor Hans R. Griem of the University of Maryland and Professor Ralph H. Lovberg of the University of California at San Diego.

It remains my pleasant task to thank the editors of this volume, the contributors, and the publishers for a well coordinated effort.

L. MARTON

*July 1968
Washington, D.C.*

PREFACE TO VOLUME 7

If the reader refers to the Preface of Volumes 5A and 5B of this treatise (Nuclear Physics), he will find much that applies to these volumes on atomic physics. In fact, by substituting the word "atomic" for "nuclear," a good part of that preface could admirably suit these volumes. Experimental atomic physics in all its branches has experienced a tremendous growth in the last two decades. There are many articles and books which give excellent reviews of basic principles and details of techniques of various detectors, methods, and specific topics in atomic physics. But indeed it is difficult to obtain comprehensive information on principal methods and their relative merits for the measurement of specific reactions. The present volumes are an attempt to unify the basic experimental techniques of what has (perhaps in the prejudiced opinion of the editors) managed to sustain itself over the years as being among the most stimulating and challenging areas of contemporary physics research.

Again, owing to the comprehensive coverage of this book, and to the enthusiastic response of a large number of contributors who treated their subject matter so thoroughly, it has been necessary to divide the work into two volumes. There is, fortunately, a natural division possible in the subject matter. Volume 7A deals primarily with material on beam-gas and beam-beam techniques, while Volume 7B deals primarily with material on experiments in bulk matter, mainly in some form of the plasma state.

As is the case in any fast-moving field, much has happened during the past two years, during which this book has been in preparation, which would, and should, have been included had there been time. For example, any subsequent edition will doubtless contain more material on high energy resolution electron spectroscopy and on polarized electron and atom scattering experiments than is contained in these volumes.

We wish to take this opportunity to express our deepest appreciation and thanks to all the contributors for their understanding and cooperation. Thanks are also due to Academic Press and to Dr. L. Marton, the Editor-in-Chief of "Methods of Experimental Physics," for invaluable help and continuous encouragement.

*New York University
University of Pittsburgh*

BENJAMIN BEDERSON
WADE L. FITE

CONTRIBUTORS TO VOLUME 7, PART A

- I. AMDUR, *Department of Chemistry, Massachusetts Institute of Technology, Cambridge, Massachusetts*
- C. F. BARNETT, *Oak Ridge National Laboratory, Oak Ridge, Tennessee*
- BENJAMIN BEDERSON, *Department of Physics, New York University, Bronx, New York*
- H. B. GILBODY, *Department of Pure and Applied Physics, The Queen's University of Belfast, Belfast, Northern Ireland*
- M. F. A. HARRISON, *Culham Laboratory, Abington, Berkshire, England*
- DOUGLAS W. O. HEDDLE, *Physics Department, University of York, Heslington, York, England*
- C. E. KUYATT, *Electron Physics Section, National Bureau of Standards, Washington, D.C.*
- E. W. McDANIEL, *School of Physics, Georgia Institute of Technology, Atlanta, Georgia*
- ROY H. NEYNABER, *Space Science Laboratory, General Dynamics Convair, San Diego, California*
- H. PAULY, *Institut für angewandte Physik, Universität Bonn, Bonn, Germany*
- A. C. RIVIERE, *Culham Laboratory, Abington, Berkshire, England*
- J. A. R. SAMSON, *G.C.A. Corporation, Bedford, Massachusetts*
- STEPHEN J. SMITH, *Joint Institute for Laboratory Astrophysics,* University of Colorado, Boulder, Colorado*
- J. P. TOENNIES, *Physikalisches Institut, Universität Bonn, Bonn, Germany*
- G. L. WEISSLER, *Department of Physics, University of Southern California, Los Angeles, California*
- W. L. WIESE, *Plasma Spectroscopy Section, National Bureau of Standards, Washington, D.C.*

* Of the National Bureau of Standards, Washington, D.C. and the University of Colorado.

5. OPTICAL PUMPING*

5.1 Introduction

The application of optical methods to the detection of transitions between the magnetic sublevels of an atomic energy state, in particular those of an excited state, was first proposed by Bitter¹ in a paper published in 1949 in which he describes the changes caused in the Zeeman effect of a radiating atom by a weak oscillatory magnetic field whose frequency is near resonance with the Zeeman transition frequency of the atom in that state. This was rapidly followed by the publication of the principle of the *double resonance technique* in 1949²; a technique which together with the related *electron impact technique*³ have since been extensively used to study the rf spectra and lifetimes of excited states.⁴ In these methods the magnetic sublevels of an excited state are selectively populated, either by using polarized exciting radiation or by impact with electrons in a collimated beam. Since the radiation from such a state will exhibit a pattern of intensity and polarization characteristic of its sublevel populations, transitions induced by a resonant magnetic field will modify these properties and are thereby detectable.

In 1950 appeared the classical paper of Kastler,⁵ in which he proposed a method of optically producing and detecting differences of population among the magnetic sublevels of the ground state of an atom; a method commonly referred to as *optical pumping*.⁶ This method utilizes the selection rules governing the absorption of radiation by the atoms from a circularly polarized collimated beam. If the total angular momentum of the atom in the ground state is F , and the projections along the light axis are M , then the absorption of right circularly polarized light will be governed

¹ F. Bitter, *Phys. Rev.* **76**, 833 (1949).

² J. Brossel and A. Kastler, *Compt. Rend.* **229**, 1213 (1949).

³ H. W. B. Skinner and E. T. S. Appleyard, *Proc. Roy. Soc. Ser. A* **117**, 224 (1928).

⁴ G. W. Series, *Rept. Progr. Phys.* **22**, 280 (1959).

⁵ A. Kastler, *J. Phys. Radium*, **11**, 255 (1950).

⁶ Numerous references will be found in "Quantum Optics and Electronics" (C. DeWitt et al., eds.). Gordon and Breach, New York, 1965; J. Brossel, *Advan. Quantum Electron.* Pt. II, (J. R. Singer, ed.). Columbia Univ. Press, New York, 1961; also F. Bitter, *Appl. Opt.* **1**, 1 (1962).

* Part 5 is by F. G. Major.

5. OPTICAL PUMPING

by the selection rule $\Delta M = +1$, and an atom originally in the sublevel M_i of the ground state must go to a level characterized by $M' = M_i + 1$ in the excited state; however, in undergoing spontaneous emission it may go to sublevels in the ground state characterized by M_i , $M_i + 1$, or $M_i + 2$, as shown in Fig. 1. Thus it is evident that if the atom continues to go through the cycle of absorption and re-emission, it will have its distribution of populations among the sublevels of the ground state increasingly favoring the sublevel with the highest positive M . An ensemble of atoms having this nonequilibrium distribution by virtue of the above process is said to be optically oriented or polarized. If, instead of a circularly polarized beam, an unpolarized beam is used, the ensemble will acquire a small degree of alignment in which the populations are a function only of the magnitude of M , so that the populations of $+M_i$ and $-M_i$ are the same.

The first experimental attempt to succeed in demonstrating the workability of the optical pumping scheme using polarized light was made on Na atoms in free flight, in the form of an atomic beam, by Brossel *et al.* and published in 1952.⁷ Further basic studies using atomic beams were carried out by the Paris group and at Princeton University by Hawkins and Dicke.⁸

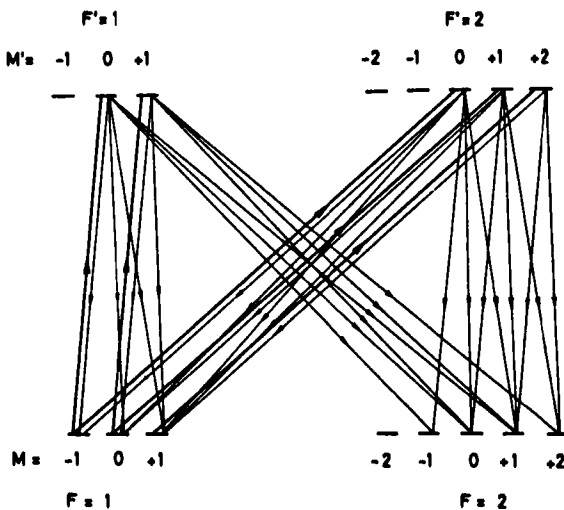


FIG. 1. Schematic representation of typical optical transitions occurring in the optical pumping cycle of an atom having a $^2S_{1/2}$ ground state, a $^2P_{1/2}$ resonant excited state, and a nuclear spin $I = \frac{1}{2}$.

⁷ J. Brossel, A. Kastler, and J. Winter, *J. Phys. Radium* **13**, 668 (1952).

⁸ W. B. Hawkins and R. H. Dicke, *Phys. Rev.* **91**, 1008 (1953); W. B. Hawkins, *ibid.* **98**, 478 (1955).

In 1955 the enhancement of ground-state atomic polarization due to the presence of foreign gases was observed,⁹ leading ultimately to an important simplification in the manner of achieving long relaxation times; one was no longer limited to the use of an atomic beam, but could observe polarization in an absorption cell containing the saturated vapor of the element and a buffer gas. However, while atoms in a spherically symmetric ground *S*-state preserve their spin state extremely well in collisions with the buffer gas atoms, considerable depolarization occurs in the excited *P*-state, leading to important changes in the properties of an optically pumped system which were reported by Dehmelt¹⁰ in 1957, who also demonstrated that high signal-to-noise ratios are obtainable by monitoring the transmission of the pumping light through the cell; a property which depends only on the ground state polarization.

In 1958, Dehmelt published a paper¹¹ which was to have a great influence in extending the range of the optical pumping technique to systems which could not conveniently be directly pumped. By the process of spin-exchange with optically oriented Na he successfully polarized free electrons, and showed that their polarization could be monitored by observing the change in the Na polarization which, through spin exchange, would accompany any change in the electron polarization. Soon after that, there came in rapid succession a large number of papers describing the successful observation of spin-exchange polarization in a variety of paramagnetic atoms. Thus apart from the experiments involving spin exchange between one alkali atom with another,¹² the method proved effective in the case of H,¹³ N,¹⁴ P,¹⁵ and Ag.¹⁶ Thus not only has the optical pumping technique contributed greatly to the study of the radio-frequency spectra of atoms which can be directly pumped, but through the spin-exchange process other systems have been studied and, in so doing, knowledge gained about the exchange mechanism itself.

The optical pumping of metastable atomic states is exemplified in the work of Colegrove and Franken¹⁷ on the 3S_1 state in He, where the transition probabilities are such that a considerable alignment is obtainable

⁹ J. Brossel, J. Margerie, and A. Kastler, *Compt. Rend.* **241**, 865 (1955).

¹⁰ H. G. Dehmelt, *Phys. Rev.* **105**, 1487 (1957).

¹¹ H. G. Dehmelt, *Phys. Rev.* **109**, 381 (1958).

¹² R. Novick and H. Peters, *Phys. Rev. Letters* **1**, 54 (1958); P. Franken, R. Sands, and J. Hobart. *ibid.* **1**, 118 (1958).

¹³ W. L. Anderson, F. M. Pipkin, and J. C. Baird, *Phys. Rev.* **120**, 1279 (1960).

¹⁴ W. W. Holloway, E. Luscher, and R. Novick, *Phys. Rev.* **126**, 2109 (1962).

¹⁵ R. H. Lambert and F. M. Pipkin, *Phys. Rev.* **128**, 198 (1962).

¹⁶ G. S. Hayne and H. G. Robinson, *Bull. Am. Phys. Soc.* **5**, 411 (1960).

¹⁷ F. D. Colegrove and P. A. Franken, *Phys. Rev.* **119**, 680 (1960).

5. OPTICAL PUMPING

using unpolarized pumping radiation. In the course of this work interference effects due to the crossing of the excited state sublevels were observed as manifested by the change in the resonance fluorescence process when the applied magnetic field assumed certain appropriate values. This formed the basis of the *level-crossing technique*¹⁸ which is basically similar to the double resonance method and in the limit of zero magnetic field becomes the familiar *Hanle effect*.

As an established technique optical pumping is being increasingly used as a tool to study the forces acting on the irradiated atoms due to their environment. Such forces will in general introduce relaxation and energy level shifts which under suitable conditions can be observed and related back to the nature of the perturbing interactions causing them. In contrast to other methods of attaining atomic and nuclear orientation, optical methods are capable of producing a high degree of polarization in both the ground state and the excited state with relative experimental simplicity and on systems consisting of nearly free atoms. By their nature they also provide a unique tool for the study of the interaction of optical radiation with matter, including such topics as energy level shifts,¹⁹ diffusion of resonance radiation,²⁰ coherence phenomena,²¹ and virtual transitions.¹⁹

The most serious practical limitation to the technique comes from the need to have an adequate source of pumping radiation, which, apart from a relatively small number of elements, is difficult to obtain. Moreover if the ground state is other than an *S*-state, or if it is a high melting point element, then presumably the only recourse in solving the containment problem is to use an atomic beam; this, however, would detract from the usefulness of the technique in the study of relaxation. Attempts to apply the technique to ions have succeeded only in one instance,^{21a} Sr^+ ; again it is undoubtedly because of the lack of a sufficiently intense pumping source to produce a polarization of the ions in a plasma. There appears some hope of overcoming this difficulty in the use of electrodynamic confinement of the ions²² in ultrahigh vacuum.

5.2 Theoretical Foundations

The application of optical pumping methods to the study of interatomic forces through their effect on the irradiated atoms requires a theory which

¹⁸ P. A. Franken, *Phys. Rev.* **121**, 508 (1961).

¹⁹ C. Cohen-Tannoudji, *Ann. Phys. (Paris)* **7**, 469 (1962); L. D. Shearer, *Phys. Rev.* **127**, 512 (1962).

²⁰ J. P. Barrat, *J. Phys. Radium* **20**, 657 (1959).

²¹ A. Corney and G. W. Series, *Proc. Phys. Soc. (London)* **83**, 213 (1964); also O. Nedelec, M. N. Deschizeaux, and J. C. Pebay-Peyroula, *Compt. Rend.* **257**, 3130 (1963).

^{21a} H. Ackermann, G. zu Putlitz, and E. W. Webber, *Phys. Letters* **24A**, 567 (1957).

²² H. G. Dehmelt and F. G. Major, *Phys. Rev. Letters* **8**, 213 (1962).

gives a full description of the interaction of the atoms with the radiation field itself. A refined theoretical description of the optical pumping cycle has been given by Barrat and Cohen-Tannoudji²³ following the spirit of the preceding notable work by Barrat²⁰ on the coherent diffusion of resonance radiation. We shall here present the theory however in a form adequate only for a good working knowledge of the technique and refer the reader to the original works for a discussion of such topics as radiation shifts of energy levels and coherence phenomena.

Consider then an aggregate of a large number of noninteracting atoms having a number density sufficiently small that there is a negligible probability that a given atom will absorb radiation resulting from the fluorescence of others; in practice this means the density must not exceed about 10^{11} cm^{-3} . Assume the atoms have a Zeeman structure in their ground state, the various substates being characterized by the quantum numbers F, M , and similarly let F', M' characterize the excited state involved in the resonance fluorescence. The axis of quantization is taken to be defined by the wave vector \mathbf{k} of the pumping radiation having a polarization vector \mathbf{e} , which will generally be involved through its spherical components $e_1 = (1/\sqrt{2})(e_x + ie_y)$, $e_0 = e_z$, $e_{-1} = (1/\sqrt{2})(e_x - ie_y)$. In practice the degeneracy with respect to M is removed with a uniform magnetic field which we will assume is parallel to the light axis, so that $H_z = H_0$, $H_x = H_y = 0$.

The manner in which M -state pumping is accomplished in order to create a preferred orientation is based on the selection rules governing the optical transitions. Thus in the dipole approximation the transition probability from state $|FM\rangle$ to $|F'M'\rangle$ is given by²⁴

$$B(FM \rightarrow F'M') = \frac{8\pi^3\nu}{hc} |\langle FM | \mathbf{e} \cdot \mathbf{D} | F'M' \rangle|^2 j_\nu \quad (5.2.1)$$

where \mathbf{D} is the electric dipole moment operator ($e\mathbf{r}$), and j_ν is the flux density of photons per unit frequency range at the frequency ν and is assumed to be constant over the frequencies of the transitions involved. Now since the matrix element is evaluated between two angular momentum eigenstates we may apply the Wigner-Eckart theorem²⁵ to obtain

$$\langle FM | D_\mu | F'M' \rangle = \langle FM | F'1M'\mu | \rangle \langle F || D || F' \rangle \quad (5.2.2)$$

where the first factor on the right-hand side is a Clebsch-Gordon coefficient, the second factor is the reduced matrix (which is independent of

²³ J. P. Barrat and C. Cohen-Tannoudji, *J. Phys. Radium* **22**, 443 (1961).

²⁴ P. A. M. Dirac, "Principles of Quantum Mechanics," 4th ed. Oxford Univ. Press, London and New York, 1958.

²⁵ D. M. Brink and G. R. Satchler, "Angular Momentum." Oxford Univ. Press, London and New York, 1962.

5. OPTICAL PUMPING

M and M'), and $\mu = 0, +1, -1$, corresponding to the spherical components of \mathbf{D} . Since the Clebsch-Gordon coefficient vanishes unless $M' = M - \mu$, and $F, F', 1$ satisfy the triangular condition, we have the selection rules

$$M' - M = 0, \pm 1; \quad F' - F = 0, \pm 1 \quad (F = F' = 0 \text{ forbidden}). \quad (5.2.3)$$

Thus if the light has a pure circular polarization, say e_{+1} , then from the matrix element for D_{-1} the absorption probability vanishes except for $M' = M + 1$, and in general the probabilities belonging to a given F, F' are proportional to $|\langle FM | F' 1 M' \mu \rangle|^2$.

Of equal importance to the pumping cycle is the process of spontaneous emission, whereby an atom, having absorbed a quantum, returns to the ground state by radiating with a probability differing from that for absorption only in the ratio of the Einstein A and B coefficients. However, in order to obtain an adequate description of the emission process, it is necessary to consider the interaction of the atom with radiation directed along any given polar angles θ, ϕ and with an arbitrary polarization \mathbf{e} . If the polarization vector is written as

$$\mathbf{e} = \mathbf{u}_1 \cos \psi + \mathbf{u}_2 \sin \psi \quad (5.2.4)$$

where $\mathbf{u}_1, \mathbf{u}_2$ are orthogonal unit vectors in the plane perpendicular to \mathbf{k} , it can be shown that the geometrical dependence of the transition probability is all contained in a factor F_μ given by²⁶

$$F_\mu = \left| \sum_P \bar{e}^{iP\psi} D_{\mu P}^1(\phi, \theta, 0) \right|^2 \quad (5.2.5)$$

where P is the polarization index and can assume only the values ± 1 , corresponding to right or left circular polarization, and $D_{MM'}^1$ is a rotation matrix. An atom in a given substate in the excited state will radiate to such substates in the ground state for which $\mu = 0, \pm 1$, each transition having a radiation pattern given by F_μ : for $\mu = 0$ the pattern is that of a classical electric dipole oscillating along the z axis (" π " radiation), and $\mu = \pm 1$ has the pattern of a dipole rotating in the x - y plane (" σ " radiation).

In the further discussion we shall limit ourselves to alkali-like atoms in a weak magnetic field for which \mathbf{F} is compounded of a nuclear spin \mathbf{I} and the electronic angular momentum \mathbf{J} , which is $\frac{1}{2}$ for the ground state and $\frac{1}{2}, \frac{3}{2}$ for the resonant excited P -states. Under the condition of broad excitation we have already assumed, the probability per unit time of an absorptive

²⁶ M. E. Rose, "Multipole Fields." Wiley, New York, 1955.

transition from state $|JFM\rangle$ to $|J'F'M'\rangle$ is given in the notation of Brink and Satchler²⁵ by

$$B(JFM \rightarrow J'F'M')$$

$$= (2F' + 1)(2J + 1) |\langle FM | F'1M'\mu \rangle W(F'FJ'J; 1I)|^2 \frac{1}{T_0} \quad (5.2.6)$$

in which $W(F'FJ'J; 1I)$ is a Racah coefficient and

$$\frac{1}{T_0} = \sum_{F'M'} B(JFM \rightarrow J'F'M') = \frac{8\pi^3 \nu e^2}{hc} |\langle J || r || J' \rangle|^2 j_\nu^\mu = \pi r_0 c f_D j_\nu^\mu \quad (5.2.7)$$

where r_0 is the classical radius of the electron, and f_D is the oscillator strength,²⁷ which, for an unpolarized beam (an incoherent and equal mixture of $\mu = \pm 1$) is nearly $\frac{1}{2}$ for $J' = \frac{1}{2}$ ("D₁" transition) and $\frac{1}{3}$ for $J' = \frac{3}{2}$ ("D₂" transition). We define the relative transition probabilities $b(JFM \rightarrow J'F'M')$ thus

$$\frac{1}{T_0} b(JFM \rightarrow J'F'M') = B(JFM \rightarrow J'F'M'). \quad (5.2.8)$$

Now let ω_{ij} represent the probability per unit time that an atom initially in the state $(F, M)_i$ will, as a result of absorbing and re-emitting one quantum, be in the state $(F, M)_j$. In computing the elements of the matrix ω_{ij} , sometimes called the *optical pumping matrix*, we shall make the simplifying assumption that there is a negligible overlap between the different P -state hyperfine (F') levels; then under broad excitation the processes of absorption and emission may be taken as independent (consistent with the conservation of energy to within the breadth of the ground state). In addition, a knowledge is needed of how the substate populations of the resonant excited state are allowed to evolve before radiative decay occurs. If, for example, the atoms diffuse through a buffer gas in which the collision frequency exceeds the natural breadth of the excited state, then the populations of these substates are equalized and there is a complete loss of memory of any selectivity in the excitation process. If t_R is the relaxation time for the excited state and $1/\Gamma$ is its lifetime, then we may write

$$\omega_{ij} = \sum_{k'} b_{ik'} a_{k'j}, \quad t_R \gg \frac{1}{\Gamma}; \quad \omega_{ij} = \frac{1}{N} \sum_{k'm'} b_{ik'} a_{m'j}, \quad t_R \ll \frac{1}{\Gamma}, \quad (5.2.9)$$

where N is the total number of substates in the upper level, and $b_{ik'}$, $a_{m'j}$ are the relative transition probabilities for absorption and emission,

²⁷ A. C. G. Mitchell and M. W. Zemansky, "Resonance Radiation and Excited Atoms." Cambridge Univ. Press, London and New York, 1934.

5. OPTICAL PUMPING

respectively. In the case of $t_R \ll 1/\Gamma$, where complete disorientation occurs, the expression for ω_{ij} is particularly simple; in fact, since $\sum_{m'} a_{m'j} = 1$, we have

$$\omega_{ij} = \frac{1}{N} \sum_{k'} b_{ik'}, \quad t_R \ll \frac{1}{\Gamma}, \quad (5.2.10)$$

which shows that it is determined solely by the absorption probabilities. This has the consequence, which is important in practice,¹⁰ that if j_r is constant over the frequencies of both D transitions, the value of ω_{ij} is the same for all i, j , and no preferred orientation can result. Henceforth we shall assume that $j_r = 0$ for the D_2 frequencies. The evolution of the M -state populations in the ground state under the action of the light alone is governed then by a set of linear equations of the form²³

$$\frac{d\rho_i}{dt} = -\frac{\rho_i}{T_0} \sum_j \omega_{ij} + \frac{1}{T_0} \sum_j \omega_{ji} \rho_j. \quad (5.2.11)$$

Assuming the pumping light has a pure circular polarization, then $f_{D^{\mu}} = 1/6$ and the mean time an atom spends in a given $(F, M)_i$ substate is given by $(\alpha_i)^{-1}$ where

$$\alpha_i = \frac{1}{T_0} \sum_j \omega_{ij}. \quad (5.2.12)$$

In practice this time must be short enough for the pumping to compete favorably with any relaxation mechanism acting on the atom, but not so short as to be a significant source of broadening of the level. This description in terms of the populations is adequate, apart from the refinements of the type discussed by Barrat and Cohen-Tannoudji²³ provided the pumping radiation is not a coherent mixture of different states of polarization. It is of the essence of optical pumping to make $\omega_{ij} \neq \omega_{ji}$ through the selectivity introduced into the absorption process, either by the use of polarized light, or, as in the case of "hyperfine pumping," by an unequal j_r distribution for the different hyperfine components. Numerical solutions of the pumping equations (usually obtained with the aid of a computer) have been given for several of the alkali elements²⁸ both for complete disorientation in the excited state, and in the absence of it. As a concrete example we choose one that can readily be solved explicitly, namely D_1 pumping with σ^+ light of a fictitious alkali atom with $I = 0$, as illustrated in Fig. 2. In this case it is easily verified that

$$\rho_{1/2} - \rho_{-1/2} = (\omega_{-1/2, 1/2} - \omega_{1/2, -1/2})[1 - \exp(-t/T_0)], \quad (5.2.13)$$

²⁸ W. Franzen and A. G. Emslie, *Phys. Rev.* **108**, 1453 (1957); W. B. Hawkins, *ibid.* **123**, 544 (1961).

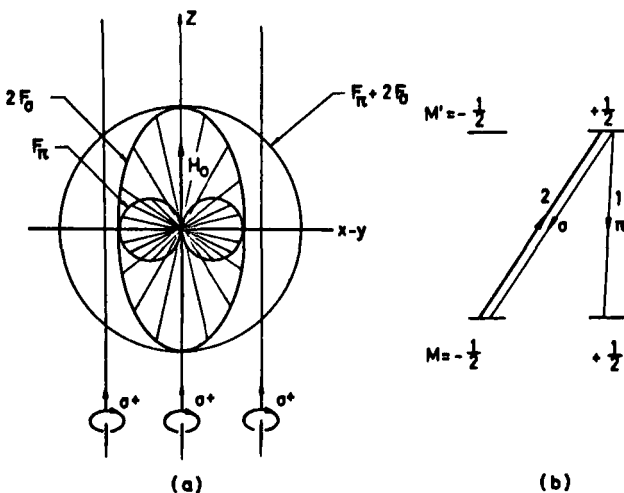


FIG. 2. Optical pumping of a fictitious alkali atom having $I = 0$ using D_{1,σ^+} pumping radiation. (a) The general character of the radiation patterns of the transitions involved; (b) the optical pumping diagram showing the relative transition probabilities for the σ and π transitions.

showing that since $\omega_{-1/2,1/2} \neq \omega_{1/2,-1/2}$ ($\omega_{1/2,-1/2} = 0$ for pure σ^+ radiation) the polarization ($\rho_{1/2} - \rho_{-1/2}$) builds up exponentially with a time constant $1/T_0$ to the value of $(\omega_{-1/2,1/2} - \omega_{1/2,-1/2})$.

Having outlined how an orientation may be obtained, we now consider the problem of observing this orientation. A direct measurement of the absorption or emission of the small Zeeman energy is impractical because of the small macroscopic moments involved; instead a "trigger" type of method is used in which transitions involving radio-frequency quanta are monitored by their effect on transitions at optical frequencies (representing in a crude sense a power gain on the order of 10^{10}). Of the optical observables, the total absorption of pumping radiation and the intensity or radiation pattern of the fluorescence have been extensively used; we will consider here only the absorption process.

The absorption probabilities will in general depend on the state of polarization of the radiation; a coherent mixture of polarization states makes the absorption sensitive to off-diagonal elements in the density matrix; however, we will retain here the restriction to light of a pure polarization, for which the total absorption probability per unit time, α , is given by

$$\alpha = \sum_i \alpha_i \rho_i . \quad (5.2.14)$$

5. OPTICAL PUMPING

It should be noted that this expression is valid even in the presence of off-diagonal elements in the density matrix, and that α_s is independent of the degree of disorientation in the excited state.

We will consider two cases of practical importance: (i) the radiation has a pure circular polarization with j_z constant over the D_1 frequencies but zero otherwise, (ii) the light is unpolarized, directed along the z axis, with j_z finite and constant over the M -states of one hyperfine component (F -state) of the D_1 transition but is small otherwise. Case (i) obtains when one monitors the absorption of the light beam used in the usual pumping of M -states. The total absorption α in this case can be shown to satisfy

$$\alpha_s = \frac{2}{3} \frac{1}{T_0} (\frac{1}{2} - \langle S_z \rangle) \quad (5.2.15)$$

and therefore monitors the spin polarization $\langle S_z \rangle$ of the atoms. It is clear from this that α approaches zero for a fully oriented system; this is physically evident since the action of the pumping radiation is to depopulate the absorbing states. Case (ii), on the other hand, as a pumping process, leads to an inequality in the populations of the two hyperfine states $F = I \pm \frac{1}{2}$, and the absorption can be shown to monitor $\langle \mathbf{I} \cdot \mathbf{S} \rangle$; thus,

$$\alpha_F = \frac{c}{T_0} (1 + k \langle \mathbf{I} \cdot \mathbf{S} \rangle) \quad (5.2.16)$$

where c, k are constants.

We shall now briefly consider the method of magnetic resonance with the particular aim of indicating how the magnetic spectral line-shape is affected by the presence of the optical pumping radiation itself; other perturbations will generally be represented by phenomenological relaxation terms of the same form.

An atom having the nuclear and electronic spins coupled by the hyperfine interaction will, when placed in a uniform magnetic field H_0 directed along the z axis, have a magnetic Hamiltonian of the form

$$\mathcal{H} = H_0(\gamma_J J_z + \gamma_I I_z) + a \mathbf{I} \cdot \mathbf{J} \quad (5.2.17)$$

whose eigenvalues for $J = \frac{1}{2}$ are given by the Breit-Rabi²⁹ formula for all field intensities. In the region of low fields where \mathcal{H} is approximately diagonal in the F, M representation, the energy levels of the different M -states are nearly equally spaced and, at sufficiently small fields, one obtains a complete overlap of transition frequencies between adjacent

²⁹ G. Breit and I. I. Rabi, *Phys. Rev.* **38**, 2082 (1931).

M -states, resembling for each F value those of a single spin with a gyro-magnetic ratio given approximately by $\gamma_F = \pm \gamma_J/(2I + 1)$ for $F = I \pm \frac{1}{2}$ and a Zeeman frequency $\omega_0 = \gamma_F H_0$. The behavior of such a spin in the presence of a circularly polarized high-frequency magnetic field H_1 as a means of inducing transitions between the various M -states has been solved by Majorana.³⁰ Being a multilevel system its exact analysis is complicated; however, Brossel³¹ has, for example, deduced theoretical line-shapes on the basis of the free spin solution of Majorana for magnetic transitions in an optically excited state of Hg. When the overlap of transition frequencies is induced by the broadening due to the application of a sufficiently intense H_1 field, multiple (radio-frequency) quantum transitions become observable.³²

The case of the two-level system, however, is a great deal simpler and is nonetheless important for two reasons: the solution for a multilevel system can be constructed from it, and, secondly, it is often possible to choose the experimental conditions where it gives an adequate description. Thus consider the case of a weak H_1 field acting on the system in the presence of an H_0 field of such intensity that a small quadratic splitting makes the overlap of frequencies negligible. In this case if the frequency of H_1 is in resonance with the transition frequency for one pair of adjacent sub-states M and $M + 1$, transitions between only these two states need be considered; the others are negligibly weak. In writing down the contribution of H_1 to the time evolution of the density matrix, one may then neglect matrix elements connecting all states except the two in resonance with H_1 .

In order to describe the effects of the radiation on the magnetic spectral lines, the equations for the full density matrix are necessary, and have been given by Barrat and Cohen-Tannoudji.²³ These authors have shown that for a system in which only one optical hyperfine component is involved, connecting to an excited state with a Zeeman frequency of ω_e , the off-diagonal elements obey equations which in the two-level approximation may be written in the following form:

$$\begin{aligned} \frac{d\rho_{MM+1}}{dt} \simeq & - \left[\frac{\alpha_{M+1} + \alpha_M}{2T_0} - i\Delta E' (\alpha_{M+1} - \alpha_M) \right] \rho_{MM+1} \\ & + \frac{\Gamma B_{M+1M}^{M+1M}}{T_0[\Gamma + i(\omega_0 - \omega_e)]} \rho_{M+1M} \end{aligned} \quad (5.2.18)$$

where the quantity B_{M+1M}^{M+1M} is a function of transition amplitudes. This

³⁰ E. Majorana, *Nuovo Cimento* **9**, 43 (1932).

³¹ J. Brossel, *Ann. Phys. (Paris)* **7**, 622 (1952).

³² J. Winter, *Ann. Phys. (Paris)*, **19**, 746 (1959).

5. OPTICAL PUMPING

equation and a conjugate one for ρ_{M+1M} have solutions of the form

$$\rho_{MM+1} = \rho_{MM+1}^0 \exp\left(-\left(\frac{1}{T_2} + i\varepsilon\right)t\right) \quad (5.2.19)$$

where

$$\frac{1}{T_2} = \frac{\alpha_{M+1} + \alpha_M}{2T_0} - \frac{1}{T_0} B_{M+1M}^{M+1M} \frac{\Gamma^2}{\Gamma^2 + (\omega_0 - \omega_e)^2} \quad (5.2.20)$$

and

$$\varepsilon = \Delta E' (\alpha_{M+1} - \alpha_M) + \frac{1}{T_0} B_{M+1M}^{M+1M} \frac{\Gamma(\omega_0 - \omega_e)}{\Gamma^2 + (\omega_0 - \omega_e)^2}. \quad (5.2.21)$$

The physical interpretation of these equations is briefly as follows: $1/T_2$, which is the time constant for decay of coherence between the substates, is made up of a contribution from the loss of coherence in the optical absorption process, and one which represents the partial preservation of coherence during the entire pumping cycle; ε represents a shift in the frequency of the Zeeman transition connecting the two states and is also a sum of two terms, the first of which represents a radiation shift due to *virtual* quantum transitions while the second relates to *real* transitions. These shifts have been studied experimentally in Hg¹⁹⁹ by Cohen-Tannoudji, and in He*(2³S₁) by Shearer.¹⁹

In order to obtain the magnetic resonance line-shape explicitly in the presence of the radiation (and a large class of other types of relaxation processes which leads to terms of a similar form) we note that the magnetic dipole transitions induced by a circularly polarized H_1 magnetic field of frequency ω may be fully represented in the steady-state equations by terms in the population equations using a transition probability per unit time given by³³

$$P(\omega) = \frac{2|h|^2 T_2}{(\omega - \omega_0 - \varepsilon)^2 T_2^2 + 1}; \quad h = \gamma_F \frac{H_1}{2} \langle M+1 | F_+ | M \rangle. \quad (5.2.22)$$

In the limit of small H_1 it can readily be shown that the changes in the populations of *all* the substates are proportional to $P(\omega)$, and therefore the optically observed line-shape under these circumstances will be a simple Lorentzian of half-width $(\pi T_2)^{-1}$, with the center frequency shifted by $\varepsilon/2\pi$.

³³ A. Abragam, "Principles of Nuclear Magnetism." Oxford Univ. Press, London and New York, 1961.

5.3. Apparatus

The problems of carrying out an optical pumping experiment center around the following: the containment of the atoms in a way free of undesirable perturbations, the means of producing and monitoring a sufficiently intense and stable beam of pumping radiation, and the provision of a controlled magnetic environment.

5.3.1. Containment

The original method of obtaining a localized concentration of free atoms was through the use of atomic beams, whose production, being a fundamental problem in the field of molecular beam spectroscopy, has long been studied.^{34*} However, since in the case of optical pumping we are not required to produce an intense narrow beam for state selection by magnetic deflection, the problem is a great deal simpler.

The beam source is an oven, with a small opening, in which the element is vaporized to a vapor pressure compatible with the well-known condition for beam formation $d \leq \lambda$ where λ is the mean free path of the atoms and d is the diameter of the opening. A refluxing type of oven for Cs, permitting degassing of the metal in an ultrahigh vacuum glass system, has been successfully used by the author.²² On emerging from the oven the atoms within a well-defined cone pass through a limiting aperture into the optical pumping region, where they are irradiated with the pumping light over a sufficient length of their trajectories to achieve the desired degree of orientation. Where low melting point elements are involved care must be taken to ensure that in the optical pumping region the background concentration of the atoms and the amount of condensation on the glass surfaces are within tolerable limits.

The body of current work on optical pumping is done with atoms contained in an absorption cell, either filled with an inert buffer gas to hinder diffusion to the walls, or lined with a magnetically inert coating³⁵ in order to reduce the relaxation rate at the walls, which would otherwise be the mean time of direct flight across the cell. The cells are generally made of Pyrex of a spherical or cylindrical geometry with a side tube, connected to

³⁴ N. F. Ramsey, "Molecular Beams." Oxford Univ. Press, London and New York, 1956.

³⁵ C. O. Alley, *Advan. Quantum Electron.* (J. R. Singer, ed.), p. 120. Columbia Univ. Press, New York, 1961.

* See also Vol. 3, Part 6.

the cell through a narrow constriction, for the purpose of containing the metal.

For wax-lined cells it is essential that the area of the constriction be a sufficiently small fraction of the total area of the envelope. The reason is that atoms coming into contact with the free metal surface lose their orientation, and therefore, even assuming that the atoms can make an infinite number of nondisorienting bounces off the wax surface, the mean disorientation time can never exceed the value given by

$$T_1 \leq 4V/\bar{v}s \quad (5.3.1)$$

where V is the volume of the cell, \bar{v} is the mean velocity of the atoms, and s is the area of the constriction.

The concentration of the atoms is controlled by maintaining the temperature of the free surface of the metal a few degrees lower than the rest of the envelope, so that, at equilibrium, the vapor pressure is the saturation value at the temperature of the metal. To maintain this temperature distribution, a constant-temperature enclosure is required, which, in cases where there is a need to avoid undesirable magnetic fields in the immediate vicinity of the cell, is usually heated from a remote source by circulating oil, or, in some cases, air.

In the construction of the cells, it has become increasingly evident that, where they are to be used for the determination of relaxation times in the noble gases,³⁶ there is a particular need to achieve a level of purity characteristic of an ultrahigh vacuum system. While the requirements on purity are not always so demanding, good experimental practice dictates that the cell envelope should be baked for a few hours at about 400°C under continuous pumping at 10^{-6} mm Hg before the metal is distilled into the reservoir and the buffer gas or wall coating material is introduced. This procedure will reduce the desorption of undesirable gases from the walls and contamination of the metal.

5.3.2. Magnetic Fields

The selection of the magnetic environment and the sophistication in the design of the field sources is of course determined by the degree of magnetic spectral resolution one is striving to attain. For low fieldwork, which has thus far received the most attention, it is advisable to minimize the presence of ferromagnetic materials in the vicinity of the absorption cell, and, if the choice exists, to set up the experiment in a location where time-varying fields from power lines and electrical machinery is minimal. The

³⁶ F. A. Franz, *Phys. Rev.* **139**, A603 (1965).

desired fields are then established with an array of coils of such a number and dimensions as will give the desired degree of field uniformity.

The simplest of such arrays is the Helmholtz pair,³⁷ which consists of two circular coils of equal radius mounted coaxially one radius apart. For coils having a constant current density over a cross section of axial width η and radial depth ξ , Maxwell has shown that the scalar potential of the field in the neighborhood of the center of the system is given (in electromagnetic units) by

$$\Phi_m = \frac{16\pi ni}{5\sqrt{5}} \left(1 - \frac{\xi^2}{60a^2}\right) \frac{r}{a} P_1(\theta) + \frac{2^5}{5^4} \frac{ni}{3\sqrt{5}} (31\xi^2 - 36\eta^2) \frac{r^3}{a^3} P_3(\theta) - \frac{2^{83^2}}{5^5} \frac{ni}{\sqrt{5}} \frac{r^5}{a^5} P_5(\theta) \quad (5.3.2)$$

where r, θ are spherical polar coordinates with the axis of the coils taken as the z axis, and a is the radius to the center of the winding. It is evident from this that if the following condition is satisfied,

$$31\xi^2 = 36\eta^2, \quad (5.3.3)$$

the third-order term in the potential drops out, as it does for conductors of infinitesimal cross section.

A considerable improvement in the uniformity of the field can be achieved by using, in addition to the main field-producing Helmholtz pair, another smaller pair³⁸ having the same current flowing in the opposite direction to the former, and having a radius a' and number of turns n' such that

$$\frac{n'}{a'^5} = \frac{n}{a^5}. \quad (5.3.4)$$

It is evident from the expression for Φ_m that, in the combined field of the two Helmholtz pairs, the fifth-order term in the potential drops out. It must be remembered, however, that the cancellation of higher-order terms implies a uniformity which can be realized in practice only if the tolerances on the dimensions are close enough that the lower-order terms make a sufficiently small contribution.

The cancellation of static field gradients due to the laboratory environment may be accomplished in an "orthogonal" manner through the use of arrays of linear conductors.³⁹ Since the atomic Zeeman frequencies depend on the magnitude of the magnetic field and not its direction, gradients

³⁷ A. E. Ruark and M. F. Peters, *J. Opt. Soc. Am.* **13**, 205 (1926).

³⁸ G. G. Scott, *Rev. Sci. Instr.* **28**, 270 (1957).

³⁹ W. A. Anderson, *Rev. Sci. Instr.* **32**, 241 (1961).

in the transverse components of the field contribute only to second order, and therefore only the three gradients in H_z are important. To produce a constant $\partial H_z / \partial z$ requires two pairs of long parallel conductors joined at their ends to form rectangles of width d , and placed in the $z = \pm d/2$ planes with the current circulating in the opposite direction in the two planes. The $\partial H_z / \partial y$ gradient requires two parallel rectangles in each of the planes $z = \pm d/2$ of width d and spacing $2^{1/2}d$, center to center. Of course the configuration for $\partial H_z / \partial x$ is that for $\partial H_z / \partial y$ rotated through 90° about the z axis.

5.3.3. Light Sources

It was realized early in the history of the study of resonance fluorescence that the intensity of the fluorescence was strongly dependent on the mode of operation of the source of exciting radiation.²⁷ The fluorescent atoms have a relatively sharp absorption line-width, and the amount of fluorescence is sensitive to the profile of the emission line from the lamp; particularly the presence of self-reversal, a condition arising usually at relatively high vapor densities of the emitting atoms, when an unfavorable distribution of excitation allows light originating from one part of the lamp to pass through cooler layers of atoms which absorb radiation from the center of the spectral line.

It was to minimize self-reversal and avoid the electrode noise of the dc arc that the high-frequency electrodeless discharge lamp was developed.⁴⁰ In this type of lamp the atoms are excited in a plasma sustained in a mixture of the atomic vapor and an inert gas at a pressure of about 2 mm Hg by a radio-frequency field. This field is generated by a radio-frequency current circulating in coils of such geometry and disposed in such a manner around the lamp that the dissipation of rf energy in the plasma and the glass envelope (glass being a lossy dielectric at elevated temperatures) determines a temperature distribution permitting the vapor pressure to come to equilibrium with the metal in the reservoir. Stable operation free from relaxation oscillations also requires that if an excursion from equilibrium occurs, with an accompanying change in the impedance of the plasma, the intensity of the rf field must compensate for it. This is satisfactorily accomplished by energizing the coils from a source of constant rf current. When these requirements are met, these lamps provide a radiated output free from self-reversal and with a spectral brightness and stability remarkably close to the theoretical limits.

⁴⁰ W. E. Bell, A. L. Bloom, and J. Lynch, *Rev. Sci. Instr.* **32**, 688 (1961); R. G. Brewer, *ibid.* **32**, 1356 (1961).

5.3.4. Photodetectors*

The choice of a photodetector is naturally dependent on the level of intensity and wavelength of the radiation, and the frequency response required. A detector with a quantum conversion efficiency ζ and collection efficiency q ($=1$ for a vacuum phototube, but generally <1 for a solid-state detector) will see the photon shot noise in the incident beam only if the following condition is satisfied:

$$\frac{\overline{i_n^2}}{e^2 \zeta^2 q^2 J} \leq 1 \quad (5.3.5)$$

where $\overline{i_n^2}$ is the mean square fluctuation in the photocurrent due to internal causes in the detector, J is the number of incident photons per second, and e is the electronic charge. It is evident from this that, for the relatively large J values involved in the transmission monitoring method, the problem of attaining the optimum ratio of signal to noise hinges less in practice on the reduction of the dark current but rather of J -dependent types of noise, such as the $1/f$ noise.⁴¹ In the case of solid-state $p-n$ junction photodiodes operating in the photovoltaic mode, a strong reduction in $1/f$ noise is achievable by choosing the operating point at $V = 0$, where V is the voltage bias. This requires that the illuminated cell either be connected to a low dc impedance load (an inductor) or be actively provided a low-impedance load at the input of a fed-back amplifier. Although vacuum photocells have commonly been used, junction photodiodes in Si, Se, and GaAs⁴² are available with high quantum efficiency (≈ 1) in the near-infrared and visible regions of the spectrum.

The essential parts of an optical pumping apparatus using optical transmission monitoring are depicted in Fig. 3. The components should be rigidly mounted on a nonmagnetic optical bench in a laboratory environment as free as possible of magnetic, mechanical, and optical sources of noise.

Thanks to the inventive genius of Land,⁴³ large sheet polarizers and $\lambda/4$ retardation sheets are readily available commercially; as are the multi-layer dielectric interference filters for isolating the D_1 wavelength in the heavier alkali elements.

⁴¹ G. R. Pruett and R. L. Petritz. *Proc. IRE* **47**, 1524 (1959).

⁴² G. Lucovsky and P. H. Cholet, *J. Opt. Soc. Am.* **50**, 979 (1960); E. G. Bylander, A. J. Hodges, and J. A. Roberts, *ibid.* **50**, 983 (1960).

⁴³ E. H. Land, *J. Opt. Soc. Am.* **41**, 957 (1951).

* See also Vol. 2, Chapter 11.1; Vol. 4A, Chapter 2.3.

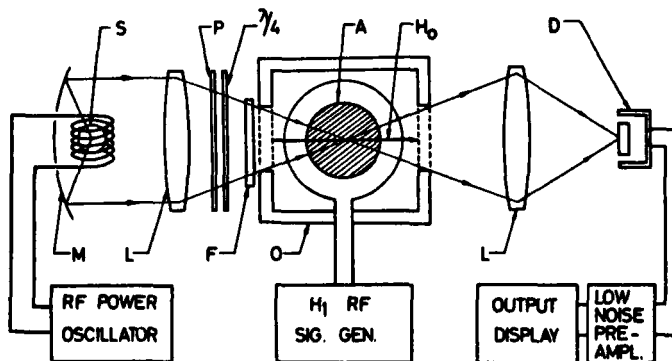


FIG. 3. Schematic diagram of typical optical pumping apparatus utilizing transmission monitoring. S is the source of pumping radiation; M , L form the optical condensing system, P is the sheet polarizer, $\lambda/4$ the quarter wave sheet, F the interference D_1 filter, H_0 the magnetic field, A the absorption cell, O the constant temperature oven, L a converging lens, and D the photodetector.

5.4. Spin Exchange

When an atomic system having an uncompensated spin angular momentum collides with another, there is, in general, a finite probability that a rearrangement of electron spins will occur;⁴⁴ a process of great interest both as a means of extending the range of application of the optical pumping technique and as a relaxation process.

In a collision between two atoms in S ground states, each with an electronic spin of $\frac{1}{2}$, it can be shown that,⁴⁵ neglecting spin-orbit interactions, the scattering is described by

$$\Psi_s \rightarrow e^{ikz} \psi_0 + \left[\frac{1}{4} (f_1 + f_0) \frac{e^{ikR}}{R} + \frac{1}{4} (f_1 - f_0)(1 - \sigma_1 \cdot \sigma_2) \frac{e^{ikR}}{R} \right] \psi_0 \quad (5.4.1)$$

where ψ_0 is the total electronic wave function for the noninteracting two-atom system, σ_1 and σ_2 are the Pauli spin operators for the two atoms, and f_1 , f_0 are the scattering amplitudes for the two possible total spin states, $S = 1$ and $S = 0$. The character of the interaction between the atoms in these two states is known from the theory of the H_2 molecule; the triplet ($S = 1$) interaction is repulsive (except for a small Van der Waals force at

⁴⁴ E. M. Purcell and G. B. Field, *Astrophys. J.* **124**, 542 (1956); J. P. Wittke and R. H. Dicke, *Phys. Rev.* **103**, 620 (1956).

⁴⁵ A. Dalgarno, *Proc. Roy. Soc. A* **262**, 132 (1961).

large nuclear separations) and the singlet ($S = 0$) interaction is attractive, becoming repulsive only at such small nuclear separations that the repulsion of the cores dominates. The scattering amplitudes are therefore expected to differ in general, leading to a finite cross section for spin exchange as computed from

$$Q_x = \frac{1}{4} |f_1 - f_0|^2. \quad (5.4.2)$$

If f_1, f_0 are written in terms of the phase shifts in a partial wave expansion, thus

$$f_{1,0} = \frac{1}{2ik} \sum_{l=0}^{\infty} (2l+1) \{ \exp(2i\delta^{1,0}) - 1 \} P_l(\theta), \quad (5.4.3)$$

the expression for the spin-exchange cross section becomes

$$Q_x = \frac{\pi}{k^2} \sum_{l=0}^{\infty} (2l+1) \sin^2(\delta_l^1 - \delta_l^0). \quad (5.4.4)$$

At low energies the numerical value of this cross section can be quite large; for example, nearly $300 \pi a_0^2$ for thermal electrons on Na,¹¹ and about $30 \pi a_0^2$ for two H atoms at 300°K.⁴⁵

As mentioned in the introduction, following the pioneering work of Dehmelt¹¹ on the polarization of free electrons through spin exchange with optically oriented Na, a large number of workers have since used the technique in the study of the magnetic resonance spectra of such systems as H, N, P, and Ag. In these experiments the atoms are allowed to interact with the alkali vapor in the absorption cell, under continuous optical pumping. In the case of H, N, and P, the atoms are formed by a partial dissociation of the molecules using an electrical discharge in a manner which minimizes the disruption of the rest of the system; this may be accomplished by carrying out the dissociation in a side tube and using a flow system to transfer the atoms to the absorption cell. The chemical activity of P necessitates a peculiar arrangement to control this element, but otherwise the same basic technique is used. As the two species of atoms are allowed to make spin-exchange collisions they will each acquire a degree of polarization determined by the relaxation processes acting in competition with the orienting processes; hence, if the unknown atoms are disoriented by a resonant H_1 field, this in effect increases the relaxation⁴⁶ for the alkali atoms, and leads to a reduction in their polarization which can be optically monitored.

To understand the behavior of systems undergoing spin exchange, and to relate the physical observables to the scattering amplitudes for the

⁴⁶ F. Grosssetete, *J. Phys. Radium* **25**, 383 (1964).

5. OPTICAL PUMPING

various total spin states, requires a theory which in its full generality would be extremely complicated, considering the large number of other interactions involved in an actual system. To bring out some of the basic properties of such systems, assume we have two spin- $\frac{1}{2}$ systems with no nuclear spin and let the spin-exchange process be characterized by a mean exchange time T_x , which will prove to be valid for a description of spin state populations; then if ρ_1^+ , ρ_1^- represent the occupation probabilities of the states $m_s = \frac{1}{2}$ and $m_s = -\frac{1}{2}$ for system (1), with similar notation for system (2), we may write

$$\frac{d\rho_1^+}{dt} = -\frac{1}{T_x} \rho_2^- \rho_1^+ + \frac{1}{T_x} \rho_2^+ \rho_1^-, \quad \frac{d\rho_1^-}{dt} = -\frac{1}{T_x} \rho_2^+ \rho_1^- + \frac{1}{T_x} \rho_2^- \rho_1^+. \quad (5.4.5)$$

Rewritten in terms of the polarizations $P_1^+ = \frac{1}{2}(1 + P_1)$ and $P_1^- = \frac{1}{2}(1 - P_1)$ these equations become

$$\frac{dP_1}{dt} = -\frac{1}{T_x} (P_1 - P_2) \quad (5.4.6)$$

with a similar equation for P_2 . It is clear from this that the system tends towards equilibrium in which $P_1 = P_2$ with a time constant $1/T_x$. If, as has been done by Balling *et al.*,⁴⁷ a full description of the process is given in terms of the scattering amplitudes (and not merely the magnitude $|f_1 - f_0|^2$) one obtains for the density matrix of system (1), when that of (2) is assumed diagonal, the following equation:

$$\frac{d\rho_1}{dt} = \begin{pmatrix} -\frac{1}{T_x} (\rho_1^+ \rho_2^- - \rho_2^+ \rho_1^-) & -\frac{1}{T_x} [1 - i\kappa(\rho_2^+ - \rho_2^-)] \rho_1^+ \\ -\frac{1}{T_x} [1 + i\kappa(\rho_2^+ - \rho_2^-)] \rho_1^- & -\frac{1}{T_x} (\rho_1^- \rho_2^+ - \rho_2^- \rho_1^+) \end{pmatrix} \quad (5.4.7)$$

where κ , the frequency shift coefficient, is given by

$$\kappa = \frac{1}{Q_x} \frac{\pi}{2k^2} \sum_{l=0}^{\infty} (2l+1) \sin 2(\delta_l^1 - \delta_l^0). \quad (5.4.8)$$

The form of this solution indicates that the magnetic spectral line-shape is Lorentzian with a half-width $\Delta_{1/2}$ and center frequency ν given by

$$\Delta_{1/2} = (\pi T_x)^{-1}, \quad \nu = \nu_0 + \frac{\kappa}{2\pi T_x} (\rho_2^+ - \rho_2^-). \quad (5.4.9)$$

⁴⁷ L. C. Balling, R. J. Hanson, and F. M. Pipkin, *Phys. Rev.* **133**, A607 (1964).

In a series of experiments on the magnetic resonance of free electrons oriented by spin exchange with Rb, Balling *et al.* claim to have observed a frequency shift amounting to 2% of the fraction of the line-width attributed to spin exchange. It should be noted that the form of the above result is unaffected by the presence of nuclear spins⁴⁸ provided the simple expression $(\rho_2^+ - \rho_2^-)$ for the electron polarization is replaced by $2 \operatorname{Tr}(S_z \rho_2)$; this has to do with the fact that during a collision the nuclear spin state does not have time to change appreciably through the hyperfine coupling to the electronic spin. Thus one may expect that in the presence of nuclear spins the following relations hold⁴⁶:

$$\langle s_{1z} \rangle_x = \langle s_{2z} \rangle, \quad \langle I_{1z} \rangle_x = \langle I_{2z} \rangle, \quad \langle F_{1z} + F_{2z} \rangle = \text{const.} \quad (5.4.10)$$

On the basis of the last relationship one is led to postulate that, for an isolated system in which angular momentum is statistically exchanged, an equilibrium distribution of angular momentum may be reached given by

$$\rho_M = \frac{e^{-\beta M}}{\sum_M e^{-\beta M}} \quad (5.4.11)$$

corresponding to the most probable distribution, ρ_M , for a constant total z component of angular momentum. This has been experimentally confirmed in the work of Anderson and Ramsey⁴⁹ on the intensities of magnetic resonance lines in Na. The characterization of the M -state polarization by a single "spin temperature" parameter β under conditions where spin exchange dominates over other spin-dependent interactions is of fundamental importance to the study of M -state relaxation. The reason is that $\langle S_z \rangle$, which is the observable monitored in the study of M -state relaxation, will also be a function of the single parameter β , and the time behavior of both $\langle F_z \rangle$ and S_z is proportional to that of β .

5.5 Relaxation Processes

5.5.1. Introduction

An optically oriented system is far from thermodynamic equilibrium with its surroundings and a study of the relaxation times characterizing the return to equilibrium provides a means of learning about the interactions involved in the relaxation process. Because the different types of such interactions impose a different time behavior on the elements of the

⁴⁸ P. L. Bender, *Phys. Rev.* **134**, A1174 (1964).

⁴⁹ L. W. Anderson and A. T. Ramsey, *Phys. Rev.* **132**, 712 (1963).

5. OPTICAL PUMPING

density matrix, it is important that the optically measured observables be chosen to yield the relaxation times as simply and unambiguously as possible. A theoretical analysis based on Bloch's theory of relaxation has been given by Bloom⁵⁰ in which he compares the relative merits in the above sense of several optical observables when the relaxation is due to one of several types of interactions, such as dipolar, electric quadrupole, spin exchange (with a large "sink" of unpolarized spins) and the pumping radiation itself. On the basis of whether a single time constant can be deduced from these observables, he concludes that, apart from magnetic resonance line-width measurements, the absorption of "hyperfine pumping" radiation is the least open to question (for the decay of $\langle \mathbf{I} \cdot \mathbf{S} \rangle$) in all cases except spin exchange.

5.5.2. Measurement of Relaxation Times

5.5.2.1. Magnetic Resonance Line-Shape. As indicated in Chapter 5.3, the shape of a magnetic spectral line is a simple Lorentzian in the limit of small H_1 intensity in the two-level approximation; it can further be shown that the line-width in the neighborhood of $H_1 = 0$ is given by

$$\Delta_{1/2}^2 = \frac{1}{T_2^2} + \frac{2|h|^2}{T_2} (T_1 + T'_1). \quad (5.5.1)$$

Thus an extrapolation to zero H_1 will yield the transverse relaxation time T_2 and the slope of the curve of $\Delta_{1/2}^2$ versus H_1^2 will yield the combined longitudinal relaxation time ($T_1 + T'_1$) for the two states. Both these relaxation times will have contributions from the pumping process, and therefore if the relaxation due to other causes is desired, the experiment must be repeated at different light intensities and an extrapolation to zero intensity made.

5.5.2.2. Transient Methods. In the form originally used by Dehmelt,⁵¹ the transmission of circularly polarized light is monitored as the spin orientation recovers after reversing its direction relative to the incident beam. This is accomplished by adiabatically turning the magnetic field through 180° in a time much longer than the Zeeman period, but still short compared to all other characteristic times in the system. Since the conditions for spin-exchange equilibrium usually obtain in these experiments, the transmission growth curves as displayed on an oscilloscope may be expected to have approximately a simple exponential character.

In the form later developed by Franzen,⁵² relaxation is allowed to occur

⁵⁰ A. L. Bloom, *Phys. Rev.* **118**, 664 (1960).

⁵¹ H. G. Dehmelt, *J. Opt. Soc. Am.* **55**, 335 (1965).

⁵² W. Franzen, *Phys. Rev.* **113**, 850 (1959).

"in the dark"; that is, the circularly polarized pumping light is interrupted with a shutter for variable lengths of time, and the transmission at the end of each dark period is displayed on an oscilloscope. This method has been extensively used to measure T_1 for the alkali atoms diffusing in various buffer gases.^{36,49,53,54} In these experiments, disorientation cross sections are deduced from the observed relaxation time as a function of the buffer gas pressure. Since complete disorientation occurs at the bare glass walls of the absorption cell, the relaxation is governed both by collisions with the gas atoms and diffusion to the walls; the rate equation for the polarization must therefore include both a diffusion term and a collision term, and be solved with the boundary condition that the polarization is zero at the walls. The relaxation time corresponding to the first-order diffusion mode is assumed to be the one observed, and is expressed as a function of gas pressure in terms of the diffusion coefficient D and the relaxation cross section, which are adjusted to fit the experimental curves.

This method has also been applied to the study of spin exchange as a relaxation process by Grosssetete,⁵⁵ who has also published a detailed theoretical account⁴⁶ of this aspect of spin exchange. This work is notable in that, in contrast to some of the other experimental work on relaxation, a systematic effort is made to control the experimental variables; thus, using enriched isotopes of Rb, the M -state relaxation is measured independently for the two hyperfine levels $F = I \pm \frac{1}{2}$ by using a rotating H_1 field to depolarize one of them.

The same procedure followed in the Franzen method may of course be used in the study of F -state relaxation if, instead of circularly polarized light, "hyperfine pumping" type of light is used. The basic experimental problem in applying this method is to find a suitable source of pumping radiation, that is, one having a large difference in the intensity of the two hyperfine components. This is generally accomplished by exploiting pressure shifts,⁵⁶ Doppler shifts,⁵⁷ or the Zeeman effect⁵⁸ to bring into closer coincidence the wavelength of a hyperfine component of another isotope or element with that of the given element. Thus the hyperfine pumping of Rb⁸⁷ can be accomplished by using a filter of Rb⁸⁵ vapor in Ar at a pressure of 77 mg Hg, while Cs¹³³ has been successfully pumped with an Ar light source in a magnetic field of 5000 G.

⁵³ R. J. McNeal, *J. Chem. Phys.* **40**, 1089 (1964); R. G. Brewer, *ibid.* **40**, 1077 (1964).

⁵⁴ F. A. Franz, and E. Luscher, *Phys. Rev.* **135**, A582 (1964).

⁵⁵ F. Grosssetete, *Compt. Rend.* **258**, 3668 (1964).

⁵⁶ P. Davidovits and N. Knable, *Rev. Sci. Instr.* **35**, 857 (1964).

⁵⁷ H. Bucka, *Z. Physik* **141**, 49 (1955).

⁵⁸ E. C. Beaty, P. L. Bender, and A. R. Chi, *Phys. Rev.* **112**, 450 (1958).

5. OPTICAL PUMPING

This form of the technique has been applied to the study of the relaxation of the Rb isotopes in an evacuated, wax-lined absorption cell by Bouchiat and Brossel.⁵⁹ It is particularly useful in the study of relaxation between the hyperfine levels in spin exchange collisions between identical atoms, a process where the original Franzen method is ineffective. An important extension of this technique has recently been developed in the work of Ardit and Carver⁶⁰ on the relaxation between $F = 2, M = 0$ and $F = 1, M = 0$ states in Rb, in which the populations are monitored by rf emission following an rf pulse.

5.5.2.3. Crossed Beam Technique. Under the action of a resonant H_1 field an optically oriented system will develop a nonzero transverse component of $\langle S \rangle$ which rotates with the Zeeman frequency about the z axis. If a relatively weak circularly polarized monitoring beam is directed along the x axis, its transmission will be modulated at the Zeeman frequency⁶¹ by an amount proportional to $\langle S_x \rangle$ and therefore provides a direct way of measuring the transverse relaxation time T_2 . Thus if H_1 is applied to give a steady-state modulation ($\gamma H_1 T_2 < 1$) and is then suddenly turned off allowing $\langle S_x \rangle$ to decay under the action of the relaxation processes, the amplitude of modulation will also decay with a time constant which can be measured with the aid of an oscilloscope. Alternatively one may apply a 90° H_1 pulse and observe the decay of $\langle S_x \rangle$ in a similar manner. In all cases where these measurements are made in the presence of the primary pumping beam, an extrapolation to zero intensity of this beam is required.

5.5.3. Relaxation Interactions

Apart from the inherent relaxation interactions arising from the pumping radiation and spin exchange between the atoms of the pumped system, studies have been made, as already mentioned, of relaxation processes involving other atomic and molecular systems, both in the gaseous state and as a solid surface layer on the walls of the absorption cell. In Table I are collected some of the results on the disorientation cross section of the alkali atoms interacting with various buffer gases. When these values are compared with the gas kinetic cross sections it becomes evident how remarkably small they are; it takes on the average nearly 10^9 collisions for a Rb atom to become disoriented in He gas. Moreover the observed phase coherence times indicate that the cross section for the loss of coherence must be also comparably small. Attempts to provide a theoretical description of the in-

⁵⁹ M. Bouchiat and J. Brossel, *Compt. Rend.* **257**, 2825 (1963).

⁶⁰ M. Ardit and T. R. Carver, *Phys. Rev.* **136**, A643 (1964).

⁶¹ H. G. Dehmelt, *Phys. Rev.* **105**, 1924 (1957).

TABLE I. Spin Disorientation Cross Sections for Alkali Elements in Various Buffer Gases*

Gas	Na (158°C)	Rb (67°C)	Cs (44°C)
He	$2.2 \times 10^{-26} \text{ a}$	$3.3 \times 10^{-25} \text{ b}$	—
Ne	$1.8 \times 10^{-24} \text{ a}$	$3.3 \times 10^{-24} \text{ b}$	$5.3 \times 10^{-24} \text{ c}$
A	$8.8 \times 10^{-23} \text{ a}$	$1.1 \times 10^{-22} \text{ b}$	$8.0 \times 10^{-23} \text{ c}$
Kr	$2.0 \times 10^{-21} \text{ a}$	$7.3 \times 10^{-21} \text{ b}$	$2.1 \times 10^{-21} \text{ c}$
Xe	$2.5 \times 10^{-20} \text{ a}$	$1.3 \times 10^{-19} \text{ b}$	$4.6 \times 10^{-20} \text{ c}$
$^{14}\text{N}_2$	$4.1 \times 10^{-24} \text{ a}$	$5.7 \times 10^{-23} \text{ d}$	$4.7 \times 10^{-23} \text{ c}$
$^{15}\text{N}_2$	—	—	$5.3 \times 10^{-23} \text{ c}$
H ₂	$2.7 \times 10^{-26} \text{ a}$	$2.2 \times 10^{-24} \text{ e}$	—
D ₂	—	$2.2 \times 10^{-24} \text{ e}$	—

* Cross sections are expressed in cm².

a A. T. Ramsey and L. W. Anderson, *Nuovo Cimento* **32**, 1151 (1964).

b F. A. Franz, *Phys. Rev.* **139**, A603 (1965).

c F. A. Franz and E. Luscher, *Phys. Rev.* **135**, A582 (1964).

d R. J. McNeal, *J. Chem. Phys.* **40**, 1089 (1964); R. G. Brewer, *ibid* **40**, 1077 (1964).

e R. G. Brewer, *J. Chem. Phys.* **37**, 2504 (1962).

teractions responsible for these cross sections have been made by Bernheim⁶² and Herman.⁶³ Since the ground state of the alkali atoms is an *S*-state and the noble gases have a closed shell structure it may be expected that a magnetic perturbation acting on the electron spin can only arise from an orbital angular momentum induced during the collision, or possibly the nuclear moment of the noble gas atom. The perturbation term involving the spin-orbit type of interaction may be written in the form

$$H'_{\text{eff}} = \gamma(R) \mathbf{K} \cdot \mathbf{S} \quad (5.5.2)$$

where \mathbf{K} is the total angular momentum of rotation of the two-atom system during the collision, \mathbf{S} is the electron spin, and $\gamma(R)$ is the strength of the interaction, and is a function of the internuclear distance R . Herman has made detailed estimates of $\gamma(R)$ and finds that for short-range interactions between the atoms the cross sections computed from

$$Q = \frac{4\pi}{3} \int_0^{\infty} \phi^2(b) b db, \quad (5.5.3a)$$

⁶² R. A. Bernheim, *J. Chem. Phys.* **36**, 135 (1962).

⁶³ R. M. Herman, *Phys. Rev.* **136**, A1576 (1964).

where ϕ is a phase shift given by

$$\phi = \frac{K}{2} \int_{\text{coll}} \gamma(t) dt, \quad (5.5.3b)$$

are in satisfactory agreement with the experimental values. This type of dipolar interaction leads to relaxation in a manner which is contained in the work of Bouchiat⁶⁴ on the dipolar relaxation of alkali atoms through an $\mathbf{S} \cdot \mathbf{I}$ interaction between the alkali electron spin and the nuclear moments in a solid surface layer of wax. Under conditions where spin-exchange equilibrium is *not* established the spin polarization $\langle S_z \rangle$ is expected to decay with two time constants: the one calculated from Q above, and one a factor of $(2I + 1)^2/2$ longer, where I is the nuclear spin of the alkali. To observe this two-mode decay using the Franzen method requires a high initial polarization and a degree of precision which has not apparently been attempted.

The problem of the interaction of the alkali spin with the nuclear moment of the gas atom has also been treated by Herman,⁶⁵ who finds that, when properly symmetrized wavefunctions are used, the contact hyperfine interaction can be several orders of magnitude larger than had previously been thought; however, the relaxation cross sections are still relatively small and are expected to make an appreciable contribution only for He for which the spin-orbit interaction is small. Even for He^3 it would seem, on comparing the measured cross section for Rb-He^4 with the value for Rb-He^3 deduced from the work of Bouchiat *et al.*⁶⁶ on the polarization of He^3 nuclei by dipolar exchange with oriented Rb, that the Rb-He^3 cross section is about a factor of 10 smaller than for Rb-He^4 . Brewer⁶⁷ has made an interesting comparison between the relaxation of Rb in H_2 and D_2 in which he finds that the nuclear spin makes no appreciable difference. This behavior is in contrast to relaxation on a solid wax surface where it is observed that the relaxation is predominantly of a dipole-dipole nature; in fact, an increase amounting to a factor of 5 in the relaxation time is observed⁶⁸ when deuterated compounds are used.

5.5.4. Hyperfine Frequency Shifts

The "field-independent" hyperfine transition $\Delta F = 1, M' = 0, M = 0$, whose frequency as a function of H_z has a vanishing first derivative at

⁶⁴ M. A. Bouchiat, *J. Phys. Radium* **24**, 611 (1963).

⁶⁵ R. M. Herman, *Phys. Rev.* **137**, A1062 (1965).

⁶⁶ M. A. Bouchiat, J. Brossel, T. R. Carver, and C. M. Varnum, *Phys. Rev. Letters* **5**, 373 (1960).

⁶⁷ R. G. Brewer, *J. Chem. Phys.* **37**, 2504 (1962).

⁶⁸ J. Brossel, in "Quantum Optics and Electronics" (C. DeWitt *et al.*, eds.), p. 264. Gordon and Breach, New York, 1965.

$H_z = 0$, is of particular importance, both intrinsically and for its use in the establishment of frequency standards. When observed in a buffer gas, the spectral line-width of this transition, being insensitive to small field gradients near $H_z = 0$ and having a Doppler width reduced by the Dicke⁶⁹ effect, is typically a few tens of cycles in a transition frequency of several gigacycles. With this degree of spectral resolution, small shifts in the hyperfine splitting due to collisions with other gas particles or the walls of the absorption cell are observable. The pressure and temperature dependence of these shifts have been studied by Ardit and Carver⁷⁰ and by Bender *et al.*⁷¹; some of the observed pressure coefficients are summarized in Table II. It is interesting to compare these hyperfine shifts with the pressure shifts observed in the optical absorption spectra of the alkali elements; apart from the obvious differences arising from the nature of the transitions, there is a strong resemblance in the dependence of the sign of the shift on the perturbing gas, particularly for the higher members of the alkali principal series.

TABLE II. Displacements in the Ground State HFS Frequencies of Alkali Elements in Various Buffer Gases*

Gas	Na ^a	Rb ^b	Cs ^a
H ₂	—	660	+1900
N ₂	+100	+520	+ 930
He	—	+720	+1600
Ne	+80	+390	+650
A	≈ 0	-51	-250
Kr	—	-580	-1300
Xe	—	—	-2400

* Displacements in the hfs frequencies are given in cps per Torr.

^a E. C. Beaty, P. L. Bender, and A. R. Chi, *Phys. Rev.* **112**, 450 (1958); M. Ardit and T. R. Carver, *Phys. Rev.* **109**, 1012 (1958); **112**, 449 (1958); M. Ardit, *J. Phys. Radium* **19**, 873 (1958).

^b P. L. Bender, E. C. Beaty, and A. R. Chi, *Phys. Rev. Letters* **1**, 311 (1958).

These shifts may be understood in terms of the changes induced in the contact hyperfine interaction through the changes in $|\psi(0)|^2$ caused by the (electrostatic) interactions during a collision. The long-range Van der Waals interaction tends to reduce $|\psi(0)|^2$ and leads to a red shift while short-range

⁶⁹ R. H. Dicke, *Phys. Rev.* **89**, 472 (1953).

⁷⁰ M. Ardit and T. R. Carver, *Phys. Rev.* **109**, 1012 (1958); **112**, 449 (1958).

⁷¹ P. L. Bender, E. C. Beaty, and A. R. Chi, *Phys. Rev. Letters* **1**, 311 (1958).

exchange interactions have the opposite effect; hence, the heavier gases, having a greater polarizability, are expected to have a stronger Van der Waals interaction and consequently a tendency to produce a red shift, whereas the reverse is true for the lighter gases. While the perturbation in the hyperfine energy levels is calculable for the dispersion forces, no such theory exists for the short-range exchange region; it is usually assumed that, since the perturbation follows the same dependence on internuclear distance in the dispersion region as the dispersion energy itself, it is reasonable to expect it to follow the same pattern as typical molecular forces at short range. Explicit derivations of the dispersion energy of an atom in a given hyperfine state, and hence the hyperfine separation in the presence of dispersion forces, have been given by Margenau *et al.*⁷² and has also been studied by Adrian⁷³; the result being of the form

$$\Delta E_{\text{hfs}} = -\frac{3(e\hbar^2)}{2m} \frac{1}{R^6} \frac{f_1 \alpha_2 I_2}{E_1(E_1 + I_2)} \left[\frac{1}{E_1 + I_2} + \frac{2}{I_1} \right] E_{\text{hfs}}^{(0)} \quad (5.5.4)$$

where I_1 , f_1 , and E_1 are the ionization energy, oscillator strength, and excitation energy of the first P -state of the given atom, α_2 and I_2 are the polarizability and ionization energy of the perturbing atom, and R is the internuclear distance. The shift in the mean frequency of the transition, that is, the center frequency for a symmetric line, is then obtained from the following statistical theorem:

$$\Delta\bar{\nu}_{\text{hfs}} = \frac{4\pi n}{h} \int_0^\infty \exp(-U(R)/kT) \Delta E_{\text{hfs}} R^2 dR. \quad (5.5.5)$$

Robinson⁷⁴ has applied this theorem to obtain the frequency shifts and their temperature dependence using for $U(R)$ Lennard-Jones molecular potentials containing R^{-6} and R^{-12} terms, and a similar R dependence with additional R^{-8} and R^{-10} terms for ΔE_{hfs} . All the coefficients in $U(R)$ and ΔE_{hfs} are expressed in terms of physical constants of the atoms except two, which are varied to fit the experimental data. He shows that good numerical agreement with experiment is obtained particularly for the lighter gases, with the resulting values for the atomic radii in reasonable agreement with accepted values.

⁷² H. Margenau, P. Fontana, and L. Klein, *Phys. Rev.* **115**, 87 (1959); R. Herman and H. Margenau, *ibid.* **122**, 1204 (1961).

⁷³ F. J. Adrian, *J. Chem. Phys.* **32**, 972 (1960).

⁷⁴ L. B. Robinson, *Phys. Rev.* **117**, 1275 (1960).

6. SWARMS

6.1. Electron Swarms*

6.1.1. Introduction

A new class of experiments involving collisions of electrons with gas atoms and molecules is now introduced. Typically, low-energy electrons are introduced at one electrode, and a potential difference V is applied between this electrode and an adjoining one. In vacuum, this arrangement would give the electrons the kinetic energy eV , if their initial energy is neglected. In the present chapter, the case is being considered in which gas is present in the system at a density high enough so that the electrons experience a great many atomic or molecular collisions in traveling through the potential fall. Under these circumstances, the electrons also acquire a distribution of velocities in magnitude and direction but a mean energy very much less than eV . Experiments in which the random motion of the electrons plays an important role are called swarm experiments. The treatment thus generally presumes that the gas pressure or density is high enough to limit mean free path lengths for the electrons to values less than about 10^{-2} of the electrode separation in order to reasonably assure a near-uniform distribution. Interest in swarm experiments exists over a large range of field strength and pressure. In addition to the general phenomenology of swarms, specific atomic properties such as collision cross sections of electrons with molecules at low electron energy not obtainable from direct, binary collision studies can be obtained. As the electron energy is raised, inelastic collisions grow in importance, and ultimately the array of phenomena of gas discharges appears.

6.1.2. The Characteristic Variables

A tube consisting of two parallel-plate electrodes about 5 cm in diameter and about 1 cm apart may be envisaged (see Fig. 1). A surrounding envelope of glass or metal for gas containment is further assumed, provided with adequate viewing ports and vacuum and gas controls. The walls must not be allowed to influence the field between the plates or in any way

* Chapter 6.1 is by R. N. Varney and L. H. Fisher.

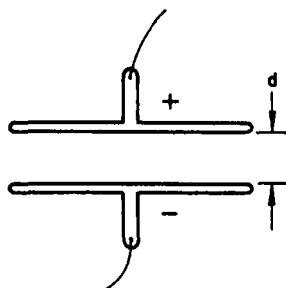


FIG. 1. Two electrodes with potential difference V , separation d , in a tube at pressure p .

disturb the electron motion. Charging of insulating walls and conduction of charges by metallic walls have in some cases in the past influenced measurements and damaged their usefulness. The two electrodes are connected to a voltage supply V . The cathode is assumed to be capable of emitting electrons on demand, for example photoelectrically under ultraviolet illumination. It is desirable to limit the electron emission to a small area at the center of the cathode in order to confine the electron motion to the uniform region of the field between the plates. Under the conditions described, the electron velocity distribution becomes independent of the initial electron energy in a very short distance from the cathode.

The applied voltage V , plate separation d , and gas pressure p are the elementary adjustable experimental parameters. The electric field strength E is, in this simple case, V/d . The field is constant throughout the gap, unless space charge causes deviations from the simple value of V/d . The force on an electron due to the field is eE . Two combinations of variables prove experimentally to be of widespread importance in controlling the behavior of currents in gases. These are E/p and pd . Their importance first appears in that if one or both of the combinations is held constant, various characteristics of the conduction become fixed. Thus, for example, the drift speed of electrons and ions in a gas is found to depend on E/p rather than on E and p separately. Other quantities depending on E/p and on pd are described as they arise. (There are exceptions, which will be pointed out.)

The dependence of various phenomena of electron and ion swarm experiments on E/p and on pd is to be regarded here as strictly experimental. Theoretical justifications become extremely complex because, among other factors, of the uncertainty of the distribution law and the dependence of mean free path on electron speed. With adequate limiting assumptions, proofs are relatively simple, but their validity ultimately falls back on experiment. The discovery of the significance of E/p rather than E/N (N is

the gas molecule number density) as a critical variable was a consequence of the fact that most experiments were done within a few degrees of the same temperature. Actually, E/N or E/ρ (ρ is the gas density) is the more critical controlling quantity; E/p is equally good provided the temperature is specified or, better still, if the pressure is corrected to a standard temperature by the equation

$$p_s = p T_s / T. \quad (6.1.1)$$

Here T and p are the absolute gas temperature and the pressure actually observed in the experiment; p_s is the pressure referred to a standard temperature T_s . The quantity p_s may be characterized as the pressure that would prevail if the density were the same as exists in the tube but the temperature were T_s . Not all authors use the same standard temperature. Some authors have failed to specify the temperature at all, which severely limits the usefulness of their measurements. Values of T_s of 273° , 288° , 295° , 298° , and 300°K have all been used.

6.1.3. Observables of Electron Swarm Experiments

The observables are remarkably unsophisticated. The current may be measured, and, with suitable timing devices, drift speed of the electron motion may be ascertained by a distance versus time observation. In some arrangements, a comparison of motions caused in one direction by an applied electric field and in a perpendicular direction either by a magnetic field or by the diffusion caused by a gradient of density of electrons can also be made. The method employing a magnetic field provides an alternate method for determining electron drift speeds. Finally, an increase or decrease of current (measured under appropriate conditions) is used to disclose information about ionizing collisions that form positive ions, or electron attachments that form negative ions. Other observations may be more intricate and involve instruments such as optical and mass spectrometers. Such observations serve to disclose how electrons may have expended their energy.

As will be seen, many basic atomic properties may be obtained from swarm experiments.

6.1.4. Nature of Drift Velocity or Mobility

When an electric field is applied to a region containing gas and a swarm of electrons, the electrons acquire a drift motion in the direction opposite to E . The electrons take on a drift speed v that is dependent on E/p_s and on the gas. Despite the highly random swarmlike motions of the electrons, the experimentally measured drift speed shows a surprisingly

sharp value. [Far more massive ionic bodies demonstrate such a sharp drift speed also, characteristic of the gas, the ion, and the value of E/p_s (see Chapter 4.1)]. The sharpness of the experimentally determined drift speed is the result of the fact that each electron travels many free-path lengths at many speeds in a centimeter of advance in the field, but when these are averaged, each electron emerges with essentially the same average advance per second. The point is treated (but not for electron drift) in standard works on probability by showing that the average of many events which individually occur with a Poisson distribution takes on a sharply defined value. The drift speeds are far below the mean thermal speeds of electrons by a factor depending on E/p_s . The factor is different for each gas and is usually near 100 at E/p_s of 1 V (cm-Torr) $^{-1}$.

Associated with drift speed, the term *mobility* may be introduced. Mobility, μ , is defined as the drift speed divided by the electric field strength, $\mu = v/E$. The mobility is dependent on the gas pressure, or more specifically on the gas density. The reduced mobility or mobility constant μ_s is, accordingly, defined as

$$\mu_s = \mu(p/P)(T_s/T), \quad (6.1.2)$$

where p and T are the pressure and absolute temperature at which observations are made of μ ; P and T_s refer to standard values, usually NTP, but sometimes with laboratory temperature in place of ice-point temperature. Introducing N and N_s as the gas particle densities at p and T and at P and T_s , respectively, and using the ideal gas law, Eq. (6.1.2) may be rewritten as

$$\mu_s N_s = \mu N. \quad (6.1.3)$$

Values of μN are sometimes quoted as findings. The value of the mobility constant μ_s is then μN divided by the number of molecules per unit volume, N_s , at the chosen standard pressure and temperature, again introducing the problem of whether to choose N_s for 0°C or for a laboratory temperature. The use of μN eliminates any possible misunderstanding but is unfortunately not yet in common practice, nor does μN appear in older literature. More commonly, the quantity described in the literature is

$$\mu_0 = \frac{1}{760} \frac{v}{(E/p_0)} = \frac{273v}{760(E/p)T}, \quad (6.1.4)$$

the pressures being in Torr and the temperature in degrees Kelvin.

The use of mobility instead of drift speed actually originated for ions for the simple reason that μ_s for ions was found to be constant, independent of E/p_s and p (see, however, Chapter 4.1 on ionic drifts). The calculation of Eq. (6.1.2) or (6.1.4) may always be made, but the reduced mobility loses

a certain element of its purpose if indeed, as is the case for electrons, it is *not* constant with E/p_s . In the range of very low values of $E/p_s \gtrsim 10^{-2}$ V (cm-Torr) $^{-1}$, the reduced mobility for electrons is, however, independent of E/p_s .

It should be noted here that both the drift speed v and the reduced mobility μ_s for electrons may be separately dependent on the gas temperature. The temperature "corrections" of Eqs. (6.1.2) and (6.1.4) are only gas-density corrections and do not influence or disclose an intrinsic dependence on T .

6.1.5. Nature of Diffusion and Diffusion Measurement

The basic law for interdiffusion of two gases is applicable without appreciable error to electrons diffusing in a gas. The law may be used to define the coefficient of diffusion D for electrons in gases by the relationship

$$\Gamma = -D \nabla n, \quad (6.1.5)$$

in which Γ is the flux density of electrons due in this case to a density gradient ∇n of the electrons. Γ is the net number of electrons crossing unit area normal to ∇n in unit time (e.g., electrons per square centimeter per second) with n the electron number density (e.g., electrons per cubic centimeter). The limitation that Γ is due only to diffusion implies that no electric fields are acting. In much of the following material, D refers to free electrons at very low density, in neutral gases. If the density of free electrons grows too high, significant space charge is produced with consequent electric fields and violation of the assumption of no fields. The presence of positive ions at suitably low densities does not alter the value of D characterizing the diffusion of electrons. In various stages of discharges and plasmas, virtually every variation of electron density, positive-ion density, space charge, and space neutrality is encountered, and these conditions are in general not treated here, but may be found where they naturally arise.

The equation of continuity indicates that in the absence of sources

$$\nabla \cdot \Gamma = -(\partial n / \partial t), \quad (6.1.6)$$

and the partial differential equation of diffusion results:

$$\nabla \cdot (D \nabla n) = \partial n / \partial t. \quad (6.1.7)$$

If D is constant throughout the region of diffusion, which it is under conditions of small values of n and ∇n , Eq. (6.1.7) takes on the simpler form

$$D \nabla^2 n = \partial n / \partial t. \quad (6.1.8)$$

Solutions of this equation for a variety of initial and boundary conditions exist in the literature. For electrons in gases, as opposed to interdiffusion of two gases, pure diffusion experiments are uncommon. A combination of diffusion with electric-field drift has been used far more commonly. Such an experiment was first designed and carried out by Townsend and Tizard¹ in 1913. In this experiment, electrons are drifting in an electric field and at the same time are diffusing at right angles to the field. For such a case, Eq. (6.1.5) must be rewritten as

$$\Gamma = -D \nabla n + n\mathbf{v}, \quad (6.1.9)$$

where \mathbf{v} is the drift velocity. The flux of electrons Γ is resolvable into the vector sum of a pure diffusion term and a pure drift term. After conversion of this equation to a second-order partial differential equation by the use of the equation of continuity, the new equation presents a more tractable one for application to realizable experiments. This type of experiment has been found of renewed interest in recent times. Its use in studying electron diffusion will be discussed later (see Section 6.1.7).

6.1.6. Experimental Determination of Electron Drift Speeds

Various methods of measuring electron drift speeds in gases have been devised over a period of some 60 years. These include (1) the magnetic deflection method introduced by Townsend and Tizard,² (2) a commutated voltage technique introduced by Rutherford³ for ions and applied by Loeb⁴ and Wahlin⁵ to electrons and very recently with modernized instrumentation by Nolan and Phelps,⁶ (3) an electron shutter method combining ideas of Loeb,⁷ Van de Graaff,⁸ Tyndall *et al.*,⁹ and Bradbury¹⁰ and extensively used by Bradbury and Nielsen,¹¹ by Phelps and associates,¹²

¹ J. S. Townsend and H. T. Tizard, *Proc. Roy. Soc. A* **88**, 336 (1913).

² J. S. Townsend and H. T. Tizard, *Proc. Roy. Soc. A* **87**, 357 (1912).

³ E. Rutherford, *Proc. Cambridge Phil. Soc.* **9**, 401 (1898).

⁴ L. B. Loeb, *Phys. Rev.* **19**, 24 (1922); **20**, 397 (1922); **23**, 157 (1924).

⁵ H. B. Wahlin, *Phys. Rev.* **21**, 517 (1923); **23**, 169 (1924); **27**, 588 (1926); **37**, 260 (1931).

⁶ J. F. Nolan and A. V. Phelps, *Phys. Rev.* **140**, A792 (1965).

⁷ L. B. Loeb, "Basic Processes of Gaseous Electronics," p. 399. Univ. of California Press, Berkeley, California, 1955.

⁸ R. J. Van de Graaff, *Phil. Mag. [7]* **6**, 210 (1928).

⁹ A. M. Tyndall, L. H. Starr, and C. F. Powell, *Proc. Roy. Soc. A* **121**, 172 (1928).

¹⁰ N. E. Bradbury, *Phys. Rev.* **44**, 883 (1933).

¹¹ N. E. Bradbury and R. A. Nielsen, *Phys. Rev.* **49**, 388 (1936); R. A. Nielsen, *ibid.* **50**, 950 (1936); R. A. Nielsen and N. E. Bradbury, *ibid.* **51**, 69 (1937).

¹² A. V. Phelps, J. L. Pack, and L. S. Frost, *Phys. Rev.* **117**, 470 (1960); J. L. Pack and A. V. Phelps, *ibid.* **121**, 798 (1961); J. L. Pack, R. E. Voshall, and A. V. Phelps, *ibid.* **127**, 2084 (1962).

and by Lowke,¹³ (4) an oscilloscopic technique first employed by Hornbeck,¹⁴ and (5) an avalanche and cloud-chamber technique developed by Raether.¹⁵

The electron shutter method has been used to obtain the bulk of the most reliable data presently available, and accordingly a typical experimental form is now described as used by Phelps *et al.*¹² Values of electron drift velocity in various gases using this method cover values of E/p_s ranging in various gases from about 20 down to nearly 10^{-4} V (cm-Torr)⁻¹. The arrangement consists, in order, of an electron source, an initial drift space, with electric field E , bounded by the source and a first grid having the "shutter" capability to be described below but also functioning as an ordinary electrode, the measuring drift space between the first grid and a second grid identical with the first, and finally, an electron collector beyond the second grid. The distance between the first and second grids is accurately measured, and the field strength E between them is also controlled and measured with precision. Fields in the auxiliary spaces, before the first grid and after the second, are usually regulated to be the same as that in the measuring space.

The "shutter" feature of the two grids is now described as used in such a typical experiment. Each grid consists of parallel wires in which all of the odd-numbered wires are connected to one side of a voltage supply and all of the even-numbered wires to the opposite side. Electrons are released continuously from the source photoelectrically and acquire a steady-state drift in the auxiliary space between the source and the first grid. A dc voltage between the odd and even grid wires of the first grid sweeps out the electrons so that none pass through the grid. A signal generator now applies a single short pulse of voltage to the grid wires of grid 1, just neutralizing the dc voltage. (Sometimes a sinusoidal voltage is used instead of a pulse and dc voltage.) While the voltage is removed, electrons pass through grid 1, and then drift in the field between grids 1 and 2. If the voltage pulse on the wires of grid 1 is short, only a burst of electrons is introduced into the principal drift space between the grids.

Grid 2 is operated exactly as is grid 1. No electrons pass through it to the collector electrode unless the pulsed voltage on grid 2 "opens" this shutter at just the time that the burst of electrons passed by grid 1 reaches grid 2. The time interval between the voltage pulses on grids 1 and 2 must be just the transit time for electrons to drift from grid 1 to 2 to obtain a peak reading on the collector.

¹³ J. J. Lowke, *Australian J. Phys.* **16**, 115 (1963).

¹⁴ J. A. Hornbeck, *Phys. Rev.* **83**, 374 (1951).

¹⁵ H. Raether, "Electron Avalanches and Breakdown in Gases." Butterworth, London and Washington, 1964.

In normal operation, the voltage pulsing process consisting of a pulse on shutter 1 followed by another on shutter 2 is repeated at a 1 to 10 kc/sec rate. An electrometer (not an oscilloscope, which under most circumstances cannot provide the necessary amplification *and* the necessary speed) displays the electron current between the second grid and the collector averaged over many pulse repetitions. The time between voltage pulses of a single cycle on the two grids is varied by the operator until the current peaks. The drift distance divided by this time interval gives the electron drift velocity.

Lest the peculiarities of the shutter bias voltages introduce an error in the drift field, it is common to determine the time interval for peak currents with two different drift distances (between grids 1 and 2) and to evaluate the drift speed of the electrons by such a differential procedure.

A variation of this method introduced by Pack and Phelps¹² consists of flashing the ultraviolet light source (flash duration $\sim 1.6 \mu\text{sec}$) so as to produce bursts of electrons from the source with the grids at zero bias. In this method, the electrometer current shows a dip associated with the closing of each shutter. It was hoped that this variation would reduce errors arising from distortion of drift fields by bias voltages.

Method 1 of electron drift speed measurement is of major historical importance, and the same apparatus is used in part for D/μ determinations (see Section 6.1.7). The device depends for drift speed measurement on the use of a magnetic field B transverse to the electric (drift) field and the detection of the resulting lateral drift by the use of a sectored electron collector electrode. No pulsating or shutter device is used. As originally used, the ratio of the transverse electron displacement x to the longitudinal drift distance z was taken to be proportional to the respective forces on the electrons in these directions. The original formulation stated

$$x/z = f_x/f_z = v_z B/cE \quad (\text{Gaussian units}), \quad (6.1.10)$$

where v_z is the drift speed caused by the applied longitudinal field E . Readers are referred to references such as Huxley and Crompton,¹⁶ which shows corrections for proper averaging of speeds. Jory¹⁷ concludes that Eq. (6.1.10) requires a correction that is a function of E/p and may be in excess of 50%. The correction factor is today the primary objective of measurements by this method as it is related to integral averages of electron distribution functions like those of Sections 6.1.9 and 6.1.10.

¹⁶ L. G. H. Huxley and R. W. Crompton, in "Atomic and Molecular Processes" (D. R. Bates, ed.), pp. 335-373. Academic Press, New York, 1962.

¹⁷ R. L. Jory, *Australian J. Phys.* **18**, 237 (1965).

6.1.7. Measurement of D/μ

The Townsend and Tizard² arrangement just described was used by them¹ without the magnetic field to compare the drift of electrons in the longitudinal direction caused by an electric field E with the lateral spread due to diffusion. An evaluation of D/μ was made from these measurements. The method has been employed recently by Warren and Parker,¹⁸ Crompton and Jory,¹⁹ and Rees *et al.*²⁰ Since the lateral diffusion is cylindrically symmetric for a small circular electron source as used in the more recent experiments, a central collecting disk surrounded by two successive concentric collector rings is used. The critical measurement is the ratio of currents to the center and first ring, respectively, or to the first and second ring, respectively. The two ratios should give the same results for D/μ ; failure to do so has led to extensive studies of the causes and the proper means of compensating for the discrepancies. Although improvements have resulted, some uncertainties still remain. Using modern techniques of gaseous purity, highly sensitive meters for current measurement, and sharply collimated electron beams, measurements have been obtained down to E/p_s values as low as 10^{-4} V (cm-Torr)⁻¹. At the lowest values of E/p_s , the ratio D/μ was found to take on a constant value equal to the gas temperature expressed in electron volts (see Section 6.1.10). With measurements of μ and D/μ , the value of the diffusion coefficient D for slow electrons in gases is thus also known.

6.1.8. Kinetic Theory of Diffusion

Relatively generalized, modern treatments of the theory of diffusion (and mobility; see Section 6.1.9) of electrons in gases have been given by Allis²¹ and by Huxley and Crompton.¹⁶ Some treatments earlier than these tend to expand on particular types of distribution laws and on particular forms of the functional dependence of the mean free path on the electron speed. Only the results from Allis²¹ or from Huxley and Crompton¹⁶ are cited here. The theoretical procedures leading to the results involve a high order of approximation and leave no concern regarding any experimental comparison, at least for the domain of elastic collisions. Extreme conditions are imaginable, for example, in discharges from very sharp points where variations of mean electron speed with position are large, under which the

¹⁸ R. W. Warren and J. H. Parker, Jr., *Phys. Rev.* **128**, 2661 (1962).

¹⁹ R. W. Crompton and R. L. Jory, *Australian J. Phys.* **15**, 451 (1962).

²⁰ J. A. Rees and R. L. Jory, *Australian J. Phys.* **17**, 307 (1964); J. A. Rees, *ibid.* p. 462; **18**, 41 (1965).

²¹ W. P. Allis, in "Handbuch der Physik" (S. Flügge, ed.), Vol. 21, pp. 383-444. Springer, Berlin, 1956.

approximations of the theory become questionable. Readers concerned with such cases should resort to the two references cited.

The coefficient of diffusion satisfies a general equation

$$D = (4\pi/3) \int c^3 l(c) f(c) dc. \quad (6.1.11)$$

The distribution function f is normalized to make $4\pi \int c^2 f(c) dc = 1$. Its form is not necessarily known and may, in fact, be determined from measurements involving D to be described in ensuing pages. Specifically, it is not necessarily Maxwellian. The mean free path $l(c)$ is assumed to be a function of the electron speed. $l(c)$ is not necessarily the mean free path that would be measured by an attenuation experiment in a beam of electrons. In diffusion (and mobility) experiments, each scattering event is weighted by its effectiveness in reducing momentum transfer by the electrons across a plane. This value of $l(c)$ is therefore called the *mean free path for momentum transfer*.²² In the interest of correlating the results of swarm experiments with those of beam experiments, a theoretical analysis is standardly made on a basis that all collisions are elastic,¹⁶ an adequate procedure for an interesting enough range of E/p_s and of a number of gases to warrant the analysis. If many inelastic collisions occur, the validity of the comparison does not appear to be adequately treated, but the comparison is probably still satisfactory in comparison with the magnitude of the experimental uncertainties.

Equation (6.1.11) may be seen to be simply $D = \bar{cl}/3$, the product cl being averaged over speeds, rather than the classical kinetic theory expression $D = \frac{1}{3} \bar{c}l$ that applies when l is independent of c or varies only slowly with c .

Since the mean free path varies inversely with the reduced pressure p_s , the quantity Dp_s is independent of the gas pressure. This product, expressed in $\text{cm}^2\text{-sec}^{-1}\text{-Torr}$, is frequently the form in which the diffusion coefficient is presented in tabulations. To analyze the experimental work that is presented in Sections 6.1.11–6.1.16, it is desirable to note at this point that Dp_s is dependent on *three* aspects of the motions of the electrons in the gas. These are (1) the form of the distribution law $f(c)$; (2) the form of the mean free path as a function of speed, $l(c)$; and (3) the effective electron temperature T_e that affects Eq. (6.1.11) by the value of a constant in the distribution law. It may be well also to note at this point what the meaning of "electron temperature" is, and some of its characteristics.

²² S. C. Brown, "Basic Data of Plasma Physics," p. 19. M.I.T. Press, Cambridge, Massachusetts, 1959.

The electrons do not exchange kinetic energy with the gas molecules at all readily, as may be recognized from considerations of the small relative mass of the electrons to that of the molecules and the requirement of conservation of momentum in collisions. The details of this exchange are treated in Section 6.1.16 and are not set out at this point, but it should be recognized that in an electric field the electrons may (in fact, usually do) have a temperature considerably higher than the gas temperature.

The electrons, behaving like a highly attenuated component of a gaseous mixture, satisfy the ideal gas law

$$p_e = nkT_e. \quad (6.1.12)$$

Here n is the number of electrons per unit volume, and k is Boltzmann's constant. The partial pressure of the electrons, p_e , satisfies the expression

$$p_e = \frac{1}{3}nm\bar{c}^2, \quad (6.1.13)$$

where \bar{c}^2 is

$$\bar{c}^2 = 4\pi \int c^4 f(c) dc. \quad (6.1.14)$$

The electron temperature is thus derived as for gases from

$$\frac{3}{2}kT_e = \frac{1}{2}mc\bar{c}^2 = 2\pi m \int c^4 f(c) dc. \quad (6.1.15)$$

As thus defined, the distribution function $f(c)$ does not need to be Maxwellian in order to give meaning to T_e .

6.1.9. Kinetic Theory of Drift Velocity and Mobility

Following the same notation and the same references^{16, 21} as in the preceding section, the electron drift speed v is shown to be

$$v = \frac{4\pi eE}{3m} \int f(c) \frac{d(lc^2)}{dc} dc. \quad (6.1.16)$$

This equation discloses that

$$v = (eE/3m)\bar{c}^{-2}(d/dc)(lc^2). \quad (6.1.17)$$

If l is independent of c so that it may be extracted from both the derivative and the integral of Eq. (6.1.16), it appears that

$$v = (2eE/3m)\bar{c}^{-1}l. \quad (6.1.18)$$

The same equation without the factor E gives the value of the mobility μ . For a Maxwellian distribution of speeds, the mobility then becomes

$$\mu = 8el/3m\bar{c}. \quad (6.1.19)$$

Small variations of l with c can be treated by averaging l and c separately. Stronger variations, and deviations from the Maxwellian distribution law, require the use of the more precise form shown in Eq. (6.1.17).

As is true for the diffusion coefficient, the mobility is dependent on the mean free path, on the electron temperature, and on the law of distribution of speeds. If one of these three characteristics is known, e.g., either the electron temperature or the distribution law, the combined experimental knowledge of μ and D/μ (hence of D) makes evaluation of $l(c)$ possible, or potentially so. The progress of such work is described in Section 6.1.13.

6.1.10. Relationship of D to μ

The experimental measurement of the ratio D/μ suggests at once that the theoretical value of D/μ should be examined by dividing the value of D by that of μ given in the two preceding sections. Analytically, both D and μ depend on $f(c)$ and $l(c)$ so that a relation of possibly meaningful form is imaginable. Finally, the diffusive nature of drift motion, involving many collisions per centimeter of advance in the field direction, gives an intuitive suggestion that a significant relationship between D and μ may exist.

The theoretical evaluation of D/μ appears in countless references, as the ratio has been recognized as interesting for many years. It seems to have been derived first for the case of charged particles in gases by Townsend²³ in 1899, although the name of Einstein is usually associated with it, arising from his work on Brownian movement (hence not charged particle drift at all) in 1905–7.

If $f(c)$ is Maxwellian, calculation of D/μ by dividing Eq. (6.1.11) by Eq. (6.1.16) shows D/μ to be independent of l , and hence independent of the functional form of $l(c)$. The result is

$$\frac{D}{\mu} = \frac{\frac{1}{2}mc^2}{\frac{3}{2}e} = \frac{kT_e}{e}. \quad (6.1.20)$$

This form, valid for the Maxwellian case, is known as the Einstein relation. For non-Maxwellian distributions, the temperature factor is sometimes retained, forcing the calculation into the form

$$\frac{D}{\mu} = \frac{3}{2F} \frac{kT_e}{e}, \quad (6.1.21)$$

where

$$F = \frac{\bar{c}^2 [\bar{c}^{-2} (d/dc)(lc^2)]}{2\bar{l}c}. \quad (6.1.22)$$

²³ J. S. Townsend, *Phil. Trans. Roy. Soc. London A* **193**, 129 (1899).

The factor F is $\frac{3}{2}$ for the Maxwellian case and 1.312 for the Druyvesteyn distribution.^{16, 24}

6.1.11. Experimental Values of D/μ

The measurements of D/μ as a function of E/p_s at several gas temperatures obtained by Warren and Parker¹⁸ are shown in Figs. 2-4. These

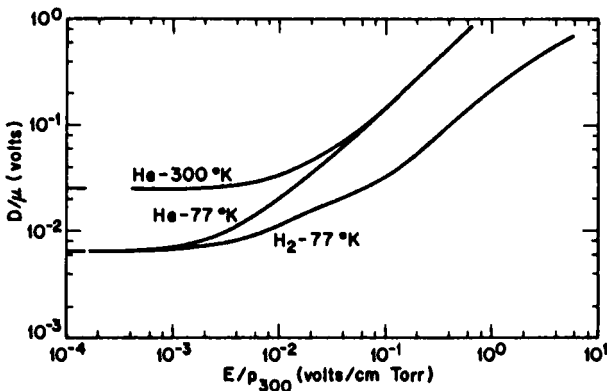


FIG. 2. Experimental values of D/μ versus E/p_{300} for electrons in helium at 77° and 300°K and in hydrogen at 77°K. [Results are those of R. W. Warren and J. H. Parker, Jr., *Phys. Rev.* **128**, 2661 (1962).] The value of D/μ is the electron temperature expressed in appropriate units ($T_e \cdot k/e$) and becomes equal to the gas temperature at low E/p .

curves disclose a value of D/μ accurately equal to kT/e , with T the gas temperature, at E/p_s below $\sim 10^{-3}$ V (cm-Torr) $^{-1}$. With increasing E/p_s , the value of D/μ rises. It should be noted that the variation of D/μ with E/p_s is extremely different from one gas to another. This sort of observation was first made by Townsend²⁵ as early as 1908 and was correctly interpreted by Townsend and Tizard¹ in 1913 as disclosing an effective increase in the electron temperature above that of the gas. It may equally well be stated that the value of D/μ discloses the mean terminal energy reached by the electrons. An alternative to the electron temperature, first introduced by Townsend, is the use of a multiplying factor K such that

$$T_e = KT, \quad (6.1.23)$$

²⁴ The Druyvesteyn distribution applies to the electrons in a gas when collisions are purely elastic and the electron temperature is appreciably different from that of the gas. It has the form $\exp(-E^2/k^2 T_e^2)$ or $\exp(-c^4/\alpha^4)$. See M. J. Druyvesteyn, *Physica* **10** 61 (1930); **1**, 1003 (1934).

²⁵ J. S. Townsend, *Proc. Roy. Soc. A* **81**, 464 (1908).

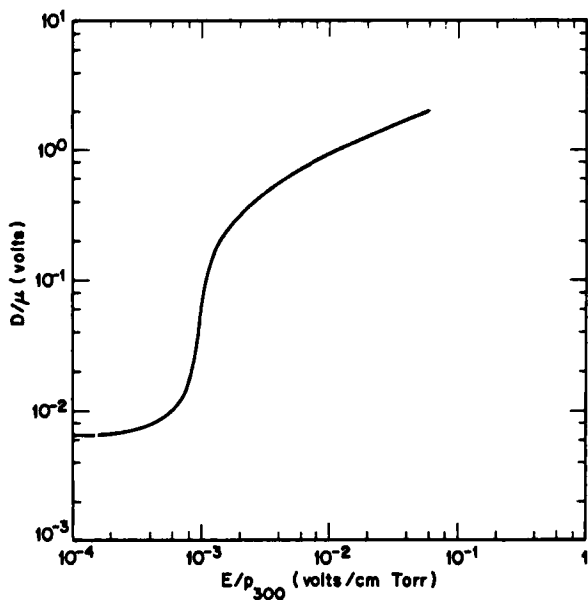


FIG. 3. Experimental values of D/μ versus E/p_{300} for electrons in argon at 77°K. [Results are those of R. W. Warren and J. H. Parker, Jr., *Phys. Rev.* **128**, 2661 (1962).]

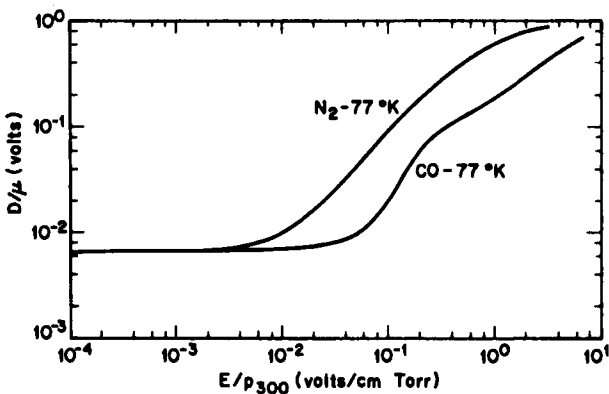


FIG. 4. Experimental values of D/μ versus E/p_{300} for electrons in nitrogen and in carbon monoxide at 77°K. [Results are those of R. W. Warren and J. H. Parker, Jr., *Phys. Rev.* **128**, 2661 (1962).] The differences between these curves reflect the different cross sections for very slow electrons in the two gases shown in Fig. 9.

where T_e is the electron temperature and T is the gas temperature. An immediate advantage of this notation is that K is also the ratio of the mean electron kinetic energy to the mean kinetic energy of the gas molecules. Its value thus shows the extent to which electrons have accumulated energy from the electric field above the value expected from equipartition. At the highest values of E/p_s , a partial leveling off of some curves is attributable to the fact that electrons are gaining so much energy that they can produce electronic excitation or even ionization. In such exciting or ionizing collisions, each electron loses a large amount of its kinetic energy and only regains it after many free paths of drift. The large losses of energy, even though occurring infrequently, are sufficient to slow the rate of rise of the mean electron energy with increasing E/p_s . Some increase of electron energy continues to occur with increasing E/p_s ; however, the measurements of D/μ become more complicated to interpret when appreciable ionization by collision occurs. The complexities of these studies of D/μ at higher values of E/p_s , with the various compensations and corrections for newly produced primary and secondary electrons, have recently been undertaken by Crompton *et al.*²⁶

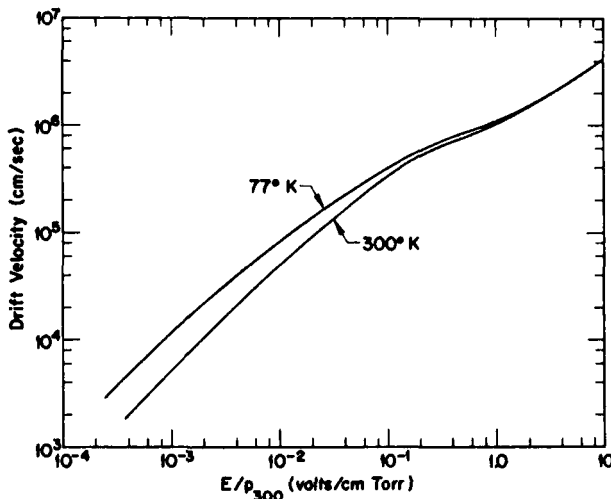


FIG. 5. Experimental values of drift velocity versus E/p_{300} for electrons in hydrogen at 77° and at 300°K. [Results are those of J. L. Pack and A. V. Phelps, *Phys. Rev.* **121**, 798 (1961).]

²⁶ R. W. Crompton, B. S. Liley, A. I. McIntosh, and C. A. Hurst, *Proc. 7th Intern. Conf. Ionized Gases, Belgrade, 1965*, Vol. 1, p. 86 (1966).

6. SWARMS

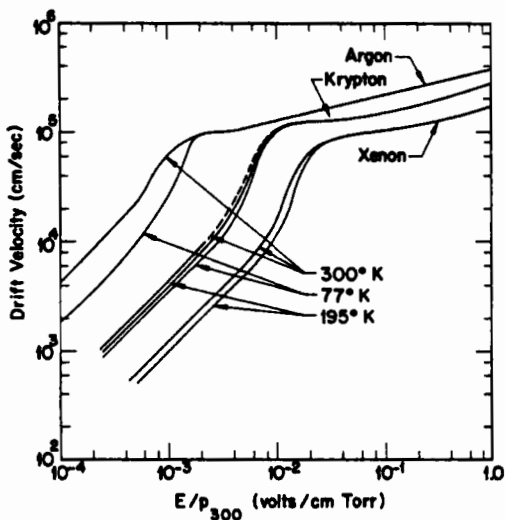


FIG. 6. Drift velocities of electrons in argon, krypton, and xenon at various temperatures. [Results are from Pack, Voshall, and Phelps, *Phys. Rev.* 127, 2084 (1962).] Note that the change with temperature is inverted to that for hydrogen shown in Fig. 5.

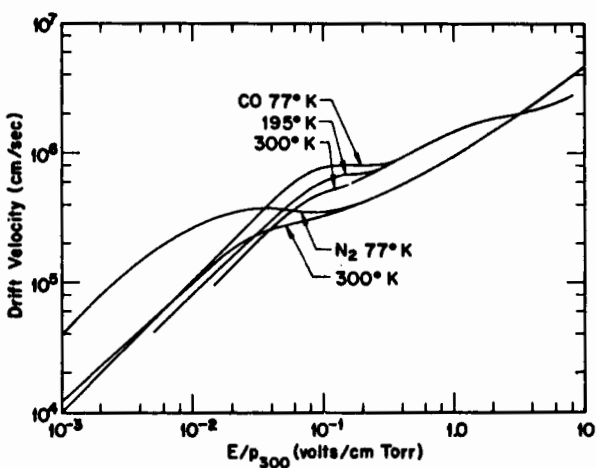


FIG. 7. Drift velocities of electrons in nitrogen and in carbon monoxide at various temperatures. [N₂ curves from J. L. Pack and A. V. Phelps, *Phys. Rev.* 121, 798 (1961); CO curves from J. L. Pack, R. E. Voshall and A. V. Phelps, *Phys. Rev.* 127, 2084 (1962).]

6.1.12. Experimental Values of Drift Velocity

Some results of Pack and Phelps¹² of electron drift velocity measurements as a function of gas temperature and of E/p_s are shown in Figs. 5-7. At such low values of E/p_s , that the electrons are in thermal equilibrium with the gas as shown by the D/μ measurements, the drift velocity is seen to be gas temperature dependent. At these low values of E/p_s , the drift velocity is accurately proportional to E/p_s , in accordance with the prediction of Eq. (6.1.16) under these conditions. At higher E/p_s , the electron temperature is far enough above that of the gas to wipe out any dependency of v on gas temperature. The curves are markedly different from one gas to another.

6.1.13. Use of Swarm Experiments to Determine Collision Cross Sections

Swarm experiments were recognized as early as 1921 in the work of Townsend and Bailey²⁷ to yield a value of the mean free path, or inversely, the collision cross section. Although in early work the simple form of the relationship between mobility and mean free path given in Eq. (6.1.19) was all that could be used, some spectacular results like the excessively long mean free path of electrons with about 0.4 eV of kinetic energy in argon were discovered by the swarm method.^{28,29} With the modern analytical as well as experimental procedures, swarm experiments continue to present measurements at very low E/p_s not yet matched by beam work. In this review, considerably more attention is given to the more recent aspects of the work. Much of the older work on cross sections and other parameters derived from swarm experiments to be discussed later may be found in Healey and Reed.³⁰

6.1.14. Collision Cross Sections from Swarm Experiments for Electrons in Thermal Equilibrium with Gases at Room Temperature and below

In the low range of E/p_s where the electrons are in thermal equilibrium with the gas, the rules for equipartition applicable to a gaseous mixture of two components apply to the mixture of electrons and gas molecules. It is standardly presumed, therefore, that the distribution function f for the electrons in this range of E/p_s is Maxwellian. The expression for drift speed given by Eq. (6.1.16) is thus freed of the uncertainty concerning f ,

²⁷ J. S. Townsend and V. A. Bailey, *Phil. Mag.* [6] **42**, 873 (1921).

²⁸ J. S. Townsend and V. A. Bailey, *Phil. Mag.* [6] **43**, 593 (1922).

²⁹ J. S. Townsend and V. A. Bailey, *Phil. Mag.* [6] **44**, 1033 (1922).

³⁰ R. H. Healey and J. W. Reed, "The Behaviour of Slow Electrons in Gases," p. 18ff. Amalgamated Wireless Press (Australasia), Ltd., Sydney, Australia, 1941.

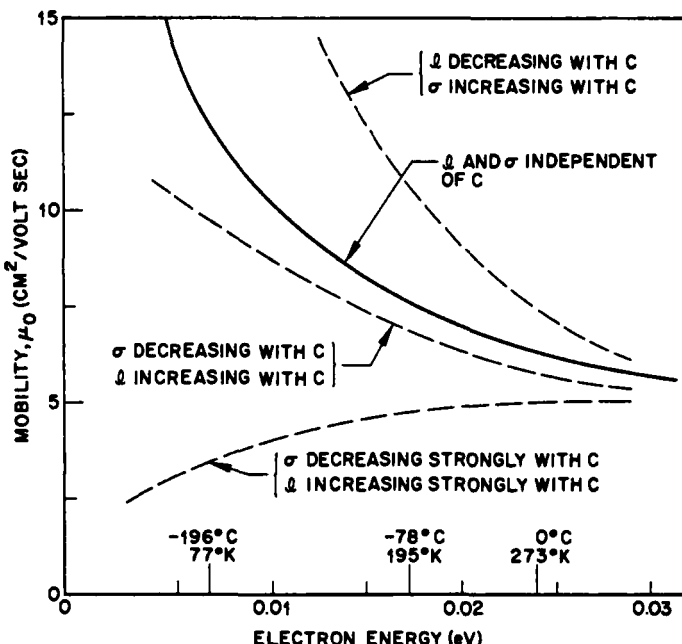


FIG. 8. Schematic plot of electron mobility versus mean electron energy and temperature for various assumed forms of the relation between cross section and electron velocity. The plot refers primarily to the domain where electron speed distributions are Maxwellian. The symbols are l for mean free path, σ for momentum transfer cross section for electrons in the gas, and c for electron speed.

but it still contains the mean free path l as a function of c . Only for the rare cases such as hydrogen and helium for which l appears to be very nearly constant with c (in the low range of c) can the simplified form of Eq. (6.1.19) be used to relate the drift velocity, mean free path, and mean speed \bar{c} .

If the Maxwellian law is inserted in Eq. (6.1.16), the mobility is seen to take the form

$$\mu(\bar{c}) = \frac{\pi^{1/2} e}{3m\alpha^5} \int l(c)c^3 \exp(-c^2/\alpha^2) dc, \quad (6.1.24)$$

where α is the most probable electron speed, $\alpha = \bar{c}\pi^{1/2}/2$. The problem is essentially to solve the integral equation (6.1.24) for $l(c)$, and this first becomes reasonably feasible with values of $\mu(\bar{c})$ for a great many values of \bar{c} . Frost and Phelps,³¹ with mobility values at only three temperatures, took $l(c)$ as a three-parameter function of c of the form $\alpha c^{-1/2} + \beta c^{-1} + \gamma c^{-3/2}$ and evaluated the three coefficients by fitting to the three values of μ . In Fig. 8, a schematic characterization of μ versus the thermal energy of the

³¹ L. S. Frost and A. V. Phelps, *Phys. Rev.* **127**, 1621 (1962).

electrons is plotted for various assumed functional forms of $l(c)$, including the case of $l(c)$ being constant, decreasing with c , increasing slowly, and increasing strongly with c . Since the mean free path is reciprocally related to the molecular or atomic cross section

$$l = 1/N\sigma, \quad (6.1.25)$$

where N is the gas particle density and σ the cross section, it is common to discuss the relationship of μ to σ rather than to l . In Fig. 9, the corresponding results to those of Fig. 8 are shown by plotting the cross sections σ against electron thermal energy obtained for several actual gases deduced from measured mobilities.¹²

In Fig. 9, the constancy of the cross sections for H₂ and He may be noted, as well as the drastic change for Ar. The last is well known as the

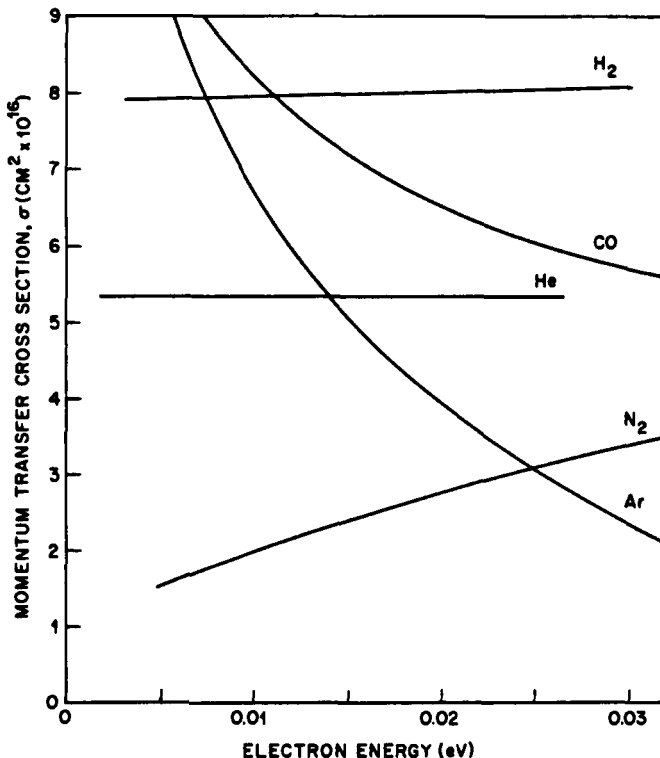


FIG. 9. Some electron momentum transfer cross sections in He, Ar, H₂, N₂, and CO. The curves are essentially from J. L. Pack and A. V. Phelps, *Phys. Rev.* **121**, 798 (1961) and from L. S. Frost and A. V. Phelps, *Phys. Rev.* **127**, 1621 (1962) and use three-parameter approximations to l as a function of c in Eq. (6.1.24). The drastically different behavior of N₂ and CO was predicted theoretically by S. Altshuler, *Phys. Rev.* **107**, 114 (1957).

"Ramsauer-Townsend effect," a change in cross section with electron speed which is drastic enough to stretch the precision of the approximations used above. Perhaps of greatest interest is the opposite trends of the curves in Fig. 9 for N₂ and CO, two gases that in many respects are strongly alike. The behavior of the electron cross sections is in accordance with predictions by Altshuler³² based on the fact that N₂ has no permanent dipole moment, whereas CO does. It is one of the triumphs of swarm experiments that these different characteristics emerge so clearly from nothing but mobility measurements as a function of temperature.

6.1.15. Use of Swarm Experiments: Electron Energies above Room Temperature

As mentioned in Section 6.1.11, as E/p_s is raised, the observed values of D/μ rise above the values of kT/e , where T is the gas temperature. The values of E/p_s at which the rise of D/μ begins, as well as the variations in the rate of rise, are of interest (see Figs. 2-4).

In the atomic gases, the rise of D/μ sets in at values of E/p_s between 10^{-3} and 10^{-2} V (cm-Torr)⁻¹. In the molecular gases, by contrast, D/μ does not depart from kT/e until E/p_s is made appreciably greater. These facts can be qualitatively correlated with the absence of low-lying energy levels in the rare gases and the relatively dense array of low-lying rotational and vibrational levels in the molecular gases which serve to remove additional energy from the electrons as they receive it in increasing amounts from the increasing field.

The shapes of the D/μ curves once they begin to rise are markedly dependent on the type of gas and are even markedly different for different atomic gases. Thus, for example, the curve for argon rises much more steeply than the one for helium. This difference in behavior appears to be associated with the extraordinarily large mean free path of electrons in argon at around 0.4 eV.

Pack and Phelps¹² and Frost and Phelps³¹ have evaluated cross sections for rotational excitation and to some degree vibrational and even electronic excitation for molecular gases by a trial-and-error method. In this range of E/p_s , the distribution law cannot be assumed to be Maxwellian. They begin by assuming certain cross sections based on theory. The detailed procedure varies. They either assume a reasonable theoretical form of the distribution law for electron energies, or evaluate one from numerical solution of the Boltzmann equation, inserting these assumed values into the Huxley integrals for v and D , Eqs. (6.1.11) and (6.1.16), and finally re-adjusting values of cross sections until the experimental values of v and D/μ

³² S. Altshuler, *Phys. Rev.* **107**, 114 (1957).

are attained. The authors emphasize that the cross sections so obtained are only *possibly* correct. The analytical methods are in a constant state of revision. Experimental data and calculations continue to be refined.³³

6.1.16. The Loss of Kinetic Energy of Electrons in Gases

A further question that has received both experimental and theoretical study for many years concerns the transfer of kinetic energy of electrons to gas atoms and molecules in collisions. From the work on binary collisions, using electron beams in gases at low pressures, it is well known that electrons can have perfectly elastic collisions or that they may have inelastic collisions in which they give up a quantum of energy corresponding to some kind of resonance excitation in the gas particle. It has already been indicated in Section 6.1.15 that, in swarm experiments on electrons in gases, the electrons can rise to a temperature above that of the gas at a lower value of E/p , if the gas does not have excitable low-lying energy levels than if it does have them. The concern of this section is to determine how elastic and inelastic energy losses can be measured in swarm experiments.

A quantity that proves to be open to evaluation is the mean fractional energy loss per collision of the entire swarm. This quantity, designated f , may be defined simply as

$$f = \overline{\Delta Q}/\bar{Q}. \quad (6.1.26)$$

\bar{Q} is the mean electron kinetic energy, and hence $\frac{1}{2}mc^2$ or $\frac{3}{2}kT_e$; $\overline{\Delta Q}$ is the mean loss of kinetic energy of an electron per collision. The mean fractional energy loss per collision may be evaluated from experimental observations of D/μ and μ such as have already been described.

The mean energy loss per unit time is the same as the mean energy gain per unit time. The latter is just eEv , with eE the electric force acting on the electron and v the drift speed or mean distance of advance of the electron in the field direction per unit time. The quantity $\overline{\Delta Q}$ that is under study here, however, is the mean loss *per collision*. A mean number of collisions per unit time is given by (c/l) , assuming that electron scattering is isotropic, so that

$$\overline{\Delta Q} = eEv/(c/l). \quad (6.1.27)$$

If Eq. (6.1.17) giving v as a function of E is used to eliminate E from Eq. (6.1.27), the result is

$$\overline{\Delta Q} = \frac{1}{2}mv^2K^*, \quad (6.1.28)$$

³³ See, for example, A. G. Engelhardt, A. V. Phelps, and C. G. Risk, *Phys. Rev.* **135**, A1566 (1964).

where

$$1/K^* = \frac{1}{6} \overline{(c/l)} \overline{c^{-2} [d(lc^2)/dc]}. \quad (6.1.29)$$

The evaluation of K^* requires theoretical decisions as to distribution laws and mean free path as a function of speed. The possible variations of K^* prove, however, not to be very large. Since $\bar{Q} = \frac{1}{2}mc^2$, the value of f becomes

$$f = \overline{\Delta Q}/\bar{Q} = K^* v^2/c^2, \quad (6.1.30)$$

or, expressed in terms of electron temperature,

$$f = K^* mv^2/(3kT_e), \quad (6.1.31)$$

or finally, expressing T_e in terms of D/μ ,

$$f = \frac{3K^* mv^2}{4Fe(D/\mu)}. \quad (6.1.32)$$

Experimental evaluation of f thus follows directly from the values of v and D/μ . The value of K^* ranges from 2 to 3, depending on the distribution and mean free path laws. The uncertainties in K^* and F give rise to only minor correction factors.

Before examining the experimental findings, the value of that part of f associated with purely elastic collisions should be noted. It takes the form¹⁶

$$f(\text{elastic}) = S \frac{Mm}{(M+m)^2} \left(1 - \frac{1}{K}\right), \quad (6.1.33)$$

where m and M are the electronic and molecular masses, respectively, and K is the electron temperature factor. S is a factor whose value would be 2 if only a single, binary collision between an electron and a molecule were being considered. It takes on a value of $\frac{8}{3}$ for a Maxwellian distribution of electron velocities and about 2.4 for a Druyvesteyn distribution.¹⁶ It may be noted that the fraction $Mm/(M+m)^2$ is for all practical purposes m/M . The fraction $f(\text{elastic})$ approaches zero as the electron temperature approaches the gas temperature. This fact reflects the definition of f as a *net* fractional energy loss per collision so that, when the electrons are in complete Boltzmann equilibrium with the gas, there is no net loss.

The fractional energy loss per collision f appears as the quantity of interest in much of the literature on electron collisions in gases.^{16, 30, 34} Because of the observations of beam experiments, and of the theoretical work, for example by Gerjuoy and Stein,³⁵ the evaluation of cross sections

³⁴ See Loeb,⁷ pp. 391–396.

³⁵ E. Gerjuoy and S. Stein, *Phys. Rev.* **97**, 1671 (1955); **98**, 1848 (1955).

for inelastic collisions of various kinds (e.g., rotational, vibrational, or electronic excitation and ionization) in swarm experiments has been undertaken as an alternative to the calculation of f . Finally, Frost and Phelps in particular³¹ have resorted to the use of "the collision frequency for inelastic collisions," to be contrasted with the collision frequency for momentum transfer collisions, as a more readily usable parameter than f . The collision frequency for inelastic collisions, expressed in the form ν_u/N , is calculated from the observations by the ratio of the energy gain per collision (shown previously to be eEv) to the energy excess $D/\mu - kT/e$, giving

$$\nu_u/N = eEv/(D/\mu - kT/e)N. \quad (6.1.34)$$

Readers are referred to the original reference for further details.

6.1.17. Experimental Values of the Mean Fractional Energy Loss per Collision

The fractional energy loss per collision was first evaluated for electrons in gases by Townsend and Bailey^{27, 28} in 1921–2. Using a form of Eq. (6.1.32) with the combined numerical coefficients evaluated at about 2.46, a number predicted for that equation for Maxwellian velocity distributions, the values of the fraction f were determined for many gases at many values of E/p_s . The findings are well summarized by Healey and Reed,³⁰ and reproduced by Loeb.^{35a} Although modern measurements are distinct improvements, the principal feature of modern work lies in the theoretical deductions from the data concerning excitations of various kinds in the gases.

In Figs. 10–12, the values of the total fractional energy loss per collision f , obtained from experimental data for He, Ar, H₂, N₂, and CO all at 77°K^{12, 18, 36} by substitution in Eq. (6.1.32), are plotted. Also plotted is that part of f which is due only to elastic collisions calculated from Eq. (6.1.33). The following comments are applicable.

For He (Fig. 10), the total and the elastic curves for f can be brought into agreement below E/p_s of 1 V (cm-Torr)⁻¹ by proper choice of the distribution law and the mean free path versus speed relationship. Above E/p_s of 1, the elastic part of f has long since reached a saturation value, but the total f by contrast starts rising steeply. The rise can only be explained on the basis of excitation of electronic energy levels in the helium. At values of E/p_s just above 1, apparently a significant percentage, probably 0.1 to 1%, of the electrons are attaining the 19.8 eV of kinetic energy needed for excitation.

^{35a} See Loeb,⁷ pp. 323–328.

³⁶ J. L. Pack, R. E. Voshall and A. V. Phelps, *Phys. Rev.* 127, 2084 (1962).

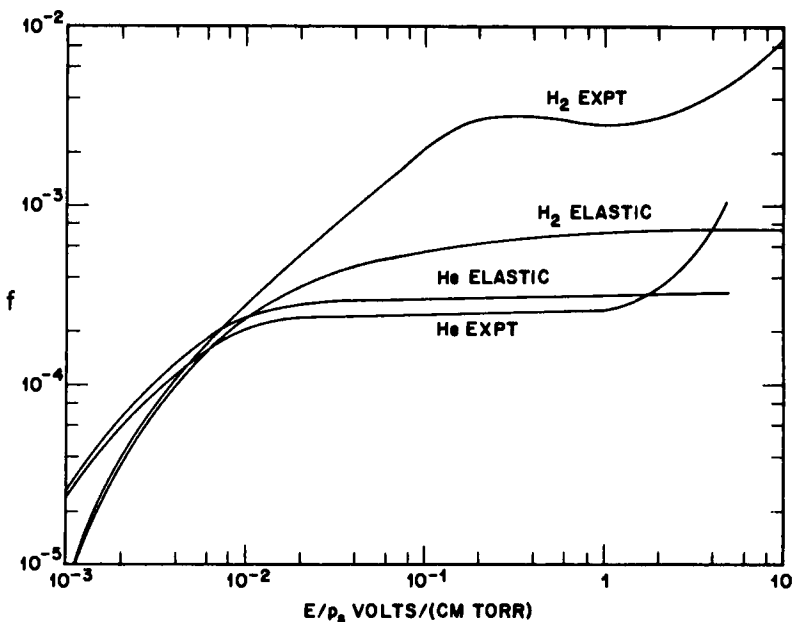


FIG. 10. Fractional energy loss per collision, and fractional loss per elastic collision only, for electrons in helium and in hydrogen at 77°K. The curves were computed from the experimental data of Figs. 2 and 5 and drift velocity data of J. L. Pack and A. V. Phelps, *Phys. Rev.* **121**, 798 (1961) for He using Eqs. (6.1.32) and (6.1.33). For H₂, the constant *S* was taken as 2.67 and the constant *K** was taken as 2.37 below E/p_s of 5×10^{-3} and 2.54 above 10^{-2} . For He, *S* was taken as 2.4, *K** as 2.37 in the low range of E/p_s below 2×10^{-3} and 2.54 for the higher range.

For argon (Fig. 11), the persistence of D/μ in retaining an elevated value at E/p_s as low as 10^{-3} V (cm-Torr)⁻¹ has the effect that $f(\text{elastic})$ remains near its saturation value even at this low E/p_s . Although there are probably almost no inelastic collisions for E/p_s below 5×10^{-2} V (cm-Torr)⁻¹, the failure of the total and the elastic f values to match should be attributed to the difficulty of properly computing the two coefficients *F* and *K** involved in the evaluation of $f(\text{total})$ from the experimental data. The difficulty arises from the extreme variations of $\ell(c)$ with *c* for argon in the range of 0.4 eV of electron energy. The odd behavior of $\ell(c)$ must be recognized to exert a complicating influence on all of the parameters; for example, the distribution function would seem to have a "hole" at 0.4 eV, as electrons in the field in this range of kinetic energy gain more energy virtually without any gas collisions. The coefficients *F* and *K** thus change for each value of E/p_s and are difficult to calculate even by machine computation, even if

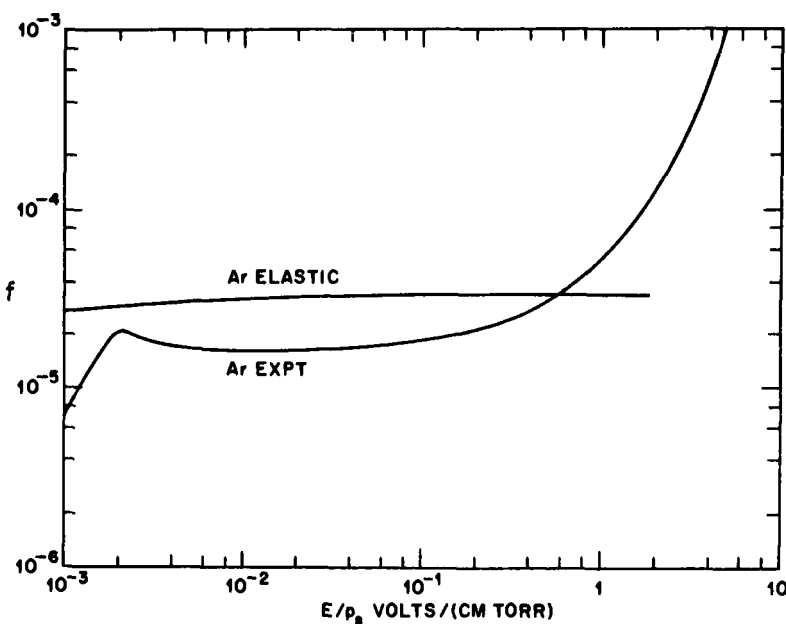


FIG. 11. Fractional energy loss per collision, and fractional loss per elastic collision only, for electrons in argon at 77°K. The curves were computed from data of Figs. 3 and 6, using Eqs. (6.1.32) and (6.1.33). A value of 2.4 was used for S and 3 for K^* .

$l(c)$ is known from electron beam experiments, because of the odd behavior of the distribution law induced by the variation of $l(c)$.

Inelastic collisions in argon set in, as noted, when E/p_s exceeds the surprisingly small value of 5×10^{-2} V (cm-Torr) $^{-1}$. Because of the Ramsauer effect, which renders the gas virtually transparent to electrons at 0.4 eV, the electrons pass very quickly to higher kinetic energies at low values of E/p_s . They continue to gain kinetic energy, as argon has no electronic energy levels below 11.6 eV which might slow down their net rate of gain of energy from the field.

For hydrogen (Fig. 10), the experimental and the elastic collision curves coincide for values of E/p_s up to 10^{-2} V (cm-Torr) $^{-1}$. As E/p_s increases, the experimental value rises above the elastic value, presumably as a result of excitation of rotations. There is something of a dip in the curve of f versus E/p_s around E/p_s of 1 before the final steep rise associated with electronic excitations; the dip vanishes at room temperature.

Curves for N₂ and CO are shown in Fig. 12. The observed fractional energy loss in nitrogen is similar to that in hydrogen except that there is

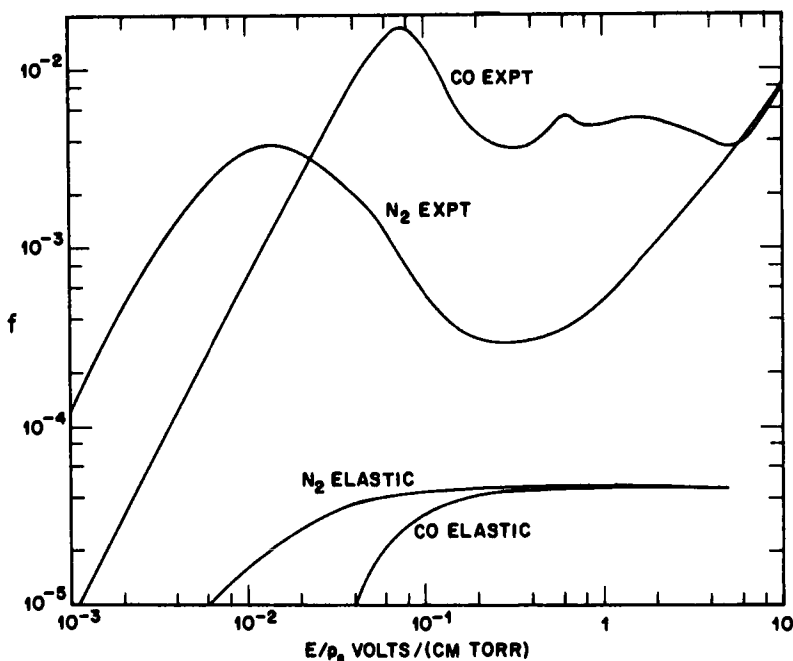


FIG. 12. Fractional energy loss per collision and per elastic collision in N₂ and CO at 77°K, computed by Eqs. (6.1.32) and (6.1.33) from data of Figs. 4 and 7. Values of S of 2.4 and K^* of 2.54 were used.

already great loss of energy to inelastic collisions at E/p_s of 10^{-3} V (cm-Torr) $^{-1}$. The sharp dip in the curve of f versus E/p_s , occurring in N₂ at low gas temperatures in the range $10^{-2} < E/p_s < 2 \times 10^{-1}$ is interesting; the dip is much less pronounced at room temperature. The behavior is parallel in CO. Some similar results were obtained by Bailey³⁷ in 1932. Bailey³⁷ found no dip in N₂ but a marked one in CO at room temperature.

The dip in N₂ at 77°K is indicated to some degree in the energy exchange plot by Frost and Phelps³¹; to make the comparison between their curves and those of Fig. 12 of the present work, it is necessary to note in both works that the experimental energy loss curves approach much nearer to the elastic collision curves and then separate again.

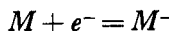
6.1.18. Attachment of Electrons to Atoms and Molecules

Before leaving the study of the motion of slow electron swarms in gases at low values of E/p_s , the phenomenon of attachment of electrons to form

³⁷ V. A. Bailey, *Phil. Mag.* [7] 13, 993 (1932).

negative ions must be examined. The subject has been reviewed most recently by Loeb,³⁸ by Prasad and Craggs,³⁹ and by Hasted.⁴⁰ An earlier exhaustive review by Massey⁴¹ is also of interest.

The attachment of an electron e^- to a molecule M signifies that a reaction of basic form



must be occurring. (No effort is made at this point to indicate the kinetic mechanism of the reaction, e.g., whether three-body collisions are essential. The heat of this reaction is the binding energy of the negative ion, or the electron affinity of the molecule. In measurements of attachment, it is normally assumed that the reaction is primarily one of attachment and that the reverse, or detachment, process occurs only to a negligible degree. Under this condition, attachment rate measurements are meaningful and are described below. It is, however, possible that experimental conditions may be such that the backward reaction or detachment in gaseous collisions becomes important. It is not always clear in experimental work that the detachment is indeed negligible, although, in much of the work in oxygen at low E/p_s , it would appear to be the case.

Electron attachment and electron affinity are associated with those substances that are electrochemically negative. In these gases, the behavior of electron swarms is more or less strongly influenced by attachment. The gases of interest include oxygen, the halogens, water, air, hydrogen chloride, ammonia, some of the common hydrocarbons, and a few gases especially employed because of their strong attachment such as carbon tetrachloride, freon, and sulfur hexafluoride.

The existence of free electrons in discharges was only recognized after low-pressure experiments were conducted or when, at high pressure, the extensive removal of water vapor and air as impurities became possible. Mobility experiments were probably the first in which negative ions were distinguished from free electrons in gases, the former having the much lower mobilities characteristic of positive ions by contrast with the high mobilities of the latter.

Many gases (like hydrogen and helium) that are not generally classified as electronegative were observed to form negative ions, but these gases

³⁸ L. B. Loeb, in "Handbuch der Physik" (S. Flügge, ed.), Vol. 21, pp. 445-470. Springer, Berlin, 1956.

³⁹ A. N. Prasad and J. D. Craggs, in "Atomic and Molecular Processes" (D. R. Bates, ed.), pp. 206-244. Academic Press, New York, 1962.

⁴⁰ J. B. Hasted, "Physics of Atomic Collisions," Chapter 8. Butterworth, London and Washington, 1964.

⁴¹ H. S. W. Massey, "Negative Ions," 2nd ed. Cambridge Univ. Press, London and New York, 1950.

often display attaching power only under special circumstances such as having been previously brought to an excited state. Cases of this type are not treated in the present context.

The ability of molecules or atoms of a given type to attach electrons is described quantitatively by three different measures. These are (1) the probability of attachment of an electron moving under the influence of an electric field for unit distance of advance in the field direction; this quantity is represented by η ; (2) the probability of attachment per collision; the symbol h is commonly used for this quantity; and (3) the collision cross section for attachment, commonly represented by σ_a with the subscript to connote attachment. (The failure of these coefficients to give adequate representation of some observations led ultimately to further understanding of attachment in cases where three-body collisions were essential; see Section 6.1.20.) The three coefficients must be related through such intermediate quantities as mean free path, drift velocity, and thermal velocity.

The attachment coefficient, η , is defined by the differential relationship

$$di_e = -\eta i_e dx, \quad (6.1.35)$$

which on integration for steady-state conditions takes the form

$$i_e = i_{e0} e^{-\eta x}. \quad (6.1.36)$$

Here i_e is the electron current crossing a plane at x in the usual parallel-plate geometry, and i_{e0} is the constant and continuous electron current at the plane $x = 0$. The current due to free electrons decreases as the electrons attach; the conduction by negative ions is supposed here to be distinguishable from that by electrons. It is reasonably apparent that Eqs. (6.1.35) and (6.1.36) could well display a factor involving the gas density or pressure. As written, η will surely increase if p_s is increased. Hence, η/p_s is in most cases the variable that depends on E/p_s . (See, however, Section 6.1.20 for a case in which η/p_s is still separately dependent on p_s .)

The relationship of η to h follows from a consideration of the number of electron collisions per unit distance of advance in the field direction. If \bar{c} and l are, respectively, the mean thermal speed and mean free path of the electrons, then \bar{c}/l gives a mean number of collisions per unit time. The drift speed v gives the distance of advance per unit time so that on this basis $\bar{c}/(lv)$ is the number of collisions per unit distance of advance. Hence it follows that

$$\eta = h\bar{c}/lv, \quad (6.1.37)$$

and this is the relationship between η and h . By use of more accurate averages over velocity distributions and mean free paths (e.g., taking \bar{c}/l as

the mean collision frequency), Eq. (6.1.37) can be converted to the form

$$\eta = (2eE/mv^2K^*)h, \quad (6.1.38)$$

where K^* is the constant between 2 and 3 which appears in the evaluation of the fractional energy loss per collision. For a Maxwellian distribution, the relationship becomes

$$\eta = 0.84(eE/mv^2)h. \quad (6.1.39)$$

The collision cross section for attachment, σ_a , is obtained by writing Eq. (6.1.36) in the form

$$i_e = i_{e0} \exp(-\sigma_a Ny). \quad (6.1.40)$$

The symbol y stands for the total path of travel of the electron rather than the advance x in the field direction. The relationship is $y = x\bar{c}/v$, so that

$$\eta = \sigma_a N \bar{c} / v. \quad (6.1.41)$$

N is the number of molecules of gas per unit volume and is related in the usual way to the pressure.

6.1.19. Measurement of Attachment at Low E/p_s

The earliest measurements, made between 1910 and 1924, are described by Loeb⁴² and are not described here. In 1925, Bailey⁴³ then used a variation of the Townsend and Tizard¹ experiment in which lateral diffusion and axial drift are compared. The electrons acquire a value of D/μ which is larger than that for negative ions. In the Bailey variation, electrons are "lost" by lateral diffusion, whereas negative ions are not lost in comparable numbers. The attachment coefficient η is accordingly evaluated. Further details of this method are also omitted.

In 1926, Loeb invented the electron filter already described in Section 6.1.6. An rf voltage on the grid wires sweeps out highly mobile electrons that drift transversely through the grid but only gives the far more sluggish negative ions a tremor as they drift through. In the hands of Loeb *et al.*,³⁸ this device produced some important results on attachment. It suffered from certain inherent difficulties. The principal one related to the influence of the relatively high values of E/p_s in the filter arising from the rf voltage. Bradbury¹⁰ improved the method by using two filters and noting the change in electron and negative ion currents as the charges drifted through the distance separating the filters. Identification of electron current and of

⁴² See Loeb,⁷ Chapter V.

⁴³ V. A. Bailey, *Phil. Mag.* [6] **50**, 825 (1925).

negative ion current depended on the removal of the electron component of the current by the filters.

The device in most recent use and built to utilize modern technology is due to Doehring⁴⁴ with further use by Chanin *et al.*⁴⁵ It is described here-with in some detail. The basic tube is equipped with two shutter-type grids such as are used for ion drift velocity measurements (see Chapter 4.1). The two shutters are separated a distance d and have a drift field between them. Contrary to the arrangement in the electron filter type of shutter, each shutter consists of two completely separate gauzes with a very small distance between them. Normally, a dc potential is applied to the two gauzes in such a direction as to prevent all negative ions and electrons from drifting through them. A brief square wave of potential of reversed sign opens the shutter, permitting negative ions and electrons to pass through.

Electrons are liberated continuously from a source, and they drift, with some attachment, to the first shutter. During a brief "shutter-open" time, n_0 electrons cross the entrance plane at $x = 0$, and those that do not attach are swept rapidly through the principal drift space and are collected by the second shutter if it is closed, or by the collector beyond the second shutter if it is open. The number of electrons actually reaching any plane x is given by $n = n_0 \exp(-\eta x)$, the balance being lost by attachment to form negative ions. On a time scale based on the time for negative ions to cross the drift space, d/v_i (v_i is the negative-ion drift speed), the electrons enter and attach or drift to the second shutter, all in a very short time. The electrons that attach produce negative ions in each slab of thickness dx of amount dn_i given by

$$dn_i = \eta n_0 \exp(-\eta x) dx, \quad (6.1.42)$$

creating a linear negative ion density N_i at the time of electron arrival at the anode (i.e., very nearly $t = 0$)

$$N_i = dn_i/dx = \eta n_0 \exp(-\eta x) \text{ ions/cm.} \quad (6.1.43)$$

This initial ion density is thus greatest near the first grid ($x = 0$) and falls off toward the second grid ($x = d$) according to Eq. (6.1.43). The negative ions drift toward the second shutter with the negative-ion drift speed v_i . If the second shutter opens at some time t after the first shutter, for an interval dt , the number of ions dn_i that reach the collector back of the shutter is

$$dn_i = N_i v_i dt, \quad (6.1.44)$$

with N_i the value taken from Eq. (6.1.43). This corresponds to ions that

⁴⁴ A. Doehring, *Z. Naturforsch.* **7a**, 253 (1952).

⁴⁵ L. M. Chanin, A. V. Phelps, and M. A. Biondi, *Phys. Rev. Letters* **2**, 344 (1959).

were at x and drifted the distance $d - x$ (i.e., from x to d) at speed v_t in the time interval t between the opening of the first and the second shutters. Thus, the essential drift distance for collection at t is $d - x = v_t t$, and the number collected in the interval dt is

$$dn_t = \eta n_0 v_t \exp[-\eta(d - v_t t)] dt \quad (6.1.45)$$

or

$$dn_t = \eta n_0 v_t \exp(-\eta d) \exp(\eta v_t t) dt. \quad (6.1.46)$$

The negative ions that penetrate the second shutter and reach the collector are recorded on a sensitive current meter. Actually, the cycle of square-wave pulses on the two shutters is repeated many times per second, so that the sensitive meter reads a smoothed average of the pulsating current amounting to dn_t multiplied by the number of repetitions per second. Finally, the operator varies the interval t between the pulses on the two shutters and plots the current as a function of this interval. The current, according to Eq. (6.1.46), should thus rise exponentially with t , and this was observed experimentally to be the case, allowing evaluation of ηv_t .

With t virtually zero, the free electrons that escape attachment reach the collector and are recorded. As t is made slightly larger, the electrons are stopped by the second shutter, but the negative ions that were formed very close to it are collected. As t is made still longer, the negative ions contained in a slab of thickness $v_t dt$ which had been formed progressively nearer to the first grid reach the collector. Finally, if t exceeds d/v_t , the current drops to zero, as no negative ions remain to be swept out, thus allowing an evaluation of v_t , and finally of η .

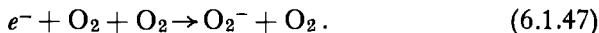
6.1.20. Results of Attachment Studies at Low E/p_s

Only the results of attachment studies in oxygen are discussed here. Readers are referred to the extensive literature summarized by Loeb⁴² or McDaniel⁴³ for results in other gases and for information obtained by other than swarm experiments.

The results described are for attachment of electrons in oxygen for $E/p_s \gtrsim 10$ obtained by Chanin *et al.*⁴⁵ using essentially the method described above. The experiments were carried out at room temperature and below. The features of interest are disclosed on examination of η/p_s as a function of E/p_s . Below $E/p_s = 3$ V (cm-Torr)⁻¹, η/p_s decreases with increasing E/p_s , at fixed pressure. However, contrary to many gas-conduction observable quantities, η/p_s proves in addition in this range of E/p_s

⁴³ E. W. McDaniel, "Collision Phenomena in Ionized Gases," Chapter 8. Wiley, New York, 1964.

to depend on p_s as well as E/p_s , the value of η/p_s rising linearly with p_s at fixed E/p_s . The pressure effect has been interpreted as disclosing that three-body impacts are essential to the attachment of electrons to O_2 to form O_2^- . Thus we may write a description of this attachment process as



The decline of η/p_s with increasing E/p_s discloses that the process of Eq. (6.1.47) becomes less efficient as the electron energy increases.

As E/p_s is increased beyond the value of $3 \text{ V (cm-Torr)}^{-1}$, the graph of η/p_s changes abruptly and instead of declining now rises steeply with E/p_s . It is furthermore *independent* of pressure in this range of E/p_s . The observations suggest that a very different attachment process is occurring, and it has been postulated to be representable by the reaction



The ion in this region is thus O^- instead of O_2^- . The reaction is called "dissociative attachment." It does not involve an outside third body and hence does not display the pressure dependence seen at lower values of E/p_s . These interpretations are in accord with nonswarm-type experiments.

In view of the following section on the subject of detachment, it is pointed out that the results of the present section prove to refer to conditions where detachment is negligible.

6.1.21. Detachment of Electrons from Negative Ions

An important concern for both the fundamentals of atomic processes and practical gas-ion considerations is the manner in which electrons may become detached from negative ions, the mechanism for such detachment, and the energy required for it. Detachment by photons, yielding a detachment energy, is the subject of Chapter 2.3 of this book. The literature on detachment in swarm experiments is limited and calls for further experimental work.

In 1935, Loeb⁴⁷ used his electron filter to remove electrons from a drifting stream of electrons and negative ions, and then passed the negative ions through a coarser electron filter in which the negative ions could presumably be "smashed" by the high values of E/p_s in the filter itself. The resulting data are highly complex but were interpreted by Loeb to show detachment of negative ions at $E/p_s \approx 90 \text{ V (cm-Torr)}^{-1}$. On the basis of present knowledge, it would appear that both O^- and O_2^- may have been involved in these experiments. The finding is extremely important and is worthy of verification and further study.

⁴⁷ L. B. Loeb, *Phys. Rev.* **48**, 684 (1935).

Phelps and Pack⁴⁸ used an apparatus of the type for attachment studies by Chanin *et al.*⁴⁵ (essentially the Doebring⁴⁴ design) in a variant procedure and studied detachment of electrons from oxygen ions. By using a value of E/p_s of about 1.25 V (cm-Torr)⁻¹, they assured formation of O_2^- rather than of O^- . As the O_2 gas temperature was raised successively to 423°, 473°, and 523°K, the detachment rate rose strongly. At room temperature, the detachment rate was apparently below a measurable value. From these measurements, combined with attachment rates for electrons at the same temperatures as the detaching negative ions, they deduced an electron affinity of 0.43 ± 0.02 eV for O_2 . This work constitutes a direct measurement in swarm experiments of O_2^- detachment.

The O^- ion that is formed at higher values of E/p_s is found from photo-detachment studies to have a binding energy of about 1.5 eV (see Chapter 2.3). As shown by the Loeb⁴⁷ experiment of 1935, and in an understandable way from thermodynamic considerations,⁴⁹ the O_2^- and the O^- ions should certainly detach the electron at high enough values of E/p_s . Frommhold⁵⁰ believes he has evidence of this detachment; he uses essentially a speeded-up version of the Hornbeck¹⁴ experiment and notes the electron pulse persisting, as negative ions liberate additional electrons during their flight. He reads a mean lifetime of the negative ions and expresses the result in the form of $p\tau$ in Torr-seconds as a function of E/p_s ranging from 10^{-4} Torr-sec at E/p_s of 35 to 2×10^{-8} at E/p_s of 200. The values of the detachment times appear to be startlingly short, implying a "detachment coefficient" more than an order of magnitude larger than the attachment coefficient. Further study is of significant interest.

6.1.22. Ionization by Electron Collisions; $E/p_s \gtrsim 1$

The analysis of early sections may be restated in a general form that the conductivity of matter may be associated with the ability of an electric field to cause electric charges in a medium to acquire a drift or directed component of their motion. Often the charges exist in the medium before the application of the electric field (metals, electrolytes, plasmas). The concern in this section is with the conductivity of gases where the gas becomes conducting only when free electric charges are caused to appear in the gas by an external source, where these free electric charges consist at least in part of electrons, and where some of these electrons accumulate enough energy from the

⁴⁸ A. V. Phelps and J. L. Pack, *Phys. Rev. Letters* **6**, 111 (1961); see also J. L. Pack and A. V. Phelps, *J. Chem. Phys.* **44**, 1870 (1966).

⁴⁹ M. W. Zemansky, "Heat and Thermodynamics," 4th ed., p. 437. McGraw-Hill, New York, 1957.

⁵⁰ L. Frommhold, *Fortschr. Physik* **12**, 597 (1964).

field to ionize neutral molecules. Thus, the discussion is an extension of previous sections to values of E/p_s , ranging from about 1 to an uncertain large value of the order of 10^3 V (cm-Torr) $^{-1}$.

The current associated with charges introduced by external means alone is referred to as the initial current, and the electrons so produced are referred to as initial electrons. Once again, unless otherwise noted, it will be assumed that all the initial electrons are liberated from the cathode as opposed to the case where electrons are liberated in the gas volume, for example by X rays. It is assumed that electrons that are released from the cathode but that are subsequently reflected back into the cathode by gas molecules (back diffusion) are not initial electrons. The initial current (and/or the applied voltage) may be a constant or a function of time. The steady state and certain transient cases have been treated extensively^{15, 51-53}. In the transient cases, it is generally assumed that either the initial current is a rectangular pulse and that the voltage is constant, or that the initial current is constant and that the voltage is a step. The present discussion, unless otherwise noted, is for the steady state. The failure to provide enough initial electrons in a controlled way leads to statistical phenomena. Thus, even for spark gaps with very high applied voltages, the breakdown has been shown in extreme cases to be delayed until a single electron is released at a suitable place in the gap, by a cosmic ray, for example. The principle of the spark chamber of nuclear and cosmic-ray studies depends in part on the provision of the initial electrons by the radiation being studied. At least one free electron is necessary to initiate ionization and breakdown processes.

There is one case in which the applied voltage itself may extract the required electrons from electrode surfaces; the process is called field emission. As a rough criterion, it may be declared that field emission requires minimum electric field strengths of 10^7 V/cm.⁵⁴ Field emission does not necessarily require enormous voltages, but can be caused by surface roughness and/or by residual surface charges.

Even at voltages below breakdown, a current larger than the initial current generally flows through the gas. If the current is larger, one may conclude that ionization by collision is occurring in the gas, and that attachment of electrons to form negative ions may or may not be occurring. (We neglect attachment for the present; the subject of negative-ion formation in the

⁵¹ See Loeb,⁷ Chapters VIII and IX.

⁵² A. von Engel, in "Handbuch der Physik" (S. Flügge, ed.), Vol. 21, pp. 504-573. Springer, Berlin, 1956.

⁵³ F. Llewellyn Jones, "Ionization and Breakdown in Gases." Methuen, London, 1957.

⁵⁴ M. von Ardenne, "Tabellen zur Angewandten Physik," 2nd ed., Vol. 1, pp. 118-120. Deuts. Verlag Wissen., Berlin, 1962.

presence of ionization by collision is discussed in Section 6.1.27.) If the initial current density is small enough, the current through the gas is found to be proportional to the initial current, all other conditions remaining the same. Such conduction seems to emit no light to the eye and is sometimes called a dark or Townsend discharge. (The term "discharge" as used here is not synonymous with breakdown.) Under such conditions, the electric field between the plane parallel electrodes is to a high degree of approximation uniform. For the preceding conditions to apply, the initial current density must be kept low enough to avoid distortion by space charge. Crowe *et al.*⁵⁵ cite various examples in which initial current density runs to 10^{-10} A/cm² without distortion. A value of initial current density of 10^{-12} is adequate for measurement yet safe from space charge distortion.

The liberation of electrons by ionizing collisions in the gas at the position where the electrons lose energy is called a primary process, and the electrons so released are called primary electrons. There is, of course, no distinction thereafter between primary electrons and initial electrons if both are at the same position in the gas; their subsequent actions are indistinguishable. The process of ionization by electron collision produces electron and positive-ion currents, which, if this were the only relevant process, would produce an amplification M_p of the initial current. M_p depends on the nature and density of the gas, on the potential difference between the electrodes, and on the electrode separation.

Electrons may also be liberated at the cathode by positive ions, photons, and excited atoms. Conceivably, electrons may also be liberated in the gas by nonprimary processes at positions other than those where electrons lose their energy. All such electrons are called secondary electrons; they appear usually to be liberated at the cathode, and, unless otherwise stated, this will be assumed. The processes by which they are emitted are called secondary processes. Any such secondary process (acting at the cathode) produces a further amplification M_s above that due to M_p . Since M_s amplifies the initial electron current from i_0 to $M_s i_0$ and the primary process amplifies the electron current leaving the cathode by a factor M_p , the total amplification of the initial current is $M_p M_s$. M_s is dependent on the nature of the cathode surface as well as on the characteristics of the impinging particles causing secondary emission, and indirectly on M_p .

The conduction of electricity in a Townsend discharge in a gas, even under steady-state conditions, is marked by ionization processes that cause a variation with distance from the cathode of ion and electron number and current densities. Despite these variations, the total current due to all

⁵⁵ R. W. Crowe, J. K. Bragg, and V. G. Thomas, *Phys. Rev.* **96**, 10 (1954).

carriers has the same value at each plane. In considerable distinction to the case for plasmas and electrolytes, the charge densities of positive and negative carriers do not cancel each other in the gas conduction case. A rather odd consequence, which will appear quantitatively below, is that the current densities of positive ions or of electrons (or of negative ions if they are present) are independent of the drift velocities of the respective carriers.⁵⁶

The quantities M_p and M_s are now characterized quantitatively. The electrons in a Townsend discharge have an energy distribution characterized by the ratio E/p_s or E/N (see Section 6.1.2). In the following, we neglect diffusion and recombination processes. In the types of dc experiments to be considered here, it is possible to neglect diffusion and recombination because electron transit times from cathode to anode are too short for these processes to be of importance. In microwave discharges, on the other hand, where the field reverses in time, and there is no net drift motion of the electrons, diffusion and recombination (and attachment in appropriate gases) play important roles.

Assume that a constant initial current i_0 of electrons is liberated from the cathode. Let $i_e(x)$ be the electron current at a distance x from the cathode. At a distance $x + dx$, the electron current is increased by $di_e(x)$, where

$$di_e(x) = \alpha i_e(x) dx. \quad (6.1.49)$$

Equation (6.1.49) contains the assumption that the ionization process is linear in i_e . The coefficient α is known as the first Townsend ionization coefficient and is found experimentally to depend on the product of p_s and some function of E/p_s . The equation is written in this form for traditional reasons; since the increase in electron current in dx is proportional to the gas pressure, the equation would be more suitably written as

$$di_e(x) = (\alpha/p_s)p_s i_e(x) dx. \quad (6.1.50)$$

The quantity (α/p_s) may be characterized as the fractional increase in electron current per unit of pressure per unit of advance of distance of the electrons in the field. Equations (6.1.49) and (6.1.50) apply whether secondary electrons (liberated at the cathode) are present or not. That aspect of the solution of the equation is governed by the boundary conditions.

Solution of Eq. (6.1.49) gives

$$i_e(x) = ce^{\alpha x}. \quad (6.1.51)$$

⁵⁶ L. H. Fisher and R. N. Varney, *Am. J. Phys.* **34**, 228 (1966).

Since the total current crossing any plane is the same, it is now possible to utilize this consideration twice:

- (1) At the anode, $x = d$, electrons enter the anode, but no positive ions leave it, so that the total current i equals the electron current at the anode, $i_e(d)$, and Eq. (6.1.51) reads

$$i = i_e(d) = ce^{\alpha d}. \quad (6.1.52)$$

- (2) At any plane, x , in the gap, i_+ , the positive-ion current, must equal the total current i less i_e , or

$$i_+(x) = i - i_e(x) = c(e^{\alpha d} - e^{\alpha x}). \quad (6.1.53)$$

If no secondary effects are occurring at the cathode, Eq. (6.1.51) gives $c = i_0$, where i_0 is the initial current. An immediate consequence in the absence of secondary emission is that the total current is

$$i = i_0 e^{\alpha d}. \quad (6.1.54)$$

The primary multiplication factor is thus

$$M_p = e^{\alpha d}. \quad (6.1.55)$$

As previously noted, electrons may also be liberated from the cathode at a rate in excess of the initial value i_0 as a consequence of the primary process going on in the gas. The so-called secondary electrons may be emitted by any or all of several mechanisms, including photoelectric emission arising from photons from the gas and emission by bombardment of the cathode by positive ions and by neutral atoms in excited states. In steady-state experiments, it is not possible to identify what particular mechanism causes the secondary electron emission. (In transient experiments, segregation of the effects is possible, since the times of transit for photons, ions, and neutrals are different.) It thus becomes practical to introduce a secondary liberation coefficient γ as the number of secondary electrons per positive ion incident on the cathode even though some of the secondary electrons *never* involved a positive ion in any stage of the primary or secondary processes. In effect, one notes that a current $i_+(0)$ of positive ions hits the cathode, and a current $\gamma i_+(0)$ of electrons other than initial electrons leaves the cathode on a continuing basis. There is no way under these conditions of establishing whether the positive ions are or are not responsible for the secondaries. If values of γ exclusively for positive ions are sought, steady-state experiments may give spuriously high findings.

Using the foregoing interpretation of γ , that γ secondary electrons are released at the cathode per positive ion striking the cathode, a new boundary condition in the presence of secondary emission may be introduced by

first noting that Eq. (6.1.53) gives $i_e(0) = c(e^{\alpha d} - 1)$, so that

$$i_e(0) = i_0 + \gamma c(e^{\alpha d} - 1), \quad (6.1.56)$$

and, at $x = d$,

$$i = i_e(d) = ce^{\alpha d} = [i_0 + \gamma c(e^{\alpha d} - 1)]e^{\alpha d}, \quad (6.1.57)$$

since $c = i_e(0)$. Solving for c gives

$$c = \frac{i_0}{1 - \gamma(e^{\alpha d} - 1)}. \quad (6.1.58)$$

The total current is thus

$$i = \frac{i_0}{1 - \gamma(e^{\alpha d} - 1)} e^{\alpha d}. \quad (6.1.59)$$

This equation marks the factor $1/[1 - \gamma(e^{\alpha d} - 1)]$ as M_s , the secondary multiplication factor, and $e^{\alpha d}$ as before, M_p . The coefficient γ is called the second Townsend coefficient.

When a single electron leaves the cathode, the primary multiplication leads to a state of affairs called an electron avalanche. The term is used interchangeably for the result of a burst of initial electrons, confined to a small area and short time compared with the electron transit time. The term *single avalanche*, particularly as used by Raether,¹⁵ refers to the avalanche initiated by a single electron. All of the electrons of a single avalanche are located at any instant t at a single value of x given by $x = vt$. Here v again stands for the electron drift speed and t the interval since emission of the single electron from the cathode. The electron density is zero at all other values of x , except for the small spread due to diffusion. The result is illustrated in Fig. 13. As noted previously, the electron current $i_e(x)$ in the steady state is given by $i_e(0)e^{\alpha x}$. The electron current at x is caused by electrons liberated from the cathode at an earlier time x/v . Thus, if one considers multiplication of a single electron emitted at a definite time, one finds that the multiplication is given by $e^{\alpha x}$, since the steady-state current is a superposition of many such electrons being emitted continuously. More properly for the case of a single electron emitted at time 0, the number of electrons in the gap should be written as $\exp(\alpha vt) \delta(x - vt)$, where δ is the Dirac delta function.

As the electron avalanche passes through the gas, it leaves behind a positive-ion residue that in contrast to the electrons is distributed at all x between 0 and vt . This array of positive ions is sometimes called a positive-ion avalanche and sometimes is treated as part of the single avalanche. Actually, the positive ions are not snowballing in the way the

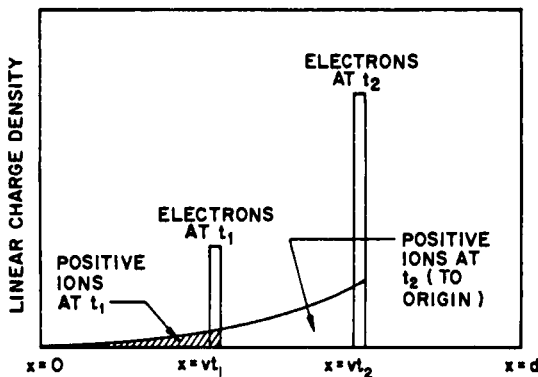


FIG. 13. Schematic graph of a single electron avalanche at two times during its history showing linear density at various distances from the cathode. The electron avalanche corresponds to a single snowball; the positive ions are spread out from the cathode to the electron snowball. The area under the single electron snowball curve diminished by one should equal the area under the corresponding positive-ion curve.

electrons are; in fact, in time intervals comparable with the electron transit time, they hardly move at all. They are distributed at all x between 0 and the electron snowball with linear density given by

$$N_i \approx \alpha e^{\alpha x}, \quad 0 \leq x \leq vt. \quad (6.1.60)$$

The total number of positive ions is $e^{\alpha x} - 1$ and hence is one less than the total number of electrons in the snowball. Except for the difference of unity, the areas under the electron peak and the positive-ion exponential are equal.

As the electron peak moves onward toward the anode, it grows higher; in the same time interval, the positive-ion distribution moves a negligible distance toward the cathode but becomes extended toward the anode, as shown schematically in Fig. 13.

When the cathode is illuminated continuously, a time integration of the preceding effects occurs. There is then an array of electrons at all values of x , although the electrons at one instant belong to different avalanches at each x . The graph of electron density in the steady state is proportional to the envelope of the single avalanche peaks. By contrast, because the positive ions associated with each avalanche are spread out in space and since the positive ions drift toward the cathode, their density distribution takes on a much altered form from that of a single avalanche, as shown in Fig. 14. At any one position, the electrons and ions are created at an equal rate; the rate is a maximum at the anode. Most of the current near the anode is due

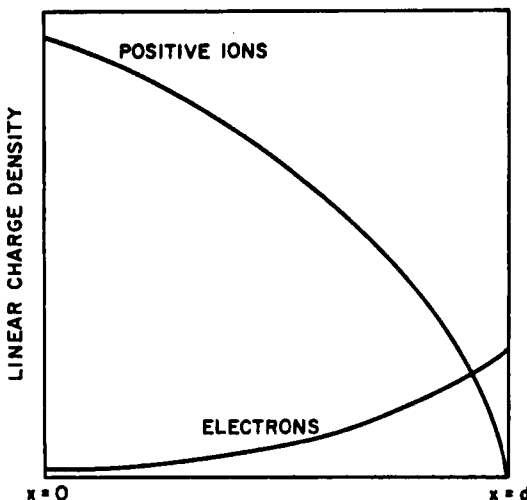


FIG. 14. Schematic graph of the densities of electrons and positive ions when a constant photoelectric current of electrons leaves the cathode. The linear electron density is given by $(i_0/v)e^{\alpha x}$; the linear positive-ion density is $(i_0/v_+)(e^{\alpha d} - e^{\alpha x})$. The maximum ion density (at $x = 0$) is thus approximately v/v_+ times greater than the maximum electron density (at $x = d$). For actual gases, the ratio of maximum positive-ion density to maximum electron density is even greater than depicted in this schematic diagram. There is *not* charge neutrality in the gap, and hence the figure and the equations can only represent experiments correctly for very low currents and charge densities for which the space charge potentials are negligible.

to electrons; most of the current near the cathode is due to positive ions, despite the fact that most of the positive ions are created near the anode. This situation arises because, in the steady state, the positive-ion current at the cathode consists of the superposition of the motion of positive ions of various ages created at all positions in the gap at various earlier or retarded times. A further remarkable fact in this type of conduction, as may be seen from Eqs. (6.1.51)–(6.1.56), is that the fractions of the total current carried by electrons and positive ions is independent of the drift velocities of these charged carriers. This is only possible because the densities of positive and negative charges are functions of position. Equations (6.1.54) and (6.1.59) have been verified experimentally for many gases over large ranges of E/p_s .

As previously mentioned, α/p_s is a function of E/p_s . Thus,

$$\alpha/p_s = F(E/p_s). \quad (6.1.61)$$

Every gas has its own characteristic function. M_p may be expressed as

$$M_p = \exp[(\alpha/p_s)(p_s d)], \quad (6.1.62)$$

pointing out that, for a given value of E/p_s for a given gas, M_p varies in an identical way with p_s and d . This is the first example of the importance of $p_s d$ as a gas discharge parameter mentioned in Section 6.1.2.

M_p may be written in the alternate form

$$M_p = \exp(\eta V), \quad (6.1.63)$$

where $\eta = \alpha/E$ and V is the potential difference across the electrodes. (The use of η in the present context is not to be confused with the attachment coefficient for which the same symbol is commonly used.) The quantity η is also occasionally called the first Townsend coefficient, causing slight confusion with its counterpart α . It is the fractional increase of electron current incurred as the electrons fall through unit potential difference. η is a function of E/p_s . All of the preceding forms for M_p are equivalent, and all may be used.

Equation (6.1.62) shows that M_p may be considered to be a function of E/p_s and $p_s d$. Equation (6.1.63) shows that M_p may alternately be considered to be a function of E/p_s and the applied voltage V . In actual fact, the parameters that are set by an observer are V , p_s , and d , and M_p can be considered to be a function of V and $p_s d$. The same functional dependences hold for M_s .

Similarly, M_s may be written in the alternate forms

$$M_s = \{1 - \gamma[\exp\{(\alpha/p_s)p_s d\} - 1]\}^{-1} \quad (6.1.64)$$

and

$$M_s = \{1 - \gamma[\exp(\eta V) - 1]\}^{-1}. \quad (6.1.65)$$

At low products of p_s and d (and hence at low values of V), the electrons may travel an appreciable distance from the cathode before reaching an energy distribution characteristic of E/p_s . In such cases, the foregoing equations all must be corrected. It is generally assumed that, for a given value of p_s and E/p_s , there exists a distance d_0 such that, for $x < d_0$, $\alpha = 0$. Thus, for example, the current through the gap with $\gamma = 0$ becomes

$$i = i_0 \exp[\alpha(d - d_0)] \quad (6.1.66)$$

or

$$i = i_0 \exp[\eta(V - V_0)]. \quad (6.1.67)$$

Here V_0 is a function of E/p_s and is, in general, about equal to the ionization potential of the gas. In cases where the applied potential is large compared to the ionization potential, these corrections may be neglected.

6.1.23. Experimental Evaluation of α and γ

We now consider methods for evaluating the first and second Townsend coefficients from steady-state gas amplified currents. In order to obtain the value of the first Townsend coefficient α (or preferably of α/p_s) at a particular value of E/p_s , it is necessary to measure currents at various values of V at that value of E/p_s . Keeping E/p_s constant ensures that i_0 , V_0 , and γ are constant, provided that the illumination of the cathode is constant and the cathode surface is stable. A voltage variation at constant E/p_s implies a variation in the product $p_s d$. The most common method that has been used to determine the first Townsend coefficient has been to measure pre-breakdown ionization currents keeping E/p_s and p_s constant and varying d . However, it is often more convenient to keep E/p_s and d constant and vary p_s . Despite the fact that values of the first Townsend coefficient have been measured for many years, there has been little agreement among different experimental values over an extended range of E/p_s for any gas.⁵⁷ It is remarkable that a rather simple experimental parameter such as α/p_s should be the subject of so much uncertainty. It has been relatively easy to ascribe differences between current and earlier work to gas impurities, and in some cases this may have been an important factor. However, in some cases, early work in "impure" gases has turned out to be more reliable than some later work in "pure" gases. Differences may arise from the method of cathode illumination, depending on whether the ultraviolet light passes through holes in the anode to the cathode, or whether illumination of the cathode at an angle occurs. The possible variation of initial current with electrode separation due to reflections must be carefully considered. But an important feature must be the method of analyzing the experimental data, assuming that gas purity is no problem and that i_0 is constant independent of electrode separation. Thus, a discussion of methods of analysis of experimental data is in order.

In the past, essentially four methods of analysis have been used to obtain values of the first Townsend coefficient in uniform fields from pre-breakdown ionization currents at constant E/p_s . The first and most common is the measurement of the slope of a plot of $\ln i$ versus V for low values of V (but for $V \gg V_0$). This method is valid only if $\gamma \ll 1$.⁵⁷ The second is a three-point method originally due to Townsend and MacCallum⁵⁸ which uses prebreakdown currents measured at three voltages $V_1 < V_2 < V_3$ such that $V_2 - V_1 = V_3 - V_2 = \delta V$. This three-point method has been generalized to the case of unequal voltage intervals.⁵⁹

⁵⁷ D. E. Golden, H. Nakano, and L. H. Fisher, *Phys. Rev.* **138**, A1613 (1965).

⁵⁸ J. S. Townsend and S. P. MacCallum, *Phil. Mag. [7]* **6**, 857 (1928).

⁵⁹ E. Jones and F. Llewellyn Jones, *Proc. Phys. Soc. (London)* **72**, 363 (1958).

The third method is due to Gosseries⁶⁰ and is a way of plotting the reciprocal of currents measured at certain values of V against the reciprocal of currents measured at certain other prescribed values of V such that a linear plot results whose slope allows the determination of the first Townsend coefficient. Linearity of the plot is assumed to assure the constancy of i_0 and γ throughout the measurements. The fourth method may be considered to encompass all iterative procedures that involve some criterion to determine all of the various parameters involved simultaneously using all of the current-voltage data.⁵⁷

One of the weaknesses of the first three methods of analysis is that they only give definite recipes for determining α/p_s (or η) and do not specify a definite procedure for determining the other three parameters, i_0 , γ , and V_0 . Under suitable circumstances, the first three methods may be used to calculate all four parameters accurately. However, in many cases, these methods have been used where they cannot be applied properly. The second method has been used to determine α/p_s without using all of the available data. Both the second and third methods have been used to evaluate α/p_s without evaluating the other three parameters. Without evaluating all four parameters, there is no guarantee that the remaining parameters will have reasonable values using the determined value of α/p_s . Thus, there is a definite risk that the values of α/p_s so obtained are spurious and would give physically meaningless values of the other parameters, such as V_0 less than the ionization potential, or $\gamma < 0$. The three-point methods lead to fluctuations in the calculated values of α/p_s , depending upon which three points are used. The fourth method is the only method that determines all four parameters simultaneously in a prescribed way using all of the data. Thus, the presentation of values of α/p_s without presentation of some raw data and an explicit description of the method of evaluation of data is not acceptable, despite the fact that this has been the practice of many authors for many years.

In addition to these static measurements, there are some other methods of interest for determining α/p_s . Wijsman⁶¹ has calculated the fluctuations to be expected in the number of electrons created in a single avalanche. By measuring the statistical distribution of such numbers, it is possible to obtain α/p_s . Frommhold⁶² and Schlumbohm⁶³ have shown that this method is not in bad agreement with results obtained from dc measurements. Frommhold⁶⁴ has also obtained some values of α/p_s by measuring time

⁶⁰ A. Gosseries, *Physica* **6**, 458 (1939).

⁶¹ R. J. Wijsman, *Phys. Rev.* **75**, 833 (1949).

⁶² L. Frommhold, *Z. Physik* **144**, 396 (1956); **150**, 172 (1958).

⁶³ H. Schlumbohm, *Z. Angew. Phys.* **11**, 156 (1959).

⁶⁴ L. Frommhold, *Z. Physik* **160**, 554 (1960).

constants in the external circuit associated with electrons and ions in single avalanches.

6.1.24. Experimental Values of the First Townsend Coefficient

Results of α/p_s have been summarized by Druyvesteyn and Penning,⁶⁵ by Loeb,⁵¹ and most recently by Prasad and Craggs.³⁹

A useful empirical formula originally introduced by Townsend⁶⁶ on very rough arguments is

$$\alpha/p_s = A \exp(-Bp_s/E). \quad (6.1.68)$$

This formula has been shown to represent the values of α/p_s in H₂ to $\pm 2\%$ for $22 < E/p_0 < 1000$.⁶⁷ Ward⁶⁸ prefers to restrict the use of Eq. (6.1.68) to molecular gases and to use for noble gases an expression of the form

$$\alpha/p_s = A \exp[-D(p_s/E)^{1/2}]. \quad (6.1.69)$$

Equations (6.1.68) and (6.1.69) predict curves for α/p_s versus E/p_s of similar shape. Thus both equations predict that α/p_s increases with increasing E/p_s to a saturation value that is approached asymptotically. Observations are in general agreement with these equations. By contrast to these curves, graphs of η versus E/p_s show a maximum. Despite frequent statements to the contrary, there is no experimental evidence that α/p_s as a function of E/p_s has a maximum for any gas.

Generally speaking, values of α/p_s reach a given value for noble gases at a lower value of E/p_s than for molecular gases. This is a manifestation of the fact that the average electron energy is much higher in noble gases than in molecular gases for a given value of E/p_s , as discussed in Section 6.1.15. Values of α/p_s appear to be measurable in the noble gases for E/p_s as low as about 5, whereas for molecular gases values of about 20 or more are required. Measured values of α/p_s range from about 10^{-4} to about 5 or 10 (cm-Torr)⁻¹. Detailed values of α/p_s are not quoted here.

Values of α/p_s in argon at low E/p_s have been found to depend on p_s as well as on E/p_s .⁶⁹ It is thus pointed out that the ionization of gases may involve a much more complicated process than simple electron collisions.

⁶⁵ M. J. Druyvesteyn and F. M. Penning, *Rev. Mod. Phys.* **12**, 87 (1940).

⁶⁶ J. S. Townsend, "Electricity in Gases," p. 292. Oxford Univ. Press (Clarendon), London and New York, 1915.

⁶⁷ D. J. Rose, *Phys. Rev.* **104**, 273 (1956).

⁶⁸ A. L. Ward, *Phys. Rev.* **112**, 1852 (1958).

⁶⁹ D. E. Golden and L. H. Fisher, *Phys. Rev.* **123**, 1079 (1961).

6.1.25. Kinetic Theory Analysis of α/p_s

The quantity α/p_s can be written in the form

$$\alpha/p_s = 4\pi \int_{C_i}^{\infty} (c/v) c^2 f(c) P_i(c) dc = \overline{c P_i(c)} / v, \quad (6.1.70)$$

where c is electron speed, v the electron drift velocity, $f(c)$ the electron distribution function (normalized as in Section 6.1.8), $P_i(c)$ the probability of ionization per electron per unit pressure, and C_i is the minimum electron speed for ionization. To calculate values of α/p_s from Eq. (6.1.70), values of v and $P_i(c)$ must be inserted, and the form of $f(c)$ must be assumed. Furthermore, the average electron energy must be inserted. Emeléus *et al.*⁷⁰ carried out this process for a number of gases by inserting experimentally determined values of P_i , v , and D/μ . (They used extrapolated values of D/μ in some cases.) They found that, by and large, a Maxwellian distribution for $f(c)$ gave reasonable values of α/p_s in the molecular gases, but gave results orders of magnitude off in argon.

Strictly speaking, Eq. (6.1.70) could be used just as well to calculate v from known values of the other parameters, including α/p_s . Thus, in the most general sense, Eq. (6.1.70) may be used as a test of whether the proper form for $f(c)$ has been chosen, assuming α/p_s , v , P_i , and D/μ have all been accurately determined. The unfolding of $f(c)$ from experimental parameters using Eq. (6.1.70) has not been developed to any extent. It should be noted that in any case only the form of $f(c)$ for $c > C_i$ is involved in the foregoing discussion. Readers are referred to reviews of Loeb⁷¹ and von Engel,⁵² where papers on this subject are discussed.

6.1.26. Experimental Values of the Second Townsend Coefficient

Values of γ have been obtained in several ways. The method outlined previously, i.e., evaluation of γ from static ionization currents, has provided the bulk of the data. A second method for determining γ is from values of α/p_s and measurement of breakdown potentials. The Townsend breakdown equation (see Section 6.1.28), then allows determination of γ . It is impossible from static measurements to determine the nature of the secondary process or processes. For the purpose of identifying the nature of the secondary processes, transient studies must be made. Such transient studies may consist of current-time measurements both below and above breakdown; the measurements of formative time lags of spark breakdown have also been of importance in revealing the nature of the secondary

⁷⁰ K. G. Emeléus, R. W. Lunt, and C. A. Meek, *Proc. Roy. Soc. A* **156**, 394 (1936).

⁷¹ See Loeb,⁷ Chapter VIII.

process. Details of the transient studies are not given here; they are summarized by Loeb,⁷² Little,⁷³ and to some extent by Raether.¹⁵

Not only is the value of E/p_s important in determining the value of γ , but the material of the cathode and its physical condition must be carefully specified. Values of γ have been obtained ranging from less than 10^{-4} to 20. The usual range, however, is narrower and lies between 10^{-3} and 10^{-1} . Transient studies have revealed the relative importance of metastable atoms, ions, and photons in secondary liberation. Control of the surface condition is so difficult that obtaining values of γ from tables is of little more than orienting significance.

6.1.27. Attachment and Ionization Occurring Simultaneously

We now consider the case where electrons, in addition to ionizing by collision, may undergo direct or dissociative attachment as well.^{74, 75} In this case, the electronic, negative-ion, positive-ion, and total currents i_e , i_- , i_+ , and i are given in the steady-state case by

$$i_e = i_0 e^{(\alpha-\eta)x}, \quad (6.1.71)$$

$$i_- = \frac{\eta i_0}{\alpha - \eta} [e^{(\alpha-\eta)x} - 1], \quad (6.1.72)$$

$$i_+ = \frac{i_0 \alpha}{\alpha - \eta} [e^{(\alpha-\eta)d} - e^{(\alpha-\eta)x}], \quad (6.1.73)$$

$$i = \frac{i_0 \alpha}{\alpha - \eta} e^{(\alpha-\eta)d} - \frac{\eta i_0}{\alpha - \eta}, \quad (6.1.74)$$

where η is the attachment coefficient as defined in Section 6.1.18.

In this case,

$$M_p = \frac{\alpha}{\alpha - \eta} e^{(\alpha-\eta)d} - \frac{\eta}{\alpha - \eta}. \quad (6.1.75)$$

It is interesting to note that M_p is no longer equal to $i_e(d)/i_0$ as it was in the absence of attachment [see Eq. (6.1.55)]. In the presence of secondary

⁷² See Loeb,⁷ Chapter IX.

⁷³ P. F. Little, in "Handbuch der Physik" (S. Flügge ed.), Vol. 21, pp. 574–663. Springer, Berlin, 1956.

⁷⁴ M. A. Harrison and R. Geballe, *Phys. Rev.* **91**, 1 (1953).

⁷⁵ J. B. Freely and L. H. Fisher, *Phys. Rev.* **133**, A304 (1964).

action, it is found that

$$M_s = (1 - [\gamma\alpha/(\alpha - \eta)]) \{ \exp[(\alpha - \eta) d] - 1 \}^{-1}. \quad (6.1.76)$$

Corrections for d_0 have generally not been made in the presence of attachment.

The statistical method previously mentioned has also been applied to the study of numbers of electrons produced in an avalanche in the presence of ionization and attachment.^{62, 63} In this case, it is necessary to make measurements at two or more different values of $p_s d$ for any given value of E/p_s in order to evaluate α and η . The results obtained for α and η by this method are in reasonable agreement with results obtained by static methods.

Recently, Frommhold⁵⁰ had adduced evidence that in O₂ electrons may not stay attached once they form negative ions. If this is an important effect, it further complicates the evaluation of coefficients from static measurements. One should also recall the experiments of Loeb⁴⁷ in which evidence was obtained that negative ions in oxygen lose their electrons at $E/p \sim 90$. One must consider that this aspect of the problem is as yet incompletely resolved.

6.1.28. Direct-Current Breakdown

A brief discussion is now given of dc parallel-plate breakdown. The electrode separation and gas densities are assumed to be large enough so that the gas plays a role in the breakdown. Consider again a uniform field geometry at a certain gas density with ultraviolet irradiation of the cathode. If the potential difference between the electrodes is increased in small increments, then at some potential the discharge can no longer be characterized as a Townsend or dark discharge. At this potential, characteristic of the nature of the gas, gas density, and nature and condition of the cathode, the current increases enormously (sometimes by many orders of magnitude), the potential across the electrodes falls (sometimes by many orders of magnitude), and light and sound are usually emitted. If it is assumed that all of these phenomena occur at the same potential, then this potential may be called the sparking potential.

Townsend⁷⁶ gave a theory whereby the sparking potential could be calculated from a knowledge of the first and second Townsend coefficients. The breakdown condition given by Townsend is that the current given by

⁷⁶ J. S. Townsend, *The Electrician*, p. 971 (April 3, 1903); see also Townsend,⁶⁶ p. 322.

Eq. (6.1.59) becomes infinite, i.e., the denominator of Eq. (6.1.59) becomes zero. This condition for determining the breakdown potential has been successful and indicates without any doubt that the threshold voltage for causing breakdown is explained in terms of the same coefficients that are used to explain currents below breakdown.

Townsend's criterion of an infinite current at breakdown has been criticized. It was considered a great advance on the Townsend formulation when it was pointed out that the vanishing of the denominator of Eq. (6.1.59) could be interpreted as the regenerative condition for an electron leaving the cathode to replace itself. In actual fact, both of these conditions are not only mathematically but physically identical. Equation (6.1.59) is a steady-state equation for the current when the cathode has a constant illumination. When the denominator vanishes, Eq. (6.1.59) indeed predicts an infinite current, but only after an infinite time. Under the regeneration condition, each electron replaces itself, and, since the cathode is continuously illuminated, this also leads to an infinite current in the steady state. The statement that one interpretation is to be preferred over the other is unwarranted. Obviously, other considerations come into play at this voltage, i.e., space charge effects and circuit parameters that control the current.

Actually, in fine detail, a number of points are inadequate in the foregoing treatment. It is tacitly assumed in the preceding that breakdown occurs before space charge effects are important. The sparking potential for most gases is independent of ultraviolet illumination at low enough illumination. Even with the absence of any ultraviolet illumination, the breakdown potential will be the same as with low illumination if one waits long enough for an electron to initiate the discharge. The time necessary is the time for an electron to appear in the discharge volume very near the cathode from either cosmic rays or natural radioactivity. With careful enough observations, one can measure a moderate decrease of breakdown potential with moderate illumination. Tremendous lowerings may be observed with strong ultraviolet illumination such as may be obtained from an auxiliary spark.

Furthermore, Townsend's treatment assumes that breakdown occurs under such conditions that the primary multiplication factor is so low that the ionization produced in a single avalanche does not seriously distort the field. For common gases, the primary multiplication factor at breakdown may be about 1000; in argon, it may be just slightly greater than unity. Space charges are virtually unimportant in these cases. A number of cases of complicated organic gases have been found where the multiplication appears to be 10^8 ; in such cases, the field distortion as the result of a single

avalanche would be important, and it would appear that the Townsend theory would require some modification for these gases.¹⁵

Static measurements of the breakdown potential do not lead to the elucidation of the nature of the secondary processes acting, any more than do static measurements of the Townsend currents. However, a measurement of the time required for the development of a spark as a function of overvoltage, once an initiating electron is provided, gives an indication of the nature of the secondary process. Such measurements indicate that the time for a spark to develop is many microseconds near the threshold and reduces, usually very rapidly, with increasing overvoltage. Such studies have indicated that, in general, at pressures above 50 Torr, the secondary mechanism is photoelectric liberation of secondary electrons from the cathode. Some authors have preferred to invoke a slight admixture of the effect of positive ions on the cathode.

For a recent review of dc breakdown near atmospheric pressure, one may refer to a paper by Marshak.⁷⁷ Marshak carries the treatment of the breakdown further in time than is done in the present section; we have preferred to limit the discussion (and the meaning of the term *breakdown*) to the initial processes leading to instability of current and voltage. Marshak is thus led into an analysis of the filamentary nature of atmospheric sparks.

With decreasing pressure, below about 10 Torr, the breakdown loses the explosive characteristics associated with atmospheric sparks. Details of the breakdown process change, e.g., the relative roles of the various secondary mechanisms may be different, but the principles that are applicable remain the same.

LIST OF UNUSUAL SYMBOLS

d	Plate separation	∇	Gradient operator
N	Gas molecule number density	c	Speed of an electron
N_s	Gas molecule number density at STP	K	Townsend electron temperature factor
p_s	Pressure corrected to standard temperature	σ	Atomic or molecular cross section
T_s	Standard temperature	\bar{Q}	Mean electron kinetic energy
v	Electron drift speed	f	Mean fractional energy loss per collision
μ	Mobility	η	Electron attachment coefficient
μ_s	Reduced mobility, mobility constant, mobility at any chosen standard temperature and pressure	h	Probability of attachment per collision
μ_0	μ_s at NTP	α	Townsend's first ionization coefficient
n	Electron number density	η'	Alternative form of Townsend's first ionization coefficient ($\eta' = \alpha/E$)
Γ	Electron flux density	γ	Townsend's second ionization co- efficient

⁷⁷ I. S. Marshak, *Soviet Phys., Usp. (English Transl.)* **3**, 624 (1961); *Usp. Fiz. Nauk* **71**, 631 (1960).

6.2 Afterglow Experiments: Atomic Collisions of Electrons, Ions, and Excited Atoms*

6.2.1. The Afterglow

The term "afterglow" is used to describe an ionized or excited gas from which the external source of ionization or excitation has been removed. In a "static" system the afterglow period follows the termination of the externally applied excitation, while in a "flowing" system the afterglow region is that part of the gas which has flowed away from the exciting region. In the afterglow the various excited atoms, ions, electrons, and normal atoms may undergo a variety of atomic collision processes, often with all species at the ambient temperature. Thus, afterglow studies have provided useful information concerning rates of electron-ion recombination, metastable atom diffusion, excited atom ionizing collisions, etc., for particles with very small mean energies ($\lesssim 0.04$ eV).

As will be discussed in detail in later subsections, a number of different experimental techniques have been employed in the afterglow studies of the behavior of electrons, ions, and excited atoms. Microwaves have been used to determine the complex conductivity of the ionized gas, and from these measurements the concentration of free electrons and their rates of collision with neutral molecules and, in some cases, with positive ions have been determined. Microwave "noise" emission measurements have been used to determine mean electron energies during the afterglow. The use of photomultipliers, together with time-sampling and noise reduction techniques, has greatly increased the sensitivity of optical emission and optical absorption apparatus, with the result that it has been possible to monitor excited atoms (molecules) and metastable atoms (molecules) at concentrations which were previously undetectable. Similarly, the application of ion multipliers at the outputs of differentially pumped mass spectrometers has permitted observation and identification of the feeble currents of ions which diffuse to the walls of the afterglow container and effuse through an orifice into the spectrometer.

These various experimental techniques are sometimes used singly in the atomic collision studies; however, they are especially useful if used in combinations which assure that the particular afterglow process under study is the only important one, or, if more than one process is of importance, that proper account is taken of all relevant processes. In the next subsections we shall develop the basic equations which describe the afterglow processes, describe in some detail several of the principal methods of

* Chapter 6.2 is by Manfred A. Biondi.

observing the species of interest, and conclude with a few illustrations of the results of afterglow atomic collision studies. It should be emphasized that these afterglow techniques have been principally employed in the study of rather weakly ionized (fractional ionization $< 10^{-3}$) plasmas.

6.2.2. Particle Continuity Equations

At the outset we shall consider that part of the afterglow in which the velocity (energy) distributions of the various particles (electrons, ions, and excited atoms) have become stationary. As a result it is sufficient to employ particle continuity equations in three-dimensional coordinate space rather than the full Boltzmann transport equation; thus much cumbersome mathematics is avoided without sacrifice of applicability to afterglow studies of rather general interest.

At a given point in space the particle species j obeys the equation

$$\frac{\partial n_j}{\partial t} = \sum_k P_k - \sum_l L_l - \nabla \cdot \mathbf{\Gamma}_j, \quad (1)$$

where n_j represents the concentration and $\mathbf{\Gamma}_j$ the particle current density of the j th species; the terms P_k represent the various processes by which the j th species may be produced (ions, for example, may be created by collisions of excited atoms), and the terms L_l represent the various processes by which the given species may be lost (e.g., positive ions disappear as a result of recombination with electrons). It is important to stress that Eq. (1) is a *point* relationship, yet essentially all of the afterglow techniques which we shall consider measure certain *space averages* of the various particle concentrations; thus, proper account must be taken of this factor in arriving at quantitative determinations of atomic collision rates (see, for example, Section 6.2.5.1).

It is in the current density term, $\mathbf{\Gamma}_j$, that the static and flowing afterglow methods exhibit a principal difference, since it is assumed that the particles under study are carried along with the mass flow of the gas in which they move. Thus, if laminar flow of the gas occurs with a velocity \mathbf{v}_M in the flowing afterglow, one contribution to the particle current $\mathbf{\Gamma}_j$ is simply $n_j \mathbf{v}_M$. If turbulence effects are small, one can transform to a coordinate system moving with the laminar streaming velocity, \mathbf{v}_M , and the flowing afterglow equation reduces to that of the static afterglow.

In a coordinate system moving with the mass flow of the background gas, the principal contribution to the current density of the particles under study is a diffusion term, i.e.

$$\mathbf{\Gamma}_j = -\nabla(D_j n_j) \simeq -D_j \nabla n_j, \quad (2)$$

where D_j is the appropriate diffusion coefficient for the particles and has been assumed to be independent of position in the afterglow in order to

bring it outside the gradient operator. For excited atoms, D_j is simply the free diffusion coefficient, while for ions and electrons in the afterglow it is the appropriate ambipolar diffusion coefficient. For example, if electrons and one type of positive ion are the only charged particles present in the afterglow, then at moderate charged particle concentrations ($>10^6 \text{ cm}^{-3}$) the mutual space charge field retards the highly mobile electrons and speeds up the flow of the slower positive ions, so that neither is moving at its "free" diffusion rate. Instead, the particle currents are essentially equal and may be represented as

$$\Gamma_{ae} \simeq \Gamma_{ai} \simeq -D_a \nabla n_{e,i}, \quad (3)$$

where the ambipolar diffusion coefficient, D_a , for electrons of kinetic temperature T_e and ions at T_i has been shown¹ to be given by

$$D_a \simeq D_+ (1 + T_e/T_i). \quad (4)$$

The quantity D_+ is the positive ion free diffusion coefficient. When "thermal" afterglow conditions prevail, i.e., $T_e = T_i = T_{\text{gas}}$, we have $D_a \simeq 2D_+$.

This rather simple situation is altered drastically when negative ion formation occurs. In this case, negative ions are essentially trapped in the plasma and electrons diffuse to the boundaries at an accelerated rate. Simplified theories taking negative ions into account^{2,3} indicate that the effective ambipolar diffusion coefficient for the electrons in a "thermal" afterglow ($T_e = T_- = T_+ = T_{\text{gas}}$) is given by

$$"D_{ae}" \simeq 2D_+ (1 + n_-/n_e), \quad (5)$$

where n_- and n_e are the negative ion and electron concentrations, respectively. We shall discuss further the complicating effect of negative ions on afterglow collision studies in Section 6.2.5.3.

We omit from consideration the response of the charged particles in the plasma afterglow to externally applied dc or low-frequency ac electric fields, since the interior of the ionized gas is largely shielded from these fields, and so the current density which flows in the volume bears no simple relationship to the applied fields.

Let us now consider the volume production and loss terms appearing in the continuity equation. Generally, such terms describe processes involving at most one-, two-, and three-body interactions between the particle under study and other particles. As an example of a one-body interaction leading

¹ W. Schottky, *Physik. Z.* **25**, 635 (1924).

² M. A. Biondi, *Phys. Rev.* **109**, 2005 (1958).

³ H. J. Oskam, *Philips Res. Rept.* **13**, 335 (1958).

to particle loss, consider spontaneous radiative decay of an excited atom. The rate R_1 of such loss is given by

$$R_1 = n_x/\tau_r = \nu_1 n_x, \quad (6)$$

where n_x is the excited atom density and τ_r is the lifetime of the excited state, which is related to the one-body rate coefficient, ν_1 , by $\nu_1 = 1/\tau_r$.

In the case of two-body interactions we can introduce the concept of a collision reaction cross section, Q , as well as a two-body rate coefficient, β . Thus, for a schematic reaction of the type

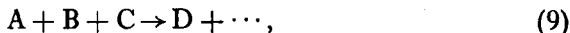


we expect a reaction rate, R_2 , of the form

$$R_2 = \beta n_a n_b, \quad (8)$$

where $\beta = \langle Qv \rangle$, and the brackets refer to averaging over the distribution of relative velocities between particles of types a and b . Examples of two-body "destruction" of particles are radiative de-excitation of metastable atoms on collisions with normal atoms and two-body dissociative recombination of electrons with positive ions. Examples of two-body reactions leading to particle production are ionization by collisions of electrons with normal atoms or by collisions of pairs of metastable atoms.

Three-body reactions are characterized by a coefficient, K ; thus, for a reaction of the form



the rate R_3 is given by

$$R_3 = K n_a n_b n_c. \quad (10)$$

An example of a three-body electron loss process is electron capture by an oxygen molecule to form a negative ion in an excited state, with a second oxygen molecule participating to stabilize the negative ion.

Account is taken of the various particle production and loss mechanisms by inserting in the continuity equation, Eq. (1), the appropriate rate terms of the forms given above for the P_k and the L_l . Using electrons as an example, the production of electron-ion pairs by metastable-metastable ionizing collisions leads to a term of the form $P_{\text{ion}} = \beta_{\text{ion}} n_M^2$, where β_{ion} is the two-body ionization rate coefficient and n_M is the metastable atom concentration. Similarly, electron loss by three-body attachment in oxygen leads to a term $L_{\text{att}} = K_{\text{att}} n^2(O_2) n_e$, where $n(O_2)$ represents the concentration of oxygen molecules.

Since it is possible that the electrons, ions, and excited atoms in an afterglow each undergo several different collision processes, some of which

couple the behavior of one species to that of another (e.g., metastable-metastable ionization), it is clear that the most general afterglow can be rather complex. The problem in attaining useful results from afterglow measurements is to achieve sufficiently simple conditions that the particles under study undergo only one or two significant atomic collision reactions. The reaction rates may then be deduced from characteristic temporal variations and/or dependences on such parameters as neutral gas density. This point is illustrated more fully in Section 6.2.5.

6.2.3. Excitation Methods*

The particular method by which the excited or ionized gas is created provides some control over the species present in the afterglow. For example for the case of ionization of a noble gas by microwave energy, the density of metastable atoms in the afterglow is found to be a rather sensitive function of the duration of the ionizing pulse.⁴ Thus, ones success in studying the behavior of a particular species during the afterglow is, in part, dependent on the choice of excitation conditions.

Historically, some of the first successful studies were carried out on afterglows following interruption of a dc (or low-frequency ac) glow or arc discharge. Such discharges, involving rather complicated electrode effects, are somewhat less satisfactory than radio-frequency or microwave electrodeless discharges, which offer a simpler plasma, akin to the positive column of the ordinary glow discharge. In all these discharges, dc through microwave, the electrons, ions, and various excited atoms are created by an electron swarm whose mean energy is of the order of one to several electron volts. Thus, in creating the particular species of interest (e.g., metastable atoms) the electron swarm also produces large numbers of other excited states and, in molecular gases, may cause significant dissociation and vibrational and rotational excitation as well.

In order to avoid complicating effects in chemically active gases such as nitric oxide, photoionization by ultraviolet photons is sometimes employed. By using photons of frequency, ν , such that $\hbar\nu \gtrsim eV_i$, where V_i is the ionization potential of the gas, it is possible to produce moderate densities of ions (e.g., NO^+) and electrons, yet avoid appreciable dissociation and excited molecule production. In addition, from considerations of energy conservation and the Franck-Condon principle, it is possible to predict the electronic and possibly the vibrational state of the molecular ion produced by the photons. Unfortunately, the ionization potentials of many of

⁴ W. H. Kasner and M. A. Biondi, *Phys. Rev.* 137, A317 (1965).

* See also Vol. 2, Chapter 4.3.

the gases of interest are so high (>12 V) that vacuum ultraviolet technology is required in order to employ photoionization; thus, photoionized plasmas have achieved only limited application in afterglow studies.

Rather specialized excitation techniques have been employed in some afterglow studies. For example, in order to approximate the excitation and ionization mechanisms occurring in the ionosphere under certain conditions (e.g., auroras), streams of high-energy electrons have been used in the laboratory to bombard a gas in order to create ionization, excitation, and dissociation which, in part, simulate the upper atmosphere processes.

Examples of the various excitation methods described in the preceding paragraphs are given in Fig. 1. The configurations shown are based on designs employed in a variety of successful afterglow experiments. In part (a) of the figure is shown a pulsed dc hot cathode arc tube. The cathode and anode are located in side arms, so that a long, clear optical absorption path via the end windows may be used for studies of metastable atom behavior. The dashed line surrounding the central portion of the tube indicates a suitable location of a microwave cavity to provide determinations of the average electron concentration within the enclosed region of the tube. Part (b) of the figure indicates another discharge tube used in metastable

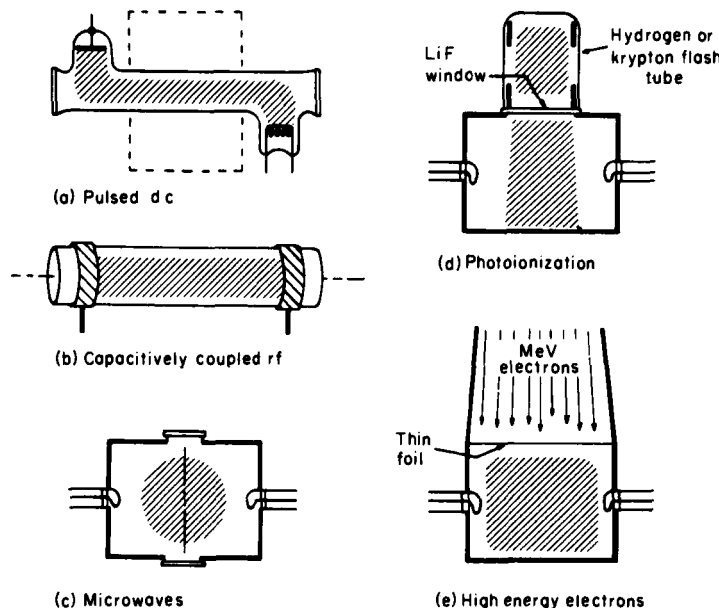


FIG. 1. Examples of the excitation methods employed in plasma generation for afterglow studies.

atom studies. Here the plasma is created by a pulse of radio-frequency energy which is capacitively coupled into the glass tube by the external ring electrodes (crosshatched). A second form of electrodeless discharge is illustrated in part (c), where the plasma is created in a gas sample within a resonant cavity by a pulse of microwave energy. The energy may be coupled into the cavity by means of a coaxial line terminating in a magnetic loop, as shown, or by a waveguide terminating in an iris in the cavity wall. The cavity may also contain windows to provide for optical emission or optical absorption studies.

In parts (d) and (e) of Fig. 1 are shown two methods of plasma generation which do not involve use of a discharge. In part (d) ultraviolet photons ($h\nu \sim 12$ eV) capable of photoionizing NO gas are generated by a hydrogen- or krypton-filled pulsed light source⁵ and admitted to a microwave cavity through a lithium fluoride window. The cavity geometry provides a convenient way of observing the electron density in the plasma and the afterglow. In a similar fashion, in part (e) a pulsed beam of million-electron-volt-energy electrons from an accelerator passes through a thin foil serving as the top wall of a microwave cavity containing the gas sample under study. The million-electron-volt electrons on collisions with gas molecules create energetic secondary electrons which in turn create additional electron-ion pairs, with the result that a moderately ionized gas is produced.

In all of the excitation methods described, the electrons' kinetic energy during the plasma-generating phase exceeds thermal energy. Thus, in order to carry out afterglow studies under "thermal" conditions, an interval must elapse during which the electrons "cool off" through elastic recoil and inelastic collisions with the neutral atoms and molecules. Since, at an elastic collision with an atom (mass M), a "hot" electron (mass m) loses, on the average, only the fraction $2m/M$ of its energy, many elastic collisions are required in the cooling process. If, in addition, the electron-atom elastic collision cross section is rather small, the electrons' energy relaxation time may be appreciable. Using neon as an example of an atom which presents a small cross section (Ramsauer effect) for elastic collisions with slow electrons, we find that, at a pressure of 1 Torr, the energy decay time constant is ~ 200 μ sec. Although other atoms offer larger elastic cross sections for electrons, the larger masses in the heavier atoms (e.g., Hg) may offset this effect, leading to similarly long energy relaxation times. Molecular gases generally offer shorter electron energy decay times, as the result of the multitude of inelastic electron collisions involving excitation of the closely spaced rotational and vibrational energy levels.

⁵ B. H. Mahan, *J. Chem. Phys.* **33**, 959 (1960); R. C. Gunton and T. M. Shaw, *Phys. Rev.* **140**, A748 (1965).

An additional complicating effect in obtaining "thermal" electrons arises when appreciable concentrations of metastable states of the neutral atoms or molecules are present during the afterglow. These metastables may act as reservoirs, feeding kinetic energy to the slow electrons as a result of "superelastic" collisions which de-excite the metastables. Since the cross section for superelastic collisions may be much greater than gas kinetic, this process is capable of "heating" the electrons well above ambient gas temperature. As mentioned in Section 6.2.4.1.4, techniques such as microwave "noise" emission measurements during the afterglow provide a means of determining the electron temperature in cases where there is reason to believe it is not at the ambient value.

6.2.4. Observational Methods*

The principal methods of afterglow measurements which we shall consider are microwave (free electrons), optical emission techniques (radiating excited atoms and molecules), optical absorption (long-lived atomic states, such as metastables and normal atoms), and mass spectrometric apparatus (positive and negative ions). A sufficiently detailed discussion of the various methods will be given to provide an understanding of the principles involved and the general forms of the apparatus employed. The reference material cited may then be used to obtain the details of design and construction of particular apparatus employed for various afterglow investigations.

6.2.4.1. Microwave Techniques. The interaction of free electrons in an ionized gas with an electromagnetic signal of appropriate frequency provides a convenient way of determining the average concentration of the electrons in the gas and their total rate of collision with atoms, ions, and other electrons. Although the precise derivation, from transport theory,⁶ of the electrons' complex conductivity is rather involved, one can obtain a good qualitative understanding of the electron behavior from a simple "one-electron" formulation given many years ago by Drude⁷ and Lorentz.⁸ Let us consider the motion of electrons in response to an ac electric field of angular frequency ω and to a viscous damping term resulting from collisions with the medium in which they move. The equation of motion is, therefore,

$$m\ddot{\mathbf{r}} = -e\mathbf{E} - \nu_e m\dot{\mathbf{r}}, \quad (11)$$

⁶ H. Margenau, *Phys. Rev.* **69**, 508 (1946).

⁷ P. Drude, *Ann. Physik* **7**, 687 (1902).

⁸ H. A. Lorentz, "The Theory of the Electron," 2nd. ed., Dover, New York, 1915.

* Consult also relevant chapters of Vols. 2, 3, and 4.

where \mathbf{r} is the displacement of the electron of charge e and mass m , \mathbf{E} is the electric field, and ν_c is to be associated with the momentum transfer collision frequency of the electrons with other particles in the medium. Equation (11) can be solved for $\dot{\mathbf{r}}$, and by introducing the complex conductivity σ_c in the equation for the current density \mathbf{J} we have

$$\mathbf{J} = \sigma_c \mathbf{E} = -ne\dot{\mathbf{r}}. \quad (12)$$

Thus, we find that

$$\sigma_c = \sigma_r + i\sigma_i = ne^2/[m(\nu_c + i\omega)]. \quad (13)$$

This so-called *Lorentz conductivity*, derived in such an elementary manner, agrees precisely with the result obtained by Margenau⁶ from a rigorous transport theory calculation when the electron momentum transfer frequency, ν_c , is assumed to be independent of the electrons' velocity.

Many of the afterglow studies of interest are carried out in the high-frequency region in which $\omega \gg \nu_c$, where the imaginary part of the conductivity (dielectric effect) outweighs the real part (resistive effect). It has been shown^{9,10} that in this region it is possible to retain the simple Lorentz conductivity form, Eq. (13), when the electron collision frequency varies with velocity v , provided that ν_c is replaced by an effective collision frequency, ν_{eff} . For example, if in the velocity region of interest the electron collision frequency is approximately proportional to v^l , then

$$\nu_{eff} = (1 + l/3)\bar{\nu}_c, \quad (14)$$

where $\bar{\nu}_c$ is obtained by averaging $\nu_c(v)$ over the electron velocity distribution.

The simple Lorentz formulation also makes clear the transition of an ionized medium from dielectric to metallic behavior as the electron density is increased. The complex dielectric constant K_c of a medium having the conductivity given in Eq. (13) may be shown to be

$$K_c = 1 - ne^2/m\varepsilon_0 \omega(\omega - i\nu_c), \quad (15)$$

where ε_0 is the permittivity of free space. Thus, in the high-frequency region, $\omega \gg \nu_c$, the dielectric constant becomes zero when the electron density is given by

$$n' \simeq m\varepsilon_0 \omega^2/e^2. \quad (16)$$

Below this critical density the ionized gas acts as a lossy dielectric, above it, as a lossy metallic reflector. Turning the argument around, we may introduce the *plasma frequency*, ω_p , above which frequency an electromagnetic

⁹ See, for example, M. A. Heald and C. B. Wharton, "Plasma Diagnostics with Microwaves," Wiley, New York, 1965.

¹⁰ A. V. Phelps, O. T. Fundingsland, and S. C. Brown, *Phys. Rev.* **84**, 559 (1951).

wave propagates into the ionized medium. Thus, for a given electron density,

$$\omega_p = (ne^2/m\epsilon_0)^{1/2}. \quad (17)$$

These relations for the complex conductivity and associated quantities apply to any charged particle. Therefore, in cases where all electrons have attached to form negative ions, the concentrations of positive and negative ions can be inferred from determinations of the conductivity of the ionized medium.¹¹

6.2.4.1.1. CAVITY METHODS. Determinations of the perturbation of the resonant frequency and the loading of a microwave cavity by electrons in an ionized gas provide one of the principal methods of measuring electron densities and collision frequencies. The analysis of the method usually starts with the following expression, which stems from a perturbation treatment given by Slater,¹²

$$\left(\frac{1}{Q} - \frac{1}{Q_0}\right) - \frac{2i(\omega - \omega_0)}{\omega_0} \simeq \frac{1}{\epsilon_0 \omega_0} \frac{\int_V \mathbf{J} \cdot \mathbf{E} dV}{\int_V E^2 dV}, \quad (18)$$

where Q represents the cavity's loaded Q and ω its resonant angular frequency in the presence of the ionized gas. The zero subscripts on the quantities refer to conditions when the ionized gas is absent. This expression is valid provided that the ionized gas does not significantly perturb the electric field distribution in the cavity. Thus, we limit ourselves to circumstances where $n \ll n'$ at all points within the cavity. Substituting for \mathbf{J} under conditions where $v_e \ll \omega$, we obtain relations for the resonant frequency perturbation and the cavity loading,

$$\frac{\omega - \omega_0}{\omega_0} = \frac{\Delta\omega}{\omega_0} \simeq \frac{e^2}{2m\epsilon_0(\omega^2 + v_{\text{eff}}^2)} \frac{\int_V nE^2 dV}{\int_V E^2 dV}, \quad (19)$$

and

$$\left(\frac{1}{Q} - \frac{1}{Q_0}\right) \simeq 2\left(\frac{v_{\text{eff}}}{\omega}\right)\left(\frac{\Delta\omega}{\omega_0}\right), \quad (20)$$

where the term v_{eff} refers to the proper *effective* electron collision frequency [see discussion relating to Eq. (14)]. Here we have taken the collision frequency from under the integral sign on the assumption that it is not position dependent within the cavity.

¹¹ C. Greaves, *J. Electron Control* **17**, 171 (1964); T. H. Y. Yeung, *ibid.* **5**, 307 (1958).

¹² J. C. Slater, *Rev. Mod. Phys.* **18**, 441 (1946).

Equation (19) shows that the frequency shift of the resonant cavity is proportional to a field-weighted average of the free electron density. Thus, in order to obtain absolute values of the electron density from the measured frequency shifts, subsidiary information is required concerning the spatial distribution of the electrons within the cavity. If we rewrite the field-weighted average of electron density of Eq. (19) in terms of an ordinary average \bar{n} and a shape factor $F(r, \theta, z)$, i.e.,

$$\bar{n} F(r, \theta, z) \equiv \int_V n E^2 dV / \int_V E^2 dV, \quad (21)$$

it is a straightforward matter to calculate $F(r, \theta, z)$ for various cavity and plasma geometries and so obtain a numerical relationship between the average electron density within the plasma container and the measured frequency shift of the cavity.¹³⁻¹⁵ Typical values of this form factor for different electron distributions within a TM₀₁₀ cavity are given in Table I.¹³

By way of contrast, it will be seen from Eqs. (19) and (20) that, for the experimental conditions considered,

$$\frac{\nu_{\text{eff}}}{\omega} = \left(\frac{1}{Q} - \frac{1}{Q_0} \right) / \frac{(2 \Delta\omega)}{\omega_0}. \quad (22)$$

That is, one obtains the electron collision frequency from measured cavity properties, without needing to know the spatial distribution of the electrons.

Simplified block diagrams of two forms of resonant cavity apparatus used in afterglow electron density determinations are given in Figs. 2 and 3. The particularly simple form of transmission apparatus which may be used when the ionization is generated by some external agent such as high-energy photons or electrons [see parts (d) and (e) of Fig. 1] is illustrated in Fig. 2. The synchronization of the various events is controlled by the master generator. The plasma is created by a pulse of ionizing radiation of suitable duration ($\sim 0.01-5$ msec) which may be repeated at regular intervals, e.g., ~ 20 msec). In this case a single-mode TM₀₁₀ cavity resonant at ~ 3 GHz contains the ionized gas under study. The resonant frequency of the cavity as a function of time is determined by transmitting a very-low-energy microwave signal through the cavity via coaxial lines and coupling loops. The signal is detected by the crystal, amplified by a video amplifier, and displayed on the y axis of an oscilloscope whose sweep

¹³ M. A. Biondi, *Rev. Sci. Instr.* **22**, 500 (1951).

¹⁴ H. J. Oskam, Microwave investigation of disintegrating gaseous discharge plasmas, Ph.D. Thesis, Univ. of Utrecht, Netherlands, 1957.

¹⁵ D. J. Rose and S. C. Brown, *J. Appl. Phys.* **23**, 1028 (1952).

TABLE 1. Shape Factor, $F(r, \theta, z)$ for Plasma Containers Placed within a Cylindrical TM₀₁₀ Cavity of Radius R and Height H

Container					
Shape	Rad.	Ht.	Electron distribution	$F(r, \theta, z)$	Remarks
Cylindrical	r	h	Uniform: $n = \bar{n}$	$3.70 \left[\frac{h}{H} \right] \rho^2 [J_0^2(2.4\rho) + J_1^2(2.4\rho)]$	$\rho = r/R$ Electron distribution characteristic of idealized recombination loss
			$n = n_0 J_0(2.4\rho) \cos(\pi z/h)$ $\bar{n} = 0.274n_0$	$2.32 \left[\frac{h}{H} \right] [1.6\rho^2 - 1.42\rho^4 + 2.58\rho^6]$	Accurate for $\rho \ll \frac{1}{2}$ Electron distribution characteristic of diffusion loss
Spherical	r	—	Any electron distribution	$3.70 \left[\frac{\text{vol. of sphere}}{\text{vol. of cavity}} \right]$	Accurate for $r \ll R$

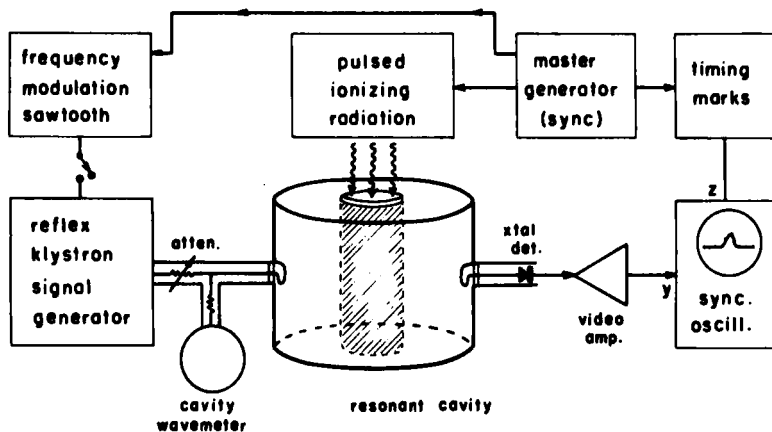


FIG. 2. Simplified block diagram of microwave resonant cavity apparatus employing transmitted signal detection to measure electron densities.

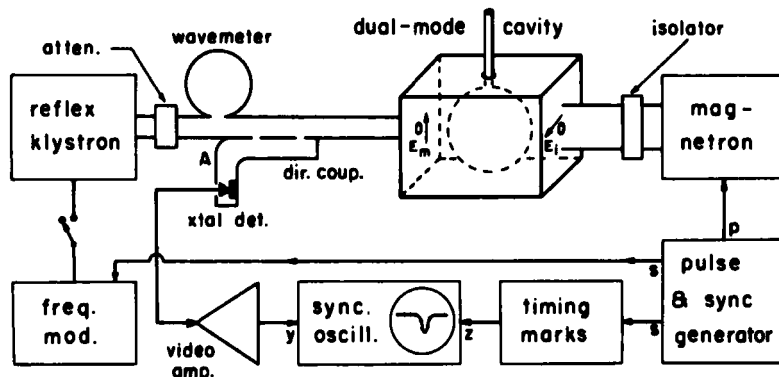


FIG. 3. Simplified block diagram of dual-mode microwave cavity apparatus employing reflected signal detection to measure electron densities. In order to measure electron collision frequencies a calibrated variable attenuator is inserted in the directional coupler waveguide at point *A* (see text for detailed discussion).

is synchronized to start at the end of the ionizing pulse and carries intensified (*z*-axis) timing marks. The frequency of the signal can be accurately determined by a precision cavity wave meter (sensitivity $\sim \pm 20$ kHz).

The timing cycle of the events is illustrated in Fig. 4. Part (a) indicates the ionizing pulse which, in most cases, is repeated at regular intervals. Part (b) illustrates the behavior of the electron density, which usually increases throughout the ionizing pulse and then decreases with time during

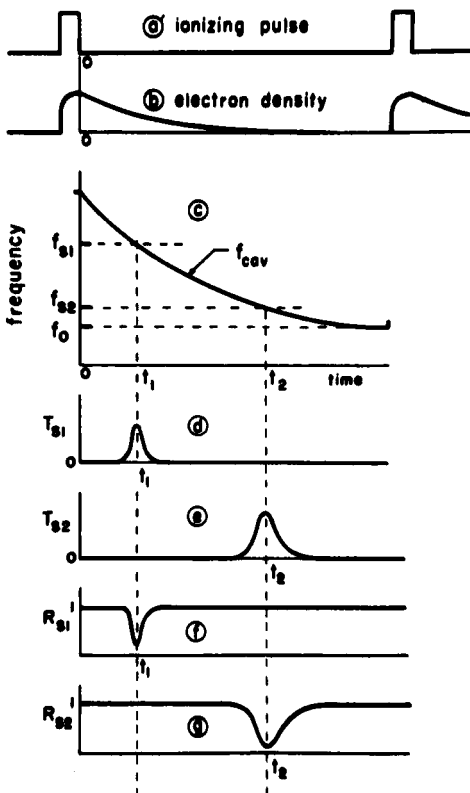


FIG. 4. Timing cycle of events in microwave cavity methods of measuring electron densities during the afterglow. Fixed probing signal frequencies are employed.

the afterglow. The changing electron density during the afterglow produces a corresponding change in the resonant frequency of the cavity, as indicated in part (c), the cavity returning to the empty resonant frequency, f_0 , when the electron density has decayed to negligibly small values.

If now a low-energy signal from the klystron, set at a fixed frequency f_{s1} , is incident in the cavity, it will be reflected strongly at all times when the cavity's resonant frequency is quite different from f_{s1} . Substantial transmission through the cavity will occur only around the time t_1 , when $f_{\text{cav}} \approx f_{s1}$, as indicated in part (d), which represents the pattern seen on the oscilloscope. By measuring the frequency f_{s1} with the wavemeter and noting the time t_1 of maximum transmission on the calibrated oscilloscope sweep, one point of the curve, f_{cav} versus t , is determined. By setting the klystron

6. SWARMS

to a new frequency f_{s2} and noting the new time of maximum transmission, t_2 , as indicated in part (e), a second point is determined, etc.

It will be noted that, as the electron density becomes rather small and f_{cav} approaches f_0 , the transmitted signal curves become very broad; therefore, it is difficult to determine the time of maximum transmission accurately. In order to obtain more precise measurements in this case, the frequency of the reflex klystron is swept by ac coupling a synchronized sawtooth wave (for example, from the oscilloscope sweep) to the reflector electrode. The resulting timing sequence is illustrated in Fig. 5. Here the changing cavity frequency with time is indicated by the curve, f_{cav} , while the synchronized, swept signal frequency is the line f_s . It will be seen that the two curves cross at the frequency f_{sc} , which is very nearly equal to f_0 . As a result of the swept signal frequency, the transmitted signal, T , shows a rather sharp maximum at the time t_{sc} . To find the frequency of the signal generator at this instant, one changes the frequency f_{wm} of the cavity wavemeter (which is connected in an absorption mode) until its sharp

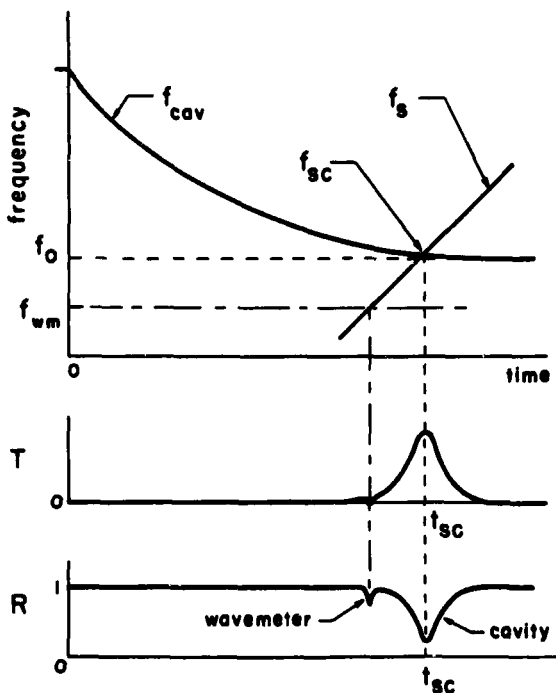


FIG. 5. Timing cycle of events when a swept-frequency probing signal is used to determine electron densities late in the afterglow.

absorption pip is exactly at the maximum of the transmitted curve; at this point, $f_{wm} = f_{sc}$.

By operation of the apparatus in either or both the fixed signal frequency and swept frequency modes one obtains point-by-point data of f_{cav} versus time. From these data and a knowledge of the relative distribution of the electrons within the cavity, Eqs. (19) and (21) permit one to obtain absolute values of the average electron density \bar{n} .

The second form of resonant cavity apparatus, involving reflected signal measurements, is illustrated in Fig. 3. Here the ionized gas is generated in a spherical quartz bottle by microwave energy from a magnetron which is waveguide coupled to a rectangular parallelepiped cavity via a ferrite isolator. In order to prevent overload of the video amplifier by the magnetron pulse, two cavity modes are used, the electric field of the ionizing mode E_i being orthogonal to that of the cavity frequency measuring mode E_m . In this way, negligible leakage of magnetron power into the measuring waveguide is achieved. The apparatus operates in analogous fashion to the transmission apparatus of Fig. 2, except that the reflection from the cavity of the low-energy klystron signal is detected by the directional coupler and crystal detector, and the amplified signal is displayed on the synchronized oscilloscope.

Referring again to the timing cycles, parts (f) and (g) of Fig. 4 show the reflected signal seen on the oscilloscope for two different fixed signal frequencies. Here, the measured times of minimum reflection and corresponding signal frequencies yield the desired curve of f_{cav} versus time. When f_{cav} approaches f_0 , the swept frequency method illustrated in Fig. 5 makes determination of the time of minimum reflection more accurate, as indicated at the bottom of the figure.

Before leaving the subject of average electron density determinations by resonant cavity techniques, it is important to consider the point at which deviations from the linear relationship between electron density and frequency shift, Eq. (19), occur.^{9,16} In general, if the plasma occupies most of the volume of the cavity, frequency shifts up to $\sim 10\%$ of the empty resonant frequency of the cavity are within the range of applicability of the linear perturbation theory. If, however, the plasma is concentrated over a limited volume of the cavity, then one violates the requirement that $n \ll n'$ at appreciably smaller fractional frequency shifts, and perturbation theory is not sufficiently accurate.

Measurements of the collision frequency of electrons in ionized gases make use of resonant cavity apparatus quite similar in form to those just

¹⁶ S. C. Brown, *Proc. U.N. Intern. Conf. Peaceful Uses At. Energy*, 2nd, Geneva 32, p. 394, 1958, Pergamon Press, Oxford, 1959.

discussed for electron density determinations. From Eq. (22), it will be seen that measurements of the change in Q and in the resonant frequency of the cavity permit determination of the electrons' effective collision frequency, ν_{eff} , from a very simple relationship, provided that certain conditions are met. For example, since the rate of collisions of electrons with atoms, ions, or other electrons may depend on the average electron energy, we assume that a sufficiently small measuring field is present in the cavity not to disturb the electron energy and therefore make it position dependent. Second, since ν_{eff} is linearly proportional to the concentration of scatterers with which the electrons collide, the simple form, Eq. (20), can not be used when electron-electron or electron-ion scattering is important, and the electron and ion densities vary with position in the cavity.

To determine the electron collision frequency at a given time in the afterglow we determine the cavity's frequency shift at that instant, using the methods already described, and then determine the change in $1/Q$ relative to the "empty" cavity conditions. There are a number of ways of determining the Q of the cavity^{10,15,17} with and without the plasma. We shall present here a simple method making use of the apparatus of Fig. 3, to which is added a calibrated attenuator in the directional coupler guide leading to the crystal detector (point *A*).

The desired quantities are obtained from determinations of the loaded Q of the empty cavity and of the reflection coefficient of the cavity on resonance, Γ^r . The loaded Q of a cavity may be thought of as resulting from contributions from the cavity itself, the plasma, and the coupling to the external world, i.e.,

$$\frac{1}{Q} = \frac{1}{Q_u} + \frac{1}{Q_1} + \frac{1}{Q_2} + \frac{1}{Q_p}, \quad (23)$$

where Q_u is the intrinsic or unloaded Q of the cavity, Q_1 and Q_2 are the Q 's associated with the two coupling irises, and Q_p represents the effect of plasma loading. Since the first three terms on the right of Eq. (23) do not change as the plasma decays in the afterglow, it will be seen that the quantities in Eq. (22) reduce to $(1/Q) - (1/Q_0) = 1/Q_p$.

To determine the loaded Q with and without the plasma we proceed as follows; with no discharge occurring in the cavity, we operate the klystron of Fig. 3 in its swept-frequency mode. Thus, the signal on the oscilloscope resembles curve (1) at the bottom of Fig. 6. If the crystal detector were truly a square law device the signal would be proportional to $(\Gamma)^2$, where Γ is the instantaneous reflection coefficient, $\Gamma = E_r/E_t$, for the wave incident on the cavity from the klystron. For a lossless waveguide we have,

¹⁷ S. C. Brown and D. J. Rose, *J. Appl. Phys.* **23**, 711 (1952).

for conditions far from resonance, $\Gamma_\infty = 1$. We now determine the value of the reflection coefficient of the empty cavity on resonance, Γ_0^r , by noting the height of the reflected signal above the base-line at resonance* and then increasing the attenuation at point *A* of Fig. 3 until the amplitude of the off-resonance reflected signal decreases to this height [curve (2) of Fig. 6]. The required attenuation is related to Γ_0^r by, $\text{atten}(db) = 20 \log \Gamma_0^r$. By use of this value of Γ_0^r and appropriate charts, such as Fig. 7 of Ref. 17, one can find the reflection coefficient at the cavity's half-power points, Γ_0^h , and thus determine the attenuator setting which locates the corresponding reflected signal amplitude [point (3) in Fig. 6]. If we now return the attenuator to its initial setting, the cavity wavemeter pip may be moved to the locations of the half-power points on curve (1) and from this the quantity Δf_h determined (top of Fig. 6). The loaded Q of the empty cavity is then $Q_0 = f_0 / \Delta f_h$.

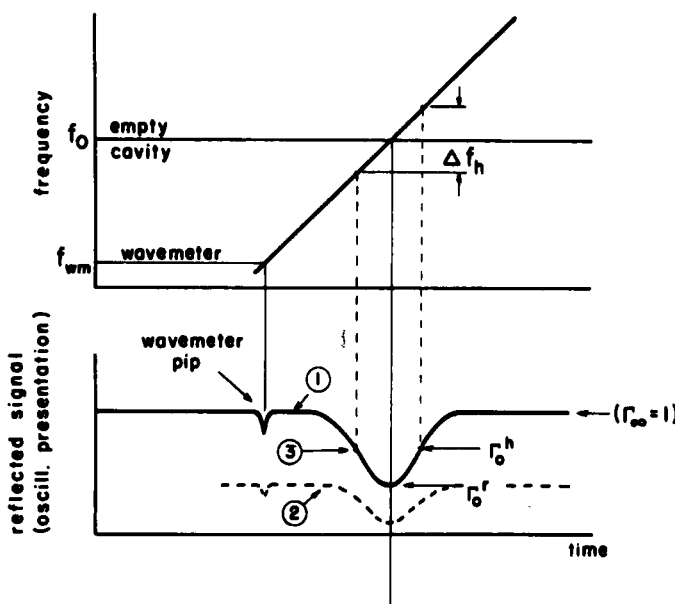


FIG. 6. Timing cycle of events in cavity reflection method (see Fig. 3) of determining electron collision frequencies during the afterglow.

* It is necessary to use direct coupled amplifiers from the detector to the oscilloscope to preserve the zero signal reference level.

It may readily be shown² that, on resonance, the reflection coefficient Γ^r is related to the loaded Q and to the input coupling Q , Q_1 , by

$$\Gamma^r = -(1 - 2Q/Q_1). \quad (24)$$

Thus, since Q_1 is unaffected by the presence of the plasma, we find that the loaded Q in the presence of the plasma is related to Q_0 by

$$Q = (1 + \Gamma_p^r)Q_0/(1 + \Gamma_0^r), \quad (25)$$

where Γ_p^r is the reflection coefficient at the instant that the signal frequency equals the cavity-plus-plasma resonant frequency. The value of Γ_p^r is determined in an analogous manner to that described earlier for Γ_0^r . With the measurement of the cavity's frequency shift at this same instant, the electron collision frequency may be calculated by use of Eq. (22).

Successful determinations of electron collision frequencies using resonant cavity techniques which differ in detail from the above method have been carried out by Phelps *et al.*¹⁰ and by Gould and Brown.¹⁸ Thus, cavity techniques offer reasonably simple and reliable methods for determining average electron densities and collision frequencies in the ranges where the linear theory applies.

6.2.4.1.2. FREE-SPACE PROPAGATION METHODS. In order to obtain measurements of successively higher electron densities, it is necessary to use successively higher microwave frequencies to assure that $n \ll n' \equiv m\epsilon_0 \omega^2/e^2$. However, as the wavelength of the microwaves decreases, smaller and smaller volumes of plasma can be enclosed within a resonant cavity operating in one of its low excitation modes. While the use of a higher mode cavity, in which the electric and magnetic fields have a number of zeros within the cavity, permits enclosing a larger plasma volume, difficulties are encountered with excitation of the many alternate cavity modes lying at nearby frequencies. Thus, one turns to "plane-wave" propagation through the plasma, as indicated schematically in Fig. 7, for a method which permits studies of higher-density plasmas occupying substantial volumes of space.

The theoretical analysis is facilitated if we consider frequencies sufficiently large that (a) the electron density is well below the critical value (i.e., $n \ll n'$) and (b) the wavelength is small compared to the dimensions of the plasma; hence, plane-wave propagation through the plasma may be assumed.

We shall consider normal incidence of a plane wave on a plasma of a size and shape which approximates a plasma "slab." Thus, we may represent the electromagnetic field by the form $\exp(iwt - \gamma cx)$, where the com-

¹⁸ L. Gould and S. C. Brown, *J. Appl. Phys.* **24**, 1053 (1953).

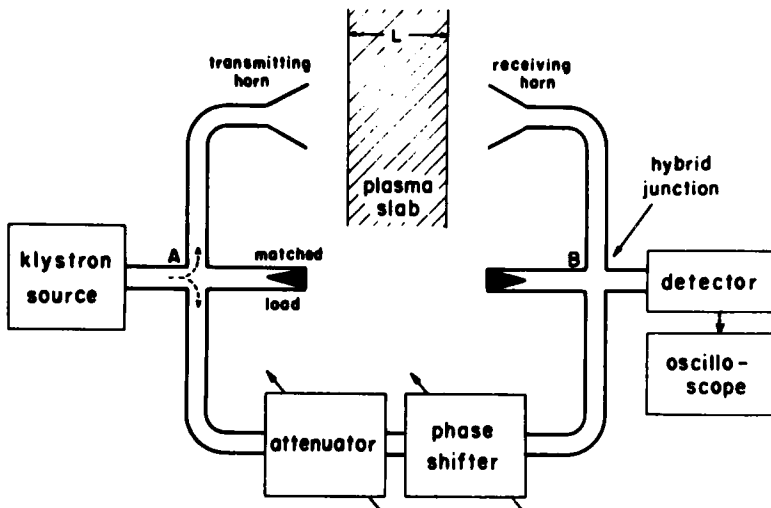


FIG. 7. Simplified diagram of microwave bridge employed in free-space propagation determinations of the electron density and collision frequency in plasma-afterglows.

plex propagation coefficient γ_c is related to the complex dielectric coefficient K_c of Eq. (15) by

$$\gamma_c \equiv \alpha + i\beta = i\omega(K_c)^{1/2}/c, \quad (26)$$

α being the attenuation coefficient and β the phase coefficient. One readily finds that

$$\beta = [1 - (n/n')]^{1/2} 2\pi/\lambda, \quad (27)$$

where λ refers to the wavelength in vacuum. The phase change $\Delta\phi$ caused by a plasma slab* introduced in the transmission path is, therefore, given by

$$\Delta\phi = - \int_{\text{path}} (\beta_p - \beta_0) dx \simeq (e^2/2m\omega\epsilon_0 c) \int_{\text{path}} n(x) dx, \quad (28)$$

where the subscripts p and zero refer to the phase coefficients with and without the plasma, respectively, and the approximation is valid to first order in (n/n') . It has been shown⁹ that, for a slab of thickness L , the average electron density \bar{n} in the slab is related to the phase shift by

$$\bar{n} (\text{cm}^{-3}) = 118.4[f(\text{Hz})/L (\text{cm})] \Delta\phi (\text{rad}). \quad (29)$$

* We shall assume that the slab has "soft" boundaries; that is, the fractional change in propagation coefficient over a distance of a wavelength is small.

Thus, for small phase shifts, the average electron density is linearly proportional to the phase shift. An example of the form of the departure from linearity is given by the following equation, which has been derived⁹ for a uniform electron density, $\bar{n} = n_u$, in the slab:

$$(n/n') = 2(\lambda \Delta\phi/2\pi L) - (\lambda \Delta\phi/2\pi L)^2. \quad (30)$$

An apparatus useful for accurate determinations of the phase shift caused by the presence of the plasma in the free-space propagation zone is shown schematically in Fig. 7. Microwave energy from the klystron divides at junction *A*, propagates in the upper branch through free space between the horns and in the lower branch through an attenuator and phase shifter in the waveguide before being reunited at the junction *B*, where the resulting combined signal goes to the detector. With the plasma absent, this microwave bridge is balanced by adjusting the attenuator and phase shifter to provide a null at the detector. The plasma is then created and the additional phase shift $\Delta\phi$ required to rebalance the bridge is noted. This procedure is suitable for determining the static phase shift resulting from the presence of a steady plasma. One then finds the average electron density in the slab by application of Eq. (29).

The microwave bridge may be used for determinations of the changing electron densities during the afterglow under the following circumstances. If the initial afterglow electron density and the plasma thickness are sufficiently large that $\Delta\phi$ is many times 2π , and if $v_c \ll \omega$, so that attenuation by the plasma is small, then as the electron density decays, the detector will register a null each time $\Delta\phi$ changes by 2π . The changing detector signal is conveniently displayed on a synchronized oscilloscope. If one observes the electron density decay until the final null at $\Delta\phi \simeq 0$ occurs, then by counting backwards through successive nulls one can determine $\Delta\phi$ absolutely and hence \bar{n} for each time at which a null signal appears on the oscilloscope trace. A disadvantage of this method relative to the cavity methods is that one can not obtain data points at arbitrary values of electron density, only at those values for which $\Delta\phi$ is a multiple of 2π . Thus, the whole range of electron densities between $\Delta\phi = 0$ and 2π can not be examined, leading to a substantially reduced range of observable electron densities relative to cavity techniques.

This free-space propagation method is elegantly simple in principle. However, because of reflections and refractions at plasma boundaries and difficulties in approximating the plane wave propagation through a plane plasma slab for which the analysis holds, in practice considerable skill and sophisticated techniques are required to attain a system which provides quantitative average electron density determinations. An excellent, detailed discussion of the various free-space propagation methods has been given

by Heald and Wharton,⁹ who consider not only bridge methods but also attenuation and reflection methods. The major advantage of these methods over cavity techniques is their suitability for study of high plasma densities ($n \gtrsim 10^{12} \text{ cm}^{-3}$) occupying substantial volumes of space (linear dimensions $> 10 \text{ cm}$).

6.2.4.1.3. GUIDED WAVE PROPAGATION. The use of electromagnetic radiation within wave guides to measure plasma properties involves principles similar to the free-space propagation method and offers certain advantages, as well as some disadvantages. Here the propagation constants are determined for a wave passing through a length of plasma within a waveguide, and thus, the complex propagation coefficient γ_c and the phase coefficient β may be represented by Eqs. (26) and (27), except that the guide wavelength must be used in Eq. (27), rather than the wavelength in vacuum.

On the assumption that the plasma uniformly fills the waveguide across its cross-sectional area with the only variation of electron density in the propagation (x) direction, the phase shift analysis presented in the previous subsection may be carried over to the guided wave case. In practice, plasma containers which only partially fill the waveguide and within which the electron density decreases toward the boundaries (see Fig. 8) are employed, leading to severe complications in the analysis.¹⁹

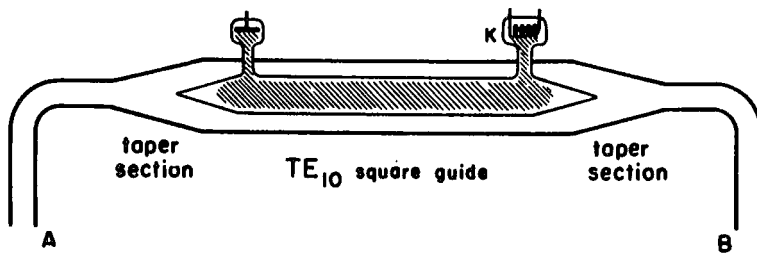


FIG. 8. Upper arm of microwave bridge employing guided wave propagation through the plasma to determine the electron density and collision frequency. The section shown replaces the upper section between points *A* and *B* in Fig. 7.

An example of a guided wave apparatus patterned after the free-space propagation bridge apparatus of Heald and Wharton⁹ involves replacing the upper path of the bridge of Fig. 7 between points *A* and *B* by the waveguide section shown in Fig. 8. Here an enlarged section of TE_{10} square guide contains a cylindrical Pyrex tube with tapered ends to minimize reflections. The plasma is created by dc voltage pulses applied between an external hot cathode and anode. (This form of guide and plasma

¹⁹ J. M. Anderson and L. Goldstein. *Phys. Rev.* **100**, 1037 (1955).

tube follows closely that employed by Anderson and Goldstein in their guided wave apparatus.¹⁹⁾ The attenuation and the phase shift introduced by the presence of the plasma are determined from the values of additional attenuation and phase shift introduced in the lower arm to rebalance the bridge.

Decaying electron densities during the afterglow are determined by pulsing the klystron "on" for a short interval at a particular time in the afterglow and noting the attenuation and phase shift at this "instant" in the afterglow.¹⁹⁾ By varying the time in the afterglow during which the klystron is "on" the electron density decay and collision frequency can be determined. This method is patterned after that developed by Anderson and Goldstein,¹⁹⁾ who used a somewhat different form of microwave bridge, employing directional couplers in place of the hybrid junctions at *A* and *B* in Fig. 7 to obtain the signal for the lower arm of the bridge. In addition, instead of the variable attenuator and phase shifter, a slotted line with standing wave detector was used in the lower line to determine the phase shift introduced by the plasma.^{19,20)}

An additional interesting feature employed by Anderson and Goldstein involves the use of a second pulsed microwave signal at a slightly different frequency which is introduced to the bridge from the left and serves to raise the electron energy during the measuring interval. In this way, the energy dependence of the electron collision frequency may be determined.¹⁹⁾ This method of electron heating by microwaves is a counterpart of that used by Gould and Brown¹⁸⁾ in their resonant cavity technique.

Historically, the guided wave method was developed before the free-space propagation techniques. While the guided wave method avoids the technical difficulties of the free-space method in achieving pure plane-wave propagation between the horns, it is generally confined to use with much smaller plasma volumes at a given microwave frequency.

6.2.4.1.4. MICROWAVE RADIATION MEASUREMENTS. Before leaving the subject of microwave methods of determining various electron properties in the afterglow, we should mention the determinations of mean electron energy ("temperature") obtained from measurements of microwave emission "noise." Since calculation of the mean electron energy from the microwave power radiated by the plasma afterglow involves a rather complicated analysis, space limitations require that we merely outline the principles involved and refer the reader to the detailed discussion given in the literature.^{9,21,22)}

²⁰⁾ L. Goldstein, M. A. Lampert, and J. Geiger, *Elec. Commun.* **29**, 243 (1952).

²¹⁾ D. Formato and A. Gilardini, *Proc. Intern. Conf. Ionization Phenomena Gases, 4th Uppsala*, 1959, **1**, pp. IA99-104. North-Holland Publ. Amsterdam, 1960.

²²⁾ G. Bekefi and S. C. Brown, *Am. J. Phys.* **29**, 404 (1961).

There are two limiting cases of radiation emitted from the afterglow for which the analysis is somewhat simplified: (a) when the medium acts as a "black-body" and (b) when the medium is essentially transparent. The "black-body" medium is the simplest to treat; however, the conditions required for the afterglow medium to approximate a black-body are very difficult to achieve in practice.

A medium approximates a black-body if (1) it is many absorption lengths ($l_a = \alpha^{-1}$) deep at the radiated frequency and (2) it is not overdense, i.e., $\omega \gg \omega_p$, so that the radiation may escape freely from the medium without reflection. Under these circumstances the Planck black-body radiation function $B(\omega, T)$ in the low-frequency (Rayleigh-Jeans) limit, $\hbar\omega \ll kT_e$, describes the unpolarized intensity radiated from an extended plasma in unit frequency interval and into unit solid angle,

$$B(\omega, T) = \frac{kT_e \omega^2}{4\pi^3 c^2}, \quad (31)$$

where we have assumed that the afterglow electron energy distribution is sufficiently close to Maxwellian to be characterized by a temperature T_e . If this radiation is detected by a dipole antenna properly located outside the plasma, then, as a result of the λ^2 dependence of its effective receiving area and its sensitivity to one polarization, the power received in a band pass $\Delta\omega$ is

$$P(\omega) \Delta\omega = kT_e \Delta\omega / 2\pi. \quad (32)$$

Thus, a determination of the absolute microwave "noise" power received by the antenna provides a direct measurement of the electron temperature when the afterglow conditions approximate black-body behavior. Unfortunately, only afterglows at rather high pressures and low ionization densities provide the circumstances, $v_{\text{eff}} > \omega \gg \omega_p$, for which the black-body conditions are readily met.

Let us now consider the other limit, that of a "completely" transparent medium, that is, one where $\alpha^{-1} \gg L$, L being the depth of the plasma in the direction of radiation propagation. We still require that the plasma be underdense, $\omega \gg \omega_p$, at the monitored "noise" frequencies to avoid reflections. In this case the emitted radiation is calculated by summing the uncorrelated free-free electron transitions resulting from accelerations during collisions. For the case of predominantly electron-ion scattering collisions, the microwave radiation from a transparent plasma has been shown⁹ to depend not only on the electron temperature, but on the electron density and the ionic charge as well. In addition, at a given frequency, the power radiated from the transparent plasma varies inversely with the

square root of the electron temperature, rather than directly with the temperature, as in the black-body case.

Since many plasma-afterglow conditions fall between these extreme cases of a black-body or a transparent medium, it will be seen that relating the measured noise power to the electron density may be an exceedingly difficult task. However, several investigators^{9,21,22} have developed a variety of techniques of microwave radiation measurements which have provided them with information concerning the average electron energy in the plasma.

6.2.4.2. Spectroscopic Methods. In this section we shall consider techniques appropriate for the study of weak optical emission from the afterglow or for the detection of very weak optical absorption by species of interest in the plasma afterglow. As a result of the need for maximum sensitivity and speed of response, photomultiplier detectors are employed in conjunction with optical elements such as interference filters, spectrographs, and interferometers. The principal novel use of the photomultiplier detector in the repetitive plasma-afterglow studies involves time-sampling methods such as are discussed in Section 6.2.4.2.1. The method is further illustrated in the discussion of emission intensity, optical absorption, and spectral line-shape studies in Sections 6.2.4.2.2-4. Finally, the use of the multiplier in either the output current mode or pulse-counting mode, with appropriate techniques for maximizing the signal/noise ratio, is discussed in Section 6.1.4.2.5.

6.2.4.2.1. TIME-SAMPLING TECHNIQUES. The use of time-sampling techniques²³ on repetitive afterglows permits one to obtain accurate values from data in which there are large statistical fluctuations. Instead of operating the photomultiplier in a continuously sensitive mode, it is electronically gated "on" for a given interval in the afterglow by application of a rectangular negative high-voltage pulse to its electrodes using a circuit of the type illustrated in Fig. 9. (The diodes and capacitors in the last two dynode circuits act to maintain steady voltages on these electrodes and thus shield the collector electrode from induced currents.) Thus, the photomultiplier responds to radiation only during the high-voltage gating pulse.

Suppose now that one wishes to observe the time dependence of very weak emission spectra from the afterglow. The measuring interval (photomultiplier "on" time) must be short compared to the decay time in order to determine accurately the shape of the curve. However, the number of quanta reaching the photomultiplier during the "on" time may be so small that statistical fluctuations in the value are very large. For a repetitively produced afterglow it is possible to reduce greatly the uncertainty in the

²³ A. O. McCoubrey, *Phys. Rev.* **93**, 1249 (1954).

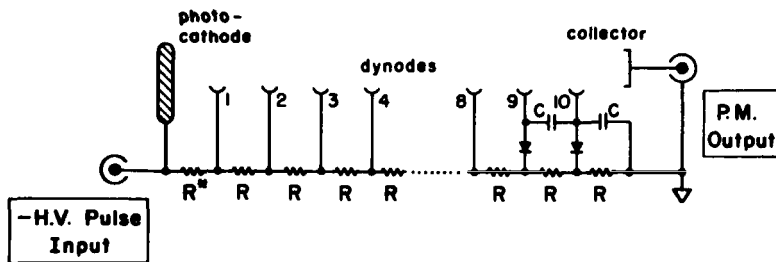


FIG. 9. Photomultiplier gating circuit. Application of a high-voltage pulse to the dynode chain makes the photomultiplier sensitive to radiation during a given interval. The values of R in the resistor chain are chosen to obtain proper voltages between the photocathode and first dynode and between adjacent dynodes. Typical values employed are $R = 100 \text{ K}$ and $C = 10 \mu\text{F}$.

value of the radiation intensity by taking the signals obtained during many afterglows at this "on" time ("time sample") and integrating them.

6.2.4.2.2. Low-Intensity Optical Emission Measurements. An apparatus making use of time sampling to permit measurements of the intensity of radiation emitted as a function of afterglow time is illustrated in the block diagram of Fig. 10. Radiation from the repetitively produced plasma

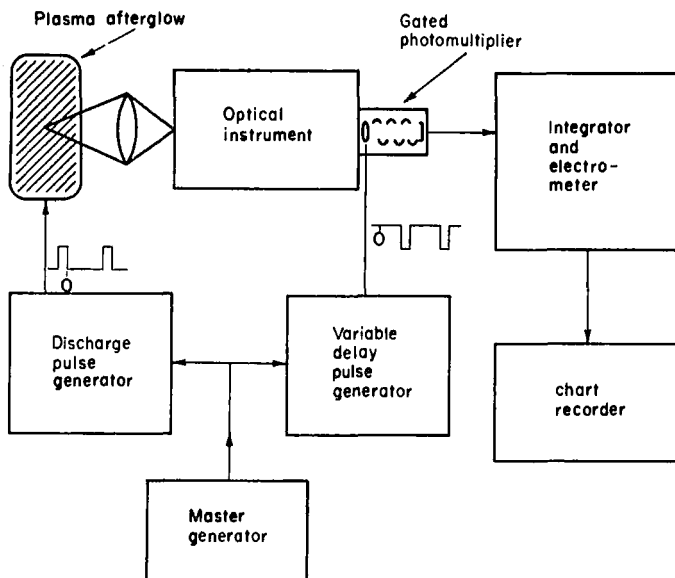


FIG. 10. Simplified block diagram of apparatus used for studies of radiation emitted during the afterglow.

and afterglow passes through the optical instrument (in this case, a spectrograph set on a given spectral line) and falls on the photocathode of the multiplier. A repetitive high-voltage pulse of appropriate width and delayed by a specified time relative to the start of the afterglow is applied to the photomultiplier to make it sensitive to radiation. The output of the photomultiplier is fed to an integrator (condenser) across the input resistor of an electrometer to add the signals received from many afterglows. For example, with discharge pulse repetition rates of 100 sec^{-1} and integrating times of $\sim 100 \text{ sec}$ it is possible to reduce the statistical fluctuations in the measured intensity value by a factor of ~ 100 relative to that obtained from a single afterglow.

By varying the time in the afterglow that the photomultiplier is gated "on", one obtains the variation of emission intensity as a function of afterglow time. Alternatively, one can obtain the emitted spectrum at a given time in the afterglow by using the output of the electrometer to drive the y axis of a chart recorder whose x axis is driven by a synchronous motor. By slowly* driving the wavelength drum of the spectrograph with a synchronous motor, the intensity versus wavelength spectrum emitted during the specified afterglow interval is obtained.

6.2.4.2.3. MEASUREMENTS OF WEAK OPTICAL ABSORPTION. If two states of an atom or molecule are connected by an optical transition of frequency ν_{ij} , then it is possible to monitor the concentration of atoms in the lower state by noting the absorption of a beam of radiation at the frequency ν_{ij} as it traverses a medium containing the atoms. Thus, one may determine the behavior of such species as metastable atoms or molecules during the afterglow. In conventional optical absorption studies of afterglows, the variation in the transmitted intensity of the selected radiation is detected by a photomultiplier, amplified, and presented on a synchronized oscilloscope. This method is satisfactory for absorptions of $\sim 1\%$ or greater. If, however, the absorption of the transmitted beam is small, owing either to a small concentration of the absorbing species or to the fact that the absorption strength per atom (i.e., the transition's oscillator strength) is small, a more elaborate system is needed.

A simplified diagram of the principal elements of a sensitive optical absorption apparatus²⁴ is given in Fig. 11. A steady source, whose spectrum contains line radiation which is selectively absorbed by the atomic states under study, is at the left. The radiation is collimated and passes through

²⁴ A. V. Phelps and J. L. Pack, *Rev. Sci. Instr.* **26**, 45 (1955).

* The time taken for the drive to scan through a spectral line must be substantially longer than the integrating time employed.

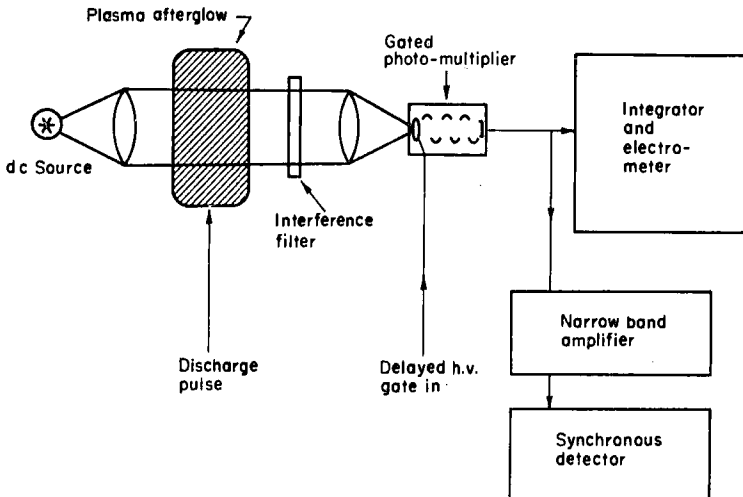


FIG. 11. Simplified block diagram of apparatus used to measure weak optical absorption during the afterglow.

the repetitively produced plasma-afterglow. The particular wavelength undergoing absorption is selected from the rest of the spectrum by a narrow-band interference filter and focused on the gated photomultiplier. The average value of the transmitted intensity $I_0(1-A)$, where I_0 is the incident intensity and A is the absorption, is recorded by the integrator and electrometer.

The use of the narrow-band amplifier and synchronous detector to detect the small, time-varying absorption is illustrated by the timing sequence of Fig. 12. The exciting pulse, repeated at intervals of τ , produces the absorbing atoms, whose concentration decreases with time in the afterglow [part (b)]. Thus, the selective absorption causes the transmitted beam intensity to be smallest early in the afterglow and increase to a maximum late in the afterglow [part (c)]. The generator which supplies high-voltage pulses to the photomultiplier operates at twice the frequency of the exciting pulse generator. Thus, the multiplier is gated on not only at the time t_1 in the afterglow but also at $t_1 + \tau/2$ [see part (d)]. The afterglow time is made sufficiently long that, after the interval $\tau/2$, essentially no absorbing atoms are present. Thus, the photomultiplier output current at $(t_1 + \tau/2)$ corresponds to zero absorption, while at t_1 it is reduced by the finite absorption. The fundamental frequency component of this signal [part (d)] is selected and amplified by the tuned narrow-band amplifier [part (e)] and synchronously rectified by a detector with a long (~ 100 sec) integrating

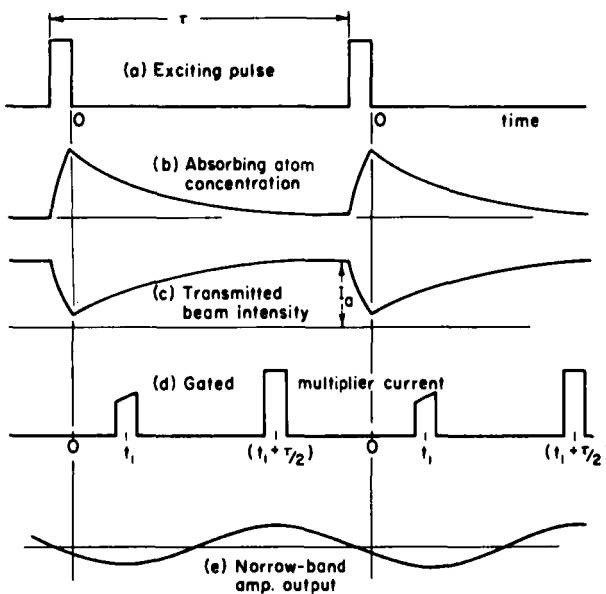


FIG. 12. Timing sequence in apparatus used to determine the time variation of optical absorption during the afterglow.

time. Comparison of the output of the detector (proportional to AI_0) with the average photomultiplier current registered on the electrometer (proportional to I_0) permits calculation of $A(t_1)$. This method of determining the variation of optical absorption during the afterglow is capable of measuring absorptions as small as 1 part in 10^4 .²⁴

6.2.4.2.4. SPECTRAL LINE-SHAPE DETERMINATIONS AT LOW INTENSITY.

In some studies it is necessary to determine the shapes of spectral lines emitted from the afterglow. Since the lines are often feeble in intensity, the optical instrument employed must offer both high resolution and high optical speed. These somewhat contradictory requirements are met by the Fabry-Perot interferometer. In order to obtain maximum sensitivity, photomultiplier rather than photographic detection of the interference pattern is employed.

The form²⁵ of Fabry-Perot interferometer used as the optical instrument in the afterglow apparatus of Fig. 10 is shown in Fig. 13. Here the Fabry-Perot plates are contained in a vacuum-tight housing. Light from the afterglow is collimated by the input lens. The spectral line to be studied is isolated from the rest of the spectrum by an interference filter and passes through the Fabry-Perot etalon. The circular fringes of the interference

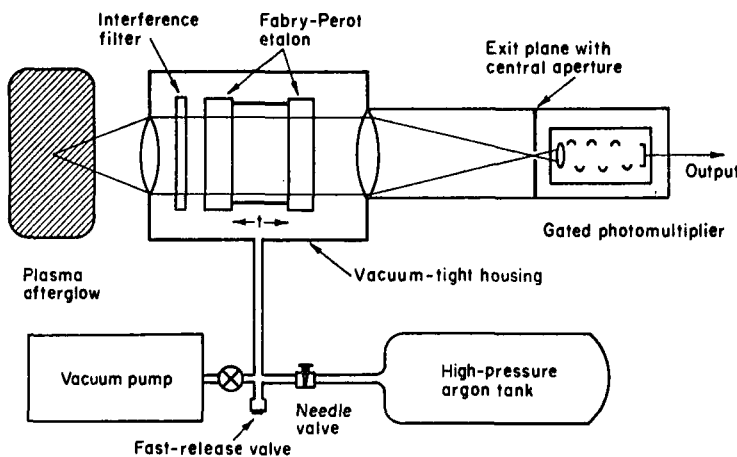


FIG. 13. Simplified diagram of the photoelectric recording Fabry-Perot interferometer. A high-pressure "pop-off" valve (not shown) opens when the gas pressure inside the housing is approximately 15 lb/in².

pattern are imaged by the output lens at the exit plane which contains a small hole aligned with the center of the pattern. Thus, light from the center of the pattern passes through to the photocathode of the gated photomultiplier. The output of the multiplier is fed to an integrator and electrometer which drives the *y* axis of a chart recorder, as in Fig. 10. In this way the intensity at the wavelength of the central spot of the Fabry-Perot pattern is recorded.

The wavelength corresponding to constructive interference among the normal incidence beams making up the central spot of the Fabry-Perot pattern is given by

$$\lambda = 2\mu t/n, \quad (33)$$

where λ is the wavelength in vacuum, μ the index of refraction of the medium between the plates, t the etalon spacer length, and n the interference order. This wavelength is made to change linearly* with time by evacuating the housing containing the etalon plates and then introducing argon gas from a high-pressure tank through a needle valve at a constant rate, thereby changing μ at a constant rate. Since the *x* axis of the recorder is

* The wavelength is changed sufficiently slowly that many seconds are required to trace the line profile, with the result that information from many afterglows is used.

driven at a constant rate by a synchronous motor, the chart record provides a direct presentation of intensity as a function of frequency (or wavelength) over the spectral line profile. The frequency scale of the chart record is calibrated by tracing the line through more than one interference order. Then, according to Eq. (33), the frequency interval (in wave numbers) between the same point in the line in each successive order is simply $\Delta\nu = 1/2t$.*

The above method of photoelectric line profile recording^{25,26} involves the use of the photomultiplier in its output current mode. In order to measure very weak afterglow line profiles it is necessary to reduce the "dark current" of the multiplier to the lowest practicable level. Methods for accomplishing this reduction are discussed in the next subsection.

Alternatively, one can operate the multiplier in a pulse-counting mode, using an electronic discriminator to accept pulse heights in the range caused by photons and to reject the rest of the output pulse spectrum as unwanted noise. In this case, a somewhat different operation of the Fabry-Perot instrument is employed. The method used involves cyclical scanning through the line and accumulation of the information from each scan in the memory of a multichannel analyzer unit.²⁷ In this case the vacuum pump (Fig. 13) is not used, and the system operates from atmospheric pressure upwards. The needle valve is adjusted to scan through one interference order in approximately one minute. At the end of this interval the fast release valve is opened to permit the housing pressure to return to atmospheric.

The pulses from the photomultiplier are fed to the multichannel analyzer, which is set to advance channels at the rate of one per second, starting at the instant that the fast release valve closes (tripping a micro-switch) and stopping when the valve is automatically opened by a solenoid one minute later. In this manner the spectral line is scanned once a minute, and as many scans as desired can be accumulated in the memory of the analyzer. Readout of the stored data is made in analog form on a strip-chart recorder and in digital form on a printer.

6.2.4.2.5. CURRENT MODE VERSUS PULSE COUNTING WITH PHOTOMULTIPLIERS. As noted in the preceding sections, the photomultiplier detector may be used in either its output current or output pulse mode. In this

²⁵ M. A. Biondi, *Rev. Sci. Instr.* **27**, 36 (1956).

²⁶ P. Jacquinot and C. Dufour, *J. Rech. Centre Natl. Rech. Sci. Lab. Bellevue (Paris)* **6**, 91 (1949).

²⁷ M. A. Biondi, and W. A. Feibelman, *Plan. Space Sci.* **16**, 431 (1968).

* Here, μ has been taken as equal to unity, since it differs by only ~ 3 parts 10^4 from that figure.

subsection we discuss the means for increasing the signal-noise ratio in each mode and the relative merits of each.

It is well known that, when operating in the current mode, it is possible to decrease the dark current of a photomultiplier by orders of magnitude by cooling the tube to dry ice (195°K), to liquid nitrogen (77°K), or to even lower temperatures.²⁸ However, in some tubes the remaining fluctuations in current are much larger than would be expected on statistical grounds,²⁹ so that one has achieved a reduction in dark current without a corresponding reduction in "noise." This noise evidently consists of large current spikes, well above the $\sim 10^6$ electrons/pulse obtained with the normal multiplication of the dynode structure.²⁹

If the full area of the photocathode is not needed for photon detection, as is the case with the Fabry-Perot instrument where only a small aperture area ($<1 \text{ mm}^2$) is viewed, then a large reduction in dark "noise" can be achieved if the tube has a linear, Venetian-blind dynode structure, as in the EMI 9558. The effective photocathode area is reduced from its large value ($\sim 20 \text{ cm}^2$ in the 9558) to the desired value by use of diverging magnetic lenses³⁰ such as are shown in Fig. 14. The diverging magnetic field lines assure that only electrons leaving a small area of the center of the photocathode can traverse the dynode structure, leading to a multiplied output signal. We have used the electromagnetic lens³⁰ shown in part (a) of Fig. 14 in laboratory afterglow studies³¹ to reduce the effective photocathode area to $\sim 1 \text{ mm}^2$, while the use of eight rod-shaped permanent magnets distributed around the perimeter of the lens of part (b) of the figure achieves the same result in a model used for aeronomy studies in the field.²⁷ In these lenses the field near the multiplier end of the light pipe is typically 200–300 G. By cooling the multiplier to the vicinity of dry-ice temperatures with these lenses in place, the dark current in the EMI 9558 is reduced from its rated value of $\lesssim 10^{-9} \text{ A}$ to $\sim 3 \times 10^{-13} \text{ A}$ without apparent loss of signal sensitivity. More important, the fluctuations in this current approach the theoretical values expected for purely statistical effects.

Although this reduction in dark "noise" has only been achieved for a reduced effective cathode area in the form of a small spot, a similar, if more modest, reduction should also be achieved when the optical image is a

²⁸ R. W. Engstrom, *J. Opt. Soc. Am.* **37**, 420 (1947).

²⁹ J. Sharpe, Dark current in photomultiplier tubes. Doc. Ref. No. CP. 5475. E.M.I. Electron. Ltd., Hayes, Middlesex, England, October, 1964, Unpublished; see also Vol. 2 of this series, Chapter 11.1.

³⁰ G. Y. Farkas and P. Varga, *J. Sci. Instrum.* **41**, 704 (1964), L. Frommhold and W. A. Feibelman, *J. Sci. Instrum.* **44** 182 (1967).

³¹ L. Frommhold and M. A. Biondi, *Bull. Am. Phys. Soc.* **11**, 493 (1966).

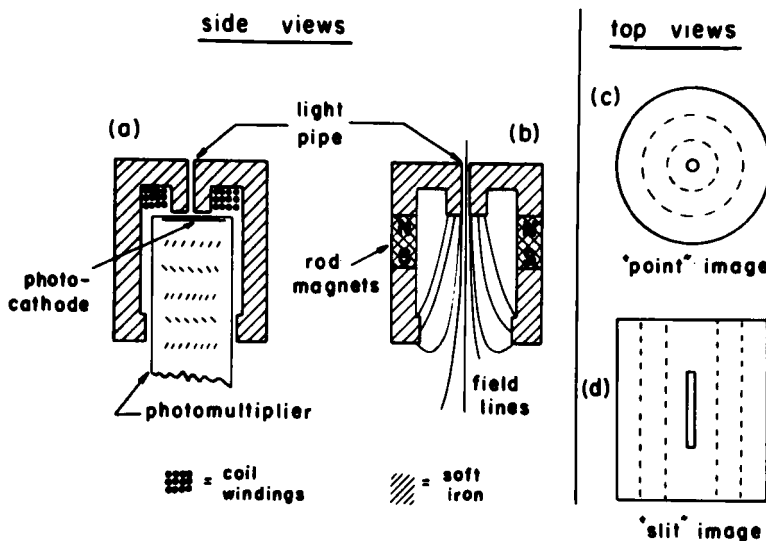


FIG. 14. Forms of magnetic diverging lenses used to reduce the effective photocathode area in order to decrease noise effects: (a) electromagnet type, (b) permanent magnet type, (c) point symmetric lens, and (d) line symmetric lens.

slit rather than a small circle. Here the lens would be made of slabs of soft iron, as shown in the top view of Fig. 14(d), to cause the field to diverge normal to the line of the slit while remaining nearly parallel along the slit direction.

While the use of diverging magnetic lenses and cooling of the multiplier has led to very important reductions in "noise" in the output of the photomultiplier operating in the current mode, use of these techniques in conjunction with a pulse-counting mode of detection leads to even smaller "noise" levels. The reason for an expected further reduction is the observation that the remaining noise still contains some large current spikes of the type already referred to. By using discriminators to pass only a "window" containing the ordinary pulse heights associated with the normal gain of the multiplier, the large spikes can be eliminated without substantial loss of signal. Even if the large spikes are accepted, in the pulse-counting mode each counts as one pulse (as do the normal signal pulses), in spite of the large current associated with the spikes. Thus, pulse-counting and multi-scaling techniques, in conjunction with the use of diverging lenses and multiplier cooling, probably lead to the most favorable signal-noise ratios in photomultiplier detection of radiation.

6.2.4.3. Mass Spectrometric Techniques. The use of a differentially pumped mass spectrometer to sample the ions diffusing to the walls of a plasma-afterglow tube permits identification of the ions undergoing ambipolar diffusion or recombination with electrons, as well as ion-molecule reactions. The latter subject is discussed by Fite in Chapter 6.3, while we shall be concerned with ion identification in studies of atomic collisions such as electron-ion recombination. Since afterglow ion densities are often rather modest, mass spectrometers of large entrance apertures are used to achieve reasonable signal levels during the afterglow. For this reason, the radio-frequency mass spectrometer³² and the quadrupole mass filter,³³ together with ion multipliers to amplify their outputs, have been employed in many afterglow studies.

One form of apparatus used in afterglow studies of electron-ion recombination⁴ is indicated in Fig. 15. In this case the plasma-afterglow tube is a microwave cavity and ionization of the gas is achieved by a pulse of microwave energy coupled into the cavity from the waveguide. The cavity is connected to an ultrahigh-vacuum gas handling system which supplies the gas under study. In one wall of the cavity there is a small (~ 0.01 -in.-

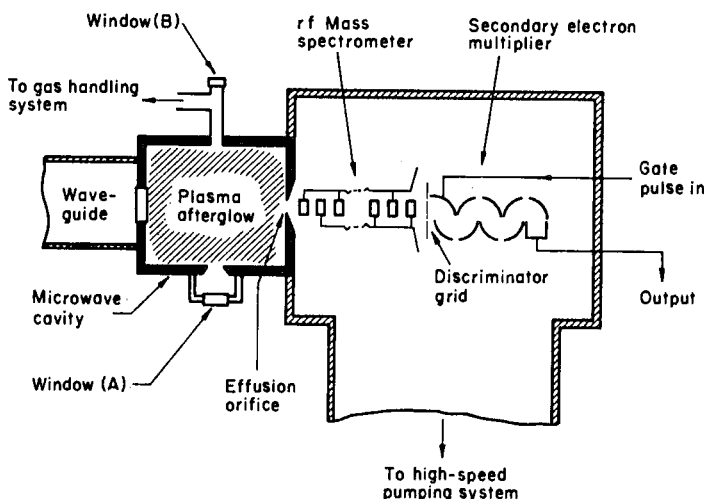


FIG. 15. Microwave afterglow apparatus employing a differentially pumped radio-frequency mass spectrometer to monitor the currents of various ions diffusing to the cavity walls.

³² R. L. F. Boyd and D. Morris, *Proc. Phys. Soc. (London)* **A68**, 1 (1955).

³³ W. Paul, H. P. Reinhard, and U. von Zahn, *Z. f. Physik* **152**, 143 (1958).

diam) effusion orifice which leads to the differentially pumped radio-frequency mass spectrometer.³²

The apparatus of Fig. 15 employs a very simple form of differential pumping in which the ion lens, mass spectrometer, and secondary electron multiplier are all enclosed in a single housing which is rapidly pumped ($\gtrsim 100$ liters/sec) with an oil diffusion pump and a zeolite isolation trap.³⁴ This system maintains an adequately low pressure in the spectrometer ($\lesssim 10^{-3}$ Torr) when the pressure in the afterglow tube is ~ 20 Torr.

The ion lens maintains a low electric field in the high-pressure region in the immediate vicinity of the effusion orifice, where ions still undergo collisions, to minimize ion conversion reactions between the accelerating ions and the neutral gas. The ions are accelerated (to ~ 400 eV energy) into the 24-element Boyd-type spectrometer, to which is applied a constant amplitude rf field whose frequency is made to change slowly with time. At a given frequency, ions of the proper charge-to-mass ratio which enter the spectrometer in the proper phase gain energy (~ 20 eV) from the rf field. A retarding field applied at the discriminator grid rejects all ions which have not gained the additional energy, thus providing "mass" selection. The ions passing the discriminator are reaccelerated into the first dynode of the secondary electron multiplier, which provides an amplified output signal proportional to the ion current striking the first dynode. For afterglow studies, the electron multiplier is electronically gated "on" for a given interval by application of a high-voltage pulse (in analogous fashion to the method described earlier for photomultiplier operation).

For typical afterglow ion densities, $\sim 10^9\text{--}10^{10}\text{ cm}^{-3}$, the mass-analyzed output currents to the electrometer are in the range $\sim 10^{-11}\text{--}10^{-10}\text{ A}$ for a $100\text{-}\mu\text{sec}$ afterglow gating interval. Thus, this method provides a means of studying the variation with time of mass-identified ion currents diffusing to the wall during the afterglow. Other investigators³⁵ have used a quadrupole mass spectrometer in place of the radio-frequency instrument with comparable detection sensitivity.

It should be noted that, in studies of ions diffusing to the wall from a plasma during the afterglow, positive and negative ions escape to the walls in very different fashion, and the negative ion wall current can not be simply related to the behavior of the ions within the plasma. The underlying reason for this statement is that in the case of ambipolar diffusion of positive ions, electrons, and negative ions to the boundaries one can show,^{2,3} as noted in Section 6.2.2. that under the action of the space-charge field the positive ions diffuse at the ordinary ambipolar rate, while negative ions are "trapped"

³⁴ M. A. Biondi, *Rev. Sci. Instr.* **30**, 831 (1959).

³⁵ H. J. Oskam, Private communication (1966).

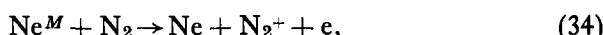
in the plasma, diffusing at $\lesssim 10^{-3}$ times the ambipolar rate until most of the electrons have disappeared. One, therefore, sees positive ions at the walls from the beginning of the afterglow onward, while negative ions do not appear at the wall until the electron density has decreased to negligible values.³⁶ Thus, only for the case of the *positive* ions does the wall current provide readily interpretable information concerning the time history of ions within the plasma volume.

6.2.5. Examples of Afterglow Atomic Collision Studies

6.2.5.1. Electron-Ion Recombination and Ionization by Metastable Atoms. As an example of afterglow studies in which microwave, mass-spectrometric, and optical absorption techniques have been simultaneously used to study electron-ion recombination and ionization by metastable atoms, let us consider recent work by Kasner and Biondi⁴ on neon-nitrogen afterglows. The aim of the experiment is to determine the rates of recombination of electrons with ions of ionospheric interest, such as N_2^+ and O_2^+ . The difficulty is that atmospheric gases form a whole series of ions, for example, N_2^+ , N_3^+ , N_4^+ , O_2^+ , O_3^+ , etc; therefore, mass identification of the ions under study is necessary to assign unambiguously a measured recombination rate to a given ion.

An apparatus of the type indicated in Fig. 15 was employed in these studies,⁴ microwaves being used to ionize the gas and to measure the electron density during the afterglow and the rf mass spectrometer to monitor the identity and time decay of the positive ions reaching the walls of the cavity. In addition, the windows at *A* and *B* in Fig. 15 provided an optical path through the plasma afterglow to permit optical absorption measurements of the metastable atom density decay with an apparatus similar to that shown in Fig. 11. Here, the absorption was sufficiently great ($>1\%$) that it was possible to measure the reduction in transmitted intensity directly from the output of the gated photomultiplier, without need for the synchronous detector described in Section 6.2.4.2.3.

To avoid complex ion (N_3^+ , N_4^+) formation, very small pressures of nitrogen ($\lesssim 10^{-3}$ Torr) were used. Since at these pressures ambipolar diffusion loss would have been extremely large, neon (at ~ 20 Torr pressure) was added as a buffer gas to inhibit diffusion of the electrons and ions. Neon was also chosen because its metastable (3P_2) state has just sufficient energy to ionize N_2 molecules by the Penning reaction



leaving the N_2^+ in its ground electronic and a low ($v \leq 3$) vibrational state.

³⁶ W. L. Fite and J. A. Rutherford, *Discussions Faraday Soc.* **37**, 192 (1964).

Under conditions in which only one ion species (N_2^+) predominates in the afterglow and electron-ion recombination is the only significant afterglow process (i.e., electron attachment, diffusion, and production processes are negligible) the particle continuity equation, Eq. (1), simplifies to

$$\frac{\partial n_e}{\partial t} \simeq -\alpha n_+ n_e \simeq -\alpha n_e^2, \quad (35)$$

where α represents the two-body electron-ion recombination coefficient and we have set $n_+ \simeq n_e$ because of the near-neutrality of the afterglow plasma. The solution of this equation yields the well-known "recombination decay" form,

$$1/n_e = 1/n_{e0} + \alpha t, \quad (36)$$

which indicates that the reciprocal of the electron density increases linearly with time, the slope of the curve yielding the recombination coefficient α .

The microwave frequency shift method yields field-weighted average electron density values; therefore, Eq. (35) should properly be integrated over the afterglow volume in the microwave cavity. When this is done, one finds⁴ that the average electron density $\langle n_e \rangle$ obeys the equation

$$\langle n_e \rangle^{-1} = \langle n_{e0} \rangle^{-1} + S\alpha t, \quad (37)$$

where $S = \langle n_e^2(r) \rangle / \langle n_e(r) \rangle^2$ is the factor which takes into account the spatial distribution of the electrons. Thus, the measured slope of the average electron density curve is ($S\alpha$), rather than α , as is often assumed.

Examples of the observations are shown in Fig. 16, where the reciprocal of the average electron density is plotted against afterglow time for several discharge pulse lengths. It will be seen that only for the longest (2 msec) pulse length (curve A) does the observed decay follow the simple recombination law of Eqs. (36) or (37).

It was suspected that metastable atoms remaining from the discharge were continuing to produce electrons and ions by the Penning reaction during the afterglow. The suspicion was confirmed by the optical absorption measurements (see Fig. 17) which showed a substantial absorption by metastable atoms during the afterglow, except in the case of the 2-msec pulse length (curve A). It will be noted that the metastable atom concentration inferred from the optical absorption decays exponentially with time in the afterglow, and therefore the rate of Penning ionization should decay in like manner.

A solution of the continuity equation has been obtained³⁷ for the case of electrons produced by such a decaying source and lost by electron-ion

³⁷ W. B. Kunkel, *Phys. Rev.* **84**, 218 (1951).

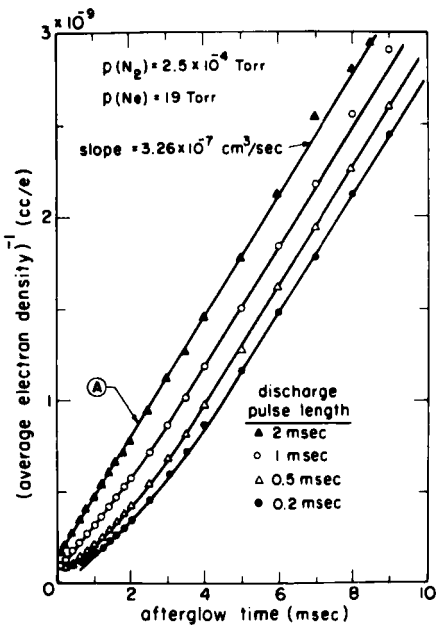


FIG. 16. Reciprocal of the average electron density as a function of afterglow time in a nitrogen-neon mixture for several discharge pulse lengths. The gas temperature is 300°K.

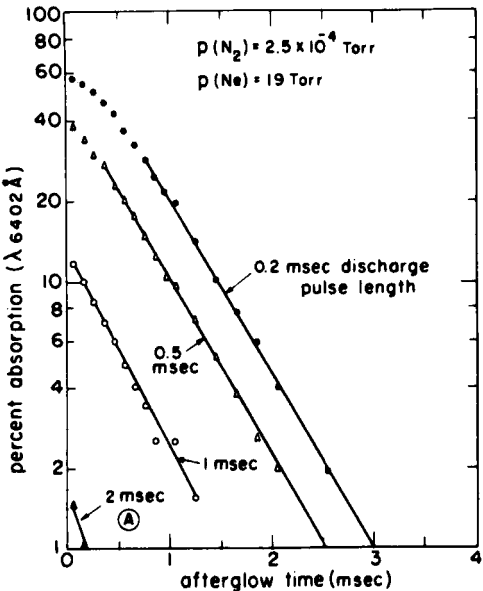


FIG. 17. Optical absorption by neon 3P_2 metastable atoms during the afterglow in a nitrogen-neon mixture. The conditions are identical to those under which the measurements of Fig. 16 were carried out.

recombination, i.e.,

$$\frac{\partial n_e}{\partial t} = b \exp[-\nu_m(t - t_0)] - \alpha n_e^2, \quad (38)$$

where b is the Penning ionization rate at $t = t_0$ and ν_m is the decay frequency of the metastable neon atoms. The solid curves in Fig. 16 are fits of the solutions of Eq. (38) to the data, using the metastable atom concentrations indicated by the optical absorption observations and a Penning ionization cross section for reaction (34) of $Q_i \sim 10^{-15} \text{ cm}^2$ at 300°K ,* together with the value $(S\alpha) = 3.26 \times 10^{-7} \text{ cm}^3/\text{sec}$ determined directly from curve *A* of Fig. 16, where metastable ionization plays a negligible role.

The procedure for obtaining the recombination coefficient α from the value $(S\alpha)$ was as follows. The frequency shift data were converted to the average electron density values given in Fig. 16 on the unrealistic assumption that the electrons were uniformly distributed throughout the cavity, then the corrections of the data for the actual electron spatial distribution were obtained from the calculations of Gray and Kerr,³⁸ who obtained computer solutions of the continuity equation for the case of an ambipolar diffusion loss term plus an electron-ion recombination term.[†] The recombination coefficient obtained in this manner was $\alpha = (2.9 \pm 0.3) \times 10^{-7} \text{ cm}^3/\text{sec}$ at 300°K . Studies of the apparent variation in α as the nitrogen and neon partial pressures were changed led to substantially smaller deviations in α than indicated by the ± 0.3 uncertainty quoted; this value represented an estimate of possible errors introduced by the imperfect knowledge of the spatial distribution of the electrons within the afterglow cavity.

The final step in the determination of the electron-ion recombination coefficient was its assignment to the particular ion responsible. For this

³⁸ E. P. Gray and D. E. Kerr, *Ann. Phys. (N. Y.)* **17**, 276 (1962).

* Since the absolute metastable concentrations deduced from the optical absorption are uncertain by a factor of ~ 2 , the Penning cross section may be similarly in error. However, the relative values of metastable atom concentrations for the different pulse lengths are accurately known. The cross section for de-excitation of the metastable atoms on collision with N_2 molecules, $Q_{\text{de-ex}}$, was determined directly from the optical absorption curves by noting the increase in metastable decay rate with increasing N_2 pressure.⁴ The value $Q_{\text{de-ex}} = (5.4 \pm 1.0) \times 10^{-16} \text{ cm}^2$ was obtained at 300°K . Therefore, within the accuracy of the determinations of the absolute values of metastable concentrations, it appears that the de-excitation of neon metastables by nitrogen molecules leads to ionization of the nitrogen molecule, although other processes such as dissociation of the nitrogen molecule may also take place.

† Note added in proof: Very recently Frommhold and Biondi have extended Gray and Kerr's results to three-dimensional geometries. See L. Frommhold and M. A. Biondi, Tech. Report, Physics Department, Univ. of Texas, Austin, Texas, 1968, unpublished and *Ann. Phys. (N.Y.)* **48** No. 3, July (1968).

purpose the ion wall currents were monitored by the mass spectrometer shown in Fig. 15. It was found that, during the afterglows in which the electron density decays were as given in Fig. 16, the principal afterglow ion was N_2^+ , with small concentrations of N_3^+ and N_4^+ . It is possible to relate the ion diffusion current to the wall to the ions' concentration within the volume, provided that the form of their spatial distribution does not change appreciably with time. Then, as can be seen from the diffusion current equation (3), $\Gamma_t \propto n_t$, since under these conditions $\nabla n_t \approx c n_t$ at the boundary.

In Fig. 18 is plotted the observed afterglow electron density and ion wall currents (on a logarithmic scale) as functions of time. The electron density data of curve *A* in Fig. 16 are replotted here, and the relative ion currents are normalized to this curve by making the N_2^+ ion current agree with the electron density at $t = 4$ msec. It will be seen that in the later afterglow, when the form of the spatial distribution has presumably become nearly constant, the N_2^+ current accurately follows the electron density decay, while no adjustment in normalization could cause the N_3^+ or N_4^+ currents to follow the electron decay. Thus, since N_2^+ was the predominant afterglow ion and followed the electron decay over a reasonable range, the measured recombination rate was assigned to N_2^+ ions.⁴

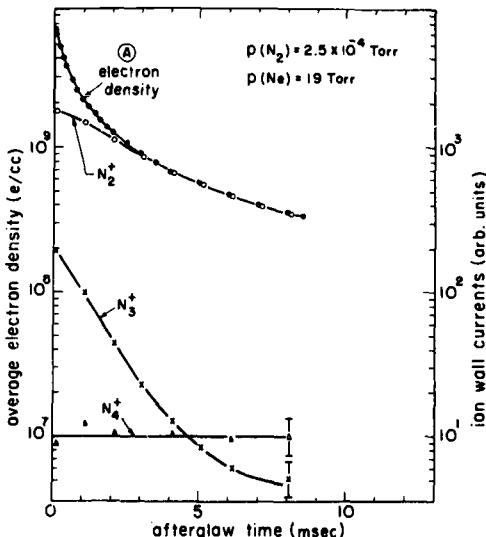


FIG. 18. Electron density and ion wall current decays in a nitrogen-neon afterglow. The conditions correspond to the 2-msec pulse length (curve *A*) in Figs. 16 and 17. The error bars at 8 msec on the N_3^+ and N_4^+ curves indicate the error in ion current measurement at low current values.

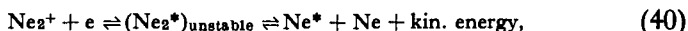
In these studies the use of optical absorption to observe the behavior of neon 3P_2 metastable atoms during the afterglow was incidental to the main recombination investigation, although the cross section for de-excitation of neon metastables by nitrogen molecules was determined to be $Q_{\text{de-ex}} = (5.4 \pm 1.0) \times 10^{-16} \text{ cm}^2$ at 300°K (by observing the effect on the metastable decay rate of varying the concentration of nitrogen molecules while holding the neon atom concentration fixed).⁴ Far more extensive studies of metastable atom and molecule diffusion, conversion, and de-excitation processes have been carried out by a number of investigators,³⁹ some of whom introduced²⁴ the more elegant techniques described in Section 6.2.4.2.3.

6.2.5.2. The Mechanism of Electron-Ion Recombination. In the previous section we discussed determinations of the two-body recombination coefficient between N_2^+ ions and electrons at 300°K. The coefficient $\alpha(\text{N}_2^+) = 2.9 \times 10^{-7} \text{ cm}^3/\text{sec}$ corresponds to the exceedingly large electron capture cross section $Q_{\text{rec}} \sim 3 \times 10^{-14} \text{ cm}^2$, which is some 10^5 times the radiative capture value; thus, some extremely efficient, nonradiative capture mechanism seems to be involved. Let us now consider how optical emission intensity and spectral line-shape determinations have been employed to determine the mechanisms of electron-ion recombination.

Two processes of electron capture which are potentially more efficient than radiative recombination are collisional and dissociative recombination, i.e.,



and



where the superscript * indicates an electronically excited state. We have used He^+ and Ne_2^+ ions as examples, since extensive studies have been made of these ions. In reaction (39) an interchange of energy between two free electrons leads to capture of one into an atomic excited state, the other electron receiving additional kinetic energy. The process is three-body in character and, for thermal (300°K) afterglows, outweighs two-body radiative recombination when the electron density exceeds 10^9 cm^{-3} .

Studies of the intensities of line radiation emitted from flowing⁴⁰ and from static helium afterglows⁴¹ have been carried out using spectrographs,

³⁹ A. V. Phelps and J. P. Molnar, *Phys. Rev.* **89**, 1202 (1953); A. V. Phelps, *ibid.* **114**, 1011 (1959).

⁴⁰ C. B. Collins and W. W. Robertson, *J. Chem. Phys.* **40**, 2202, 2208 (1964); E. E. Ferguson, F. C. Fehsenfeld, and A. L. Schmeltekopf, *Phys. Rev.* **138**, A381 (1965).

⁴¹ F. E. Niles and W. W. Robertson, *J. Chem. Phys.* **40**, 2909 (1964).

interference filters, and photomultiplier detectors. The electron temperature was inferred from the relative intensities of transitions whose upper levels lay near the ionization continuum⁴⁰ on the assumption that the populations of these states were in "Saha equilibrium" with the electrons which were causing many transitions among these levels as a result of inelastic and superelastic collisions with the excited atoms. The electron density was estimated from the measured absolute line intensities and a calculation of the atomic/molecular ion concentration ratio, together with the Saha equation. These observations were shown to be consistent with capture of electrons by ions, with other electrons acting as the third body, in accordance with the predictions of collisional-radiative recombination theory.⁴²

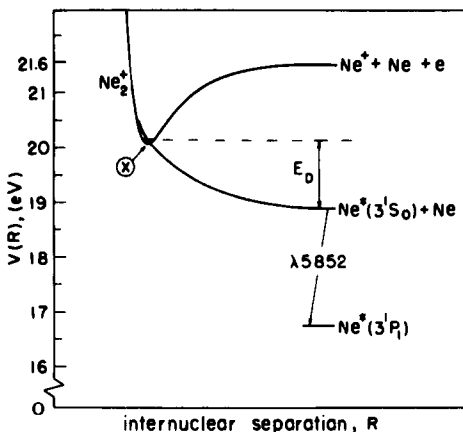


FIG. 19. Schematic representation of the potential energy $V(R)$ between two neon atoms as a function of their internuclear separation. Only two of the many possible curves are shown: one for a stable state of the molecular ion, Ne_2^+ , and one for an unstable state of the excited molecule, Ne_2^* .

The second recombination process, reaction (40), is two-body in character and can be better understood with the aid of Fig. 19, which shows schematic potential curves for the states involved. The initial step is the capture of an electron by a molecular ion, without change of energy of the system, to form an excited molecule in an unstable state. For such capture, a favorable curve crossing of the type indicated is required. The unstable molecule begins to dissociate, and if the internuclear separation increases

⁴² D. R. Bates, A. E. Kington, and R. W. P. McWhirter, *Proc. Roy. Soc. A* **267**, 297; **A270**, 155 (1962).

beyond point X , it is no longer energetically possible for the electron to be released by autoionization [i.e., the first half of reaction (40) going to the left]. The dissociation then proceeds to completion, producing two neon atoms, one probably in an electronically excited state, moving apart with kinetic energies totally E_D , the change of potential energy in the reaction.

Unlike the case of collisional recombination, reaction (39), where extensive theoretical calculations have produced detailed predictions of the recombination coefficient,⁴² the theory of dissociative recombination is at best qualitative at present and can only suggest that the dissociative process may be sufficiently efficient to explain the large two-body recombination coefficients deduced from laboratory and ionospheric measurements. In order to determine experimentally whether dissociative capture is responsible for the large electron-ion recombination rates measured in laboratory studies of noble-gas afterglows, we have sought to measure the kinetic energies of the excited atoms produced by recombination.^{31,43} The method employed involves determinations of the spectral line shapes emitted by the excited atoms, since if the fast atoms radiate before losing their excess kinetic energy, a pronounced Doppler effect is expected in the emitted lines.

The high-resolution studies of the weak afterglow radiation were provided by the Fabry-Perot instrument of Fig. 13 employed in an afterglow apparatus of the type indicated in Fig. 10. For the studies of the neon $\lambda 5852$ ($2p_1 \rightarrow 1s_2$) transition an interference filter was used to separate that line from the rest of the afterglow spectrum,⁴³ while for the studies of other lines the interference filter was removed and the Fabry-Perot exit plane aperture made the entrance "slit" of a small grating monochromator,³¹ thereby permitting the desired line to be selected from the rest of the spectrum by appropriate setting of the monochromator's wavelength dial.

Let us consider the expected shapes of the spectral lines emitted from a neon plasma and afterglow, using the $\lambda 5852$ line as an example. During the microwave discharge used to create the plasma the excitation of the $2p_1$ state is expected to occur predominantly by electron impact. The excited atoms should, therefore, have ambient ($\sim 300^{\circ}\text{K}$) thermal velocities and should emit a thermal Doppler line. The expected Doppler profile is indicated at the top of Fig. 20, a half-width $\Delta\nu_T = 0.05 \text{ cm}^{-1}$ corresponding to 300°K . Although $\lambda 5852$ is a singlet transition, natural neon contains principally two isotopes, $\sim 91\%$ Ne_{20} and $\sim 9\%$ Ne_{22} . The predicted isotope shift between the two components is 0.075 cm^{-1} , as indicated in the middle of Fig. 20; thus, the line profiles involve superpositions of these two components.

⁴³ T. R. Connor and M. A. Biondi, *Phys. Rev.* **140**, A778 (1965).

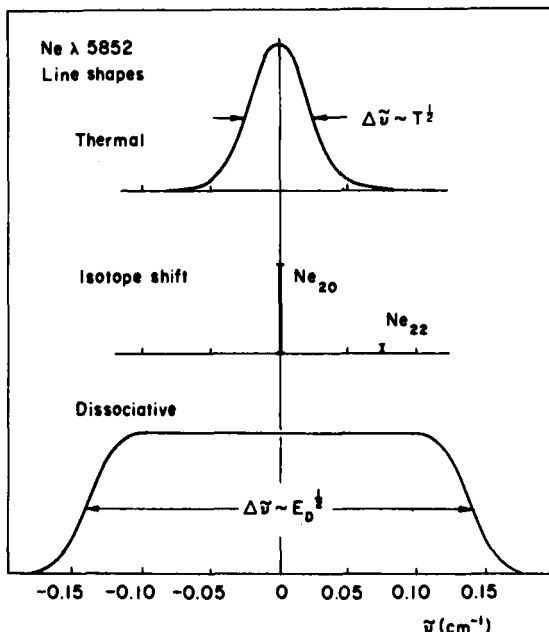


FIG. 20. Predicted line shapes for the neon $\lambda 5852$ transition. Top: thermal Doppler profile for one isotopic component (Ne_{20}) at 300°K . Middle: expected isotope shift and abundance ratio ($\sim 10 : 1$) for natural neon. Bottom: line profile for excited atoms produced by dissociative recombination with $E_D = 1.3$ eV and $T = 300^\circ\text{K}$.

During the afterglow, the excited atoms are produced predominantly by recombination. If dissociation from a single initial molecular ion state occurs (as in Fig. 19), then the excited atoms have a single speed of dissociation ($\sim E_D^{1/2}$). Since all directions of dissociation relative to a given observer are equally probable, the resulting Doppler shifts lead to a flat-topped, broad spectral line. The predicted form of the line to be expected under these circumstances, with $E_D \approx 1.3$ eV and including the effect of the thermal (300°K) motion of the molecular ions from which the excited atoms are produced, is shown at the bottom of Fig. 20.

The remaining question concerning the afterglow line shape involves consideration of what fraction of the fast, dissociatively produced excited atoms radiate before they transfer their excitation to the normal neon atoms by the reaction



If such transfer takes place, the radiation from the slow atoms will, of course

be the thermal Doppler profile, and this will be superposed on the broad, flat-topped, fast-atom profile. Since the rate of transfer of excitation varies directly with the concentration of normal atoms, while the radiative lifetime of the excited state is constant, one expects to see the fast excited atom recombination radiation most readily at low neon pressures ($\sim 1\text{-}10$ Torr).

Figure 21 represents photographs of the chart records of the $\lambda 5852$ line profiles during the discharge and during the afterglow.³¹ (The Fabry-Perot pattern repeats itself in going through each interference order—this provides the frequency scale, $\Delta\nu = 1/2t = 0.500 \text{ cm}^{-1}$, indicated at the top of the figure.) It will be seen that during the discharge the line exhibits the expected two-isotope-component shape but is slightly broader than a 300°K thermal Doppler width. This effect is the result of pronounced pressure broadening of this transition, whose lower state is a resonance state and therefore is highly perturbed by collisions with normal atoms.

During the afterglow the line profile evidently consists of a narrow thermal atom core on top of a broad pedestal of the type expected for dissociatively produced atoms. Thus, the afterglow line shape confirms the dissociative recombination production of fast excited atoms, a fraction of which transfer their excitation to thermal neon atoms before radiating.

The favorable signal/noise ratios in the line profile tracings of the weak afterglow radiation, which is evident in the upper half of Fig. 12, result from the use of the magnetic diverging lens on the cooled ($\sim 200^\circ\text{K}$)

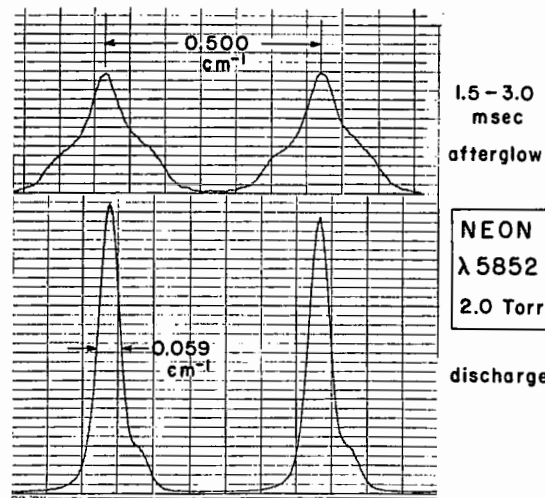


FIG. 21. Photographs of recorder tracings of the $\lambda 5852$ line profile obtained with the Fabry-Perot interferometer. Top: during the period 1.5–3.0 msec in the afterglow. Bottom: during the microwave discharge, at a pressure of 2 Torr and $T = 300^\circ\text{K}$.

photomultiplier. Without the lens and cooling the noise level was more than 10 times greater.

6.2.5.3. Other Afterglow Studies. There are many other interesting examples of atomic collision studies carried out using afterglow techniques which, because of space limitations, can only be mentioned by title. Studies of photoionized NO plasmas and afterglows, using microwave and mass spectrometric techniques, have yielded rates of ambipolar diffusion and electron-ion recombination of NO^+ ions and electrons, as well as three-body attachment of electrons to NO molecules.^{44,45} Here, because of the trapping in the plasma of negative ions formed by electron attachment, it was necessary to operate in a "single-pulse" fashion, in effect obtaining data from a single plasma-afterglow. In this way the accumulation of negative ions from pulse to pulse which would occur in a repetitive plasma-afterglow cycle was avoided, and therefore the effect of negative ions on ambipolar diffusion loss of electrons (discussed in Section 6.2.2) was minimized. Further, since the "single-pulse" operation assured that $n_e \gg n_-$ during the early afterglow, one could set $n_e \approx n_+$ (plasma neutrality), thereby greatly simplifying the analysis of electron decays in electron-ion recombination studies in electronegative gases (see Section 6.2.5.1).

Microwave afterglow studies following ionization of O_2 and N_2 mixtures by energetic ($\sim \text{MeV}$) electrons have yielded accurate values of the three-body attachment rates of electrons to O_2 with either O_2 or N_2 molecules acting as third-bodies in stabilizing the reaction.⁴⁶ Microwave discharge-afterglow studies of the noble gases⁴⁷ have provided ambipolar diffusion and recombination rates between electrons and (presumably) diatomic positive ions, e.g., Ar_2^+ .

Electron collision frequencies with neutral atoms or molecules have been determined by a variety of microwave techniques.^{10,18,19} In addition, in higher-density plasma-afterglows, the electron-ion collision rate has been deduced from microwave conductivity measurements.¹⁹

In cases where attachment quickly removes free electrons, yielding an afterglow in which positive and negative ions are the only charge carriers, radio-frequency conductivity measurements of ion density decays (quite analogous to the microwave measurements of free electrons) have been used to determine positive ion-negative ion recombination rates for ions such as I_2^+ and I^- .¹¹

⁴⁴ R. C. Gunton and T. M. Shaw, *Phys. Rev.* **140**, A756 (1965).

⁴⁵ C. S. Weller and M. A. Biondi, *Bull. Am. Phys. Soc.* **11**, 495 (1966); **13** 199 (1968).

⁴⁶ V. A. J. van Lint, J. Perez, M. E. Wyatt, and L. K. Nichols, U.S. Air Force Weapons Lab. Rept. RTD TDR-63-3076, December 1963. Kirtland Air Force Base, Albuquerque, New Mexico, Unpublished.

⁴⁷ H. J. Oskam and V. R. Mittelstadt, *Phys. Rev.* **132**, 1435, 1445 (1963).

From the foregoing examples, it is evident that afterglow studies permit a wide variety of atomic collision processes involving electrons, positive and negative ions, and excited atoms or molecules to be studied. Since the energies of the particles are usually very small (<0.1 eV), afterglow techniques provide a means for low-energy atomic collision studies.

6.3. Mass Spectrometry of Afterglows^{†*}

For the study of collision processes at thermal energies involving ions and neutrals, mass spectrometric monitoring of afterglows in gases has been employed in order both to identify processes which occur and, in a number of cases, to measure rate coefficients. Both stationary and flowing afterglows have been used. These are considered in turn.

6.3.1. Stationary Afterglows

6.3.1.1. Apparatus. The first instance of the coupling of afterglow techniques and mass spectrometry appears to be that of Phelps and Brown¹ in connection with their research on electron-ion recombination in helium. Presented with their microwave results indicating a recombination coefficient several orders of magnitude greater than expected if their primary ion were He^+ , with the knowledge from earlier mass spectrometric studies of Tüxen that He_2^+ is a stable ion,² and with the considerations of D. R. Bates indicating that the molecular ion would recombine rapidly through the dissociative recombination process,³ Phelps and Brown mass spectrometrically examined the ions in their afterglow and found that indeed He_2^+ was the dominant ion. The sampling was accomplished by allowing the gas in the afterglow to flow out through a small hole in the cavity into a rapidly pumped mass spectrometer, accelerating the ions and magnetically analyzing them. Phelps and Brown also studied the growth of the He_2^+ ion as a function of time and pressure in the cavity and therefrom were able to determine an effective rate for production through the process $\text{He}^+ + \text{He} \rightarrow \text{He}_2^+ + \text{He}$.

¹ A. V. Phelps and S. C. Brown, *Phys. Rev.* **86**, 102 (1952).

² O. Tüxen, *Z. Physik* **103**, 463 (1936).

³ D. R. Bates, *Phys. Rev.* **77**, 718 (1950); **78**, 492 (1950).

[†] For a general discussion of methods in mass spectrometry see Volume 3, Part 5, or Volume 5B, Section 2.3.1.

* Chapter 6.3 is by Wade L. Fite.

Some years elapsed before the technique was again put to use. Prompted by the need for thermal energy rate coefficients for processes in the ionosphere, groups at the University of Birmingham, University College London, and General Atomic revived the method independently. Dickinson and Sayers⁴ first reported on $O^+ + O_2 \rightarrow O + O_2^+$; Langstroth and Hasted⁵ considered this reaction as well as $O^+ + N_2 \rightarrow NO^+ + N$; and Fite *et al.*⁶ presented values for several other reactions including those of nitrogen ions with molecular oxygen.

Although the details of the three sets of experiments and the methods of obtaining rate coefficients differed, the basic experimental approach was identical. A gas in a chamber is excited by some pulsed means and ions in the afterglow emerge through a hole in the wall of the chamber, entering an ion mass spectrometer. The signal of each ion species, recorded as a function of time, is the basic experimental information.

In the Birmingham experiments by 1964 the apparatus had evolved to the form described by Sayers and Smith.⁷ The afterglow chamber was a cylinder of Kodial glass with a diameter 14.5 cm and an over-all length of about 30 cm. The electrode system consisted of two parallel flat nickel disks of 11 cm diam inside the vessel placed about 16 cm apart and two external sleeves of copper about 5 cm wide placed about 7 cm apart. The mass spectrometer was of the miniature rf linear accelerator type and was contained in a side arm of the afterglow chamber, the ions entering the mass spectrometer through a small circular orifice of 0.18 mm diam at the center of a Nilo-K disk of 2.5 cm diam which was effectively sealed to the wall of the chamber.

The excitation was provided by rf pulses† at a frequency of 7 Mc/sec and of duration 10 μ sec. The power in the pulses could be varied continuously from the minimum required to initiate a discharge to about 200 kVA. Normally a power of about 25 kVA was used, and the pulses were applied repetitively at a rate of about 50 pulses per second. Subsequently provision has been made to use single pulsing in order to minimize cleanup of gas and other undesirable effects which will be discussed later.

Particular attention was paid to having good vacuum conditions and conditions of high gas purity.‡ The Kodial glass was selected over Pyrex,

⁴ P. H. G. Dickinson and J. Sayers, *Proc. Phys. Soc. (London)* **76**, 137 (1960).

⁵ G. F. O. Langstroth and J. B. Hasted, *Discussions Faraday Soc.* **33**, 298 (1962).

⁶ W. L. Fite, J. A. Rutherford, W. R. Snow, and V. A. J. van Lint, *Discussions Faraday Soc.* **33**, 264 (1962).

⁷ J. Sayers and D. Smith, *Discussions Faraday Soc.* **37**, 167 (1964).

† For pulse techniques see different chapters of Volume 2; in particular, see Chapter 9.6.

‡ Vacuum techniques and gas purification are discussed in Volume 4B, Part 5.

for example, because of the belief that Cl^- ions are evolved from Pyrex in a discharge. Similarly, greaseless joints were used and rubber gaskets were excluded entirely from the system. The entire apparatus could be baked and additionally the metal parts were outgassed using eddy current heating. Cold traps were used above the mercury diffusion pumps and in the gas circulating system. The ultimate vacuum of the entire system was about 10^{-7} Torr.

The apparatus of Langstroth and Hasted was similar to that of Sayers and his collaborators. A large afterglow chamber was used as was a linear accelerator type mass spectrometer. The mass spectrometer was located in a re-entry arm so that sampling was made near the axis of the afterglow chamber rather than at a wall. The other major difference between the two apparatus was the method of pulsing. While Sayers' group used pulses of rf, Langstroth and Hasted employed a pulsed dc discharge.

In the apparatus of Fite *et al.*⁸ a magnetic mass spectrometer was used. This instrument is shown in Fig. 1. Constructed entirely of stainless steel with copper gaskets, the entire apparatus could be baked out. Mercury diffusion pumps were used to minimize oil buildup in the apparatus and double liquid nitrogen trapping was employed in the interests of achieving good vacuum. The ultimate pressure in the instrument was about 10^{-8} Torr.

In contrast to the equipment of the English workers, the afterglow chamber itself was quite small (linear dimensions of the order of 4 cm) and was equipped to use excitation either by rf pulses or by a 40-MeV pulsed electron beam from a linear accelerator. The pusher electrode of Fig. 1 was used as an electrode for rf excitation (the other electrode being the

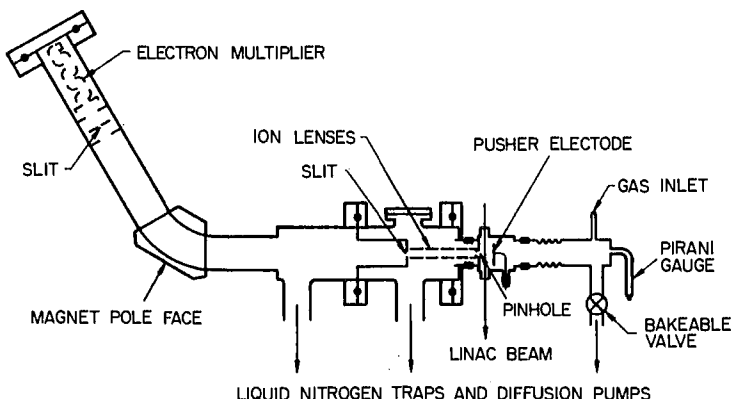


FIG. 1. Stationary afterglow apparatus of W. L. Fite, J. A. Rutherford, and W. R. Snow, and V. A. J. Van Lint, *Discussions Faraday Soc.* **33**, 264 (1962).

metallic wall of the afterglow chamber), and also to provide a weak dc field during the afterglow to move ions toward the pinhole. The pinhole itself was circular of approximately $\frac{1}{4}$ mm diam, sufficiently small to give a pressure drop of about 4 orders of magnitude between the afterglow chamber and the first differentially pumped stage of the mass spectrometer itself.

In the first stage of the mass spectrometer the ions emerging from the pinhole were accelerated to about 400 eV and focused onto the slit between the first and second differentially pumped stages. Also in the first stage, not shown in the diagram, was a small electron gun whose beam was directed across the gas flowing out of the afterglow chamber. By using this gun direct mass analysis of the neutral gases in the afterglow chamber could be made and, coupled with the total pressure as read on a Pirani gauge, the partial pressures of the gases in the afterglow chamber could be determined with reasonable accuracy.

Typical data output, the ion signals as a function of time, are shown in Fig. 2. In this case 1% of oxygen was added to spectroscopically pure nitrogen and the mixture was excited using 20-MeV electron pulses. The gas was completely exchanged between pulses and the time history of one ion was obtained per pulse. Superposing the oscilloscope traces, it is evident that initial N_2^+ ions are being exchanged for O_2^+ ions and N^+ ions are generating NO^+ . The total ion signals decay with time because of ambipolar diffusion of the plasma as a whole to the walls.

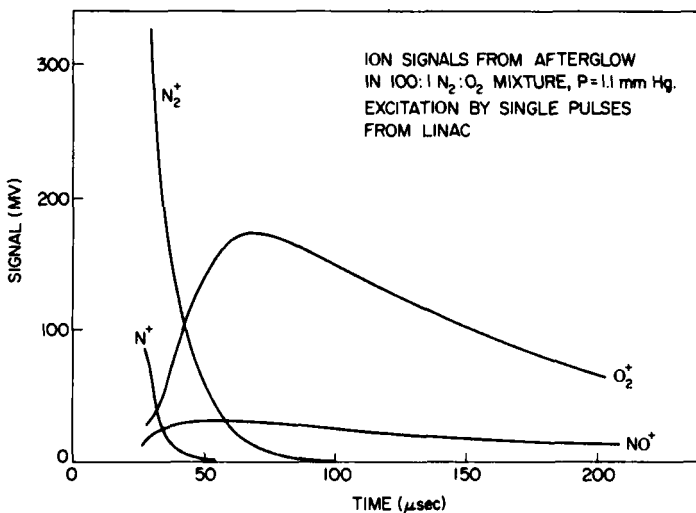


FIG. 2. Oscilloscope traces of mass peaks in a stationary afterglow. The gas mixture was N_2 and O_2 mixed in the ratio of 100 to 1. The excitation pulse was provided by 20 MeV electrons.

6.3.1.2. Data Analysis Methods. The basic experimental information obtained in stationary afterglow mass spectrometry is the time history of any given ion species to which the mass spectrometer is tuned. It is assumed that the instantaneous current of any ion is proportional to the number density of that ion in the immediate vicinity of the sampling aperture. Of interest in the study of ion-neutral processes is the effect on the time history of a given ion when a small amount of a particular reactant gas is present in the afterglow, with the aim to determine the rate coefficient, k .

The rate of change of number density, N_1 , of a primary ion at any position in the afterglow (including the immediate vicinity of the sampling aperture) can be described by

$$\frac{\partial N_1}{\partial t} = -\alpha_1 n_e N_1 - k N_1 n_2 - \left(\sum_i \gamma_i n_i \right) N_1 + D_1 \nabla^2 N_1 \quad (1)$$

where α_1 is the electron-ion recombination coefficient, n_2 is the number density of the neutral reaction of interest, γ_i is the rate coefficient for reaction with other species of number density n_i which alter the primary ion concentration, and D_1 is the ambipolar diffusion coefficient. Two methods are used to determine k .

In the method of Dickinson and Sayers,⁴ data are taken only rather late in the afterglow and at such time that the recombination term has become negligibly small and the ambipolar diffusion has settled into its fundamental mode. If a search with the mass spectrometer fails to reveal other ionic products due to reactions other than with n_2 , then the third term vanishes and Eq. (1) becomes

$$\frac{\partial N_1}{\partial t} = -k N_1 n_2 - \frac{D_1}{\Lambda^2} N_1 \quad (2)$$

where Λ is the "diffusion length" determined from solving the diffusion equation subject to vanishing of N_1 at the boundary for the particular geometry of the afterglow chamber.

Equation (2) is immediately integrated to give

$$N_1 \propto \exp(-t/\tau) \quad (3)$$

where $1/\tau = kn_2 + (D_1/\Lambda^2)$. If one finds time intervals late in the afterglow which are described by an exponential decay, then the decay rate, $1/\tau$, can be plotted as a function of n_2 to yield a straight line. The slope of this line will be the decay constant, k , and the intercept can be used in conjunction with the calculated Λ for a given geometry in order to determine D_1 .

This simple and appealing analysis method requires that measurements be made late in the afterglow, after the higher diffusion modes have decayed

out. For reasonably rapid reactions, k is sufficiently high that the primary ions would be completely gone before this situation would obtain. The reaction loss of primary ions must therefore be slowed down and this is done by the use of buffer gases, of which helium is most common. With of the order of 1% of reactive gas in helium, conditions are such that measurements can be made using this approach. In this case D_1 is of course the ambipolar diffusion coefficient of the primary ion diffusing through the buffer gas.

In practice, with chambers the size used by Sayers' group,^{4,7} measurements are made several milliseconds in the afterglow, so that fast electronic circuitry is not required. At such late times one can be assured that both the electrons and ions have cooled to room temperature. Ample time is allowed for excited species, except for the most stubborn metastables, to decay and one can feel reasonably sure that the process is taking place between ground-state species at the ambient temperature.

The reactions most studied using this approach have involved O^+ as the primary ion. Using helium as the buffer gas is an excellent choice because the initial discharge produces He^+ which reacts within tens of microseconds to form O^+ through the reaction $He^+ + O_2 \rightarrow He + O + O^+$. In the later portions of the afterglow O^+ reacts with O_2 and any other neutral reactants added.

The second method of data analysis is that used by Fite *et al.*, who chose to balance the loss of primary ion against the appearance of secondary ions and so obtain a reaction rate. In addition to Eq. (1), a second equation describing the change of the number density, N_2 , of a secondary ion was written so that two equations,

$$\frac{\partial N_1}{\partial t} = -\alpha_1 n_e N_1 - k N_1 n_2 - \left(\sum_i \gamma_i n_i \right) N_1 + D_1 \nabla^2 N_1. \quad (1)$$

and

$$\frac{\partial N_2}{\partial t} = -\alpha_2 n_e N_2 + k N_1 n_2 - \left(\sum_i \delta_i n_i \right) N_2 + D_2 \nabla^2 N_2, \quad (4)$$

described the process. In the second equation δ_i are the rate coefficients for processes which cause depletion of the secondary ions and form tertiary ions. Defining $R = N_2/N_1$, one obtains by combining these equations

$$\begin{aligned} \frac{\partial R}{\partial t} = & \left\{ (\alpha_1 - \alpha_2) n_e + \sum_i (\gamma_i - \delta_i) n_i + \left(D_2 \frac{\nabla^2 N_2}{N_2} - D_1 \frac{\nabla^2 N_1}{N_1} \right) \right\} R \\ & + k n_2 (1 + R). \end{aligned} \quad (5)$$

This analysis should be appropriate at any point in the gas inside the afterglow chamber and therefore in the immediate vicinity of the aperture

through which the ions emerge. Assuming that the ion currents are proportional to the number densities in the immediate vicinity of the aperture, R was therefore taken also to be the ratio of observed ion currents.

In the limit of very small R , Eq. (5) clearly degenerates only to $R = kn_2 t$, so that k should be determinable from the slope at the origin of a plot of R versus t . It should be noted also that, since the coefficient of R in Eq. (5) is a series of differences in similar terms, one might expect the first term to contribute little for primary and secondary ions of similar recombination coefficients, ambipolar diffusion coefficients, etc. Experimentally this seems to be the case. The second term appears to dominate in such cases for R up to 0.3 or more.

The necessity of obtaining the value of k at small values of R and therefore at small values of t imposes some uncertainty in the results. At small times, i.e., of the order of tens of microseconds in the afterglow, the gas may not have yet cooled down following the excitation pulse and metastable states of both the reacting ion and neutral gas may be present. The temperature and metastable state content has not been assayed. Fast-response circuitry is required and Fite *et al.*⁸ used circuitry with a rise time of about 0.5 μ sec. Offsetting these disadvantages is the fact that, since measurements are made at short times, there is no need either to use buffer gases or to use large afterglow chambers.

Both approaches to the measurement of thermal reaction rates in stationary afterglows suffer from several additional problems, foremost of which is that of gas purity. For a fast reaction between the ions of a primary gas and a secondary gas neutral, e.g., $\text{He}^+ + \text{O}_2$, it is necessary to keep the partial pressure of the secondary gas to about 1% that of the primary gas in the fast methods used by Fite *et al.*, and in the slow methods of Sayers *et al.* even smaller secondary gas pressures are maximal. Since any impurities should be present in amounts very small compared to the secondary gas, extreme requirements are placed on the purity of the primary gas and on cleanliness of the apparatus.

Bakeout has been found to be not an unmixed blessing and has in fact generated problems. In Birmingham, the adsorption of the secondary gas to freshly baked glass surfaces made difficult the determination of the secondary gas pressure. In the stainless-steel chamber used at General Atomic, baking appeared to introduce impurities, particularly CO, into the afterglow chamber.

Generation of impurities by chemical reactions is also a problem. As a case in point, it is found that repetitive pulsing of gas mixtures of N_2 and O_2 produces nonnegligible amounts of almost all the known oxides of nitrogen. To avoid this problem, it is necessary to completely change gas in the chamber after only a few pulses.

Yet another problem is that the stationary afterglow techniques have not been successful at studying negative ion reactions. Fite and Rutherford⁸ working without buffer gases found that negative ions could not be extracted from the afterglow until about a millisecond had elapsed. Presumably sheaths at the exit aperture formed fields which prohibited the escape of negative ions for this period of time. The negative ion mass spectra observed at late times indicated that a rich collection of processes occur in atmospheric gases, for a wide variety of ions up to about mass 130 were found, but the absence of negative ion signals early in the afterglow prevented the determining of any negative ion rate coefficients.

The longer-time methods of stationary afterglow mass spectrometry, e.g., as practiced by Smith and Sayers,⁷ have evidently not been applied to negative ion reaction problems.

6.3.2. Flowing Afterglows

6.3.2.1. General Considerations Flowing afterglow techniques as compared to stationary afterglow methods in general substitute spatial resolution in a rapidly flowing gas for time resolution in a static gas. The success of flowing afterglows for the study of neutral chemical and free radical reactions using spectroscopic monitoring led naturally to their application for the study of ion-neutral reactions as well. The development of the technique for ion-neutral reaction studies was made at the Environmental Sciences Services Administration (ESSA) Laboratories in Boulder, Colorado, by the group headed by Ferguson.

Figure 3 shows a sketch of one of their experiments.⁹ The tube is either Pyrex or quartz, typically about 1 meter in length and 8 cm i.d. The tube can be equipped with flat optical windows of quartz on the side for spectroscopic observations. The discharge electrodes consist of a large cylindrical cathode and a small wire anode when a dc discharge is to be used. The porous plug is inserted to smooth the gas flow; although it can be omitted, shock patterns in the gas flow from the nozzle can be set up in its absence and perhaps lead to interpretational complications.

In earlier versions of the experiment, the initial ionization was produced by an electrodeless microwave discharge in a converging-diverging deLaval nozzle which exhausted into the large tube. In this case a porous plug was not used.

The usual mode of operation introduces helium gas into the tube at a flow rate of around $200 \text{ cm}^3 \text{ sec}^{-1}$ at atmospheric pressure and a flow speed

⁸ W. L. Fite and J. A. Rutherford, *Discussions Faraday Soc.* **37**, 192 (1964).

⁹ F. C. Fehsenfeld, E. E. Ferguson, and A. L. Schmeltekopf, *J. Chem. Phys.* **44**, 3022 (1966).

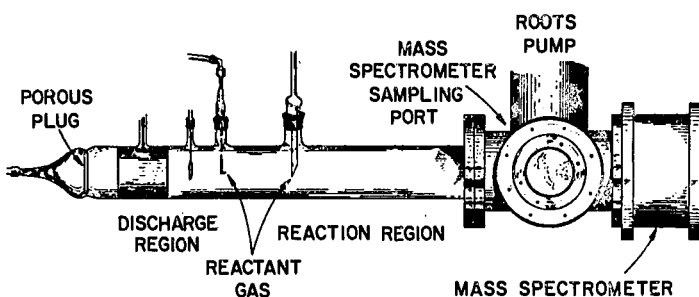


FIG. 3. Flowing afterglow apparatus used at the Environmental Sciences Services Laboratory in Boulder, Colorado.

of about 10^4 cm sec^{-1} , giving a pressure in the flow tube of about 0.3 Torr. A large Roots blower backed by a large mechanical forepump exhausts the helium upward at the right in Fig. 3. In the discharge region about $10^{11} \text{ ions cm}^{-3}$ are produced along with a comparable density of metastable helium atoms.

To the weakly ionized gas flowing down the tube neutral reactants are admitted through side arms located downstream from the discharge region. As the mixed gases travel the remaining length of the flow tube, reactions between the various ions, metastables, and neutral reactant gases occur. Finally at the end of the flow tube the ion composition is monitored by means of an ion mass analyzer. Ferguson and his collaborators chose as their ion analyzer a small frequency-scanned radio-frequency quadrupole mass filter. It is located in a separately pumped vacuum chamber which is connected to the flow tube through a 0.5 mm-diam hole in shim stock of thickness from 0.025 to 0.125 mm. Typical ion currents under dc operating conditions ranged from 10^{-14} to 10^{-11} A .

In addition to dc operation of the discharge, pulsed operation of the discharge is often used. When the pulsed discharge is used, the ion detection system is gated on about 6 msec after the breakdown, the time it takes for the plasma to flow down the length of the tube. By so gating, the detection of photoions produced down the tube by the helium resonance radiation from the discharge is obviated. These photoions have been observed directly by an oscilloscopic display of the ion current versus time after the discharge pulse. There is seen a prompt pulse of ions which evidently corresponds to ions formed by photoionization in the immediate proximity of the aperture to the mass filter. This first pulse decays rapidly as the discharge itself ceases and then a second pulse appears after the time required for the gas to flow down the tube. Gating the detection system excludes the detection of photoions.

The ion detection system utilizes pulse-counting techniques in the case of the Ferguson experiments.

6.3.2.2. Chemical Considerations The object of afterglow mass spectrometry is to study reactions between ions and neutrals of specific chemical natures. In the stationary afterglow approach the chemical control of the afterglow is limited to the selection and the partial pressures of the neutral gases which will be subjected to the ionizing pulse and from which both the ionic and neutral reactants will be generated. In the flowing afterglow considerably more control is available. One can choose the gas through which the discharge will be run and which will later become the buffer gas in the experiment. Each of the subsequent reactant gases are fed in separately and are not subjected to the discharge. If one wishes the subsequent reactant gases either excited or partially dissociated, this can be achieved by subjecting these gases to separate discharges prior to their admission to the flow tube. This flexibility is the major reason for the versatility of flowing afterglow techniques as compared to stationary afterglow methods.

Each reaction problem presents its own chemical problems and we here summarize a few cases drawn from the experience of the ESSA group.

6.3.2.2.1. REACTIONS WITH CARRIER GAS IONS. The simplest type of reaction involves ions of the carrier gas with the neutrals of a single chemically stable ground-state reactant gas, for example, $\text{He}^+ + \text{O}_2$.¹⁰ When the carrier is helium, the discharge produces a plasma of density near 10^{11} ions cm^{-3} and a comparable number of metastable helium atoms. The electron temperature rapidly thermalizes as the gas moves downstream; spectroscopic studies have indicated that 30 cm downstream from the discharge the electron temperature is less than 350°K and the Doppler temperature of the neutral helium is approximately 300°K. X-band microwave interferometry has indicated that electron loss is by ambipolar diffusion to the walls and absorption spectroscopy has indicated that downstream the metastable atoms were effectively all in the $2\ ^3S$ state. The absence of $2\ ^1S$ metastables is understood on the basis of supereastic collisions of electrons which convert the $2\ ^1S$ atoms into $2\ ^3S$ atoms. As the helium plasma moves downstream He_2^+ ions are formed, evidently in three-body collisions, resulting in a ratio of molecular-to-atomic ions of about 0.1 at the entrance to the mass filter tube.

When a reactant gas, e.g., O_2 , is introduced through one of the side arms downstream, the mass filter detects a diminution of He^+ ions; concurrently the ionic products of the reactions with O_2 appear. Figure 4 shows the signal intensities as a function of flow of O_2 .

¹⁰ F. C. Fehsenfeld, A. L. Schmeltekopf, P. D. Goldan, H. I. Schiff, and E. E. Ferguson, *J. Chem. Phys.* **54**, 4087 (1966).

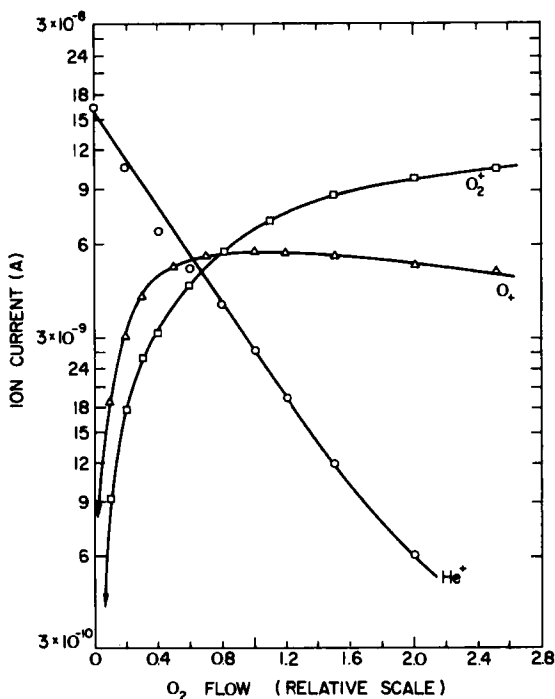


FIG. 4. Positive ion currents observed in a flowing afterglow in helium upon the addition of O_2 . From these date the rate coefficient for $\text{He}^+ + \text{O}_2 \rightarrow \text{He} + \text{O}^+ + \text{O}$ is deduced. [F. C. Fehsenfeld, A. L. Schmeltekopf, P. D. Goldan, H. I. Schiff, and E. E. Ferguson, *J. Chem. Phys.* **44**, 4087 (1966).]

The first problem upon presentation of data such as shown is the identification of the processes. Qualitatively the matching of the rate of loss of He^+ with the rise of O^+ suggests that the principal reaction is $\text{He}^+ + \text{O}_2 \rightarrow \text{He} + \text{O} + \text{O}^+$. The slower rise of O_2^+ suggests that it is either the product of a reaction involving something other than He^+ or of the Penning ionization reaction $\text{He}^* + \text{O}_2 \rightarrow \text{He} + \text{O}_2^+ + e^-$. Penning ionization also admits of producing O^+ as well, i.e., $\text{He}^* + \text{O}_2 \rightarrow \text{He} + \text{O} + \text{O}^+ + e^-$. Another possibility is that the O_2^+ is a tertiary ion formed in a reaction with the secondary ions; in this case, for example, the charge transfer reaction $\text{O}^+ + \text{O}_2 \rightarrow \text{O} + \text{O}_2^+$.

The problem of identification of processes must in each case be approached through a variety of means. If the rates for variously postulated side reactions are known then each can be evaluated separately. Additionally one can manipulate the experiment to enhance or eliminate certain

reactions. For example, by the addition of Ar to the helium, the He^+ ions are unaffected but Penning ionization, $\text{He}^* + \text{Ar} \rightarrow \text{He} + \text{Ar}^+ + \text{e}$, quenches out the helium metastables. After a separate experiment is performed to see the effects of $\text{Ar}^+ + \text{O}_2$, one can conclude that the O_2^+ in the data of Fig. 4 does indeed arise from Penning ionization by the helium metastables and that the O^+ is the only product of the reaction between He^+ and O_2 .

Having identified the ionic reaction occurring, the method used to obtain a rate coefficient is similar in philosophy to that of the Birmingham group in stationary afterglow experiments, i.e., the rate of loss of the primary ion as the secondary neutral is added constitutes the basic data. Recalling that the reaction rate constant, k , is defined by

$$\frac{\partial N_1}{\partial t} = -kN_1 n_2$$

where N_1 is the primary ion number density and n_2 is the reactant neutral number density, N_1 as a function of time is given by

$$N_1 = N_{1,0} \exp(-kn_2 t).$$

In the stationary afterglow experiments, t is the time of flow of the gas between the point of injection of the neutral reactant gas and the point of sampling. It can be varied in two ways: (1) by changing the flow speed and (2) by changing the position of injection of the second gas. In practice, it is more convenient to leave these two quantities, and therefore t , fixed and vary n_2 by varying the amount of secondary gas being flowed into the system. By keeping the flow speed constant, one avoids problems of changing diffusion to walls, flow profiles, etc.; the variation of distance between entry of the second gas and the sampling point has been quantized in the ESSA experiments and clearly it is desirable to have a continuously varying parameter to ensure that the function form of the loss of primary ions is indeed exponential.

The number density, n_2 , is obtained most simply from measuring the amount of flow of the second gas and equating it to $n_2 A v$, where A is the cross-sectional area of the tube and v is the flow velocity. Corrections to this simple analysis have been made allowing for diffusing and mixing associated with the neutral introduction by a small "point-source" nozzle on the axis of the tube. This numerical analysis leads to corrections of the order of 30% over the simpler analysis indicated above and also shows that one effect of the point-source nozzle for introduction of the second gas is to give a very slight deviation from perfectly linear plots, the deviation depending very little on the particular neutral reactant when helium is the

carrier gas. In cases where marked curvature of the primary ion signal is observed (for example, at the highest flow rates in Fig. 4), it appears that chemical processes are complicating the experiment. In Fig. 4 the curvature is believed to be due to He^+ production in the collision of two metastable helium atoms. This process becomes significant only when most of the originally formed He^+ has been removed in the reaction with O_2 .

6.3.2.2.2. REACTIONS WITH SECONDARY IONS. Many of the more interesting cases involve reactions involving ions of gases not particularly suitable for use as carrier gases. To illustrate the handling of such a problem we consider reactions of nitrogen ions with oxygen. In such gases, flowing afterglow mass spectrometry as practiced by the ESSA group takes the form of using a carrier gas discharge (e.g., He) and the injection of a second gas in which reactions occur to form a group of secondary ions at the expense of the primary helium gas ions. Then at a point even farther downstream a third gas is injected and reactions occur between the secondary ions and the tertiary neutrals to form tertiary ions. Mass analysis of the tertiary ion spectrum is used to deduce the processes occurring and the rate of loss of each of the secondary ions as a function of the third gas addition is used to deduce the rate coefficient.

Typical results of such an experiment are shown in Fig. 5. In this experiment¹¹ nitrogen gas is first added to the afterglow in helium and the second gas is oxygen. Both the N^+ and N_2^+ react with the O_2 . From the rate of decay with O_2 flow it is evident that N^+ reacts by about an order of magnitude faster than does N_2^+ . Further the initial rise of the tertiary ions O_2^+ and NO^+ which correlates well with the decay of the N^+ indicates that charge transfer, $\text{N}^+ + \text{O}_2 \rightarrow \text{N} + \text{O}_2^+$, and the ion-atom interchange process, $\text{N}^+ + \text{O}_2 \rightarrow \text{NO}^+ + \text{N}$, proceed at nearly equal rates, and the total decay rate of the N^+ must arise from both processes. Since the total loss rate constant of N^+ is about $1 \times 10^{-9} \text{ cm}^3 \text{ sec}^{-1}$, a branching ratio of one half gives a rate constant of $5 \times 10^{-10} \text{ cm}^3 \text{ sec}^{-1}$ for the process $\text{N}^+ + \text{O}_2 \rightarrow \text{NO}^+ + \text{O}$. This value agrees well with the result obtained from stationary afterglow data of the type shown in Fig. 2.

From the total rate of formation of O_2^+ and from the portion made from N^+ , the amount formed in charge transfer of N_2^+ and O_2 can be readily deduced. The data of Fig. 5 yield a charge transfer rate of about $1 \times 10^{-10} \text{ cm}^3 \text{ sec}^{-1}$. This value is about half the value obtained from the stationary afterglow data of Fite *et al.*⁶

This factor of 2 discrepancy is perhaps not outside the combined possible errors in the two experiments, but it gives a reason to compare the stationary

¹¹ P. D. Goldan, A. L. Schmeltekopf, F. C. Fehsenfeld, H. I. Schiff, and E. E. Ferguson, *J. Chem. Phys.* **44**, 4095 (1966).

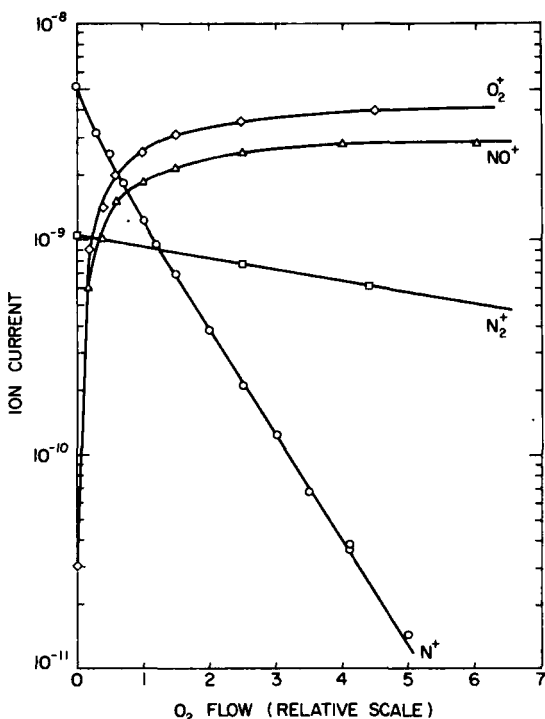


FIG. 5. Positive ion currents observed with O_2 added to a flowing afterglow containing N^+ and N_2^+ ions. Balancing of the currents yields rate coefficients for the charge transfer reactions $N_2^+ + O_2 \rightarrow N_2 + O_2^+$ and $N^+ + O_2 \rightarrow N + O_2^+$ and the ion-molecule reaction $N^+ + O_2 \rightarrow NO^+ + O$. [P. D. Goldan, A. L. Schmeltekopf, F. C. Fehsenfeld, H. I. Schiff, and E. E. Ferguson, *J. Chem. Phys.* **44**, 4095 (1966).]

and flowing afterglow techniques on a very important point. This is the question of excited states. In the stationary afterglow method all the gases are subjected to the initial energy pulse and neutral as well as ionic reactants may be in excited states as well as in the ground state. In the flowing afterglow the neutral reactants are introduced downstream of the point of energy input and where the neutral reactants are chemically stable they are certain to be in only the ground state when introduced. It may very well be that the factor of 2 discrepancy in the case of charge transfer between N_2^+ and O_2 arises because excited O_2 , present in unknown amounts in the stationary afterglow, may have a larger cross section for charge transfer than the purely ground state O_2 in the flowing afterglow experiment.

It is to be pointed out that excited states of the ionic reactants are also relevant to the question of obtaining proper rates. In afterglow experiments where secondary ions react with tertiary neutrals the method of producing the secondary ions allows some control over the ionic states. In both the flowing afterglow experiments and in the stationary afterglow experiments of Sayers^{4,7} and his collaborators reactions between the inert gas ions and metastables and the secondary neutrals produce the secondary ions. By proper choice of the inert gas, the state population of the secondary can be controlled to some extent.

Yet another advantage of flowing afterglow methods over stationary afterglow techniques resides in its capability to use neutral reactants which are not chemically stable. To produce nitrogen atoms a gas discharge is run in nitrogen before its admission to the flow tube. Although the dissociation is rather weak, the concentration of atoms can be determined through titration with NO. In this process NO is admitted downstream of the point where the N is admitted. The fast reaction $N + NO \rightarrow N_2 + O$ occurs to replace N by O. As the amount of NO is increased the color of the afterglow changes from yellow (pure nitrogen) to dark blue (as the NO bands are excited) to black and then to green (from O + NO reactions). At the NO flow rate for which the afterglow is black the amount of NO introduced is equal to the amount of N. By measuring the flow of NO under these conditions, the amount of N being introduced upstream is determined. Cutting off the NO now leaves this N in known amounts which can be used to react with ions introduced even farther upstream.

For the study of atomic oxygen in ion-neutral reactions one can simply leave the NO flow turned on at the flow rate which gives the dark afterglow. The titrating reaction with N converts each NO into an O so that measuring the NO flow gives directly the O atom flow.

The use of a separate discharge acting on a secondary or tertiary gas admitted to the stream permits some additional studies of the effects of excited states. The approach is exemplified by the measurements of Schmeltekopf *et al.*¹² of the rate coefficient for $O^+ + N_2 \rightarrow NO^+ + N$ as a function of the vibrational temperature of the nitrogen. In this experiment fixed conditions were used to produce O⁺ ions and the nitrogen which was added was previously subjected to a separate gas discharge in which the power could be varied. An electron beam in the flow tube was used to excite the first negative band spectrum of N₂⁺. From the vibrational temperature of the spectrum observed, the vibrational temperature of the N₂ was obtained, and then the reaction of the O⁺ with the N₂ was studied.

¹² A. L. Schmeltekopf, R. C. Fehsenfeld, G. I. Gilman, and E. E. Ferguson, *Planetary Space Sci.* **15**, 401 (1967).

It was found that the rate increases sharply with vibrational temperature of the N₂ ranging from about 1.8×10^{-12} cm³ sec⁻¹ at 300°K to about 6×10^{-11} cm³ sec⁻¹ at a vibrational temperature of 6000°K.

6.3.2.2.3. NEGATIVE ION REACTIONS. Reactions involving negative ions and neutrals are fully as interesting for the upper atmosphere information needs as are the reactions involving positive ions. In addition to charge transfer and ion-neutral reactions leading to new chemical species, the associative detachment reaction A + B⁻ → AB + e becomes of interest.

In principle the performance of any afterglow experiment detecting negative ions should be identical with one detecting positive ions, with of course polarities of electrostatic potentials being reversed. In practice, the situation is more complicated, presumably because of sheath problems at the wall where the ions are removed through the aperture. As noted earlier in stationary afterglow experiments involving electronegative gases with no buffer gases, Fite and Rutherford⁸ found that negative ions could not be extracted during the early portions of the afterglow. While they could be removed late in the afterglow, all the simple reactions had already occurred and all that could be seen were quite heavy negative ions which evidently were the result of several reactions including the clustering of water molecules onto the simpler ions.

In the flowing afterglow extraction of the ions is made sufficiently far downstream to correspond to the late portions of a stationary afterglow, and the large amount of buffer gas compared to the reactive gases slows things down to where the simple reactions can be observed. All types of negative ion reactions have been studied in the flowing afterglow experiments at ESSA, and the rates for associative detachment reactions¹³ have commanded particular attention for upper atmospheric interest.

¹³ F. C. Fehsenfeld, E. E. Ferguson, and A. L. Schmeltekopf, *J. Chem. Phys.* **45**, 1844 (1966).

7. SHOCK TUBES*

7.1. Introduction

In studying the physics and chemistry of gases in the temperature range between about 0.2 and 50 eV, one has very limited experimental techniques available for producing gas samples in known thermodynamic states. Shock tubes provide a means of achieving this capability. In this part we shall discuss the nature of shock-tube flows with emphasis on their capabilities and limitations. Existing instrumentation for measuring the state of the shock-processed gas sample will be described and many examples of the application of shock tubes in studying the physics and chemistry of high-temperature gases will be given. Owing to space limitations, the present treatment can be considered introductory only. The interested reader is referred to the more extensive treatment of two quite recent books on the subject.^{1,2}

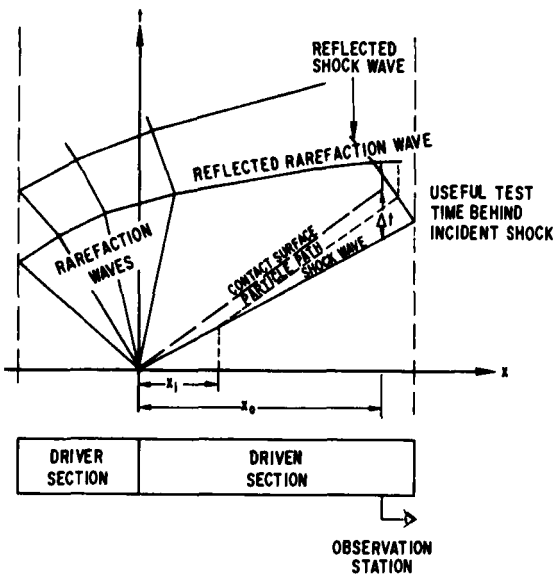
7.2. Production of Shock Waves in Shock Tubes

The shock tube is an extremely simple device with which one-dimensional shock waves traveling at essentially uniform speed are produced. The shock wave adiabatically compresses and heats to a higher temperature the test gas into which it propagates. This gas is typically at rest and at room temperature, prior to being shocked. The shock wave itself is very thin; in fact, only several mean free paths thick of the gas into which it propagates. For most practical purposes, then, the hot gas sample to be examined is immediately behind the shock wave. Indeed, to make any measurements within the shock itself requires considerable effort and unique experimental techniques. The facility is nothing more than a long (compared to its diameter) tube, two sections of which are separated by a diaphragm; see Fig. 1. In the shorter section a gas is added at high pressure, while the other section contains the test gas at a lower pressure. The former

¹ J. N. Bradley, "Shock Waves in Chemistry and Physics." Wiley, New York, 1962.

² E. F. Greene and J. P. Toennies, "Chemical Reactions in Shock Waves." Academic Press, New York, 1964.

* Part 7 is by R. A. Hartunian.

FIG. 1. x - t diagram and shock tube.

is called the driver and the latter the driven section. When the diaphragm is suddenly caused to burst, the high-pressure gas expands into the driven section driving a shock wave ahead of it. At the same time an expansion (rarefaction) wave propagates into the driver gas causing this gas to start moving down the tube. The rarefaction wave also decreases the pressure of the driver gas. The speed of the shock wave depends on the pressure ratio across the diaphragm, the speed-of-sound ratio of the driver and driven gases, and the diameter ratio of the two sections. Formulas to establish this dependence will be given later in this section.

It is convenient to follow events in shock-tube flows with the assistance of an x - t diagram (Fig. 1). This figure gives the position of any waves or particles at any time. The origin is positioned at the diaphragm and time begins with its bursting. The slope of any line on this diagram is the inverse of the velocity of the wave or particle. The shock always travels faster than the interface between the driver and driven gases (also called the contact surface), so the slopes are as indicated in the figure. The useful test time at the observation station is the time between shock arrival and the arrival of the contact surface, reflected rarefaction (expansion) wave, or reflected shock wave from the end wall of the driven section (see Fig. 1). During the useful test time, the shocked gas sample is uniform in its

thermodynamic and flow properties and provides an excellent environment in which to study the chemical and physical properties of the high-temperature gas.

Let us now consider the events which interrupt this uniform flow situation. First, the contact surface may arrive, which brings behind it the driver gas to end the test. Under most design conditions, this is the primary test time limitation. For this case, the useful test time is

$$\Delta t_{\text{test}} = x_{\text{os}} \left(\frac{1}{u_s} - \frac{1}{u_p} \right) \quad (7.2.1)$$

where x_{os} represents the position of the observation section measured relative to the diaphragm, u_s is the shock velocity, and u_p is the velocity of the gas behind the shock relative to the tube wall. It is clear that the farther one goes from the diaphragm to make observations, the longer is the useful test time. The other factors which typically end the useful test time are the arrival of either the reflected rarefaction wave from the end of the driver section or the reflected shock from the end wall of the driven section. Both situations can be calculated with fairly high accuracy. Using Eq. (7.3.13) of the following chapter, the velocity of the shock wave reflected from the driven section end wall is known, so that its time of arrival at the observation section is easily calculated. For the reflected rarefaction wave, the process is more complicated, but following the methods indicated by Hall³ its time of arrival at the observation station may also be determined. After reflecting from the driver end wall, the rarefaction travels faster than both the contact surface and shock, so that for a long enough driven tube it will pass both. To prevent the reflected shock from ending the test time, the distance between the observation station and the end wall of the driven section is made sufficiently long, while the length of the driver section must be increased to assure that the reflected rarefaction does not limit the useful test time.

Also indicated on Fig. 1 is the time history of a particle of gas originally in the driven section of the shock tube. Upon being shocked, such a particle travels at velocity u_p and crosses the observation section in a time interval behind the shock wave easily calculated from the sketch in Fig. 1, viz.,

$$t_L = (x_{\text{os}} - x_t) \left(\frac{1}{u_p} - \frac{1}{u_s} \right) \quad (7.2.2)$$

This time is called the laboratory time. Actually, that particle has been subjected to the post-shock high-temperature environment for a larger

³ J. G. Hall, UTIA Rept. No. 26 (1954); *J. Appl. Phys.* **26**, 698 (1955).

time (called the particle time) equal to

$$t_p = t_L \left(\frac{u_s}{u_s - u_p} \right) = t_L \frac{\rho_2}{\rho_1} \quad (7.2.3)$$

where ρ_2/ρ_1 is the density ratio across the shock [see Eq. (7.3.8) of the following chapter].

On the basis of the information given above, the lengths of the driven and driver sections of the shock tube are selected to give test times which have been computed to be comfortably long for the particular experiments in question. For ordinary limitations of laboratory space, the length of the driven section goes up to about 15 meters. The average driver length is about 1.5 meters. For this case, Table I indicates the time after shock arrival at an observation station 12.2 meters from the diaphragm that the contact surface, rarefaction wave, and reflected shock arrive for a range of shock Mach numbers. (Mach number is defined as the ratio of the shock velocity to the speed of sound of the gas into which it propagates.) In these calculations, the driven gas has been assumed to be diatomic ($\gamma = 1.4$) and two driver gases have been used, N₂ and He. From the table, it is seen that only for very weak shocks and with He as the driver gas does the rarefaction wave arrive before the contact surface to end the test. Otherwise the contact surface always limits the test time. It is also seen that test times vary from tens of microseconds up to a couple of milliseconds. Accordingly, measurement techniques must be gauged to these short times. The major developments in electronics technology in the past 30 years have made it possible to obtain the required measurements well within this time.

TABLE I. Test Time for Shock, Rarefaction, and Reflected Shock

Shock Mach number	$t_{\text{contact surface}}$ (msec)	Arrival time after shock arrival at $X = 12.2$ meters, $t_{\text{shock}} = 0$		
		$t_{\text{reflected rarefaction wave}}$ He driver (msec)	$t_{\text{reflected rarefaction wave}}$ N ₂ driver (msec)	$t_{\text{reflected shock}}$ (msec)
1.60	21.8	-1.7	5.0	15.2
2.00	10.9	-1.3	8.3	13.7
2.50	6.3	-0.8	11.0	12.0
3.00	4.2	-0.2	12.6	10.5
4.00	2.5	0.9	—	8.3
5.00	1.8	2.0	—	6.8
6.00	1.4	3.1	—	5.8
7.00	1.2	4.0	—	5.1

It is to be stressed that the discussion and formulas provided above apply to the ideal situation in which effects on the flow due to the boundary layer on the shock-tube walls are negligible. In a later chapter (Chapter 7.4), it will be seen that these effects can substantially affect the useful test time in many cases. In general, one finds the actual test time to be about one-half to one-third of the ideal calculated time. For operation in cases where the driven gas is at very low initial pressure, less than 1 mm Hg, say, the actual test time is considerably less than even these factors.

The strength of the shock which is produced is determined by the pressure ratio of the driver gas to that of the driven, p_4/p_1 . It also depends on the ratio of sound speeds, (a_4/a_1), and the isentropic exponents, γ_4, γ_1 , in the two gases. The following equation permits calculation of the strength of the shock produced [p_2/p_1 , or, using Eq. (7.3.7), this may be expressed in terms of M_s] as a function of these initial conditions:

$$\frac{p_4}{p_1} = \frac{p_2}{p_1} \left[1 - \frac{a_1(\gamma_4 - 1)(p_2/p_1 - 1)}{a_4(\gamma_1 - 1) \left[\frac{2\gamma_1}{\gamma_1 - 1} \frac{p_2}{p_1} \left(\frac{\gamma_1 + 1}{\gamma_1 - 1} \right) + \frac{p_1}{p_2} \right]^{1/2}} \right]^{-(2\gamma_4)/(\gamma_4 - 1)} \quad (7.2.4)$$

The derivation of this equation is given on p. 48 of Bradley's work.¹ It may easily be deduced from Eq. (7.2.4) that stronger shocks are obtained for larger initial pressure ratios across the diaphragm, p_4/p_1 , for larger values of a_4/a_1 and for larger γ_1 . Inasmuch as the speed of sound is inversely proportional to the square root of the molecular weight, it follows that lighter driver gases such as He and H₂ give much stronger shocks than N₂, say, for the same p_4/p_1 . Figure 2 illustrates the shock Mach numbers generated in nitrogen as a function of p_4/p_1 with H₂, He, and Ar taken as the driver gases. It is obvious that significantly higher shock strengths are obtained when H₂ or He are used.

If the temperature or pressure of the gas behind the incident shock wave is not adequate for a particular experiment, several techniques are available to extend this range. First, a small concentration of the gas to be studied is mixed with a large concentration of an inert monatomic dilutent (Argon or Neon, for example). Later, it will be seen that for the same strength shock much higher temperatures are obtained. Another very frequently used technique is to examine the gas behind a reflected shock wave. With no additional effort, considerably higher temperatures and pressures are obtained (see Figs. 9 and 11). A word of caution regarding the nonuniformity of this gas sample under some experimental conditions is in order. Additional details of this effect are given below (see Chapter 7.4). Still another way of obtaining strong shocks is to heat the driver gas in order

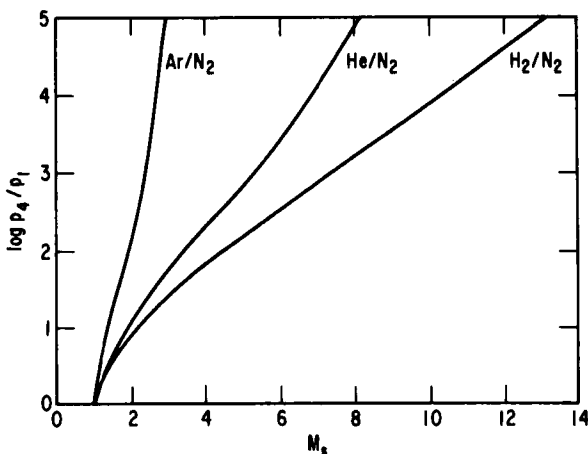


FIG. 2. $\log P_4 / P_1$ versus shock mach number for shock waves in nitrogen with various driver gases.

to obtain higher values of $a_4/a_1 \sim (T_4/T_1)^{1/2}$. The heating may be achieved in several ways. First, ordinary electrical resistance heaters may be wrapped around the driver to raise the temperature a few hundred degrees centigrade. Secondly, a combustible mixture of H_2 and O_2 may be mixed with a large amount of He (Nagamatsu and Martin,⁴ for example). The mixture is ignited by an electrical spark which results in the driver gas being heated to temperatures on the order of 2000°C. The accompanying increase in pressure causes the diaphragm to burst. Thirdly, a large amount of electrical energy stored in a capacitor bank may be rapidly discharged into the driver gas.⁵ By this method, temperatures on the order of 8000°C are obtained. Figure 3 provides a comparison of the various driver techniques as they are typically employed. For experiments involving the measurement of chemical reaction rates or some detailed physical property of the shocked gas, the role of impurities on the measurement must be evaluated. The combustion and electrical drivers typically deposit impurities in the shock tube following each run. For this reason, the simple resistance heated drivers are to be preferred.

Stronger shocks may also be generated by changes in shock-tube geometry. The primary change is to employ a larger-diameter driver section than the driven section.⁶ The gains achieved by this method are quite small,

⁴ H. T. Nagamatsu and E. D. Martin, *J. Appl. Phys.* **30**, 1018 (1959).

⁵ J. C. Camm and P. H. Rose, *Phys. Fluids* **6**, 663 (1963).

⁶ R. A. Alpher and D. R. White, *J. Fluid Mech.* **3**, 457 (1958).

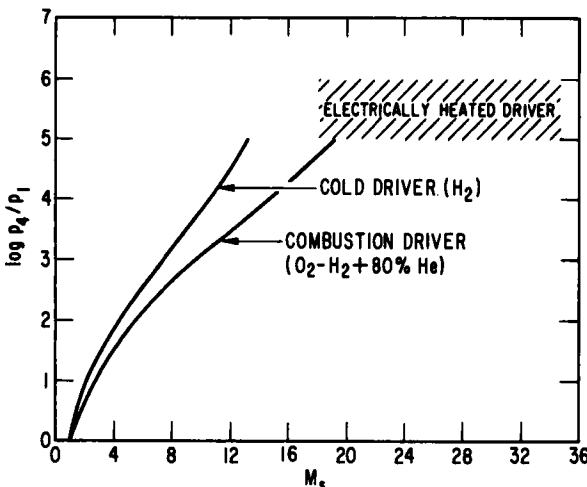


FIG. 3. Comparison of cold, electrically heated, and combustion drivers.

however. It should be pointed out that at times it becomes necessary to use a smaller-diameter driver than driven section. In this case, much weaker shocks are generated for the same initial conditions in a uniform cross-section shock tube. Figure 4 illustrates this loss in performance for typical shock-tube cases.

For the generation of extremely strong shock-waves (Mach number of about 100), a class of shock tubes utilizing electromagnetic forces has been developed. In these tubes, no diaphragm is used, so that only one gas exists at a uniform pressure. A large amount of electrical energy is deposited extremely rapidly into the gas at one end of the tube. The heating and expansion of this gas then drives a shock wave into the remainder of the test gas. To further accelerate the shock, the electrical current which runs from the capacitor bank and through the gas is passed through a lead situated outside of the glass shock tube but near the driver end. The electromagnetic field generated about this lead serves to accelerate the heated, ionized driver gas. Fowler *et al.*⁷ and Atkinson and Holden⁸ were among the first to investigate this technique. Two simple geometries of these electromagnetic shock tubes are illustrated in Fig. 5. A third configuration is the magnetic annular shock tube (MAST), the details of which

⁷ R. G. Fowler, W. R. Atkinson, W. D. Compton, and R. J. Lee, *Phys. Rev.* **88**, 137 (1952).

⁸ W. R. Atkinson and W. R. Holden, Ionized gas flow in electrically energized shock tubes. Res. Inst. Tech. Rept. Proj. 87. Univ. of Oklahoma, Stillwater, Oklahoma, 1954.

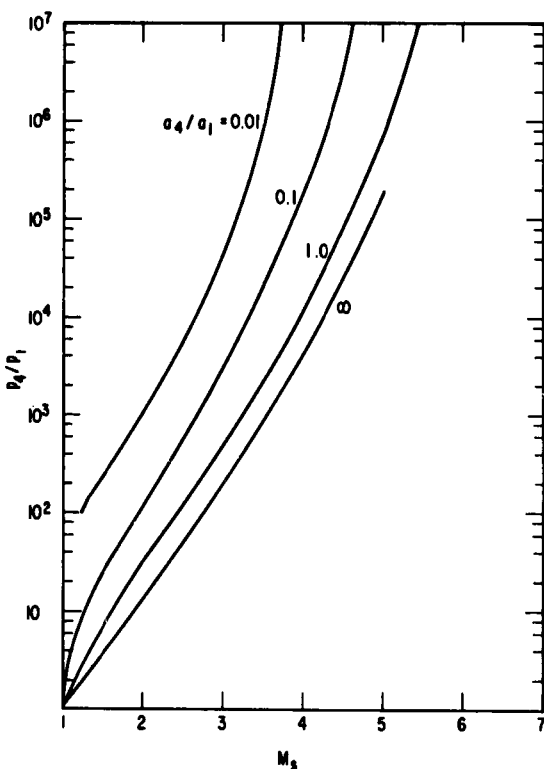


FIG. 4. Shock-tube performance for nitrogen-air shock tube for various driver-driven chamber area ratios.

may be found in the work of Patrick.⁹ Up to the present time, electromagnetic shock tubes have not been used to make basic measurements of the shocked gas sample. The extent of the uniform region behind the shock has not been as thoroughly established as for pressure-driven tubes. For some cases, nonplanar shocks have been observed, which together with rapid attenuation of the shock speed result in a nonuniform gas sample. Owing to the importance of these tubes in producing such strong shocks, additional effort in obtaining uniform gas samples behind the shock is warranted.

The shock tubes discussed in this chapter are those most commonly employed. Many other special-purpose tubes and flow techniques, may be used to produce shock waves. Some of these are discussed by Greene and Toennies² on pp. 96-102.

⁹ R. M. Patrick, *Phys. Fluids* **2**, 589 (1959).

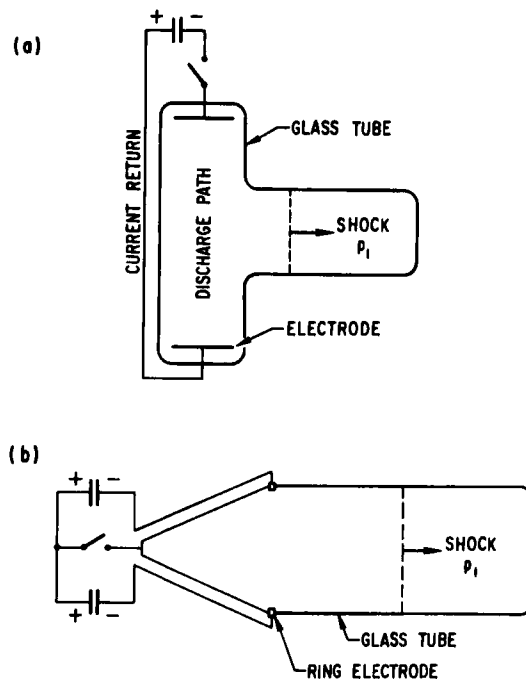


FIG. 5. Geometries of electromagnetic shock tubes: (a) T tube; (b) conical tube.

7.3. Shock-Wave Relations

In this chapter, the equations relating thermodynamic and flow quantities behind a normal shock to their values ahead of the shock will be indicated. A complete derivation of these relations may be found in several sources.¹⁻³

If the effects of viscosity and heat transfer (either by conduction or radiation) are neglected, the conservation equations which govern the one-dimensional motion of a gas are

$$\begin{aligned} \frac{\partial \rho}{\partial t} + \frac{\partial(\rho u)}{\partial x} &= 0 && \text{(conservation of mass),} \\ \frac{\partial u}{\partial t} + u \frac{\partial u}{\partial x} &= -\frac{1}{\rho} \frac{\partial p}{\partial x} && \text{(conservation of momentum),} \quad (7.3.1) \\ \frac{\partial H}{\partial t} + u \frac{\partial H}{\partial x} &= 0 && \text{(conservation of energy),} \end{aligned}$$

where ρ is the density, u the velocity in the x direction, p the pressure, and H the total enthalpy, defined as $h + u^2/2$, with h being the specific enthalpy. The coordinate x is parallel to the direction of fluid motion and t is the time. If one enters a coordinate system moving with the shock wave, these equations may be integrated for steady flow ($\partial/\partial t = 0$) across a normal shock wave to give

$$\rho_2 u_2 = \rho_1 u_s, \quad (7.3.2a)$$

$$p_2 + \rho_2 u_2^2 = p_1 \gamma \rho_1 u_s^2, \quad (7.3.2b)$$

$$h_2 + u_2^2/2 = h_1 + u_s^2/2. \quad (7.3.2c)$$

In these equations the subscript 1 refers to conditions ahead of the shock wave while the subscript 2 refers to post-shock conditions. The velocity u_2 is that relative to the shock velocity. In laboratory coordinates, the gas actually sweeps by an observation station at velocity $u_p = (u_s - u_2)$, which is usually much greater than u_2 itself. It is to be stressed that while the shock process occurs adiabatically under the assumptions of no thermal conduction or radiation, it is not a reversible process. There is an increase in entropy across the shock. In fact, $\Delta S = c_v \ln[(p_2/p_1)(\rho_1/\rho_2)]$. The increase is due to energy and momentum transport in the shock. Since conditions ahead of a shock wave are generally known it is seen that there are four unknowns, p_2 , ρ_2 , u_2 , and h_2 , with only three equations. Actually two more relations are required to specify the state of the gas. These are the equation of state $p = p(\rho, T)$ and the caloric equation of state $h = h(\rho, T)$. For a perfect gas without dissociation or ionization, the equation of state is

$$p = \rho RT \quad (7.3.3)$$

where R is the gas constant obtained by dividing the universal gas constant by the molecular weight. It is seen that use of this equation has introduced the temperature T as another variable, which necessitates the use of caloric equation of state to complete the system of equations. For an ideal gas with a constant (independent of temperature) heat capacity the caloric equation is

$$h = c_p T (+ \text{const}) \quad (7.3.4)$$

or in terms of the internal energy

$$e = c_v T (+ \text{const}) \quad (7.3.5)$$

where c_p and c_v are the heat capacities per unit mass at constant pressure and volume, respectively. It is recalled that $c_p - c_v = R$ and that the symbol γ is used to denote c_p/c_v . It will be seen below that, for the ideal gas, thermodynamic and flow quantities behind the shock in ratio to their

values ahead are functions only of γ and the shock Mach number $M_s = u_s/a_1$, where a_1 is the speed of sound of the gas ahead of the shock wave. Before presenting these formulas, a discussion of the perfect and ideal gas assumptions is required. The perfect gas assumption is valid so long as molecular interactions are negligible. At very high pressures or low temperatures, an equation of state such as van der Waal's must be used. For most shock-tube applications these particular effects are negligible and will not be considered further here. Other deviations from ideal gas behavior are important, however, For stronger shocks where temperatures are high enough to cause dissociation or ionization, the equation of state must reflect the increase in number of moles accompanying these processes as follows:

$$p = Z(\alpha, \alpha') \rho RT \quad (7.3.6)$$

where Z is the increase in number of moles, α, α' are the degrees of dissociation and ionization, respectively, and are complicated functions of temperature and pressure. For a diatomic gas $Z = (1 + \alpha)$, while for single ionization it is $(1 + \alpha')$. Further, even in the absence of dissociation or ionization, the heat capacities become a function of temperature. This is due to the excitation of internal degrees of freedom, such as rotation and vibration in molecules, for example. All of these effects are called real gas effects. In most shock-tube experiments these effects are important in determining the thermodynamic state of the shocked gas. Regarding the solution of the conservation equations, together with the two equations of state [Eqs. (7.3.3) and (7.3.4)], explicit relations can be derived easily for the ideal gas, whereas numerical techniques are resorted to when real gas effects are significant. Many iterations must be performed due to the complicated dependence of α, α' and c_p on both temperature and pressure. Several methods of conducting these numerical calculations efficiently are described by Greene and Toennies,² on p. 47. However, it should be stressed that most organizations engaged in shock-tube research possess electronic computer programs capable of determining conditions across shock waves in any gas or gas mixture. In addition, tables and graphs of these solutions are available in published form for some of the more common gases (Ar ,¹⁰ air,¹¹ N_2 ,¹² O_2 ,¹²).

¹⁰ E. L. Resler, S. C. Lin, and A. Kantrowitz, *J. Appl. Phys.* **23**, (1952).

¹¹ S. Feldman, Hypersonic gas dynamic charts for equilibrium air. Avco/Everett Res. Rept. No. 40 (1957).

¹² R. A. Alpher and H. D. Greybar, Calculation of shock hughoniots and related quantities for nitrogen and oxygen. Gen. Elec. Res. Lab. Rept. No. 58-RL-1915. Gen. Elec. Corp., 1958.

The real gas effects will be discussed in somewhat more detail in a later chapter devoted to a description of the relaxation zone behind the shock. The following, however, are the results derived for an ideal gas of arbitrary isentropic exponent γ :

$$\frac{p_2}{p_1} = \frac{2\gamma M_s^2 - (\gamma - 1)}{\gamma + 1}, \quad (7.3.7)$$

$$\frac{p_2}{\rho_1} = u_1/u_2 = \frac{(\gamma + 1)M_s^2}{(\gamma - 1)M_s^2 + 2}, \quad (7.3.8)$$

$$\frac{T_2}{T_1} = \left[\frac{2\gamma M_s^2 - (\gamma - 1)}{\gamma + 1} \right] \left[\frac{(\gamma - 1)M_s^2 + 2}{(\gamma + 1)M_s^2} \right]. \quad (7.3.9)$$

Thus, it is seen that if the speed of the shock wave u_s is measured as it propagates into a gas of known thermodynamic state, i.e., p_1 , ρ_1 , T_1 , γ , and $a_1 [=(\alpha\gamma RT_1)^{1/2}]$ are known, then $M_s = u_s/a_1$ is established and the thermodynamic state and velocity of the gas behind the shock are easily determined. Equations (7.3.7)–(7.3.9) are plotted in Figs. 6 to 8 for a range of

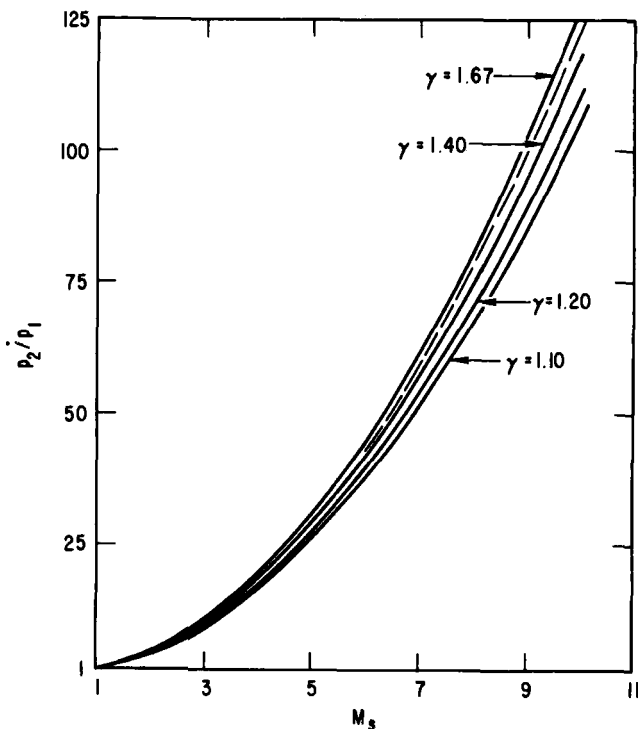


FIG. 6. Pressure ratio across a normal shock wave as a function of shock mach number.

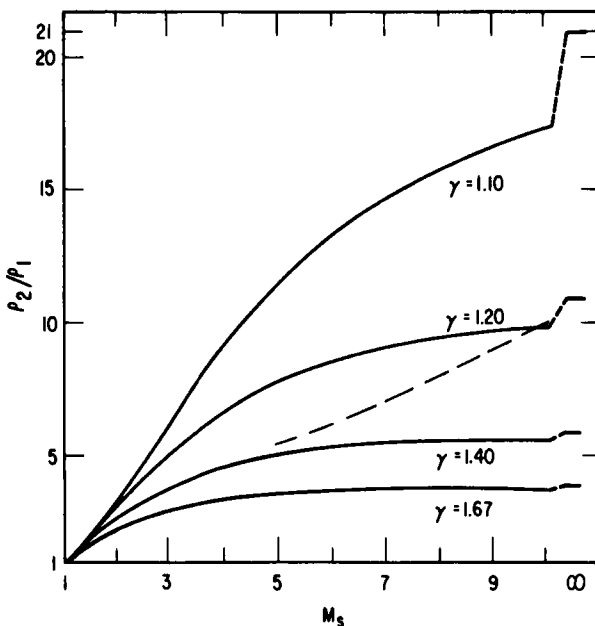


FIG. 7. Density ratio across a normal shock wave as a function of shock mach number.

values of γ . It is recalled that γ is 1.67 for a monatomic gas, 1.4 for a diatomic gas with no vibrational heat capacity, and as the molecules become more complex γ approaches unity. It is seen that the pressure ratio is much less sensitive to γ , while the temperature and density ratios are extremely sensitive. Regarding the temperature, the physical reasoning leading to the indicated dependence on γ is as follows: from the normal shock-wave relations it is seen that the specific enthalpy and not the temperature appears explicitly. It can be shown that the specific enthalpy ratio across the shock is nearly independent of γ for a given shock Mach number, M_s . Temperature is obtained from enthalpy by dividing by c_p . For more complex molecules c_p is larger, since these molecules can absorb more energy in internal degrees of freedom, so that the translational temperature T_2 is correspondingly smaller than for a monatomic or diatomic gas. As an example, consider a shock of Mach number ten which propagates into Argon ($\gamma = 1.67$) or ideal air ($\gamma = 1.4$) at room temperature ($T_1 = 300^\circ\text{K}$). For Argon, the post-shock temperature would be 9000°K , while for the ideal air it would be approximately 6000°K . This is one of the reasons that mixtures of a test gas and a monatomic gas (typically Argon) are often

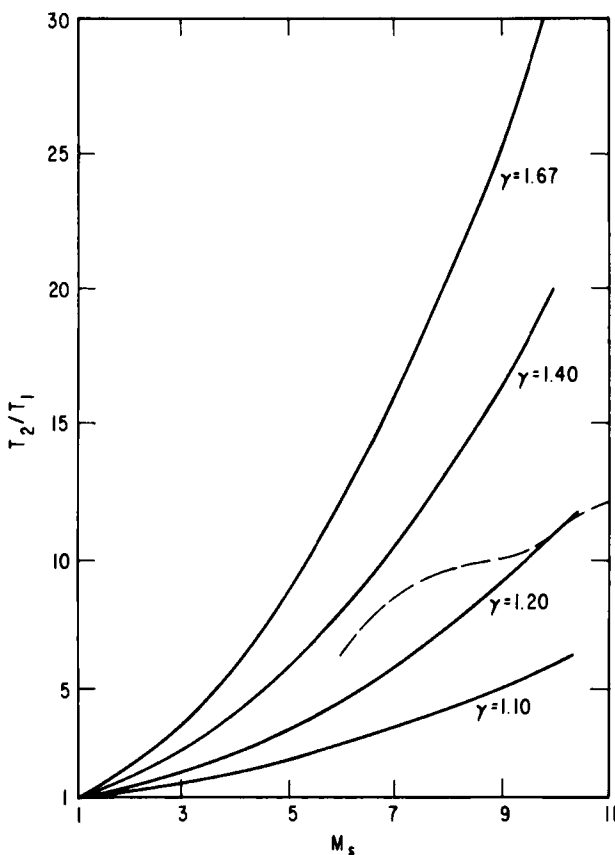


FIG. 8. Temperature ratio across a normal shock wave as a function of shock Mach number.

used; viz., to increase the test gas temperature without resorting to a stronger shock. Finally, on each of Figs. 6 to 8, the dashed line indicates the values obtained for real air in thermochemical equilibrium, which now includes excitation of internal degrees of freedom, dissociation and ionization. These curves are to be compared to the $\gamma = 1.4$ curves. For the example cited above, it is seen that the temperature for real air in equilibrium would be only about 3000°K. This dramatic reduction is due largely to the fact that energy was extracted from translation of the molecules to cause dissociation. This clearly depicts the significance of real gas effects.

As mentioned earlier, if the temperature and pressure behind an incident shock wave are not high enough for the experimenter's purpose, a significant gain in both can be obtained by allowing the shock to strike and reflect

from a plane surface, typically the end wall of a shock tube. Upon doing so, the gas which has been shocked once by the incident wave is shocked a second time by the reflected wave which causes the temperature and pressure to rise still further. In addition, the gas behind the reflected shock is brought to rest with respect to the laboratory as required by the boundary condition at the wall. Relations for conditions behind a reflected shock in terms of the original incident shock Mach number and the thermodynamic state of the gas into which the incident shock is propagating are given below for the same gases considered above (the derivation of these relations may be found in the work of Greene and Toennies,² on pp. 26, 27):

$$\frac{p_5}{p_1} = \left[\frac{\left(\frac{3\gamma - 1}{\gamma - 1} \right) M_s^2 - 2}{M_s^2 + \frac{2}{\gamma - 1}} \right] \left[\frac{\left(\frac{2\gamma}{\gamma - 1} \right) M_s^2 - 1}{\frac{\gamma + 1}{\gamma - 1}} \right], \quad (7.3.10)$$

$$\frac{p_5}{\rho_1} = \frac{\left(\frac{\gamma + 1}{\gamma - 1} \right) M_s^2 \left[\frac{2\gamma}{\gamma - 1} M_s^2 - 1 \right]}{\left[M_s^2 + \frac{2}{\gamma - 1} \right] \left[2M_s^2 + \frac{3 - \gamma}{\gamma - 1} \right]}, \quad (7.3.11)$$

$$\frac{T_5}{T_1} = \frac{\left[\left(\frac{3\gamma - 1}{\gamma - 1} \right) M_s^2 - 2 \right] \left[2M_s^2 + \frac{3 - \gamma}{\gamma - 1} \right]}{\left[\left(\frac{\gamma + 1}{\gamma - 1} \right)^2 M_s^2 \right]}. \quad (7.3.12)$$

The reflected shock velocity in ratio to the speed of sound in the original test gas prior to any shocking is

$$\frac{u_5}{a_1} = \frac{\left[2M_s^2 + \frac{3 - \gamma}{\gamma - 1} \right]}{\left(\frac{\gamma + 1}{\gamma - 1} \right) M_s}. \quad (7.3.13)$$

Figures 9–12 plot these quantities as before.

In closing this chapter, it should be remarked that the solution of Eqs. (7.3.2) and (7.3.3) is valid in regions far upstream and downstream of the shock wave, where viscous forces and thermal conduction parallel to the direction of flow are negligible. To complete the description of the shock wave, it is essential to know the thickness of the region where these transport terms are not negligible, i.e., to evaluate the shock thickness. In the present brief treatment, a detailed description of the derivation of shock

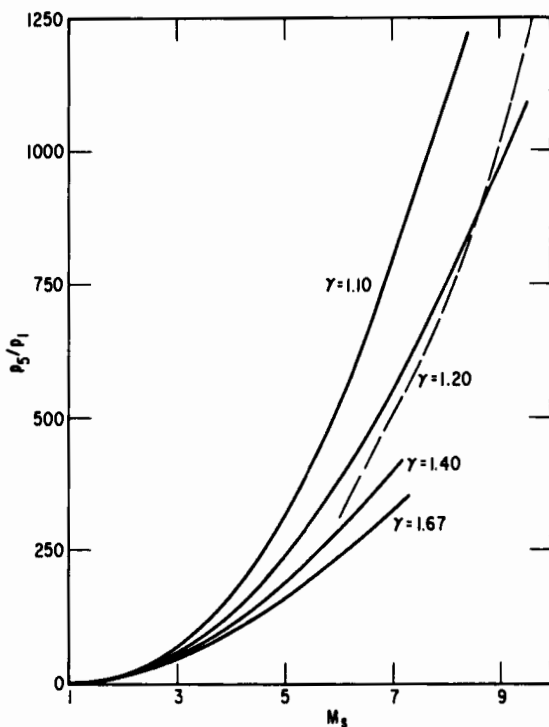


FIG. 9. Pressure ratio behind a reflected shock wave as a function shock Mach number.

thickness relations is not warranted; rather, the reader is referred to Bradley¹ and Talbot.¹³ Suffice it to say that shock thicknesses at which the translational temperature or density go from their initial to post-shock values is on the order of several mean free paths in the original test gas. Accordingly, under most conditions of initial density in shock-tube experiments, the shock wave is extremely thin and usually beyond the time response capability of instruments. On the other hand, it is clear that if an instrument were devised which was capable of following the density or temperature rise within the shock wave, one would provide valuable information on basic molecular forces which go into transport properties, as well as a good test of kinetic theories attempting to predict flow phenomena occurring with very few collisions among the particles. As will be pointed out in a later chapter, an electron beam technique has been successfully applied to this end.

¹³ L. Talbot, *ARS (Am. Rocket Soc.) 32*, 1009 (1962).

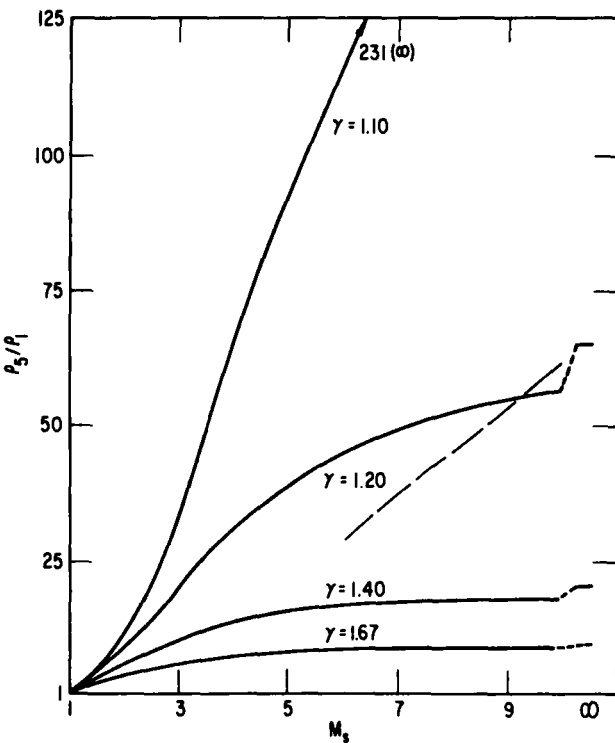


FIG. 10. Density ratio behind a reflected shock wave as a function of shock Mach number.

7.4. Deviations of Shock Tube Flows from Ideal Calculations

Up to this point all the calculations of shock-tube flows, including test time, shock properties, and shock strengths generated from given initial conditions, have assumed that the flow is one-dimensional, that the diaphragm bursting time is negligibly small, and that the contact surface between the driver and driven gases is a clearly defined line. Under many conditions these assumptions are good and shock-tube performance is found to agree adequately with these calculations. The major discrepancy is usually in the test time. As mentioned earlier, the experimental test time is found to be a factor of two to three less than ideal under most circumstances and considerably less when very low initial pressures are required. This discrepancy is due to two major factors. First, during the finite diaphragm opening time, the high-pressure gas jets through the opened part.

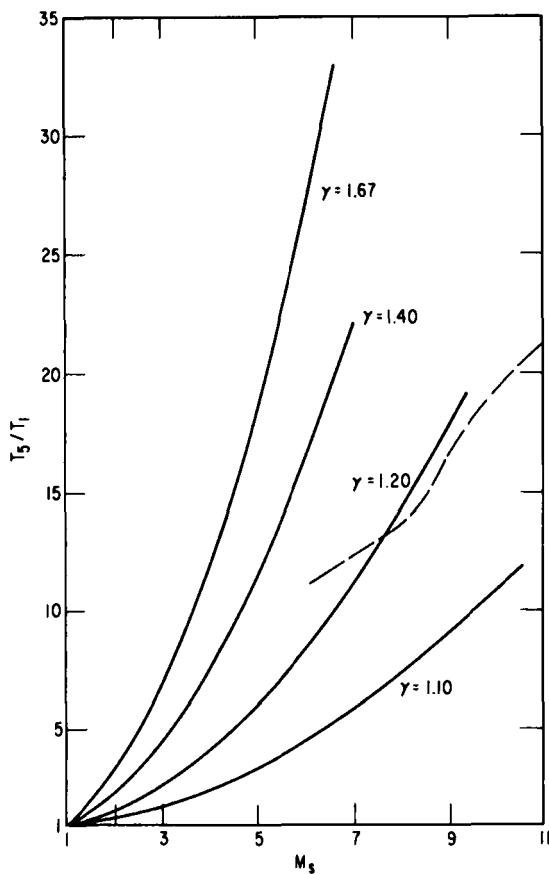


FIG. 11. Temperature ratio behind a reflected shock wave as a function of shock Mach number.

This jetting causes mixing of the driver and driven gases which results in broadening of the contact surface. The leading edge of this broadened contact surface arrives at the observation station earlier than estimated from the ideal calculation. A more important effect in limiting the test time is the deviation from one-dimensional flow. This deviation is due to the growth of a boundary layer along the walls behind the shock wave (see Fig. 13). The boundary layer is the region of flow where viscous forces and thermal conduction in the gas cause the velocity and temperature to

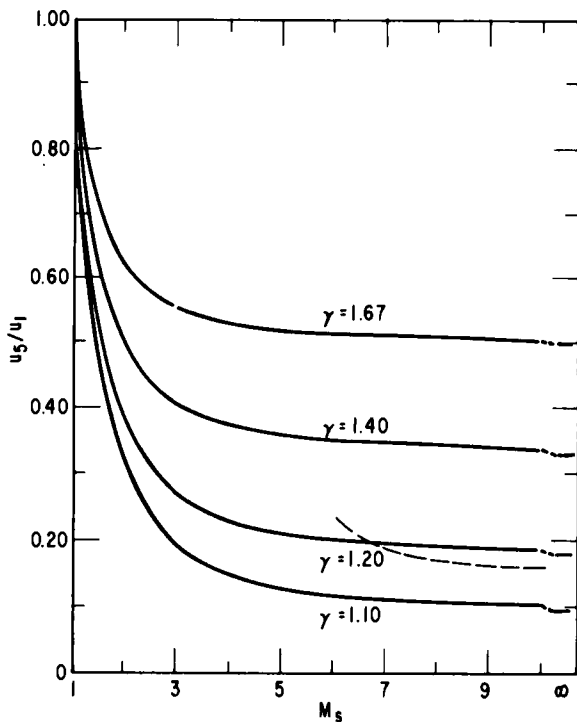


FIG. 12. Reflected shock velocity in ratio to original shock velocity as a function of shock Mach number.

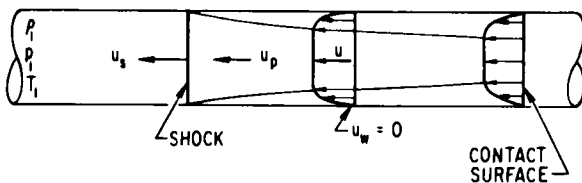


FIG. 13. Shock-wave boundary layer in nonsteady coordinates.

go from their high values behind the shock to the required values at the walls. These wall boundary conditions are zero velocity and near room temperature. The boundary layer grows as the square root of the distance behind the shock wave, but, in general, is very thin. The characteristics of the boundary layer have been studied extensively both theoretically and experimentally, and are quite predictable. To analyze this flow, it is

convenient to go into a coordinate system fixed in the shock wave, since this renders the flow steady in time. To transform into these coordinates, one simply subtracts the shock velocity, u_s , from all flow velocities indicated in Fig. 14. The wall, which was stationary in the previous coordinate system, is now seen to translate at shock velocity. Figure 14 shows the situation which is then analyzed using the conservation equations for fluid motion including viscous and thermal conduction terms. It can be shown that the pressure is uniform across these thin fluid layers. Typical profiles of other thermodynamic and flow variables are shown in Fig. 15. It is seen that the distribution of mass flow per unit area, ρu , is such that it increases monotonically from the edge of the layer to the wall. This additional mass flow comes from the external stream. Regarding the influence of the boundary layer on the external flow behind the shock wave, it is due to this removal of mass from the stream into the boundary layer. A direct measure of the mass removal is a quantity known as the displacement thickness, δ^* , which is defined as

$$\delta^* = \int_0^\delta \left(1 - \frac{\rho u}{\rho_2 u_2}\right) dy \quad (7.4.1)$$

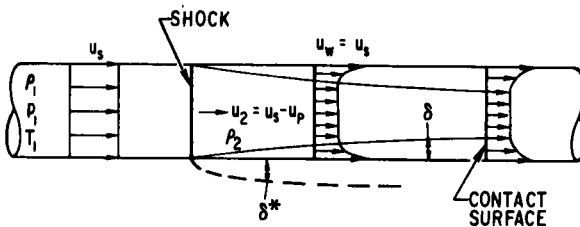


FIG. 14. Shock-wave boundary layer in steady coordinates.

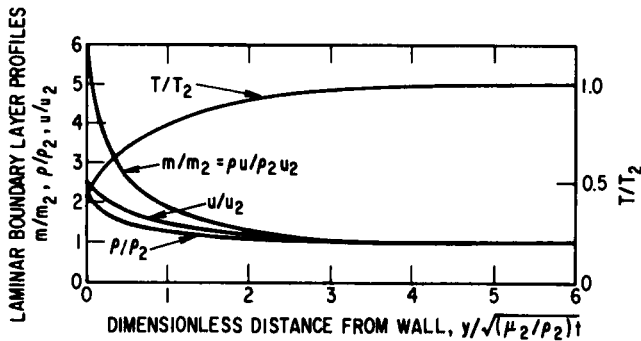


FIG. 15. Profiles of velocity, density, temperature, and mass flow in shock-tube laminar boundary layer for $M_s = 1.5$ in argon.

where δ is the boundary layer thickness. The displacement thickness grows parabolically with distance behind the shock, and is negative in this flow case (since ρu is everywhere greater than $\rho_2 u_2$). The displacement thickness is sketched schematically in Fig. 14. As far as the external flow is concerned, it is as though it were flowing through a diverging tube whose diameter is $d + (-2\delta^*)$, where d is the geometric diameter. The flow through this effective diverging channel causes both axial and radial gradients in all the flow and thermodynamic variable. The deviations in these quantities from the uniform values they would have if the boundary layer were neglected is obviously dependent upon the magnitude of $-\delta^*/d$. A useful formula for δ^* is

$$(-1)\delta^* = A(M_s) (x/p_1)^{1/2} \quad (7.4.2)$$

where p_1 is in atmospheres and x is in feet. In this expression the coefficient $A(M_s)$ is plotted in Fig. 16. The evaluation of δ^* comes from detailed

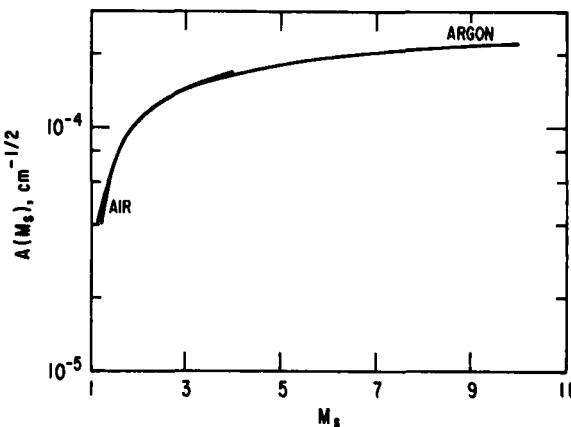


FIG. 16. Laminar boundary layer displacement thickness function.

solutions of the boundary layer equations, which have been solved for a broad variety of gases by Mirels.¹⁴ Real gas effects have been included as well. It is seen that δ^* is inversely proportional to the square root of the initial pressure p_1 of the test gas. It is for this reason that the boundary layer effects are most pronounced when the experiment must be conducted at low initial pressures. Further, it is obvious that the problem can be overcome to a large extent by using a large-diameter shock tube, such that $-\delta^*/d \ll 1$ for all initial pressures.

¹⁴ H. Mirels, *Phys. Fluids* **6**, 1201 (1963).

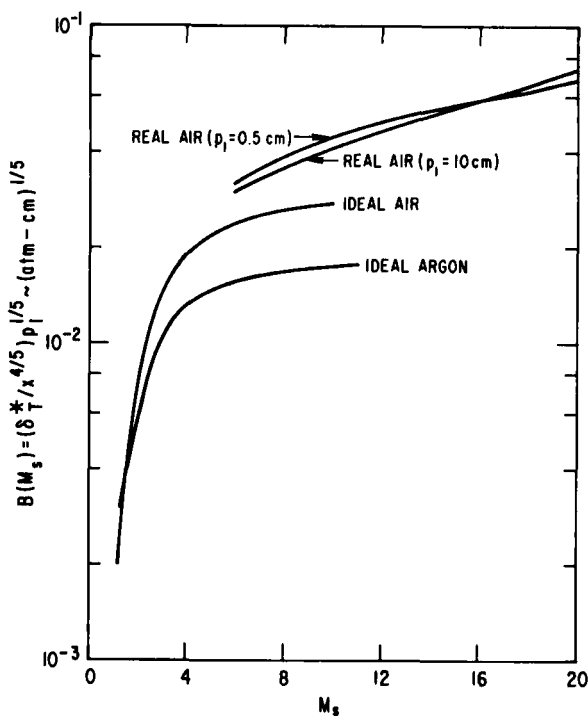


FIG. 17. Turbulent boundary layer displacement thickness function.

The expression for $-\delta^*$ given in Eq. (7.4.2) is valid so long as the boundary layer remains laminar. This is always the case immediately behind the shock, but under many conditions the laminar boundary layer becomes unstable and undergoes transition to turbulent flow a certain distance behind the shock. The significance of this transition is that the turbulent boundary layer grows at a more rapid rate, with an accompanying larger influence on the uniformity of the external stream. An expression for δ^* for a turbulent boundary layer is¹⁵

$$\delta^*_T = \frac{x^{4/5}}{p_i^{1/5}} B(M_s) \quad (7.4.3)$$

where the function $B(M_s)$ is plotted in Fig. 17. The process of transition is extremely complicated, and, although it has been studied fairly extensively for shock tube flows, its detailed prediction for any given shock tube to an accuracy of better than a factor of two or three is still not possible.

¹⁵ H. Mirels, *AIAA J.* **2**, (1964).

The distance behind the shock at which transition occurs may be estimated to this accuracy by the relation

$$x_{tr} \text{ (cm)} = \frac{C(M_s)}{p_1 \text{ (atm)}} \text{ ft} \quad (7.4.4)$$

where $C(M_s)$ is indicated in Fig. 18. Factors such as roughness of the shock-tube walls, protuberances, small mismatches in the shock-tube wall at joints of sections, and extraneous waves which are propagated forward

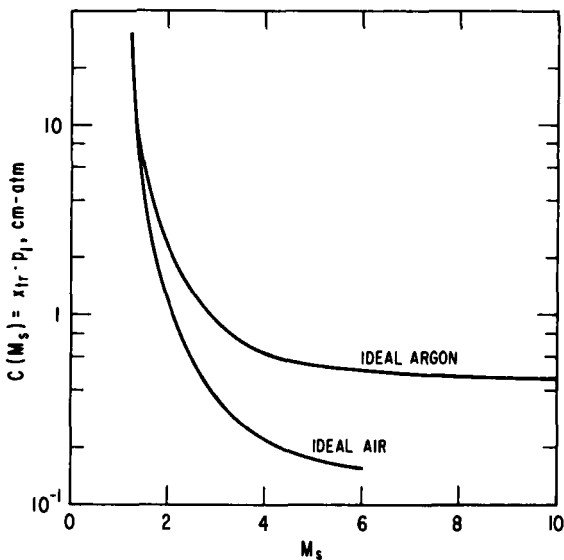


FIG. 18. Turbulent transition distance function based on $(Re)_{tr} = 10^6$.

from the nonuniform contact surface can all contribute to premature transition. In the interest of better control of this phenomenon, it is advisable that the interior of the shock tube be finished to approximately 100 μin . or less. It is further advisable to actually measure the transition time (simply related to the distance; $x_{tr} = u_s t_r$) for those experiments in which boundary layer corrections may be significant. Several techniques are available to make this measurement.¹⁶⁻¹⁸

¹⁶ A. J. Chabai and R. J. Emrich, *Bull. Am. Phys. Soc.* **3**, 291 (1958).

¹⁷ I. R. Asbridge, An interferometric study of shock tube boundary layers. Inst. of Res. Tech. Rept. No. 14. Lehigh Univ., Bethlehem, Pennsylvania, 1959.

¹⁸ R. A. Hartunian, A. L. Russo, and P. V. Marrone, *J. Aerospace Sci.* **27**, 587 (1960).

Using Eqs. (7.4.2)–(7.4.4), the significant characteristics of the boundary layer may be calculated. The boundary layer affects the shock-tube flow in the following ways: first, waves generated from the boundary layer may cause the shock to attenuate (slow down with time); second, it causes the shock wave to be curved; and, third, it contributes significantly to a reduction of test time. Again these effects are negligible when $\delta^*/d \ll 1$, or at high initial pressures. We will now consider each of these effects briefly. Regarding attenuation, it is to be emphasized that the velocity of the shock is measured at several stations along the tube in every run. With the degree of attenuation established, it is possible to estimate the changes with time in the flow and thermodynamic properties at the observation station. The estimate may be made as follows: Consider two particles of gas, one originally far upstream of the observation station and the second only a short distance upstream. Due to attenuation, the former particle is shocked by a stronger shock wave than the latter. Since the latter particle sweeps across the observation point first, the observer would see a lower-temperature, pressure, etc., gas at early times. By following the two particles in time and having known the shock strengths of each, the time history of temperature, etc., can be calculated. The magnitude of the attenuation depends on many factors as described above, but typical values like 0.5–5% per meter of travel are experienced. The detailed prediction of shock attenuation has been examined by several authors.^{19,20} In the latter two references contributions to attenuation from both the laminar and turbulent boundary layers as well as the boundary layer in the region behind the contact surface have been considered. Reasonable agreement with experimental results is found. These analyses may be used to obtain more accurate distributions of flow and thermodynamic properties than the simple one indicated above.

Regarding shock curvature, this boundary layer effect was first analyzed by Hartunian.²¹ The presence of only one plane wall was considered there. This treatment was later extended to include shock tubes of circular cross section.²² Figure 17 illustrates a curved shock together with the obvious difficulty this causes in any measurements which integrate across the whole shock tube (light emission or absorption, e.g.). The following simple relation may be used to estimate the magnitude of the bowing out of the shock front:

$$\Delta = F(M_s, p_1) \frac{\sqrt{y}}{\sqrt{p_1}} \quad (7.4.5)$$

¹⁹ R. L. Trimpf and N. B. Cohen, *NACA Tech. Note* 3944 (1957).

²⁰ H. Mirels and W. H. Braun, *NACA Tech. Note* 4021 (1957).

²¹ R. A. Hartunian, *Phys. Fluids* 4, 1059 (1961).

²² P. C. T. de Boer, *Phys. Fluids* 6, 962 (1963).

where the function $F(M_s, p_1)$ is shown in Fig. 19 both for ideal and real air. Measurements of shock curvature have been made over a wide range of pressures and Mach numbers. Values of Δ on the order of 1 mm were obtained at $p_1 = 0.34$ mm Hg and $1.8 < M_s < 6.3$ and 1 cm for $p_1 = 0.01$ mm Hg at $M_s \approx 20$. Good agreement is obtained between theory and experiment. The major problem which is influenced by shock curvature is that related to measurements of the thickness of the shock front itself by a technique which integrates across the tube. Special care must be taken to eliminate this effect from the measurement.

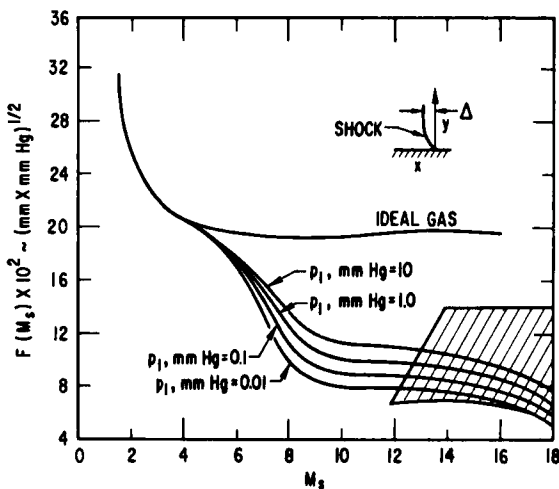


FIG. 19. Shock shape as a function of shock Mach number for air; //// represents experimental data.

Under more extreme conditions of low pressure, a condition is reached where all the mass flowing across the shock eventually flows into the boundary layer at the position of the contact surface. This situation is illustrated in Fig. 20. For this case, no mass flow accumulates between the shock and contact surface, as it does in ideal flow. Accordingly, in this limit the separation between the shock and contact surface remains constant, instead of growing linearly with distance from the diaphragm. Obviously, the test time becomes much shorter than ideal calculations would predict. This phenomenon was first identified in the experiments of Duff,²³ who also provided the explanation just given. Detailed analysis of this flow was first

²³ R. E. Duff, *Phys. Fluids* 2, 207 (1959).

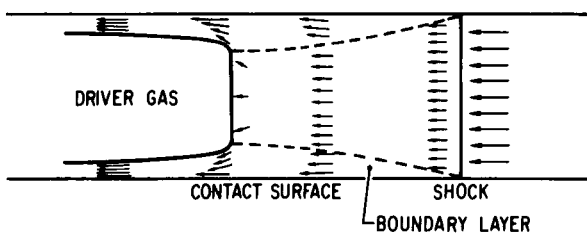


FIG. 20. Limiting condition of mass flow in the boundary layer in steady coordinates. The lengths of the arrows indicate the flow velocity with respect to the shock.

given by Roshko.²⁴ Since that time other experimental results have become available,^{25,26} and a more complete theoretical treatment has been developed by Mirels.¹⁴

The maximum possible separation distance in a low-density shock tube, l_m , can be expressed as

$$\frac{1}{p_1} \frac{l_m}{d^2} = G(M_s) \quad (7.4.6)$$

for a given test gas. This function is plotted in Fig. 21 for air and argon. The variation of separation distance, l , with shock distance from the diaphragm, x_s , is estimated from

$$\frac{X}{2} = \ln(1 - T^{1/2}) + T^{1/2} \quad (7.4.7)$$

when $X = (\rho_1/\rho_2)(x_s/l_m)$, $T = l/l_m$. This equation is plotted in Fig. 22. Agreement between theory and experiment is good.

In the experiments, it has been noticed that once the limiting condition is achieved the shock travels at uniform speed. One would erroneously conclude from this lack of attenuation that conditions in the test gas are uniform. Actually, the axial gradients in properties are quite severe. It is very important to correct basic data taken under low-pressure conditions for these effects. Mirels²⁷ has calculated the magnitude of these corrections for some typical measurements made in shock tubes.

²⁴ A. Roshko, *Phys. Fluids* **3**, 835 (1960).

²⁵ W. J. Hooker, *Phys. Fluids* **4**, 1451 (1961).

²⁶ J. C. Camm and P. H. Rose, *Phys. Fluids* **6**, 663 (1963).

²⁷ H. Mirels, Flow nonuniformity in shock tubes operating at maximum test time. Rept. No. TDR-669(6240-10)-4. Aerospace Corp. Los Angeles, California.

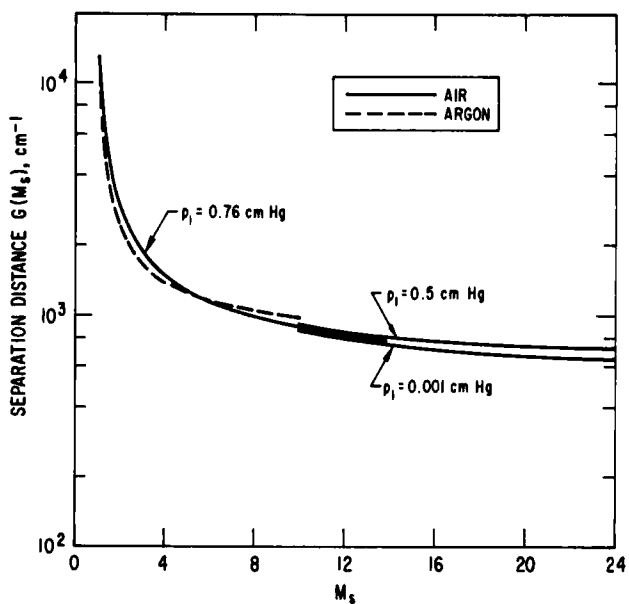


FIG. 21. Shock Mach number versus separation distance between shock and contact surface.

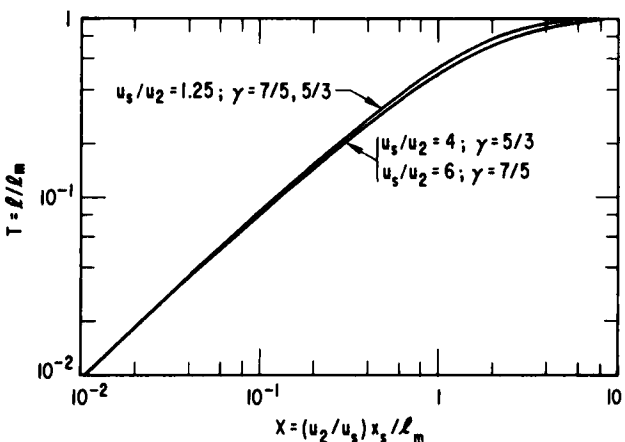


FIG. 22. Variation of T with X for ideal gas.

7.5. Reflected Shock Nonuniformities

Under many conditions, the interaction of a reflected shock wave with the boundary layer caused by the incident shock results in a configuration shown in Fig. 23. The shock puts feet out in front of its direction of propagation (bifurcates). Pockets of gas exist behind these bifurcations and move along with the shock wave. This situation was first analyzed by Mark.²⁸

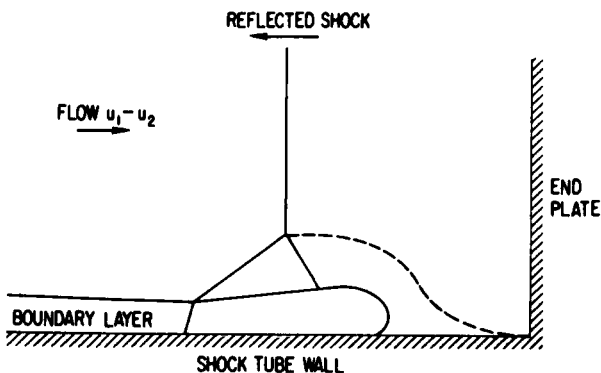


FIG. 23. Interaction of reflected shock with the boundary layer behind the incident shock (Mark).

The bifurcation occurs for those cases in which the total pressure in the boundary layer is lower than the pressure behind the reflected shock. This accounts for the boundary layer fluid forming the pockets behind the bifurcated shock. The oblique shock waves assure that the supersonic flow properly negotiates the turns about the pocket. The dashed line is the contact surface between the gas which has passed through the normal shock and that through the two oblique shocks (different entropy). It is clear that when this flow situation is achieved the test gas behind the reflected shock will not be uniform. Analysis, including the extension of Mark's work by Byron and Rott,²⁹ indicates those conditions under which the shock bifurcates (M_s from 2.3 to 6.5 for $\gamma = 1.4$, for example). Prediction of the detailed distributions of quantities in the region behind the reflected shock is quite approximate.

²⁸ H. J. Mark, *J. Aeron. Sci.* **24**, 304 (1957); *NACA Tech. Memo.* 1418 (1958).

²⁹ S. R. Byron and N. Rott, *Proc. Heat Transfer Fluid Mech. Inst.*, Stanford Univ. Press, Stanford, California, 1961.

General agreement between theory and experiment is found regarding the regimes in which bifurcation occurs. However, several experiments indicate that the temperature behind the reflected wave may be as much as 300 to 500°K below the calculated value for incident shocks in the Mach number range ~ 2.75 to 3.60. This result is based on measurement of the incident and reflected shock velocities, and is for that reason indirect. Indeed, direct measurements of the temperature and density behind reflected shocks indicate that the temperatures achieved are only 50°K below the expected value. It is clear that more understanding of the fluid dynamics behind reflected shock waves is essential before that region can be used with a high degree of reliability for chemical and physical measurements. Certainly, direct measurements of density and temperature should accompany present experiments.

7.6. Measurement Techniques in Shock-Tube Flows

One of the major obstacles in the measurement of shock-wave properties is the short duration of the observation. Well-developed steady-state measurement techniques are often inapplicable for this reason. It has been the development of rapid-response instruments which has made the shock tube a useful research tool. To be sure, there are still several fundamental quantities which cannot be measured over a wide range of shock-tube conditions. The use of auxiliary measurements together with the application of shock-wave theory has made it possible to overcome some of the inadequacies in direct measurement.

In all shock-tube experiments, two measurements are made which define the state of the gas immediately behind the shock (before any relaxation phenomena have occurred); these are the shock speed and the initial pressure of the test gas. Both are quite easy to measure. Standard methods are used to measure initial pressure, so nothing more will be said of this except to warn that continual calibration of the particular gage employed is essential; especially in the range from 10 to 1000 μHg . There are many techniques^{1,2} available to measure shock speed, only the most common of which will be discussed here. Most indicate the time of shock passage past each of several measured stations along the tube. By recording the time difference between two successive stations an average speed is deduced for this interval. The electronic circuitry which permits a simple single display of shock passage time for all stations is given by Rabinowicz *et al.*³⁰ Thin film resistance thermometers are used most often to detect the shock wave.

³⁰ J. Rabinowicz, M. E. Jessey, and C. A. Bartsch, *J. Appl. Phys.* **23**, 97 (1955).

An exception to this fact is that whenever electric discharge systems are used to drive shock waves. The electrical noise is so great that spurious signals are picked up by the thin film thermometers (or any other electrical pickup) which trigger them prematurely. Accordingly, for these cases optical systems are used to detect the shock. The thin film is most popular because of its simplicity, rapid response ($0.1 \mu\text{sec}$) and accuracy. This instrument is nothing more than a small resistance element (typically 1 mm wide by 5 mm long, and with a resistance from 100 to 1000Ω) mounted on the surface of a small glass disk which is then mounted flush with the i.d. of the shock tube. The resistance of the thin film is linearly proportional to its temperature. When the shock wave passes over the film the heat transfer from the shocked gas instantaneously raises the temperature of the glass disk surface, which the thin film senses. By having a steady current (about 20 mA) through the thin film and a large load resistor to ground, the change in resistance causes a significant voltage change across the load resistor which is recorded on an oscilloscope. Amplification is used when necessary. The thin films are very easy to fabricate. Platinum is used most commonly and it is most easily applied to the glass disk by methods used in the decorative glass industry.³⁰ If the shock gas temperature is extremely high, its electrical conductivity can be sufficient to provide a shorting path for the current through the gage. This effect may be minimized by evaporating a thin insulating film (SiO, for example) over the gage.³¹

Another simple electrical detector is an ionization gage.³² This may be a spark plug or any two closely spaced electrodes, one of which is held at a potential near breakdown. Passage of the shock causes breakdown to occur and the discharge current is used to generate a potential jump across a resistor. This method is not as uniformly dependable as the thin film thermometers, and becomes inadequate for weak shocks.

Optical methods are sometimes used to detect shock passage. Two general modes of operation are employed; one is based on using the change in index of refraction across the shock to deflect a light beam through a narrow slit onto a photomultiplier,³³ while the second mode detects the radiation emitted from the high-temperature gas behind the shock or a change in the absorption of a beam of light.³⁴ By placing the appropriate detectors at several positions along the shock tube and recording the time of shock passage at each, the shock velocity is easily derived. A continuous time history of shock velocity may be obtained when the shock front is

³¹ P. V. Marrone and R. A. Hartunian, *Phys. Fluids* **2**, 719 (1959).

³² H. Harrison, H. S. Johnston, and E. R. Hardwick, *J. Am. Chem. Soc.* **84**, 2478 (1962).

³³ J. B. Toennies and E. F. Greene, *J. Chem. Phys.* **26**, 655 (1957).

³⁴ H. B. Palmer and D. F. Hornig, *J. Chem. Phys.* **26**, 98 (1957).

luminous. A long narrow slit is arranged parallel to the axis of a window section of the shock tube. The light emitted through the slit may be recorded as a function of time by a rotating drum camera.³⁵ In this camera, film is placed on the periphery of a drum rotating at a known constant speed in a plane perpendicular to the slit. The resulting photograph is an x - t diagram of the shock motion, the time coordinate having been provided by the drum motion. Any curvature of the shock line on this photograph is immediate evidence of shock attenuation. If the shock front is not luminous enough, schlieren photography can be used.

7.7. Density Measurements

Measurement of the density distributions behind shock waves is important to the complete understanding of both the uniformity of flow behind the shock wave and the rate of chemical reactions. The techniques employed most frequently are optical although electron beam and X-ray absorption techniques have also been used. Each of these general techniques will be described briefly in the following paragraphs.

7.7.1. Optical Methods

For accurate quantitative measurements of the density distribution behind shock waves, interferometric methods are used most frequently. The Mach-Zehnder interferometer is used extensively in shock-tube work because of its over-all flexibility. The principle of the interferometer in this application is illustrated in Fig. 24. Essentially, a monochromatic parallel beam of light is obtained by filtering the output of a light source. The parallel beam is then split by a half-silvered mirror and one of the resultant beams is passed through the shock tube and the other through a compensating section. A compensating section allows for the difference in optical path due to passage through the windows of the shock tube and the gas at initial conditions before arrival of the shock wave. The two resultant beams are then brought together and focused on a photographic plate by the mirror system indicated in Fig. 24. A uniform field of fringes is obtained by slightly rotating the half-silvered mirrors. Arrival of the shock wave causes a density change and an accompanying change in the index of refraction of the gas. This, in turn, results in a change in the optical path for the beam going through the shock tube of an amount given by the relation $\Delta N_1 \cdot l_1 = K \Delta \rho l_1 = S\lambda$ where S is the number of fringes shifted, N_1 is the index of refraction of the gas, ρ the gas density, l_1 the length of the test

³⁵ H. Edels and D. Whittaker, *J. Sci. Instr.* **32**, 103 (1955).

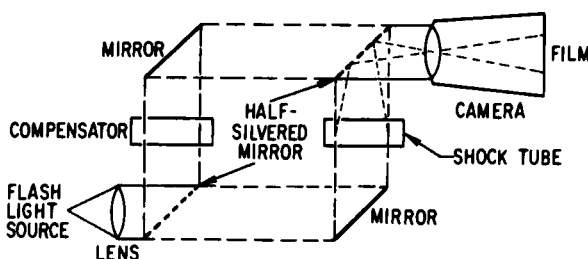


FIG. 24. Experimental arrangement for Mach-Zehnder interferometer.

section, and K is the Gladstone-Dale constant ($N_1 - 1/10$). The constant K , which is usually determined experimentally, depends on the wavelength of the light and nature of the gas but is essentially independent of the pressure. Immediately behind the shock wave a sudden large shift of the fringes is produced which is then followed by a smaller variation of fringe shifts due to either fluid dynamic variation of the density or chemical reaction. A typical interferogram of a shock wave in nitrogen is shown in Fig. 25. The slow variation of density behind the shock wave in this case

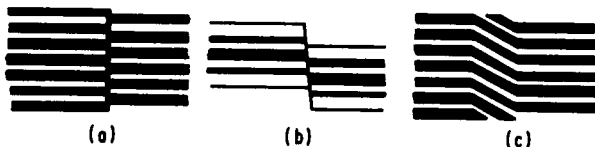


FIG. 25. Interferograms for three methods of tracing interference fringes: (a) normal appearance; (b) using "white" light source; (c) by means of offset fringes.

is due to vibrational relaxation of the nitrogen. The major limitation of interferometric techniques is that very small fringe shifts are obtained at low gas densities. The minimum fringe shift which can be measured is about 0.02 fringes. This implies density changes of the order of 0.0004 of the density of air at NTP. Since chemical reactions proceed more slowly at lower densities it is clear that many fast reactions cannot be investigated using this technique. The Mach-Zehnder arrangement has the advantage of a large field of view. Accordingly, the density distribution in the flow about models placed in the shock tube can be examined.

A different type of instrument is the chronointerferometer designed by Curtiss *et al.*³⁶ By the experimental arrangement shown in Fig. 26, a single

³⁶ C. W. Curtiss, R. J. Emrich, and J. Mack, *J. Rev. Sci. Instr.* **25**, 679 (1954).

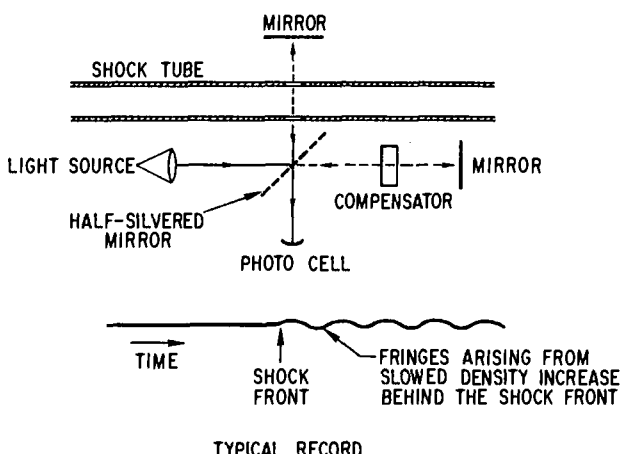


FIG. 26. Chronointerferometer.

fringe can be obtained over the entire field of view. The intensity of the fringe is then followed with a photomultiplier which records the maxima and minima in light output due to density changes across the test section. Density changes of the order of 10^{-5} gm/cm³ can be measured with this system. Although this is considerably less sensitive than the Mach-Zehnder interferometer it has the advantage that the density change can be followed for a longer time without loss in accuracy. Further, it is considerably lower in cost. For more details on interferometers the reader is referred to Greene and Toennies.²

7.7.2. Schlieren and Shadowgraphs*

Visualization of the shock wave formed about a model in a supersonic or hypersonic flow is of importance to aerodynamicists. Two relatively simple photographic techniques which permit this to be accomplished are the schlieren and shadowgraph techniques. The two methods depend on the refraction of light due to density gradients associated with the shock front. The refraction follows Snell's law; that is, $1/\bar{r} = \bar{N}$.

The shadowgraph method is illustrated in Fig. 27. A point light source and lens are used to produce a parallel beam of light which is passed through the test section. A very short duration flash lamp or spark is used to prevent smearing of the rapidly moving shock. A shock front passing through the test section will appear as two closely spaced lines, one being lighter and

* See also Volume 1, Sections 4.2.3.3 and 4.2.3.4, as well as Section 7.1.4.

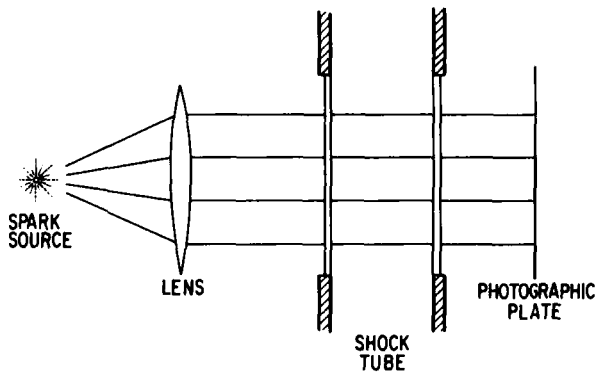


FIG. 27. Optical set-up for shadowgraph photography.

the other darker than the background and is accordingly easily visualized. For flow about models placed in a shock tube the shape of the shock wave can be seen.

The schlieren system is illustrated in Fig. 28. Here, the light source is focused at the center of the test section and passed through a second lens to a camera. A knife edge is placed behind the second lens so as to cut off approximately one-half of the cone of light. When a density gradient exists in the test section, due to a shock wave, say, the light is refracted and strikes more or less of the knife blade causing a change in the light intensity received by the camera. It can be shown that the change in light density on the photographic plate is related to the integrated gradient of the density in the test section. Figure 29 is a typical schlieren photograph.

The major limitation of both shadowgraph and schlieren photography is that relatively high gas densities are required. Accordingly, they cannot be used in hypersonic wind tunnels where the flow is expanded to very low

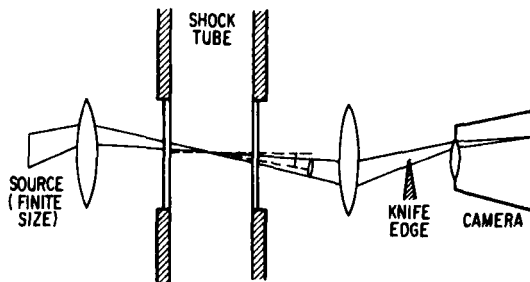


FIG. 28. Apparatus used for schlieren photography.

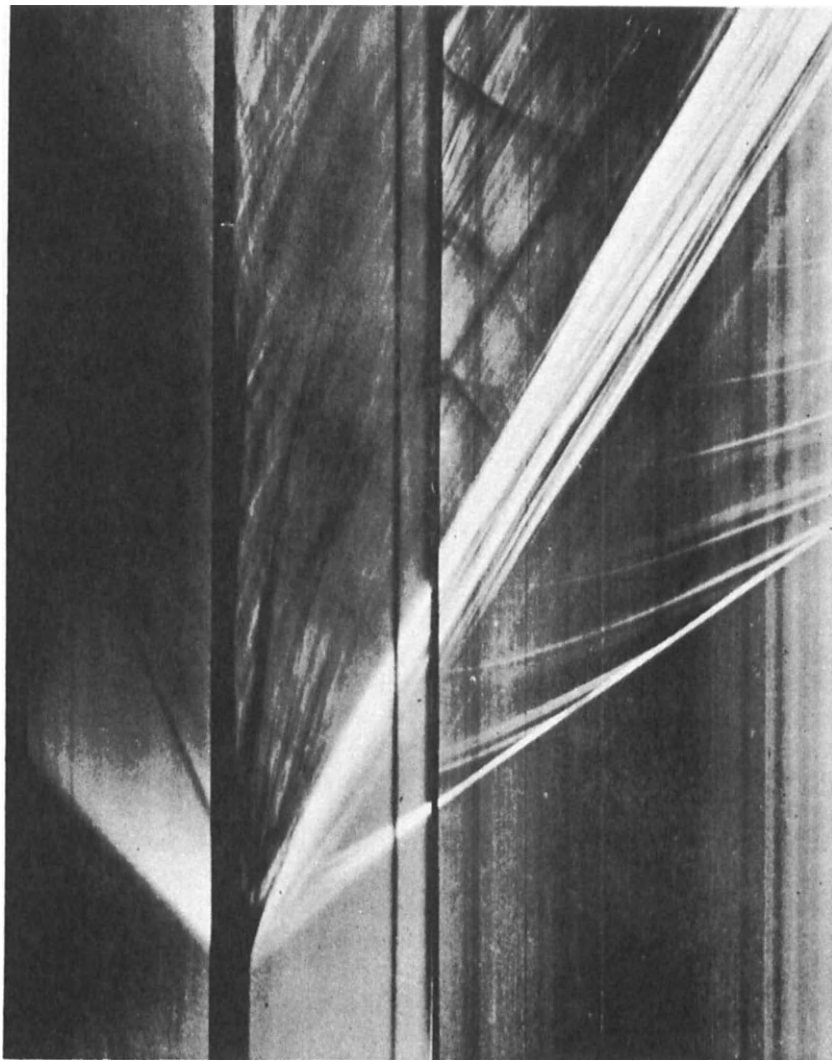


FIG. 29. A typical schlieren photograph.

densities, nor to visualize very weak shock waves. Additional details on these systems are given by Bradley¹ and Greene and Toennies.²

7.7.3. Optical Absorption Methods

The density of a gas may be determined by the amount of absorption of a light beam passed through it. The absorption coefficient of the particular molecules or atoms must be known as a function of temperature. The absorption is governed by the Beer-Lambert law,

$$\frac{I}{I_0} = \exp(-\alpha_t \rho_t x), \quad (7.7.1)$$

where α_t is the absorption coefficient, ρ_t the partial density of the particular species, x the path length, I the transmitted intensity, and I_0 the incident intensity. Use of this technique in the visible and ultraviolet regions is most prevalent because high-intensity light sources are readily available and absorption coefficients are large. In practice, an appropriate light source is well collimated in a narrow beam passed through the test section and received by a photomultiplier. For absorption continua, filters are used to isolate the appropriate spectral region, while for line spectra either a light source emitting the same lines or a high-resolution monochromator are used.

Absorption techniques in the vacuum ultraviolet have been used extensively. In this region of the spectrum absorption coefficients are large. Special windows must be used on the shock tube in order to transmit the vacuum ultraviolet radiation. CaF or LiF are used most often. The latter permits transmission down to 1000 Å. For still shorter wavelengths windowless techniques must be devised. Such a system is described by Gruszczynski *et al.*³⁷

Regarding the infrared region of the spectrum, considerable work has been done in recent years. The absorption coefficients in this spectral region are generally quite small. The development of rapid response, sensitive infrared detectors (such as gold-doped germanium and indium antimonide cells) has been largely responsible for the increased activity in this area.

Although optical absorption methods have been used to measure the total gas density behind shocks, they are primarily used to measure vibrational relaxation and chemical reaction rates. In these experiments the absorption of a particular species is measured as a function of time behind

³⁷ J. S. Gruszczynski, W. R. Warren, Jr., and D. A. Rogers, *Proc. Intern. Shock Tube Symp. 5th*, Preprint No. 317. U.S. Naval Ordnance Laboratory, Maryland, 1965.

a shock. The rate of formation or disappearance of the species is then readily deduced from these measurements.

Measurement of the radiation emitted from a shocked gas is also used to determine the high-temperature characteristics of gases and to obtain reaction rates. For cases where more than one species is present it must be assured that the other species do not contribute to the radiation being examined. Also, to establish concentration of the species of interest it must be demonstrated that there is no self-absorption of the radiation by the gas; that is, the gas must be optically thin to the particular radiation. Techniques for verifying this are described by Watson.³⁸ Examples of the use of absorption and emission techniques for the rate measurements in the various spectral regions are contained in the literature.³⁹⁻⁴¹

7.8. Electron Beam Densitometers

The absorption of an electron beam as it passes through a gas is related to the density by the Beer-Lambert law. This fact was first used to measure the density behind shocks by Venable and Kaplan.⁴² The method was then used by Duff⁴³ to study the flow behind shocks at low pressures. The electron beam enters the shock tube through a small hole, 0.1 mm diam, and its intensity after passing through the gas is measured by a photomultiplier coated with a liquid phosphor. Densities as low as 10^{-4} of NTP have been measured. It is to be remembered that the density measured is that integrated over the entire path. In attempts to measure shock-wave thickness using this method, the effects of shock curvature can lead to erroneous interpretation of the data. To circumvent this problem Camac⁴⁴ recently devised an ingenious method which measures the scattering of electrons from a small region of the shock front in the center of the tube. In this way, he was able to make the most accurate measurements of shock thickness available today.

Still another mode of utilizing electron beams to measure gas density is to measure the radiation emitted by the gas due to excitation by the electron beam.⁴⁵ The intensity of the radiation has been shown to depend

³⁸ R. Watson, *Proc. Intern. Shock Tube Symp. 5th*, Preprint No. 417, U.S. Naval Ordnance Lab., Maryland, 1965.

³⁹ S. A. Losev, *Dokl. Akad. Nauk. SSSR.* **120**, 1291 (1958).

⁴⁰ M. Camac and A. Vaughan, *J. Chem. Phys.* **34**, 460 (1961).

⁴¹ R. W. Patch, *J. Chem. Phys.* **36**, 1919 (1962).

⁴² D. Venable and D. E. Kaplan, *J. Appl. Phys.* **26**, 639 (1955).

⁴³ R. E. Duff, *Phys. Fluids* **2**, 207 (1959).

⁴⁴ M. Camac, *Phys. Fluids* **7**, 1076 (1964).

⁴⁵ E. P. Muntz, *Phys. Fluids* **5**, 80 (1962).

nearly linearly on the gas density. By focusing optics on a small portion of the beam path, very local measurements can be made. This method has been used very successfully in low-density arc tunnels and shock tunnels.⁴⁶ It is limited to use at very low densities, where the absorption of the electron beam is negligibly small.

It should be pointed out that if the electron beam is to be used to follow density changes due to chemical reaction, the absorption coefficient of each of the species formed must be known.

7.9. X-Ray Absorption

X-ray absorption as a means of gas density measurements was demonstrated by Kistiakowsky and Kydd.⁴⁷ Knight and Venable,⁴⁸ using a flash X-ray source, developed the method for shock tubes. Typically, higher densities are required to obtain measurable absorption than are determined by either optical or electron beam absorption. Accordingly, high mass number gases, such as Xenon, are used to increase the absorption.

7.10. Partial Density of Particular Species

It has been pointed out above that measurement of the concentration of a particular species behind a shock wave can be measured by optical absorption or emission. Another direct method for doing this is to use a time-of-flight mass spectrometer connected to the shock tube. In an early version of this experiment, Bradley and Kistiakowsky⁴⁹ put a small hole in the end wall of the shock tube through which the gas behind the reflected shock was passed into a time-of-flight mass spectrometer. The mass spectrum is sampled every 25 μ sec, so that reactions taking considerably longer than this can easily be followed. A major difficulty of this method is to assure that the gas reaching the spectrometer has not changed its composition in passing through the cool thermal boundary layer which grows with time from the end wall. Very careful design of the collection system and pressure range of the experiment is required. Bradley and Kistiakowsky established the useful range of their experiment by measuring the known dissociation rate of N_2O . Since their experiments, others have used this technique to measure molecule dissociation rates,⁵⁰ and to qualitatively identify intermediate radicals during the dissociation of complicated molecules.⁵¹

⁴⁶ E. P. Muntz and E. J. Softley, *AIAA J.* **4**, 961 (1966).

⁴⁷ G. B. Kistiakowsky and P. H. Kydd, *J. Chem. Phys.* **25**, 824 (1956).

⁴⁸ H. T. Knight and D. Venable, *Rev. Sci. Instr.* **29**, 92 (1958).

⁴⁹ J. N. Bradley, and G. B. Kistiakowsky, *J. Chem. Phys.* **35**, 256 (1961).

⁵⁰ R. W. Diesen and X. Felmlee, *J. Chem. Phys.* **39**, 2115 (1963).

⁵¹ A. Modica, *J. Chem. Phys.* **43**, 3383 (1965).

7.11. Temperature Measurement

Measurement of the temperature behind incident and reflected shock waves would be invaluable in establishing the true state of the gas as a function of time. Unfortunately, it is one of the more difficult measurements to obtain. Three broad techniques have been employed with varying degrees of success: (a) optical; (b) speed of acoustic waves; and (c) hot wires. The capability of each method to function over a wide range of temperatures and densities, as well as its spatial resolution, is an important consideration.

7.11.1. Optical Methods

One of the earliest approaches in this category is the line reversal technique.⁵² In this method the test gas is seeded with NaCl, which, upon being shocked, dissociates to give Na. If sodium line radiation is then passed from a light source (external to the shock tube) through the shocked gas, the atoms in the latter either emit or absorb radiation, depending upon whether the gas temperature is higher or lower than that of the source. By varying the source temperature for successive, identical shocks one encounters a case where the radiation from the light source is unaffected by the shocked gas. When this case is achieved, the temperature of the gas is that of the light source. Particular geometries of the optics are described by Bradley¹ and Greene and Toennies.²

The line reversal technique has been used to measure temperatures from about 2000–8000°K.⁵³ Recent experiments using Na in N₂ shocks indicate that the sodium line reversal temperature is the vibrational temperature of the nitrogen and not its translational temperature. In fact several other methods which rely on measurement of radiation from excited electronic states of trace contaminants introduced in a molecular test gas show that either the translation or vibrational temperature of the molecule is measured, depending upon the particular species involved.⁵⁴

Another optical method of measuring temperature is to determine the relative intensity of two lines of a known radiator. Some examples are the violet and green lines of Cr, rotational lines of CN, violet bands of OH, and vibrational lines of O₂.

⁵² J. G. Clouston, A. G. Gaydon, and I. I. Glass, *Proc. Roy. Soc. A248*, 429 (1958).

⁵³ A. R. Fairbairn, *Proc. Roy. Soc. A267*, 88 (1962); S. A. Losev and N. A. Generalov, *Instr. Exptl. Tech.(USSR)* (English Transl.) p. 454 (1959).

⁵⁴ A. G. Gaydon, Energy transfer in hot gases. *Natl. Bur. Std. Circ.* No. 523, 1 (1954).

7.11.2. Speed of Acoustic Waves

The speed of sound in a single component gas with a constant ratio of specific heat, γ , is

$$a = \left(\frac{\gamma RT}{M} \right)^{1/2}$$

where R is the universal gas constant and M the molecular weight. The time required for an acoustic wave generated by a spark, for example, to travel a known distance establishes the temperature. The sound wave can be followed by a pulsed schlieren system.⁵⁵ A more elaborate arrangement has been recently developed by Carnevale *et al.*⁵⁶ In this method a continuous train of acoustic waves is propagated across a square shock tube in the gas behind a reflected shock. The transit time to a receiver on the opposite wall is measured. Temperatures in argon up to 8000°K have been measured. For a dissociated gas, or one undergoing vibrational relaxation, the acoustic wave is dispersed⁵⁷ and the measurement becomes very difficult.

The absorption of the acoustic wave train has been used to determine the thermal conductivity of the gas behind a reflected shock.⁵⁶ This absorption is determined by the relation

$$\alpha = \frac{2\pi^2 f^2}{\gamma p a} \left[\frac{4}{3} \mu + \frac{(\gamma - 1)k}{c_p} \right]$$

where μ is the viscosity coefficient, k the thermal conductivity, and f the frequency of the acoustic wave.

7.11.3. Hot Wires

A more difficult method of determining temperature is to measure the heat transfer to hot wires placed in the flow.⁵⁸ This method requires considerable interpretation and is subject to errors in the transport coefficients which determine the heat transfer and uncertain atom recombination rates on the surface of the wire. A somewhat simpler application of hot wires is to measure temperature in the nonflowing region behind a reflected shock. In this case, the heating current through the wire is adjusted for a series of identical runs until no heat is transferred between the gas and wire. Under this condition, the gas and wire temperatures are equal.

⁵⁵ W. Smith, H. Glick, A. Hertzberg, and W. Squire, *Phys. Rev.* **98**, 1141 (1955).

⁵⁶ E. H. Carnevale, C. Carey, and T. Marshall, *Proc. Intern. Shock Tube Symp.* 5th U.S. Naval Ordnance Lab., Maryland, 1965.

⁵⁷ E. L. Resler, Jr., *J. Chem. Phys.* **25**, 1287 (1956).

⁵⁸ F. C. Dewey, Jr., *ARS (Am. Rocket Soc.) J.* **31**, 1709 (1961).

7.12. Application of Shock Waves to the Measurement of Basic Physical Properties

From the preceding chapters in this part, it is clear that the shock wave may be used to study many basic physical processes which elucidate both the structure of molecules and their interactions with atoms and electrons. The significant ingredient which shock waves add is the examination of these properties at high temperatures. Along with this, of course, is the fact that species characteristic of higher temperatures (atoms, radicals, and electrons) are easily produced behind shock waves. That they are produced thermally simplifies the analysis of their production.

The studies of high-temperature gas properties may be divided into two general categories: first, those where the gas is known to be in thermochemical equilibrium; and, second, the study of processes which lead to the approach to equilibrium. In the former category, one may establish the dissociation energy, radiation characteristics, and transport properties of high-temperature gases. While the latter may be used to determine the rates of chemical reactions including the rates of excitation of vibration and rotation of molecules. In the following paragraphs examples of each of these studies will be given. A much more detailed listing of these studies is given in Ref. 2.

7.13. Equilibrium Gas Studies

If a high-temperature gas is known to be in equilibrium, its chemical composition is known to be determined by any two thermodynamic variables (temperature and density, for example) if the dissociation (ionization) energies of all the molecules involved are known. Conversely, if any two thermodynamic variables and the species present at high temperature are known, dissociation (ionization) energies may be deduced. To determine this energy, it would be sufficient to shock a gas to such high temperatures and densities that one is assured equilibrium is achieved in the available test time, and measure the density behind the shock and velocity of the shock. The measured density is then compared to equilibrium shock calculations of its value behind that velocity shock assuming a variety of dissociation energies, D . Figure 30 illustrates such a comparison for the N_2 system. To cross check such a determination it would be advisable to measure some other sensitive thermodynamic variable (temperature, for example) or species concentrations. In the absence of the cross-check measurements, it is possible to assure that equilibrium has been achieved

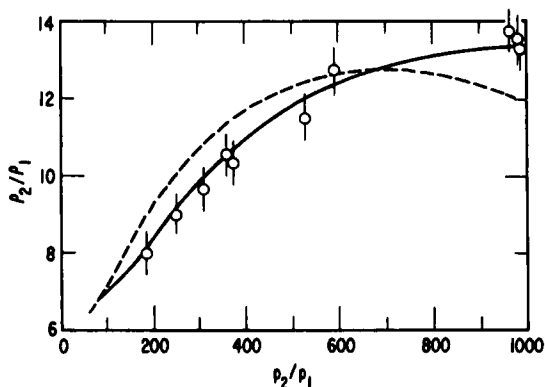


FIG. 30. Comparison of calculated shock relations for N_2 with experimental points. The solid curve is for $D(N_2) = 225$ and the dashed curve is for $D(N_2) = 170$ kcal/mole.

by significantly increasing the initial pressure of the experiment (thus reducing the dissociation relaxation time) and demonstrate that the same dissociation energy is derived. For very complicated molecules, where several dissociation processes of unknown energies take place, it becomes imperative to accompany the density measurements with those of species concentrations.

Transport properties of high-temperature gases may also be determined by shocking a gas to a known state of equilibrium. Several techniques are available to determine these properties. First, measurement of the heat transfer to the end wall of a shock tube (using thin film resistance thermometers) has been shown to lead to a measurement of the thermal conductivity of the gas. In this way, the thermal conductivity of high-temperature, partially dissociated oxygen⁵⁹ and partially ionized argons^{60,61} has been measured. In another series of experiments,⁶² it has been shown that the viscosity coefficient of high-temperature gases may be determined from measurements of the heat transfer to the side wall of a shock tube. Very recently a technique for determining thermal conductivity by measuring the absorption of acoustic waves across a gas sample behind a reflected

⁵⁹ F. C. Hansen, R. A. Early, F. E. Alsofon, and F. C. Witteborn, *NASA Tech. Rept. TR-R-27* (1959).

⁶⁰ E. F. Smiley, *The measurement of the thermal conductivity of gases at high temperature with a shock tube*. Thesis, Catholic Univ. of America Press, 1957.

⁶¹ M. Camac, J. A. Fay, R. M. Feinberg, and N. H. Kemp, *Proc. Heat Transfer Fluid Mech. Inst.* Paper No. 58. Stanford Univ. Press, Stanford, California, 1963.

⁶² R. A. Hartunian and P. V. Marrone, *Phys. Fluids* **4**, 535 (1961).

shock has been demonstrated.⁵⁸ Finally, a technique of generating a molecular beam in the 1-eV range has been under development.⁶³ In this method, the gas behind the reflected shock is permitted to escape through a small hole in the end wall of the shock tube and is then rapidly expanded to very low densities. A system of collector nozzles is then used to form the beam. By allowing such a beam to impinge upon a gas sample and measuring the scattering angles, basic cross sections may be derived for use in transport property calculations. This technique complements more classical molecular beam methods, which are generally limited to a fraction of one or many tens of electron volts.

Another class of basic measurements to which shock-tube techniques are particularly amenable is that of radiative characteristics of high-temperature gases. A very extensive literature exists on this subject.^{1, 2} Specifically, absorption and emission spectra may be obtained and in many cases the *f* number of certain radiative transitions may be determined. Again, the ability of the shock tube to produce radicals characteristic of high-temperature gases gives it a unique position which complements the more classical electron beam excitation-radiative lifetime measurements approach. The latter method is limited to those species characteristic of room, or, at best, oven temperatures. It should be pointed out that to obtain spectra of very-high-temperature gases in the far ultraviolet, windowless techniques must be developed, since the best windows available at present transmit radiation only down to about 1000 Å. Methods of making these measurements have recently been developed.^{37, 64} Many precautions must be observed in such methods, as discussed in these references.

7.14. Approach to Equilibrium

One of the largest contributions of shock-tube techniques to the understanding of atomic and molecular processes has been its application to the measurement of the time required to achieve molecular vibrational, dissociation, and ionization equilibrium behind the shock wave. The process of going from some nonequilibrium state to equilibrium is called relaxation. As mentioned in an earlier section, energy transfer processes within and immediately behind the shock wave lead to the achievement of translational relaxation and, most generally, rotational relaxation (for molecules). Although some measurements of the rotational relaxation time have been made, most experiments have been concerned with vibrational, dissociation, and ionization relaxation. For a diatomic molecule, then, collisions at

⁶³ G. T. Skinner, *Phys. Fluids* **8**, 452 (1965).

⁶⁴ J. S. Gruszynski *et al.*, Fast response total radiation gage for measurement of radiant emission from high temperature gas, *IEEE Paper* CP 63-438 (1963).

the high temperature right behind the shock cause the vibrational levels to become populated. The rate at which this occurs and the fundamental processes involved are the subject of several theories.⁶⁵⁻⁶⁷ Of course, each theory has assumptions related to the mechanism itself, as well as the nature of basic molecular forces. The temperature dependence of vibrational relaxation is one important result of each theory which can be tested. It is this aspect which shock-tube measurements over a wide range of temperatures can be most useful, since other techniques for measuring vibrational relaxation times⁶⁸ have been limited to the low-temperature range. Vibrational relaxation times have been determined in shock tubes by measuring the density⁶⁹ or temperature⁷⁰ profiles behind the shock. Details of how these profiles are employed to deduce the relaxation time are given in those references and have been briefly reviewed by Bradley¹ on p. 190. A more direct approach to establishing the basic mechanism of vibrational relaxation is to measure the rate of population of specific vibrational levels. This can be done by measuring the light emission or absorption of transitions involving these levels.^{71,72} Of course, such measurements are quite difficult and must be carefully interpreted. The development of more sensitive detectors is making these measurements feasible for a broader range of gases. Still another technique for measuring vibrational relaxation times for some systems was developed by Millikan and White.⁷³ In one particular case, CO was used as a tracer to follow N₂ vibrational relaxation. Because of a resonance in the vibrational energies between the two molecules, the N₂ vibrational energy is rapidly transferred to CO. The latter conveniently emits radiation in the infrared of a magnitude which is easy to follow. This general method of using appropriate tracers is very promising. Although existing measurements have not been able to evaluate the validity of any one theory, they are generally correlated on the basis of the relaxation time varying as $\tau = A \exp(T^{-1/3})$ where τ is the relaxation time, p the pressure, and A is a constant peculiar to the particular molecules and gas. The latter may be obtained for many systems from the compilation given by Millikan and White.⁷³

⁶⁵ L. Landau and E. Teller, *Physik. Z. Sowjetunion* **10**, 34 (1936).

⁶⁶ J. M. Jackson and N. F. Mott, *Proc. Roy. Soc. A* **317**, 703 (1932).

⁶⁷ Z. Slawsky, R. N. Schwartz, and K. F. Herzfeld, *J. Chem. Phys.* **20**, 1591 (1952).

⁶⁸ K. F. Herzfeld and T. A. Litovitz, "Absorption and Dispersion of Ultrasonic Waves," Academic Press, New York, 1959.

⁶⁹ V. Blackman, *J. Fluid Mech.* **1**, 61 (1956).

⁷⁰ J. G. Clouston, A. G. Gaydon, and I. I. Glass, *Proc. Roy. Soc. A* **248**, 429 (1958).

⁷¹ M. W. Windsor, N. Davidson, and R. L. Taylor, *J. Chem. Phys.* **27**, 315 (1957).

⁷² J. P. Appleton and M. Steinberg, Tech. Rept. 60-01M. Gen. Motors Defense Res. Lab. 1966.

⁷³ R. C. Millikan and D. R. White, *J. Chem. Phys.* **39**, 98 (1963).

Dissociation relaxation times are measured most generally by following the decay of one of the reactants or the rate of formation of a product by optical emission or absorption. To make these measurements quantitative it is essential to know the emissivity or absorptivity of the species in the temperature range of the experiments. These are generally obtained as an adjunct to the dissociation rate measurements. It is desirable to operate the shock tube under conditions such that the dissociation reaction goes to complete equilibrium within the available test time, since the number density of each species can be calculated quite accurately (for those gases where the thermodynamic data are not in doubt). This measurement of the equilibrium number density can then serve as a calibration for the measurement during the nonequilibrium part of the trace. Supporting measurements of the density and temperature profiles are certainly advisable whenever they can be made. In many cases^{74,75} these measurements have been used alone to deduce the dissociation rate. The dissociation rate, k_f , for simple molecules varies with temperature as $k_f \sim T^{-n} \exp(-E/kT)$ where E is the activation energy and k is Boltzmann's constant. Since the exponential factor overwhelms the pre-exponential temperature dependence, a plot of $\log k$ versus $1/T$ (an Arrhenius plot) provides an essentially straight line whose intercept yields the activation energy. Although the activation might be thought to be the dissociation energy, this is not generally the case. The activation energy turns out to be less by a couple of kT , which represents energy absorbed in filling vibrational levels. The exponent n is generally evaluated by comparing high-temperature measurements with room-temperature values. The recombination rate, k_r , for a simple molecule is deduced from the measured dissociation rate and the known equilibrium constant, K , where $K = k_r/k_f$. Since K has an exponential temperature dependence similar to k_f , it follows that $k_r \sim T^{-m}$, where m is a constant related to n . It is clear that any method of measuring the recombination rate of atoms to form a molecule over a significant temperature range is an inherently more accurate way of establishing the pre-exponential temperature dependence of k_f . It is this factor over which the various theories disagree. Several methods exist for measuring the recombination rate at high temperature directly, but few measurements have actually been made to date. In the work of Wray,⁷⁶ O_3 was shocked, which rapidly produced O atoms behind the shock. The atoms then recombined to form O_2 , which was followed by optical techniques. Other methods use a reflected shock to get the gas in a state of dissociated equilibrium and then rapidly

⁷⁴ S. R. Byron, *J. Chem. Phys.* **30**, 1380 (1959).

⁷⁵ A. G. Gaydon and I. R. Hurle, *Symp. Combustion, 8th Pasadena, Calif.*, 1960, p. 309. Williams & Wilkins, Baltimore, Maryland, 1962.

⁷⁶ K. L. Wray, *J. Chem. Phys.* **38**, 1518 (1963).

cool this gas to force recombination. The cooling may be achieved by rapidly expanding the gas through a flow nozzle⁷⁷ or by using a steady⁷⁸ or nonsteady⁷⁹ expansion wave. The latter technique has the advantage that only one observation station is required. Although only preliminary data have been obtained using these techniques, they appear to afford one of the few methods of accurately obtaining the pre-exponential temperature dependence. Still another method is described by Hartunian and Thompson.⁸⁰ In this approach, a classical glow discharge tube, in which a gas is flowed slowly past a microwave or rf discharge section to produce some atoms, is used. The predissociated gas is then shocked, which causes the temperature and density to rise. The density increase forces recombination to proceed.

One important factor to consider in both dissociation and recombination measurements is that during these reactions the gas temperature is changing by the heat absorbed or released by the reaction. These changes must be factored into the data reduction. A technique used most often to minimize the temperature change is to use a small percentage of the reacting species in a large concentration of a monatomic gas (Argon, e.g.). The latter serves as an isothermal heat bath. The disadvantage of this method is that the dissociation rate depends on the collision partner, which in these cases would be largely the monatomic gas. By increasing the concentration of reactants in succeeding runs and carefully correcting for temperature changes the effect of other collision partners may be evaluated.

It should be pointed out that at high temperatures, the various relaxation times become of the same order of magnitude. In such cases the various processes become coupled. This seriously complicates the reduction of data, but, of course, provides very fundamental information related to the entire process by which a gas dissociates. Experiments clearly showing this coupling are reported by Wray,⁸¹ and theories are being developed to explain it.^{82,83}

The determination of ionization rates proceeds along the same lines described for the other relaxation processes. For monatomic gases (Argon,

⁷⁷ I. R. Hurle, A. L. Russo, and J. G. Hall, Experimental studies of vibrational and dissociative nonequilibrium in expanded flows. *AIAA Conf. Phys. Entry Planetary Atmospheres, Boston*, 1963.

⁷⁸ J. Wilson, *J. Fluid Mech.* **15**, 497 (1963).

⁷⁹ T. A. Jacobs, R. A. Hartunian, R. R. Giedt, and R. Wilkins, *Phys. Fluids* **6**, 972 (1963).

⁸⁰ R. A. Hartunian and W. P. Thompson, *Proc. Intern. Shock Tube Symp.* 5th p. 209. U.S. Naval Ordnance Lab., Maryland, 1965.

⁸¹ K. L. Wray, *J. Chem. Phys.* **37**, 1254 (1962).

⁸² J. Keck and G. Carrier, *J. Chem. Phys.* **43**, 2284 (1965).

⁸³ C. E. Treanor and P. V. Marrone, *Phys. Fluids* **5**, 1022 (1962).

Xenon, etc.) the process is more straightforward than for diatomic gases. For the latter, the dissociation process is involved and the ionization may occur from the molecules or atoms. An examination of Ref. 84 indicates how complicated the process gets for even so apparently simple a system as air. In most cases, the rate of ionization is deduced from measurements of the rate of formation of electrons behind the shock wave. Earliest experiments used probes which measured the gas conductivity as a function of time.^{84,85} The use of microwave absorption and optical techniques is becoming more widespread.⁸⁶⁻⁸⁸ Since the ionization potential of many trace contaminants, such as the alkali metals, is much lower than many molecules extra care as to the purity of the gas sample must be exercised. Indeed, in all of the relaxation processes, trace contaminants of any type can lead to serious error, so that strong efforts must be made to minimize or, hopefully, evaluate these effects.

It is clear that the interpretation of measurements for all the relaxation processes is quite complicated in most cases, since many things are changing during relaxation. The use of computer programs for nonequilibrium flow behind shock waves has contributed significantly in this area. These programs solve simultaneously the equations of motion, energy continuity, and state, together with those governing the rates of chemical reactions (law of mass action) as a function of distance behind the shock. Typically, the programs are written to include many arbitrary reactions (vibrational relaxation is included as a reaction), with the rate constants expressed as functions of temperature. The thermodynamic information (dissociation and vibration energies, specific heats, etc.) for most known molecules are carried on a separate tape. As an input to the computer, one merely states the gas, initial pressure, and shock velocity, and the computer reads out profiles of species, flow, thermodynamic properties behind the shock. By varying estimates of the assumed rates, those which lead to agreement with the experimental measurement are obtained. Sensitivity of the results to uncertainty in the rates is also easily assessed.

ACKNOWLEDGMENT

The author would like to express his appreciation to Drs. W. P. Thompson and T. A. Jacobs for critically reviewing the manuscript. He is also grateful to Dr. H. Mirels for his contribution to the chapter. Finally, thanks are due to Miss S. E. Chambers and Mrs. R. J. Nichols for assistance in preparation of the manuscript.

⁸⁴ L. Lamb and S. C. Lin, *J. Appl. Phys.* **28**, 754 (1957).

⁸⁵ H. E. Petschek and S. Byron, *Ann. Phys. (N.Y.)* **1**, 270 (1957).

⁸⁶ R. G. Jahn, *Phys. Fluids* **5**, 678 (1962).

⁸⁷ K. Harwell and R. G. Jahn, *Phys. Fluids* **7**, 214 (1964).

⁸⁸ R. A. Alpher and D. R. White, *Phys. Fluids* **2**, 162 (1959).

8. FLAME KINETIC STUDIES*†

8.1. Introduction

In recent years flames have become a reliable source for high-temperature chemistry studies and for chemical kinetic data. This relatively new branch of chemistry derives from the different thermodynamic stabilities that may arise at elevated temperatures. Different oxidation states become stable as compared with the commonly known ones existing at lower temperatures. Ionization and electronic excitation can occur, thus changing the flame into a gaseous flowing plasma. At present the greatest interest is in study of simple collision processes which occur in flames, aimed at obtaining values for reaction cross sections at elevated temperatures (1000–5000°K).

"Flame" is a rather loosely used expression and covers such phenomena as atomic flames and afterglows, cool flames, diffusion flames, flash photolysis, and plasma jets, besides the common "hot" self-propagating flame. Although the latter type will be emphasized, kinetic studies in other systems will be included where relevant to the general discussion.

In order to extract kinetic data from flames it is necessary to simplify the system as much as possible. Consequently, simple fuels (some of which result in far from simple systems) have been used in the hope that not too great a mixture of species exist in the burnt gases. It is possible to burn flames in a variety of ways. The gas flow can be laminar or turbulent; the fuel and oxidant can either be premixed or mix as they burn. The pressure of the surrounding atmosphere can be varied over a wide pressure range (0.1 Torr to 50 atm) and the temperature is variable from 1000 to 6000°K. The most readily interpretable flame is steady, flat, and premixed.

Flame kinetic studies depend upon knowledge of the flame system, of the species present, and of the reactions involved. Little progress had been made until mass spectrometry and probe techniques came to the aid of the optical spectroscopist and the analytical chemist. A good understanding of some flames now exists. For example, the hydrogen-oxygen system is sufficiently understood so that studies of the basic flame itself are no longer

† Supported in part by the Advanced Research Projects Agency and the Office of Naval Research.

* Part 8 is by K. Schofield and H. P. Broida.

necessary. Instead, this flame can be used as a high-temperature, gaseous, wall-less vessel containing species of known behavior and concentration. Controlled amounts of trace additions to the flame initiate new reactions but leave the basic flame unperturbed.

Until recently there were few books pertinent to this field except those of Gaydon¹ and Wolfhard.² However, two new books have been published by Fenimore³ and by Fristrom and Westenberg.⁴ Each tends to be confined to the authors' particular interests, techniques, and research experience but are quite useful as reference works. In addition, the bound volumes of papers presented at the biannual international symposia on combustion⁵ are an invaluable source of information on all aspects of combustion.

8.2. Flames and Their Composition

8.2.1. General

Many techniques are used in combustion studies. Spectroscopy is a major tool and the spectral regions now in use range from the ultraviolet through to the infrared in both absorption and emission. However, it is the mass spectrometer† which has given the recent impetus to combustion research. Coupled with the microprobe method of sampling from flames,

¹ A. G. Gaydon, "The Spectroscopy of Flames." Chapman & Hall, London, 1957.

² A. G. Gaydon and H. G. Wolfhard, "Flames, Their Structure, Radiation and Temperature," 2nd ed. Chapman & Hall, London, 1960.

³ C. P. Fenimore, Chemistry in premixed flames. "The International Encyclopedia of Physical Chemistry and Chemical Physics," Vol. 5, Topic 19. Macmillan, New York, 1964.

⁴ R. M. Fristrom and A. A. Westenberg, "Flame Structure." McGraw-Hill, New York, 1965.

⁵ *Symp. Combust.*

1st, Massachusetts, 1928. Combust. Inst., Pittsburgh, Pennsylvania, 1965;

2nd, Rochester, New York, 1937. Combust. Inst., Pittsburgh, Pennsylvania, 1965;

3rd, Madison, Wis., 1948. Williams & Wilkins, Baltimore, Maryland, 1949;

4th, Cambridge, Mass., 1952. Williams & Wilkins, Baltimore, Maryland, 1953;

5th, Pittsburgh, 1954. Reinhold, New York, 1955;

6th, Yale Univ., 1956. Reinhold, New York, 1957;

7th, London, Oxford, 1958. Butterworths, London, 1959;

8th, Pasadena, Calif., 1960. Williams & Wilkins, Baltimore, Maryland, 1962;

9th, Cornell Univ., Ithaca, N.Y., 1962. Academic Press, New York, 1963;

10th, Univ. Cambridge, Cambridge, Engl., 1964. Combust. Inst., Pittsburgh, Pennsylvania, 1965;

11th, Univ. of California, Berkeley, Calif., 1966. Combust. Inst., Pittsburgh, Pennsylvania, 1967.

† See Vol. 3, Part 5.

mass spectroscopy allows analysis of a flame's stable species concentrations at any point. Moreover, charged species in flames can be observed readily. Gas chromatography can also be used to analyze the stable species while electron spin resonance† permits detection of free radicals. Langmuir probes have been successful in several investigations to give estimates of electron and ion concentrations throughout the flame. Radio-frequency and microwave methods also are available for electron concentration determinations.

Reaction zones of premixed stationary flames generally are thin at atmospheric pressure (0.1 mm in a H₂/O₂ flame). However, the thickness of the reaction zone is a function of burning velocity and pressure. Low-burning-velocity (10 cm sec⁻¹) flames have reaction zones several millimeters thick while for faster burning mixtures reaction zones are thin unless the flame is at reduced pressure. In the short distance of the reaction zone, very fast bimolecular reactions raise the temperature from the slightly preheated temperature to a value very close to the final flame temperature. Downstream from this is the burnt gases region, which can extend for many centimeters, and in which the final approach to full equilibrium takes place.

Fast-burning atmospheric mixtures are generally used for burnt gas studies while slow-burning atmospheric mixtures and low-pressure flames are used for reaction zone studies.

8.2.1.1. Flame Sources. The common burners producing flat flames suitable for kinetic studies are those of Gaydon,⁶ Powling,⁷ Egerton and Thabet,⁸ Botha and Spalding,⁹ and Padley and Sugden.¹⁰ The first burner is useful only at low pressure, the middle two at both low and atmospheric pressure, while the last is limited to atmospheric pressure studies. These burners are illustrated in Fig. 1.

For low-pressure studies, ordinary tube-type burners have been used a great deal. Owing to the quenching effects as the pressure is lowered, tubes of wide diameter are required to maintain stable flames. Such a basic burner, developed by Gaydon and Wolfhard,⁶ is shown in Fig. 1a. By controlling the flow, the flame can be varied from a cone or a hemisphere to a flat disk.

The Egerton-Powling burner,^{7, 8} Fig. 1b, produces a flat and disk-shaped flame. Since the flame burns under approximate adiabatic conditions, care

⁶ A. G. Gaydon, *Quart. Rev. (London)* **4**, 1 (1950).

⁷ J. Powling, *Fuel* **28**, 25 (1949).

⁸ A. Egerton and S. K. Thabet, *Proc. Roy. Soc. A211*, 445 (1952).

⁹ J. P. Botha and D. B. Spalding, *Proc. Roy. Soc. A225*, 71 (1954).

¹⁰ P. J. Padley and T. M. Sugden, *Proc. Roy. Soc. A248*, 248 (1958).

† See also Vol. 3, Chapter 4.2.

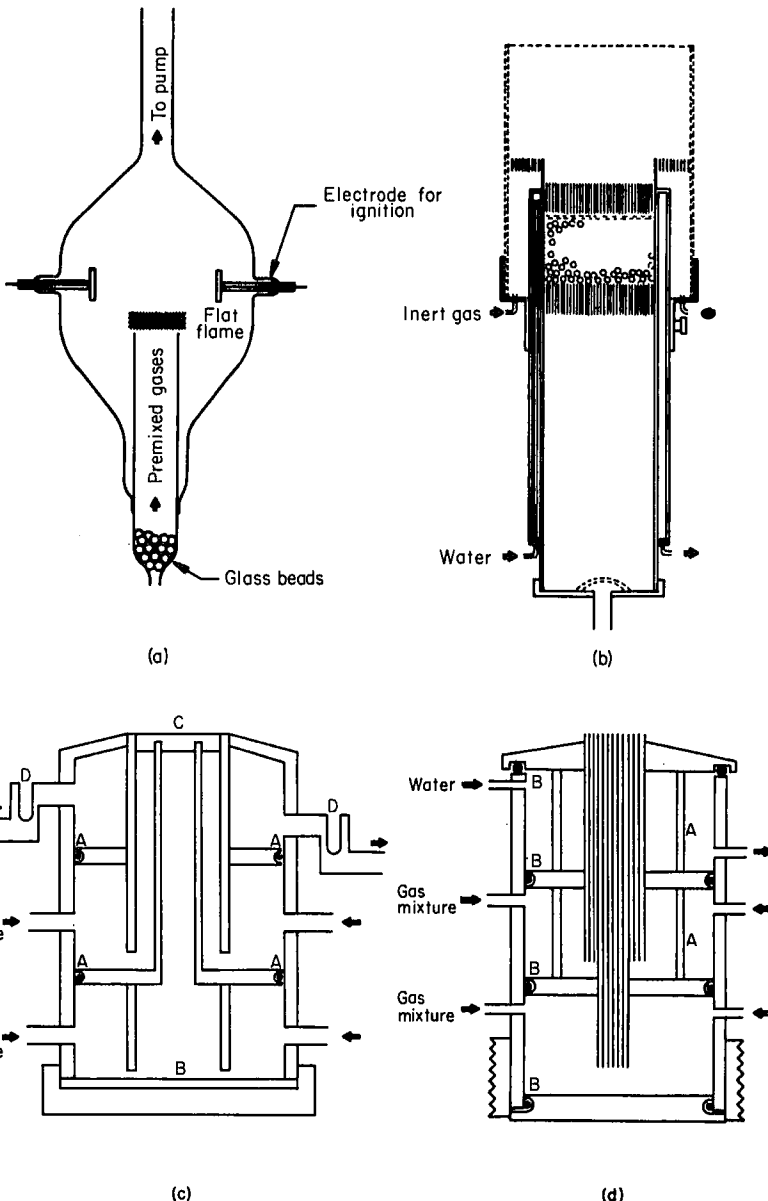


FIG. 1a. Gaydon-Wolfhard burner for low-pressure flames [from A. G. Gaydon, *Quart. Rev. (London)* 4, 1 (1950)]. FIG. 1b. Egerton-Powling burner [from J. Powling, *Fuel* 28, 25 (1949)]. FIG. 1c. Botha-Spalding burner: A, "O" ring seals; B, neoprene pad; C, brass sinter disk; D, thermocouple cups [from J. L. J. Rosenfeld and T. M. Sugden, *Combust. Flame* 8, 37 (1964)]. FIG. 1d. Modified Sugden burner: A, rod supports; B, "O" ring seals.

has to be taken to balance the stream velocity against the burning velocity. Mixtures having burning velocities from 4 to 12 cm sec⁻¹ can be maintained on such a burner. Dixon-Lewis¹¹ and co-workers have used such a burner with the modification of an electrically heated top gauze.

The Botha-Spalding burner,⁹ Fig. 1c, is more versatile and since the flame is under nonadiabatic conditions it can maintain flames of burning velocities in the range 4–38 cm sec⁻¹. Laminar flat flames are produced by having a water-cooled porous metal plate for the top of the burner. The flame sits downstream from this plate, stabilized by heat loss to the burner. Fristrom has used a modification which forms spherical flames.¹² The burner can be used at reduced pressure as shown in Fig. 2.

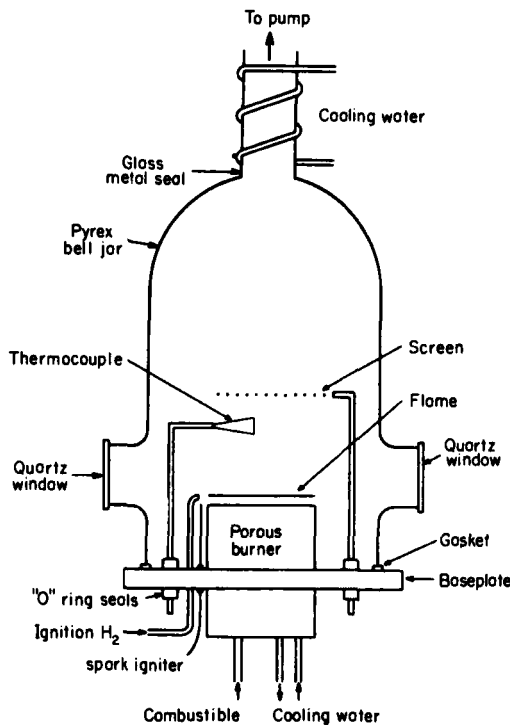


FIG. 2. Low-pressure burner [from W. E. Kaskan, *Combust. Flame* 2, 229 (1958)].

The Sugden¹⁰ burner, Fig. 1d, used for atmospheric pressure studies, produces laminar flow for flames covering a wide range of burning velocity, up to many hundreds of centimeters per second. Small primary cones

¹¹ G. Dixon-Lewis and G. L. Isles, *Trans. Faraday Soc.* 53, 193 (1957).

¹² R. M. Fristrom, *Combust. Flame* 2, 103 (1958).

emerge from each of the hypodermic tubes and are adjusted to be about 0.5 mm high. Under these conditions it is found that the tops of the cones tend to merge together to produce a relatively flat reaction zone. It is helpful to surround the experimental flame with one of the same composition, so that the inner flame is shielded from indrawn air and no discontinuity exists on its boundary.

In many kinetic studies, additives are introduced into the flame, generally only as trace quantities of the flame gases (i.e., 1 part in 10^5 to 10^9). Salts can be added as an aqueous spray,¹³ and liquids by saturating a fraction of the gas flow with the vapor.

8.2.1.2. Equilibria and Nonequilibria in Flames. Since flames do not attain but only approach full thermodynamic equilibrium, chemical thermodynamic calculations can be made at best with only a limited and known error. Sugden¹⁴ pointed out that, for chemical reactions, generally it is possible to make sensible estimates for the time to approach close to equilibrium. For fast chemical reactions such as



in atmospheric flames, approximately 1 μsec is required.

There are several distinguishable types of nonequilibria in flames that are important under different flame conditions.

8.2.1.2.1. CHEMICAL NONEQUILIBRIUM. This generally arises through the large buildup of atoms and radicals that can take place in the reaction zone of flames and through the slow recombination reactions that remove such excesses.

8.2.1.2.2. THERMAL NONEQUILIBRIUM. At atmospheric pressure, flame particles suffer around 10^9 collisions/sec. Since translation and rotational energies relax rapidly, needing only 1 to 10 and 1 to 100 collisions, respectively, to attain a thermal or Maxwell-Boltzmann distribution, such energy is equipartitioned quickly. Vibrational relaxation can be a considerably slower process. However, in a medium containing effective collision relaxers, such as H_2O , vibrational relaxation is more rapid than in simple gases.

¹³ R. Herrmann and C. T. J. Alkemade, "Chemical Analysis by Flame Photometry," 2nd ed., p. 97 (translated by P. T. Gilbert, Jr.). Wiley (Interscience), New York, 1963.

¹⁴ T. M. Sugden, *Trans. Faraday Soc.* **52**, 1465 (1956).

Consequently vibrational nonequilibrium can only exist in the early stages of the reaction zone of atmospheric pressure flames.¹⁵

As the pressure is lowered, and so the number of gas collisions, it is possible to observe a breakdown of equipartition; temperature measurements^{1, 2} based on rotational or vibrational populations can give meaningless "effective" temperatures or the system can show a non-Maxwellian distribution.¹⁶

8.2.1.2.3. RADIATIVE NONEQUILIBRIUM. Gaydon^{1, 2} stresses the importance, particularly at low pressure, of radiation from flames not being balanced by absorption as a cause of nonequilibrium. In most atmospheric pressure flames, however, the radiation process is of small importance compared to the activation and deactivation processes.

8.2.1.2.4. ELECTRONIC NONEQUILIBRIUM. This is very common in the reaction zone of flames, but also can exist in the burnt gases. It results from the chemiluminescent formation of excited electronic states.

8.2.1.2.5. ELECTRON NONEQUILIBRIUM. Two types of electron non-equilibrium concentrations exist in flames; excesses and deficiencies. The former result from chemi-ionization processes, the latter from kinetically slow ionization processes.

8.2.1.3. Flame Composition. **8.2.1.3.1. MAJOR STABLE SPECIES.** In some mixtures, major stable species concentrations can be calculated by assuming chemical and thermodynamic equilibrium; in others, experimental determinations are required. Provided reactions are fairly well equilibrated, as in the burnt gases of atmospheric pressure H_2/O_2 , CO/O_2 , and $CO/H_2/O_2$ flames, the major species concentrations are readily calculated from available thermodynamic data.² A lack of chemical equilibrium amongst the small concentrations of atomic and radical species will often have only a small effect, and is generally negligible. Results of such calculations for a series of fuel-rich $H_2/O_2/N_2$ flames are illustrated in Fig. 3. If carbon fuels are considered, it is assumed that these are burnt completely and no partially oxidized species other than CO are considered. Weinberg¹⁷ has modified the method, establishing explicit equations for C/H/O and C/H/O/N systems which are free of solid matter.

Reaction zone regions require direct measurements and in low-pressure and low-burning-velocity atmospheric pressure flames, stable species concentrations have been obtained through microprobe sampling which "freezes" the high-temperature reactions. Analytical means such as mass spectrometry, gas chromatography, gravimetric, or volumetric analysis are

¹⁵ K. E. Shuler and H. P. Broida, *J. Chem. Phys.* **20**, 1383 (1952).

¹⁶ H. P. Broida and D. F. Heath, *J. Chem. Phys.* **26**, 223 (1957).

¹⁷ F. J. Weinberg, *Proc. Roy. Soc. A* **241**, 132 (1957).

then applied to the sample.¹⁸⁻⁴⁰ With the exception of infrared absorption,^{41, 42} optical spectroscopy has been little used to determine stable species.

8.2.1.3.2. ATOMS AND RADICALS. Although atoms and radicals in flames are minor constituents, a knowledge of their concentrations and life history is essential for an understanding of combustion itself, and also for providing a means of obtaining collision cross sections for reactions involving these species with other particles at flame temperatures. Owing to their activity, concentration determinations are difficult, but in recent years several methods have been developed. Except for electron spin resonance techniques and certain spectroscopic determinations, most of the

- ¹⁸ G. Dixon-Lewis and A. Williams, *Symp. Combust., 9th, Cornell Univ., Ithaca, N.Y., 1962*, p. 576. Academic Press, New York, 1963.
- ¹⁹ G. Dixon-Lewis, M. M. Sutton, and A. Williams, *Symp. Combust., 10th, Univ. Cambridge, Cambridge, Engl., 1964*, p. 495. Combust. Inst., Pittsburgh, Pennsylvania, 1965.
- ²⁰ G. Dixon-Lewis, M. M. Sutton, and A. Williams, *Trans. Faraday Soc.* **61**, 255 (1965).
- ²¹ R. M. Fristrom, R. Prescott, and C. Grunfelder, *Combust. Flame* **1**, 102 (1957).
- ²² R. M. Fristrom, W. H. Avery, and C. Grunfelder, *Symp. Combust., 7th, London, Oxford, 1958*, p. 304. Butterworths, London, 1959.
- ²³ R. M. Fristrom and A. A. Westenberg, *Symp. Combust., 8th, Pasadena, Calif., 1960*, p. 438. Williams & Wilkins, Baltimore, Maryland, 1962.
- ²⁴ R. M. Fristrom, C. Grunfelder, and S. Favin, *J. Phys. Chem.* **64**, 1386 (1960).
- ²⁵ A. A. Westenberg and R. M. Fristrom, *J. Phys. Chem.* **64**, 1393 (1960).
- ²⁶ R. M. Fristrom, *Symp. Combust. 9th, Cornell Univ., Ithaca, N.Y., 1962*, p. 560. Academic Press, New York, 1963.
- ²⁷ R. M. Fristrom, *Science* **140**, 297 (1963).
- ²⁸ A. A. Westenberg and R. M. Fristrom, *Symp. Combust., 10th, Univ. Cambridge, Cambridge, Engl., 1964*, p. 473. Combust. Inst., Pittsburgh, Pennsylvania, 1965.
- ²⁹ C. P. Fenimore and G. W. Jones, *J. Phys. Chem.* **61**, 651 (1957).
- ³⁰ C. P. Fenimore and G. W. Jones, *J. Phys. Chem.* **62**, 178 (1958).
- ³¹ C. P. Fenimore and G. W. Jones, *J. Phys. Chem.* **62**, 693 (1958).
- ³² C. P. Fenimore and G. W. Jones, *J. Phys. Chem.* **63**, 1154 (1959).
- ³³ C. P. Fenimore and G. W. Jones, *J. Phys. Chem.* **63**, 1834 (1959).
- ³⁴ C. P. Fenimore and G. W. Jones, *Symp. Combust., 8th, Pasadena, Calif., 1960*, p. 127. Williams & Wilkins, Baltimore, Maryland, 1962.
- ³⁵ C. P. Fenimore and G. W. Jones, *J. Phys. Chem.* **65**, 298 (1961).
- ³⁶ C. P. Fenimore and G. W. Jones, *J. Phys. Chem.* **65**, 993 (1961).
- ³⁷ C. P. Fenimore and G. W. Jones, *Symp. Combust. 9th, Cornell Univ., Ithaca, N.Y., 1962*, p. 597. Academic Press, New York, 1963.
- ³⁸ R. Prescott, R. L. Hudson, S. N. Foner, and W. H. Avery, *J. Chem. Phys.* **22**, 145 (1954).
- ³⁹ R. Friedman and J. A. Cyphers, *J. Chem. Phys.* **23**, 1875 (1955).
- ⁴⁰ T. A. Milne and F. T. Greene, *Symp. Combust., 10th, Univ. Cambridge, Cambridge, Engl., 1964*, p. 153. Combust. Inst., Pittsburgh, Pennsylvania, 1965.
- ⁴¹ R. C. Millikan, *Combust. Flame* **5**, 349 (1961).
- ⁴² R. C. Millikan, *J. Phys. Chem.* **66**, 794 (1962).

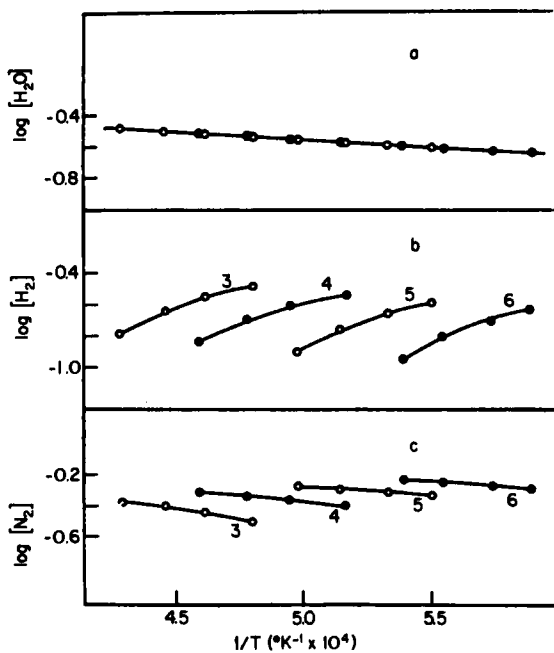


FIG. 3. Composition of burnt flame gases for the major constituents (a) H_2O , (b) H_2 , and (c) N_2 as functions of temperature. Concentrations are expressed as partial pressures in atmospheres. The fuel-rich atmospheric $\text{H}_2/\text{O}_2/\text{N}_2$ flames are grouped into sets, clearly visible in (b) and (c). In each set N_2/O_2 unburnt volume ratios take the value given by the number on the curve; within each set H_2/O_2 unburnt volume ratios take the successive values 4.5, 4.0, 3.5, and 3.0 towards increasing temperatures [from R. W. Reid and T. M. Sugden, *Discussions Faraday Soc.* **33**, 213 (1962)].

methods involve an addition to the flame to establish reactions involving the particular species, or the addition of a scavenger to a gas sample immediately after the sample has been taken.

Foner and Hudson⁴³ and more recently Milne and Greene,^{40, 45} Greene *et al.*,⁴⁴ and Vriens *et al.*⁴⁶ have attempted to detect the atoms and radicals directly by rapidly producing a fast-flowing molecular beam from a sample and analyzing with a mass spectrometer.

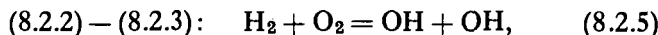
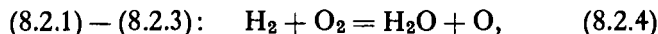
⁴³ S. N. Foner and R. L. Hudson, *J. Chem. Phys.* **21**, 1374 (1953).

⁴⁴ F. T. Greene, J. Brewer, and T. A. Milne, *J. Chem. Phys.* **40**, 1488 (1964).

⁴⁵ T. A. Milne and F. T. Greene, *J. Chem. Phys.* **44**, 2444 (1966).

⁴⁶ L. Vriens, A. L. Boers, and J. A. Smit, *Appl. Sci. Res. Sect. B*, **12**, 65 (1965).

In the case of H₂/O₂ systems, it is known⁴⁷⁻⁴⁹ that in the burnt gases reactions (8.2.1)–(8.2.3) are kinetically equilibrated. This means that algebraic additions and subtractions of these equations must also be effectively balanced; viz.,



In the burnt gases, the radical and atomic concentrations can be calculated from the stable species concentrations, since the necessary equilibrium constant values are available. There is a snag, however, that makes it necessary to develop experimental methods for these determinations. In fuel-rich flames [O₂] is extremely small, while in lean flames [H₂] is small. Consequently the low concentrations limit accuracy and only approximate values for [H], [OH], and [O] can be obtained. In the burnt gas region, owing to the interrelation of the atoms and radicals in Reactions (8.2.1–8.2.3) it is necessary to measure only one atom or radical concentration since this will then enable the others to be obtained from the available data.

8.2.1.3.3. IONS AND ELECTRONS. The fact that flames contain charged particles has been known for a very long time.⁵⁰ Early measurements were based on the conductivity of the flame medium, and, although excessive ionization was recorded in the reaction zones of certain flames, the concept of chemi-ionization was not formulated until the middle of this century.^{51, 52} Flame ionization occurs in natural flames and also as a result of flame additives. Concentrations can vary over a wide range from 10⁶ to 10¹⁵ ions/cm³ in the flame gases.

The mass spectrometer has become a necessary tool for flame ionization studies. Other methods give total ion concentrations but do not give the nature of the ions present. Initially, studies of only the positively charged species were undertaken,⁵³⁻⁶⁹ but recently interest has turned to their negative counterparts^{55, 69-73} which are more important than previously believed.

⁴⁷ W. E. Kaskan, *Combust. Flame* **2**, 229 (1958).

⁴⁸ W. E. Kaskan, *Combust. Flame* **2**, 286 (1958).

⁴⁹ E. M. Bulewicz, C. G. James, and T. M. Sugden, *Proc. Roy. Soc. A* **235**, 89 (1956).

⁵⁰ H. F. Calcote, *Prog. Astronaut. Aeron.* **12**, 107 (1963).

⁵¹ H. F. Calcote, *Symp. Combust.*, 3rd, Madison, Wis., 1948, p. 245. Williams & Wilkins, Baltimore, Maryland. 1949.

⁵² H. F. Calcote, *Combust. Flame* **1**, 385 (1957).

⁵³ H. F. Calcote, *Symp. Combust.*, 9th, Cornell Univ., Ithaca, N.Y., 1962, p. 622. Academic Press, New York, 1963.

⁵⁴ H. F. Calcote and J. L. Reuter, *J. Chem. Phys.* **38**, 310 (1963).

Single and double Langmuir probes have been used to investigate the spatial distribution of the positive ion concentration in flames from 1 to 760 Torr.^{53, 55, 74-83} Although interpretation of probe data is subject to error,⁷⁷ ion recombination rates determined from such studies appear to be verified by other techniques of measurement.†

⁵³ H. F. Calcote, S. C. Kurzus, and W. J. Miller, *Symp. Combust., 10th, Univ. Cambridge, Cambridge, Engl.*, 1964, p. 605. Combust. Inst., Pittsburgh, Pennsylvania, 1965.

⁵⁴ A. Fontijn, W. J. Miller, and J. M. Hogan, *Symp. Combust., 10th, Univ. Cambridge, Cambridge, Eng.*, 1964, p. 545. Combust. Inst., Pittsburgh, Pennsylvania, 1965.

⁵⁵ J. Deckers and A. van Tiggelen, *Combust. Flame* **1**, 281 (1957).

⁵⁶ J. Deckers and A. van Tiggelen, *Bull. Soc. Chim. Belges* **66**, 664 (1957).

⁵⁷ J. Deckers and A. van Tiggelen, *Nature* **182**, 863 (1958).

⁵⁸ J. Deckers and A. van Tiggelen, *Symp. Combust., 7th, London, Oxford*, 1958, p. 254. Butterworths, London, 1959.

⁵⁹ S. De Jaegere, J. Deckers, and A. van Tiggelen, *Symp. Combust., 8th, Pasadena, Calif.*, 1960, p. 155. Williams & Wilkins, Baltimore, Maryland, 1962.

⁶⁰ A. Cooper, K. Littlewood, and J. H. Wilson, *Nature* **210**, 946 (1966).

⁶¹ P. F. Knewstubb and T. M. Sugden, *Symp. Combust., 7th, London, Oxford*, 1958, p. 247. Butterworths, London, 1959.

⁶² P. F. Knewstubb and T. M. Sugden, *Nature* **181**, 474 (1958).

⁶³ P. F. Knewstubb and T. M. Sugden, *Nature* **181**, 1261 (1958).

⁶⁴ P. F. Knewstubb and T. M. Sugden, *Proc. Roy. Soc. A255*, 520 (1960).

⁶⁵ K. N. Bascombe, J. A. Green, and T. M. Sugden, *Advan. Mass Spectrometry, Proc. Conf., 2nd, Oxford*, 1961, **2**, p. 66. Pergamon Press, Oxford, 1962.

⁶⁶ J. A. Green and T. M. Sugden, *Symp. Combust., 9th, Cornell Univ., Ithaca, N.Y.*, 1962, p. 607. Academic Press, New York, 1963.

⁶⁷ A. N. Hayhurst and T. M. Sugden, *Proc. Roy. Soc. A293*, 36 (1966).

⁶⁸ W. J. Miller and H. F. Calcote, *J. Chem. Phys.* **41**, 4001 (1964).

⁶⁹ W. J. Miller and A. Fontijn, *Nature* **204**, 679 (1964).

⁷⁰ A. Feugier and A. van Tiggelen, *Symp. Combust., 10th, Univ. Cambridge, Cambridge, Engl.*, 1964, p. 621. Combust. Inst., Pittsburgh, Pennsylvania, 1965.

⁷¹ P. F. Knewstubb and T. M. Sugden, *Nature* **196**, 1311 (1962).

⁷² H. F. Calcote and I. R. King, *Symp. Combust., 5th, Pittsburgh*, 1954, p. 423. Reinhold, New York, 1955.

⁷³ H. F. Calcote, *Symp. Combust., 8th, Pasadena, Calif.*, 1960, p. 184. Williams & Wilkins, Baltimore, Maryland, 1962.

⁷⁴ H. F. Calcote, *Discussion. Symp. Combust., 10th, Univ. Cambridge, Cambridge, Engl.*, 1964, p. 668. Combust. Inst., Pittsburgh, Pennsylvania, 1965.

⁷⁵ B. E. L. Travers and H. Williams, *Symp. Combust., 10th, Univ. Cambridge, Cambridge, Engl.*, 1964, p. 657. Combust. Inst., Pittsburgh, Pennsylvania, 1965.

⁷⁶ I. R. King, *J. Chem. Phys.* **27**, 817 (1957).

⁷⁷ I. R. King, *J. Chem. Phys.* **29**, 681 (1958).

⁷⁸ I. R. King, *J. Chem. Phys.* **31**, 855 (1959).

⁷⁹ I. R. King, *J. Chem. Phys.* **35**, 380 (1961).

⁸⁰ I. R. King, *J. Chem. Phys.* **36**, 553 (1962).

⁸¹ I. R. King, *J. Chem. Phys.* **37**, 74 (1962).

† See also Vol. 2, Chapter 4.3.

In one or two isolated cases it has been possible to measure ion concentrations in flames by optical spectroscopy.^{84, 85} Another indirect method, depending on the depletion of the free atomic concentration if ionization occurs, has been used^{85, 86} and thermal ionization collision cross sections obtained.

Electron concentrations in flames have been measured by single Langmuir probes, by radio-frequency and microwave methods, and by two spectroscopic techniques. Single probe measurements^{53, 55, 76, 77} have been criticized⁷⁷ and give unreliable values for the electron temperature as well as too low values for $[e^-]$. At present, however, no other method is available for measuring $[e^-]$ on a point-to-point basis throughout a flame.

Radio-frequency and microwave methods essentially measure the electrical conductivity of the flame which can be related to $[e^-]$. These methods suffer from poor spatial resolution but have the advantage of not disturbing the flame, since the power absorbed is negligible. Radio-frequency resonance⁸⁷⁻⁹² (10–100 Mc/sec, sensitivity $\geq 10^8$ electrons/cm³) and direct microwave attenuation methods⁹³⁻⁹⁶ (1–100 Kmc/sec, sensitivity $\geq 10^{10}$ electrons/cm³) have spatial resolution of 1 to 2 cm. The microwave cavity method⁹⁷⁻¹⁰⁰ (3–10 Kmc/sec) is the most useful of the electromagnetic radiation methods for flame studies, having a spatial resolution as small as 3 mm length of flame with a sensitivity $\geq 10^8$ electrons/cm³.

Electron cyclotron resonance has been observed in low-pressure flames.^{94, 101-106} With a magnetic field of several kilogauss, radiation of

⁸⁴ F. W. Hofmann and H. Kohn, *J. Opt. Soc. Am.* **51**, 512 (1961).

⁸⁵ K. Schofield and T. M. Sugden, *Symp. Combust., 10th, Univ. Cambridge, Cambridge, Engl.*, 1964, p. 589. *Combust. Inst.*, Pittsburgh, Pennsylvania, 1965.

⁸⁶ T. Hollander, P. J. Kalff, and C. T. J. Alkemade, *J. Chem. Phys.* **39**, 2558 (1963).

⁸⁷ H. Smith and T. M. Sugden, *Proc. Roy. Soc. A211*, 31 (1952).

⁸⁸ A. J. Borgers, *Symp. Combust., 10th, Univ. Cambridge, Cambridge, Engl.*, 1964, p. 627. *Combust. Inst.*, Pittsburgh, Pennsylvania, 1965.

⁸⁹ P. F. Knewstubb and T. M. Sugden, *Trans. Faraday Soc.* **54**, 372 (1958).

⁹⁰ P. F. Knewstubb and T. M. Sugden, *Res. Correspondence* **9**, A1 (1956).

⁹¹ H. Williams, *Symp. Combust., 7th, London, Oxford*, 1958, p. 269. Butterworths, London, 1959.

⁹² H. Williams, *Symp. Combust., 8th, Pasadena, Calif.*, 1960, p. 179. Williams & Wilkins, Baltimore, Maryland, 1962.

⁹³ H. Belcher and T. M. Sugden, *Proc. Roy. Soc. A201*, 480 (1950).

⁹⁴ J. Schneider and F. W. Hofmann, *Phys. Rev.* **116**, 244 (1959).

⁹⁵ K. E. Shuler and J. Weber, *J. Chem. Phys.* **22**, 491 (1954).

⁹⁶ F. M. Page, *Discussions Faraday Soc.* **19**, 87 (1955).

⁹⁷ B. A. Thrush and T. M. Sugden, *Nature* **168**, 703 (1951).

⁹⁸ T. M. Sugden and R. C. Wheeler, *Discussions Faraday Soc.* **19**, 76 (1955).

⁹⁹ F. M. Page and T. M. Sugden, *Trans. Faraday Soc.* **53**, 1092 (1957).

¹⁰⁰ P. J. Padley and T. M. Sugden, *Symp. Combust., 8th, Pasadena, Calif.*, 1960, p. 164. Williams & Wilkins, Baltimore, Maryland, 1962.

microwave frequencies is required to observe the resonance. By this method both electron concentrations and electron-molecule collision frequencies can be determined.

For strong flame plasmas, Stark-broadening and the "series-limit" method of Inglis and Teller¹⁰⁷ have been used¹⁰⁸ to obtain approximate values for $[e^-]$.

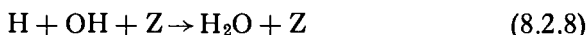
8.2.2. Premixed Flames

The hydrogen-oxygen flame system is reasonably well understood from a chemical viewpoint, and for this reason is a useful medium for additive investigations. In such flames, excess H, OH, and O concentrations are produced in the reaction zone and, with increasing distance from the reaction zone, decay relatively slowly towards their thermodynamic equilibrium values. It is now established that although these atomic and radical concentrations are in excess they are interrelated through the very fast reactions (8.2.1)–(8.2.3) such that a quasi-equilibrium is established even in the reaction zone^{47–49} of low-pressure flames. Thus

$$\frac{(H)}{(H)_{\text{equil.}}} = \frac{(OH)}{(OH)_{\text{equil.}}} = \left(\frac{(O)}{(O)_{\text{equil.}}} \right)^{1/2}$$

and, according to the conditions, these ratios can vary from unity to many thousands.

Generally speaking, the atom and radical concentrations increase in excess of their thermodynamic equilibrium values as flames become more hydrogen-rich and lower in temperature. Excess atom and radical concentrations decay via



where Z is any third body. Fuel-rich H_2/O_2 flames are generally used since

¹⁰¹ J. Schneider and F. W. Hofmann, *Phys. Rev. Letters* **1**, 408 (1958).

¹⁰² E. M. Bulewicz and P. J. Padley, *Combust. Flame* **5**, 331 (1961).

¹⁰³ E. M. Bulewicz, *J. Chem. Phys.* **36**, 385 (1962).

¹⁰⁴ E. M. Bulewicz and P. J. Padley, *J. Chem. Phys.* **36**, 2231 (1962).

¹⁰⁵ E. M. Bulewicz and P. J. Padley, *Symp. Combust.*, 9th, Cornell Univ., Ithaca, N.Y., 1962, p. 638. Academic Press, New York, 1963.

¹⁰⁶ E. M. Bulewicz and P. J. Padley, *Symp. Combust.*, 9th, Cornell Univ., Ithaca, N.Y., 1962, p. 647. Academic Press, New York, 1963.

¹⁰⁷ D. R. Inglis and E. Teller, *Astrophys. J.* **90**, 439 (1939).

¹⁰⁸ R. Friedman and A. Macek, *Symp. Combust.*, 10th, Univ. Cambridge, Cambridge, Engl., 1964, p. 731. Combust. Inst., Pittsburgh, Pennsylvania, 1965.

these are of constant size for many centimeters after the reaction zone. Temperatures from 1000 to 3000°K can be achieved.

Another useful medium for additive investigations is CO/O₂ flames diluted with N₂ or Ar. Owing to the difficulty of getting ultrapure hydrogen, the natural ionization level in H₂/O₂ flames, particularly in the reaction zone, is large,^{67, 68} whereas that of dry CO/O₂ is known to be extremely low.⁸⁰ OH concentrations also are very low in such flames, so that additions will not result in hydroxide formation. Spectroscopically, pure CO/O₂ flames suffer from a fairly strong banded and continuous emission in the visible region which reduces sensitivity for emission observations.

These two flames, the H₂/O₂ and CO/O₂, constitute the basis for most flame additive work. Variations, such as H₂/O₂ flames containing small amounts of hydrocarbons⁶⁸ or carbon monoxide,¹⁰⁹ have occasionally been used. At present most other combustible mixtures are still studied for their own basic kinetic problems.

8.2.3. Low-Pressure and Small-Burning-Velocity Atmospheric Pressure Flames

At low pressures, owing to the smaller number of collisions, only fast reactions can become equilibrated and consequently thermodynamic calculations are not generally applicable. Recent improvements in experimental technique have made it possible to examine the microstructure of low-pressure and low-burning-velocity atmospheric flames. It is now possible to interpret quantitatively some individual collision processes. For a full treatment it is necessary to know flame compositions, temperature profiles, and the local aerodynamics^{24, 110} of regions of the flame. Quartz microprobes used with an analytical tool such as the mass spectrometer can sample regions of the flame (Fig. 4). Although initially limited to the detection of only the stable species,^{21, 29, 39, 111} atom and radical concentrations can now be determined under some conditions (q.v., Section 8.3.2). Temperature patterns can be obtained by using very small silica-covered thermocouples,^{24, 112-114} which have no disturbing influence on the flame and are very reliable. The appropriateness of certain chemical reactions is

¹⁰⁹ W. E. Kaskan, *Combust. Flame* 3, 49 (1959).

¹¹⁰ R. M. Fristrom, W. H. Avery, R. Prescott, and A. Mattuck, *J. Chem. Phys.* 22, 106 (1954).

¹¹¹ R. M. Fristrom and A. A. Westenberg, *Combust. Flame* 1, 217 (1957).

¹¹² W. E. Kaskan, *Symp. Combust.*, 6th, Yale Univ., 1956, p. 134. Reinhold, New York, 1957.

¹¹³ R. Friedman, *Symp. Combust.*, 4th, Cambridge, Mass., 1952, p. 259. Williams & Wilkins, Baltimore, Maryland, 1953.

¹¹⁴ R. Friedman and E. Burke, *J. Chem. Phys.* 22, 824 (1954).

tested by observing the species and noting their concentration profiles with respect to time. If the rates of growth and decay are measurable, and suitably corrected for diffusion and conduction, the validity of the reactions can be checked and rate constants determined. Owing to a lack of data, one difficulty for such a full interpretation is the necessary corrections for molecular diffusion, thermal diffusion, and thermal conduction. Complications also arise from the multicomponent nature and temperature variation within a flame. One method to bypass this problem is the use of gas

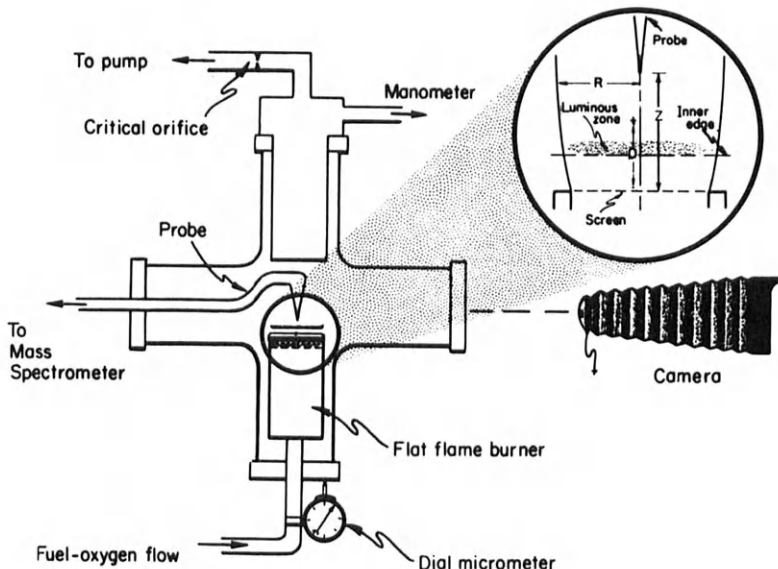


FIG. 4. Microprobe flame sampling technique [from R. M. Fristrom, W. H. Avery, and C. Grunfelder, *Symp. Combust.*, 7th, London, Oxford, 1958, p. 304. Butterworths, London, 1959].

mixtures having one component in large excess and the treatment of the flame as a binary mixture of this component with each species in turn.²⁵ Although experimental values of diffusion coefficients at high temperatures are particularly scarce, there is a summary¹¹⁵ of molecular diffusion and thermal conductivities with particular reference to flames. The situation

¹¹⁵ A. A. Westenberg, *Combust. Flame* 1, 346 (1957).

has recently improved with new experimental values.¹¹⁶⁻¹²⁵ Thermal diffusion is negligible in most cases, as compared with molecular diffusion,²⁵ and is generally ignored. In most flame studies, thermal conductivities have been calculated by a method due to Lindsay and Bromley¹²⁶ using the conductivities for pure constituents.

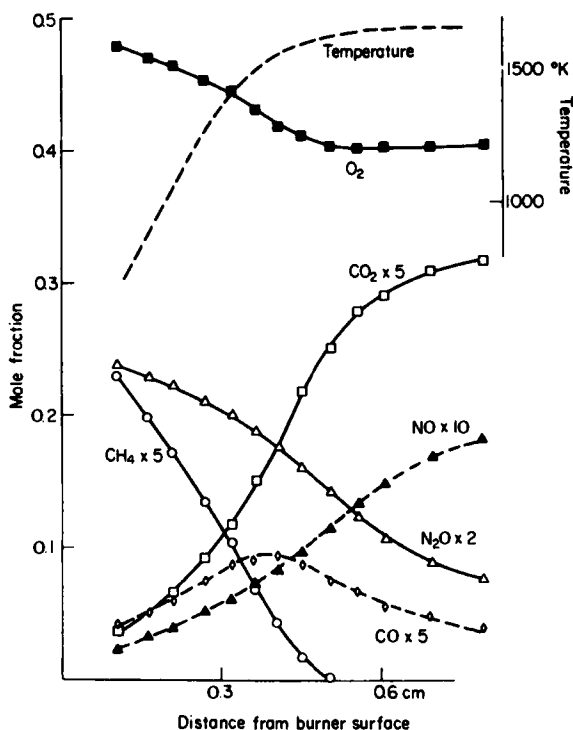


FIG. 5. Traverses through a fuel-lean flame; $\text{CH}_4 + 7.54\text{O}_2 + 1.80\text{N}_2\text{O} + 4.13\text{Ar}$, burnt at 14 cm of pressure [from C. P. Fenimore and G. W. Jones, *J. Phys. Chem.* **65**, 2200 (1961)].

The need for transport corrections has been discussed in papers by Dixon-Lewis and Williams,¹⁸ Dixon-Lewis *et al.*,¹⁹ Fristrom and Westenberg,^{23, 25} and Peacock and Weinberg.¹²⁷ Errors in the transport data constitute the main uncertainties in this technique. Typical corrected profiles obtained are illustrated in Fig. 5.

¹¹⁶ A. A. Westenberg and R. E. Walker, *J. Chem. Phys.* **26**, 1753 (1957).

¹¹⁷ R. E. Walker and A. A. Westenberg, *J. Chem. Phys.* **29**, 1139, 1147 (1958); **31**, 519 (1959); **32**, 436 (1960).

A technique used with low-pressure or small-burning-velocity atmospheric flames is the study of the heat release profile. In H_2/O_2 flames at low temperatures, a large discrepancy between measured and predicted profiles^{18, 128} could only be rectified by considering the importance of the HO_2 radical.¹²⁹

Peacock and Weinberg¹²⁷ and Frazier *et al.*¹³⁰ have investigated the H_2/Br_2 atmospheric pressure flame system. [Br] unfortunately was not measured in either case but calculated assuming a steady state. Although there is a complete lack of accurate transport property data for this flame,¹³¹ the large disagreement between measured and calculated heat release profiles shows that there is insufficient time available in the flames for the establishment of a steady state. If the [Br] can be measured, a complete experimental description would be achieved.

8.2.4. High-Pressure Flames

Spectroscopic investigations of hydrocarbon-oxygen or air and CO/O_2 flames up to 40 atm^{132, 133} showed that equipartitioning of the energy occurred faster than at normal pressure and the increase in pressure reduced the extent of dissociation. Thus flames are several hundred degrees hotter at high pressure than at atmospheric pressure, since dissociation of molecules into atoms and radicals absorbs a fraction of the heat resulting from the fast exothermic chemical reactions.

- ¹¹⁸ A. A. Westenberg and G. Frazier, *J. Chem. Phys.* **36**, 3499 (1962).
- ¹¹⁹ R. E. Walker, N. de Haas, and A. A. Westenberg, *J. Chem. Phys.* **32**, 1314 (1960).
- ¹²⁰ R. E. Walker, L. Monchick, A. A. Westenberg, and S. Favin, *Planetary Space Sci.* **3**, 221 (1961).
- ¹²¹ R. E. Walker, *J. Chem. Phys.* **34**, 2196 (1961).
- ¹²² G. Ember, J. R. Ferron, and K. Wohl, *J. Chem. Phys.* **37**, 891 (1962).
- ¹²³ R. E. Walker, N. de Haas, and A. A. Westenberg, *Phys. Fluids* **3**, 482 (1960).
- ¹²⁴ A. A. Westenberg and N. de Haas, *Phys. Fluids* **5**, 266 (1962).
- ¹²⁵ A. A. Westenberg and N. de Haas, *Phys. Fluids* **6**, 617 (1963).
- ¹²⁶ A. L. Lindsay and L. A. Bromley, *Ind. Eng. Chem.* **42**, 1508 (1950).
- ¹²⁷ F. Peacock and F. J. Weinberg, *Symp. Combust., 8th, Pasadena, Calif.*, 1960, p. 458. Williams & Wilkins, Baltimore, Maryland, 1962.
- ¹²⁸ G. Dixon-Lewis and A. Williams, *Nature* **196**, 1309 (1962).
- ¹²⁹ C. P. Fenimore and G. W. Jones, *Symp. Combust., 10th, Univ. Cambridge, Cambridge, Engl.*, 1964, p. 489. Combust. Inst., Pittsburgh, Pennsylvania, 1965.
- ¹³⁰ G. C. Frazier, R. M. Fristrom, and J. F. Wehner, *A.I.Ch.E. (Am. Inst. Chem. Engrs.) J.* **9**, 689 (1963).
- ¹³¹ E. S. Campbell and R. M. Fristrom, *Chem. Rev.* **58**, 173 (1958).
- ¹³² J. Diederichsen and H. G. Wolfhard, *Trans. Faraday Soc.* **52**, 1102 (1956).
- ¹³³ J. Diederichsen and H. G. Wolfhard, *Proc. Roy. Soc. A* **236**, 89 (1956).

8.2.5. Diffusion Flames

Recently, complicated diffusion flames¹³⁴ have been studied with a stable flat flame established with a counterflow opposed-jet burner (Fig. 6). Flow patterns, spectra, temperature distributions, and gas composition profiles were obtained. This burner has an advantage compared to low-pressure, premixed flame kinetic investigations in that it has a much wider range of conditions over which it is useful. It not only permits the study of fuel-oxidant ratios with high burning velocities but even of reactants too reactive to permit their premixing.

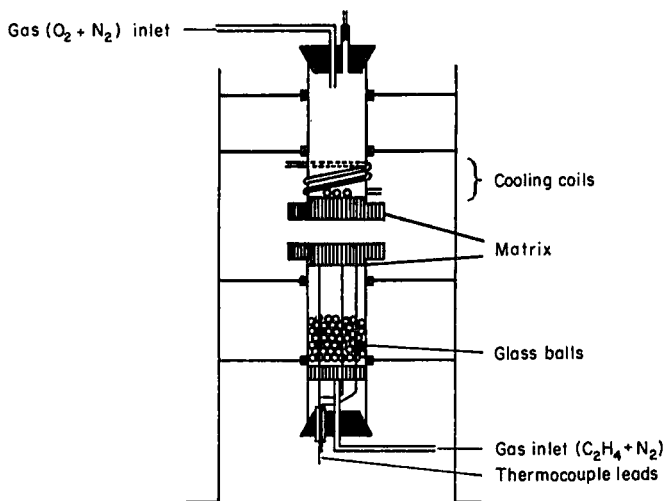


FIG. 6. Opposed jet burner [from T. P. Pandya and F. J. Weinberg, *Proc. Roy. Soc. A279*, 544 (1964)].

Some 30 years ago, Polanyi developed several classic diffusion flame techniques to study fast reactions; these techniques have been successfully used to obtain kinetic data.

8.2.5.1. Dilute Flame Method. Beutler and Polanyi¹³⁵ in 1925 introduced this simple method, applicable to reactions proceeding on almost every collision. Vapor streams of reactants at low pressures are introduced from opposite ends into an evacuated tube at pressures such that the mean free path is greater than the diameter of the tube and diffusion is therefore the

¹³⁴ T. P. Pandya and F. J. Weinberg, *Proc. Roy. Soc. A279*, 544 (1964).

¹³⁵ H. Beutler and M. Polanyi, *Naturwissenschaften* 13, 711 (1925).

predominant method of mixing. The two reactants (e.g., alkali metal atoms with the halogen gases) interpenetrate until they are consumed. The involatile product deposited on the walls can be used to measure the extent of interpenetration. It is quite easy to relate the half-width of this deposit, together with the diffusion coefficients of the two reactants, to the rate of the reaction. The range of reactions that can be covered with this technique is limited, however, owing to the fact that the distribution half-width cannot be too large or the technique no longer becomes feasible. Also, since the wall of the vessel is present, care must be taken to prevent wall reactions.

Although little used at present, the technique did show that certain alkali metal atom-halogen reactions were indeed very fast, some being faster than then considered possible, using generally accepted gas-kinetic collision diameters. Reaction cross sections $\geq 100 \text{ \AA}^2$ in magnitude, or up to 10 times the gas-kinetic cross sections were found.

8.2.5.2. Diffusion Flame Technique. For slightly slower reactions, those occurring every 10 to 10^5 collisions, von Hartel and Polanyi¹³⁶ developed another method, still in use. In this procedure it is observed as to how far one reactant (sodium has been extensively used) diffuses into an excess of a reacting atmosphere (e.g., a halide) before being consumed. By diluting the reactants, a convenient diffusion path can be produced so that the alkali metal is consumed before reaching the wall, hence removing any wall complications. An expression for the rate constant was derived.¹³⁶ An extensive critical investigation by Heller¹³⁷ established that, provided certain experimental conditions were satisfied, the method would approach the simplifying assumptions made in the original treatment and rate data would be reliable to within a factor of two. More recently, Cvetanovic and LeRoy,¹³⁸ Smith,¹³⁹ Reed and Rabinovitch,¹⁴⁰ and Cvetanovic¹⁴¹ have reconsidered the theoretical aspects.

Over the years a great wealth of information on the relative and absolute rates of sodium atoms with organic and inorganic halides has accumulated. Reviews by Bawn¹⁴² (1942), Warhurst¹⁴³ (1951), and Steacie¹⁴⁴ (1954) cover the field extensively.

¹³⁶ H. von Hartel and M. Polanyi, *Z. Physik Chem.* **B11**, 97 (1930).

¹³⁷ W. Heller, *Trans. Faraday Soc.* **33**, 1556 (1937).

¹³⁸ R. J. Cvetanovic and D. J. LeRoy, *Can. J. Chem.* **29**, 597 (1951).

¹³⁹ F. T. Smith, *J. Chem. Phys.* **22**, 1605 (1954).

¹⁴⁰ J. F. Reed and B. S. Rabinovitch, *J. Phys. Chem.* **59**, 261 (1955).

¹⁴¹ R. J. Cvetanovic, *Can. J. Chem.* **34**, 54 (1956).

¹⁴² C. E. H. Bawn, *Ann. Rept. Progr. Chem. (Chem. Soc. London)* **39**, 36 (1942).

¹⁴³ E. Warhurst, *Quart. Rev. (London)* **5**, 44 (1951).

¹⁴⁴ E. W. R. Steacie, Systems containing sodium. In "Atomic and Free Radical Reactions," 2nd ed., Vol. II, Chapter 13. Reinhold, New York, 1954.

The determination of activation energies of reactions is rather difficult with this technique. As a consequence, until recently, rather than obtain reaction cross sections, a normal frequency factor (i.e., a normal gas kinetic cross section plus unit steric factor) was assumed so that the activation energy could be calculated from a single rate constant determination.¹⁴⁵⁻¹⁴⁷ The reaction cross section used, 35 Å², was based on measurements carried out in 1930 by von Hartel and Polanyi¹³⁶ and confirmed by Cvetanovic and LeRoy.¹⁴⁸ Molecular beam studies^{149, 150} find that this somewhat arbitrary value is high but that, for reactions of the type M + RX, reaction cross sections do remain about the same ($\gtrsim 10 \text{ Å}^2$) and suffer no apparent steric interference as the R group becomes larger. For this class of reactions the collision cross sections agree well with gas kinetic values.

8.2.5.3. "Life-Period" Method. This third method by Frommer and Polanyi¹⁵¹ was introduced owing to the doubt about approximations made in the diffusion flame technique. This method kept the same experimental arrangement but was based on a different set of measurements. Under steady-state conditions, by determining the number of metal atoms introduced in unit time into the vessel and the total number of atoms throughout the flame, the effective lifetime of the atoms, and hence the rate of the reaction, can be determined. Since these methods depend on strong absorption or emission, their application has been limited to alkali metals.

8.2.5.4. Other Methods. In more recent times, two new variants on the diffusion flame technique have appeared, widening its scope and application. The first of these, credited to Kistiakowsky, removes the optical detection and is based on the determination of the steady-state temperature pattern through the spherical reaction zone using a very fine thermocouple probe.¹⁵²⁻¹⁵⁵

The second is Garvin's "product emitter method" for chemiluminescent reactions. The method rests on the same assumptions as those underlying the temperature pattern method and a mathematical model has been

¹⁴⁵ J. W. Hodgins and R. L. Haines, *Can. J. Chem.* **30**, 473 (1952).

¹⁴⁶ J. F. Reed and B. S. Rabinovitch, *J. Phys. Chem.* **61**, 598 (1957).

¹⁴⁷ E. D. Kaufman and J. F. Reed, *J. Phys. Chem.* **67**, 896 (1963).

¹⁴⁸ R. J. Cvetanovic and D. J. LeRoy, *J. Chem. Phys.* **20**, 1016 (1952).

¹⁴⁹ D. R. Herschbach, *Discussions Faraday Soc.* **33**, 149 (1962).

¹⁵⁰ D. R. Herschbach, *Appl. Opt. Suppl.* **2**, 128 (1965).

¹⁵¹ L. Frommer and M. Polanyi, *Trans. Faraday Soc.* **30**, 519 (1934).

¹⁵² D. Garvin, V. P. Guinn, and G. B. Kistiakowsky, *Discussions Faraday Soc.* **17**, 32 (1954).

¹⁵³ D. Garvin and G. B. Kistiakowsky, *J. Chem. Phys.* **20**, 105 (1952).

¹⁵⁴ G. B. Kistiakowsky and R. Williams, *J. Chem. Phys.* **23**, 334 (1955).

¹⁵⁵ F. T. Smith and G. B. Kistiakowsky, *J. Chem. Phys.* **31**, 621 (1959).

developed¹⁵⁶ to interpret such flames in which a product molecule emits the radiation which is monitored. Examples of its use include investigations of the infrared emission from vibrationally excited ground electronic OH,¹⁵⁷ and the reaction of active hydrogen and sodium.^{158, 159} Rapp and Johnston¹⁶⁰ have investigated a NO/F₂ diffusion flame and Markstein¹⁶¹⁻¹⁶³ a Mg/O₂ flame.

8.3. Experimental Techniques

8.3.1. Optical Studies

Optical spectroscopy has been a major tool in flame investigations with its main use being the detection of electronically excited species—atoms, atomic ions, and simple radicals. The spectroscopic technique has not succeeded in extracting much kinetic data from low-pressure flames. Research in this field has been mainly concerned with the detection of species and an analysis as to their rotational, vibrational, and electronic population distributions.

In atmospheric pressure flames, however, more quantitative investigations have been carried out. Kinetic rates and reaction cross sections are determined through obtaining the concentrations of the ground states of the species directly from intensity measurements. Such methods are limited to systems in which thermal equilibrium prevails, i.e., the burnt gases of atmospheric flames.

8.3.1.1. Spectroscopic Methods of Measuring Atomic and Radical Concentrations. 8.3.1.1.1. NO ADDITION TO THE FLAME. 8.3.1.1.1.1. *Electron-Spin Resonance (ESR)*. The Russian schools have made great use of ESR. They have reported detecting H, D, O, OH, HO₂, and halogen atoms in various

¹⁵⁶ D. Garvin, P. P. Gwyn, and J. W. Moskowitz, *Can. J. Chem.* **38**, 1795 (1960).

¹⁵⁷ D. Garvin and J. D. McKinley, *J. Chem. Phys.* **24**, 1256 (1956).

¹⁵⁸ J. C. Polanyi and C. M. Sadowski, *J. Chem. Phys.* **36**, 2239 (1962).

¹⁵⁹ E. M. Nemeth, J. C. Polanyi, and C. M. Sadowski, *J. Chem. Phys.* **40**, 2054 (1964).

¹⁶⁰ D. Rapp and H. S. Johnston, *J. Chem. Phys.* **33**, 695 (1960).

¹⁶¹ G. H. Markstein, *Symp. Combust.*, 9th, Cornell Univ., Ithaca, N.Y., 1962, p. 137. Academic Press, New York, 1963.

¹⁶² G. H. Markstein, *Progr. Astronaut. Aeron.* **15**, 177 (1964).

¹⁶³ G. H. Marstein, *Discussion. Symp. Combust.*, 10th, Univ. Cambridge, Cambridge, Engl., 1964, p. 682. Combust. Inst., Pittsburgh, Pennsylvania, 1965.

low-pressure flames.¹⁶⁴⁻¹⁷⁷ The technique generally consists of burning the flame in a quartz tube which passes through the resonant microwave cavity, placed between the poles of the magnet. In such work, spatial resolution is low, and an average concentration is obtained within the cavity. Obtaining absolute concentrations is difficult, but if possible the technique has wide scope through its ability to detect electrons of unpaired spin, i.e., many atoms, radicals, and molecules such as OH, NO, NO₂, and O₂. Westenberg and De Haas^{178, 179} have now laid the foundation for such measurements, since confirmed,¹⁸⁰ and attempts, although criticized,¹⁸¹ to measure [H], [O],²⁸ and [OH]^{182, 183} have been made.

8.3.1.1.1.2. Ultraviolet Absorption. Pure spectroscopic methods of analysis have a great advantage of not disturbing the flame. Experimental difficulties do, however, restrict this method to very few strongly absorbing

¹⁶⁴ V. N. Panfilov, Yu. D. Tsvetkov, and V. V. Voevodskii, *Kinetics Catalysis (USSR) (English Transl.)* **1**, 305 (1960).

¹⁶⁵ V. V. Azatyan, L. A. Akopyan, A. B. Nalbandyan, and B. V. Ozherelev, *Proc. Acad. Sci. USSR Phys. Chem. Sect. (English Transl.)* **141**, 815 (1961).

¹⁶⁶ V. V. Azatyan, V. N. Panfilov, and A. B. Nalbandyan, *Kinetics Catalysis (USSR) (English Transl.)* **2**, 276 (1961).

¹⁶⁷ V. V. Azatyan, L. A. Akopyan, and A. B. Nalbandyan, *Kinetics Catalysis (USSR) (English Transl.)* **2**, 857 (1961).

¹⁶⁸ L. I. Avramenko and R. V. Kolesnikova, *Proc. Acad. Sci. USSR Phys. Chem. Sect. (English Transl.)* **140**, 750 (1961).

¹⁶⁹ V. V. Azatyan, L. A. Akopyan, and A. B. Nalbandyan, *Dokl. Akad. Nauk. Arm. SSR* **35**, 123 (1962).

¹⁷⁰ V. N. Panfilov, *Kinetics Catalysis (USSR) (English Transl.)* **3**, 559 (1962).

¹⁷¹ V. P. Balakhnin, Yu M. Gershenson, V. N. Kondratev, and A. B. Nalbandyan, *Proc. Acad. Sci. USSR Phys. Chem. Sect. (English Transl.)* **154**, 114 (1964).

¹⁷² V. P. Balakhnin, Yu M. Gershenson, V. N. Kondratev, and A. B. Nalbandyan, *Proc. Acad. Sci. USSR Phys. Chem. Sect. (English Transl.)* **154**, 158 (1964).

¹⁷³ G. A. Sachyan and A. B. Nalbandyan, *Bull. Acad. Sci. USSR Div. Chem. Sci. (English Transl.)*, p. 1250 (1964).

¹⁷⁴ V. V. Azatyan, A. B. Nalbandyan, and E. N. Sarkisyan, *Proc. Acad. Sci. USSR Phys. Chem. Sect. (English Transl.)* **158**, 869 (1964).

¹⁷⁵ V. N. Panfilov, *Kinetics Catalysis USSR (English Transl.)* **5**, 185 (1964).

¹⁷⁶ L. Yu. Rusin, A. M. Chaikin, and A. E. Shilov, *Kinetics Catalysis USSR (English Transl.)* **5**, 998 (1964).

¹⁷⁷ V. N. Panfilov and V. V. Voevodskii, *Kinetics Catalysis USSR (English Transl.)* **6**, 519 (1965).

¹⁷⁸ A. A. Westenberg and N. de Haas, *J. Chem. Phys.* **40**, 3087 (1964).

¹⁷⁹ A. A. Westenberg, *J. Chem. Phys.* **43**, 1544 (1965).

¹⁸⁰ K. M. Evenson and D. S. Burch, *J. Chem. Phys.* **44**, 1715 (1966).

¹⁸¹ Discussion. *Symp. Combust., 10th, Univ. Cambridge, Cambridge, Engl., 1964*, p. 483. Combust. Inst., Pittsburgh, Pennsylvania, 1965.

¹⁸² A. A. Westenberg and N. de Haas, *J. Chem. Phys.* **43**, 1550 (1965).

¹⁸³ G. Dixon-Lewis, W. E. Wilson, and A. A. Westenberg, *J. Chem. Phys.* **44**, 2877 (1966).

radicals or molecules. So far, quantitative measurements have been reported for OH, CH, and C₂.¹⁸⁴ Earlier determinations of OH^{185, 186} did not have the most suitable flames for optical studies and the method was more fully developed by Kaskan.^{47, 48} Good spatial resolution is obtained and radical profile decay measurements on the burnt gases of flames may be carried out. From a knowledge of the *f*-numbers of the absorption bands, absolute measurements can be made. The method is restricted to regions of thermal equilibration, i.e., the burnt gases. Generally, multiple-reflection absorption techniques are required to observe the absorption. Del Greco and Kaufman¹⁸⁷ have confirmed the reliability of this method by obtaining an independent check on an [OH] so measured.

8.3.1.1.2. ADDITION TO THE FLAME. 8.3.1.1.2.1. *The Sodium-Lithium Method⁴⁹ for Absolute [H].* Trace quantities of sodium and lithium salts are added to a hydrogen-rich flame and the resulting strong resonant line emissions are measured. Under these flame conditions, sodium exists as atoms and ions. Lithium, however, also undergoes extensive compound formation which produces gaseous LiOH. The hydroxide is formed in the reaction



Order-of-magnitude calculations^{14, 49} show that reasonable equilibration is obtained in the burnt gases. Consequently, since the equilibrium constant

$$K_{(8.3.1)} = \frac{[\text{LiOH}][\text{H}]}{[\text{Li}][\text{H}_2\text{O}]},$$

knowledge of $K_{(8.3.1)}$, $[\text{H}_2\text{O}]$, and the ratio $[\text{LiOH}]/[\text{Li}]$ enables $[\text{H}]$ to be calculated. The $[\text{LiOH}]/[\text{Li}]$ ratio can be evaluated from a comparison of the sodium and lithium resonant line emission, using known *f*-values and spectral sensitivity factors. $K_{(8.3.1)}$ is not known but can be calculated by standard statistical thermodynamic methods.^{188, 189}

Since thermal excitation is necessary for such an emission comparison, this method as such is restricted to the burnt gas region of flames of temperatures above 1500°K. However, the recent use of atomic absorption spectroscopy for the determination of the $[\text{LiOH}]/[\text{Li}]$ ratio¹⁹⁰ has now extended the applicability of the technique to low-temperature regimes

¹⁸⁴ R. Bleekrode and W. C. Nieuwpoort, *J. Chem. Phys.* **43**, 3680 (1965).

¹⁸⁵ H. J. Kostkowski and H. P. Broida, *J. Opt. Soc. Am.* **46**, 246 (1956).

¹⁸⁶ A. G. Gaydon and H. G. Wolfhard, *Proc. Roy. Soc. A* **194**, 169 (1948).

¹⁸⁷ F. P. Del Greco and F. Kaufman, *Discussions Faraday Soc.* **33**, 128 (1962).

¹⁸⁸ H. Smith and T. M. Sugden, *Proc. Roy. Soc. A* **219**, 204 (1953).

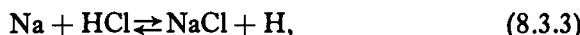
¹⁸⁹ P. J. Th. Zeegers and C. T. J. Alkemade, *Combust. Flame* **9**, 247 (1965).

¹⁹⁰ M. J. McEwan and L. F. Phillips, *Combust. Flame* **9**, 420 (1965).

where chemiluminescent emission is recorded. Figure 7 shows values obtained for [H] in several fuel-rich $H_2/O_2/N_2$ flames; corresponding values for OH, O, and O_2 have been calculated through the interrelation of the atoms and radicals, due to the fast reactions (8.2.1)–(8.2.3).

8.3.1.1.2.2. *The Sodium-Chlorine Method⁴⁹ for Absolute [H].* A sodium salt is sprayed into the flame in low concentration, and controllable amounts of chlorine are added to the unburnt flame gases in quantities up to 0.5% of the gas flow.

Balanced reactions are established in the burnt gases,



and it can be readily shown¹⁹¹ that (assuming thermal excitation of sodium)

$$\frac{I_{Na}^0}{I_{Na}'} = 1 + \frac{K_{(8.3.3)}[Cl]_0}{[H]}$$

where I_{Na}^0 and I_{Na}' are the sodium resonance emission intensities in the absence and presence of chlorine, respectively. $[Cl]_0$ is the effective concentration of total chlorine being added to the flame gases. Consequently, [H] can be obtained from the straight line plot of I_{Na}^0/I_{Na}' against $[Cl]_0$. The required $K_{(8.3.3)}$ is readily calculable from statistical thermodynamics.

It might be noted that although chlorine is added in quantities up to 0.5%, far from a trace additive, it appears to have little effect on the general flame kinetics. Experimental verification of this was found by Bulewicz *et al.*,¹⁹¹ who reversed the technique on knowing [H], and determined the bond energy of many gaseous diatomic metal halides formed by adding metal salts together with halogens to the flame.

8.3.1.1.2.3. *CuH Emission as a Measure of Relative [H].* Bulewicz and Sugden¹⁹² found that on the addition of copper salts to flames, *inter alia*, copper hydride bands are emitted, the strongest being the (0, 0) band at 4280 Å. It was shown that this band intensity varied directly with [H] and was fairly independent of temperature.¹⁹³ The intensity of the CuH band can be used throughout the flame as a measure of [H].

8.3.1.1.2.4. *The Sodium Continuum as a Measure of Relative [OH].* James and Sugden¹⁹⁴ showed that a continuous emission from the ultraviolet

¹⁹¹ E. M. Bulewicz, L. F. Phillips, and T. M. Sugden, *Trans. Faraday Soc.* **57**, 921 (1961).

¹⁹² E. M. Bulewicz and T. M. Sugden, *Trans. Faraday Soc.* **52**, 1475 (1956).

¹⁹³ R. W. Reid and T. M. Sugden, *Discussions Faraday Soc.* **33**, 213 (1962).

¹⁹⁴ C. G. James and T. M. Sugden, *Proc. Roy. Soc. A* **248**, 238 (1958).

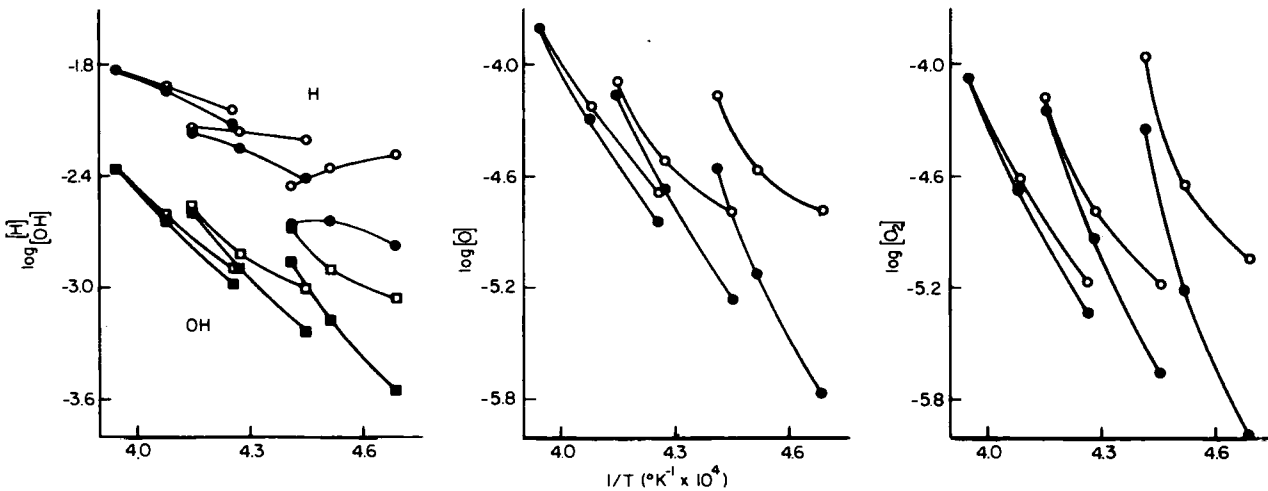
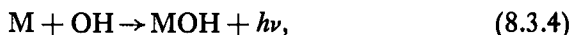


FIG. 7. Minor constituent concentrations in the burnt gases, 1.25 msec downstream of the reaction zone, of fuel-rich $\text{H}_2/\text{O}_2/\text{N}_2$ flames. Points ● and ■ represent thermodynamic equilibrium concentrations; points ○ and □ experimental values. Concentrations expressed as partial pressures in atmospheres. Each set of three flames has a N_2/O_2 unburnt volume ratio of 2, 3, or 4, respectively, towards lower temperatures. The members of each set have H_2/O_2 unburnt volume ratios of 3.5, 4, 4.5 ($\text{N}_2/\text{O}_2 = 2$); 3, 3.5, 4 ($\text{N}_2/\text{O}_2 = 3$); and 2.5, 3, 3.5 ($\text{N}_2/\text{O}_2 = 4$) in the direction of decreasing temperature.

through to the red, apparent when an alkali metal salt is added to a H₂/O₂ flame, arises through radiative recombination,



where M represents an alkali metal atom. The intensity of the continuum can be taken as a relative measure of the [OH] and has only a slight temperature dependence. The intensity observed depends on the rate of (8.3.4) and not on the establishment of a steady state, so that measurements can be taken even in the reaction zone. Of the alkali metal salts, sodium is usually used since it is free from complication in flames and gives a reasonably strong continuum.

Under some conditions the emission from bands of CuOH can be used for [OH]¹⁹⁵ but is unreliable.¹⁹³

8.3.1.1.2.5. Flame Photometric Determinations of [O]. The IO method¹⁹⁶ is now the recognized method for obtaining relative values for [O]. It entails observing the emission of the (0, 4) band of IO at 5307 Å, produced when iodine, either elemental or as methyl iodide, is added to hydrogen-rich flames to the extent of up to 0.25% of the unburnt gas mixture flow. The emission is thermal in origin and the intensity of the (0, 4) IO band is a direct measure of [O] for a constant amount of iodine.

The NO method^{197, 198} previously used is unreliable since the NO affects the kinetic system.^{199, 200}

8.3.1.1.2.6. The Chemiluminescent Method. Chemiluminescent excitation of metal atoms in flames is now well established. Determining factors^{10, 201} for chemiluminescent excitation predominating over thermal processes are

- (i) low temperature,
- (ii) high electronic excitation energy,
- (iii) close proximity to the reaction zone.

The importance of these factors is well illustrated in Figs. 8 and 9.

Chemiluminescent emission of metal atoms in H₂/O₂/N₂ flames results from the reactions



¹⁹⁵ E. M. Bulewicz and T. M. Sugden, *Trans. Faraday Soc.* **52**, 1481 (1956).

¹⁹⁶ L. F. Phillips and T. M. Sugden, *Trans. Faraday Soc.* **57**, 914 (1961).

¹⁹⁷ A. G. Gaydon, *Proc. Roy. Soc. A* **183**, 111 (1944).

¹⁹⁸ C. G. James and T. M. Sugden, *Nature* **175**, 252 (1955).

¹⁹⁹ T. M. Sugden, E. M. Bulewicz, and A. Demerdache, Chemical reactions in the lower and upper atmosphere. *Proc Intern. Symp., Stanford*, 1961, p. 89. Wiley (Interscience), New York, 1961.

²⁰⁰ E. M. Bulewicz and T. M. Sugden, *Proc. Roy. Soc. A* **277**, 143 (1964).

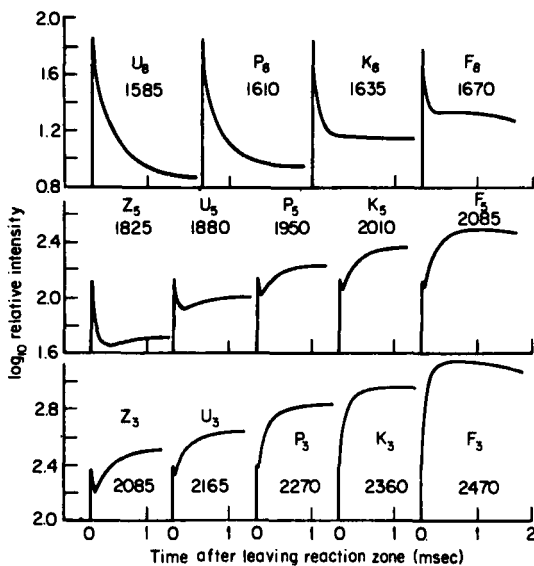


FIG. 8. Variation of sodium *D*-line intensity with time from primary reaction zone. *F, K, P, U, Z* denote flames with H_2/O_2 unburnt volume ratios of 2.5, 3.0, 3.5, 4.0, 4.5, respectively. The subscript numeral denotes the N_2/O_2 unburnt volume ratio. The temperatures quoted are the line-reversal temperature reached where the curves become nearly horizontal [from P. J. Padley and T. M. Sugden, *Proc. Roy. Soc. A* **248**, 248 (1958)].

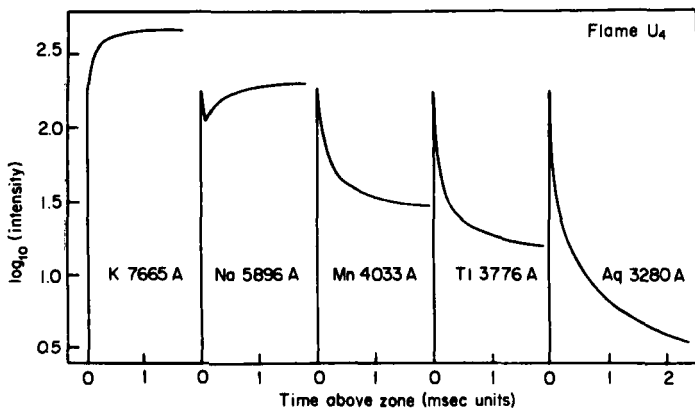


FIG. 9. Variation of intensity with time for lines with different excitation energies in a given flame (U_4), $4H_2 + O_2 + 4N_2$. All are resonance lines, so that the wavelength is simply related to the excitation energy [from P. J. Padley and T. M. Sugden, *Symp. Combust., 7th, London, Oxford, 1958*, p. 235. Butterworths, London, 1959].

For the case of thallium, the 3776 Å emission line is excited predominantly by the type (8.3.5) mechanism, while for lead the 4058 Å emission is due to reaction (8.3.6) in such flames.²⁰¹ Other metals studied are intermediate in nature between these two extremes. Further studies on Tl and Pb chemiluminescence have been reported.²⁰²

If a metal is electronically excited by a chemiluminescent reaction of type (8.3.5) or (8.3.6) in a H₂/O₂/N₂ flame, wherever H + H₂O ⇌ H₂ + OH is balanced, the atomic emission intensity of the relevant electronic transition may be used for relative values of [H]. Rosenfeld and Sugden²⁰³ have used the intensity of the 4058 Å Pb line for this purpose, and Dixon-Lewis,^{18, 204} burning hydrogen flames at around 1000°K, the sodium D-lines.

8.3.1.2. "Van der Held" Dilution Curves. Generally in flames, conditions are such that the contour of an emission line is governed by Doppler and pressure (Lorentz) broadenings. Under conditions of thermal excitation and negligible self-absorption it can be shown²⁰⁵⁻²⁰⁷ that the intensity of emission is directly proportional to the concentration of the ground electronic state. As self-absorption becomes important a change from a linear to square-root dependence on concentration occurs, as illustrated in Fig. 10. The region of change depends on the ratio of Lorentz to Doppler broadening, and the location of this region allows an estimate of the mean collision cross section between the particular electronically excited atoms and the flame gas molecules. By this means, Hinnov²⁰⁸ obtained 64 Å² for the cross section of Na in the ²P_{3/2} state in a C₂H₂/air flame. James and Sugden²⁰⁹ determined values for the other alkali metals. Hofmann and Kohn,⁸⁴ Hinnov and Kohn,²¹⁰ and van Trigt *et al.*²¹¹ have further pursued this type of study, obtaining values for the alkali, the alkaline-earth, and several transition metals in various flames. Recently, investigations have

²⁰¹ P. J. Padley and T. M. Sugden, *Symp. Combust.*, 7th, London, Oxford, 1958, p. 235. Butterworths, London, 1959.

²⁰² L. F. Phillips and T. M. Sugden, *Trans. Faraday Soc.* **57**, 2188 (1961).

²⁰³ J. L. J. Rosenfeld and T. M. Sugden, *Combust. Flame* **8**, 44 (1964).

²⁰⁴ G. Dixon-Lewis, M. M. Sutton, and A. Williams, *Discussions Faraday Soc.* **33**, 205 (1962).

²⁰⁵ E. F. M. Van der Held, *Z. Physik* **70**, 508 (1931).

²⁰⁶ A. C. G. Mitchell and M. W. Zemansky, "Resonance Radiation and Excited Atoms," 2nd Impression. Cambridge Univ. Press, London and New York, 1961.

²⁰⁷ C. G. James and T. M. Sugden, *Proc. Roy. Soc. A* **227**, 312 (1955).

²⁰⁸ E. Hinnov, *J. Opt. Soc. Am.* **47**, 151 (1957).

²⁰⁹ C. G. James and T. M. Sugden, *Nature* **171**, 428 (1953).

²¹⁰ E. Hinnov and H. Kohn, *J. Opt. Soc. Am.* **47**, 156 (1957).

²¹¹ C. van Trigt, Tj. Hollander, and C. T. J. Alkemade, *J. Quant. Spectry. Radiative Transfer* **5**, 813 (1965).

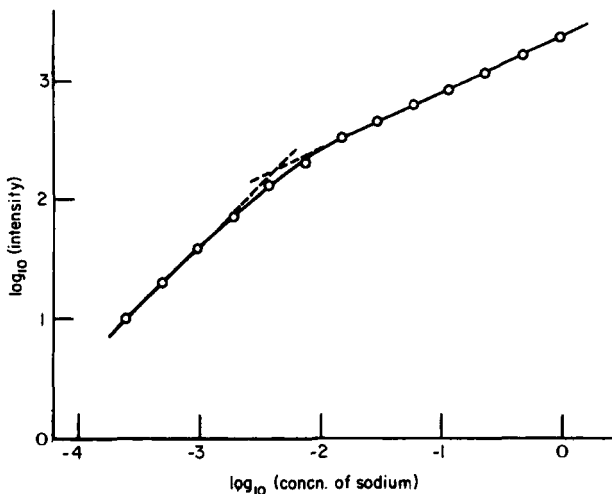


FIG. 10. The variation of the intensity of the *D*-lines of sodium in emission from the burnt gases of a flame, showing the transition of the order of dependence on concentration from 1.0 to 0.5 as self-reversal becomes important.

been made of the dependence of the collision half-width of a spectral line on the nature of the gas molecule perturbing the radiating atom.²¹²⁻²¹⁴ Na($^2S_{1/2}$ - $^2P_{3/2}$) and Sr(1S_0 - 1P_1) resonance lines have been observed in C₂H₂/O₂ flames with N₂, He, Ar, and CO₂ as the major species diluent.

In quantitative flame photometric work, the ratio of the intensities in emission (I_1, I_2) of two atomic lines of wavelengths (λ_1, λ_2) given by²⁰⁷

$$\frac{I_1}{I_2} = \frac{N_1 f_1}{N_2 f_2} \left(\frac{\lambda_2}{\lambda_1} \right)^3 \exp \left(-\frac{hc}{kT} \left(\frac{1}{\lambda_1} - \frac{1}{\lambda_2} \right) \right)$$

allows either concentrations (N) or *f*-values²¹⁵ to be compared, or the temperature (T) to be determined.²¹⁶

"Van der Held" dilution curves (Fig. 10) also can give an insight into the behavior of an element in a flame. Processes such as ionization or association (dimers, etc.) can readily be detected since the extent of these varies with the partial pressure of the additive and so will deform the plot,

²¹² W. Behmenburg, H. Kohn, and M. Mailander, *J. Quant. Spectry. Radiative Transfer* **4**, 149 (1964).

²¹³ W. Behmenburg and H. Kohn, *J. Quant. Spectry. Radiative Transfer* **4**, 163 (1964).

²¹⁴ W. Behmenburg, *J. Quant. Spectry. Radiative Transfer* **4**, 177 (1964).

²¹⁵ E. F. M. Van der Held and J. H. Heierman, *Physica* **2**, 71 (1935); **3**, 31 (1936).

²¹⁶ L. Huldt, *Spectrochim. Acta* **7**, 264 (1955).

decreasing or increasing the linear gradient, respectively. It was through not observing this deformation that Schofield and Sugden⁸⁵ realized the slow kinetic ionization mechanism operative for sodium in flames. However, the kinetic ionization rate for K, Rb, and Cs is such that the ionization effect is apparent.⁸⁴ Compound formation involving only one atom of the additive has no effect on the intensity-concentration curve shape but will move the curve as a whole.²⁰⁹

8.3.1.3. Flame Intensity Profiles. Since the detected solid angle of emission can be reduced to a very narrow section, the resolution in a flame on a Sugden burner¹⁰ is very good. The optical arrangement is generally such that radiation from a less than 0.5 mm strip can be detected and intensity profiles can be obtained along a distance or time axis (Figs. 8 and 9). Determination of the mode of excitation is a main use of intensity profile studies. Band systems can similarly be observed. However, for these the chemiluminescent nature may not always be obvious, since intensities may depend on other factors which are changing rapidly with time.¹⁹⁶

Occasionally intensity profiles can determine the rate or cross section for a reaction. Schofield and Sugden⁸⁵ and Hollander *et al.*⁸⁶ have shown that the potassium resonance line emission as a function of time in high-temperature flames represents the progress of the thermal ionization

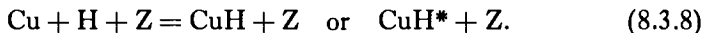


and have obtained a reaction cross section for the process.

In elucidating the reaction by which a molecule is formed, intensity profiles can be very helpful. In H₂/O₂/N₂ flames, diatomic molecules are formed either by bimolecular or by termolecular reactions.¹⁴ Taking the example of CuH in flames, possible reactions for its formation are



or



[Cu], [H₂], and the [Z] concentrations are sensibly constant throughout the burnt gases, so that by comparing the profile of the CuH emission with the known composition profile of [H] the two reactions may be distinguished. Reaction (8.3.7) predicts [CuH] to vary as 1/[H] while (8.3.8) predicts [CuH] is proportional to [H]; the latter is found to be true.^{192, 193}

8.3.1.4. Isothermal Flames—"Family Effect." Although this technique is not responsible for the determination of cross sections directly, it establishes which reactions are occurring in the burnt gases. The basis of the method is to use several flames of differing composition in which some of the flames have the same temperatures but very different compositions.

The particular emission under investigation is observed in all the flames at the same time after combustion. From the observations it can be inferred as to whether the flame's temperature alone is the deciding feature or whether the flame composition plays a part. If the latter is true it is then generally possible to elucidate as to which flame reactants are involved.

A classic case of this is the measurement of Na and Li resonance line intensities in several $H_2/O_2/N_2$ flames at equitme points (Fig. 11). It is

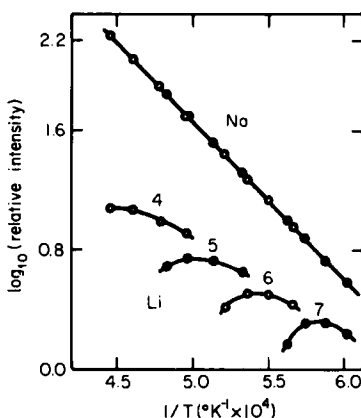
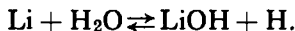


FIG. 11. The variation of the intensity I of the sodium and lithium resonance lines as a function of flame-gas temperature. Measurements made in atmospheric pressure flames at regions 1.25 msec from the reaction zone. Groups of flames with N_2/O_2 unburnt volume ratios 4, 5, 6, and 7 are shown. Within each group points represent H_2/O_2 unburnt volume ratios of 2.5, 3, 3.5, and 4 towards lower temperatures.

apparent that Na shows no isothermal effect but Li does. This implies that the sodium emission is solely a function of temperature and otherwise unaffected, whereas lithium undergoes extensive compound formation. Since intensity-concentration plots for lithium are linear, a compound of the type LiX appears to be formed. It is a relatively easy matter^{14, 207} to establish that this is $LiOH$ formed via



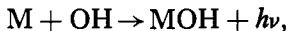
This technique has been used many times. It established the hydroxide emission bands of calcium, strontium, and barium,^{217, 218} later confirmed

²¹⁷ C. G. James and T. M. Sugden, *Nature* **175**, 333 (1955).

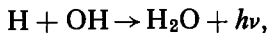
²¹⁸ E. M. Bulewicz, *Nature* **177**, 670 (1956).

by Charton and Gaydon,^{219, 220} and discovered MgOH²²¹ and MnOH²²² bands, as confirmed by Pesic and Gaydon.²²³ Other work has led to the correct assignment of certain continua observed in flames:

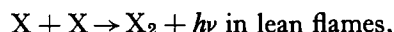
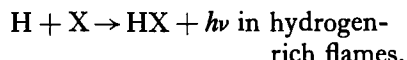
the alkali continuum¹⁹⁴



the hydrogen flame continuum²²⁴



the halogen continua²²⁵



and has established



as being the predominant excitation reaction for these metals in hydrogen-rich flames.²⁰¹

8.3.1.5. Measurement of Collisional Deactivation. Boers *et al.*²²⁶ irradiated a flame containing sodium with a modulated sodium line emission source. The amount of absorption in the flame was measured, and by rotating the detector system about the flame as center the resonance fluorescence from the flame at various angles was observed. From such measurements the importance of collisional deactivation as compared to the radiation process was evaluated. From the probability of collisional deactivation the collision cross section for the $3\ ^2P$ state of sodium was calculated.²²⁶ Since this preliminary work, the dire need for quenching data at high temperatures has promoted further research, basically using this same technique. Hooymayers and Alkemade²²⁷ report quenching cross sections for sodium and potassium with N_2 , CO_2 , CO, O_2 , H_2 , Ar, and H_2O as quenchers and have investigated their temperature dependencies. Jenkins²²⁸ and Carabetta and Kaskan²²⁹ give values for sodium with H_2 , N_2 , H_2O , CO, CO_2 , O_2 , He, Ar, and N_2 , O_2 , H_2O as quenchers, respectively.

This method is limited to strong absorbers.

²¹⁹ M. Charton and A. G. Gaydon, *Proc. Phys. Soc. (London)* **A69**, 520 (1956).

²²⁰ A. G. Gaydon, *Proc. Roy. Soc. A* **231**, 437 (1955).

²²¹ E. M. Bulewicz and T. M. Sugden, *Trans. Faraday Soc.* **55**, 720 (1959).

²²² P. J. Padley and T. M. Sugden, *Trans. Faraday Soc.* **55**, 2054 (1959).

²²³ D. Pesic and A. G. Gaydon, *Proc. Phys. Soc. (London)* **73**, 244 (1959).

²²⁴ P. J. Padley, *Trans. Faraday Soc.* **56**, 449 (1960).

²²⁵ L. F. Phillips and T. M. Sugden, *Can. J. Chem.* **38**, 1804 (1960).

²²⁶ A. L. Boers, C. T. J. Alkemade, and J. A. Smit, *Physica* **22**, 358 (1956).

²²⁷ H. P. Hooymayers and C. T. J. Alkemade, *J. Quant. Spectry. Radiative Transfer* **6**, 501 (1966).

²²⁸ D. R. Jenkins, *Chem. Commun.* p. 171 (1966); *Proc. Roy. Soc. A* **293**, 493 (1966).

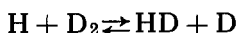
²²⁹ R. A. Carabetta and W. E. Kaskan, *Symp. Combust.*, 11th, *Univ. of California, Berkeley, Calif.*, 1966, p. 321. *Combust. Inst.*, Pittsburgh, Pennsylvania, 1967.

8.3.2. Microprobe Sampling and Mass Spectroscopy

8.3.2.1. Atom and Radical Concentration Determinations by Means of Microprobe Sampling and Mass Spectrometric Analysis. 8.3.2.1.1. D₂O METHOD FOR ABSOLUTE [H]. This method, developed by Fenimore and Jones,³¹ is applicable to the burnt gases of fuel-rich, 1000–2000°K flames, at any pressure. D₂O is added in small amounts of 0.1 to 1% to the unburnt premixed gases. Formation of HD and other stable products is followed by using a high spatial resolution microprobe technique coupled with a mass spectrometer. This data enables $k[H]$ to be evaluated; the k represents the rate constant for the reaction of H + D₂O and is required for an absolute determination of [H]. By using the burnt gases of certain hydrocarbon flames, in which, unlike most hydrogen flames, [H] is at its equilibrium value, k was determined.³¹ More recently, Dixon-Lewis *et al.*^{19, 20, 204, 230} also have obtained values from flames at 1072°K by various methods, confirming Fenimore and Jones' value to within a factor of two. However, a much lower activation energy for k is now recommended.²³¹ Other research by Fenimore and Jones³³ and by Bascombe²³² further illustrates the method.

8.3.2.1.2. H₂O¹⁸ METHOD FOR [H] ABSOLUTELY. If flames are too lean, [H] becomes too small for the previous method. A similar method³⁴ using addition of H₂O¹⁸ to the premixed unburnt gases is more applicable. The technique requires the formation of O¹⁶O¹⁸ to be monitored and is limited to the burnt gases of flames since certain equilibrations have to be established for the analysis.

8.3.2.1.3. D₂ METHOD FOR [H] ABSOLUTELY. On addition of D₂ to a flame, the fast reaction



occurs. Although this is equilibrated in the burnt gases of the flame, its progress can be followed in the reaction zone of low-pressure flames,³² and in slow-burning atmospheric pressure flames.²⁰⁴ The technique is to add a little D₂ to the unburnt, premixed gases and, by microprobe sampling and mass spectrometric analysis, follow the growth of HD, together with the other stable species throughout the reaction zone. From this data values for [H] in the reaction zone region can be obtained.

²³⁰ G. Dixon-Lewis, M. M. Sutton, and A. Williams, *J. Chem. Soc.*, p. 5724 (1965).

²³¹ K. Schofield, *Planetary Space Sci.* **15**, 643, 1336 (1967).

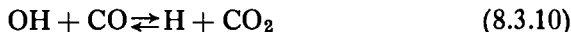
²³² K. N. Bascombe, *Symp. Combust.*, **10th**, Univ. Cambridge, Cambridge, Engl., 1964, p. 55. *Combust. Inst.*, Pittsburgh, Pennsylvania, 1965.

8.3.2.1.4. N₂O METHOD FOR [H] ABSOLUTELY. In rich flames, N₂O is consumed predominantly by the fast reaction



Fenimore and Jones,³² through measurements of [H] in the burnt gases by the D₂O method, obtained the rate constant. Since the reaction with H atoms is irreversible, observations of the decay of N₂O are now sufficient to enable [H] to be determined. The method is particularly useful in the reaction zone. An example of the method³⁵ determines [H] in a H₂/N₂O/NH₃/NO flame. Generally about 0.5% of N₂O is added to the unburnt gas mixture. Dixon-Lewis *et al.*^{19, 230} have redetermined the rate constant of (8.3.9) using the D₂ method for [H] in the reaction zone and confirmed the value obtained by Fenimore and Jones.

8.3.2.1.5. CO₂ METHOD FOR [OH] ABSOLUTELY. The reaction



has been shown to be effectively equilibrated in the burnt gases of flames^{109, 233} and is now generally accepted as being the main reaction responsible for CO₂ formation in hydrocarbon-oxygen flames.³⁷ Fenimore and Jones^{32, 233} obtained a value for the rate constant of (8.3.10) by measuring [H] and the stable species concentration profiles in a H₂/O₂/CO₂ flame. This has since been redetermined.^{19, 20} These values, together with other independent determinations, have now established $k_{(8.3.10)}$ over the temperature range 300–2000°K to well within a factor of two.²³¹

With the kinetics established, the method is now under no restriction and has been found most useful in the reaction zone region, particularly of hydrocarbon-oxygen flames. From the rate of formation of CO₂ and the CO profile, [OH] can be determined if (8.3.10) is regarded as irreversible, the approximate case in lean flames.^{37, 234, 235} If [H] is such that the reverse reaction does have to be taken into account, since its concentration is required before [OH] can be determined, the method is of no use.

8.3.2.1.6. N₂O METHOD FOR [O] ABSOLUTELY. This method is restricted to lean flames where [O] ≫ [H] and [OH]. Under these conditions the major reaction for the disappearance of N₂O is the irreversible reaction³⁰



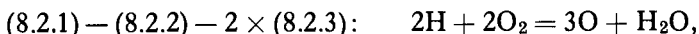
rather than the fast reaction with H atoms (8.3.9).³² Since rate constant

²³³ C. P. Fenimore and G. W. Jones, *J. Phys. Chem.* **62**, 1578 (1958).

²³⁴ A. A. Westenberg and R. M. Fristrom, *J. Phys. Chem.* **65**, 591 (1961).

²³⁵ C. P. Fenimore and G. W. Jones, *J. Phys. Chem.* **65**, 2200 (1961).

data for reaction (8.3.11) was lacking, Fenimore and Jones³⁰ initially obtained an approximate value through calculating [O] in the burnt gases of an atmospheric pressure flame from the effective balance (8.2.4). Since lean flames were concerned, [H₂] was small and only approximately measurable. A reinvestigation of the rate,³⁴ measuring [H] in the burnt gases of a low-pressure flame by the H₂O¹⁸ method and converting this to a more accurate estimate of [O] via the effective balance



confirmed the original estimate. The method with the rate data established has been used mainly in the reaction zone region.³⁶

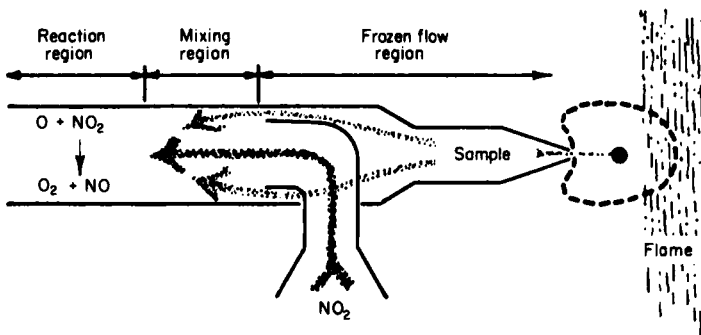
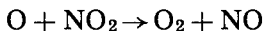


FIG. 12. Schematic diagram of scavenger probe [from R. M. Fristrom, *Symp. Combust., 9th, Cornell Univ., Ithaca, N.Y., 1962*, p. 560. Academic Press, New York, 1963].

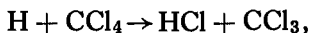
8.3.2.2. Atom and Radical Concentration Determinations by Applying Scavenger Methods to a Microprobe Sample. This is an extension of the microprobe-mass spectrometric technique, whereby atom and radical concentrations may be obtained without making any additions to the flame. The method, developed by Fristrom and co-workers,^{26, 27} depends on finding chemical scavengers, which, if added immediately to a sample, undergo a rapid quantitative reaction with the atom or radical of interest, to yield stable analyzable products. Radical concentrations then are calculated from known relations to the product species. The main requirement is that the scavenger reacts rapidly before other reactions can occur. Figure 12 illustrates the method of applying the technique.

[O] has been detected by adding an excess of NO₂ to the sample so that the quantitative reaction²³⁶



²³⁶ F. Kaufman, *Proc. Roy. Soc. A* **247**, 123 (1958).

occurs. However, H also reacts with NO_2 ,²³⁷ so the method is only of use when $[\text{O}] \gg [\text{H}]$. For [H] the only scavenger used so far has been CCl_4 ,



but since the reaction is not quantitative it yields only approximate values. Other scavengers are now being sought, e.g., I_2 seems suitable for the determination of CH_3 radicals.

8.3.2.3. Direct Mass Spectrometry of Ions in Flames. The ions present in flames may be readily detected by a mass spectrometer, having no ionization chamber, but a small sampling hole against which the flame is directed. Three schools of research have applied this technique to the study of flame ionization processes. Calcote^{53, 54} has concentrated on low-pressure (1–6 Torr) hydrocarbon-oxygen flames and studied the reaction zone in detail. Van Tiggelen^{57, 60} has worked in the intermediate pressure range (10–100 Torr) investigating a wide variety of flames. Sugden^{66, 69} uses atmospheric pressure flames. Knewstubb²³⁸ has recently reviewed these three experimental systems. King and Scheurich²³⁹ have modified Sugden's technique through the use of a time-of-flight mass spectrometer.

After initial problems as to whether the detected ions were a true representation of the flame sample, it is now possible to establish the flame ions.⁶⁷ These mass spectrometric techniques are quite sensitive, being able to detect $\geq 10^5$ to 10^6 ions cm^{-3} in the flame gases. Consequently, with such a level of detection, the natural isotopes, e.g., C^{13} (1.1% abundant), O^{18} (0.20%), and N^{15} (0.36%) can usually be detected and used to determine the correct ions for the detected masses. If difficulties do arise, deuterium or substituted reactants can be used.^{54, 58, 59} Useful techniques for small amounts of the isotopic species are available.^{56, 68} Likewise, inert diluents can be changed (e.g., Ar for N_2) to facilitate ion identifications.

Many surprising results have come from the study of hydrocarbon flames. For a long time it had been known that ionization in the reaction zone of these flames was very high, in fact, higher than could be explained on a thermal basis. On analysis, samples of the reaction zone region of such flames showed ions of mass up to and possibly greater than 150.^{61, 63, 65} H_3O^+ surprisingly was the most abundant ion and persisted into the burnt gases; C_3H_3^+ was the most abundant hydrocarbon ion. Profiles of several ions are shown in Fig. 13. A very extensive and rapid polymerization of the fuel is apparent and is greatest for the unsaturated hydrocarbon fuels.

²³⁷ M. A. A. Clyne and B. A. Thrush, *Trans. Faraday Soc.* **57**, 2176 (1962).

²³⁸ P. F. Knewstubb, Mass spectrometry of ions from electric discharges, flames and other sources. In "Mass Spectrometry of Organic Ions" (F. W. MacLafferty, ed.), Chapter 6, p. 255. Academic Press, New York, 1963.

²³⁹ I. R. King and J. T. Scheurich, *Rev. Sci. Instr.* **37**, 1219 (1966).

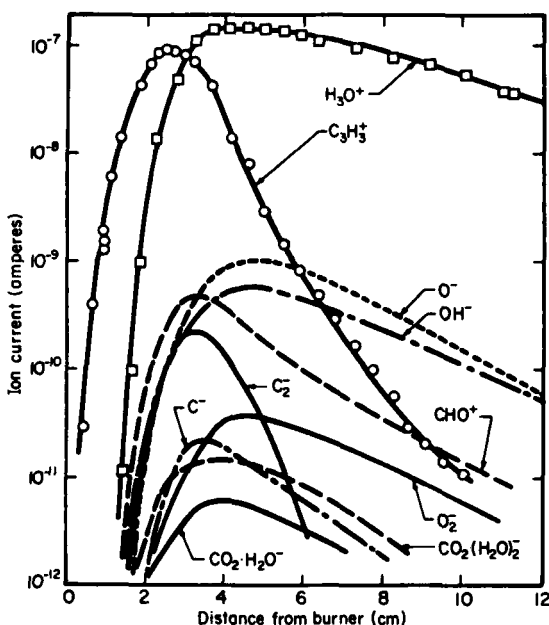
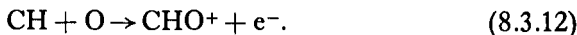


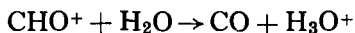
FIG. 13. Positive and negative ion profiles for an acetylene-oxygen flame. Equivalence ratio 1.0; pressure 1 Torr; total flow $70 \text{ cm}^3/\text{sec}$ STP [from H. F. Calcote, S. C. Kurzus, and W. J. Miller, *Symp. Combust.*, 10th, Univ. Cambridge, Cambridge, Engl., 1964, p. 605. Combust. Inst., Pittsburgh, Pennsylvania, 1965].

These ions are short lived, however, and confined to the reaction zone region; the burnt gases of such flames generally only show H_3O^+ .

The precise mechanism by which the initial ionization occurs is



It was initially proposed by Calcote⁷⁵ and has been established by Bascombe *et al.*⁶⁷ and Green and Sugden⁶⁸ investigating $\text{H}_2/\text{O}_2/\text{N}_2$ flames to which controlled additions of C_2H_2 were made. The ion profiles were investigated as a function of added C_2H_2 , and it was found (Fig. 14) that $[\text{H}_3\text{O}^+] \propto [\text{C}_2\text{H}_2]^{1/2}$ and $[\text{CHO}^+] \propto [\text{C}_2\text{H}_2]$, so that such relationships had to be satisfied by proposed mechanisms. The CHO^+ ion is the precursor for H_3O^+ ,



which rate has been measured in flames.^{67, 68} As yet, the reactions by which the remaining multitude of ions are formed have not been firmly established.⁵⁵ Fontijn *et al.*⁵⁶ have attempted to set up and study these kinds of

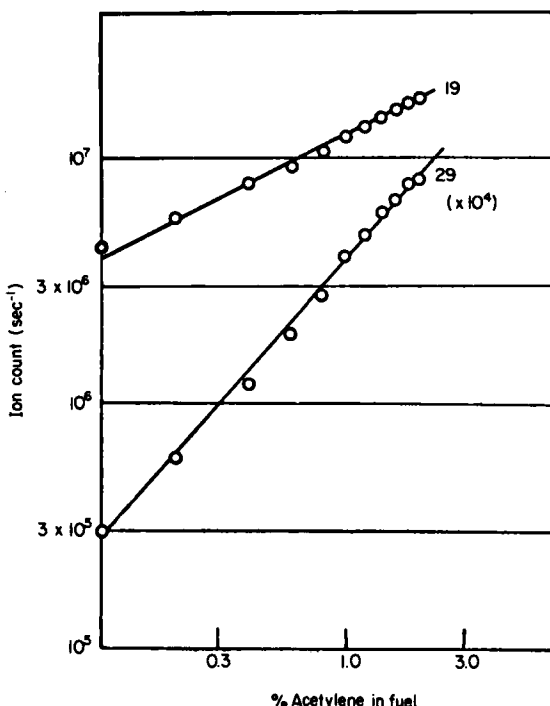
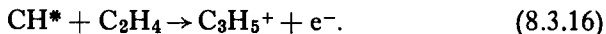
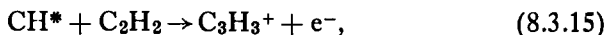
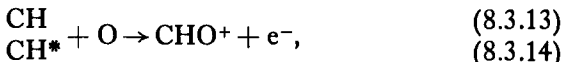


FIG. 14. Dependence of maximum ion counts at mass 19 (H_3O^+) and mass 29 (CHO^+) on the percentage acetylene in the fuel of a $\text{H}_2/\text{O}_2/\text{N}_2$ flame [from J. A. Green and T. M. Sugden, *Symp. Combust., 9th, Cornell Univ., Ithaca, N.Y., 1962*, p. 607. Academic Press, New York, 1963].

reactions in low-pressure flow systems, which are less complex than the usual flame, and have studied the atomic oxygen with C_2H_2 and C_2H_4 reactions. Owing to the lack of water in their system, CHO^+ is the dominant ion. They conclude that there are two basic chemionization processes:

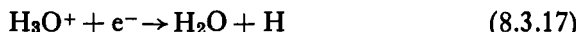


However, more recent work by Miller²⁴⁰ on low-pressure flames shows that (8.3.14) and (8.3.15) are unimportant and that C_3H_3^+ is probably

²⁴⁰ W. J. Miller, *Symp. Combust., 11th, Univ. of California, Berkeley, Calif., 1966*, p. 311. Combust. Inst., Pittsburgh, Pennsylvania, 1967.

formed by proton transfer and/or ion molecule reactions involving C_3H_2 or C_2H_2 . An estimate of $k_{(8.3.18)}$ has been made.^{67, 68}

In hydrocarbon-oxidant flames, H_3O^+ is the dominant ion, particularly in the burnt flame gases, and its concentration approximates to that of the electron concentration (negative ions considered negligible). Disappearance of ions follows

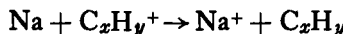
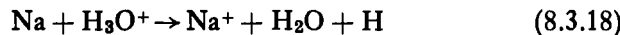


and the simple bimolecular law

$$\frac{1}{[H_3O^+]_1} - \frac{1}{[H_3O^+]_2} = k(t_2 - t_1)$$

where k is the rate constant for (8.3.17). Values for the recombination rate have been established.^{67, 68}

The ionization of metal atoms in flame gases has been studied by many workers. An interesting point is that addition of quantities of sodium and potassium causes the natural flame ion peaks to disappear. Evidence for charge transfer reactions



is gradually accumulating.^{54, 60, 66, 69} Hayhurst and Sugden⁶⁹ have recently quoted a value for $k_{(8.3.18)}$ at 2000°K.

Calcote,⁵³ using Langmuir probes, determined both the positive ion and electron concentrations in flames at various pressures. Since the positive ion concentration was found to exceed that of the electrons by a significant amount, the formation of negative ions was apparent. Initial attempts to observe negative ions in flames failed, but recently several reports have appeared wherein numerous ions have been detected.^{55, 70, 72} A typical set of profiles appears in Fig. 13. Miller and Fontijn⁷¹ have also detected these ions in an atomic oxygen-acetylene flow system.

8.3.3. Electron Measurements

Van Tiggelen and co-workers²⁴¹⁻²⁴⁴ have developed circular and rectangular slit burners in which a flame burns between two edges which are electrically insulated from one another. In this way, the conductivities

²⁴¹ J. Poncelet, R. Berendsen, and A. van Tiggelen, *Symp. Combust., 7th, London, Oxford, 1958*, p. 256. Butterworths, London, 1959.

²⁴² R. Berendsen and A. van Tiggelen, *Bull. Soc. Chim. Belges* **68**, 620 (1959).

²⁴³ R. Berendsen, G. Taelemans, and A. van Tiggelen, *Bull. Soc. Chim. Belges* **69**, 32 (1960).

²⁴⁴ A. van Tiggelen, *Progr. Astronaut. Aeron.* **12**, 165 (1963).

in the flame fronts of a number of flames have been measured. However, it is not possible to deduce from the apparent conductivity the absolute concentration of ions and electrons in the flame. Assumptions made by van Tiggelen in attempting to do so are not justified.²⁴⁵

When weak plasmas are measured, the "saturation current" method,²⁴⁶ however, is convenient and absolute. The maximum electrical current which can be drawn from a flame is equal to the rate of electron production. The technique has also been used recently in low-pressure flow systems.²⁴⁷⁻²⁴⁹

8.3.3.1. Langmuir Probes. In spite of the difficulties associated with the use of probes and the uncertainty concerning the absolute values obtained, probes are invaluable for high spatial resolution studies in flames. With the development of small probes,^{53, 77} flame disturbances, cooling effect on the surrounding gases, and too extensive a depletion of the flame's supply of ions (electrons) can be reduced to a minimum.

Probe theory strictly applies to low pressures, such that the mean free path of the species is much larger than the probe dimensions (never the case in combustion studies), and until recently^{74, 77} both the practical and theoretical problems were such to prohibit the use of probes at high temperatures and pressures. The initial work of Calcote resulted in low values for the positive ion concentration since corrections for the pressure effect and probe size,^{78, 250} later found to be necessary, were not included.

If only a single ion is known to be involved, a value for the recombination coefficient in the burnt gases may be obtained from the positive ion profile.⁵⁵ It has been found necessary to correct for the ambipolar diffusion to the walls of the burner,^{55, 75} particularly at low pressure. Values obtained for the recombination coefficient are considered to refer to the dissociative recombination reaction (8.3.17). Using flames over a range of pressures (33-760 Torr) and temperatures (1740-2130°K), Calcote has found the recombination rate to be independent of pressure and temperature.^{55, 75} King⁸³ failed to establish this independence of pressure through his neglect of the ambipolar diffusion.

²⁴⁵ C. R. Gatz, W. A. Rosser, and F. T. Smith, Study of radar beam attenuation in rocket exhaust gases, Pt. 2: The chemistry of ionization in rocket exhausts. Tech. Final Rept. AFBMD-TR-61-39, Pt. 2, Contract AF 04(647)-221, February 1961.

²⁴⁶ K. G. Payne and F. J. Weinberg, *Symp. Combust., 8th, Pasadena, Calif., 1960*, p. 207. Williams & Wilkins, Baltimore, Maryland, 1962.

²⁴⁷ C. R. Gatz, F. T. Smith, and H. Wise, *J. Chem. Phys.* **35**, 1500 (1961).

²⁴⁸ C. R. Gatz, R. A. Young, and R. L. Sharpless, *J. Chem. Phys.* **39**, 1234 (1963).

²⁴⁹ C. A. Arrington, W. Brennen, G. P. Glass, J. V. Michael, and H. Niki, *J. Chem. Phys.* **43**, 1489 (1965).

²⁵⁰ I. R. King, and H. F. Calcote *J. Chem. Phys.* **23**, 2203 (1955).

The flame ion profile can also be used to establish the rate of ion formation. If it is assumed that the recombination process is the same throughout the flame, then the maximum ion concentration will occur when the rate of recombination equals the rate of ion formation. Rates of ion formation therefore may be obtained and can be useful in checking proposed mechanisms. Calcote⁷⁵ established that the rate of ion formation in hydrocarbon flames was proportional to the square of the pressure, inferring a second-order ion-producing reaction.

8.3.3.2. Electromagnetic Absorption Methods. Radio-frequency and microwave absorption methods (cf. Section 8.2.1.3.3) essentially measure the electrical conductivity of the flame, which is related to $[e^-]$. A knowledge of the collision frequency of electrons with flame gas molecules is required before this can be evaluated. This limits the accuracy as such values are still quite scattered.^{53, 88, 251, 252}

Since ionization in flames without additives is in general rather small or confined to the reaction zone region, these methods have been used mainly to study effects of small additions of ionizable metallic salts to flames, since there is then extensive ionization in the burnt gases. Techniques center around either electron profile measurements or studies of $[e^-]$ as a function of the additive concentration.

Electron cyclotron resonance has been observed in low-pressure flames.^{84, 101-106} From the shape of the resonance absorption line, both the electron-molecule collision frequency and $[e^-]$ can be obtained. At low pressures, the reaction zone of certain flames becomes extensive and $[e^-]$ has been measured in this region,^{102, 105, 106} but no profiles throughout the flame have been obtained.

Bulewicz¹⁰³ burnt low-pressure acetylene-oxygen flames diluted with amounts of either N_2 , Ar, He, or Ne. By suitably varying the amount of the diluent it was possible to isolate the electron-molecule collision cross sections for the individual constituents. Values of $80 \pm 4 \text{ \AA}^2$ for H_2O and $37 \pm 2 \text{ \AA}^2$ for CO_2 were obtained at about 2200°K . Other values determined were N_2 , 30 \AA^2 ; He, 27 \AA^2 ; Ar, 7 \AA^2 ; Ne, 5 \AA^2 . The correctness of the values for H_2O and CO_2 was tested¹⁰⁴ by burning many stoichiometric hydrocarbon-oxygen flames for which these are the burnt gases major constituents. Great care, however, must be taken in order to obtain reliable values for collision cross sections using such techniques.²⁵³

²⁵¹ D. L. Turcotte and W. Friedman, *Symp. Combust., 10th, Univ. Cambridge, Cambridge, Engl.*, 1964, p. 673. Combust. Inst., Pittsburgh, Pennsylvania, 1965.

²⁵² E. M. Bulewicz, *Discussion. Symp. Combust., 10th, Univ. Cambridge, Cambridge, Engl.*, 1964, p. 683. Combust. Inst., Pittsburgh, Pennsylvania, 1965.

²⁵³ F. C. Fehsenfeld, L. R. Megill, and L. K. Dippleman, *J. Chem. Phys.* **43**, 3618 (1965).

8.4 Rate Constants (Cross Sections) from Flame Studies

Schofield²³¹ has recently drawn up a critical evaluation of rate data for many simple bimolecular and termolecular reactions of neutral species. Closer inspection of the analysis shows the contribution that flame studies have made to the determination of rate constants and their temperature dependencies. The temperature regime of flame studies, 1000–2500°K, couples well the higher-temperature shock-tube data to the lower-temperature data from such sources as discharge-flow systems, photolyses, and thermal studies. Although undoubtedly a complex one, the flame medium generally is beset with problems no worse than those occurring in the other mentioned basic techniques.

9. INTERACTIONS OF PARTICLES WITH SOLIDS

9.1. Interactions of Heavy Particles with Solids*

9.1.1. Introduction

At sufficiently high energies, where the effective range of interatomic repulsive forces is small compared to lattice spacings, the interactions of heavy particles with solids are not very different than they would be with a dense gas or, more properly in the case of conductors, with a dense plasma. An energetic ion entering a solid may lose its energy through elastic collisions with lattice atoms, by inelastic collisions with bound electrons through ionization and excitation, or by inelastic collisions with conduction electrons through the generation of plasmons.

Lattice atoms liberated by these collisions can cause secondary collision cascades which may result in generation of permanent lattice defects (radiation damage)[†] or in the ejection of atoms from the solid surface (sputtering). Manifestations of the electronic interaction may be observed in such processes as the ejection of secondary electrons, the formation of electron-hole pairs in semiconductors, and the change of the ionic charge of an energetic projectile in the target.

At lower incident energies, the interatomic repulsive forces of the lattice atoms with respect to an incoming particle tend to merge. The penetration of the particle becomes more limited, and at sufficiently low energies pure surface interactions predominate. Secondary electron ejection may still exist but only because of Auger emission of electrons from the conduction band due to neutralization of an incident ion. At thermal energy, an incoming particle may be trapped and adsorbed on the surface, or it may be reflected with the exchange of some energy with lattice phonons. In this case, the translational energy of the surface atoms in their lattice sites can no longer be ignored.

It is quite clear that any attempt at a complete treatment of the experimental methods used in the investigation of all the phenomena mentioned would be quite impossible within the confines of this chapter. Instead, in

[†] See also Vol. 6A, Chapter 4.4.

* Chapter 9.1 is by S. Datz and H. O. Lutz.

keeping with the content of this volume, we will concentrate on primary particle collisions which can be most clearly described in terms of atomic collision processes. For example, the reflection behavior of beams from well-ordered surfaces has been explained in terms of single collisions with surface atoms; the penetration of energetic ions in noncrystalline targets is determined by statistical collisions with the target atoms and their electrons, while channeling phenomena have been shown to arise from correlated collisions in ordered lattices. As a result, we will mostly be dealing with directed beams of atoms or ions incident on solid targets. If the target preparation is specific for a technique, it will be discussed under individual experiments.

9.1.2. Penetration Experiments

9.1.2.1. General Theory for a Random Solid. A particle (nuclear charge Z_1) moving through a lattice with a speed lower than the orbital velocity of the least tightly bound electron is in the neutral state for an appreciable fraction of the time. Its kinetic energy is dissipated predominantly by momentum transfer in collisions with lattice atoms (nuclear stopping). Since the binding energy of the outermost electron for most elements is in the order of 10 eV, the particle velocity v can as well be referred to the Bohr orbital velocity of the hydrogen electron $v_B = e^2/\hbar$. Thus nuclear stopping should predominate when $\xi_0 \equiv v/v_B = \hbar v/e^2 \ll 1$.

At higher velocities ($\xi_0 \sim 1$), outer electrons will be stripped off with a finite probability and the ion will lose energy through ionization and excitation of the target electrons (electronic stopping). The actual ionic charge will oscillate about a most probable value which is dependent on the ion energy.

A steady-state charge distribution is attained which is dependent on the relative values of the charge loss and gain cross sections. In general it is observed that the most probable charge state of a fast ion in a solid is significantly higher than those obtained in gases. This phenomenon, dubbed "condensation effect", is probably attributable to the high collision frequency in solids.

Some collisions may lead to excitation of bound electrons. Similarly, electron capture into excited states is possible. In the case of a diffuse gaseous medium the time between succeeding collisions may be long enough to permit de-excitation by radiative processes, whereas in condensed media the next collision can occur before relaxation takes place. Since the ionization cross section is expected to be greater for excited states, the higher collision frequency in solids should lead to higher average charge states.

If the ion velocity greatly exceeds the orbital velocities of all of its electrons ($\xi_0/Z_1 \gg 1$), they will be stripped off and only the bare nucleus proceeds through the medium. The energy loss is dominated by electronic stopping.

Bohr¹ was the first to outline the theoretical aspects of the passage of fast particles through matter. If dynamical effects, such as polarization of the medium by the moving particle, are neglected, the elastic collision between it and a lattice atom can be described in terms of the Coulomb potential of the nuclei, screened by their electron clouds. The general form of this potential can be written as

$$V(r) = \frac{Z_1 Z_2 e^2}{r} \cdot \phi(r) \quad (1)$$

where Z_1, Z_2 are the nuclear charges of the ion and the target atoms, r the radial distance, and $\phi(r)$ the screening function. The crucial problem in calculating the potential is to find a reasonable expression for $\phi(r)$. Generally it is calculated from the electron density distribution of the neutral atoms. Bohr assumed exponential screening,

$$\phi(r) = e^{-r/a} \quad (2)$$

where the screening radius $a = a_H \cdot (Z_1^{2/3} + Z_2^{2/3})^{-1/2}$, and $a_H = 5.29 \cdot 10^{-9}$ cm, the classical radius of the hydrogen atom. This Bohr screening function is an approximation to the Thomas–Fermi screening function of a neutral atom. The values for the potential given by this function are generally too small, especially at larger distances r . Other forms of $\phi(r)$ have also been used in theoretical calculations. The mathematically simple $1/r$ screening as used by Nielsen² gives a relatively good approximation to the Thomas–Fermi potential at lower particle energies; the nuclear stopping power becomes

$$-\left(\frac{dE}{dx}\right)_n = \frac{\pi^2 N a Z_1 Z_2 e^2 M_1}{2.718(M_1 + M_2)} \quad (3)$$

and is independent of the particle energy E . N is the concentration of target atoms and M_1, M_2 are masses of the collision partners. A more realistic solution can be obtained if the Thomas–Fermi screening function is used. Lindhard *et al.*³ calculated a general stopping power curve (Fig. 1) by

¹ N. Bohr, *Kgl. Danske Videnskab. Selskab Mat. Fys. Medd.* **18**, 8 (1948).

² K. O. Nielsen, "Electromagnetically Enriched Isotopes and Mass Spectrometry," p. 68. Butterworths, London, and Washington D.C., 1956.

³ J. Lindhard and M. Scharff, *Phys. Rev.* **124**, 128 (1961); J. Lindhard, M. Scharff, and H. E. Schiøtt, *Kgl. Danske Videnskab. Selskab Mat. Fys. Medd.* **33**, 14 (1963).

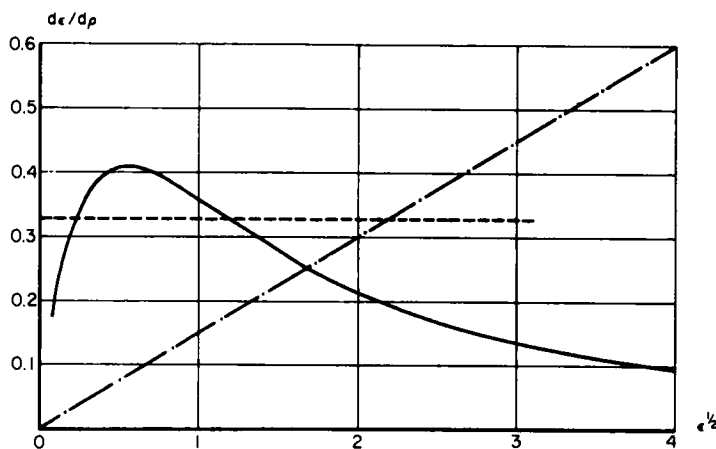


FIG. 1. Theoretical stopping cross sections in ρ - ϵ variables [J. Lindhard and M. Scharff, *Phys. Rev.* **124**, 128 (1961); J. Lindhard, M. Scharff, and H. E. Schiøtt, *Kgl. Danske Videnskab. Selskab Mat. Fys. Medd.* **33**, 14 (1963)]. —, elastic stopping, Thomas-Fermi interaction potential; - - -, elastic stopping, r^{-3} interaction potential; - · -, inelastic stopping, $k\sqrt{\epsilon}$, for $k = 0.15$.

introducing the dimensionless variables

$$\rho = 4\pi RN(0.8853 \cdot a)^2 \cdot \frac{M_1 M_2}{(M_1 + M_2)^2}, \quad (4)$$

$$\epsilon = \frac{0.8853 \cdot a}{b}.$$

R is the particle range, and b the distance of closest approach in a head-on collision. In this case the nuclear stopping power $(d\rho/d\epsilon)_n$ decreases with energy after reaching a maximum at $\epsilon \sim 0.25$.

The problem of electronic stopping has been attacked by several authors; the most recent discussion has been given by Fano.⁴ The general form of the electronic stopping power can be written as

$$\left(\frac{dE}{dx}\right)_e = \frac{4\pi Z^2 e^4}{m_e v^2} \cdot N \cdot B \quad (5)$$

where Z is the ionic charge, m_e the electron mass, and B the dimensionless "stopping number." Bohr⁵ calculated the stopping number B on the basis of classical mechanics assuming a Rutherford model of the atom. The first

⁴ U. Fano, *Ann. Rev. Nucl. Sci.* **13**, 1 (1963).

⁵ N. Bohr, *Phil. Mag.* **25**, 10 (1913).

purely quantum mechanical solution for B was obtained by Bethe,⁶ using the Born approximation:

$$B = Z_2 \cdot \ln \frac{2m_e v^2}{I} \quad (6)$$

with I the mean excitation energy of the target atoms. Bloch⁷ combined the theories of Bethe and Bohr, taking into account the perturbation of the wave functions of the atomic electrons caused by the moving particle. His result reduces to Bohr's solution for B in the limit of low ion velocities $\xi_0/Z \ll 1$, and to Bethe's solution in the limit of high ion velocities $\xi_0/Z \gg 1$. Bloch⁸ showed that for Thomas-Fermi atoms with atomic number Z_2 , the mean excitation energy I is approximately given by

$$I = K \cdot Z_2 \quad (7)$$

where K is an empirical number ("Bloch constant") in the order of 10 eV for a wide range of Z_2 values.

The Bethe-Bloch stopping formula gives a v^{-2} dependence at high ion velocities [$\xi_0/Z_1 \gg 1$ with $Z \sim Z_1$ in Eq. (5)]. At intermediate velocities ($\xi_0/Z^{2/3} \sim 1$) the gradual neutralization of the ion [decreasing Z in Eq. (5)] starts to dominate this dependence, and at lower velocities the electronic stopping power decreases proportional to velocity after going through a maximum. Lindhard *et al.*⁹ obtained in a theoretical treatment for $\xi_0/Z_1^{2/3} < 1$ the relationship.

$$\frac{d\varepsilon}{d\rho} = k \cdot \sqrt{\varepsilon}, \quad (8a)$$

$$k = Z_1^{1/6} \cdot \frac{0.0793 \cdot Z_1^{1/2} \cdot Z_2^{1/2} (A_1 + A_2)^{3/2}}{(Z_1^{2/3} + Z_2^{2/3})^{3/4} \cdot A_1^{3/2} \cdot A_2^{1/2}}, \quad (8b)$$

with A_1 and A_2 the dimensionless mass numbers of the ion and the target atoms. For ε, ρ see Eq. (4).

The total stopping of an ion in a medium is given by the sum of the elastic "nuclear" and inelastic "electronic" stopping. The fact that the moving particle can also lose energy by other processes (e.g., nuclear reactions with the target) will not be discussed here. The total range of the particle can be obtained by integrating the differential energy loss over all possible energies,

$$R = \int_0^{E_0} \left(-\frac{dE}{dx} \right)^{-1} dE. \quad (9)$$

⁶ H. A. Bethe, *Ann. Physik* **5**, 325 (1930).

⁷ F. Bloch, *Ann. Physik* **16**, 285 (1933).

⁸ F. Bloch, *Z. Physik* **81**, 363 (1933).

The measured range is usually a "projected range" or "penetration depth" R_p along the direction of beam incidence. At lower energies where the large angle scattering cross section is not small compared to the total scattering cross section, total and projected range may differ considerably. The total range then has to be deduced from the penetration depth from theoretical considerations; for example, Lindhard *et al.*³ give for an interaction potential $V(r) \sim r^{-n}$

$$\bar{R}/\bar{R}_p \simeq 1 + \frac{M_2}{M_1} \cdot \frac{n^2}{4(2n-1)}. \quad (10)$$

In deriving this formula, only elastic collisions are considered; the energy range of validity is $\epsilon \lesssim 1$. In general, it will be necessary to work with the averages \bar{R} and \bar{R}_p . Because of the statistical nature of the energy loss process the penetration depth, as well as the deflection from the initial beam direction, will scatter about most probable values. If the individual events are uncorrelated, the average square fluctuation of the energy loss ("straggling") can be written as

$$\Delta^2 = N \cdot dR \cdot \int d\sigma \cdot T_t^2 \quad (11)$$

where $d\sigma$ is the differential cross section for energy transfer T_t to atoms and atomic electrons. Here dR is used instead of dx to emphasize that the energy loss occurs along the particle path. Lindhard *et al.*³ presented a rather comprehensive study of the energy straggling and the resulting range straggling for various forms of the interaction potential $V(r)$.

9.1.2.2. Ionic Charges of Heavy Particles Passing through Solids. A fast particle moving through a solid target picks up and loses electrons, its ionic charge fluctuating about a most probable value which depends on the particle energy. The charge of the ion *in* the solid cannot be measured directly, and present stopping theory is not precise enough to permit the deduction of the ionic charge from a measurement of the stopping power. One is therefore limited to the measurement of charge distributions of the ions emerging from the target which may be affected by charge transfer processes taking place as the particle leaves the surface. In general the charge distribution of an ion beam with energy E_0 is analyzed by deflecting the beam in a magnetic or electrostatic field. Ions with different charge q are deflected differently; the charge groups can be detected, e.g., with an array of solid-state counters placed after the deflecting system giving the relative population of each charge state. The relative energy spread $\Delta E/E_0$ in the beam should be small to avoid overlapping of the charge groups. Overlapping of a group q , e.g., with the next lower group ($q-1$), will occur

for particles with an energy different from E_0 by $\pm \Delta E$, given by

$$\frac{\Delta E}{E_0} = \frac{2q + 1}{2q^2 + 2q + 1} \quad (12a)$$

for a magnetic field, and correspondingly

$$\frac{\Delta E}{E_0} = \frac{1}{2q + 1} \quad (12b)$$

for an electrostatic field.

Instead of using an array of counters to detect the charge groups, the deflected beam can be swept across a single detector by changing the deflecting field intensity. If the change in deflecting field intensity, dE/dt , is constant with time, the dwell time of different charge groups on the detector is proportional to q^{-1} . The number of counts registered in each group has to be corrected accordingly. Another possibility would be to keep the field constant and to move the detector in controlled steps across the deflected charge groups. A multichannel analyzer can be addressed by the field intensity or the position of the moving detector, to record the charge spectrum automatically. A difficulty is that the initial beam intensity can vary during the experiment; it has to be monitored, e.g., by counting a known fraction of the initial or deflected beam. This problem can be avoided, if a position-sensitive solid-state detector is used.⁹ The deflection is adjusted so that at least two charge groups, preferably the whole charge spectrum, can be recorded at one time. This decreases the time duration of an experiment considerably and makes a beam monitor unnecessary.

9.1.2.3. Energy Loss in Thin Layers of Material. A direct method for studying the stopping of fast particles in solids is to measure their energy degradation in thin foils. A beam of known energy E_0 is passed through a thin foil, and the energy E and the spread δE of the emerging particles are analyzed. Here again, position-sensitive solid-state detectors may be used to measure the positional dispersion of an electrostatically or magnetically analyzed ion beam. Particularly convenient devices for the energy analysis of highly ionizing particles are the solid-state detector¹⁰ (see Section 9.1.2.5.8) and scintillation crystals which eliminate the necessity of electric or magnetic deflection fields. When the energy resolution of the detector itself is insufficient (as is the case for heavy ions), time-of-flight techniques

⁹ E. Norbeck and R. C. Carlson, Instrumentation techniques in nuclear pulse analysis, *Natl. Acad. Sci.—Natl. Res. Council Publ.* No. 1184, p. 42 (1964).

¹⁰ J. W. T. Dabbs and F. J. Walker, ed., Semiconductor particle detection. *Natl. Acad. of Sci.—Natl. Res. Council Publ.* No. 871 (1961).

utilizing fast timing electronics (time resolution ~ 1 nsec) can be used.^{11, 11a} The energy versus energy loss relationship can be obtained by changing the foil thickness d in small steps and plotting the emergent ion energy against d , or by varying E_0 and keeping d constant. The energy loss $-\Delta E$ can also be determined directly if the energy deposition in the foil is measured calorimetrically. This technique has been used by Anderson *et al.*¹² to determine with very high precision ($\sim 0.3\%$) the stopping power of aluminum for 5–12-MeV protons and deuterons.

The thin foils are usually grown by vacuum evaporation or electrolytic deposition (e.g., Hass and Turner¹³); mechanically thinned foils (hammered and rolled) can show large nonuniformities in thickness (10% or more). The thickness can be determined with high accuracy by weighing; if the specimen is too small, interference microscopy (e.g., Tolansky¹⁴) can be used. Another very convenient method is to measure the energy loss of α -particles (emitted from a natural source) in the foil, once their stopping power has been determined by other techniques. The accuracy here is $\sim 5\%$ for a foil thickness of around $300 \mu\text{g}/\text{cm}^2$.

It facilitates the analysis if the energy loss, $-\Delta E$, is low enough to allow equating the measured difference quotient, $-\Delta E/\Delta x$, with the differential stopping power, $-dE/dx$, in the energy interval E_0 to $E_0 - \Delta E$. At low energies, and especially with heavy ions, this requires very small values of Δx , in the order of a few atom layers, and is a practical limitation in many cases. Slight nonuniformities of the foil thickness will introduce an appreciable error in the determination of Δx . Thus, the method of measuring the energy loss of ions in thin foils is generally used only if the particle ranges are at least $100 \mu\text{g}/\text{cm}^2$. With films of organic materials a higher degree of uniformity can be maintained down to thicknesses of $1 \mu\text{g}/\text{cm}^2$. Plastic films, however, are very susceptible to radiation damage; the structure of complex organic molecules is destroyed irreversibly under ion bombardment, and the films become very fragile.

The disadvantages of thin films can be avoided by analyzing the energy spectra of ions which are elastically backward scattered from a thick target (Fig. 2). A particle with initial energy E_1^0 penetrates the solid and at a distance d from the surface its energy is given by

$$E_1 = E_1^0 - \int_0^{d/\cos \theta_1} \left(-\frac{dE}{dx} \right) dx \quad (13)$$

¹¹ C. W. Williams, W. E. Kiker, and H. W. Schmitt, *Rev. Sci. Instr.* **35**, 1116 (1964).

^{11a} See also Vol. 2, Section 9.3.1; Vol. 5A, Section 2.2.1.3; Vol. 5B, Section 2.6.2.2.

¹² H. H. Andersen, A. F. Garfinkel, C. C. Hanke, and H. Sørensen, *Kgl. Danske Videnskab. Selskab Mat. Fys. Medd.* **35**, 4 (1966).

¹³ G. Hass and A. F. Turner, *Methods Exptl. Phys.* **A6**, 122 (1959).

¹⁴ S. Tolansky, "Surface Microtopography." Wiley (Interscience), New York, 1960.

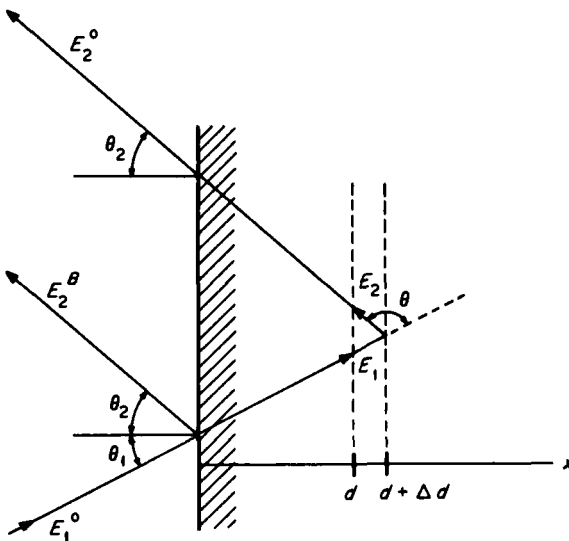


FIG. 2. Backscattering of energetic ions.

where (dE/dx) is the energy-dependent stopping power of the target for the incident ions. At a depth d some particles suffer large-angle collisions (laboratory angle θ) and leave the target again at an angle θ_2 . The fixed observation angle, θ_2 , defines the amount of energy lost in the large-angle collision:

$$E_1 - E_2 = \frac{4M_1 M_2}{(M_1 + M_2)^2} \cdot E_1 \cdot \sin^2 \frac{\vartheta}{2} \quad (14)$$

where M_1, M_2 are the masses of the ions and the target atoms. The scattering angle in the center-of-mass system is related to θ in the laboratory system:

$$\tan \theta = \frac{\sin \vartheta}{\cos \vartheta + M_1/M_2}. \quad (15)$$

The energy of the particles, detected at the angle θ , is then given by

$$E_2^0 = E_2 + \int_0^{d/\cos \theta} \left(-\frac{dE}{dx} \right) dx. \quad (16)$$

The energy spectrum observed is continuous and fairly flat near its upper limit. The lowest possible energy loss $E_1^0 - E_2^B$ of the detected particles is suffered by those which are scattered directly by surface atoms and can be calculated with Eq. (14).

To relate the depth d to the number of scattered and detected particles, cases must be chosen in which the differential scattering cross section is known. For pure Coulomb forces the inelastic energy loss of the back-scattered particles in the target material can be written as¹⁵

$$(dE/dx)_{E_1^0} = \frac{N(E_1^0)}{N(E_2^0)} \cdot n_s \cdot \sigma_R \cdot \Delta\Omega \cdot \frac{\Delta E}{K(\theta) + \cos \theta_1/\cos \theta_2}, \quad (17)$$

$$K(\theta) = 1 - \frac{2M_1 M_2}{M_1 + M_2} (1 - \cos \theta),$$

where $N(E_1^0)$ is the number of incident particles, $N(E_2^0)$ the number of scattered particles per energy interval, n_s the concentration of scattering centers, σ_R the Rutherford cross section, and $\Delta\Omega$ the solid angle subtended by the detecting system.

Frequently a thin contamination layer is formed on the target surface. It causes the scattering edge E_0^B to shift to lower energies because of the additional energy loss in the contaminant. This can be used to determine the stopping power of the contaminant for the ions.

9.1.2.4. Ranges of Heavy Particles in Solids. 9.1.2.4.1. COLLECTION OF RECOIL ATOMS EMERGING FROM A TARGET. Fast charged particles emitted from a target as a result of a nuclear reaction can be collected in stacks of thin catcher foils. Analysis by radiochemical methods then gives the range distribution of the recoil atoms in the catcher material. However, since the particle may lose some energy in the target itself it is necessary to make the target layer thin compared to the expected range of the emitted particles. This requirement limits the applicability of this method because of the small attainable yield.

An alternative is the use of the thick-target technique. In this case, the target layer is thick compared to the range of the radioactive nuclear reaction product; the particle yield is greater than in the thin-target technique. The target itself is surrounded by a thick catcher foil in which the emitted recoils are collected. At the energies in question (100 keV or higher) the collection efficiency of metal catcher foils is practically 100%. The fraction of emitted and collected recoils relative to the total number of reaction products created in the target can be measured with radiochemical methods (determination of the total radioactivity in the catcher foil and the target). From this fraction, the average recoil range in the target material can be calculated. In general the momentum vector distribution of nuclear reaction products is not isotropic in the laboratory system, especially if the nuclear reaction is induced by a fast ion. The fraction F_f of particles emitted from the target

¹⁵ K. Bethge, P. Sandner, and H. Schmidt, *Z. Naturforsch.* **21a**, 1052 (1966).

in the forward direction is then different from the fraction F_b in the backward direction. The recoil range has been discussed for isotropic and non-isotropic fragmentation by Sugarman *et al.*¹⁶ and by Porile and Sugarman.^{16a} For straight particle paths in the target the average range of the recoils in the target material is $\bar{R} = 4 dF_f/(1 + \eta)^2 = 4 dF_b/(1 - \eta)^2$, where $\eta = (\sqrt{F_f} - \sqrt{F_b})/(\sqrt{F_f} + \sqrt{F_b})$, if the range is proportional to $E^{1/2}$. It is assumed that the fragmentation of the nucleus is isotropic in the center-of-mass system. In the special case where the vector distribution of the recoils is practically isotropic in the laboratory system, e.g., in spontaneous α -decay, or (γ, n) reaction, one obtains $\bar{R} = 4 dF$, with $F_b = F_f = F$. Employing this basic technique, the ranges of numerous recoil atoms from different nuclear reactions have been determined (compare Ref. 17).

9.1.2.4.2. THE THICK-ABSORBER TECHNIQUE. This method can be applied if the ion energy can be varied continuously. The beam strikes the absorber foil which is made somewhat thicker than the expected ion range. A particle detector is placed behind the foil. Maximum ranges and mean ranges can be determined by increasing the beam energy until the detector begins to register particles, or until half of the beam is transmitted.

9.1.2.4.3. SPECTROMETRIC METHODS. In the techniques described below, a target (mass M_0) is bombarded (generally along the x axis perpendicular to its surface) with ions of mass M_2 . The ions penetrate into the lattice and come to rest within a concentration distribution (range distribution) $f(x)$. The concentration distribution can be measured by several methods.

If the target is an insulator, and the ion energy loss is mainly due to elastic collisions with the target atoms, the range may be approximated by measuring the depth of the surface layer with altered refractive index caused by the ion bombardment. Since the depth of this layer is also influenced by the range of the secondary knocked-on target atoms, this method is in general not very reliable. It has been used by Hines and Arndt¹⁸ to measure the range of 7.5 to 52-keV H_2^+ , D_2^+ , He^+ , and Ne^+ ions in quartz.

The analysis of the momentum distribution of light ions (e.g., protons) scattered from a solid surface can be used to determine the composition of the surface layers as a function of depth.¹⁹ After implantation the target is exposed to a beam of around 1-MeV protons. The backscattered protons

¹⁶ N. Sugarman, M. Campos, and K. Wielgoz, *Phys. Rev.* **101**, 388 (1956).

^{16a} N. Porile and N. Sugarman, *Phys. Rev.* **107**, 1410 (1957); **111**, 1746 (1958).

¹⁷ V. A. J. Van Lint, R. A. Schmitt, and C. S. Suffredini, *Phys. Rev.* **121**, 1457 (1961); W. Wiechmann, D. Ertel, and K. E. Zimen, *Nukleonik* **6**, 235 (1964).

¹⁸ R. L. Hines and R. Arndt, *Phys. Rev.* **119**, 623 (1960); R. L. Hines, *ibid.* **120**, 1626 (1960).

¹⁹ S. Rubin, *Nucl. Instr. Methods* **5**, 177 (1959); S. Rubin, T. O. Passel, and L. E. Bailey, *Anal. Chem.* **29**, 736 (1957).

are analyzed in a high-precision spectrometer. The analysis of the energy spectra of the detected protons follows in principle the treatment for heavier ions, given in Section 9.1.2.3. This technique was used, e.g., by Powers and Whaling²⁰ to measure the ranges of N, Ne, Ar, Kr, and Xe ions of 50–500-keV energy in Be, B, C, and Al.

Frequently the probing proton beam induces a nuclear reaction in the heavy ions which are embedded in the target. Phillips and Read²¹ and Barker and Phillips,^{21a} determined the ranges of 0.4–6.4-MeV ^{15}N ions in Au, Ni, and Ag by observing the γ -yield of a resonance in the $^{15}\text{N}(\text{p}, \alpha\gamma)^{12}\text{C}$ reaction. A proton, inducing this reaction in a ^{15}N nucleus, first has to penetrate a target layer of thickness Δx , being the penetration depth of the ^{15}N ion. The energy lost by the proton in penetrating this layer is therefore a measure of the range of the ^{15}N ion. This technique is especially valuable in the case of light ions, where the differential scattering cross section for protons may be too small for the use of the backward scattering method described above, or in the case of substitutionally located particles with masses about equal to the mass of the target atoms.

If the bombarding ion species is available as a radioactive isotope, the energy spectrum of the emitted decay product may be used to determine the depth distribution. Monoenergetic α -particles from nuclei embedded in a target will lose energy in escaping from the source. The amount of energy depends on the thickness of the material to be traversed [compare with Eq. (16); the α -decay energy corresponds to E_2]. The energy spectrum of the emerging α -particles is determined by the depth distribution of the parent nuclei. With this technique Domeij *et al.*²² measured the depth distribution of ^{222}Rn ions, injected with energies between 70 and 210 keV into targets of Al, Ag, W, and Au. The energy of the emerging α -particles (decay energy 5.486 MeV) was analyzed with a solid-state detector.

Similar considerations are applicable if the light particle emitted in the decay of the radioactive ion is an electron. Graham *et al.*²³ measured the mean depth of ^{125}Xe injected with kiloelectron-volt energies into metal targets. The radioactive ^{125}Xe emits monoenergetic conversion electrons. The manner in which these conversion line shapes vary with the depth d of the ^{125}Xe atoms beneath the surface was calibrated by covering some targets with layers of known thickness. It was found that the peak heights decreased in an approximately exponential manner with increasing d .

²⁰ D. Powers and W. Whaling, *Phys. Rev.* **126**, 61 (1962).

²¹ W. R. Phillips and F. H. Read, *Proc. Phys. Soc. (London)* **81**, 1 (1963).

^{21a} P. H. Barker and W. R. Phillips, *Proc. Phys. Soc. (London)* **86**, 379 (1965).

²² B. Domeij, I. Bergström, J. A. Davies, and J. Uhler, *Arkiv Fysik* **24**, 399 (1963).

²³ R. L. Graham, F. Brown, J. A. Davies, and J. P. S. Pringle, *Can. J. Phys.* **41**, 1686 (1963).

9.1.2.4.4. CONTROLLED REMOVAL OF THIN SURFACE LAYERS. This technique can be used with advantage if the bombarding ion species is available as a radioactive isotope. The ions (usually a mixture of radioactive and non-radioactive isotopes) penetrate into the target. The total radioactivity $\phi(0) = 100\%$ of the target is measured. Thin layers of target material (thickness $\Delta x \ll$ maximum ion range in the target) are then removed successively, and the removed quantity of radioactive material, $f(x)$, or the residual activity $\phi(x)$ of the target is measured. The curve of $\phi(x)$ versus x gives the number of radioactive ions which have penetrated into the target to a depth larger than x . Differentiating $\phi(x)$ again yields the range distribution, $f(x)$, of the radioactive ions.

The radioactive isotopes chosen have to fulfill some requirements. The lifetime has to be long enough to allow repeated accurate activity measurements over periods of several hours. The decay product should have a range which is much larger than the maximum penetration depth of the radioactive heavy ions. Backscattering of the decay products must not influence the measured function $\phi(x)$. This causes no problem in case of α - and γ -activity; in case of β -active parent nuclei the total target thickness has to be greater than the backscattering saturation thickness. The only effect of backscattering on the residual activity $\phi(x)$ is then multiplication by a constant factor, but this does not have to be considered because of the normalization of $\phi(0)$ to 100%.

The following techniques have been applied to remove thin target surface layers in controlled steps.

9.1.2.4.4.1. Chemical Etching. Bredov *et al.*²⁴ and Davies *et al.*²⁵ used chemical etching to measure the range distribution of ^{137}Cs ions of kilo-electron-volt energies in germanium disks. The disks were pre-etched before bombardment to clean the surfaces and to prepare them for the controlled etching process. The thin surface layers were removed by immersion in 3% aqueous H_2O_2 . After each immersion, the disks were weighed on a microbalance to determine the average thickness of the germanium layer removed ($\sim 10 \mu\text{g}/\text{cm}^2$). It was found that the etching rate depended strongly on the configuration of the germanium surface; too high a dose of ^{137}Cs ions ($> 3 \cdot 10^{13}/\text{cm}^2$) can cause nonuniform etching of the surface and, therefore, a distortion of the measured range distribution.²⁵

9.1.2.4.4.2. Electrolytic Peeling. This method was developed by Davies *et al.*²⁶ to measure range distributions of radioactive ions in Al. Thin surface

²⁴ M. M. Bredov, R. F. Komareva, and A. R. Regel, *Dokl. Akad. Nauk. SSSR* **99**, 69 (1954); M. M. Bredov and N. M. Okuneva, *ibid.* **113**, 795 (1957); M. M. Bredov, I. G. Lang, and N. M. Okuneva, *Zh. Tekhn. Fiz.* **28**, 252 (1958).

²⁵ J. A. Davies, J. D. McIntyre, and G. Sims, *Can. J. Chem.* **40**, 1605 (1962).

²⁶ J. A. Davies, J. Friesen, and J. D. McIntyre, *Can. J. Chem.* **38**, 1526 (1960).

layers are removed by anodizing the Al targets electrolytically in an aqueous solution of ammonium nitrate (30 gm/liter), at $25 \pm 0.5^\circ\text{C}$. The thickness of the aluminum oxide layer formed ($\sim 40 \text{ \AA}$ or more) is very uniform and reproducible. It increases linearly with the applied anodic voltage and is about $8 \mu\text{g Al/cm}^2$ for 30 V. The oxide layer is then removed by rapid dissolution in a hot aqueous solution ($T > 90^\circ\text{C}$) of orthophosphoric acid (50 gm/liter) and chromium trioxide (30 gm/liter). Using Al single crystals, Selig and Sizmann²⁷ found that the peeling rate depends on the crystallographic orientation of the surface. It is about 5% greater in the $\langle 111 \rangle$ direction than in the $\langle 110 \rangle$ direction.

Immediately before bombardment with radioactive ions, the Al target surface is cleaned and smoothed by the anodizing-peeling technique. The resulting surface has a mirror-like finish. This method was extended later to other materials such as W,^{28, 29} where no dependence of the peeling rate on the crystallographic surface orientation was found, Au,³⁰ Ta, UO₂,³¹ and Si,³² using electrolytes and solvents of different chemical composition.

9.1.2.4.4.3. Low-Energy Cathode Sputtering. The method was developed by Lutz and Sizmann³³ to measure the range distribution of ⁸⁵Kr ions in Cu. The thin surface layers are removed by sputtering the targets with 2.9-keV inactive Kr ions (current density $\sim 10 \mu\text{A/cm}^2$). The range of the sputtering ions has to be much smaller than the range of the radioactive ions. The thickness of the layers (10 \AA or more) removed increases linearly with sputtering time and depends on the sputtering yield of the target material. It can be calibrated by bombarding one-half of a specimen with a known number of 2.9-keV inactive Kr ions, while the other half is covered. The depth of the step which appears between the eroded and the uneroded area can be measured very accurately by interference microscopy.¹⁴ (It should be noted that the sputtering yield of single crystals generally depends on the crystallographic directions.) Oil deposits on the sputtered surface must be carefully avoided; they decompose to a thin carbon film which can stop the sputtering process.

The method allows removal of very uniform and reproducible surface layers if the Cu specimens are etched and electropolished immediately before

²⁷ O. Selig and R. Sizmann, *Nukleonik* **8**, 303 (1966).

²⁸ M. McCargo, J. A. Davies, and F. Brown, *Can. J. Phys.* **41**, 1231 (1963).

²⁹ E. V. Kornelsen, F. Brown, J. A. Davies, B. Domeij, and G. R. Piercy, *Phys. Rev.* **136**, A849 (1964).

³⁰ J. L. Whitton and J. A. Davies, *J. Electrochem. Soc.* **111**, 1347 (1964).

³¹ F. Brown, G. C. Ball, D. A. Channing, L. M. Howe, J. P. S. Pringle, and J. L. Whitton, *Nucl. Instr. Methods* **38**, 249 (1965).

³² J. A. Davies, G. C. Ball, F. Brown, and B. Domeij, *Can. J. Phys.* **42**, 1070 (1964).

³³ H. Lutz and R. Sizmann, *Z. Naturforsch.* **19a**, 1079 (1964).

use. Prebombardment with a high dose of the low-energy sputtering ions ($\sim 10^{18}/\text{cm}^2$) also helps to smooth the surface.³⁴ In case of a single crystal specimen the latter should be avoided if the surface crystal structure is likely to be altered by this prebombardment, unless it can be annealed later on.

The method of removing thin surface layers by controlled low-energy sputtering is in principle applicable to all solid targets and has been used to study ion penetration in Cu,³³ W,³⁵ GaAs,³⁶ and Au.³⁷

9.1.2.5. Crystal Lattice Effects on Penetration; "Channeling."³⁸ In the foregoing parts of this chapter we have treated collisions in a solid much as we would handle collisions in a dense random gas. As in the case of any multiple-collision process the information obtained from an experiment can only be a complex statistical average over many processes. The relation of the observables to the detailed contributions of individual collisions to the over-all process is therefore diffuse. The complexity of the problem can be reduced considerably when one realizes that the target atoms in solids are arranged in a well-defined spatial configuration.

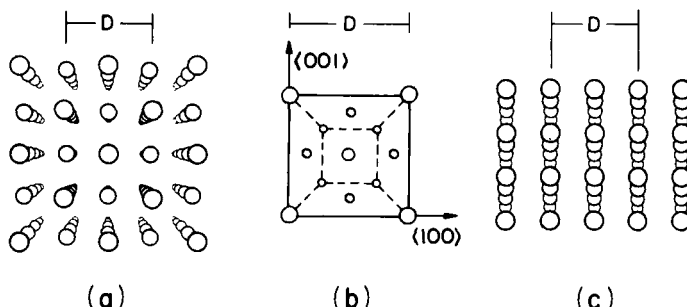


FIG. 3. (a) Perspective view of a fcc lattice along $\langle 010 \rangle$. (b) Elementary cube of a fcc lattice. (c) Rotating the crystal about the $\langle 100 \rangle$ direction shows $\{100\}$ planar channels.

That directional effects should exist can easily be visualized from the lattice model pictured in Fig. 3. If the crystal is viewed along a low-index direction, the lattice appears to be highly transparent. For the face-centered cubic lattice of Fig. 3, the most transparent direction is $\langle 101 \rangle$, the face

³⁴ H. Heinen, H. Lutz, and R. Sizmann, *Z. Naturforsch.* **19a**, 1131 (1964).

³⁵ H. Herrmann, H. Lutz, and R. Sizmann, *Z. Naturforsch.* **21a**, 365 (1966).

³⁶ C. Pöhlau, H. Lutz, and R. Sizmann, *Z. Angew. Phys.* **17**, 404 (1964).

³⁷ R. D. Schuckert, H. Lutz, and R. Sizmann, *Z. Naturforsch.* **21a**, 1296 (1966).

³⁸ For an extensive review see S. Datz, C. Erginsoy, G. Leibfried, and H. O. Lutz, *Ann. Rev. Nucl. Sci.* **17** 129 (1967).

diagonal on the front of Fig. 3b. The second best direction is $\langle 010 \rangle$. Figure 3a, a perspective view of the crystal along this axis, shows the $\langle 010 \rangle$ atomic rows. Four neighboring rows form an axial $\langle 010 \rangle$ channel. Rotating the crystal of Fig. 3a about the $\langle 100 \rangle$ axis leads to configurations of the type shown in Fig. 3c. The transparency does not disappear because open planes are maintained between the densely packed sheets of atoms.

For crystals of finite thickness, the angular aperture for transparency is vanishingly small, and one would not expect that any appreciable effects would be observed in penetration experiments using beams with large angular divergence. However, when energetic particles enter the lattice with small angles to either the rows or planes, they undergo a set of correlated small-angle collisions which tend to "channel" their directions so as to avoid close collisions with lattice atoms. These particles will penetrate more deeply into the lattice than those entering in a more "random" direction.

These effects were actually anticipated by Stark and Wendt in 1912³⁹ and rediscovered in the computer calculations of Robinson and Oen^{40, 41} in 1963. They investigated the slowing down of 1–10-keV heavy ions in a lattice model which included realistic repulsive interactions and obtained very large penetrations for particles with initial velocities nearly parallel to close-packed directions. Experimentally, this effect was first seen in studies on the penetration of kiloelectron-volt ions into crystals by Piercy *et al.*⁴² and by Lutz and Sizmann.⁴³ They measured the distribution of penetration distances and found that a significant fraction of the ions incident along low-index directions had anomalously long range. Nelson and Thompson⁴⁴ observed anomalously high transmission of 50-keV protons in channel directions.

In Fig. 4, we give a simple example of the motion of a channeled particle. The incoming particle enters in a symmetry plane containing a channel axis. Only the forces exerted by the atoms in the symmetry plane matter; the other forces cancel. Figure 4 shows only the effect of the two neighboring rows in the symmetry plane. The particle enters the crystal at z_0 and is deflected towards the axis because the forces at these distances are repulsive and the closest atoms decide the sign of the force. The next collision still tends towards the axis but the deflection is somewhat smaller. After the third collision the z values become negative, and the forces due to

³⁹ J. Stark and G. Wendt, *Ann. Phys.* **38**, 921 (1912); J. Stark, *Physik. Z.* **13**, 973 (1912).

⁴⁰ M. T. Robinson and O. S. Oen, *Appl. Phys. Letters* **2**, 30 (1963).

⁴¹ M. T. Robinson and O. S. Oen, *Phys. Rev.* **132**, 2385 (1963).

⁴² G. R. Piercy, F. Brown, J. A. Davies, and M. McCargo, *Phys. Rev. Letters* **10**, 399 (1963).

⁴³ H. Lutz and R. Sizmann, *Phys. Letters* **5**, 113 (1963).

⁴⁴ R. S. Nelson and M. W. Thompson, *Phil. Mag.* **8**, 1677 (1963); **9**, 1069 (1964).

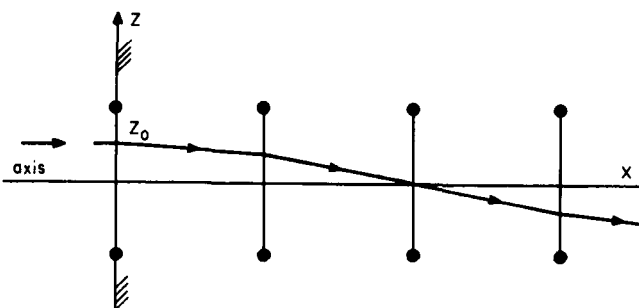


FIG. 4. Path of a particle for axial channeling in a symmetry plane.

the lower row of atoms are directed upwards. Consequently, the path $z(x)$ is a sort of sinusoidal curve and larger impact parameters near the channel axis are weighted more heavily. This "governed" motion therefore supports smaller energy losses. The "wavelength" λ of this motion for high-energy particles is usually many lattice distances in contrast to the motion shown in Fig. 4. The paths are still almost straight, the angular deviations being of the order $4z_0/\lambda$. Initial values of z_0 nearer to the atomic rows can lead to large angular deflections such that the subsequent history of the particle is more or less random.

The most important quantity determining the slowing-down history is the energy loss of the incoming particles to the atoms and electrons of the solid. For low energies the energy transfer to the lattice atoms will prevail; for high energies ionization and excitation of the electrons predominate. In any event, the energy losses will be smallest if the particle moves near a channel axis or near the middle of atomic planes where its distance to the nuclei and the atomic electrons is relatively large.

The lattice arrangement can also show an effect which, in a sense, is opposite to channeling. This occurs, for instance, if a nucleus on a lattice site emits an α -particle, or in large-angle scattering of incoming beams where the scattered particle comes close to the nucleus. In this case, the particle starts from a lattice site, and the lattice is blocking its motion in channeling directions with the result that the intensity for these directions is suppressed. The simplest case is an α -emitter on a lattice site where one considers only the blocking by the nearest neighbor (Fig. 5). For sufficiently high initial energies, E_0 , and for small initial and scattering angles, ϕ and ϕ' , we have Rutherford scattering $\psi = \phi + C/b = \phi + C/(D\phi)$ with $C = Z_1 Z_2 e^2 / E_0$ where Z_1 and Z_2 are the nuclear charges of the emitted particle and lattice atoms. The distribution in ϕ is isotropic and the distribution

$$w(\phi) = (2\psi^2 - \psi_c^2) / 4(\psi^2 - \psi_c^2)^{1/2}$$

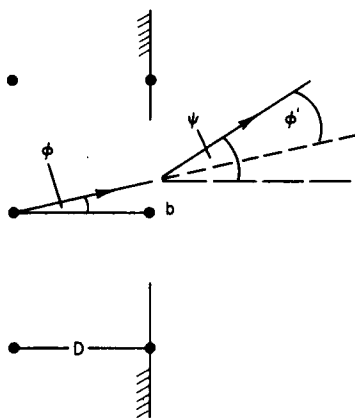


FIG. 5. Coulomb scattering of an α -particle emitted from a lattice site near the surface.

for $\psi > \psi_c = 2(C/D)^{1/2} = 2Z_1 Z_2 e^2 / E_0 D$. All outgoing particles are emitted with angles larger than the critical angle ψ_c , i.e., the emission is blocked for angles smaller than ψ_c about the crystal direction.

9.1.2.5.1. RANGES IN AXIAL CHANNELS. In this section range measurements will be discussed and illustrated by some specific examples. Figure 6 shows the results of bombarding Al crystals with 40-keV ^{85}Kr ions.⁴⁵ The bombarded surface normal is close to the indicated crystallographic directions and the incident velocity is parallel to the surface normal (axial channeling). The incident ions are radioactive, and the distribution function $w(x)$ is obtained by etching (see Section 9.1.2.4) of thin surface layers and measuring the remaining radioactivity which is proportional to $f(x) = \int_x^\infty w(x') dx'$. The quantity $f(x)$, the fraction of incident particles having come to rest at distances larger than x from the surface, is plotted for various crystallographic directions. The most open channel in a fcc lattice, such as Al, is the $\langle 101 \rangle$ channel. It gives the largest penetration depth (Fig. 6).

For a given channel, the penetration increases with initial energy. Figure 7 shows this for Xe ions of various energies incident on a $\{110\}$ surface of W.²⁹ The long tails, so called "supertails," are due to diffusion^{35, 46} and should be disregarded. The maximum range in the channel $R_0(f(R_0) = 0)$ can be expected to be least influenced by elastic collisions between ion and lattice atoms because of the larger impact parameters involved. Since R_0 cannot be

⁴⁵ G. R. Piercy, M. McCargo, F. Brown, and J. A. Davies, *Can. J. Phys.* **42**, 1116 (1964).

⁴⁶ J. A. Davies and P. Jespersgaard, *Can. J. Phys.* **44**, 1631 (1966).

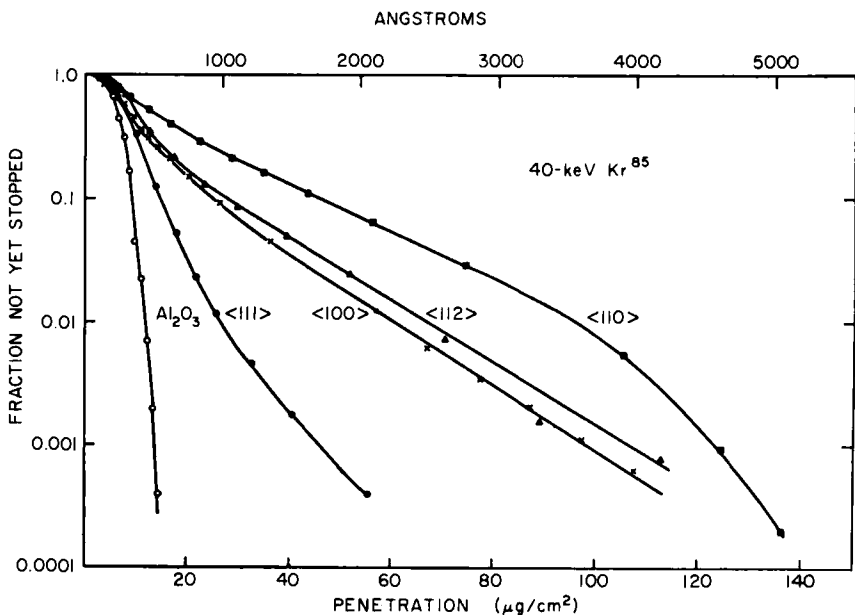


FIG. 6. $f(x) = \int_x^\infty w(x') dx'$ for axial channeling along various crystallographic directions [G. R. Piercy, M. McCargo, F. Brown, and J. A. Davies, *Can. J. Phys.* **42**, 1116 (1964)].

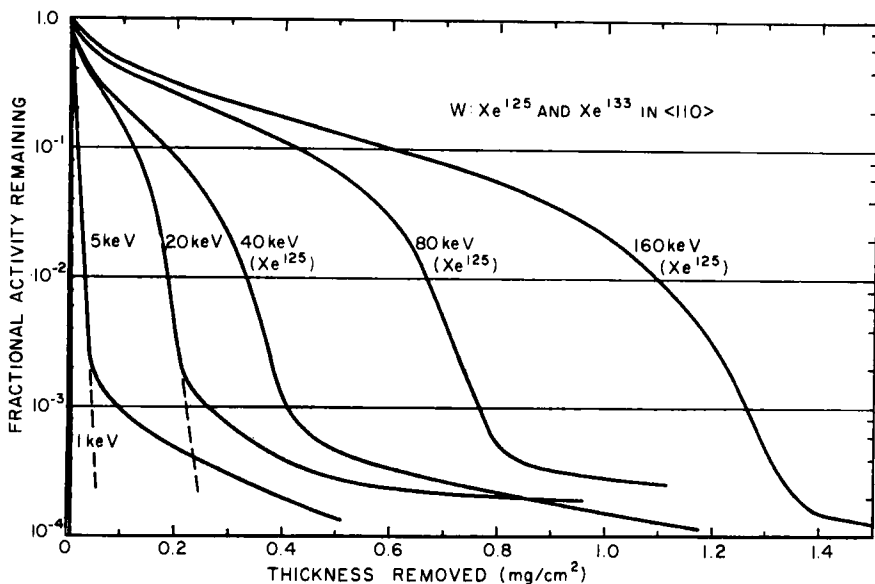


FIG. 7. $f(x)$ for Xe ions in $\langle 110 \rangle$ channels of W for various energies [E. V. Kornelsen, F. Brown, J. A. Davies, B. Domeij, and G. R. Piercy, *Phys. Rev.* **136**, A849 (1964)].

observed directly, one takes instead the range $R_{f_0}(f(R_{f_0}) = f_0)$ for sufficiently small f_0 . Figure 8 shows $R_{0.001}$ versus energy again for Xe ions in W.⁴⁷ Some points are taken from Fig. 7, neglecting the "supertail" (dashed curves). The slope is proportional to $\sqrt{E_0}$ for higher energies (electronic stopping) and increases for smaller energies by loss of energy in elastic

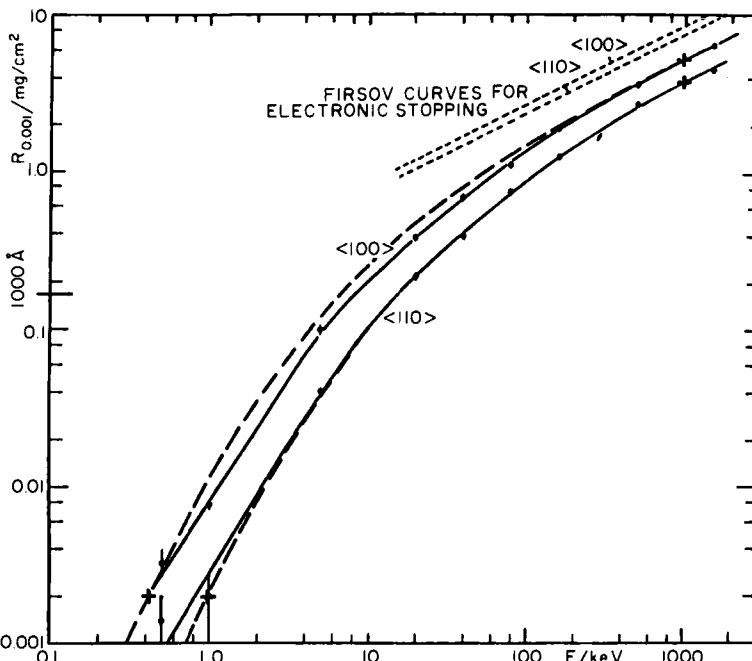


FIG. 8. $R_{0.001}$ versus incident energy E_0 for Xe in W. The dashed curve is fitted by assuming an energy loss $-dE/dx = \alpha/E + \beta\sqrt{E}$ [G. R. Piercy, M. McCargo, F. Brown and J. A. Davies, *Can. J. Phys.* **42**, 1116 (1964)].

potential interaction (nuclear stopping). The difference between the two channels should mainly be due to different nuclear losses. Firsov's⁴⁸ electronic loss curves are also shown for comparison, as well as the different losses in the two channels. For much higher energies, the channeled and unchanneled particles show separate peaks.

The influence of temperature on penetration is important. Figure 9 shows the range of 40-keV Xe ions in the $\langle 110 \rangle$ axial channel of Au for different

⁴⁷ J. A. Davies, L. Eriksson, and P. Jespersgaard, *Nucl. Instr. Methods* **38**, 245 (1965).

⁴⁸ O. B. Firsov, *Soviet Phys. JETP (English Transl.)* **9**, 1976 (1959).

temperatures.³¹ A crude theory of the temperature dependence has been given⁴⁹ in which it is assumed that the changes are due only to nuclear energy loss. The ranges should then be proportional to $\exp(-2\bar{u}^2/a^2)$, where \bar{u}^2 is the mean square fluctuation of one coordinate of a lattice atom, and a is the screening length of the interatomic potential. The results are ex-

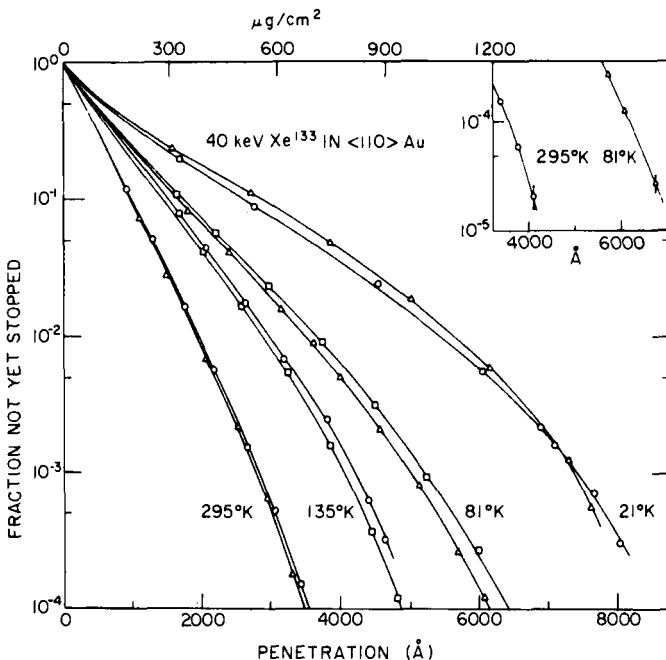


FIG. 9. Ranges of 40-keV Xe ions in Au along the $\langle 110 \rangle$ axial channel³¹ at different temperatures. [F. Brown, G. C. Ball, D. H. Channing, L. M. Howe, J. P. S. Pringle, and J. L. Whittom, *Nucl. Instr. Methods* **38**, 249 (1965).]

tremely sensitive to the values in the exponent. Consequently, only qualitative agreement between the experimental points and the fitted curves can be expected.

9.1.2.5.2. TRANSMISSION AND REFLECTION. Studies of the transmission of energetic particles through thin films were first reported by Nelson and Thompson.⁴⁴ Beams of 75-keV protons and He^+ ions ($\simeq 0.5 \mu\text{A}/\text{mm}^2$) were passed through a monocrystalline gold foil of approximately 3000-Å thickness. The foil was rotated about an axis perpendicular to its surface, thus changing the crystallographic orientation relative to the incident beam

⁴⁹ C. Lehmann and G. Leibfried, *J. Appl. Phys.* **34**, 2821 (1963).

direction while the thickness to be penetrated remained constant. The transmitted ion current increased sharply whenever the incident beam was parallel to a $\langle 110 \rangle$ axial channel. The maxima for protons were more pronounced than for He^+ ions. Measurements of the yields of backscattered particles also indicated enhanced transmission in open crystal directions: the reflection of 50-keV H^+ , He^+ , Ne^+ , and Xe^+ ions from the surface of a copper single crystal diminished markedly whenever incidence occurred along low-index directions or parallel to low-index planes. The experiment suggested that the most effective axial channels are $\langle 110 \rangle$ and $\langle 100 \rangle$, the most effective planar channels (111) and (100) . In the case of light ions, a square well potential could be used as an approximation to the actual channel potential.

After a prolonged irradiation (around $10^{18} \text{ He}^+ \text{ ions/cm}^2$), it was found that the transmission maxima disappeared. This was attributed to the blocking of channels by dislocation loops formed during the ion bombardment.

9.1.2.5.3. ENERGY LOSS. The first channeling transmission experiment with an energy analysis of the transmitted beam was reported by Dearnaley.⁵⁰ A collimated proton beam from a Van de Graaff accelerator ($E = 2.1 \text{ MeV}$) was passed through a $37\text{-}\mu$ -thick silicon single crystal. A surface barrier detector stopped the transmitted protons and was used to analyze their energy. It was found that the energy spectrum of the transmitted protons showed a pronounced high-energy tail for certain orientations which were identified as two of the main crystallographic axes of the silicon lattice, $\langle 110 \rangle$ and $\langle 114 \rangle$. Almost 50% of the particles were found to have lower than normal energy loss. The lowest observed energy loss, around 0.9 MeV , was about one-half the "normal" (random) energy loss, around 1.8 MeV .

The orientation dependence of this effect was studied by counting only the particles in the high-energy tail. Changing the orientation of the thin crystal, the counting rate showed strong peaks when a low-index direction was parallel to the incident beam direction. The angular widths of the transmission peaks depend on mass and energy of the projectile.

Scattering from axial into planar channels has been investigated by Appleton *et al.*⁵¹ Protons of 4.85-MeV energy were passed through a $50\text{-}\mu$ -thick silicon single crystal. The fraction of protons with low-energy loss was measured for beam incidence parallel to the (111) , (110) , and (100) planes, as well as parallel to the $\langle 110 \rangle$ axis. The authors showed that the fraction of the beam suffering a lower energy loss than normal could be

⁵⁰ G. Dearnaley, *IEEE Trans. Nucl. Sci.* **NS-11**, No. 3, 249 (1964).

⁵¹ B. R. Appleton, C. Erginsoy, H. E. Wegner, and W. M. Gibson, *Phys. Rev.* **19**, 185 (1965).

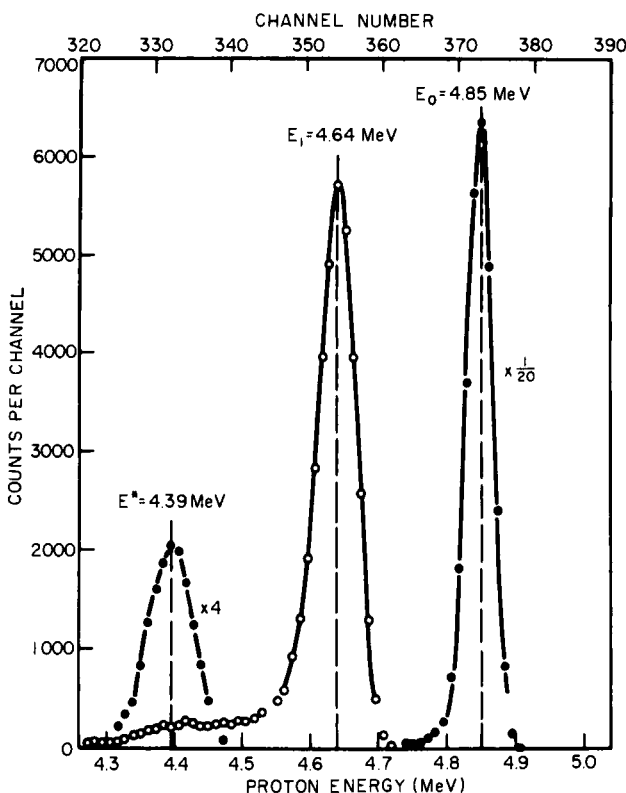


FIG. 10. Energy spectra of protons ($E_0 = 4.85$ MeV) transmitted through $50\text{-}\mu$ thick Si crystal (detector aperture = 0.07°). E_1 is obtained with the beam directed along a $\{111\}$ plane and E^* is obtained in a random direction [W. M. Gibson, C. Erginsoy, H. E. Wegner, and B. R. Appleton, *Phys. Rev. Letters* **15**, 357 (1965)].

reconstructed, for the $\langle 110 \rangle$ axial channeling, from a knowledge of the corresponding fractions for the (111) , (110) , and (100) planar channeling. Gibson *et al.*⁵² found a sharp energy loss group for 4.85-MeV protons channeled between low-index planes of a $50\text{-}\mu$ -thick silicon single crystal (Fig. 10). The surface barrier detector subtended an angle of about 0.07° . The spectrum of the protons emerging from the crystal parallel to the incident beam exhibited an energy peak with very little dispersion and an almost complete absence of "normal" particles; the (111) channel energy loss was 210 keV, the normal energy loss 460 keV. Keeping the orientation

⁵² W. M. Gibson, C. Erginsoy, H. E. Wegner, and B. R. Appleton, *Phys. Rev. Letters* **15**, 357 (1965).

of the thin crystal fixed, but moving the detector from the beam direction, caused a rapid drop in intensity of the channeled peak; simultaneously it broadened and shifted to lower energies. Besides this low energy loss component, particles with anomalously high energy loss were observed. This had been reported earlier by the same authors,⁵³ and confirmed by Sattler and Dearnaley.⁵⁴ It was concluded⁵⁵ that the high loss component was associated with particles that penetrate deeply into the dense atomic planes and are scattered out of these by a process of multiple scattering. Such trajectories sample a high electron density as well as a high nuclear density compared to the average; they are essentially "blocked" trajectories.

Datz *et al.*⁵⁶ investigated the channeling of fast heavy ions in gold single crystals. Multicomponent beams of Br and I ions⁵⁷ were produced in a Van de Graaff tandem accelerator: the negative ions were accelerated in the first stage of the tandem, stripped of some of their electrons, and stripped further during acceleration in the second stage. The resulting continuous high-energy spectrum of particles was analyzed in a 90° magnet which gave a beam consisting of a series of known sharply defined energies. This beam was highly collimated (0.01°) and passed through a single crystalline gold foil of 0.57 μ thickness. The transmitted beam was again collimated to a cone of approximately 3° half angle, and detected in a solid-state surface barrier detector, which limited the energy resolution to around 2 MeV. With this multicomponent beam technique, it was possible to obtain in one spectrum the energy dependence of the penetration of Br and I ions through gold single crystals between two energy limits, here approximately 20 and 90 MeV. Angular scans along the (100) and (110) planes across the <100>, <110>, and <112> axial channels were made. For beam incidence parallel to an axial channel, a single sharp low energy loss peak was observed skewed to lower energy. With beam incidence parallel to a planar channel, but well away from a low-index direction, two energy loss groups appeared, one having the normal loss and the other having a lower loss. Because of the reduced probability of small-impact-parameter collisions, it was suspected that channeling leads to lower charge states, which also tends to decrease the energy loss of channeled particles. The lower ionic charge of channeled

⁵³ C. Erginsoy, H. E. Wegner, and W. M. Gibson, *Phys. Rev. Letters* **13**, 530 (1964); H. E. Wegner, C. Erginsoy, and W. M. Gibson, *IEEE Trans. Nucl. Sci.* **NS-12**, No. 1, 240 (1965).

⁵⁴ A. R. Sattler and G. Dearnaley, *Phys. Rev. Letters* **15**, 59 (1965).

⁵⁵ C. Erginsoy, *Phys. Rev. Letters* **15**, 360 (1965).

⁵⁶ S. Datz, T. S. Noggle, and C. D. Moak, *Phys. Rev. Letters* **15**, 254 (1965); *Nucl. Instr. Methods* **38**, 221 (1965).

⁵⁷ C. D. Moak, J. H. Neiler, H. W. Schmitt, F. J. Walter, and G. F. Wells, *Rev. Sci. Instr.* **34**, 853 (1963).

ions has been demonstrated later by Lutz *et al.*⁵⁸ A 40-MeV I beam was passed through a $0.35\text{-}\mu$ -thick gold single crystal and deflected in an electrostatic analyzer. The charge distribution was measured for beam incidence in a random lattice direction, and in the $\langle 110 \rangle$ channel direction. In the first case, a Gaussian distribution with a most probable charge 14.3 was obtained; the second case showed a distribution skewed to higher charges with a most probable charge 12.5.

With fast heavy ions, it was observed for the first time⁵⁹ that structure exists in the energy spectrum between the most channeled and the normal energy loss. Well-collimated multicomponent beams of ^{127}I ions, as described earlier, were passed through a $0.25\text{-}\mu$ -thick single crystalline gold foil. Time-of-flight techniques¹¹ were used to obtain improved energy and angular resolution. The detecting system was aligned with the original beam direction. Detailed angular scans were made across planar channels. At the center of the channel, the normal energy loss group was almost completely replaced by a lower energy loss characteristic of the plane. Slightly off planar channel directions (around 0.2°) additional sharp groups with intermediate energy loss were found. Although their populations varied with tilt angle, the peak position did not change. No difference was observed between the (111) planar energy loss and the energy loss in the $\langle 110 \rangle$ or the $\langle 112 \rangle$ axial channels.

These experiments were repeated later⁶⁰ with 60-MeV ^{127}I ions, as well as 3-MeV α -particles. A magnetic analyzer, fitted with a position-sensitive solid-state detector, gave still better angular (0.02°) and energy resolution ($\Delta E/E \simeq 2 \times 10^{-3}$) for the I ions. Angular scans were made across and along the (111) and (100) planar channels. Right on channel the energy spectra of the transmitted I ions and α -particles showed a peak, sharp on the high-energy side and more gradually decreasing on the low-energy side. For the ^{127}I ions the normal energy loss was 16 MeV for 7000 Å crystal thickness, about twice as much as the most channeled loss. When the gold crystal was tilted in intervals δ ($\ll 1^\circ$) from the channeled orientation, the populations of this peak decreased and very pronounced peaks with higher energy loss appeared, about 1.2 MeV apart (Fig. 11). The explanation of this structure in the energy loss spectra was found to lie in the nature of the transverse oscillations of the particles in the channels. Ions entering the interplanar region are acted on by a symmetric repulsive planar potential and undergo oscillatory motion on the way through the lattice. The amplitude

⁵⁸ H. O. Lutz, S. Datz, C. D. Moak, T. S. Noggle, and L. C. Northcliffe, *Bull. Am. Phys. Soc.* **11**, 177 (1966).

⁵⁹ S. Datz, H. O. Lutz, C. D. Moak, T. S. Noggle, L. C. Northcliffe, and H. W. Schmitt, *Bull. Am. Phys. Soc.* **11**, 126 (1966).

⁶⁰ H. O. Lutz, S. Datz, C. D. Moak, and T. S. Noggle, *Phys. Rev. Letters* **17**, 285 (1966).

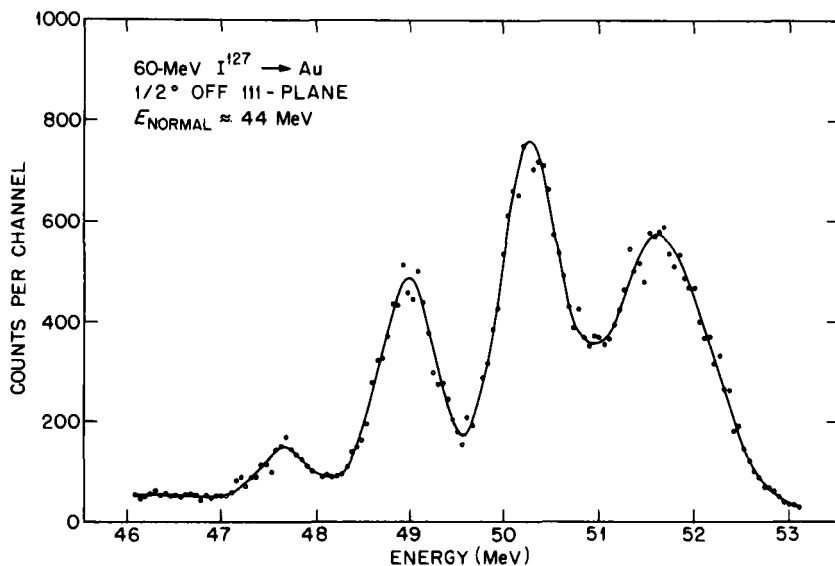


FIG. 11. Energy spectrum of 60-MeV I^{127} ions obtained after transmission through a 7000-Å thick Au single crystal. The (111) plane was tilted 0.5° from the beam direction [H. O. Lutz, S. Datz, C. D. Moak, and T. S. Noggle, *Phys. Rev. Letters* 17, 285 (1966)].

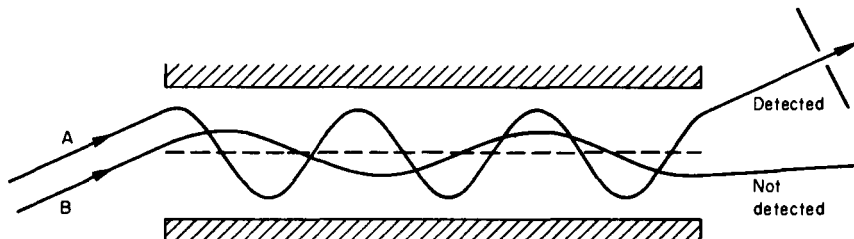


FIG. 12. Particle trajectories in a planar channel. Particle *A* will be detected if the detector is aligned with the initial beam direction. Particle *B* will not be detected [H. O. Lutz, S. Datz, C. D. Moak, and T. S. Noggle, *Phys. Rev. Letters* 17, 285 (1966)].

of the oscillation depends upon the entrance position and angle with respect to the channel midplane. Since the motion of the particle is characterized by an anharmonic oscillation, the wavelength is a function of the amplitude. The detector was in line with the incoming beam direction. Only particles having wavelengths λ , satisfying the condition $l = n\lambda$, could be detected, where l is the channel length (Fig. 12). These sets of particles with distinct wavelengths λ have distinct amplitudes; they have, therefore,

different distinct energy losses. Further studies along these lines hold promise to give information on interatomic potentials and stopping powers.

9.1.2.5.4. BACKSCATTERING FROM THICK TARGETS. Particles backscattered from different depths in a thick target can be separated by their energy¹⁸ and, therefore, the yields from thin zones at chosen depths below the surface can be measured conveniently. Bøgh and Uggerhøj^{61, 62} were the first to use this technique with low-*Z* (Al) and high-*Z* (Ta) targets and protons of 400 keV to 1.7 MeV. Figure 13 shows the scattering yields from a tantalum

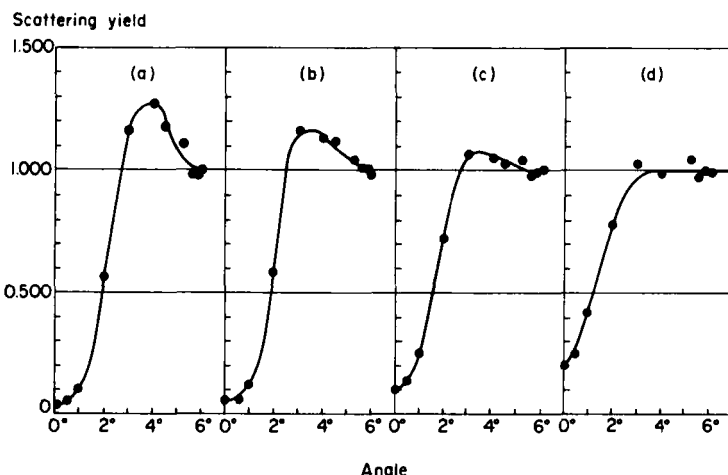


FIG. 13. Rutherford scattering yield in Ta versus angle between incident proton beam ($E_0 = 400$ keV) and the $\langle 100 \rangle$ axis. Thickness of scattering zone ~ 300 Å. Depth: (a) 600 Å; (b) 1200 Å; (c) 3000 Å; (d) 6000 Å [E. Bøgh and E. Uggerhøj, *Phys. Letters* **17**, 116 (1965)].

single crystal as a function of incidence angle with respect to the $\langle 100 \rangle$ axis. As the scattering zone (approximately 250 Å thick for 400-keV protons scattered to 116°) moves deeper inside the crystal, the minimum yield at zero incidence angle increases but the excess yield observed just outside the dip decreases rapidly to zero. Both effects have been attributed to the multiple scattering of the particles prior to the backscattering event. A very interesting application of backscattering yield measurements was pointed out by Bøgh and Uggerhøj.⁶² A dip in the yield can only be expected if the backscattering atoms are located at lattice sites. Therefore, the depth of the

⁶¹ E. Bøgh and E. Uggerhøj, *Phys. Letters* **17**, 116 (1965).

⁶² E. Bøgh and E. Uggerhøj, *Nucl. Instr. Methods* **38**, 216 (1965).

dip can be used as a measure of lattice disorder due to radiation damage or thermal vibrations. Moreover, since the energy of the backscattered particle is a function of the mass of the scattering atom, energy analysis coupled with angular scans can be used to determine the positions of impurity atoms in a crystal lattice.^{63, 64}

9.1.2.5.5. EMISSION FROM LATTICE SITES. Domeij and Björqvist⁶⁵ bombarded tungsten single crystals with alpha-active ions (^{222}Rn) and detected the three groups of alphas (5.49 MeV, 6.0 MeV, and 7.68 MeV) emitted from the decay of ^{222}Rn and the daughter products ^{218}Po and ^{214}Po . The intensity of α -particles showed strong dips in axial and planar directions, indicating that a large fraction of the Rn ions were substitutionally situated at lattice sites of the crystal. The angular widths were found to agree reasonably well with the predicted critical angle of Lindhard.⁶⁶ The minimum intensity of α -particles at the center of the dip was $\sim 25\%$ of the normal. This may be caused by an appreciable number of interstitial ^{222}Rn atoms, or by the multiple scattering of emitted particles which are fed into a channel before emerging. A low resolution energy analysis confirmed that these particles have suffered a reduced energy loss. On the other hand, it was observed that particles emerging at the intensity maxima just outside the dip have an anomalously large energy loss. As in Rutherford back-scattering, yield measurements of the emitted α -particles can be used to determine the location of the emitting atom in the lattice. Matzke and Davies⁶⁴ found that the yields of α -particles emitted from Rn atoms in KCl, CaF_2 , and UO_2 lattices do not show any orientation dependence. The Rn atoms are, therefore, not located at lattice sites. However, α -particles emitted from Po, the daughter product of Rn, show a 2.5-fold dip in intensity in the $\langle 100 \rangle$ direction, indicating that the Po atoms are substitutionally located.

9.1.2.5.6. SECONDARY PARTICLE YIELDS. The channeling process confines the ion trajectory to regions away from the atomic rows and planes, with the consequence that the probability of violent collisions with lattice atoms is reduced. It follows, therefore, that the rates of processes requiring close encounters should be suppressed for channeled ions. This suppression may be investigated either by the measurement of decreased large-angle scattering of the primary particle (Rutherford scattering), or by a decrease

⁶³ L. Eriksson, J. A. Davies, J. Denhartog, J. W. Mayer, O. J. Marsh, and R. Markarious, *Appl. Phys. Letters*. To be published.

⁶⁴ H. Matzke and J. A. Davies, *J. Appl. Phys.* **38**, 805 (1967).

⁶⁵ B. Domeij and K. Björqvist, *Phys. Letters* **14**, 127 (1965); B. Domeij, *Nucl. Instr. Methods* **38**, 207 (1965); B. Domeij, *Arkiv Fysik* **32**, 179 (1966).

⁶⁶ J. Lindhard, *Kgl. Danske Videnskab. Selskab Mat. Fys. Medd.* **34**, No. 14 (1965); *Phys. Letters* **12**, 126 (1964).

in the yield of secondary particles. Since the probability of scattering out of channels increases with crystal thickness, many investigators have chosen reactions with energy thresholds or resonant reactions that occur only over a limited range of energies, i.e., over a limited section of the particle trajectory.

9.1.2.5.6.1. *Nuclear Reactions.* Thompson⁶⁷ investigated the effect of proton channeling on the rate of neutron production from the $^{65}\text{Cu}(\text{p}, \text{n})^{65}\text{Zn}$ reaction, using an incident beam of 2.8-MeV protons. The reaction has a threshold near 2.1 MeV. Protons which remain channeled until they are slowed down to below threshold energy are less likely to cause nuclear reactions. A decrease of about 5% in the (p, n) yield was observed when the beam was parallel to the (110) and the (001) planes.

Much larger effects were observed by Bøgh *et al.*⁶⁸ in their study of the (p, γ) yields from ^{27}Al and ^{29}Si . In both of these reactions, there are sharp resonances in the region of 400 keV. Therefore, the range of penetration depths in which reactions could occur was strongly limited since collisions either above or below the resonance energy could not lead to reaction. With proton energies only slightly higher than the resonance energy, the investigators were able to restrict the reaction zone to the initial portion of the proton trajectory. By increasing the incident energy, they were able to increase the depth of the reaction zone. With a 410-keV proton beam incident on ^{27}Al (i.e., only a few kiloelectron volts above resonance), they observed a fivefold decrease in the (p, γ) yield, for incidence along a $\langle 110 \rangle$ axis. This attenuation effect decreased with increasing proton energy, i.e., with increasing depth of the reaction zone below the surface.

The opposite effect, i.e., an increase in nuclear reaction yield for ion incidence in channel directions, can be expected if the reacting target nuclei are located interstitially. This effect was found by Iferov *et al.*⁶⁹ when bombarding a deuterium-doped Nb single crystal with deuterium ions. The p yield from the $^2\text{H}(\text{d}, \text{p})^3\text{H}$ reaction showed a pronounced increase when incidence occurred along the 111-channel direction. Simultaneously, the number of elastically scattered deuterium ions decreased markedly.

9.1.2.5.6.2. *Characteristic X-Ray Yields.* With a logical extension of the string model, the electrons belonging to different atomic shells may be viewed as being distributed in discrete annuli around the axis of a densely packed row, or, in the case of planar symmetry, in layers extending out from the plane. Thus, for example, it would be expected that highly channeled particles, which are constrained to motion close to the midplane, will

⁶⁷ M. W. Thompson, *Phys. Rev.* **15**, 756 (1964).

⁶⁸ E. Bøgh, J. A. Davies, and K. O. Nielsen, *Phys. Letters* **12**, 129 (1964).

⁶⁹ G. A. Iferov, G. P. Pokhil, and A. F. Tulinov, *JETP Letters (English Transl.)* **5**, 201 (1967).

fail to encounter any electrons of the inner electron shells, while those which travel on paths with higher amplitude may, in fact, interact with inner shells and still remain channeled. Collisions of these particles with the inner shell electrons could cause ejection and the consequent emission of a characteristic X ray.

The possibility of this phenomenon was first investigated by Brandt *et al.*⁷⁰ who used proton beams at energies from 75 to 115 keV to study the yields of *K* X rays from Al and *L* X rays from Cu single crystal targets. They observed dips in the X-ray yields (about a factor of 2) when the beam was aligned with the $\langle 110 \rangle$ channel. The half widths of the dips (6.7° at 75 keV and 5.7° at 115 keV for Cu *L* X rays and 3.8° at 110 keV for Al *K* X rays) were in reasonable agreement with the predictions. In a systematic study of these systems, Khan *et al.*⁷¹ observed both planar and axial effects and investigated the effects of surface contamination on the magnitude of the dips. For the low-energy protons used in this work, even small amounts of surface contaminants can cause a great deal of scattering before the ions enter the lattice. With their cleanest surface conditions, the yield in the $\langle 110 \rangle$ direction was a factor of 15 less than the normal polycrystalline values.

9.1.2.5.7. EMERGENCE PATTERNS. The effect of crystalline potentials on the trajectories of penetrating ions has been demonstrated most graphically in experiments which record the spatial distribution of ion beams following their emergence from single crystal targets. In the first of these experiments, Schiffer and Holland⁷² interposed a $75\text{-}\mu$ -thick Si crystal into a 3.6-MeV proton beam, and photographed the fluorescence produced on a quartz plate placed some distance behind the Si target. They observed effects which were attributable to both channeling and blocking phenomena. When the $\langle 111 \rangle$ axis of the crystal was aligned with the beam, a central bright spot was observed, and bright lines corresponding to preferential scattering parallel to $\{110\}$, $\{101\}$, and $\{011\}$ planes were also seen.

A slight rotation of the crystal (2°) caused the entire pattern to shift without a measurable increase in the divergence of the deflected particles. This observation was interpreted as evidence that the beam was being steered by the crystal. Experiments with protons and α -particles with crystals of similar thickness have disclosed three general features in the emergence patterns which are represented in Fig. 14a: First, when the beam is aligned with an axial channeling direction, there is a concentration of intensity in the axial channel and a spreading in the open planar directions

⁷⁰ W. Brandt, J. M. Khan, D. L. Potter, R. D. Worley, and H. P. Smith, Jr., *Phys. Rev. Letters* **14**, 42 (1965).

⁷¹ J. M. Khan, D. L. Potter, R. D. Worley, and H. P. Smith, Jr., *Phys. Rev.* **148**, 413 (1966).

⁷² J. P. Schiffer and R. E. Holland, *Bull. Am. Phys. Soc.* **10**, 54 (1965).

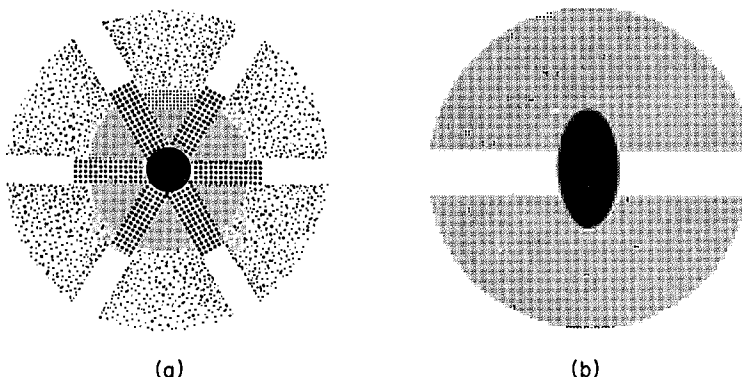


FIG. 14. Schematic pictures of transmission emergence patterns: (a) protons through an axial $\langle 111 \rangle$ channel of Si $\sim 75 \mu$ thick [J. P. Schiffer and R. E. Holland, *Bull. Am. Phys. Soc.* **10**, 54 (1965)]; (b) 40-MeV ^{127}I ions through a planar (111) channel of Au $\sim 0.5 \mu$ thick [T. S. Noggle, C. D. Moak, H. O. Lutz, and S. Datz, *Bull. Am. Phys. Soc.* **11**, 177 (1966)].

which intersect the axis; second, the contribution of the particles which have been dechanneled (random beam) to an over-all background; and third, the light streaks extending out in the planar directions. These light streaks are caused by blocking effects, i.e., the dense atom planes deter the randomly scattered ions from a chance re-entry into a planar channel.

Studies using thinner crystals ($0.5\text{-}\mu$ Au) and 40-MeV ^{127}I ions⁷³ gave somewhat different results. Transmission through the crystal with the incident beam parallel to $\{111\}$, $\{100\}$, or $\{110\}$ produced emergent beam which registered as an elliptical spot whose major axis was perpendicular to the particular plane being examined (Fig. 14b). This could be explained from a consideration of the forces acting on the ion. If one assumes a planar potential, ions which do not enter at the midplane should be deflected in a direction perpendicular to the plane; however, if the potential is perfectly smooth, there are no forces present which would deflect the ions parallel to the plane. The angular dimensions of the major axes of the spots observed could be correlated with the critical channeling angles inferred from the planar potential,⁵⁵ and the shapes of the patterns observed in low-index axial directions could be accounted for on the basis of a superposition of the elliptical spots obtained from planar channels.

The photographic technique used in these experiments permits simultaneous recording of virtually all of the emerging particles over a wide

⁷³ T. S. Noggle, C. D. Moak, H. O. Lutz, and S. Datz, *Bull. Am. Phys. Soc.* **11**, 177 (1966).

range of angle. Measurement of the energies of the particles emerging at any particular part of the pattern is generally done with solid-state detectors. An interesting new technique developed by Nelson *et al.*⁷⁴ utilized color film emulsions which gave a semiquantitative energy analysis as well as the spatial distribution of protons ($E_0 = 1.5$ MeV) emerging from single crystal foils. The color of the developed emulsion depends on the depth of penetration which in turn depends on the particle energy. Different energy loss groups associated with the different scattering processes involved in the pattern were observable as different colors.

Tulinov and co-workers⁷⁵ investigated the effect of blocking on the spatial distribution of 200 to 500-keV protons which were backscattered from thick single crystal targets. In this technique, the beam enters a crystal in a non-channeling direction, and the Rutherford-scattered protons strike a photographic plate parallel to the surface. Figure 15 shows a photographic recording of the system of "shadows" cast by crystallographic planes in tungsten obtained by the elastic scattering of 200-keV protons from a tungsten single crystal (bcc structure). The spot in the center is due to blocking by the $\langle 100 \rangle$ close-packed rows. The vertical and horizontal lines are formed by blocking from the $\{111\}$ planes. To enhance the contrast, the photographic plate was covered with a thin absorber which stopped low-energy multiple-scattered protons. The lowest-index directions give more pronounced spots since the angular dimensions of the excluded regions are directly related to the nearest-neighbor distance in the plane or row.

Nelson and Holloway⁷⁶ obtained back-reflection patterns with proton beams at energies as low as 20 keV. To enhance the detection efficiency, the Rutherford-scattered protons impinged on a fluorescent screen held parallel to the crystal surface. The lower proton energies used in this work limit the penetration depth and provide a method for the study of crystal structures of thin surface layers.

9.1.2.5.8. SURFACE BARRIER DETECTORS. Solid-state surface barrier devices which are used to detect energetic particles and determine their energies operate in much the same manner as ionization chambers. An energetic particle is stopped within a carrier-depleted region of a semiconductor. All the energy lost through electronic stopping results in the creation of electron-hole pairs, and the number of pairs in a pulse created

⁷⁴ R. S. Nelson, B. W. Farmery, G. Dearnaley, and I. V. Mitchell, UKAEA Harwell Rept. AERE-R5335.

⁷⁵ A. F. Tulinov, B. G. Akhmedova, A. A. Puzanov, and A. A. Bednyakov, *JETP Letters (English Transl.)* **2**, 30 (1965); A. F. Tulinov, *Soviet Phys. Usp. (English Transl.)* **8**, 864 (1966).

⁷⁶ R. S. Nelson and D. F. Holloway, UKAEA Harwell Rept. AERE-R5372.

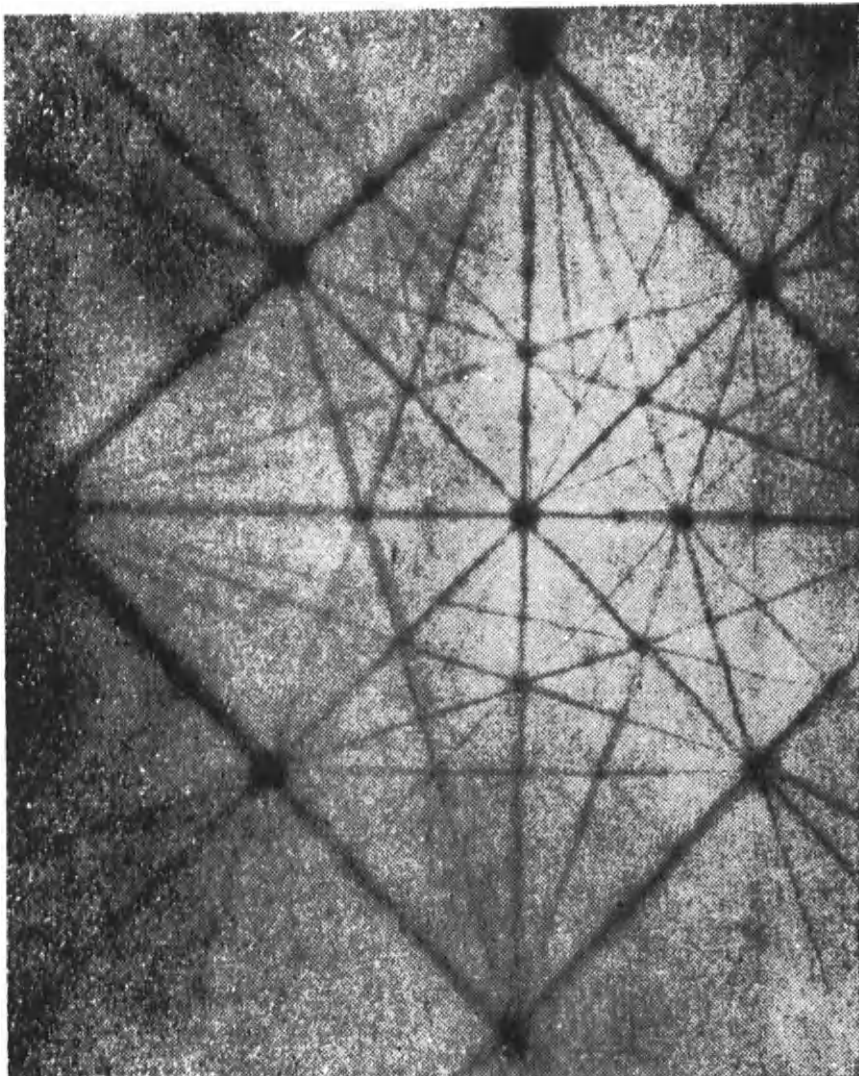


FIG. 15. Rutherford backscattering pattern of 200-keV protons from *W*. Film perpendicular to a [110] direction [A. F. Tulinov, B. G. Akhmedova, A. A. Puzanov, and A. A. Bednyakov, *JETP Letters (English Transl.)* 2, 30 (1965); A. F. Tulinov, *Soviet Phys. Usp. (English Transl.)* 8, 864 (1966)].

by the ion is used as a measure of its energy. Since these detectors are themselves single crystals, channeling phenomena can have two effects on their performance: first, on the depth of the depletion layer required to stop the ions and, second, on the relative amount of energy loss due to elastic collisions with lattice. These concerns were, in fact, among the primary motivations for Dearnaley's first studies of proton channeling in silicon.⁵⁰ The increased range of protons in Si channels and the attendant increased requirement of depletion depth for stopping were well-established by his work; however, he was unable to observe any difference in the total number of electron-hole pairs produced and collected for channeled and unchanneled protons. The practical result of this is that workers using Si surface barrier detectors for energetic protons should be careful not to orient their detectors in low-index directions with respect to the beam lest the proton range exceeds the depletion depth.

The situation with heavy ions is quite different. It has been observed that the number of electron-hole pairs created and collected by the stopping of energetic heavy ions in the crystal was considerably less than that obtained for protons of the same energy.¹⁰ One possible reason for this discrepancy (called the "pulse-height defect") lay in the contribution of elastic scattering by lattice atoms to the stopping of the ion. Since there is also a statistical spread in the amount of nuclear stopping, it could also lead to the decreased energy resolution obtained in heavy ion detection. These suppositions were confirmed by the experiments of Moak *et al.*⁷⁷ in which they investigated the effect of detector orientation of the pulse-height spectra obtained from bombardment of silicon surface barrier detectors with 10 to 120-MeV ^{127}I ions. They found that as the crystal was rotated from a random direction to the $\langle 110 \rangle$ axis a second peak developed which came from ions which had been channeled in the detector. These peaks showed no pulse-height defect and a threefold increase in the energy resolution was observed. Since nuclear stopping is only expected to be significant at lower ion energies, this result implies that the ^{127}I ions are channeled in Si over almost their entire range.

9.1.3. Interactions with Surface Atoms

9.1.3.1. High-Energy Collisions. A number of investigators have observed that fast "secondary" ions are emitted from ionically bombarded solid surfaces.^{78, 79} Moreover, some recent observations have indicated that—in some cases—a measurable fraction of the reflected ions possesses energies

⁷⁷ C. D. Moak, J. W. T. Dabbs, and W. W. Walker, *Rev. Sci. Instr.* **37**, 1131 (1966).

⁷⁸ For a general review see M. Kaminsky, "Atomic and Ionic Impact Phenomena on Metal Surfaces." Springer, New York, 1965.

⁷⁹ A review of fast ion surface scattering is given by C. Snoek and J. Kistemaker, *Advan. Electron. Electron Phys.* **21**, 67 (1965).

which are characteristic of simple two-atom collision processes.⁸⁰⁻⁸³ The latter result may be understood when one considers that the interaction times relevant to collisions involving ions in the 1 to 100-keV energy region are in the order of 10^{-16} to 10^{-17} sec, whereas vibration times of the target atoms in their lattice are in the order of 10^{-13} to 10^{-14} sec. Thus, when the energy transferred in the collision exceeds the binding energy of the target atom, one might expect decoupling from lattice interactions. This leads to the interesting possibility that a detailed study of these ions might yield fundamental information concerning the nature of high-energy interatomic scattering processes. These results might then be used to augment the information which has already been obtained by other investigators who have studied large-angle scattering of ion beams from gaseous targets.

The experimental arrangements in these experiments with solid targets are almost identical with those for gas scattering. The analysis of scattered particles can be performed with sector-type instruments using either electrostatic or magnetic deflecting systems or a combination of both as used in a parabola mass spectrograph.⁸¹ Fast neutrals can be analyzed by using pulsed beams and measuring the time of flight over a known distance.⁸⁴ In this energy range, particle multipliers or simple secondary electron emitters serve as detectors.

The two major experimental difficulties encountered in the use of solid targets are surface impurities and the contributions of multiple scattering from collisions below the surface layers. The problem of surface impurities can be avoided by the use of ultrahigh-vacuum techniques and baking (see Section 9.1.3.2) or by maintaining a sufficiently high current density in the ion beam. Since most of the incoming particles penetrate the lattice and eject 2-10 surface atoms by the sputtering process, the surface is continually refreshed during the reflection experiment. Thus, for example, a current density of $100 \mu\text{A}/\text{cm}^2$ removes $\sim 10^{16}$ atoms/ cm^2/sec while the flux of ambient gas molecules at easily attainable pressures of 10^{-6} Torr which can contaminate the surface is only $\sim 10^{14}$ molecules/ cm^2/sec .

The problem of interfering multiple scattering can be minimized by the use of oriented single crystal targets.⁸² The probability that a reflected particle will have made more than one collision with lattice atoms is strongly dependent on the depth of its first collision partner; i.e., an entering particle making its first collision in the third or fourth lattice layer has a much

⁸⁰ B. V. Panin, *Soviet Phys. JETP (English Transl.)* **15**, 215 (1962).

⁸¹ V. Walther and H. Hintenberger, *Z. Naturforsch.* **18a**, 843 (1963).

⁸² S. Datz and C. Snoek, *Phys. Rev.* **134**, A347 (1964).

⁸³ E. S. Mashkova and V. A. Molchanov, *Soviet Phys. "Doklady" (English Transl.)* **7**, 829 (1963).

⁸⁴ J. M. Fluit, J. Kistemaker, and C. Snoek, *Physica* **30**, 870 (1964).

greater chance of making other collisions before leaving the lattice than one which has made its first collision in the first lattice layer. However, the probability of escape from the lattice decreases with increasing initial penetration depth. Thus, the contribution of multiple-collision events to the spectrum can be greatly reduced by arranging the target so that only particles striking the first atomic layer emerge from the target. This effect was demonstrated by Datz and Snoek⁸² in their work on the reflection of 10 to 100-keV Ar⁺ from Cu and is shown in Fig. 16. These spectra were taken under identical bombardment and detection conditions; the only difference is that spectrum *B* was obtained by bombarding a Cu single crystal in a low-index [110] direction. The peak-to-valley ratio increases dramatically, an observation which is related to reduced Rutherford scattering for channeled particles (see Section 9.1.2.5.4). The splitting of the argon ion lines into doublets corresponds to scattering from ⁶³Cu and ⁶⁵Cu atoms at the crystal surface.

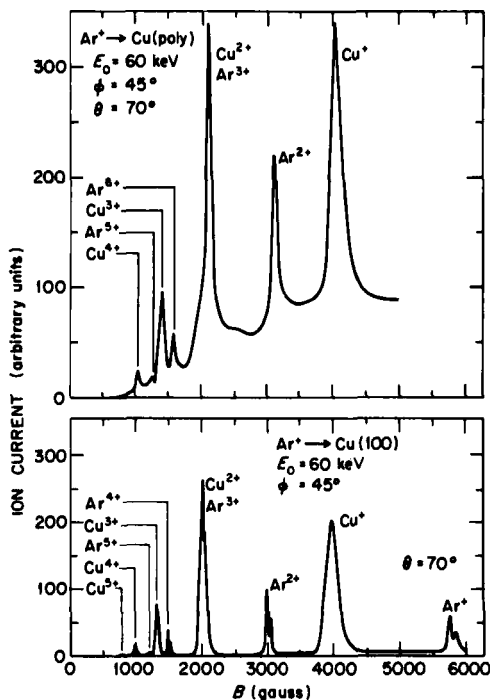


FIG. 16. Magnetic analysis of scattered ion currents for the Ar⁺ (60 keV) on Cu. The upper curve was obtained with polycrystalline Cu target. The lower curve was obtained with (100) Cu single crystal with the beam incident in the [100] direction [S. Datz and C. Snoek, *Phys. Rev.* **134**, A347 (1964)].

The results obtained in this work are qualitatively similar to those obtained in studies of large-angle atomic scattering in gases. They have demonstrated that these collisions are predominantly inelastic and lead to multiple ionization of the colliding particles. A detailed energy analysis of the emitted Cu and Ar ions gave values for the inelastic energy losses which were in close agreement with the results obtained by scattering from copper vapor⁸⁵ (see Fig. 17). A comparison of the charge state distributions obtained from solid and vapor targets showed that with solid targets there is a

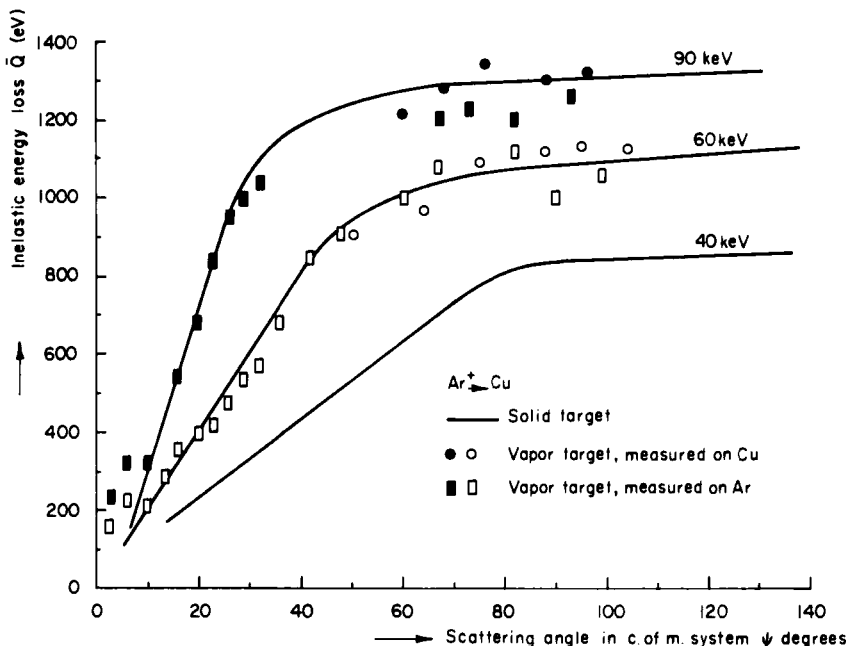


FIG. 17. Mean inelastic energy loss, \bar{Q} , for Ar^+ on Cu as measured by gas scattering and solid target techniques [C. Snoek, Ph. D. Thesis, Univ. of Amsterdam, Amsterdam, 1966].

decrease in the relative populations of higher charge groups. This effect is probably due to partial neutralization of the ions by electron transfer from the solid. The use of a solid target technique potentially possesses two advantages over gas scattering techniques. The first is the increase in target atom density, which yields an equal increase in signal and attainable angular

⁸⁵ C. Snoek, Ph. D. Thesis, Univ. of Amsterdam, Amsterdam, 1966.

resolution, and the second is the increase in the number and type of target atoms which may be used.

9.1.3.2. Thermal Energy Collisions. When the particle impinging on a solid surface has an energy less than a few electron volts, its penetration capability is nil, and it may be considered to interact directly only with atoms in the surface layer of the solid. At first sight, this would seem to simplify the considerations which govern the behavior of such systems. Under certain conditions, this is in fact the case. For example, at very low thermal energies, the associated de Broglie wavelengths of light molecules such as hydrogen and helium become long enough to be comparable to lattice spacings and, diffraction from the atomic surface grating of the crystal is observed. In general, however, thermal energy interactions are more complex than those studied at higher energies. Coupling of lattice atoms, their thermal oscillations, and the relatively weak interatomic attractive forces which were either negligible or small perturbing influences at higher energies now dominate the interaction.

To understand the nature of the problem, consider first the interaction of a cold solid with a gas in the absence of appreciable attractive forces (e.g., hot helium on a cold metal). Energy can be transferred in collisions from the gas to the solid. The maximum energy transferred in a single collision with a single surface atom would be simply $E_{\max} = (4M_g M_s)/(M_g + M_s)^2$ where M_g is the mass of the gas and M_s is the mass of a surface atom. That this is the case for high-energy surface collisions where the impulse is rapid compared with lattice oscillation times was shown in the previous section. However, for molecular velocities at thermal energies, this assumption is not valid, and the nature of the coupling of the motion of the struck atom with its neighbors becomes important. For example, if we consider just the next neighbor of the struck atom, the problem is similar to that of collisional excitation of vibrations in a diatomic molecule. In this case, there is a high probability that a large portion of the energy transferred to vibration, will be restored to translation before the termination of the collision event. If all of the possible oscillations in the lattice are coupled, there are so many vibrational modes that the probability of relocalization of all of the transferred energy is remote. The actual situation lies between these two extremes and is controlled by the detailed coupling of the surface atom with the remainder of the solid (i.e., on the mechanism for generation of lattice phonons).

Now reverse the conditions and consider a cold molecule colliding with an atom on a hot surface; the energy transferred to the gas molecule will depend on the instantaneous velocity of the bound surface atom and hence upon the lattice force constants and the phase of the particular lattice oscillations. If an appreciable binding energy of the molecule to the surface is

now introduced, the situation becomes even more complex. At the least, the trajectory of the molecule is perturbed and, if the binding energy exceeds the kinetic energy of the reflected particle, the molecule is trapped in the attractive potential and adsorbed on the surface. The adsorbed molecule may at some later time dissociate, ionize, react with the substrate, other adsorbed species, or with bombarding gas molecules. All of these latter phenomena represent secondary processes which occur after the initial adsorption process in which the incident particle has substantially lost its identity as a gas molecule and hence will not be treated here. We shall only concern ourselves with the primary collision process, in which the incoming particle is reflected from the surface.

These experiments deal with energy and momentum exchange between impinging gas molecules and solids. The results of these collisions have an important bearing on such diverse problems as heat exchange, gaseous diffusion rates, adsorption, condensation, and nucleation.

A parameter which has proven convenient in the description of these processes is the "accommodation coefficient," α , which characterizes the fraction of the energy difference transferred from a surface at temperature T_s to a gas at temperature T_g in a single collision:

$$\alpha = \frac{T_g' - T_g}{T_s - T_g}$$

where T_g' is the temperature of the gas molecule after leaving the surface. The classical method for determining α is the measurement of the heat conductivity of a gas at low pressure in the vessel whose dimensions are less than one mean free path. Typically, a thin wire of the solid in question, heated to some fixed temperature T_s , is positioned in the center of an evacuated tube which is thermostated at T_g . The gas is admitted, and the additional power Q necessary to maintain the temperature is measured. The accommodation coefficient is then obtained from

$$\alpha = Q(2\pi M_g k T_g)^{1/2} / 2pk(T_s - T_g) \quad (18)$$

where p is the gas pressure. Several other bulk methods have been developed for measuring α , but these as well as the thermal conductivity method do not give unambiguous information on the dynamic collision process. For example, if a portion of the gas is adsorbed, the measured accommodation coefficient will be a weighted average between that for reflected molecules which may exchange little energy and molecules desorbing at complete thermal equilibrium with the solid.

The most detailed information has been obtained from molecular beam experiments. The appeal of beam techniques for application to studies of gas-surface phenomena is, of course, the simplicity of the experimental

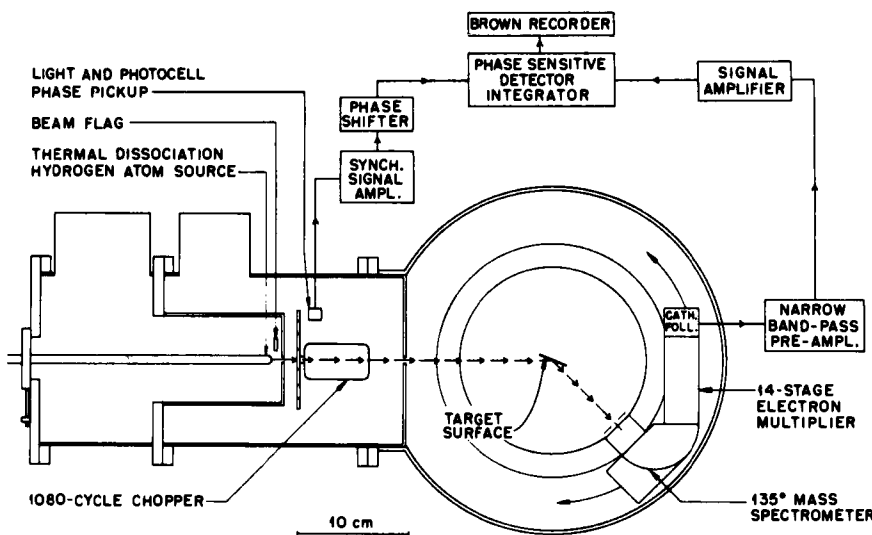


FIG. 18. Modulated molecular beam apparatus for surface reflection studies. Phase shift may be used to measure change in group velocity [S. Datz, G. E. Moore, and E. H. Taylor, in "Rarefied Gas Dynamics" (J. A. Laurmann, ed.), Vol. I, p. 347, Academic Press, New York, 1963].

concept, along with the possibility of simple interpretation of experimental results. In consequence, gas-surface phenomena have been under study since the earliest days of beam research. The early work on gas-surface work with beams has been described by Fraser⁸⁶ and by Datz and Taylor.⁸⁷ More recent work has been reviewed by Fite and Datz⁸⁸ and by Stickney.⁸⁹ The molecular beam techniques and apparatus components used in these experiments are, in most ways, identical to those used in the gas scattering experiments described in Part 4 of this volume, except that a solid target is used in place of the scattering gas. An example of the type of apparatus used is shown in Fig. 18. A modulated beam of gas strikes a surface at a given angle, and the intensity and velocity of the reflected stream of molecules are measured as a function of reflection angle. Ideally, the primary

⁸⁶ R. G. J. Fraser, "Molecular Rays," Cambridge Univ. Press, London and New York, 1931.

⁸⁷ S. Datz and E. H. Taylor, Some applications of molecular beam techniques to chemistry. In "Recent Research in Molecular Beams," Academic Press, New York, 1959.

⁸⁸ W. L. Fite and S. Datz, *Ann. Rev. Phys. Chem.* 13, 61 (1964).

⁸⁹ R. E. Stickney, *Advan. At. Mol. Phys.* 3, 143 (1967).

beam should be velocity selected, and the target should be a clean, well-oriented single crystal surface. Unquestionably, the worst difficulty in gas-surface beam work is the uncertainty of the condition of the surface due to the presence of adsorbed gases.

The fact that beam experiments are carried out in high-vacuum systems with streams of gas that are no more dense than the residual gas concentrations aids immensely in the retention of clean surface conditions, but generally this is not sufficient. This can be seen from a brief consideration of the factors which control the degree of surface contamination. A surface in contact with the ambient residual gas in a vacuum system is bombarded by a molecular flux ϕ equal to $n\bar{c}/4$ where n is the number density and \bar{c} is the most probable speed of the gas molecules. The number of available lattice sites N per square centimeter of surface is about 10^{15} . Thus if all the molecules striking a surface were to stick and remain adsorbed, an initially clean surface in contact with a gas at 10^{-10} Torr would be completely covered in about an hour. With the more readily achieved pressure of 10^{-8} , the time involved is in the order of seconds. However, the adsorbed molecules re-evaporate from the surface at a rate determined by the surface temperature T and the heat of adsorption ΔH . The mean residence time on the surface τ can be approximated by

$$\tau = \tau_0 \exp(\Delta H/kT)$$

where τ_0 is in the order of a lattice vibration time (10^{-13} to 10^{-14} sec). At equilibrium, the fraction, f , of the surface which is covered by an adsorbed layer is

$$f \simeq [1 + (N/\tau\gamma\phi)]^{-1}$$

where γ is the sticking probability. With ambient pressure of 10^{-8} Torr and with $\gamma = 1$, the fraction covered will be less than 0.1 if $\Delta H/kT < 30$. Clearly one way to maintain a pure surface is to keep it hot enough to meet this criterion. Since ΔH can vary from 0.1 kcal/mol to 100 kcal/mol, the temperature required for a clean surface can vary from 300 to 3000°K depending on the system involved. With metals such as tungsten which strongly adsorb oxygen, high temperatures ($>2000^{\circ}\text{K}$) are required. On the other hand, alkali halide surfaces prepared by cleaving the crystal in vacuum seem to remain remarkably clean for relatively long periods.

In practice, four methods can be used to obtain surfaces free of adsorbed gases. The first is to use surfaces at temperatures sufficiently high that the rate of evolution of adsorbed gas greatly exceeds the rate of arrival of background gas particles at the surface. Surface diffraction of He beams was observed from cleaved LiF crystals as early as 1930⁸⁶ with pressures no

lower than 10^{-5} Torr. The observation of diffraction requires an atomically clean surface, and, since these experiments took considerable time, it can be inferred that these surfaces are very stable with respect to adsorbed gas contamination. An alternative method is to initially clean the surface by thermal flashing or ion bombardment and to keep the target in an ultrahigh-vacuum region. However, high pumping speeds are required with this method when using beams of noncondensable gases which can interact strongly with the surface.

Another approach to the problem is to continuously renew the surface either by deposition or by removal of the surface layers at a more rapid rate than the surface can be contaminated by background gas. This method was used by Brackmann and Fite⁹⁰ in studying the reflection of atomic and molecular hydrogen at frozen gas and water surfaces by probing with a modulated hydrogen beam while a second, more intense dc beam deposited the surface. In this case the crystal form of the surface is not well defined. A variation of the continuous condensation method which overcomes this difficulty has been developed by Smith and Salzberg.⁹¹ In their work, they continuously form single crystal surfaces by epitaxial growth on a suitable substrate. Using a mica substrate, they have succeeded in forming and maintaining clean single crystal surfaces of gold and silver. A crucible containing either gold or silver is located near the target, and the deposition rate is controlled by the temperature of the crucible. If the substrate is held at $\sim 580^{\circ}\text{K}$ during deposition, the resulting epitaxial film is highly oriented with the (111) plane parallel to the substrate surface. In the case of silver it was observed that, when the deposition stopped, the reflection pattern did not change as long as the vacuum (10^{-7} Torr) was maintained. This implies that some metal surfaces remain clean for remarkably long periods.

Although atomically clean surfaces of high crystallographic order can be maintained with continuous sputtering by ion bombardment, as was demonstrated in the high-energy surface experiments⁸² (Section 9.1.3.1), this approach has not yet been used for the maintenance of clean surfaces during thermal beam reflection experiments.

The remaining difficulties in these experiments are identical with those encountered in differential scattering measurements with crossed molecular beams. Here again the detection and velocity analysis of a small number of scattered molecules is the major problem.

The use of beam modulation with phase sensitive detection can appreciably improve the sensitivity of detection, and, with a proper choice of

⁹⁰ R. T. Brackmann and W. L. Fite, *J. Chem. Phys.* **34**, 1572 (1961).

⁹¹ J. N. Smith, Jr. and H. Salzberg, *J. Chem. Phys.* **40**, 3585 (1964); **45**, 2175 (1966).

modulating frequency, Datz *et al.*⁹² demonstrated that phase sensitive detection can also be used to measure the group velocity of reflected ions. If the frequency is chosen such that the flight time of the molecule from the reflecting surface is comparable to an oscillation period, the particle velocity will be observed as a phase shift in the modulated signal (see Fig. 18). With the target withdrawn, an arbitrary zero in phase angle is established by adjusting the phase shifter to lock-in on the direct beam. Then with the target in place at the desired incidence angle and the mass spectrometer rotated to a given reflection angle, the shift in phase angle, $\Delta\phi$, of the reflected signal is measured. The group velocity of the reflected beam \bar{v}_2 is then obtained from

$$1/\bar{v}_2 = 1/\bar{v}_1 - \Delta\phi/2\pi f d \quad (19)$$

where d is the distance from the scattering center to the ion source and f is the modulating frequency. The initial mean velocity \bar{v}_1 is determined by the temperature at the beam source.

Another method used to measure the group velocity is the "stagnation detector" developed by Smith and Fite.⁹³ This device is pictured in Fig. 19. The technique involves the measurement of both the number density and the flux of the reflected beam. The first measurement is made by passing the beam directly through the electron beam of a mass spectrometer ion source. The beam can leave the region through an open slit opposite the beam entrance slit without touching the walls of the source. The ion signal S obtained with this geometry is proportional to the number density, n , of neutral particles in the beam, which is in turn equal to the ratio of the total particle flux, j , to the mean velocity of the particles, \bar{v} . The second measurement is made by closing the in-line entrance slit and letting the neutral particles enter through an aperture displaced from the ion source center line. The beam strikes a baffle located directly behind the aperture so that a neutral beam particle is forced to collide many times with the wall before reaching the electron beam. The signal obtained in this mode of operation is dependent only on the flux j . By comparing the signals obtained in the two modes, the effects of j and \bar{v} can be separated. The device can be calibrated by measuring the direct beam from a source at known temperature. Using a beam modulated at 100 cycles, a considerable phase lag was observed in the stagnation caused by the impedance of the baffle. This method would therefore lead to serious beam demodulation at higher frequencies.

⁹² S. Datz, G. E. Moore, and E. H. Taylor, in "Rarefied Gas Dynamics" (J. A. Laurmann, ed.), Vol. I, p. 347. Academic Press, New York, 1963.

⁹³ J. N. Smith, Jr. and W. L. Fite, in "Rarefied Gas Dynamics" (J. A. Laurmann, ed.), Vol. I, p. 347. Academic Press, New York, 1963.

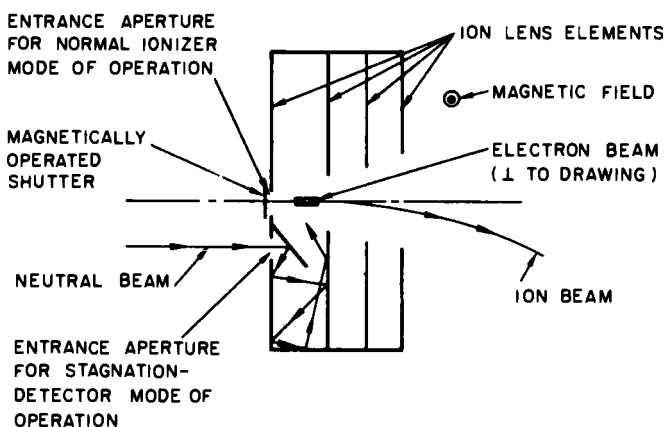


FIG. 19. Stagnation detector which determines group velocity by measuring both the number density and flux of the scattered beam [J. N. Smith, Jr. and W. L. Fite, in "Rarefied Gas Dynamics" (J. A. Laurmann, ed.), Vol. I, p. 430, Academic Press, New York, 1963].

Both of these schemes measure a weighted average of velocities of the detected particles. They suffer from the same uncertainties as those involved in thermal conductivity measurements of the accommodation coefficient, since the group velocity can only be associated with a temperature if the distribution is Maxwellian. A complete velocity analysis of a reflected potassium atom beam was carried out by Marcus and MacFee⁹⁴ using a slotted disk velocity analyzer. This was made possible by the extremely sensitive surface ionization method available for alkali atoms.

A new method which has been developed by Scott *et al.*⁹⁵ utilizes time-of-flight techniques to give the complete velocity spectrum of reflected atoms (Fig. 20). A dc atomic beam strikes the surface, and the reflected beam is chopped. It then passes through a collimator and is ionized by electron bombardment. The time shape of the ionized pulse is directly related to the velocity distribution. The ion signal from the pulsed reflected beam is much smaller than the dc ion signal from the background gas and is of the same order as the noise. The beam signal can be electronically enhanced by taking the same segment of the periodic signal during each cycle and integrating over several cycles.

⁹⁴ P. M. Marcus and J. H. McFee, "Recent Research in Molecular Beams." Academic Press, New York, 1959.

⁹⁵ P. B. Scott, P. H. Bauer, H. Y. Wachman, and L. Trilling, in "Rarefied Gas Dynamics" (J. H. de Leeuw, ed.), Vol. II, p. 1353. Academic Press, New York, 1967.

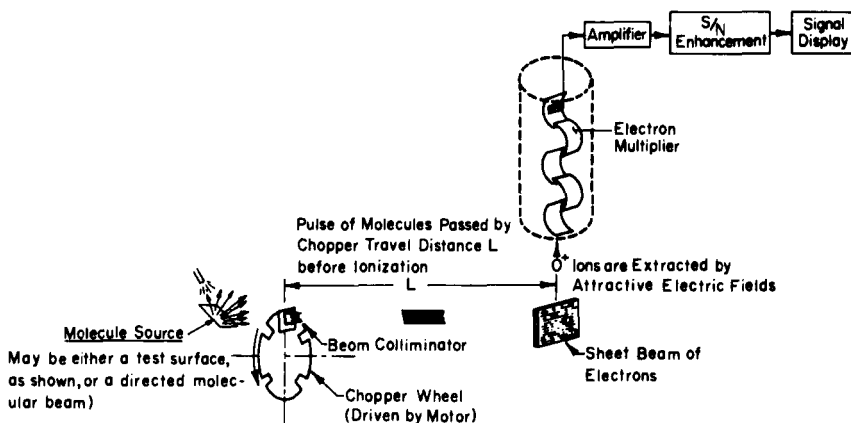


FIG. 20. Velocity analysis of the reflected beam is achieved by measuring the time distribution of the chopped reflected beam [P. B. Scott, P. H. Bauer, H. Y. Wachman, and L. Trilling, in "Rarefied Gas Dynamics," Vol. II, (J. H. de Teeuw, ed.) p. 1353, Academic Press, New York, 1967].

9.2. Interaction of Electrons with Solids*†

9.2.1. Introduction

The processes by which electrons interact with solids have been studied by many workers for over half a century. The complexity of the interaction, however, is such that while the processes involved are generally understood, there is inadequate quantitative data available to describe particular processes in particular materials.

In an earlier article in this series, Sternheimer¹ has presented the theory describing the interaction of charged particles with an assemblage of atoms. An attempt will be made in the present article to present those techniques and methods germane to electron interaction in solids. In particular, interactions involving electrons of energy between near zero and about 100 keV will be considered. At higher energies, the methods described in Vol. 5A of this series become more appropriate.

A given interaction can be described in terms of the momentum and/or energy change suffered by the incident or primary electron in a scattering

¹ Vol. 5A, Chapter 1.1.

† Contribution of the National Bureau of Standards, not subject to copyright.

* Chapter 9.2 is by C. J. Powell.

event. Inelastic processes are defined as those for which there are changes in both energy and momentum of the primary electron. Elastic processes are those for which there is significant change only in primary electron momentum; the "recoil" energy, of the order of 20 meV, is absorbed by the lattice of the solid. Information is generally desired on the cross sections for particular momentum and/or energy changes that may occur in a given solid.

Several types of experiments may be distinguished. One may be concerned with the differential or total cross sections[†] for elastic or inelastic scattering of primary electrons which may be either incident on a surface, transmitted through a thin film, or released in some way in a given specimen. Single, plural, or multiple scattering phenomena may be involved, depending on the specimen geometry and the initial electron energy. Alternatively, one may be concerned with the single, plural, or multiple scattering characteristics, elastic or inelastic, of secondary (or higher-order) electrons that may be released following interactions involving the primary electrons.

One reason for the complexity involved in determining the characteristics of the various interactions and for some of the experimental limitations is that the mean free path between interactions can vary between about 1 and 10^3 atomic spacings in the energy range under consideration. Thus if single scattering events in a transmission experiment (electrons transmitted through a thin specimen film) are to be studied, the electron energy will be limited to a range where the mean free paths are $\gtrsim 100 \text{ \AA}$. It is not generally feasible to prepare self-supporting specimens of thickness less than some hundreds of angstroms, and in many cases films of thickness between 100 and 1000 \AA are known to have properties different from the corresponding bulk material. For electron energies where the mean free path is less than 100 \AA , a reflection scattering geometry must generally be adopted in which the behavior of electrons scattered by a comparatively massive specimen is investigated. In both transmission and reflection experiments, the most meaningful data will be obtained only if the specimen can be characterized on an atomic scale.

The literature dealing with electron interaction with solids is extensive, and it is only possible to give here a summary of the more important methods and techniques and, in so doing, to offer a guide to the relevant literature. The current status of theory and experiment may be found by reference to a number of books and review articles.²⁻¹³ Surveys of certain aspects

² H. A. Bethe and J. Ashkin, in "Experimental Nuclear Physics" (E. Segrè, ed.), Vol. 1, p. 166. Wiley, New York, 1953.

³ R. D. Birkhoff, in "Handbuch der Physik" (S. Flügge, ed.), Vol. 34, p. 53. Springer, Berlin, 1958.

† For cross section definitions, see Chapter 1.1.

of electron beam spectroscopy have been given by Marton¹⁴ and by Klemperer.¹⁵

9.2.2. General Experimental Requirements

Most experimental studies of electron scattering are performed using variations of the schematic arrangements shown in Fig. 1. Electrons from the electron gun *G* interact with a specimen *S*, either in transmission through a thin film or reflection from a surface. In the first case, the electron path length in the specimen is greater than or equal to the film thickness, depending on the number of scattering events, while in the second case the path length generally cannot be determined. Electrons scattered elastically or inelastically and secondary electrons may be separated (if desired) by an energy analyzer *A* and recorded using the detector *D*. Transmission experiments are advantageous when it is desired to measure angular distributions of the scattered intensity, while reflection experiments are necessary when it is desired to investigate scattering phenomena that might be dominated by the state of the surface. For some materials, it may be easier to obtain a clean surface than to obtain comparable bulk purity in a thin film. For other materials, a high degree of volume purity in a thin film may be easily attained although it may be necessary to tolerate some surface impurities. Most experiments have been performed with polycrystalline specimens though single crystals of known orientation are necessary for a detailed interpretation of most scattering experiments.

The scattering geometry, the types of specimen that can be analyzed in an unambiguous manner, and the characteristics of the experimental

⁴ U. Fano, *Ann. Rev. Nucl. Sci.* **13**, 1 (1963).

⁵ R. D. Heidenreich, "Fundamentals of Transmission Electron Microscopy." Wiley (Interscience), New York, 1964.

⁶ B. W. Schumacher, *Proc. Intern. Conf. Electron Ion Beam Sci. Technol.*, 1st, Toronto, 1964 (R. Bakish, ed.), p. 5. Wiley, New York, 1965.

⁷ C. J. Calbick, *Phys. Thin Films* **2**, 63 (1964).

⁸ R. Gevers, in "The Interaction of Radiation with Solids" (R. Strumane, J. Nihoul, R. Gevers, and S. Amelinckx, eds.), p. 471. North-Holland Publ., Amsterdam, 1964.

⁹ S. Amelinckx, *Solid State Phys. Suppl.* **6**, 1 (1964).

¹⁰ Studies in penetration of charged particles in matter. *Natl. Acad. Sci. Natl. Res. Council Publ.* No. 1133.

¹¹ H. Raether, *Ergeb. Exakt. Naturw.* **38**, 84 (1965).

¹² F. Pradal, C. Gout, and D. Fabre, *J. Phys. (Paris)* **26**, 372 (1965).

¹³ P. B. Hirsch, A. Howie, R. B. Nicholson, D. W. Pashley, and M. J. Whelan, "Electron Microscopy of Thin Crystals." Butterworths, London and Washington, D. C., 1965.

¹⁴ L. Marton, *Rev. Mod. Phys.* **18**, 172 (1956); L. Marton, L. B. Leder, and H. Mendlowitz, *Advan. Electron. Electron Phys.* **7**, 183 (1955).

¹⁵ O. Klemperer, *Rept. Progr. Phys.* **28**, 77 (1965).

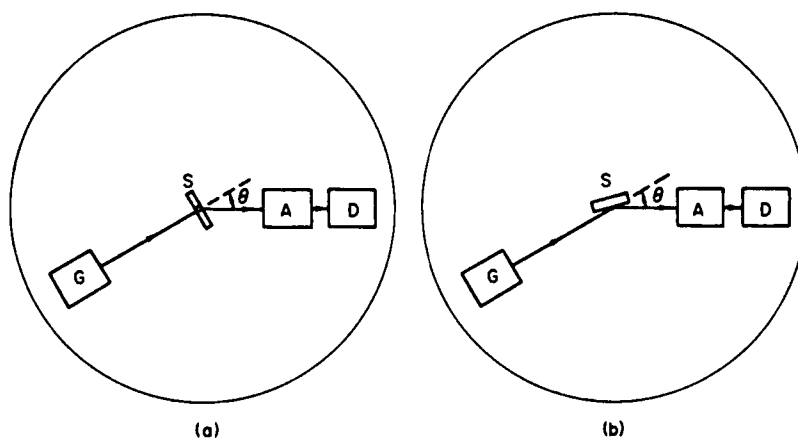


FIG. 1. Schematic arrangements for an electron scattering experiment. An electron gun G produces a beam of specified current, mean energy, energy distribution, area, and angular divergence at a specimen S , which can be either a thin film mounted on a suitable holder for "transmission" experiments (a) or a relatively thick (semi-infinite) material for "reflection" experiments (b). The energy analyzer A accepts electrons from a specified area of the specimen within a given solid angle for a mean scattering angle θ . Electrons transmitted by the analyzer reach the detector D of suitable sensitivity and should be recorded with a system signal-to-noise ratio sufficient to detect a scattering process of specified minimum cross section. Additional electron-optical elements beyond those schematically shown may be needed for beam formation, acceleration or deceleration, or for preventing electrons scattered by aperture edges or possibly low-energy secondary electrons from reaching the detector; the total number of elements and their design depends on the objectives of the experiment, as discussed in the text.

components will vary depending on the experimental objectives, as described in Sections 9.2.3 and 9.2.4. It will be convenient to discuss in this section some general characteristics and procedures.

9.2.2.1. Guns, Analyzers, Detectors. **9.2.2.1.1. GUNS.** The principles of electron gun design and the characteristics of some common guns have already been described in this series¹⁶; further information may be found in several review articles.^{15, 17} The most generally useful electron source has been the thermionic tungsten cathode for which a half-width in the energy distribution of the emitted electrons of about 0.6 eV can be expected,¹⁸ depending on the cathode temperature. However, Boersch¹⁹

¹⁶ Vol. 4, Sections 1.1.5, 1.1.6.

¹⁷ C. Süsskind, *Advan. Electron. Electron Phys.* **8**, 363 (1956); S. Leisegang, in "Handbuch der Physik" (S. Flügge, ed.), Vol. 33, p. 396. Springer, Berlin, 1958.

¹⁸ Vol. 4, Section 1.1.7.

¹⁹ H. Boersch, *Z. Physik* **139**, 115 (1954); J. A. Simpson and C. E. Kuyatt, *J. Appl. Phys.* **37**, 3805 (1966). See also T. E. Everhart, *J. Appl. Phys.* **38**, 4944 (1967), for an analysis of the characteristics of several point-cathode electron sources.

and others have shown that the observed half-width can be greater than that predicted assuming a Maxwellian energy distribution and that the "anomalous" breadth depends on the operating parameters of the gun and the beam system. Should the energy breadth in a beam for a given gun and electron-optical system be excessive for a given application, the techniques described in another chapter¹⁸ can be adopted to provide a more monoenergetic beam, albeit at a considerable sacrifice in usable current.²⁰

9.2.2.1.2. ANALYZERS. The properties of a number of electron energy analyzers have been described elsewhere in this series.²¹ For some applications, where it is desired only to separate inelastically scattered electrons from elastically scattered or no-loss electrons, a retarding-field analyzer may be sufficient. The characteristics of these analysers have been discussed by Simpson²² who has shown that their apparent simplicity is often offset by limitations in performance; the latter can, however, be reduced by careful design. A more serious disadvantage for many applications is that the integral of an energy distribution is measured. The energy distribution can be obtained by either graphical or electrical²³ differentiation, though in practice the sensitivity for detection of small signals in the integral current is limited by noise and variation of the transmission function of the device over an extended range of retarding voltage.

The energy distribution of the scattered electrons can generally be obtained more satisfactorily by a deflection analyzer, consisting of pure electric or magnetic fields or various combinations.† The focusing characteristics of several common analyzers have been computed by Henneberg²⁴ and discussed further by Bainbridge²⁵ and Grivet.²⁶ The performance of many types of analyzers has been described in reviews by Klemperer¹⁵ and Siegbahn.²⁷

At high electron energies ($\gtrsim 10^4$ eV) it is generally convenient to use a magnetic analyzer to avoid the insulation difficulties and stability problems associated with high voltages and to avoid the additional aberrations in

²⁰ See also, C. E. Kuyatt and J. A. Simpson, *Rev. Sci. Instr.* **38**, 103 (1967).

²¹ See Vol. 4, Chapter 1.1.7; Vol. 7, Chapter 1.1.

²² J. A. Simpson, *Rev. Sci. Instr.* **32**, 1283 (1961).

²³ L. B. Leder and J. A. Simpson, *Rev. Sci. Instr.* **29**, 571 (1958).

²⁴ W. Henneberg, *Ann. Physik* **19**, 335 (1934).

²⁵ K. T. Bainbridge, in "Experimental Nuclear Physics" (E. Segrè, ed.), Vol. 1, p. 559. Wiley, New York, 1953.

²⁶ P. Grivet, "Electron Optics." Pergamon Press, Oxford, 1965.

²⁷ K. Siegbahn, in "Alpha-, Beta-, and Gamma-Ray Spectroscopy" (K. Siegbahn, ed.), Vol. 1, p. 79. North-Holland Publ., Amsterdam, 1965.

† The Wien filter is a special case where an electric field E and a magnetic field B mutually perpendicular to the central electron trajectory allow undeflected transmission for an electron velocity $v = E/B$.

electrostatic analyzers at energies where relativistic mass corrections are necessary.²⁸ For lower electron energies, electrostatic analyzers are useful as the potential distributions can be closely controlled, and the necessary deflection field is a linear function of the electron energy; in a magnetic analyzer, the deflection field is proportional to the electron momentum which may not be a linear function of the magnet excitation current. With an iron-cored magnetic analyzer, there may be difficulties at low excitations,²⁹ and it is necessary to measure the field directly rather than the excitation current on account of hysteresis effects.

The fringing fields of electrostatic analyzers may be corrected using the curves of Herzog.³⁰ An estimate of the tolerances required in the construction of the field plates of electrostatic analyzers may be obtained from the work of Hoyaux and Geets³¹ who showed that accuracy in the spacing of the plates of a 127° electrostatic analyzer was more important than accuracy in the radius of curvature. For magnetic analyzers, the effect of the fringing fields can be evaluated using the results of Enge³² and of Wollnik and Ewald.³³

The energy resolution δE of a deflection analyzer is a function of the electron energy. A desired value of δE at high energies can be directly obtained by a reduction in the sizes of the various apertures and hence with a reduction in usable current. A more desirable method of achieving the given δE without necessarily decreasing the current is to decelerate the electron beam to a relatively low energy before energy analysis.^{29, 34} It is then necessary to ensure that the increased angular divergence and/or size of the beam after deceleration is not large enough to cause undesirably large energy aberrations in the analyzer section. Further, there should be no modifications to the transverse momentum components of the beam that may cause unknown but possibly significant changes in the effective angular acceptance of the decelerator-analyzer system.³⁵ A discussion of the limiting factors in decelerator-analyzer systems and of the optimizations possible has been given by Kuyatt and Simpson,³⁶ while the performance of several systems has been described by Klemperer.¹⁵

²⁸ F. T. Rogers and C. W. Horton, *Rev. Sci. Instr.* **14**, 216 (1943); F. T. Rogers, *ibid.* **22**, 723 (1951).

²⁹ L. Marton and J. A. Simpson, *Rev. Sci. Instr.* **29**, 567 (1958).

³⁰ R. Herzog, *Physik. Z.* **41**, 18 (1940); A. F. Malov and E. P. Fedoseev, *Zh. Tekh. Fiz.* **36**, 1351 (1966) [English transl.: *Sov. Phys.-Tech. Phys.* **11**, 1008 (1967)].

³¹ M. Hoyaux and J. Geets, *J. Sci. Instr.* **31**, 149 (1954).

³² H. A. Enge, *Rev. Sci. Instr.* **35**, 278 (1964).

³³ H. Wollnik and H. Ewald, *Nucl. Instr. Methods* **36**, 93 (1965).

³⁴ A. W. Blackstock, R. D. Birkhoff, and M. Slater, *Rev. Sci. Instr.* **26**, 274 (1954).

³⁵ H. Mendlowitz, *Rev. Sci. Instr.* **29**, 701 (1958).

³⁶ C. E. Kuyatt and J. A. Simpson, *Rev. Sci. Instr.* **38**, 103 (1967).

There is an additional advantage in the use of preanalysis deceleration when it is desired to measure the energy losses of primary electrons after interaction with the specimen. It is then possible to decelerate the scattered electrons by a voltage $V_0 - V_f$, as shown in Fig. 2, where V_0 is the accelerating voltage applied to the gun and eV_f is the small, fixed energy at which the electrons are transmitted through the analyzer. The effects of fluctuations in the voltage V_0 cancel to first order, and it is not usually necessary for the V_0 supply to be regulated. Energy-loss distributions may be conveniently obtained by interposing a variable sweep voltage between the V_0 supply and the gun cathode.

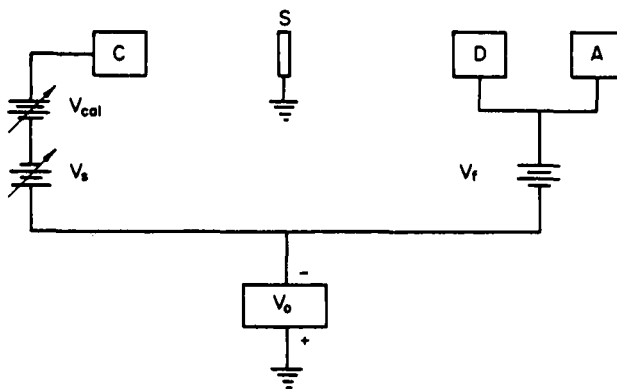


FIG. 2. Schematic diagram of a high-voltage circuit useful in experiments to measure electron energy losses where the energy loss is much smaller than the primary electron energy. The specimen S is usually desired to be at ground potential and the high voltage V_0 is applied to the gun cathode C , the decelerator D , and the analyzer A . V_f is a small fixed voltage determining the mean energy of analysis and V_s is a variable sweep voltage to obtain the energy loss spectrum. By increasing the negative voltage on C to compensate for energy losses in S , electrons reaching the detector traverse the same electric and residual magnetic fields (after leaving S); the loss spectrum is recorded with essentially constant energy and angular resolution. V_{cal} is a variable known voltage that may be inserted to vary the recorded position of the spectrum (usually the peak of elastically scattered or no-loss electrons) to calibrate the energy loss scale.

Möllenstedt³⁷ has described a compact analyzer in which deceleration, dispersion and reacceleration occur in a single element. In this analyzer use is made of the high off-axis chromatic aberration of a cylindrical einzel lens and an energy resolution of 0.5 eV with 35 keV electrons from an oxide cathode has been obtained. The electron trajectories in the lens are

³⁷ G. Möllenstedt, *Optik* 5, 499 (1949); G. Möllenstedt and W. Dietrich, *ibid.* 12, 246 (1955).

relatively complex, and it is consequently difficult to design and optimize a lens with desired optical properties.³⁸

Electrons of low energy are susceptible to deflection by small magnetic fields, particularly in the analyzer. To avoid unwanted energy-dependent deflections, it is generally necessary to neutralize the earth's field to about 1% of its normal value. A simple calculation shows that the maximum field H_{\max} (oersted) that can be tolerated at right angles to an electron path of length s (cm) is given by

$$H_{\max} = 6.74E^{1/2}d/s^2,$$

where E is the electron energy (eV) and d (cm) is the maximum tolerable beam deflection (which might arbitrarily be set equal to 10% of the width of an analyzer aperture). Simple coil systems that provide suitable field uniformity over toroidal and cylindrical volumes have been described by Ference *et al.*³⁹ and by Lyddane and Ruark,⁴⁰ respectively.

9.2.2.1.3. DETECTORS. Early electron detectors were the photographic plate, the Geiger counter, the phosphor screen, and the Faraday cage. Photographic detection and the phosphor screen are useful when electrons with a wide range of energies need to be recorded simultaneously or when it is desired to record a two-dimensional scattering pattern in a reasonable time. It may, however, be difficult or time consuming to establish a satisfactory intensity scale with a photographic detector though the light output from a phosphor screen may be measured with a photometer or by a photomultiplier. A phosphor screen viewed by a photomultiplier is a convenient method of measuring current to electrodes at high potentials where the electron energy is $\gtrsim 1$ keV. The use of the Geiger counter has been limited by the requirement of a minimum electron energy of about 5 keV to penetrate the thinnest practicable window and by the relatively long dead times ($\sim 100 \mu s$). The Faraday cage collector coupled to a suitable amplifier is often a simple and convenient detector. By making the hole in the collector small compared with the inside surface area, it is possible to minimize the error in the current measurement caused by electron back-scattering and secondary electron emission (see Chapter 1.1). Other factors limiting the performance of the Faraday collector in a retarding field analyzer have been discussed by Simpson.²²

Improved sensitivity and signal-to-noise ratio may be obtained with an electron multiplier detector having one of several geometries and one of a number of active surfaces. There is an extensive literature, and a review

³⁸ A. J. F. Metherell and M. J. Whelan, *Brit. J. Appl. Phys.* **16**, 1038 (1965); *J. Appl. Phys.* **37**, 1737 (1966).

³⁹ M. Ference, A. E. Shaw, and R. J. Stephenson, *Rev. Sci. Instr.* **11**, 57 (1940).

⁴⁰ R. H. Lyddane and A. E. Ruark, *Rev. Sci. Instr.* **10**, 253 (1939).

of the earlier devices is given by Schaetti.⁴¹ One of the more commonly used multipliers is the Allen-type,⁴² in which the dynodes are fabricated from either a Be-Cu or a Ag-Mg alloy which is activated by controlled surface oxidation.⁴³ These surfaces have a work function of about 4.5 V with the advantages that they do not respond to visible light and that thermionic emission is negligible. Other multiplier geometries which may be useful are the "Venetian blind" type,⁴⁴ the Sternglass transmission-type,^{45, 46} and the semiconductor strip⁴⁷ or channel types.⁴⁸

The fringing field of the permanent magnets needed in an early form of the semiconductor strip multiplier would be undesirable in an apparatus for low-energy electrons. The resistance per unit length of the strip or channel of the semiconductor multipliers should be as low as possible to avoid saturation effects at high intensities and long RC time-constants. On the other hand, the semiconductor resistance per unit length should be as high as possible to increase the applied high voltage to maximize the gain (without exceeding a maximum power dissipation appropriate to a material of given negative temperature coefficient of resistivity). A compromise must therefore be made between these conflicting requirements.

The detection efficiency of electron multipliers is a function of the energy of the incoming electron and has been measured to be a maximum of about 60% for electrons of about 350 eV energy for Be-Cu and Ag-Mg multipliers (see Chapter 1.1; Ref. 49). The gain per stage for multipliers with Be-Cu and Ag-Mg dynodes is about 2.5, depending on the interstage potential difference. Both the gain and the efficiency will be degraded if the surfaces are contaminated, for example, by polymerization of condensed

⁴¹ N. Schaetti, *Z. Angew. Math. Phys.* **2**, 123 (1951).

⁴² J. S. Allen, *Rev. Sci. Instr.* **18**, 739 (1947).

⁴³ A. H. Sonner, *J. Appl. Phys.* **29**, 598 (1958).

⁴⁴ R. Kalibjian, *IRE Trans. Electron Devices* **ED-9**, 454 (1962); *J. Sci. Instr.* **39**, 535 (1962).

⁴⁵ E. J. Sternglass, *Rev. Sci. Instr.* **26**, 1202 (1955).

⁴⁶ W. W. Sapp and E. J. Sternglass, *IEEE Trans. Nucl. Sci.* **NS-11**, No. 3, 108 (1964).

⁴⁷ G. W. Goodrich and W. C. Wiley, *Rev. Sci. Instr.* **32**, 846 (1961); W. W. Hunt, K. E. McGee, and M. J. Kennedy, *ibid.* **36**, 1662 (1965); C. E. F. Misso and J. Z. Karpinski, *IEEE Trans. Nucl. Sci.* **NS-11**, No. 3, 72 (1964); C. A. Spindt and K. R. Shoulders, *Rev. Sci. Instr.* **36**, 775 (1965).

⁴⁸ P. K. Oshchepkov, B. N. Skvortsov, B. A. Osanov, and I. V. Siprikov, *Pribory i Tekh. Eksp.* **4**, 89 (1960) [English Transl.: *Instr. Exptl. Tech. (USSR)* **4**, 611 (1961)]; G. W. Goodrich and W. C. Wiley, *Rev. Sci. Instr.* **33**, 761 (1962); D. S. Evans, *Rev. Sci. Instr.* **36**, 375 (1965); D. A. Bryant and A. D. Johnstone, *ibid.* **36**, 1662 (1965).

⁴⁹ J. A. Cowan, *Can. J. Phys.* **32**, 101 (1954); W. P. Alford and D. R. Hamilton, *Phys. Rev.* **105**, 673 (1957); C. Julliot, M. Cautin, R. Ducros, and C. Jehanno, *IEEE Trans. Nucl. Sci.* **NS-11**, No. 3, 160 (1964); G. C. Baldwin and S. I. Friedman, *Rev. Sci. Instr.* **36**, 16 (1965); L. A. Dietz, *ibid.* **36**, 1763 (1965).

hydrocarbon vapors under electron bombardment.^{50, 51} Multipliers with dynodes made from brass⁵² or aluminum⁵³ (without any activation) may have a more stable (though lower) gain than multipliers with Be-Cu or Ag-Mg dynodes on repeated exposure to the atmosphere, though gain changes of this type may not be serious unless absolute measurements of intensity are required.

Electron multipliers can be operated as current amplifiers or the voltage pulses at the collector can be amplified and counted. In the former mode, the device can be connected to have either a linear or a logarithmic response.⁵⁴ The noise limitations of multipliers have been discussed by Fain.⁵⁵

9.2.2.2. Specimen Preparation. The preparation and purification of solid materials have already been discussed in this series.⁵⁶ In electron scattering experiments, it is generally necessary to prepare either thin films of thickness about 10^2 to 10^4 Å for transmission experiments or more massive specimens of known surface condition for reflection experiments. The preparation and characterization (e.g., in purity, structure, and crystalline orientation) of the specimen is often the most critical part of an electron scattering experiment.

Thin films for electron microscope experiments are frequently prepared by etching or preferably electropolishing material first mechanically thinned by rolling or beating.^{13, 56a, 57} This technique is limited to single-phase materials and has the disadvantage that the surface will generally be oxidized or contaminated before being examined. The method is useful, however, in that a sample of a massive specimen can be obtained without serious sample artifacts being caused by the preparation technique.

Many other techniques exist for the preparation of thin films,⁵⁷⁻⁶² the

⁵⁰ A. E. Ennos, *Brit. J. Appl. Phys.* **4**, 101 (1953); **5**, 27 (1954).

⁵¹ H. G. Heide, *Lab. Invest.* **14**, 1134, 1140 (1965).

⁵² D. T. F. Marple, *Rev. Sci. Instr.* **36**, 1205 (1955).

⁵³ R. A. Bingham, *J. Sci. Instr.* **43**, 74 (1966).

⁵⁴ R. E. Bell and R. L. Graham, *Rev. Sci. Instr.* **23**, 301 (1952).

⁵⁵ D. L. Fain, *J. Opt. Soc. Am.* **55**, 206 (1965).

⁵⁶ Vol. 6A, Chapter 2.

^{56a} G. Thomas, "Transmission Electron Microscopy of Metals." Wiley, New York, 1962.

⁵⁷ "Techniques for Electron Microscopy" (D. H. Kay, ed.). First edition, Blackwell, Oxford, 1961. Second edition, F. A. Davis, Philadelphia, 1965.

⁵⁸ Vol. 6, Chapter 2.5.

⁵⁹ P. R. Rowland, *Vacuum* **3**, 136 (1953).

⁶⁰ R. Castaing, *Rev. Metall.* **52**, 669 (1955).

⁶¹ L. Yaffe, *Ann. Rev. Nucl. Sci.* **12**, 153 (1962).

⁶² W. Parker and H. Slatis, in "Alpha-, Beta-, and Gamma-Ray Spectroscopy" (K. Siegbahn, ed.), p. 279. North-Holland Publ., Amsterdam, 1965.

most common being vacuum evaporation.⁶³ The latter method is relatively simple and convenient, though there is ample evidence that thin films prepared in this way may have some structural properties different from the corresponding bulk material.⁶⁴ The film properties depend critically on the deposition conditions^{65, 66} as well as on contamination from either the evaporation source⁶⁷ or the residual atmosphere of the vacuum system. The most satisfactory results are obtained by rapid evaporation ($\sim 100 \text{ \AA/sec}$) in an ultrahigh vacuum system (pressure $\sim 10^{-9} \text{ Torr}$) onto a clean substrate. Depending on the experimental objectives, the substrate may be glass, glass covered with a layer of a material (e.g., NaCl, Victawet) soluble in water or some other solvent for easy removal of the film, a single crystal (e.g., NaCl) that may also be subsequently removed, or of a thin, ideally "inert" material that remains attached to the film (e.g., collodion, Formvar⁶¹).⁶⁸ Single-crystal films may be prepared under certain conditions, for example, by epitaxy.^{65, 68-70} The specimen can be mounted over a small aperture in a suitable holder or on an electron microscope specimen grid, depending on the film strength.

It is often desired to measure the thickness or mass per unit area of thin films and preferably to monitor and control the film thickness during deposition. For electron scattering experiments, the mass per unit area (mass thickness) is the more significant parameter. Thicknesses may be measured by many techniques,⁶³ for example, by a mechanical microbalance,⁷¹ the quartz crystal microbalance,⁷² microchemical analysis, the absorption of visible light, X rays, α - or β -particles, or optical methods.^{73, 74} The measurement should be made in the same vacuum in which the film was formed to minimize the effects of surface oxidation or contamination that would occur on exposure to the atmosphere. Ideally, the thickness

⁶³ L. Holland, "Vacuum Deposition of Thin Films." Wiley, New York, 1956; S. H. Maxman, *Nucl. Instr. Methods*, **50**, 53 (1967).

⁶⁴ "Structure and Properties of Thin Films" (C. A. Neugebauer, J. B. Newkirk and D. A. Vermilyea, eds.). Wiley, New York, 1959.

⁶⁵ D. W. Pashley, *Advan. Phys.* **14**, 327 (1965).

⁶⁶ K. H. Behrndt, *Vacuum* **13**, 337 (1963).

⁶⁷ H. L. Rook and R. C. Plumb, *Appl. Phys. Letters* **1**, 11 (1962).

⁶⁸ "Single-Crystal Films" (M. H. Francombe and H. Sato, eds.), Macmillan, New York, 1964.

⁶⁹ J. W. Matthews, *Phil. Mag.* **12**, 1143 (1965).

⁷⁰ R. Speidel and K. Fraz, *Optik* **19**, 434 (1962).

⁷¹ "Vacuum Microbalance Techniques" (M. J. Katz, ed., Vol. 1; R. F. Walker, ed., Vol. 2; K. H. Behrndt, ed., Vol. 3; and P. M. Waters, ed., Vol. 4). Plenum, New York, 1961-1965.

⁷² G. Sauerbrey, *Z. Physik* **155**, 206 (1959); W. H. Lawson, *J. Sci. Instr.* **44**, 917 (1967).

⁷³ S. Tolansky, "Surface Microtopography." Wiley (Interscience), New York, 1960.

⁷⁴ O. S. Heavens, *Rept. Progr. Phys.* **23**, 1 (1960).

measurement should not depend on an implicit assumption that an evaporated film has properties (e.g., density) identical to those of the bulk material, particularly if the thickness is known to be less than 1000 Å.^{63, 64, 75} Films with average thickness less than about 100 Å are generally not continuous, and consequently thickness measurements have little meaning. The two most reliable methods in common use are the Tolansky⁷³ multiple-beam interferometric technique with which the height of a "step" due to a film edge can be measured with an accuracy of about 20 Å and the quartz crystal microbalance⁷² with which mass per unit area of a film can be determined with an accuracy of about 10^{-7} gm cm⁻² (depending on the crystal and the extent to which correction is made for heating effects from the evaporation source). Thickness or mass thickness measurements may be subject to an additional systematic error if the specimen film and the film which is actually measured are not deposited on identical substrates, due to differing sticking coefficients of vapor atoms on the separate substrates and to different nucleation conditions.^{65, 76}

Specimen films for transmission experiments may be most conveniently prepared by evaporation either in the vacuum of the scattering apparatus onto a suitable substrate or in an auxiliary system in which case the substrate can be removed before the scattering measurement. The first method has the disadvantage that the substrate contributes to the scattering distribution in possibly an unknown manner, while the second method has the disadvantage of oxidation or contamination of the specimen between preparation and measurement. The substrate may also be responsible for artifacts, either directly by its contribution to the electron scattering distribution or indirectly by contamination of the specimen through volume diffusion.⁷⁷

Specimens for reflection scattering experiments require the generation of a clean, well-characterized surface. Methods for preparing such surfaces and the limitations involved have been discussed by Dillon,⁷⁸ by Roberts,⁷⁹ and by Menzel⁸⁰; techniques useful for reflection experiments include vacuum deposition (with or without epitaxial growth), cleavage of crystals,

⁷⁵ S. Aisenberg, *Natl. Vacuum Symp. of the American Vacuum Society, Tenth, Boston, 1963, Transactions* (G. H. Bancroft, ed.), p. 457. Macmillan, New York, 1963; T. E. Hartman, *J. Vacuum Sci. Technol.* **2**, 239 (1965); A. R. Wolter, *J. Appl. Phys.* **36**, 2377 (1965); J. Edgecumbe, *J. Vacuum Sci. Technol.* **3**, 28 (1966).

⁷⁶ L. Bachmann and J. J. Shin, *J. Appl. Phys.* **37**, 242 (1966).

⁷⁷ D. H. Tomboulian and E. M. Pell, *Phys. Rev.* **83**, 1196 (1951).

⁷⁸ J. A. Dillon, *Trans. Natl. Vacuum Symp.*, 1961, (L. E. Preuss, ed.), **8**, p. 113. Pergamon, New York, 1962.

⁷⁹ R. W. Roberts, *Brit. J. Appl. Phys.* **14**, 537 (1963).

⁸⁰ E. Menzel, *Rept. Progr. Phys.* **26**, 47 (1963); E. Menzel and O. Schott, *Surface Sci.* **8**, 217 (1967).

high-temperature heating (of refractory metals), ion bombardment, and solidification from the melt. There is controversy over the degree of surface cleanliness achieved for particular materials by these various techniques, and it is often necessary to perform several surface-sensitive experiments to be reasonably certain that a clean surface has in fact been obtained.

For some work, a smooth surface may be desired. Crystal cleavage produces surfaces which may be atomically smooth for hundreds or thousands of angstroms separated by steps of varying heights. Heat treatment of surfaces may cause thermal faceting⁸¹ and surfaces prepared by evaporation are often rough, depending on the deposition conditions.⁸² The Menzel technique⁸⁰ of solidification from the melt can be used to generate surfaces with a high degree of smoothness.^{82a}

It is possible to get at least a qualitative measure of the electron penetration distance for a given elastic or inelastic process in a reflection geometry by measuring the amount of some material deposited on a given substrate needed to give the scattering distribution characteristic of thick layers of that material. In practice, the thicknesses involved are generally only one or several atomic layers (for electron energies up to several hundred electron volts) and the interpretation of the results depends on knowing the nucleation and growth behavior of the deposit.⁶⁵

9.2.2.3. Experimental Strategy. In most situations, the experimentalist desires the maximum possible current from the gun, consistent with a specified beam energy, cross section, angular divergence, and energy distribution at the specimen. The analyzer should accept electrons from a specified area of the specimen within a given solid angle, and should have a specified energy resolution. The detector should have a sensitivity, commensurate with the above signal limitations, sufficient to detect electrons undergoing a process of a specified minimum cross section with an adequate signal-to-noise ratio. In most experiments it is desired to obtain data (peak positions, intensity distributions, etc.) of a given statistical significance in the shortest possible time,⁸³ particularly if the specimen may be degraded under electron bombardment or an initially clean surface contaminated during operation.

It is usually if not always difficult to satisfy all of the above requirements. If energy and/or angular resolution in the system has to be sacrificed for increased signal current, it is possible to use unfolding procedures to derive spectral distributions from smeared experimental

⁸¹ A. J. W. Moore, in "Metal Surfaces: Structure, Energetics and Kinetics" (W. D. Robertson and N. A. Gjostein, eds.), p. 155. Am. Soc. for Metals, Metals Park, Ohio, 1962.

⁸² J. W. Swaine and R. C. Plumb, *J. Appl. Phys.* **33**, 2378 (1962).

^{82a} C. J. Powell, *Phys. Rev.* (to be published).

⁸³ M. D. Hersey, *J. Res. Natl. Bur. Std.* **B69**, 139 (1965).

data.⁸⁴ These procedures, however, are often laborious (if executed manually) and depend for their success on a high signal-to-noise ratio in the experimental data as well as knowledge of the smearing function. The latter may be difficult to determine with sufficient accuracy; analyzer line shapes, for example, have been obtained only for several types of instrument in an approximate or non-analytic form.²⁷

Discussions of the expected counting losses and probable errors associated with the arrival of a given number of counts at a scaler or with a reading of a counting-rate meter have been given earlier in this series⁸⁵ and by Parrish.⁸⁶ Parrish also considers several counting strategies. Depending on the experimental objectives, it may be desired to obtain intensity data over a given distribution with constant relative error or constant absolute error. An intermediate strategy is to accumulate counts for a fixed time for each setting of the independent variable, thereby compromising between accuracy and measurement time at the lower levels of intensity. The Cooke-Yarborough strategy, in which counts are added to the signal at a small, known, periodic rate, may be useful in an automatic instrument where there is a wide range of intensities to be measured.^{86, 87}

In some electron scattering experiments it is difficult to improve the statistical significance of low-intensity signals merely by increasing the observation time. It appears that the noise power is often not independent of frequency and that relatively large low-frequency contributions to the noise power spectrum can arise from variation of amplifier or electron multiplier gain with time, or from variation of current density at the specimen on that region "seen" by the analyzer. Under these conditions, Ernst⁸⁸ has shown that the signal-to-noise ratio can be improved by making a large number of relatively rapid sweeps over the spectrum (compared to a single, slow sweep in the same total observation time). Count data may be conveniently stored in successive channels of a multichannel pulse-height analyzer operated as a multichannel scaler.⁸⁹ Time averaging may be

⁸⁴ J. O. Porteus, *J. Appl. Phys.* **33**, 700 (1962); C. P. Flynn, *Proc. Phys. Soc. (London)* **78**, 1546 (1961); J. McL. Emmerson, *Nucl. Instr. Methods* **39**, 163 (1966); W. C. Sauder, *J. Appl. Phys.* **37**, 1495 (1966); J. T. Grissom, D. R. Koehler, and B. G. Gibbs, *Nucl. Instr. Methods* **45**, 190 (1966); R. H. Ritchie and V. E. Anderson, *ibid.* **45**, 277 (1966); J. D. Morrison, *J. Chem. Phys.* **39**, 200 (1963); G. E. Ioup and B. S. Thomas, *ibid.* **46**, 3959 (1967); A. F. Jones and D. L. Misell, *Brit. J. Appl. Phys.* **18**, 1479 (1967); K.-H. Zörner, *Z. angew. Phys.* **22**, 239 (1967); J. O. Porteus, *J. Appl. Phys.* **39**, 163 (1968).

⁸⁵ Vol. 2, Chapter 9.1.

⁸⁶ W. Parrish, *Philips Tech. Rev.* **17**, 206 (1956).

⁸⁷ F. H. Cooke-Yarborough, *J. Brit. Inst. Radio Engrs.* **11**, 367 (1951).

⁸⁸ R. R. Ernst, *Rev. Sci. Instr.* **36**, 1689 (1965).

⁸⁹ M. P. Klein and G. W. Barton, *Rev. Sci. Instr.* **34**, 754 (1963); J. B. Swan, *Phys. Rev.* **135**, A1467 (1964); M. O. Krause, *ibid.* **140**, A1845 (1965).

simply and more cheaply accomplished by use of a photographic detector, though with inferior sensitivity, linearity, and without being able to inspect the data during accumulation. Alternatively, the effects of low-frequency noise may be minimized by ac modulation of the signal and the use of phase-sensitive detection (see, for example, Chapter 1.3).

It seems likely that there will in the future be an increasingly large number of experiments controlled by computer during execution. While there are obvious dangers of further isolating an experimentalist from his apparatus, it is possible that a computer can be used in real time to test various hypotheses or to calculate the optimum positions of the independent variables at which data of a given significance should be obtained for a specified objective.^{83, 90, 91} On-line control of an experiment has the significant advantage that data can be reduced and tested during accumulation and that additional data can be obtained if necessary under essentially identical conditions of operation.

9.2.3. "Atomistic" Description of Solids

An account will be given in this section of methods and techniques that have been used to investigate electron interactions with solids which have often been implicitly assumed to be a set of atoms, characterized only by a particular density and atomic number Z . Variations of angular intensity distributions with angle of incidence of the primary beam on the specimen have either been ignored or the angular resolution of the apparatus has been poor so that structure in angular intensity distributions has been smeared out.

Many experimentalists have assumed that the scattering can be interpreted in terms of various statistically independent elastic and inelastic atomic scattering processes. The adoption of these assumptions leads to considerable simplification in the theoretical description and analysis of the problem, and in fact the results of such analyses are often at least in order of magnitude agreement with experiment as far as the gross characteristics of the scattering are concerned. While the neglect of diffraction effects cannot generally be justified, Fano^{5, 92} has shown that the inelastic scattering in a solid can be described by a macroscopic dielectric constant and that this approach is equivalent to the Bethe⁹³ description of inelastic electron-atom scattering.

⁸⁰ J. E. Monahan and A. Langsdorf, *Ann. Phys. (N.Y.)* **34**, 238 (1965).

⁸¹ D. J. Wilde, "Optimum Seeking Methods." Prentice-Hall, Englewood Cliffs, New Jersey, 1964.

⁸² U. Fano, *Phys. Rev.* **103**, 1202 (1956).

⁸³ H. Bethe, *Ann. Physik* **5**, 325 (1930).

9.2.3.1. Interactions at High Electron Energies. Consideration will be given firstly to describing elastic and inelastic scattering processes involving the primary (incident) electrons. It will be assumed that the primary electron velocity is high compared to the velocity of electrons in atomic shells yet low enough so that relativistic corrections for the formulas are small; these assumptions can only be valid for elements of low Z . The measurement of differential and total cross sections requires a transmission-type scattering geometry and a primary electron energy above about 1 keV for useful transmission with self-supporting specimens. Reflection scattering geometries are useful in studying inelastic processes in materials where surface oxidation or contamination may modify the interactions.

9.2.3.1.1. ELASTIC SCATTERING. Various expressions for the differential cross section for elastic scattering of electrons by single atoms have been summarized by Motz *et al.*⁹⁴ who also give information concerning the relevant conditions of validity of the cross-section formulas and references to various evaluations and tabulations.⁹⁵ For electron energies less than 100 keV and for the thinnest practicable specimens, there will often be more than one elastic scattering event, and it is necessary to consider the angular distributions expected for plural or multiple scattering,⁹⁶ the theory for which has recently been reviewed by Scott.⁹⁷

The most extensive analyses of multiple and plural scattering of electrons in solids for energies less than 100 keV have been performed by Lenz⁹⁸ and by Burge and Smith.⁹⁹ To obtain tractable expressions, Lenz used the simple Wentzel differential cross section for elastic scattering,

$$\frac{d\sigma_e}{d\Omega} = \frac{Z^2 e^4}{E_0^2} \cdot \frac{1}{[4 \sin^2(\frac{1}{2}\theta) + \theta_0^2]^2}, \quad (1)$$

where $E_0 = \frac{1}{2}mv^2$ is the primary electron energy, θ the scattering angle, and θ_0 a screening angle given by

$$\theta_0 = \lambda/2\pi R, \quad (2)$$

⁹⁴ J. W. Motz, H. Olsen, and H. W. Koch, *Rev. Mod. Phys.* **36**, 881 (1964).

⁹⁵ See also: E. Zeitler and H. Olsen, *Phys. Rev.* **136**, A1546 (1964); E. Zeitler, *Lab. Invest.* **14**, 774 (1965); E. Zeitler and H. Olsen, *Phys. Rev.* **162**, 1439 (1967).

⁹⁶ V. E. Cosslett and R. N. Thomas, *Brit. J. Appl. Phys.* **15**, 235 (1964). The transition between plural and multiple scattering is not uniformly defined in the literature. Cosslett and Thomas find experimentally that multiple scattering becomes established (angular distribution becomes Gaussian) after about 25 elastic scattering events for electrons of about 20 keV energy.

⁹⁷ W. T. Scott, *Rev. Mod. Phys.* **35**, 231 (1963).

⁹⁸ F. Lenz, *Z. Naturforsch.* **9a**, 185 (1954).

⁹⁹ R. E. Burge and G. H. Smith, *Proc. Phys. Soc. (London)* **79**, 673 (1962); G. H. Smith and R. E. Burge, *ibid.* **81**, 612 (1963).

where λ is the electron wavelength. The single adjustable parameter R has been evaluated by Lenz for several atoms, but many authors have assumed that it can be expressed with sufficient accuracy by $R = a_0 Z^{-1/3}$, where a_0 is the Bohr radius (0.529 Å); such an assumption, however, appears to be inadequate.⁹⁹ A number of experiments have been performed to test the Lenz multiple scattering theory, using both polycrystalline metal and rare gas scatterers.^{98, 100} These experiments, together with others to test the applicability of Eq. (1) for single scattering by atoms,¹⁰¹ have shown that the Wentzel formula is inadequate to describe the observed angular distributions.

Burge and Smith⁹⁹ have fitted calculated values¹⁰² of the atomic scattering amplitude for electrons f_e to an analytic expression for each element (except K) using six adjustable constants. The elastic scattering cross section may then be written.

$$d\sigma_e/d\Omega = |f_e|^2. \quad (3)$$

This procedure has the advantage that the cross sections can be easily modified as more refined calculations of f_e become available. Burge and Smith have also considered multiple scattering in a similar way, though the computations involved are more complex.

It should be emphasized that the above theory should only be applicable to isolated and neutral atoms. Even in an amorphous solid, there will be a certain degree of short-range order, as indicated by the atomic radial distribution function, and diffraction effects cannot be ignored. In addition, the shielding parameters used for free atoms would not be expected to be applicable for long-range collisions in condensed matter. Fink and Kessler^{102a} have in fact found different elastic differential cross sections for silver in the solid and vapor states, and Brünger and Menz¹⁰³ have reported different variations of the differential cross section with angle in amorphous and crystalline germanium. While Eq. (2) indicates that an angular resolution better than θ_0 would be required in a scattering experiment designed to measure elastic scattering cross sections, it can be shown by diffraction theory and by experiment that an improvement of at least one order of magnitude in angular resolution is necessary.^{98, 100, 103}

¹⁰⁰ J. Kessler, *Z. Physik* **182**, 137, 153 (1964); W. Hilgner and J. Kessler, *ibid.* **187**, 119 (1965).

¹⁰¹ J. Geiger, *Z. Physik* **177**, 138 (1964).

¹⁰² J. A. Ibers and B. K. Vainshtein, in "International Tables for X-ray Crystallography" (C. H. MacGillavry, G. D. Rieck, and K. Lonsdale, eds.), Vol. 3, p. 216. Kynoch Press, Birmingham, England, 1962.

^{102a} M. Fink and J. Kessler, *Z. Physik* **196**, 504 (1966).

¹⁰³ W. Brünger and W. Menz, *Z. Physik* **184**, 271 (1965).

9.2.3.1.2. INELASTIC SCATTERING. The theory of inelastic scattering of electrons has been reviewed recently by Fano.⁴ Most experimental work has been concerned with the excitation of valence-band electrons (the so-called characteristic energy losses), and a review of the current theoretical and experimental situation has been published by Raether.¹¹

Consideration will be given firstly to excitations in an infinite medium or for thin film specimens of thickness greater than \hbar/q_{\min} , where the minimum momentum transfer $q_{\min} = \Delta E_n/v$ and ΔE_n is the n th energy loss. It can be shown that the doubly differential cross section *per atomic electron* for an excitation involving energy loss $\hbar\omega$ and momentum transfer q can be expressed in the form^{92, 104-106}

$$\frac{d^2\sigma_i}{d\omega dq} = -\frac{2e^2}{\pi N\hbar v^2} \cdot \text{Im} \left[\frac{1}{\epsilon(\omega, q)} \right] \cdot \frac{1}{q}, \quad (4)$$

where $\text{Im}[1/\epsilon(\omega, q)]$ is the imaginary part of the reciprocal (macroscopic) dielectric constant $\epsilon(\omega, q)$ (which is a function both of ω and q) and N is the total electron density.

The shape of an energy-loss spectrum depends principally on the factor $\text{Im}[1/\epsilon(\omega, q)]$ in Eq. (4), and is closely related to the spectrum of optical excitations¹¹ and to the electronic band-structure of the solid.¹⁰⁷ Maxima will occur in $-\text{Im}[1/\epsilon(\omega, q)]$ at frequencies near maxima in $\text{Im}[\epsilon(\omega, q)]$ (single-electron excitations) and at frequencies near those for which the real and imaginary parts of $\epsilon(\omega, q)$ are zero or small (compared to unity). A maximum of the latter type corresponds to plasmon excitation, a collective excitation of the valence electrons in a solid, and may be observed at frequencies near ω_p (energy loss $\approx \hbar\omega_p$), where $\omega_p = (4\pi Ne^2/m)^{1/2}$ and n is the valence electron density. The energy resolution needed in an analyzer to detect the structure in $\text{Im}[1/\epsilon(\omega, q)]$ is generally about 1 eV for metallic and some semiconductor specimens while an improvement of one to two orders of magnitude may be necessary for ionic and molecular solids.

Equation (4) may be related^{92, 105} to microscopic theories⁹³ of excitation by defining a differential oscillator strength

$$\frac{df}{d\omega} = -\frac{\omega \text{Im} [1/\epsilon(\omega, q)]}{(\pi\Omega_p^2/2)}, \quad (5)$$

where $\Omega_p = (4\pi Ne^2/m)^{1/2}$. An oscillator strength $f(q)$ for one or more

¹⁰⁴ J. Hubbard, *Proc. Phys. Soc. (London)* **A68**, 976 (1955).

¹⁰⁵ A. J. Glick and R. A. Ferrell, *Ann. Phys. (N.Y.)* **11**, 359 (1960).

¹⁰⁶ D. Pines, "Elementary Excitations in Solids." Benjamin, New York, 1963.

¹⁰⁷ J. C. Phillips, *Solid State Phys.* **18**, 55 (1966).

energy loss processes may be obtained by integration of Eq. (5) over appropriate regions of ω . It can also be shown that

$$\int_0^\infty \frac{df}{d\omega} d\omega = 1.$$

Using Eq. (5), Eq. (4) can be written

$$\frac{d\sigma_i}{dq} = \frac{4\pi e^4}{mv^2} \cdot \frac{1}{q} \int \frac{1}{\hbar\omega} \cdot \frac{df}{d\omega} d\omega. \quad (6)$$

For a relatively narrow energy loss peak,

$$\int \frac{1}{\hbar\omega} \cdot \frac{df}{d\omega} d\omega \approx \frac{1}{\hbar\omega_n} \int \frac{df}{d\omega} d\omega = \frac{f_n(q)}{\Delta E_n}, \quad (7)$$

where the integration has been performed over a region of $(df/d\omega)$ appropriate to an energy loss centered at $\Delta E_n = \hbar\omega_n$. For peaks with a full-width at half-maximum intensity of 0.2 ΔE_n , for example, the value of $f_n(q)/\Delta E_n$ would be about 3% lower than the value of the integral in Eq. (6). Thus

$$\frac{d\sigma_i}{dq} \approx \frac{4\pi e^4}{mv^2} \cdot \frac{1}{\Delta E_n} \cdot \frac{f_n(q)}{q}. \quad (8)$$

The function $f_n(q)$ is not well known, except for the case of plasmon excitation in a free-electron gas.^{105, 108} For other excitations, it may have to be assumed that $f_n(q) \approx f_n(0)$ for $q < q_m$, where $f_n(0)$ represents the value of f_n for $q = q_{\min} = \Delta E_n/v$ and $q_m = (2m \Delta E_n)^{1/2}$; this approximation is reasonably valid¹⁰⁹ for optically allowed transitions in free atoms (the approximation becomes better with increasing E_0) but has not been generally established for solids.

For momentum transfer q small compared to the primary electron momentum P , $q = P(\theta^2 + \theta_E^2)^{1/2}$, where θ is the electron scattering angle and $\theta_E = \Delta E_n/mv^2$. To establish experimentally the form of the differential cross section [Eq. (6)], an angular resolution better than θ_E is required. For small θ_E , it may be more convenient to deflect electrostatically the scattered electrons (with two pairs of deflection plates) rather than to mechanically drive the gun and specimen or, less desirably, the detector.¹¹⁰ The experimental determination of $f_n(q)$ for discrete energy losses is difficult for $q > \frac{1}{2}q_m$. In this region, there generally are significant intensity contributions from a background continuum¹⁰⁵ and from electrons that

¹⁰⁸ A. J. Glick, *Phys. Rev.* **129**, 1399 (1963).

¹⁰⁹ For example: E. N. Lassettre, M. E. Krasnow, and S. M. Silverman, *J. Chem. Phys.* **40**, 1242 (1964).

¹¹⁰ W. Legler, *Z. Physik* **171**, 424 (1963).

have been elastically scattered through a relatively large angle and inelastically scattered through a small angle ($\approx \theta_E$). Ambiguities in intensity measurements have made measurements of $f_n(q)$ unreliable except in special cases (involving relatively sharp energy-loss peaks), and hence it is unlikely that useful measurements of $\epsilon(\omega, q)$ for large q can be obtained from electron scattering experiments. The dielectric constant can, however, be found in the region of small q , as described by LaVilla and Mendlowitz.¹¹¹

The determination of a total cross section implies that Eq. (6) can be integrated over q with a meaningful upper limit. For plasmon excitation, such a limit exists at $q = q_c$ where q_c is defined as a critical momentum transfer at which $f(q_c) = 0$;¹¹² q_c is of the same order as q_m . This limit, however, can only be detected experimentally for relatively few materials which have narrow loss peaks. For other materials and for other types of excitation, it is not possible to make meaningful intensity measurements at large q because of interference from large-angle elastic scattering. As no theoretical predictions have been made concerning the general form of $f_n(q)$ and of values of q_c for plasmon losses in materials for which free-electron theory would be invalid, it is only possible to measure total cross sections for $q \lesssim q_m$, and then generally by assuming $f_n(q) \approx f_n(0)$. This latter assumption should not lead to an error in σ_i greater than about 10% as $(d\sigma_i/dq)$ is relatively small for $q > \frac{1}{2}q_m$.

The relative probability of M inelastic scatterings of the same type occurring in a specimen of thickness t is given by the Poisson distribution

$$P_M(t/\lambda_i) = \frac{1}{M!} \left(\frac{t}{\lambda_i} \right)^M \exp(-t/\lambda_i), \quad (M = 0, 1, 2, 3, \dots) \quad (9)$$

where λ_i is the appropriate inelastic mean free path; $\lambda_i = 1/n\sigma_i$ where n is here the density of electrons that can be excited. It is assumed that the primary electron energy and the specimen thickness are such that the average pathlength of the transmitted electrons in the specimen is not significantly greater than t . Equation (9) can be readily generalized, if desired, to obtain absolute excitation probabilities if the cross sections for all inelastic processes are known.

The several methods of measuring cross sections have been critically discussed by Swanson and Powell.¹¹³ The specimen thickness should

¹¹¹ R. E. LaVilla and H. Mendlowitz, *Phys. Rev. Letters* **9**, 149 (1962); *Appl. Opt.* **4**, 955 (1965); **6**, 61 (1967).

¹¹² R. A. Ferrell, *Phys. Rev.* **107**, 450 (1957).

¹¹³ N. Swanson and C. J. Powell, *Phys. Rev.* **145**, 195 (1966). See also: L. Marton, J. A. Simpson, H. A. Fowler, and N. Swanson, *Phys. Rev.* **126**, 182 (1962); C. J. Powell, *Health Phys.* **13**, 1265 (1967).

normally be appreciably less than λ_{\min} , where λ_{\min} is the shortest inelastic mean free path to be measured; plural inelastic scattering may otherwise distort the energy loss spectrum though corrections to a spectrum based on Eq. (9) could be applied. For some materials, the energy loss spectrum due to excitation of the valance electrons may be due almost entirely to a single loss process (i.e. $f_n(0) \approx 1$). In such cases, t may be greater than the appropriate λ_i , and the intensities of the several loss peaks, each integrated over suitable ranges of q , may be fitted to a Poisson distribution to derive the ratio t/λ_i .

For materials with narrow loss peaks, it is possible to measure $(d\sigma_i/dq)$ for $q < q_m$ from measurements of loss intensity as a function of θ . Multi-point fits to a Poisson distribution (when $t > \lambda_i$) can be obtained by computing the shape of the angular distributions of plural loss peaks for the larger scattering angles where unambiguous intensity measurements cannot be made. These computed distributions, based on either an experimental or a theoretical form of $f_n(q)$, can be fitted to experimental distributions in the small-angle region where reliable intensity measurements are possible, as illustrated in Fig. 3.

If $f_n(q)$ cannot be measured and it has to be assumed that $f_n(q) \approx f_n(0)$, total cross sections can be determined from an energy-loss spectrum measured at $\theta = 0$, correction being made for that fraction of the angular distribution not measured.^{113,113a} This measurement should preferably be made under conditions of good angular resolution ($\approx \theta_B$). Less-accurate knowledge of the apparatus angular characteristics is required if a comparison can be made with the loss spectrum of a standard material measured under the same conditions.¹¹³

The dielectric description of optical absorption and of inelastic electron scattering is only expected to be valid for photon wavelengths (and hence for corresponding energy losses) large compared with the interatomic separation. It would, however, be expected from the Bethe theory of inelastic electron-atom scattering that a cross-section equation like Eq. (8) would be applicable for large ΔE_n .

Consideration of the finite boundaries of a specimen leads to the possibility of the excitation of surface states and to the excitation of surface plasmons. Surface states have not, as yet, been detected in electron scattering experiments, but surface plasmon oscillations have been predicted^{114, 115} and observed at the interface of two media. If the two media are semi-infinite and are of dielectric constant $\epsilon_A(\omega, q)$ and $\epsilon_B(\omega, q)$, the condition

^{113a} M. Creuzburg, *Z. Physik* **196**, 433 (1966).

¹¹⁴ R. A. Ritchie, *Phys. Rev.* **106**, 874 (1957).

¹¹⁵ E. A. Stern and R. A. Ferrell, *Phys. Rev.* **120**, 130 (1960).

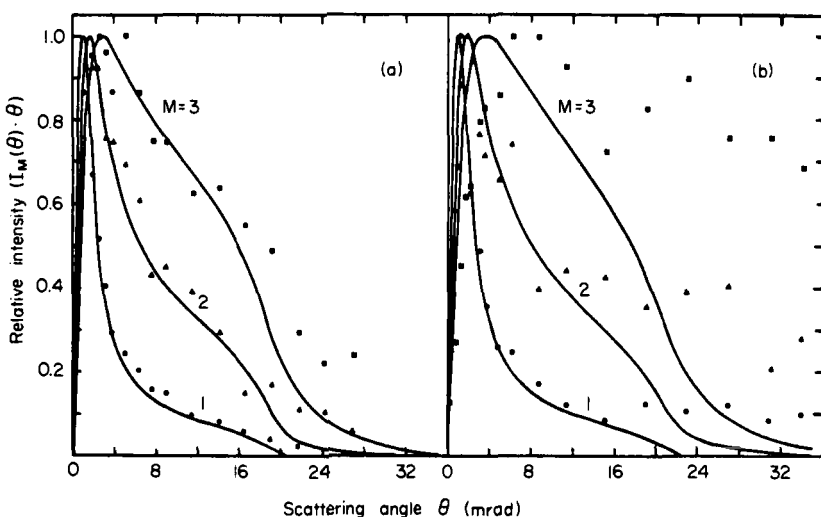


FIG. 3. First moments $I_M(\theta) \cdot \theta$ of intensity $I_M(\theta)$ as a function of electron scattering angle θ for the M th multiple of the 14.8 eV energy loss in Al (a) and of the 18.4 eV energy loss in Be (b). The points are derived from experimental measurements made with an 880 Å Al film and a 1420 Å Be film (primary electron energy = 20 keV). The energy loss peaks in Be are broader than those of Al, and the measurements at the large angles for Be include an unresolved component due to combined large-angle-elastic and small-angle-inelastic scattering. The smooth curves were computed from successive two-dimensional "folding" integrations using Eq. (8) with $f_n(q)$ obtained from the free-electron Ferrell¹¹² expression. All distributions have been normalized so that each maximum in $I_M(\theta) \cdot \theta$ is unity. The computed curves can be fitted to the experimental distributions in the 2 to 8 mrad region and the areas under the composite curves can be fitted to a Poisson distribution (Eq. (9)) to obtain an inelastic scattering cross section. [After N. Swanson and C. J. Powell, *Phys. Rev.* **145**, 195 (1966).]

for a surface plasmon resonance is that $(\varepsilon_A + \varepsilon_B)$ be equal to zero or be small compared to unity. For a metal for which $\varepsilon_A(\omega)$ can be described adequately by the free-electron formula $\varepsilon_A(\omega) = 1 - \omega_p^2/\omega^2$, the surface plasmon energy loss at a plane interface is given by

$$\hbar\omega_s = \hbar\omega_p / (1 + \varepsilon_B(\omega))^{1/2}. \quad (10)$$

For a metal bounded by a vacuum, $\omega_s = \omega_p/\sqrt{2}$. The differences between the observed values of the volume and surface plasmon losses and the corresponding values of $\hbar\omega_p$ and $\hbar\omega_p/\sqrt{2}$ are a measure of the contribution of interband transitions to $\varepsilon_A(\omega)$.^{116, 117}

¹¹⁶ D. Pines, *Physica Suppl.* **26**, 103 (1960).

¹¹⁷ C. J. Powell, *Phys. Rev. Letters* **15**, 852 (1965).

The interaction probability for an electron traversing the interface between a solid and vacuum can be expressed in the form^{115, 117a}

$$\frac{d^2P}{d\omega dq} = \frac{-2e^2}{\pi v^2} \cdot \frac{[q^2 - (\hbar\omega/v)^2]^{1/2}}{q^3} \cdot \text{Im} \left[\frac{(\varepsilon - 1)^2}{\varepsilon(1 + \varepsilon)} \right] \cdot f, \quad (11)$$

where $\varepsilon = \varepsilon_A(\omega, q)$, $\varepsilon_B = 1$, and f is a factor determined by the scattering geometry; $f = 1$ for normal incidence. The differential probability of Eq. (11) can be separated into two parts; one part represents the probability of excitation of the surface plasmon while the other represents a decrease in the probability of excitation of the "volume" plasmon loss considered previously. Equation (11) can also be applied to each of the two surfaces of a specimen film much thicker than \hbar/q_{\min} . For smaller film thicknesses, there is a coupling between the charge oscillations on the separate surfaces, and there is a surface plasmon resonance at two frequencies which are a function of q and the film thickness.^{11, 114, 115}

The requirements for measurements of the characteristics of surface plasmons are similar to those necessary for investigations of the bulk characteristics. In addition, particular care has to be given to surface cleanliness; surface layers of oxide, substrate, or other contaminants of only about 10 Å thickness will lead to a change in the surface plasmon energy loss.^{115, 118} The reflection scattering geometry is useful in that fresh surfaces can be prepared by repetitive evaporation *in situ*; frequent evaporation of Al or Ti may also be effective in reducing the oxidation rate of the surface under study to a satisfactorily low level even if the total pressure in the system is as high as $\approx 10^{-6}$ Torr.

9.2.3.2. Interactions at Low Electron Energies. The determination of the parameters associated with the interaction of low-energy (0–10³ eV) electrons with solids is much more difficult, both experimentally and theoretically, and the state of the art is consequently less well developed than with the case of electrons of higher energy considered previously.

Two approaches have been made to calculate the elastic scattering of low-energy electrons incident on a surface. One is to calculate the reflection coefficient as a function of electron energy for various estimates of the shape of the surface potential barrier, assumed one-dimensional, as discussed by Cutler and Davis.¹¹⁹ The other is to compute, as indicated in Section 9.2.3.1.1, the differential elastic scattering cross section for a surface atom in terms of an elastic scattering amplitude which is assumed

^{117a} A. Otto, *Phys. Stat. Sol.* **22**, 401 (1967).

¹¹⁸ C. J. Powell and J. B. Swan, *Phys. Rev.* **118**, 640 (1960).

¹¹⁹ P. H. Cutler and J. C. Davis, *Surface Sci.* **1**, 194 (1964).

to be that of a free atom.¹²⁰ As the interaction is confined principally to one or two surface layers of atoms, there is difficulty in testing either model due to uncertainty about the adequacy of a one-dimensional potential and to uncertainty regarding the arrangement of atoms near a surface.¹²¹

The theory of the inelastic scattering of low-energy electrons has been discussed by Ritchie and Ashley.¹²² The interaction can be described in the dielectric constant formalism of Section 9.2.3.1.2, and Quinn¹²³ has derived a formula for the cross section corresponding to plasmon excitation,

$$\sigma_p = \frac{e^2 \omega_p}{\hbar v^2} \ln \left[\frac{(E_F + E_p)^{1/2} - E_p^{1/2}}{E_0^{1/2} - (E_0 - E_p)^{1/2}} \right], \quad (12)$$

where $E_0 = \frac{1}{2}mv^2$ is the primary electron energy, E_F is the Fermi energy, and $E_p = \hbar\omega_p$. For $E_0 \gg E_p$, Eq. (12) is closely equal to the integral of Eq. (8) (from $q = \hbar\omega_p/v$ to $q = q_c$) in the limit $f_n(q) \rightarrow 1$. Expressions for the cross section due to single electron excitation, differential in scattering angle, and in the energies of the primary and secondary electron, may be found in the paper by Ritchie and Ashley.¹²²

The interaction of low-energy electrons with solids has been studied both by the impact of externally produced beams on specimens and by the use of electrons generated in the interior of a sample. Becker¹²⁴ has measured the transmission ($\approx 10^{-5}$) of 6 to 100-eV electrons incident on thin (200–400 Å) Ni films. Nakai and co-workers¹²⁵ have attempted to overcome the difficulty of preparing thin, self-supporting specimens by using a three-layer target structure. A thick support base (e.g., Al of about 2000 Å thickness) is covered with a thin insulating layer on one surface (e.g., Al_2O_3 prepared by anodic oxidation) and a thin specimen layer is evaporated onto the insulator. Nakai *et al.* bombarded the composite film with electrons of energy from 5 to 1500 eV and determined the fractional current stopped in the top specimen layer as a function of energy. It should be noted that the interpretation of this type of experiment is not straightforward; at high energies, one is in the region of single or plural inelastic scattering while at the lower energies multiple inelastic scattering prevails.

¹²⁰ N. F. Mott and H. S. W. Massey, "The Theory of Atomic Collisions," 3rd ed., Chapter 18. Oxford Univ. Press, London and New York, 1965.

¹²¹ J. J. Lander and J. Morrison, *J. Appl. Phys.* **34**, 1403 (1963); R. Seiwatz, *Surface Sci.* **2**, 473 (1964); N. R. Hansen and D. Haneman, *ibid.* **2**, 566 (1964).

¹²² R. H. Ritchie and J. C. Ashley, *J. Phys. Chem. Solids* **26**, 1689 (1965). See also: R. H. Ritchie, M. Y. Nakai, and R. D. Birkhoff, *Advan. Radiobiology* **3**. To be published.

¹²³ J. J. Quinn, *Phys. Rev.* **126**, 1453 (1962).

¹²⁴ A. Becker, *Ann. Physik* **2**, 249 (1929).

¹²⁵ Y. Nakai, F. W. Garber, R. H. Ritchie, and R. D. Birkhoff, *J. Phys. Chem. Solids* **26**, 1621 (1965).

Further, there is the possibility of systematic error in the measurements due to secondary electron emission and to the scattering of primary and secondary electrons in the insulating layer and in the interfacial regions.

The measurement of electron reflection at very low energies is associated with additional complications due to contact potential differences, the spread in energy of the primary beam, and to spurious currents caused by multiple scattering and secondary emission from electrode and detector surfaces, as discussed by several authors.^{126,127,127a} In exclusively electrostatic systems, it is possible to determine the angular characteristics of the scattered electrons unambiguously except for that fraction scattered back in a finite solid angle about the direction of the electron source. Measurement of this latter fraction can be accomplished if a magnetic field is applied.¹²⁸

Less-direct information on the electron-solid interaction at low energies can be obtained by studying photoemission (principally the photoelectron energy distribution) from bulk samples¹²⁹ and from thin films,¹³⁰ by "hot-electron" emission in thin-film diodes and triodes,¹³¹ and by photoelectric emission in sandwich films.¹³² As the inelastic mean free path varies rapidly with the electron energy in the range of these experiments,^{122, 123} it is usually possible to obtain information only on the gross characteristics of the electron scattering, especially as most of the features in photoelectron energy distributions, for example, appear to be determined by the band structures of the solids concerned.^{132a}

9.2.3.3. Multiple Scattering. In principle, measurements of differential cross sections for elastic and inelastic scattering would be sufficient to describe completely the interaction of an electron beam entering, for example,

¹²⁶ H. A. Fowler and H. E. Farnsworth, *Phys. Rev.* **111**, 103 (1958).

¹²⁷ J. Burns, *Phys. Rev.* **119**, 102 (1960).

^{127a} H. Heil and J. V. Hollweg, *Phys. Rev.* **164**, 881 (1967).

¹²⁸ R. J. Zollweg, *Surface Sci.* **2**, 409 (1964).

¹²⁹ F. G. Allen and G. W. Gobeli, *J. Appl. Phys.* **35**, 597 (1964); G. W. Gobeli, F. G. Allen, and E. O. Kane, *Phys. Rev. Letters* **12**, 94 (1964); C. N. Berglund and W. E. Spicer, *Phys. Rev.* **136**, A1030, A1044 (1964). A discussion of methods and techniques in photoemission experiments is given in Vol. 4, Chap. 1.1.3.

¹³⁰ H. Thomas, *Z. Physik* **147**, 395 (1957); S. Methfessel, *ibid.* **147**, 442 (1957).

¹³¹ T. W. Hickmott, *J. Appl. Phys.* **36**, 1885 (1965); O. L. Nelson and D. E. Anderson, *ibid.* **37**, 66 (1966); E. D. Savoye and D. E. Anderson, *ibid.* **38**, 3245 (1967).

¹³² A. I. Braunstein, M. Braunstein, and G. S. Picus, *Phys. Rev. Letters* **15**, 956 (1965). Electroluminescence may lead to photoemission in these experiments, as described by J. F. Delord, K. H. Johnston, R. E. Coovert, B. Pistoulet, C. Roustant, and M. Rouzeyre, *Appl. Phys. Letters* **11**, 287 (1967).

^{132a} A review of experiment and theory concerning the transport of very low-energy electrons in solids has been published by C. R. Crowell and S. M. Sze, *Phys. Thin Films* **4**, 325 (1967).

a semi-infinite specimen. In practice, however, measurements have not been made either with sufficient accuracy or over an adequate range of the independent variables; in any case, it is doubtful whether the theoretical problem could be solved by other than a Monte Carlo calculation on a large digital computer. It has therefore been found desirable to describe interactions with thick targets in terms of the gross observables (backscatter, absorption, and transmission coefficients; range; rate of energy loss; and probable scattering angle) which are usually considered to be a function only of the primary electron energy, the specimen thickness, and the atomic number of the specimen, if of one component. For mixtures and compounds, suitable averages are taken over the parameters of the individual components, depending on their concentration.

Theories of multiple elastic scattering of high-energy electrons have been reviewed by Scott.⁹⁷ To simplify the analysis, it is often assumed that angular deflection of the electrons results entirely from elastic scattering, while the effects of inelastic scattering can be satisfactorily represented by the Bethe stopping power equation,^{2, 4, 10†}

$$-\frac{dE}{dx} = \frac{4\pi e^4 N}{mv^2} \ln \left[\frac{mv^2}{2I} \left(\frac{\varepsilon}{2} \right)^{1/2} \right]. \quad (13)$$

In this equation, N is the electron density, ε is the base of natural logarithms, and $-(dE/dx)$ is the average rate of energy loss at the electron energy $\frac{1}{2}mv^2$ due to all inelastic processes characterized by the mean excitation energy I ($\approx 11Z$ eV). The effects of straggling (i.e., statistical variations in the number and kinds of inelastic processes) have been ignored in Eq. (13); the most probable energy loss in electron scattering is considerably less than the average energy loss. It has also been assumed that the electron energy is appreciably higher than the largest excitation energy of the system ($\approx K$ -shell binding energy). Such is often not the case in the energy range under present consideration and "inner-shell corrections" have to be applied to the parameter I .¹³³ Lenz has also shown that the theory of multiple elastic scattering has to be modified on account of electron energy loss at low electron energies (or for thick specimens).¹³⁴

Berger¹³⁵ has reviewed the Monte Carlo methods for calculating the

¹³³ U. Fano and J. E. Turner, *Natl. Acad. Sci. Natl. Res. Council Publ.* No. 1133, p. 49, (1964).

¹³⁴ F. Lenz, *Proc. Phys. Soc. (London)* **76**, 714 (1960).

¹³⁵ M. J. Berger, in "Methods in Computational Physics" (B. Alder, S. Fernbach, and M. Rotenberg, eds.), Vol. 1, p. 135. Academic Press, New York, 1963. See also: H. Paul and W. Tatzber, *Acta Physica Austriaca* **25**, 36 (1967).

† More exact expressions for the stopping power and evaluations of mean energy-loss and mean range for 40 materials and 80 energies between 10 keV and 1000 MeV are presented on p. 205 of Ref. 10.

backscattering, transmission, energy dissipation, and "slowing-down spectrum" of fast electrons for either semi-infinite or thin-film specimens. Some corrections to Berger's work and some further discussion of the Monte Carlo technique have been described by Whittle.¹³⁶ The uncertainties in the validity of the theoretical parameters used in the Monte Carlo calculations can be eliminated and the calculations can be simplified by the incorporation of experimental electron scattering data, as shown by Green and by Bishop.¹³⁷ It should be noted, however, that the results of such Monte Carlo calculations are sensitive to both the accuracy and the representation of the input data.¹³⁶ While there is qualitative agreement in the two approaches, it is not as yet clear whether it is preferable as the basis for a Monte Carlo calculation to use theoretical expressions of unknown validity (which can be used for all solids) or to adopt experimental data of unknown accuracy (from a necessarily limited number of types of specimen); the latter method would appear more useful at low electron energies (<1 keV) though it is just in this region that sufficient data is difficult to obtain on account of the short mean free paths. A Monte Carlo analysis of the motion of low-energy electrons in solids has been described by several authors.¹³⁸

Suitable experimental methods for the measurement of transmission, backscatter and absorption coefficients, range and probable angles of scatter or backscatter for thin-film specimens of varying thicknesses, and electron energies >1 keV have been described in detail in recent series of papers by Kanter¹³⁹ and by Cosslett and Thomas.¹⁴⁰ An experiment to measure the mean energy loss per inelastic event of electrons transmitted through thin specimens has been described by Rauth and Simpson.¹⁴¹ The requirements on energy and angular resolution are not stringent, as one is concerned with the average and most probable effects rather than with the details of particular processes.

9.2.3.4. Secondary Processes. The excitations produced by "primary" electrons interacting with solids lead to the emission of Auger and secondary electrons, to the emission of photons over a wide spectral range, to the

¹³⁶ J. Whittle, Australian Defense Std. Lab. Rept. No. 276, August 1965 (unpublished). Copies available on request from Defense Std. Lab., Victoria, Australia.

¹³⁷ M. Green, *Proc. Phys. Soc. (London)* **82**, 204 (1963); H. E. Bishop, *ibid.* **85**, 855 (1965).

¹³⁸ R. Stuart, F. Wooten, and W. E. Spicer, *Phys. Rev.* **235**, A495 (1964); R. N. Stuart and F. Wooten, *ibid.* **156**, 364 (1967); E. O. Kane, *ibid.* **159**, 624 (1967); E. D. Savoye and D. E. Anderson, *J. Appl. Phys.* **38**, 3245 (1967).

¹³⁹ H. Kanter, *Phys. Rev.* **121**, 461, 677, 681 (1961); H. Kanter and E. J. Sternglass, *ibid.* **126**, 620 (1962); H. Kanter, *Brit. J. Appl. Phys.* **15**, 555 (1964).

¹⁴⁰ V. E. Cosslett and R. N. Thomas, *Brit. J. Appl. Phys.* **15**, 235, 833, 1283 (1964); **16**, 779 (1965).

¹⁴¹ A. M. Rauth and J. A. Simpson, *Radiation Res.* **22**, 643 (1964).

possibility of change in the physical and chemical structure of the solid, and ultimately to the dissipation of heat.

9.2.3.4.1. SECONDARY ELECTRON EMISSION. Reviews on the theory and experimental characteristics of secondary electron emission have been published recently by Dekker¹⁴² and by Hachenberg and Brauer,¹⁴³ and a discussion of relevant methods and techniques has been published in this series.¹⁴⁴ While many experiments show that the secondary electron yield varies relatively slowly and monotonically with primary electron energy, angle of incidence of the primary beam on a surface, and with take-off angle and that the secondary electron energy distribution is relatively broad and structure-free, there are some experiments which have shown "fine-structure" in curves of yield versus primary energy,¹⁴⁵ in the secondary electron energy distribution,¹⁴⁶ in curves of the number of secondary electrons with a particular energy as a function of primary energy,¹⁴⁷ and in the secondary yield as a function of primary electron angle of incidence.^{147a} Further work is needed to identify the discrete processes involved and to determine the necessary energy and angular resolution in a particular experiment.

9.2.3.4.2. AUGER ELECTRON EMISSION. Though it is well known that an atom with an electron removed from an inner shell may return to its ground state by single or multiple Auger transitions, relatively few measurements have been made of the relative intensities and energies of Auger electrons emitted from solids.¹⁴⁸ It would be expected that an energy resolution ≈ 1 eV would be sufficient in an experiment to study the characteristics of Auger electrons and that it would be advantageous to choose a geometry such that there would be minimum absorption of the Auger electrons emerging from the specimen.

9.2.3.4.3. ELECTRON SLOWING-DOWN SPECTRUM. As primary electrons lose energy in a specimen and successive generations of secondary electrons are created and also interact with the medium, it is of considerable interest to determine the electron flux as a function of energy and path-length and the spatial variation in the energy dissipation. Theory and numerical

¹⁴² A. J. Dekker, *Solid State Phys.* **6**, 251 (1958).

¹⁴³ O. Hachenberg and W. Brauer, *Advan. Electron. Electron Phys.* **11**, 413 (1959).

¹⁴⁴ Vol. 4, Section 1.1.4.

¹⁴⁵ H. S. W. Massey and E. H. S. Burhop, "Electronic and Ionic Impact Phenomena," p. 326. Oxford Univ. Press; London and New York, 1952.

¹⁴⁶ V. Evtuhov, G. F. Smith, and L. S. Yaggy, *Rev. Sci. Instr.* **32**, 1362 (1961).

¹⁴⁷ J. Hözl, *Z. Physik* **184**, 50 (1965).

^{147a} R. W. Soshea and A. J. Dekker, *Phys. Rev.* **121**, 1362 (1961).

¹⁴⁸ G. A. Harrower, *Phys. Rev.* **102**, 340 (1956); O. Hörnfeldt, A. Fahlman, and C. Nordling, *Arkiv Fysik* **23**, 155 (1962); O. Hörnfeldt, *ibid.* **23**, 235 (1962); R. Päschke, *Z. Physik* **176**, 143 (1963).

calculations have been reported by Spencer and others,^{135, 149} while an experiment designed to measure the flux of electrons emerging from an approximately "black-body" source over a wide range of energy has been described by McConnell *et al.*¹⁵⁰

9.2.3.4.4. RADIATION. The interaction of electrons with matter leads to the direct or indirect emission of radiation⁷: characteristic X-ray production, bremsstrahlung, "transition" radiation (excited by electrons crossing the boundary of two media), fluorescence, and Smith-Purcell radiation¹⁵¹ (excited by electrons moving parallel to the surface and perpendicular to the rulings of a diffraction grating). The spectral and other characteristics of the radiations may be determined using techniques described elsewhere in this series.¹⁵² Stimulated by the need to interpret meaningfully X-ray intensities in the electron probe microanalyzer, new measurements are being made of the absolute quantum yields of characteristic X rays for particular geometries.¹⁵³

9.2.3.4.5. STRUCTURAL AND CHEMICAL CHANGE. Electron irradiation may cause specimen decomposition (e.g., the photographic process), polymerization, recrystallization, desorption of adsorbed gas, and perhaps also the generation and motion of lattice defects.¹⁵⁴ The various processes are not well understood,¹⁵⁵ and the possibility of specimen change during an electron scattering experiment should not be overlooked.

The polymerization of condensed hydrocarbon vapors under electron bombardment is a common annoyance in typical high-vacuum systems.^{50, 51} The rate of formation of such high-resistance polymer films may be reduced by heating the critical parts (e.g., specimen and analyzer apertures) to about 200°C and by the installation of an efficient cold-trap.

¹⁴⁹ L. V. Spencer and F. H. Attix, *Radiation Res.* **3**, 239 (1955); L. V. Spencer, *Natl. Bur. Std. (U.S.) Monograph No. 1* (1959); R. J. McGinnies, *Natl. Bur. Std. (U.S.) Circ. No. 597* (1959).

¹⁵⁰ W. J. McConnell, H. H. Hubbell, R. N. Hamm, R. H. Ritchie, and R. D. Birkhoff, *Phys. Rev.* **138**, A1377 (1965).

¹⁵¹ C. W. Barnes and K. G. Dedrick, *J. Appl. Phys.* **37**, 411 (1966).

¹⁵² Vol. 6B, Chapters 10, 11.

¹⁵³ V. Metchnik and S. G. Tomlin, *Proc. Phys. Soc. (London)* **81**, 956 (1964); D. B. Brown and R. E. Ogilvie, *J. Appl. Phys.* **35**, 309 (1964); W. Hink, *Z. Physik* **182**, 227 (1965).

¹⁵⁴ J. W. Mitchell, *Rept. Progr. Phys.* **20**, 433 (1957); M. Creuzburg, *Z. Naturforsch.* **20a**, 1732 (1965); L. Reimer, *Lab. Invest.* **14**, 1082 (1965); K. Kobayashi and K. Sakaoku, *ibid.* **14**, 1097 (1965); G. A. Bassett, A. J. Forty, and M. R. Tubbes, *Proc. Intern. Congr. Electron Microscopy*, 5th, Philadelphia, 1962, (S. S. Breese, ed.), Vol. 1, paper G2. Academic Press, New York, 1962; D. Menzel and R. Gomer, *J. Chem. Phys.* **41**, 3311, 3329 (1964); L. Fliermans and J. Vennik, *Phys. Letters* **25A**, 687 (1967); P. D. Townsend and J. C. Kelly, *ibid.* **26A**, 138 (1967).

¹⁵⁵ A. J. Forty, *Brit. J. Appl. Phys.* **14**, 3 (1963).

It is often important to determine the temperature rise in a specimen under given conditions of electron bombardment. Pittaway¹⁵⁶ has derived temperature distributions for both thin-film and semi-infinite targets and for both stationary and moving incident beams. Though an analysis of this type may be a useful guide, there are generally significant uncertainties in the spatial distribution and the amount of energy dissipation due to the reduction of absorbed energy by electron backscattering and by electron transmission in thin-film specimens.¹⁵⁷

9.2.4. Crystalline Solids

It is well known that solids are anisotropic with respect to electron interaction and that the degree of anisotropy is a function of the crystalline order and size. Electron diffraction, which occurs at both high and low electron energies,¹⁵⁸ is responsible for angular anisotropies in the elastic scattering. Kikuchi lines and bands are observed for thick crystals in transmission and for reflection scattering geometries, again at high and low energies.¹⁵⁹ It has also become clear in recent years that anisotropies exist also in the inelastic electron scattering.¹⁶⁰ No description will be given here of methods and techniques directly associated with electron diffraction and electron microscopy as these subjects have been already discussed in this series.¹⁶¹

The theory of electron interaction in crystals is still in development, particularly in the interpretation of electron micrographs of defects in crystals^{5, 8, 9, 13, 162} and of the so-called anomalous absorption. The latter appears to be associated with electron-phonon scattering.¹⁶³

¹⁵⁶ L. G. Pittaway, *Brit. J. Appl. Phys.* **25**, 967 (1964). See also: J. Ling, *Brit. J. Appl. Phys.* **18**, 991 (1967).

¹⁵⁷ L. Reimer and R. Christenhusz, *Lab. Invest.* **14**, 1158 (1965).

¹⁵⁸ H. Raether, in "Handbuch der Physik" (S. Flügge, ed.), Vol. 32, p. 443. Springer, Berlin, 1957. J. M. Cowley and A. L. G. Rees, *Rept. Progr. Phys.* **21**, 165 (1958); J. J. Lander and J. Morrison, *J. Appl. Phys.* **34**, 3517 (1963); J. J. Lander, *Progr. Solid State Chem.* **2**, 26 (1965); I. H. Khan, J. P. Hobson, and R. A. Armstrong, *Phys. Rev.* **129**, 1513 (1963); E. G. McRae, *J. Chem. Phys.* **45**, 3258 (1966); E. G. McRae and C. W. Caldwell, *Surface Sci.* **7**, 41 (1967).

¹⁵⁹ M. N. Alam, M. Blackman, and D. W. Pashley, *Proc. Roy. Soc. A* **221**, 224 (1954); J. L. Robins, R. L. Gerlach, and T. N. Rhodin, *Appl. Phys. Letters* **8**, 12 (1966); D. C. Johnson and A. U. MacRae, *J. Appl. Phys.* **37**, 1945 (1966).

¹⁶⁰ H. Hashimoto, A. Howie, and M. J. Whelan, *Proc. Roy. Soc. A* **269**, 80 (1962); A. Howie, *ibid.* **A271**, 268 (1963); P. Duncumb, *Phil. Mag.* **7**, 2101 (1962); R. Uyeda and M. Nonoyama, *Japan J. Appl. Phys.* **4**, 498 (1965); F. Bell and R. Sizmann, *Phys. Letters* **19**, 171 (1965); A. Fukuhara, *J. Phys. Soc. Japan* **18**, 496 (1963); K. Zeppenfeld, *Phys. Letters* **25A**, 335 (1967).

¹⁶¹ Vol. 6A, Chapters 2.9, 3.3.

¹⁶² Y. Kainuma, *J. Phys. Soc. Japan* **20**, 2263 (1965).

There is at present a need for quantitative measurements of the interaction parameters discussed in Section 9.2.3 to be made with single-crystal specimens of known orientation.^{163a} The energy-selecting electron microscope is a tool with which it is possible to determine the energies of electrons contributing to the image contrast for various positions of the objective aperture.¹⁶⁴ An angular resolution of 10^{-3} to 10^{-4} rad is required at a primary electron energy of 50 keV. An energy resolution of about 1 eV would be sufficient to discriminate against electrons involved in inelastic events of the type discussed in Section 9.2.3.1.2, but an improvement of two orders of magnitude in energy resolution would be required to distinguish electron-phonon interactions.^{164a} Less-detailed information of the electron-phonon interaction may be obtained by measuring the temperature dependence of the absorption coefficients for electrons in various regions of the diffraction pattern.¹⁶⁵

The real and imaginary Fourier coefficients of crystal potential are used extensively in the analysis of diffraction intensities. These potentials are closely related to the elastic and inelastic scattering cross sections and to the corresponding atomic scattering amplitudes. Frankl¹⁶⁶ has shown that the real part of the Fourier coefficient of potential may be obtained from the intervals between extinction contours for a strong Bragg reflection in a wedge-shaped crystal. Similar measurements over a wider range of Bragg angles can be made from the angular half-widths of Kikuchi lines or band-edges.¹⁶⁷

¹⁶³ C. R. Hall and P. B. Hirsch, *Proc. Roy. Soc.* **A286**, 158 (1965); M. J. Whelan, *J. Appl. Phys.* **36**, 2103 (1965); J. Gjønnes, *Acta Cryst.* **20**, 240 (1966); M. J. Goringe, A. Howie, and M. J. Whelan, *Phil. Mag.* **14**, 217 (1966); A. J. F. Metherell and M. J. Whelan, *ibid.* **15**, 755 (1967); A. J. F. Metherell, *ibid.* **15**, 763 (1967); Y. H. Ohtsuki; *Phys. Letters* **24A**, 691 (1967).

^{163a} A. Tonomura and H. Watanabe, *Japan J. Appl. Phys.* **6**, 1163 (1967); A. J. F. Metherell, *Phil. Mag.* **16**, 1103 (1967); K. Ishida, M. Mannami, and K. Tanaka, *J. Phys. Soc. Japan* **23**, 1362 (1967).

¹⁶⁴ H. Watanabe and R. Uyeda, *J. Phys. Soc. Japan* **17**, 569 (1962); Y. Kamiya and R. Uyeda, *ibid.* **17**, Suppl. B-II, 191 (1962); S. L. Cundy, A. J. F. Metherell, and M. J. Whelan, *J. Sci. Instr.* **43**, 712 (1965); S. L. Cundy, A. J. F. Metherell, and M. J. Whelan, *Phil. Mag.* **15**, 623 (1967); R. Castaing, A. El Hili, and L. Henry, *Compt. rend. Acad. Sci. 262*, 1051 (1966).

^{164a} H. Boersch, J. Geiger, and W. Stickel, *Phys. Rev. Letters* **17**, 379 (1966).

¹⁶⁵ M. Horstmann, *Z. Physik* **188**, 124, 412 (1965); G. Meyer, *Phys. Letters* **20**, 240 (1966); M. J. Goringe, *Phil. Mag.* **14**, 93 (1966); W. Glaeser and H. Niedrig, *J. Appl. Phys.* **37**, 4303 (1966); J. Hansen-Schmidt, *Z. Physik* **198**, 433 (1967); W. W. Albrecht and H. Niedrig, *Phys. Letters* **26A**, 14 (1967).

¹⁶⁶ D. R. Frankl, *J. Appl. Phys.* **35**, 217 (1964).

¹⁶⁷ H. A. Fowler and L. Marton, *J. Appl. Phys.* **36**, 1986 (1965).

10. ELECTRIC ARCS*

Electric arcs are widely used for the study of atomic constants and parameters. Principally the strong radiation and the fact that most arc sources are in the regime of local thermal equilibrium have made them important research tools in quantitative spectroscopy, specifically for the study of transition probabilities, line broadening parameters, and continuum absorption coefficients. In the following, the properties of arcs and the analysis of arc plasmas will be mainly discussed from this viewpoint of applications in atomic physics. Thus a detailed description of the experimental methods for the determination of particle densities and temperatures in arc plasmas is presented, the question of local thermal equilibrium is examined, and the various applications in atomic physics are discussed. The arc types to be described are also selected from this point of view. Other aspects of arc physics are generally not considered, since it would be rather irrelevant to include here detailed discussions of electrode mechanisms, anode- and cathode-falls, particle flows in arcs, convection, energy balance, etc. A detailed article on these subjects has been recently written by Finkelnburg and Maecker,¹ and it may be noted that Maecker² as well as Schmitz and Uhlenbusch³ have been quite successful in deriving transport properties of stabilized arcs from the basic theory of the arc column in conjunction with available electrical input data and consideration of radiation losses.

10.1. Description of the Various Arc Sources

Among the different types of arcs we shall discuss those that have attained importance in quantitative spectroscopy, and specifically in the areas mentioned above. It should not be overlooked, however, that certain

¹ W. Finkelnburg and H. Maecker, in "Handbuch der Physik" (S. Flügge, ed.), Vol. 22. Springer, Berlin, 1956.

² H. Maecker, *Proc. Intern. Conf. Ionization Phenomena Gases, 5th. Conf., Munich, 1961*, II, p. 1793. North-Holland Publ., Amsterdam, 1962.

³ G. Schmitz and J. Uhlenbusch, *Z. Naturforsch.* **18a**, 772 (1963); J. Uhlenbusch, *Z. Physik* **179**, 347 (1964).

* Part 10 is by W. L. Wiese.

other arc types have also been of great value for other areas of atomic spectroscopy. Especially worth mentioning are the iron-vapor arc developed by Pfund⁴ that has served for a long time to generate the line-rich iron spectrum for wavelength comparisons and the low-current carbon arc in which the crater of the anode is used as a radiation standard.⁵

10.1.1. Low-Current Atmospheric Arcs

This simple research tool has been typically operated with currents of 3–10 A dc and electrode separations less than 10 mm which have resulted in over-all voltages which are typically 30–60 V. Because the arc voltage decreases with increasing current in this current range, an ohmic ballast resistor is used in series with the arc for stable operation with constant-voltage power supplies. The electrodes may be of metal—mostly employed are Cu, Fe, W—or of graphite into which small amounts of the element to be studied are admixed. A trace of this element is thus continuously evaporated into the arc column. The radiation from the latter, i.e., usually from the total gap between the electrodes, is admitted to the spectrograph. Practically all spectroscopic measurements have been performed with photographic techniques, so that time and space integrated spectra are obtained.

The low-current atmospheric arc suffers from three major shortcomings. It is unstable with respect to position and time, its temperature range is quite limited, and thermodynamic equilibrium does not exist (see Chapter 10.4). The often violent fluctuations in the arc are its most severe shortcoming, since they prevent in practice spatial analysis of the radiation. This analysis, however, is essential to obtain the physically meaningful local values of temperature and densities. But normally no attempt at spatial resolution has been made and the local source properties are approximately replaced by “effective” values. It is evident that with this procedure serious systematic errors in the determination of atomic parameters may be introduced. Thus this source cannot be considered suitable for high-precision work.

Furthermore, the typical temperature range of 4000–8000°K is somewhat low for many studies of lighter elements, but it is quite appropriate for most metals (neutral and singly ionized atoms) and molecular species.

According to several experimental investigations and to the equilibrium criteria for arcs (for details see Chapter 10.4), only partial thermal equilibrium is established in low-current arcs. Therefore the application of some

⁴ A. H. Pfund, *Astrophys. J.* **27**, 297 (1908).

⁵ J. Euler, *Ann. Physik* (6) **11**, 203 (1953); M. R. Null and W. W. Lozier, *J. Opt. Soc. Am.* **52**, 1156 (1962).

equilibrium relations, e.g., the Saha equation, becomes doubtful. The deviations from local thermal equilibrium are primarily due to the low electron densities, which are typically below 10^{15} cm^{-3} .

10.1.2. High-Current, Controlled Atmosphere Arcs

A significant improvement in the stability of the atmospheric arc as well as a higher temperature range is obtained when the arc is operated at higher currents, roughly from 50 A on up. Raising the current will at first only result in an increase of the diameter of the arc column (bulging), but above 50 A a hotter, inner core is formed in the column, starting from the cathode. At the same time current density and temperature in the core are increased and the column becomes more stable. The higher stabilization is caused by axial gas motion in the direction away from the cathode where the self-magnetic field generated by the arc current reaches its highest value and causes a slight overpressure.¹ With the increased arc temperature, gaseous convection currents due to gravitational forces become more pronounced, too. This effect may be used for additional stabilization of the arc column if a suitable geometric configuration is chosen. A further stabilizing effect is obtained when the arc is operated in an inert atmosphere, since chemical reactions on the hot electrodes are then eliminated.

Busz and Finkelnburg⁶ were the first to investigate in detail the properties of high-current arcs operated in controlled atmospheres. They ran arcs in argon and nitrogen with water-cooled electrodes at currents up to 500 A and obtained axis temperatures as high as 30,000°K.

Olsen⁷ has applied a similar arc to spectroscopic investigations of neutral and singly ionized argon. A design of his arc chamber is given in Fig. 1. His cathode is of thoriated tungsten, ground to a conical tip, and his anode is a copper plate. Both electrodes are water cooled to prevent metal vapor contamination of the argon plasma. Olsen reports extremely good positional stability of this arc over periods of several hours and very good rotational symmetry which enables him to spatially resolve the arc radiation by applying the Abel inversion process (Chapter 10.2) to side-on observations.

10.1.3. Gas- and Fluid-Stabilized Arcs

These arc types, as well as the wall-stabilized arc, to be discussed later, have been developed mainly for the determination of atomic constants and parameters. They have been designed to overcome the major shortcomings of the simple low-current arc which, as has been pointed out before, are

⁶ G. Busz and W. Finkelnburg, *Z. Physik* **140**, 540 (1955).

⁷ H. N. Olsen, *Phys. Fluids* **2**, 614 (1959).

its positional instability, its limited temperature range, and deviations from local thermodynamic equilibrium.

The gas-stabilized arc⁸ was the earliest type of arc which provided a significant improvement with respect to column stability. The arc column is enclosed in a long and relatively wide tube, usually of glass or quartz,

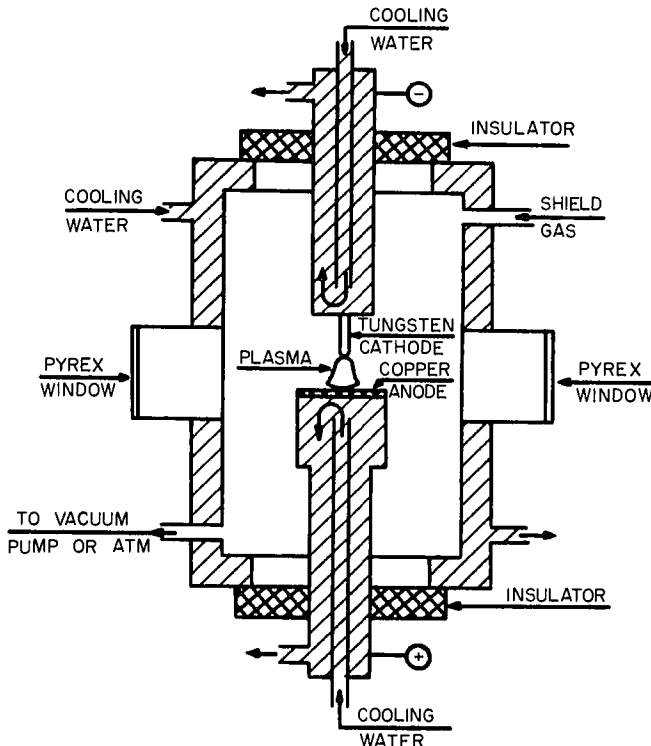


FIG. 1. Schematic diagram of Olsen's high-current argon arc chamber [H. N. Olsen, *Phys. Fluids* 2, 614 (1959)].

which may be cooled from the outside. The gas to be investigated is tangentially blown in at one end of the tube, streams through the tube in a vortex, and exits at the other end (vortex arc). The gas flow rates are kept quite low to prevent turbulent flow. Conversely, attempts have been made with good success to rotate the tube.⁹

Gas-stabilized arcs have not only been a step forward with regard to stability, but have also made possible investigations over a much-increased

⁸ O. Schönherr, *Elektrotech. Z.* 30, 365 (1909).

⁹ H. Schnautz, *Spectrochim. Acta* 1, 173 (1939).

temperature range. For example, Pfender¹⁰ reported recently that he has reached axis temperatures of about 25,000°K with an arc operating in a hydrogen atmosphere at a current of 300 A.

Even higher temperatures may be achieved by replacing the gas vortex with a fluid vortex because of the more efficient cooling of the tube walls. For a given current the tube diameter may be decreased and the stronger constriction leads to higher current densities and field strengths and ultimately to higher axis temperatures.

A typical water-stabilized arc, representing closely the original design by Maecker,¹¹ is shown in Fig. 2. Water, under normal pressure, is intro-

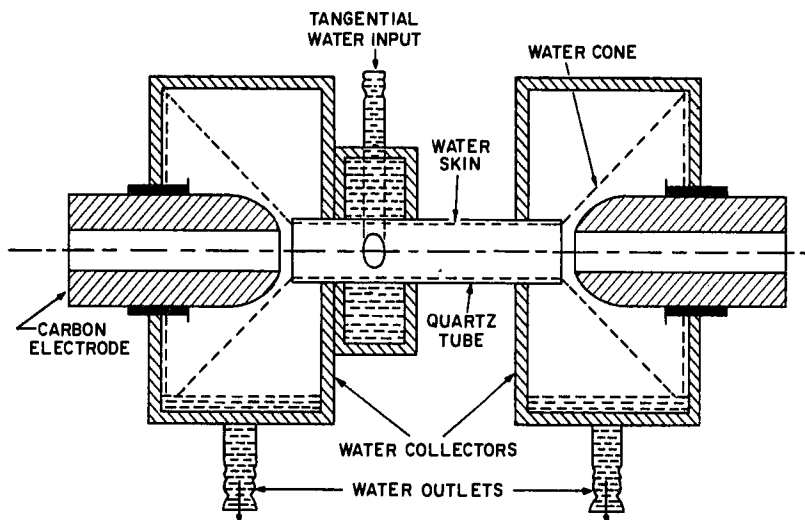


FIG. 2. Schematic diagram of a water-stabilized arc [after H. Maecker, *Z. Physik* 129, 108 (1959); G. Jürgens, *Z. Physik* 134, 21 (1952)].

duced tangentially into a cylinder in which it rotates around rapidly because of centrifugal forces. When the inner water level reaches the inner radius of the quartz tube, the water acquires an axial velocity component and develops a vortex into the tube. The resulting water skin inside the tube is only a few tenths of a millimeter thick, compared to a typical tube diameter of 8 mm. At the ends of the quartz tube the water exits in cones and is collected in two hollow chambers which also serve to cool the graphite

¹⁰ E. Pfender, *Proc. Intern. Conf. Ionization Phenomena Gases, 6th Conf.*, Paris 1963, 2, p. 369. S.E.R.M.A. Publ., Paris, 1963.

¹¹ H. Maecker, *Z. Physik* 129, 108 (1951).

electrodes. The latter have a central bore of a few millimeters to permit end-on observations as well as the ignition of the arc by short-circuiting it with a thin metal or graphite rod. Maecker¹¹ modified this arc for extremely high power consumption by eliminating the quartz tube and by enlarging and extending the cylinder so that the whole length of the arc column was surrounded by a thick layer of water. With a channel diameter of 2.3 mm and a current of 1500 A, Burhorn *et al.*¹² reached an axis temperature of 55,000°K, which still appears to be the highest attained by any stationary source under atmospheric pressure. To further increase the versatility of this arc, Peters¹³ developed a high-pressure version capable of operating at pressures up to 1000 atm, which may be employed for high-density studies.

Spectroscopic observations have been performed both end-on through the hollow electrodes and side-on through the water skin and quartz tube. The side-on observations require, of course, an Abel inversion analysis for the determination of local values of densities and temperatures. The water skin causes a certain amount of optical distortion which significantly impairs the rotational symmetry. Furthermore, from streak camera photographs^{14, 15} it has become apparent that the short time stability of the water-stabilized arc is quite poor. The arc suffers violent fluctuations and may change its position sideways by as much as its diameter due to local inhomogeneities and nonuniform evaporation and heating of the water.¹⁵ Consequently the arc appears to be smeared out and the results, obtained predominantly photographically, must be considered as average values only. The same situation, but not as marked, applies to the gas-stabilized arc. Because of this shortcoming, these two arc types are no longer in general use for atomic physics applications.

10.1.4. Wall-Stabilized Arcs

In the search for an arc source that is quiescent and stable as well as capable of sustaining the necessary high power inputs to reach high temperatures, Maecker¹⁶ in 1956 returned to the idea of a wall-stabilized arc. The simple concept of stabilizing the arc column by a solid wall had been always appealing, but presented a basic difficulty: In order to withstand

¹² F. Burhorn, H. Maecker, and Th. Peters, *Z. Physik* **131**, 28 (1951).

¹³ Th. Peters, *Z. Physik* **135**, 573 (1953).

¹⁴ H. Maecker, Th. Peters, and H. Schenk, *Z. Physik* **140**, 119 (1955).

¹⁵ P. Bogen, *Z. Physik* **149**, 62 (1957).

¹⁶ H. Maecker, *Naturforsch.* **11a**, 457 (1956).

the heat generated by the arc plasma, the wall material had to be a good thermal conductor, and, at the same time, had also to fulfill the requirement of being a good electrical insulator to prevent arcing between the electrodes and the wall. Maecker reconciled these divergent requirements by subdividing the wall into a number of sections that are electrically insulated from each other. These sections may then be constructed of effective thermal conductors, like copper, and may be water cooled to achieve a high thermal load capacity.

A recent arc design used for a number of atomic physics applications is shown schematically in Fig. 3. The arc chamber consists of ten hollow, water-cooled copper disks with a bore a few millimeters wide in the center, separated by insulating rings, which may be made, e.g., of Bakelite or anodized aluminum. The cooled metal (e.g., tungsten) electrodes are about 15 cm apart. The arc is sealed from the surrounding atmosphere by O-ring seals at all appropriate positions. Following a suggestion by Shumaker,¹⁷ argon gas is gently blown in at positions 2 and 8 as well as behind the electrodes in order to blanket these regions and to minimize the erosion and chemical reactions on the hot electrodes. (It should be noted also that carbon electrodes have been successfully used.) The gas to be studied (denoted in the figure by "study gas") is introduced at points 4 and 6. Common exit pipes, wide enough to prevent the buildup of overpressure in the arc, are positioned at 3 and 7. No gas is blown in or out of section 5, where the side-on observations take place. The gas flows may be precisely regulated with flowmeters or variable leak valves, and the flow rates are normally quite small, of the order of 10^{-1} liter/min. With a simple cooling arrangement the arc withstands input power levels of up to 2 kW/cm in stationary operation without damage. With inserts in the copper disks to direct high-velocity water flows to the most critical areas, the cooling effectiveness is greatly increased. If also well-cooled metal electrodes are employed, the power levels may be raised to about 10 kW/cm.[†]

The wall-stabilized arc fulfills quite closely the requirements of an ideal stationary source for the generation of dense, moderate-temperature plasmas. Its useful temperature range is approximately 6000–25,000°K. This range suffices for the excitation of lines from all neutral atoms and for many second and third spectra of metals and other heavier elements. Indeed, wall-established arcs have been operated with various permanent

¹⁷ J. B. Shumaker, Jr., *Rev. Sci. Instr.* **32**, 65 (1961).

[†] H. Maecker and S. Steinberger (*Z. angew. Physik* **23**, 458 (1967)) have recently described an improved design for a wall-stabilized arc capable of operating at an input level of 18 kW/cm.

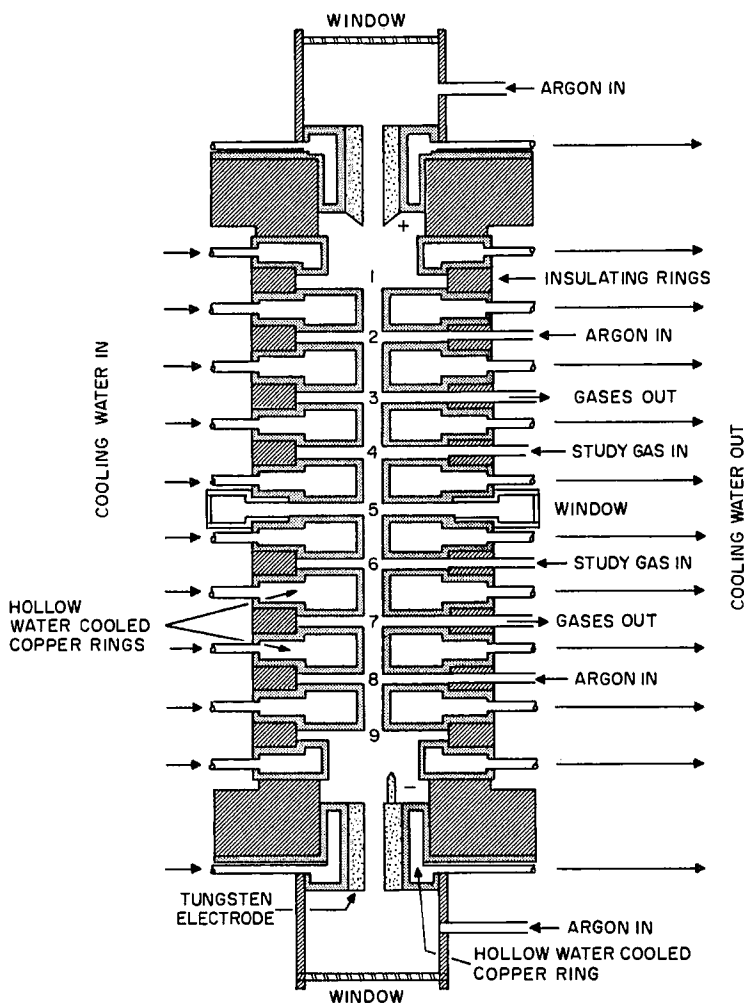


FIG. 3. Schematic diagram of a wall-stabilized arc [after W. L. Wiese, D. R. Paquette, and J. E. Solarski, Jr., *Phys. Rev.* **129**, 1225 (1962)].

gases, like H, N, O, Ne, Ar, CO₂, SO₂, but also with gaseous mixtures consisting of permanent gases and substances of fairly high vapor pressure such as Ni(CO)₄, TiCl₄, FeCl₃, and with the aerosol Cu(NO₃)₂ × 3H₂O. The latter substances, evidently, have been employed for the production of spectra of Ni I and II, Ti I and Ti II, etc.

The arc stability and reproducibility must be considered excellent. With argon blanketing the electrode regions and with effectively cooled tungsten electrodes, the arc has been operated continuously for many hours without

any noticeable deterioration or changes in condition. A quantitative test has been made with a hydrogen arc source operated at 40 A with a constant-current power supply (constant to within 20 mA) over a period of about 1½ hours. The electron density and temperature were determined from data taken about every 5 minutes, and the standard deviations of the mean values turned out to be 0.3% and 0.03%, respectively. Also, the rotational symmetry of the arc column has been found to be excellent, as was shown by scanning the arc image across two spectrometers set at right angles to each other.¹⁸ However, the length of the open, unstabilized spaces between the copper disks should be limited to about one or two times the arc diameter, otherwise kinks in the arc column may appear. In addition, some bulging of the arc in the open spaces may occur. This is of no concern in the side-on measurements, since the slit height of the observing spectrometer may be properly masked, but the resulting slight inhomogeneities in axial direction may reduce the precision of end-on measurements.

Boldt¹⁹ has significantly extended the range of arc applications by adapting the wall-stabilized arc to spectroscopic investigations in the vacuum ultraviolet region. The vacuum spectrograph is normally separated from the atmospheric pressure arc by an interlock. When the interlock, which also serves as the photographic shutter, is opened, large buffer volumes maintain the pressure difference for about 10 sec, while photographic exposures may be made.†

10.2. The Abel Inversion Process

The radiation of arc sources may be observed either from the side or from the end through the hollow electrodes. In both kinds of measurements the radiant intensity integrated over the entire depth of the arc plasma is observed. In side-on observations the recorded intensity is a mixture of contributions from many different radial zones of various temperatures and particle densities and must be reduced to local radial values, since only these are physically meaningful. Under the assumption of rotational symmetry the radial distribution of intensities may be obtained via a mathematical transformation process, the so-called Abel inversion.

In end-on measurements, on the other hand, the approximately homogeneous axial region of constant temperature and electron density is observed. End-on measurements offer therefore the great convenience of a

¹⁸ W. L. Wiese, D. R. Paquette, and J. E. SolarSKI, Jr., *Phys. Rev.* **129**, 1225 (1962).

¹⁹ G. Boldt, *Proc. Intern. Conf. Ionization Phenomena Gases*, 5th Conf., Munich, 1961, 1, 925. North-Holland Publ., Amsterdam, 1962.

† J. C. Morris and R. L. Garrison [J. Quant. Spectry. and Radiative Transfer 6, 899 (1966)] have recently made vacuum uv observations on a continuous basis by employing a differential pumping system between the wall-stabilized arc and the spectrometer.

much simpler data analysis. However, the precision of end-on observations is impaired by a number of inherent error sources, of which the most important are inhomogeneities in the end zones. In wall-stabilized arcs, slight temperature and electron density variations are also encountered along the arc column, since the arc is alternately constricted in the copper disks and widened in the insulating pieces. Furthermore, for the earlier arc types the stabilization has normally not been too good so that one may not safely assume a straight arc column. Thus, side-on measurements are normally given the first consideration in high-precision experiments. Another advantage of side-on measurements is that temperatures and densities over an extended range corresponding to the different radial layers are obtained simultaneously.

For the following, the arc plasma is assumed to be a circular disk in the x - y plane of thickness Δz , which is determined by the height of the spectrometer slit. It is further assumed that the radiation is isotropic and that there is no absorption (optically thin layer). Then, with an emission coefficient ϵ (energy radiated per unit volume, time, and solid angle), the total intensity L emitted in the y direction as a function of position x becomes, as seen from Fig. 4,

$$L(x) \Delta z = \Delta z \int_{-y_0}^{+y_0} \epsilon(r) dy. \quad (10.1)$$

Application of the rotational symmetry of the arc and substitution of $(r^2 - x^2)^{1/2}$ for y results in

$$L(x) = \int_x^{r_0} \frac{\epsilon(r) r dr}{(r^2 - x^2)^{1/2}}, \quad (10.2)$$

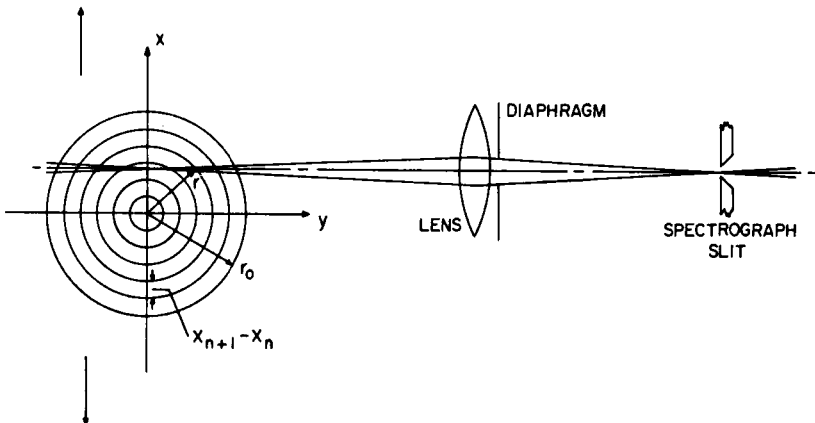


FIG. 4. Schematic optical arrangement for side-on arc observations.

where r_0 is the radius of the arc. This is a special form of Abel's integral equation and has the solution^{20, 21}

$$\epsilon(r) = -\frac{1}{\pi} \int_r^{r_0} \frac{(dL/dx) dx}{(x^2 - r^2)^{1/2}}. \quad (10.3)$$

Many different practical solutions for the evaluation of $\epsilon(r)$ have been reported in the literature.²²⁻³⁴ Since the experimental intensity curves $L(x)$ or the equivalent set of discrete numerical data for various positions x may not normally be obtained in analytical form, Eq. (10.3) [or Eq. (10.2)] must be either solved numerically²²⁻³⁰ or else the experimental curve must be approximated by a series of functions, e.g., a power series, which then may be integrated in analytical form.³¹⁻³⁴ Both approaches have found many applications.

In the first approach, i.e., the numerical solution of Eq. (10.3), the x axis and hence r is subdivided into a large number of equal increments, so that $x_n = kr_0/n$ with $k = 1, 2, \dots, n$ and $r_j = jr_0/n$ with $j = 1, 2, \dots, n$. In each interval $x_n - x_{n-1}$ the experimental curve $L(x)$ is replaced by an approximate simple function, for example a polynomial, or in the simplest approach it is set constant.²⁴

The integral equation, Eq. (10.3), may then be replaced by a sum of subintegrals. Analytical integration of the subintegrals over each zone may be performed and leads always to a solution of the form

$$\epsilon_j = r_0^{-1} \sum_k a_{jk} L_k. \quad (10.4)$$

Different sets of coefficients a_{jk} have been tabulated, which depend on the various degrees of refinement used for the representation of L_k and the

²⁰ E. C. Titchmarsh, "Introduction to the Theory of Fourier Integrals," 2nd ed. Oxford Univ. Press, New York, 1948; L. A. Pipes, "Applied Mathematics for Engineers and Physicists," 2nd ed. McGraw-Hill, New York, 1964.

²¹ H. R. Griem, "Plasma Spectroscopy," McGraw-Hill, New York, 1964.

²² H. Hörmann, *Z. Physik* **97**, 539 (1935).

²³ O. H. Nestor and H. N. Olsen, *SIAM Rev.* **2**, 200 (1960).

²⁴ H. Maecker, *Z. Physik* **136**, 119 (1953); **139**, 448 (1954).

²⁵ W. J. Pearce, *Proc. Conf. Extremely High Temp., Boston 1958* (H. Fischer and L. C. Mansur, eds.), p. 123. Wiley, New York, 1958.

²⁶ J. Friedrich, *Ann. Physik* [7] **3**, 327 (1959).

²⁷ W. L. Barr, *J. Opt. Soc. Am.* **52**, 885 (1962).

²⁸ K. Bockasten, *J. Opt. Soc. Am.* **51**, 943 (1961).

²⁹ H. Edels, K. Hearne, and A. Young, *J. Math. and Phys.* **41**, 62 (1962).

³⁰ W. Frie, *Ann. Physik* [7] **10**, 332 (1963).

³¹ M. P. Freeman and S. Katz, *J. Opt. Soc. Am.* **50**, 826 (1960).

³² S. I. Herlitz, *Arkiv Fysik* **23**, 571 (1963).

³³ R. N. Bracewell, *Australian J. Phys.* **9**, 198 (1956).

³⁴ C. R. Yokley and J. B. Shumaker, *Rev. Sci. Instr.* **34**, 551 (1963).

number of intervals employed (the normal range for n is between 10 and 40).

In the other approach, the approximate analytical solution, the experimental data $L(x)$ are first fitted by a least-squares program to a simple function like a polynomial³¹ or a Chebychev function.³² This in turn permits analytical integration of Eq. (10.3). For example, a power series of the form

$$L(x) = \sum_{i=0}^m F_i(r_0^2 - x^2)^i \quad (10.5)$$

has given excellent results. It has been found that $m = 6$ provides a very accurate representation for all cases of practical interest. Higher-order polynomials, even up to $m = 12$, give only insignificant improvement in the precision.

The numerical approaches have been the first which were employed and described in the literature. Among them, Bockasten's method²⁸ must be considered the most precise one. If the noise in the data is fairly large, say of the order of 1% or more, preference should be given to the approach of Barr,²⁷ which is designed to be relatively insensitive to random errors.

It is evident from Eq. (10.4) that the numerical effort for obtaining $\epsilon(r)$ becomes quite formidable if high precision is to be obtained or, in other words, if a fine zoning grid with many increments x_n or r_j has to be chosen.† Fortunately, with the advent of electronic computers the earlier existing need for compromises between time invested and precision has been largely eliminated. In cases where high experimental precision is obtained and needs to be preserved to the fullest extent, the best solution evidently is to employ a large digital computer. In other cases where high precision is not quite as critical, analog computers designed especially for Abel inversion calculations are of great convenience.³⁵⁻³⁷

Even if the transformation scheme is programmed for a digital or an analog computer, the amount of labor and time required to transfer and adapt the experimental data to the computer input is still appreciable. Thus for precise high-volume work, fully automatic data processing systems have been developed.^{34, 38, 39} Two basically different systems have been reported: analog^{34, 38} and analog-to-digital³⁹ systems. While the former may

³⁵ G. Boldt, Tech. Rept., Max Planck Inst., Munich, 1961.

³⁶ L. Becker and H. W. Drawin, *Z. Instrumentenk.* **72**, 251 (1964).

³⁷ W. Bötticher and K. J. Repenning, *Z. Angew. Phys.* **14**, 536 (1962).

³⁸ J. B. Shurnaker, Jr. and C. R. Yokley, *Appl. Opt.* **3**, 83 (1964).

³⁹ D. R. Paquette and W. L. Wiese, *Appl. Opt.* **3**, 294 (1964).

† This of course is meaningful only if the experimental data $I(x)$ are sufficiently precise.

be readily linked with an analog computer and designed in such a way that it records—in conjunction with a spectrometer scanning in wavelength—radially resolved spectra instantly in the laboratory, the second system may do this only to a certain degree if it is hooked up with a digital computer. On the other hand, the digital system is inherently capable of higher accuracy. Its laboratory part is basically a preprogrammed multichannel data recorder, where the data channel contains an integrating analog-to-digital voltmeter for the conversion of the photomultiplier signals, and the other channels record auxiliary information pertaining to the identification and enumeration of the data. The channel transfer to paper tape is accomplished via a high-speed (10 μ sec) solid-state shift register to allow continuous recording of the signal without appreciable dead time. The tape output is made compatible with a digital computer.

With the just-mentioned automatic data processing systems, curve fitting methods have been exclusively used, since they are much more adaptable and flexible for handling large amounts of data, and, furthermore, various computer programs for curve fitting techniques exist and data noise is effectively smoothed.

The foregoing discussion has assumed perfect rotational symmetry in the arc sources. This condition needs to be always checked and has been found very closely fulfilled only for the wall-stabilized arc sources. Freeman and Katz, in two recent papers,^{31, 40} have discussed solutions for the generalized case of a slight asymmetry in the arc and also for the case of some self-absorption.[†]

10.3. Temperature and Density Determinations

Many methods have been developed to determine temperatures and densities in arc sources. The most successful and consequently most widely applied techniques are the spectroscopic ones, which are based on the interpretation of line and continuum radiation. These methods are particularly attractive because they do not interfere with the arc discharge and they are readily applied due to the strong arc radiation.

The formula for the intensity of a spectral line is of central importance and has found many applications. This relation, applied to a line of chemical

⁴⁰ M. P. Freeman and S. Katz, *J. Opt. Soc. Am.* **53**, 1172 (1963).

[†] Recently P. Elder, J. Jerrick, and J. W. Birkeland (*Appl. Optics* **4**, 589 (1965)) have described an iterative Abel inversion technique which may be used in cases with higher self-absorption.

element a and stage of ionization z which is emitted from a homogeneous plasma source of length l , may be written as

$$I_{ki} = \int_{-\infty}^{+\infty} I(\lambda) d\lambda = \frac{1}{4\pi} \frac{hc}{\lambda_0} A_{ki} N_{k,a}^{(z)} l \quad (10.6)$$

[see also Eq. (2.1.8) of Chapter 2.1, where the other symbols are explained]. By combining it with Eq. (2.1.9), one obtains

$$I_{ki} = \frac{1}{4\pi} \frac{hc}{\lambda_0} A_{ki} N_a^{(z)} (g_k / U(T)_a^{(z)}) l \exp(-E_k / k_B T). \quad (10.7)$$

This formula (as well as most other relations still to be discussed) is valid for the case of emission from an optically thin layer and under the assumption that the arc source is in local thermal equilibrium (LTE). In the following, both conditions are assumed to be fulfilled unless it is explicitly stated otherwise. The validity criteria and experimental investigations on LTE will be examined and discussed in Chapter 10.4 and tests for the optically thin condition will be discussed in Section 10.3.1.2.

The frequently applied temperature measurement methods are now described in order of increasing complexity. They may be divided into two categories. First, there are some methods which permit direct temperature determinations without knowledge of densities. Second, there is another, normally more powerful class of temperature measurement methods for which also the knowledge of the electron density or an atomic density is required.

10.3.1. Temperature Determinations without Knowledge of Densities

10.3.1.1. Relative Line Intensities within the Same Atomic Species. By rearranging Eq. (10.7), so that all quantities related to an individual line except its upper energy level E_k appear on the same side, one obtains

$$\frac{I_{ki} \lambda_0}{A_{ki} g_k} = \exp\left(-\frac{E_k}{k_B T}\right) \frac{1}{4\pi} \frac{hcN_a^{(z)}}{U(T)_a^{(z)}} l = \exp\left(-\frac{E_k}{k_B T}\right) \times C, \quad (10.8)$$

where for a given temperature C is a constant for all lines within an atomic species (i.e., for neutral atoms of element a , singly ionized atoms, etc.). Conversion to a logarithmic scale results in

$$\log_e \left(\frac{I_{ki} \lambda_0}{A_{ki} g_k} \right) = -\frac{E_k}{k_B T} + \log_e C. \quad (10.9)$$

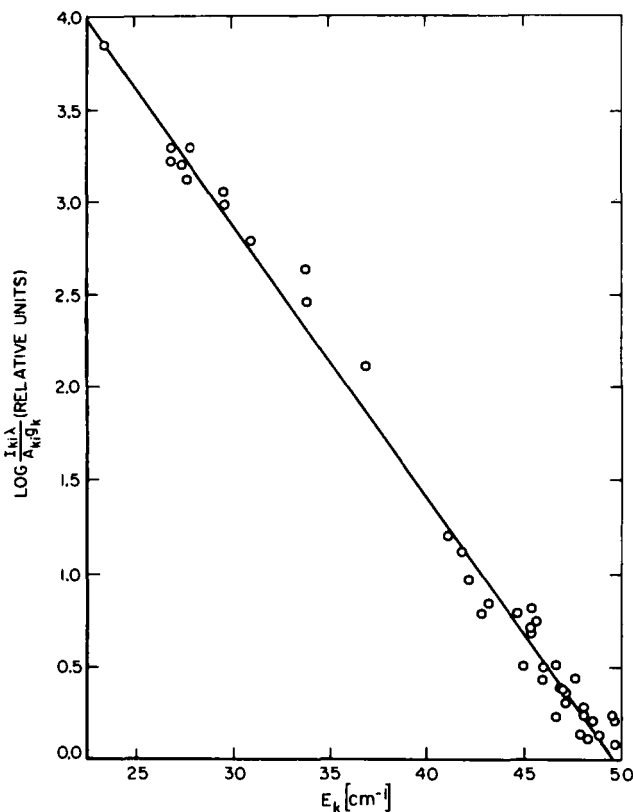


FIG. 5. Illustration of temperature determination using relative line intensities within the same species. A 10-A arc in air with copper electrodes has been used into which a trace of Cr has been admixed [C. H. Corliss, *Astrophys. J.* **136**, 916 (1962)]. The Cr I line intensities give a temperature of 4280°K.

This may be interpreted as the equation for a straight line with E_k as variable and a slope of $-1/k_B T$, from which the temperature may be determined. Thus, for the application of this method relative intensity measurements of a number of lines with various known energy levels E_k and (relative) transition probabilities A_{kt} are needed. To obtain high precision, the excitation potentials E_k should be spread out over a significant energy range, as shown in Fig. 5, which illustrates this method for the case of a low-current atmospheric arc into which a trace of chromium has been introduced.⁴¹

⁴¹ C. H. Corliss, *Astrophys. J.* **136**, 916 (1962).

This is probably the oldest and most often applied spectroscopic temperature determination. Wavelengths, energy level data, and statistical weights g (related to the total angular momentum quantum number J by $g = 2J + 1$) are readily available for thousands of lines to a very high precision.⁴² However, the numerical material for transition probabilities is still scarce.⁴³ Their availability will be consequently the decisive factor for the application of this method. In addition, they are usually not too reliable so that they may often be the limiting factor in determining the accuracy. A favorable circumstance is that transition probabilities are only required on a relative scale. The relative values are often much more accurate than absolute values, especially when they are from experimental sources (see Chapter 2.1).

Since the energy range for the bulk of excited atomic energy levels of a species is normally quite small, except for the transition elements, this method is not a very sensitive one. Its over-all accuracy is usually not better than 5%, although in exceptional cases it may be as good as 1%. For the transition elements, e.g., elements of the iron group, this approach is particularly suitable, because of the richness of their spectra and the relatively wide range of energy levels (see Fig. 5). But at present it still suffers from the large uncertainties in the transition probability data.

Quite similar is another technique to determine the temperature from relative intensity measurements of the lines of a rotational molecular band. This method is capable of higher precision, since within a band the transition probabilities are constant and the line intensities are proportional to the rotational quantum numbers. However, this method has found only a very limited range of applications because most molecules are dissociated at the high temperatures encountered in the arc column. Very few applications have been reported in the literature.⁴⁴

10.3.1.2. Peak Intensities of Optically Thick Lines. While the above-discussed method has a wide range of applications, the following approach is more restricted. First, its application is limited to homogeneous plasma

⁴² C. E. Moore, A multiplet table of astrophysical interest, rev. ed., *Natl. Bur. Std. (U.S.) Tech. Note* 36 (1959); An ultraviolet multiplet table, *Natl. Bur. Std. (U.S.) Circ.* No. 488, Sec. 1 (1950), Sec. 2 (1952), Secs. 3-5 (1962); Selected tables of atomic spectra, *NSRDS-Natl. Bur. Std.* 3, Sec. 1 (1965); Atomic energy levels, *Natl. Bur. Std. (U.S.) Circ.* No. 467, Vol. I (1949), Vol. II (1952), Vol. III (1958). All available from the U.S. Govt. Printing Office, Washington, D.C.

⁴³ B. M. Glennon and W. L. Wiese, Bibliography on atomic transition probabilities, *Natl. Bur. Std. (U.S.) Misc. Publ.* No. 278 (1966), and Supplement (1968); W. L. Wiese, M. W. Smith, and B. M. Glennon, Atomic transition probabilities, *NSRDS-Natl. Bur. Std.* 4 (1966) (Elements H through Ne). Available from the U.S. Govt. Printing Office, Washington, D.C.

⁴⁴ W. Lochte-Holtgreven and H. Maecker, *Z. Physik* 105, 1 (1937); L. S. Ornstein and H. Brinkman, *Proc. Koninkl. Akad. Wetenschap. Amsterdam* 34, 498 (1931).

layers, which means that it can be applied only in end-on arc observations. Second, spectral lines have to be found that are optically thick or completely self-absorbed in their central parts. (This means that sufficient spectral resolution must be provided to resolve the profile of the line.) The probability of self-absorption is normally very high for the strongest lines in a spectrum, especially if the source conditions are such that the lower energy level is strongly populated.

The equation of radiative transfer for a *homogeneous* plasma column of length l may be written in its integrated form as

$$I(\lambda) = B_T(\lambda) [1 - \exp(-\kappa(\lambda) l)]. \quad (10.10)$$

$I(\lambda)$ is again the intensity per unit wavelength interval, $\kappa(\lambda)$ is the (effective) absorption coefficient, and $B_T(\lambda)$ the Planck function. The product $\kappa(\lambda) l$ is called the optical depth τ . For very large optical depths one obtains

$$\lim_{\tau \rightarrow \infty} I(\lambda) = B_T(\lambda) = \frac{2hc^2}{\lambda^5} \frac{1}{\exp\left(\frac{hc}{\lambda k_B T}\right) - 1}. \quad (10.11)$$

Thus an absolute intensity measurement in the central wavelength interval of a line that approaches an optical depth of infinity may be simply used in conjunction with Planck's law to obtain the temperature (optically thick case). An example of a measurement is presented in Fig. 6 for the hydrogen line H_α . This line was emitted end-on by a pure hydrogen plasma generated in a wall-stabilized arc. The line has lost its characteristic shape for its central part, has assumed a flat top and follows the black-body curve over a wavelength interval of several angstroms. Within this interval, the absorption coefficient varies from large values [$\kappa(\lambda) l > 1$] to the highest values [$\kappa(\lambda) l \rightarrow \infty$] at the line center, and consequently the dominant intensity contributions for the various wavelength positions come from different depths of the plasma. The flatness of the region indicates a good axial homogeneity of the arc source.

Two approaches are used to determine if the center of a strong line is optically thick. First, one may scan the profile of the same line end-on as well as side-on, i.e., at two very different plasma lengths l , and observe if at a certain wavelength distance from the line center the intensity ratio becomes significantly less than the geometrical ratio $l_{\text{end-on}}/l_{\text{side-on}}$. From this point on towards the line center self-absorption becomes significant and the end-on line intensity approaches the black-body limit. An example is given by Jürgens.⁴⁵ Second, one may place a concave mirror into the extension of the optical axis to reflect the image of the arc back into the source and measure the intensity increase while scanning across the line.

⁴⁵ G. Jürgens, *Z. Physik* **134**, 21 (1952).

This method of temperature determination does not rank among the very precise ones, principally because of the following reasons: for lines in the visible or near ultraviolet, the black-body intensity is not a strong function of temperature at typical arc conditions. This may be readily seen by deriving the relative temperature error from Eq. (10.11),

$$\frac{dT}{T} = \frac{\lambda k_B T}{hc} \times \frac{dI(\lambda)}{I(\lambda)} = p \frac{dI(\lambda)}{I(\lambda)}. \quad (10.12)$$

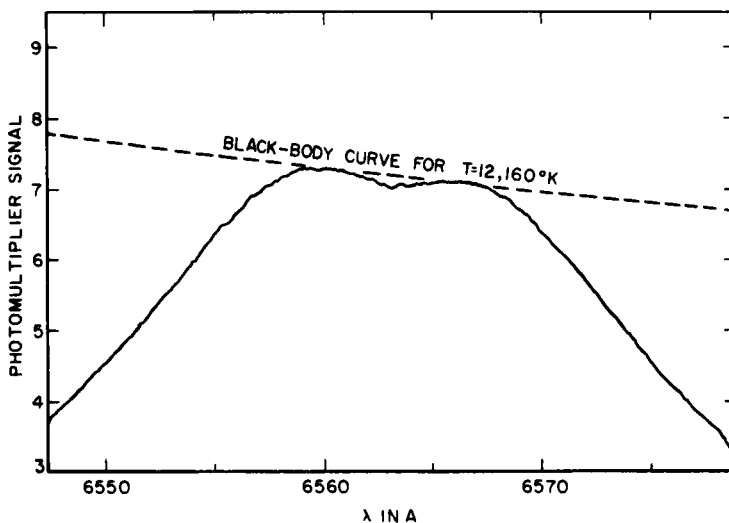


FIG. 6. Illustration of temperature determination using the peak intensity of an optically thick line. The graph shows a photoelectric recording of the central part of H_{α} , emitted end-on from a wall-stabilized arc. The slight dip in the line center is due to traces of hydrogen in the cooler electrode regions which are blanketed by argon [after W. L. Wiese, D. R. Paquette, and J. E. Solarski, Jr., *Phys. Rev.* **219**, 1225 (1962)].

For an arc temperature of 1.2×10^4 °K and wavelengths in the visible, i.e., $4000 \text{ \AA} < \lambda < 7500 \text{ \AA}$, the factor p assumes values between 0.33 and 0.63. Since uncertainties in the intensity measurements are difficult to keep below a few percent, and uncertainties in the radiation standards, including possible discrepancies between the thermodynamic and the international practical temperature scale (IPTS), are also of the same order of magnitude,⁴⁶ the relative uncertainties dT/T may be at best as low as 2%, but are normally more like 5%.

⁴⁶ H. J. Kostkowski and R. D. Lee, Theory and methods of optical pyrometry, *Natl. Bur. Std. (U.S.) Monograph No. 41* (1962).

This method becomes evidently more sensitive for lines in the vacuum ultraviolet, but there are no suitable radiation standards available for this region as yet. For this reason Boldt¹⁹ has inverted the method and has used optically thick lines as radiation standards in conjunction with a temperature measurement obtained by some other technique.

The above-discussed checks for determining the optical depth of a line may also be used to verify the optically thin condition assumed, e.g., in Eqs. (10.6) and (10.7). In this case of $\tau(\lambda) \rightarrow 0$ one obtains

$$\lim_{\tau(\lambda) \rightarrow 0} I(\lambda) = B_T(\lambda) \kappa(\lambda) l = \epsilon(\lambda, T) l, \quad (10.13)$$

using Kirchhoff's law [$\epsilon(\lambda, T)$ is the emission coefficient]. The required proportionality between $I(\lambda)$ and the depth l of an arc plasma may be readily checked with the previously quoted mirror arrangement if the line profile can be resolved.

For unresolved line profiles, however, the optical depth $\kappa(\lambda)l$ and thus the absorption-coefficient $\kappa(\lambda)$ at peak intensity must be found from calculations. An upper limit for τ is obtained if one assumes that only Doppler broadening is present. In this case the absorption coefficient is readily calculated, provided certain plasma quantities and the f -value are known.⁴⁷ However, if for the upper limit the condition $\tau \ll 1$ is not fulfilled, the line may nevertheless be subject to significant additional broadening, particularly due to the interatomic Stark effect, so that it is optically thin everywhere. This may be ascertained with more elaborate estimates by including the additional broadening mechanism. Absorption coefficients for many Stark-broadened lines may be derived by utilizing recent numerical material.²¹

10.3.1.3. Special Methods. Besides the above two methods which have found many applications, some other approaches are occasionally applied, when special suitable conditions exist in the arc source. For example, Burhorn⁴⁸ determined the temperature of a low-current iron arc from the Doppler half-widths of some iron lines by employing the relation⁴⁹

$$\Delta\lambda_{1/2}^{\text{Dopp}} = 7.16 \times 10^{-7} \lambda(T/\mu)^{1/2}, \quad (10.14)$$

where μ is the atomic weight of the species. ($\Delta\lambda_{1/2}^{\text{Dopp}}$ is obtained in angstroms if λ is in angstroms and T is in degrees Kelvin.)

Normally this method cannot be applied, since pressure broadening, particularly Stark broadening, produces the dominant contribution to the line widths in arc plasmas. Doppler broadening is usually a small effect, so

⁴⁷ See, e.g., G. D. Bell, D. R. Paquette, and W. L. Wiese, *Astrophys. J.* **143**, 559 (1966).

⁴⁸ F. Burhorn, *Z. Physik* **140**, 440 (1955).

⁴⁹ See, e.g., W. L. Wiese, in "Plasma Diagnostic Techniques" (R. H. Huddlestone and S. L. Leonard, eds.), Chapter 6. Academic Press, New York, 1965.

that the Doppler widths may not be obtained from the observed widths with sufficient accuracy. However, for elements of the iron group, certain lines originate and end in levels of the inner half-filled $3d$ electron shell. Here the situation is different. Very effective shielding occurs from the $4s$ electrons against external fields, the lines are very narrow, and are predominantly broadened by thermal Doppler effect. Of course, high-resolution spectroscopic equipment must be employed to make the effects of instrumental broadening negligible. Burhorn⁴⁸ combined therefore a Fabry-Perot interferometer with a spectrograph. His measured half-widths were typically of the order of 0.05 \AA , and resulted in a kinetic temperature of 6300°K .

Another approach which may be of particular value for high-pressure arcs is the temperature determination from the maxima of self-reversed lines. It employs the same principal idea as the method described under Section 10.3.1.2, but with the difference that now the emission from an inhomogeneous plasma layer is analyzed, as is the case for side-on observations. The rather complex theory has been developed by Bartels,⁵⁰ and an application for a high-pressure mercury arc is reported by Göing.⁵¹ Still other very specialized techniques are described by Finkelnburg and Maecker.¹

Finally, a few comments may also be in order about a temperature measurement method that is still in the development stage, but carries significant future potential. This method, proposed by Burgess⁵² and Burgess and Cooper,^{52a} is based on the measurement of the ratio between the width and the shift of a Stark-broadened line of a heavier element. While the shift and width are functions of temperature and electron density, their ratio is a function of temperature only. The method may find many future applications, but its usefulness is at the present time very severely limited by our inadequate knowledge of Stark-broadening parameters, particularly reliable Stark shifts. (This scheme is not applicable to hydrogenic lines which do not exhibit shifts.) The errors in the theoretical parameters, i.e., the shifts and to a lesser degree the widths, are rarely below 10% ^{21, 49} and thus make precise temperature determinations at the present time practically impossible. But some fairly precise experimental width and shift data have become available recently, e.g., for O I⁵³ and Ar I,⁵⁴ and more are expected in the near future.

⁵⁰ H. Bartels, *Z. Physik* **127**, 243; **128**, 546 (1950).

⁵¹ W. Göing, *Z. Physik* **131**, 603 (1952).

⁵² D. D. Burgess, *Phys. Letters* **10**, 286 (1964).

^{52a} D. D. Burgess and J. Cooper, *Proc. Phys. Soc. (London)* **86**, 1333 (1965).

⁵³ W. L. Wiese and P. W. Murphy, *Phys. Rev.* **131**, 2108 (1963).

⁵⁴ C. H. Popenoe and J. B. Shumaker, Jr., *J. Res. Natl. Bur. Std.* **A69**, 495 (1965).

10.3.2. Temperature Determinations Involving the Knowledge of Densities

Some of the most powerful and general methods of temperature measurement require the knowledge of particle densities. For one-element plasmas, these methods permit the simultaneous self-consistent determination of temperatures and densities, if also the plasma equilibrium relations are utilized. The measurement of only one suitable spectroscopic quantity, even one which yields primarily a density, is then sufficient for the temperature determination. We shall therefore first discuss all important temperature and density determinations for the instructive case of one-element plasmas. We shall see later that for the general case of multi-element plasmas many of these approaches remain applicable, but some with modified objectives.

As an essential part of these methods, a set of equilibrium and conservation equations is employed. The equations are Dalton's law (conservation of particles),

$$P = k_B T(N_e + \sum_z N_a^{(z)}), \quad (10.15)$$

the condition of local electrical neutrality,

$$\sum_z z N_a^{(z)} = N_e, \quad (10.16)$$

and chemical equilibrium expressions,

$$N_B N_C / N_A = Q_B Q_C / Q_A, \quad (10.17)$$

for reversible reactions of the type $A \rightleftharpoons B + C$, i.e., principally ionization. P is the total pressure (which is readily measured); $N^{(z)}$ is the number density of the ion of charge z ($z = 0$ for neutral, $z = 1$ for singly ionized atoms, etc.); N_e is the electron density; a denotes the chemical element, and Q_A is the partition function (translational and internal) per unit volume for the constituent A, etc. For many arc plasmas, dissociation is practically complete and only the ionization reactions have to be considered. Then Eq. (10.17) becomes specifically the Saha equation†

$$\frac{N_a^{(z+1)} N_e}{N_a^{(z)}} = 2 \frac{U(T)_a^{(z+1)}}{U(T)_a^{(z)}} \left(\frac{2\pi m_e k_B T}{h^2} \right)^{3/2} \exp\left(-\frac{\chi_{\text{eff}, a}^{(z)}}{k_B T}\right). \quad (10.18)$$

$U(T)_a^{(z)}$ and $U(T)_a^{(z+1)}$ are the internal partition functions of ions of charges z and $z + 1$ [see also Eq. (2.1.10) in volume 7A], i.e.,

$$U(T)^{(z)} = \sum_{k=0}^{k^*} g_k^{(z)} \exp(-E_k^{(z)}/k_B T), \quad (10.19)$$

† Analogous relationships apply to dissociation reactions.

where $g_k^{(z)}$ is the statistical weight and $E_k^{(z)}$ the excitation potential of atomic level k of the ion of charge z (the two quantities are available from general spectroscopic tables⁴²⁾. The effective ionization potential χ_{eff} is given by

$$\chi_{\text{eff}} = \chi - \Delta\chi, \quad (10.20)$$

where χ is the unperturbed ionization potential [tabulated for various ions, e.g., in Ref. 42] and $\Delta\chi$ is the lowering of the ionization potential.

This lowering results from perturbations on the potential distribution of a plasma atom or ion by the surrounding free electrons and ions. As a consequence, atomic electrons in high quantum states may leave the atom and may be considered as free, if the Coulomb interaction energy becomes larger than the binding energy for these states.

The lowering of the ionization potential is the most important of the high-density effects in plasmas. The literature on this subject is quite extensive, and much of the discussion has centered around the question of whether only the collective effect from all charged particles has to be considered, which gives rise to a slight polarization of the plasma, or if also the "nearest-neighbor" interaction has to be included. It appears that under normal arc plasma conditions, i.e., below a critical electron density N_e^{cr} , the nearest-neighbor interaction has only the effect that a loosely bound electron may transfer from one ion to its nearest neighbor. This electron may therefore not be considered "free" in the sense that it contributes to the plasma pressure. (But it contributes to the electrical conductivity.) Recent summaries have been given by Griem,²¹ Ecker and Kröll,⁵⁵ McChesney,⁵⁶ and Cooper.⁵⁷ The Debye correction due to plasma polarization, first advanced by Rompe and Steenbeck,⁵⁸ and Theimer,⁵⁹

$$\Delta\chi^{(z)} = (z + 1)e^2\rho_D^{-1}, \quad (10.21)$$

is now the generally accepted result of the theoretical treatments for densities below N_e^{cr} . z is again the ionic charge and ρ_D is the Debye length, which is given by

$$\rho_D = \left[\frac{k_B T}{4\pi e^2 (N_e + \sum_{z,a} z^2 N_a^{(z)})} \right]^{1/2}. \quad (10.22)$$

The critical electron density is according to Duclos and Cambel⁶⁰ given by the condition

$$N_e^{\text{cr}} + \sum_{z,a} N_a^{(z)} = (8\pi\rho_D^3)^{-1}, \quad (10.23)$$

⁵⁵ G. Ecker and W. Kröll, *Phys. Fluids* **6**, 62 (1963).

⁵⁶ M. McChesney, *Can. J. Phys.* **42**, 2473 (1964).

⁵⁷ J. Cooper, *Rept. Progr. Phys.* **29**, 35 (1966).

⁵⁸ R. Rompe and M. Steenbeck, *Ergeb. Exakt. Naturw.* **18**, 257 (1939).

⁵⁹ O. Theimer, *Z. Naturforsch.* **12a**, 518 (1957); **13a**, 568 (1958).

where the summation is over all charged species, starting with $z = 1$. Ecker and Kröll⁵⁵ arrive at a similar result.

For arc plasmas the electron densities stay usually well below this critical density, which has, for example, the value $N_e^{\text{cr}} = 3.4 \times 10^{19} \text{ cm}^{-3}$ for a plasma at a temperature of $10,000^\circ\text{K}$ with only singly ionized atoms present. If N_e^{cr} should be surpassed, which is possible for very-high-pressure arcs, the nearest-neighbor effect comes into play and a different relation becomes valid. Details are found in the work of Ecker and Kröll⁵⁵ and Duclos and Cambel.⁶⁰

Experimental attempts to measure the amount of the lowering have been inconclusive until now, but are not inconsistent with the Debye result.^{61, 62}

For the calculation of the partition function (10.19) various procedures have been proposed, principally for obtaining the limiting level E_{k^*} . The generally used approach is to apply the unperturbed energy levels up to a limiting level E_{k^*} which is given by

$$E_{k^*} \leq \chi - \Delta\chi = \chi_{\text{eff}}, \quad (10.24)$$

where $\Delta\chi$ is the same as given in Eq. (10.21). There are other, more advanced calculations for the determination of the cut-off level available,⁵⁷ but in practice the differences among the different approaches are extremely small so that their application does not seem to be justified.

Still other high-density corrections enter into the equation of state, Eq. (10.15)—namely, a slight decrease of the plasma pressure due to the attraction of positive and negative charges—and into the line and continuum intensities—namely, shifts in the positions of atomic energy levels.²¹ However, these corrections are negligible for all practical situations and have usually not been considered. For example, under typical conditions ($N_e = 10^{17} \text{ cm}^{-3}$; $T = 10^4^\circ\text{K}$), the pressure correction amounts to about 0.5% for atmospheric pressure arcs.

In this connection it may be noted that additional small-pressure corrections in arcs may arise due to radial momentum transfer^{21, 63} or due to magnetic self-compression.¹ Both effects give contributions above 1% only for very-high-current arcs.

The above set of equilibrium and conservation equations shall be now applied to the determination of temperatures in one-element arc plasmas. As the first step, the plasma composition is normally calculated as a

⁵⁵ D. P. Duclos and A. B. Cambel, *Z. Naturforsch.* **16a**, 711 (1961).

⁶¹ W. L. Wiese and J. B. Shumaker, Jr., *J. Opt. Soc. Am.* **51**, 937 (1961).

⁶² H. N. Olsen, *Phys. Rev.* **124**, 1703 (1961).

⁶³ V. V. Yankow, *Soviet Phys. Tech. Phys. (English Transl.)* **6**, 965 (1962).

function of temperature. This is possible since in the system of Eqs. (10.15)–(10.17) the number of unknowns, i.e., the $N_a^{(z)}$, N_e , and T , exceeds the number of equations always only by one. For example, if neutral and singly and doubly ionized atoms of one element are present in significant quantities, Eqs. (10.15), (10.16), and two Saha-equations (10.18) are available, that is four equations for the four densities (including the electron density) and the temperature, so that the former may be expressed in terms of the latter. In solving the set of equations for the temperature, an iterative procedure has to be used since, to start with, numerical values for N_e have to be estimated and inserted in the high-density corrections. Usually one or two iterations are sufficient. A typical graphical presentation of such a solution, for the case of a pure argon plasma in temperature range 7500–25,000°K, is shown in Fig. 7.⁵⁴

To determine then the temperature, it is necessary to measure, as the second step, just one quantity that depends either solely on the temperature or on one of the densities or a combination of these.

10.3.2.1. Absolute Line Intensities. The intensity of a spectral line may be used for the temperature determination in a variety of ways. First, the most direct approach is to apply Eq. (10.7) in a straightforward way. But instead of solving it explicitly for T , it is more convenient and instructive to calculate the line intensity for a number of temperatures and construct the intensity versus temperature curve, as has been done in Fig. 8 for several argon lines by employing the density-temperature relationships of Fig. 7 and using available transition probabilities.⁶⁴ The graphical presentation shows instructively the most suitable temperature ranges for the various lines. For example, for the Ar I lines at 9123 and 6032 Å the upper limits would lie roughly at 14,000 and 15,000°K, respectively, while the lower temperature limits are given by the sensitivity of the experimental detection equipment. It may be observed from Fig. 8 that below the 14,000°K limit for the 9123 Å line an uncertainty of 10% in the intensity measurement leads to a temperature error of only 1.5% or less.

There are two major error contributions in this method. The first comes from uncertainties in the absolute intensity measurements, which are difficult to keep below 5%, even if the best radiation standards are employed and detailed corrections for the intensity contributions of the far line wings are made, as discussed in Ref. 49. The second contribution comes from uncertainties in the transition probabilities, which have to be available on an absolute scale. The majority of these values for lighter

⁶⁴ W. E. Gericke, *Z. Astrophys.* **53**, 68 (1961); J. B. Shumaker and C. H. Popenoe, *J. Opt. Soc. Am.* **57**, 8 (1967); H. N. Olsen, *J. Quant. Spectry. & Radiative Transfer* **3**, 59 (1963) (for Ar II only).

elements is still uncertain to about 25%,⁴³ and for heavier elements the uncertainties increase quite drastically. Consequently, the relative temperature error, approximately given by

$$\frac{\Delta T}{T} = \pm \frac{k_B T}{E_k} \left(\frac{\Delta I_{kt}}{I_{kt}} + \frac{\Delta A_{kt}}{A_{kt}} \right), \quad (10.25)$$

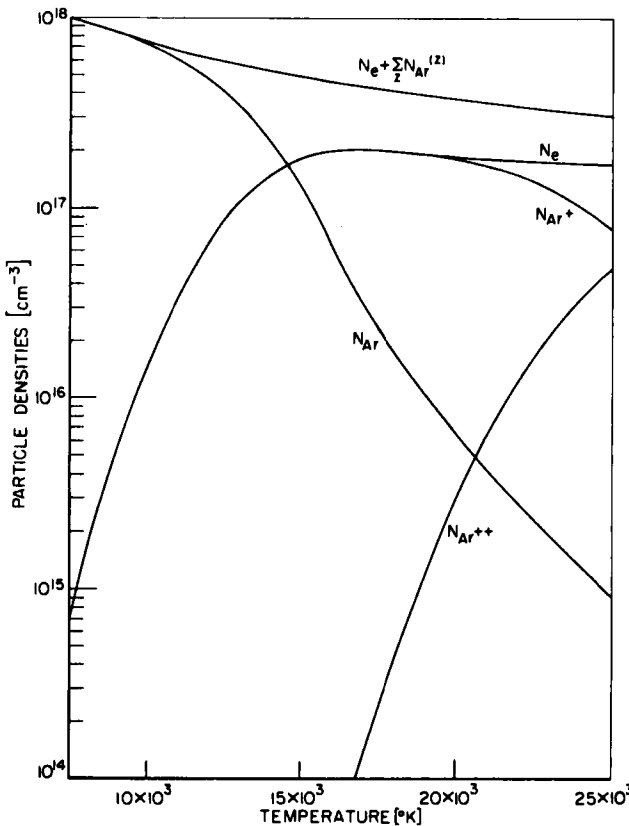


FIG. 7. Particle densities in an argon plasma at atmospheric pressure as functions of temperature.

amounts usually to about 3% for most of the higher excited lines of the lighter elements and up to 10% or more for the heavier elements. However, one may sometimes be able to select prominent lines within a spectrum with transition probability errors as small as 10% (e.g., for N, O, and Ne),⁴³ in which case uncertainties in the temperature may be decreased to about 1%.

10.3.2.2. Intensity Ratio of Lines of Subsequent Ionization Stages within the Same Element. For this slightly different approach, Eq. (10.7) is applied to two lines L and L' of successive stages of ionization z and $z + 1$ of the same element. In arcs principally the case of neutral ($z = 0$) and singly ionized atoms ($z = 1$) is encountered. The intensity ratio follows from Eqs. (10.7) and (10.18) as

$$\frac{I_{L'}^{(z+1)}}{I_L^{(z)}} = 2 \left(\frac{2\pi m_e k_B T}{h^2} \right)^{3/2} \frac{A_{L'} \lambda_L g_{k'}^{L'} 1}{A_L \lambda_L g_k^L N_e} \exp\left(\frac{E_k^L - E_k^{L'} - \chi_{\text{eff}}^{(z)}}{k_B T}\right). \quad (10.26)$$

(The element index has been omitted.) Because of the rather different temperature dependence for the intensities of lines of subsequent stages of ionization, which arises from the large energy difference $E_k^{(z)} - E_k^{(z+1)}$, this

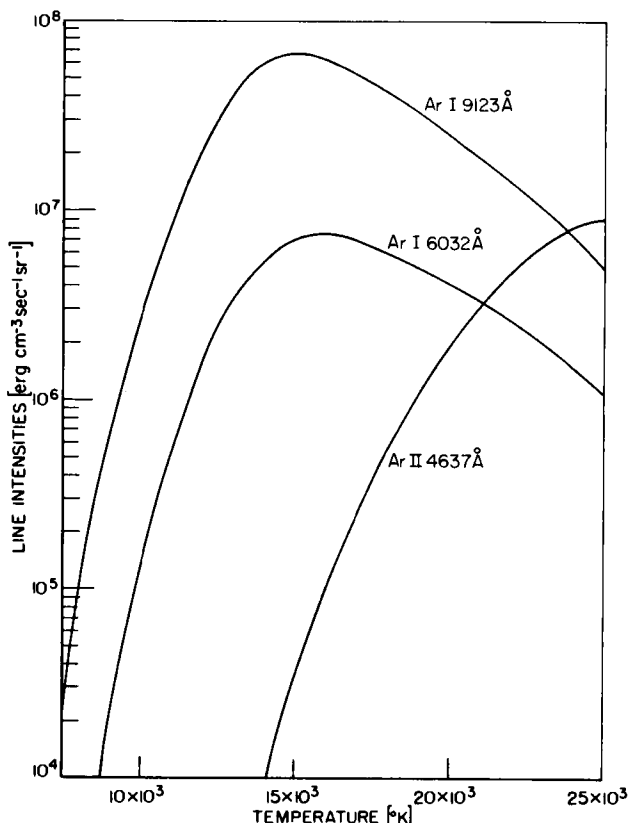


FIG. 8. Intensities of atomic and ionic argon lines as functions of temperature for an atmospheric argon plasma.

method is much more sensitive and precise than the earlier discussed, somewhat similar method based on the intensity ratios between lines of the same stage of ionization (Section 10.3.1.1). In the former case the various lines exhibit quite similar behavior with temperature. The main advantage of the present method is that only relative intensities are required. However, for the limited range of arc temperatures it is difficult to obtain strongly excited ionic lines. Only occasional applications have been reported.²⁴

A method very similar in principle would be to utilize the intensity ratio between a line and the continuum. No applications have been reported as yet, due to the scarcity of the relevant continuum data.

10.3.2.3. The Modified Fowler-Milne Method. The population of any excited atomic or ionic state [Eq. (2.1.9)] reaches a maximum at a certain temperature T_M , where the increase due to the term $\exp(-E_k/k_B T)$ is balanced by the decrease in $N_a^{(z)}/U(T)_a^{(z)}$. Beyond T_M the term $N_a^{(z)}/U(T)_a^{(z)}$ decreases rapidly due to thermal ionization, which strongly diminishes the number density of the species of charge z . This dependence is of course reflected in the line intensity versus temperature curves, as, e.g., seen in Fig. 8, where all line intensities run through maxima.

This intensity maximum may be exploited for temperature measurements, because if the temperature at the arc axis is higher than T_M for a line, the peak intensity is reached at some radial distance, and the temperature at this position may be identified with the "maximum" temperature T_M . Starting from this point the whole radial temperature distribution may be then obtained by measuring the line intensities at other positions in terms of the maximum intensity and by comparing the fractional intensities with those calculated for various temperatures below and above T_M .

Fowler and Milne⁶⁵ developed this method first for temperature determinations in stellar atmospheres, and Larenz⁶⁶ modified it later for arc sources. Typical applications are those of Olsen,⁷ Burhorn *et al.*¹² and Larenz.⁶⁷

This technique provides accurate results because it does not require knowledge of transition probabilities and involves only relative intensity measurements. However, its range of application is severely limited by the condition that the temperature at the arc axis must be higher than T_M . This is difficult to fulfill for many lighter elements, where the temperatures T_M are typically between 15,000 and 20,000°K, i.e., at the upper end of

⁶⁵ R. H. Fowler and E. A. Milne, *Monthly Notices Roy. Astron. Soc.* **83**, 403 (1923); **84**, 499 (1924).

⁶⁶ R. W. Larenz, *Z. Physik* **129**, 327 (1951).

⁶⁷ R. W. Larenz, *Z. Physik* **129**, 343 (1951).

the useful temperature range of arcs. Also, this method becomes unreliable for multielement plasmas due to local demixing effects (see Section 10.3.4).

In a recent application by Richter,⁶⁸ the Fowler-Milne method is generalized further. Again the fact is employed that the functional relationship between line or continuum intensity and temperature changes drastically as one approaches T_M .

10.3.3. Density Determinations

10.3.3.1. Stark Widths and Shifts. The number of suitable density measurement methods is much smaller than the number of temperature determinations. Among them, the most powerful and convenient approach to determine electron (or ion) densities in arcs is to apply line-broadening theory to measured line widths, especially since the recent theoretical advances by Griem and others.²¹

At the fairly high electron densities of typical arc plasmas, spectral lines are predominantly broadened by interatomic Stark effect due to the electric microfields of the electrons and ions surrounding the emitting atoms. It is evident that the line widths depend then primarily on the density of the perturbing particles. For hydrogen and hydrogenlike lines the electron density and the full half-width (i.e., the width at half-maximum intensity) of a Stark-broadened line are related by

$$N_e = C(N_e, T) (\Delta\lambda_{1/2})^{3/2}. \quad (10.27)$$

The coefficients $C(N_e, T)$, which depend only weakly on the electron density and temperature, are tabulated by Griem²¹ for a number of hydrogen and hydrogenlike lines for various electron densities and temperatures. For the most important Balmer line H_β this relationship is graphically presented in Fig. 9. It should be noted that at a given electron density the variation of width with temperature over the range from 5000 to 40,000°K is so small that it is within the thickness of the drawn line.

Figure 9 shows that for the range of electron densities encountered in stabilized arcs, typically from 10^{15} to 10^{17} cm^{-3} , the Stark half-width of H_β becomes appreciable and is precisely measurable even with fairly low resolution spectrometers. On the other hand, the Doppler half-width, namely 0.35 Å at $10^4 \text{ }^\circ\text{K}$ [Eq. (10.14)], is negligible for all practical purposes. Since, furthermore, experimental comparison studies^{18, 69} have borne out that the Stark-broadening calculations of Griem *et al.*⁷⁰ describe the H_β profile exceedingly well, i.e., with an accuracy of a few percent for the half-width,

⁶⁸ J. Richter, *Z. Astrophys.* **61**, 57 (1965).

⁶⁹ E. A. McLean and S. A. Ramsden, *Phys. Rev.* **140**, A1122 (1965).

⁷⁰ H. R. Griem, A. C. Kolb, and K. Y. Shen, *Astrophys. J.* **135**, 272 (1962).

this method of determining the electron density has emerged as one of the most precise and convenient ones. (Further comments on the experimental comparison material are found in Section 10.5.3.)

Some experimentalists have therefore extensively employed half-width measurements of H_{β} for the determination of electron densities in stabilized

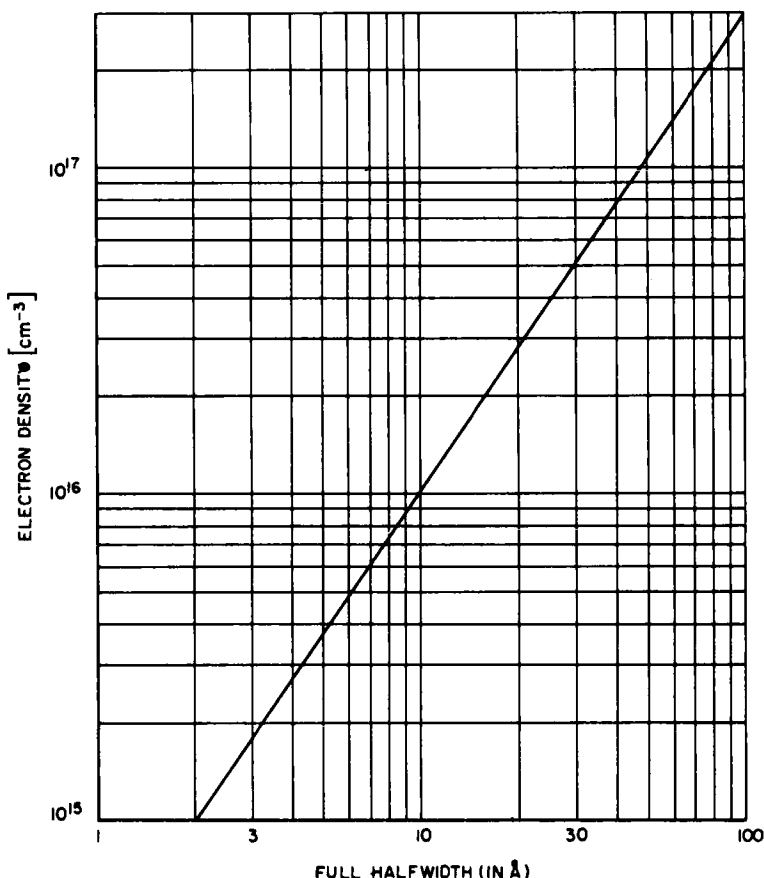


FIG. 9. Calculated (full) half-width of the Balmer line H_{β} as a function of electron density for temperatures between 5000 and 40,000°K.

arcs. It should be emphasized that this approach is not only applicable to one-element plasmas, but also to arc plasmas of arbitrary chemical composition. In the latter case a trace of hydrogen has to be added. Due to the strong intensity of H_{β} , a hydrogen ad-mixture of 1% will usually suffice, which will not significantly change the plasma properties.

If the H_{β} line cannot be observed due to lower or higher temperatures in the arc source, as, e.g., in low-current arcs, or if the H_{β} line should be strongly blended with other lines so that its profile may not be isolated (difference methods, measuring intensities with and without hydrogen added, are quite effective), one may utilize the Stark-broadened profiles either of other Balmer lines or of isolated lines of other elements. Stark-broadening parameters for these have also been calculated by Griem,^{21, 71} which, however, do not possess the same accuracy as those for the H_{β} line. In the case of isolated lines of heavier elements it has been found that the accuracy is vastly improved if the averaged result of several lines is employed.⁵³

Instead of using line widths, one may also employ the Stark shifts of isolated lines. This is even more attractive from the experimental point of view, but unfortunately the calculated shift parameters are at present quite unreliable.

For a one-element plasma one may also utilize line-width (or shift) measurements for indirect temperature determinations via the equilibrium and conservation relations [Eq. (10.15)–(10.17)]. In those temperature ranges where the degree of ionization increases rapidly, the electron density changes drastically with temperature, so that Stark-broadening measurements represent under these conditions one of the most precise approaches for temperature measurement in arcs. The accuracy may reach 1%, if the Balmer line H_{β} can be employed. Observation of H_{β} is again easily achieved by adding a trace of hydrogen to the one-element plasma. Several recent applications are reported in the literature.^{54, 61, 72}

10.3.3.2. Other Density Determinations. While there are several other methods to determine densities which have potentially wide ranges of applications, only a few actual measurements have been reported. For the continuum intensity measurements to be discussed below the principal setback is at present the scarcity of emission coefficients and the poor quality of the few available data. In another method, to be discussed later, the major disadvantages are the relative complexity of the experimental equipment and at least partly the insensitivity of the method. It should be noted that still other special methods for measuring total intensities are mentioned in the article by Finkelnburg and Maecker,¹ but they will not be reported here since they have found only one or two isolated applications.

The total continuum intensity, due to free-bound as well as free-free

²¹ H. R. Griem, *Phys. Rev.* **128**, 515 (1962).

²² J. B. Shumaker, Jr. and W. L. Wiese, in "Temperature—Its Measurement and Control in Science and Industry" (C. M. Herzfeld, ed.), Vol. 3, Pt. 1, 575. Reinhold, New York, 1962.

transitions of electrons in the field of ions, is a function of the product of ion and electron density and depends also weakly on the temperature. For the case where only singly ionized atoms ($z = 1$) of one element are present in significant numbers, as often encountered in arc plasmas, the expression converts into one where the square of the electron density is involved. If furthermore the free-bound contributions come only from recombination continua ending in closely spaced higher excited atomic levels, which is best fulfilled at long wavelengths, then one may apply the semiclassical hydrogenic Kramers–Unsöld formula^{73, 74}

$$I_{\nu,c}^{(z)} = BN_e^2(k_B T)^{-1/2} z^{*2}, \quad (10.28)$$

where $I_{\nu,c}^{(z)}$ is the continuum intensity per unit frequency interval, z^* is the effective ionic charge⁷⁴ ($z^* \approx z = 1$), and B is a constant. Consequently this relation may be used to obtain the electron density if T is approximately known. Several recent arc studies^{24, 62, 75, 75a} have shown that in the visible region of the spectrum the conditions for the application of this formula are usually not fulfilled, since an important part of the observed free-bound transitions ends in moderately excited energy levels which are far from being closely spaced and hydrogenic.^{21, 76, 77, 78} Another complication, especially for low-temperature arcs, is the appearance of continua originating from negative ion formation, such as H^- , O^- , N^- , C^- , etc., which may give substantial contributions. The present knowledge of the emission coefficients for these radiative attachment processes and also for the free-free transitions of electrons in the field of neutral atoms is still quite incomplete.⁷⁹

Another method to determine densities is to exploit the dependence of the index of refraction on density. In arc plasmas this leads usually to a determination of the atomic density since this is the dominant one, often being an order of magnitude higher than the electron density. Several interferometric density measurements have been reported in the literature. This method gives the most precise results for the outer arc zones where the total density has the highest value.⁸⁰

⁷³ A. Unsöld, "Physik der Sternatmosphären," 2nd ed. Springer, Berlin, 1955.

⁷⁴ W. Finkelnburg and Th. Peters, in "Handbuch der Physik" (S. Flügge, ed.), Vol. 28. Springer, Berlin, 1957.

⁷⁵ D. Schlüter, *Z. Astrophys.* **56**, 43 (1962).

^{75a} B. Wende, *Z. Physik* **198**, 1 (1967).

⁷⁶ M. J. Seaton, *Monthly Notices Roy. Astron. Soc.* **118**, 504 (1958).

⁷⁷ A. Burgess and M. J. Seaton, *Monthly Notices Roy. Astron. Soc.* **120**, 121 (1960).

⁷⁸ L. M. Biberman, G. E. Norman, and K. N. Ulyanov, *Opt. Spectry. (USSR)* (English Transl.) **10**, 297 (1961).

⁷⁹ L. M. Branscomb, in "Atomic and Molecular Processes" (D. R. Bates, ed.), Chapter 4. Academic Press, New York, 1962.

⁸⁰ G. Schmitz, *Z. Physik* **126**, 1 (1949).

10.3.4. Temperature and Density Determinations of Multielement Arc Plasmas

We now proceed to discuss temperature and density determinations for the general case of a multielement plasma. It is tempting to assume that the relative particle concentrations are conserved throughout the arc, so that one may consequently utilize the initial composition of the gas mixture for additional relationships in the system of equilibrium and conservation equations described under Section 10.3.2. For plasmas with X different elements one would have then $X - 1$ additional relations available describing the initial mixing ratios. For example, for chemical compounds one would use the stoichiometric ratios. Since also $X - 1$ elements are added to the one-element plasma, the system of equations is then again complete to the same degree as before, i.e., all plasma quantities, densities and temperature, may be uniquely expressed in terms of one.

This procedure had been general practice until it was detected that in the quiescently running wall-stabilized arcs the local plasma composition values may strongly deviate from the initial mixing ratios.⁸¹ The mass separation or "demixing" effects have thus invalidated the application of the initial mixing values and have made necessary the use of different approaches to find atomic densities.

Before these are discussed it should be mentioned that the mass separation effects follow readily from the dynamic theory of arc plasmas. However, it was only recently realized that the condition for a stationary state in an arc column with strong radial temperature gradients is not the previously assumed constancy of the concentration ratios, but the requirement that the sum of all forces on each constituent of the plasma must vanish. Frie and Maecker⁸² as well as Richter⁸³ could explain and roughly calculate the earlier observed effects. As forces working on each particle they included frictional forces, pressure gradients, and thermal diffusion forces, as well as those due to the axial electric field. A precise quantitative theoretical treatment does not appear to be possible as yet, partly due to the complexity of the problem (e.g., it is difficult to exactly define the boundary conditions) and partly due to the scarcity of friction coefficients, which are in turn based on atomic and ionic cross sections, etc. However, the observed mass separation effects have all found a semi-quantitative explanation in the above-quoted work.

It is instructive to consider with Frie and Maecker⁸² the simple case of an arc plasma consisting of two monatomic gases with very different ioniza-

⁸¹ H. Maecker, *Ann. Physik* [6] **18**, 441 (1956); F. Mastrup and W. L. Wiese, *Z. Astrophys.* **44**, 259 (1958).

⁸² W. Frie and H. Maecker, *Z. Physik* **162**, 69 (1961); W. Frie, *ibid.* **172**, 99 (1963).

⁸³ J. Richter, *Z. Astrophys.* **53**, 262 (1961).

tion potentials. The plasma is assumed to have an axis temperature such that only one element becomes significantly ionized, while the other remains neutral throughout (buffer gas). At temperatures below the ionization zone the temperature gradients will cause particle currents due to thermal diffusion, which usually have the effect of moving the element of smaller mass to regions of higher temperature and the heavier component to regions of lower temperature. Within the ionization reaction zone, strong concentration gradients arise between the atoms and ions of the reacting gas.

In the resulting two radial-diffusion currents, namely one with the inbound atoms and the other with the outbound ions, the buffer gas is dragged along, with the net effect that its concentration will be increased in the direction in which the friction forces are greater. Equilibrium is reached when the forces on the buffer gas balance. This requirement is of course not identical with the one assumed earlier that the concentration of the buffer gas should remain constant throughout the arc.

The demixing effect has obviously made the determination of atomic densities in complex arc plasmas very difficult, while the temperature and electron density determinations are normally not much affected. It is evident that all the temperature measurement methods of Section 10.3.1 may still be employed. Also, several of the temperature determinations involving densities may still be utilized and some others may be applied for somewhat different purposes. Thus, the intensity ratio of lines of subsequent stages of ionization (Section 10.3.2.2) may be used for temperature measurements, if the electron density can be independently determined, e.g., from Stark broadening. Absolute line intensity measurements, discussed under Section 10.3.2.1, are quite useful too. If the temperature can be determined by some other method, then these may be employed to determine atomic or ionic densities. However, the application of the modified Fowler-Milne method (Section 10.3.2.3) will give now little useful information. Among the electron density determinations, the Stark width measurements remain as useful as before, while the analysis of continuum intensity measurements becomes too complex for most practical situations.

Since the determination of atomic and ionic densities is now the most difficult problem, we shall in the following emphasize these density determinations. Let us first consider solutions for the often-encountered but somewhat restricted case of a two-element plasma, typically represented by CO_2 , SO_2 , SiCl_4 , SF_6 , TiCl_4 , etc. For the two elements and Y species (including the free electrons), we have available $Y - 1 - 2$ Saha equations, the quasi-neutrality condition, and Dalton's law, that is, altogether $Y - 1$ equations for $Y + 1$ unknowns, namely Y densities plus the temperature (as before, the total pressure is assumed to be known). Thus at least two independent measurements are required to uniquely determine the plasma

composition. For example, one may measure the electron density and temperature, or an absolute line intensity (which contains the atomic density and the temperature) plus the electron density. Bridges⁸⁴ has applied this approach to diagnose a SO_2 plasma. It is important to select carefully the quantities to be determined. For example, the combination of temperature and electron density is not useful if the two elements have approximately the same ionization potential and partition function ratio, because then the electron density would be almost independent of the mixing ratio. A case where this applies is an H_2O plasma, where the ionization potentials are: $\text{H} = 13.60 \text{ eV}$ and $\text{O} = 13.61 \text{ eV}$ and where the partition function ratios are approximately 2 and 9/4, respectively.

In the general case one has to consider a plasma consisting of X elements and Y species. Then $Y - X - 1$ Saha equations, the quasi-neutrality condition, and Dalton's law—altogether $Y - X + 1$ equations—are available relating $Y + 1$ unknowns, namely Y particle concentrations and the temperature.

Boldt⁸⁵ has recently given the following solution. He assumes first that the temperature as well as the electron density may be determined by one of the previously quoted methods so that the number of unknowns is reduced to $Y - 1$. In the two-element case, $X = 2$, the solution is then normally complete, and has been already discussed above. (However in situations like the above quoted H_2O plasma, where the electron density is nearly independent of the mixture ratio, one has either to measure a quantity other than the electron density or one has to apply the full formalism of Boldt's method. A recent example for the latter approach is described by Labuhn^{85a} for a mixture of argon and nitrogen.) For the general case Boldt proceeds to measure the absolute intensities [Eq. (10.7)] of one line each from Q constituents, so that Q additional equations of the type

$$N_b = \frac{4\pi}{hc} \times \left(\frac{I_{kt} \lambda_0 U(T)}{A_{kt} g_k l} \exp(E_k/k_B T) \right)_b, \quad (10.29)$$

with $b = 1, 2, \dots, Q$, are obtained. The transition probabilities A_{ki} are treated as unknowns, so that there is no net gain at this point. Then he employs a system of M arc plasmas which all contain the same elements but in different unknown mixing ratios. In all of these M different plasmas of known electron density and temperature, the same line intensity measurements [Eq. (10.29)], altogether of number $Q \times M$, are carried out. The M

⁸⁴ J. M. Bridges, Thesis, Univ. of Maryland, College Park, Maryland, 1966; J. M. Bridges and W. L. Wiese, *Phys. Rev.* **159**, 31 (1967).

⁸⁵ G. Boldt, *Z. Naturforsch.* **18a**, 1107 (1963).

^{85a} F. Labuhn, *Z. Naturforsch.* **20a**, 998 (1965).

incomplete systems of equations are then related through the unknown A_{ki} values and combined into one system of equations. This system of $M(Y - X + 1 + Q)$ equations and $M(Y - 1) + Q$ unknowns has a solution when the condition

$$Q \leq M(Q - X + 2) \quad (10.30)$$

is fulfilled. For example, for three elements ($X = 3$) one obtains

$$Q \leq M(Q - 1); \quad (10.31)$$

that is, if one employs $M \geq 2$ equations, this system of equations may be solved. Boldt recommends overdetermination of the system to achieve higher precision, and has illustrated his method with the example of a plasma mixture containing Ar, O, and C.⁸⁵

10.4. Local Thermal Equilibrium (LTE) in Arc Plasmas

The majority of the methods discussed for electron density and temperature determinations is based on the assumption that a state of local thermal equilibrium (LTE) prevails in the arc plasma. The regime of LTE is very attractive, since it makes the plasma analysis and the interpretation of the emitted radiation relatively simple, as we have seen in Chapter 10.3. Furthermore, with LTE plasmas it is also relatively easy to determine atomic constants and parameters (Section 2.1.2 and Chapter 10.5). The value of arcs for quantitative spectroscopy is therefore to a large part due to the fact that the high density plasmas generated with these sources are generally in a state of LTE, as we shall see below.

LTE may be defined as a state in which equilibria in the kinetic distributions of the various particles as well as in the distributions of bound atomic and ionic states and in the ionization reactions are established, and in which all these equilibria, described by Maxwellian velocity distributions and Boltzmann and Saha distribution functions, may be expressed as functions of the same unique local temperature, namely that which would be obtained for a system in complete thermal equilibrium.

Complete thermal equilibrium is, of course, only realized in a black-body e.g., a cavity, where each kind of atomic process, collisional as well as radiative, is balanced by its inverse according to the principle of detailed balancing. Thus collisional ionization is balanced by three-body recombination, photoionization by radiative recombination, etc. Such complete equilibrium cannot be realized in an arc plasma because energy losses occur constantly and act as perturbations on the equilibrium. Specifically the

emission processes are not balanced by absorption processes and lead to radiation losses. A state very close to complete thermal equilibrium may nevertheless be achieved if the energy exchange processes are much more frequent than the energy loss processes, and if the energy gained by the electrons (and ions) from the applied electric field is instantly and effectively redistributed among all particles. Thus, to establish LTE in an arc, two conditions must be fulfilled: (a) The collision rates between the electrons, which constantly receive most of the energy from the axial electric field, and the heavy particles must be so high that the electrons may transfer essentially all of this surplus energy to the heavy particles. Only this insures that the difference between the kinetic electron temperature and the lower "gas" temperature is negligible or, in other words, that a unique temperature is maintained. (b) The arc plasma must be collision dominated; i.e., the collision processes must be much more frequent than the radiative ones to insure a high rate of energy exchange processes.

Condition (a) is a special one for arc sources. It has been first considered by Mannkopff⁸⁶ and Ornstein and Brinkman,⁸⁷ and has been later in detail discussed by Finkelnburg and Maecker¹ and most recently by Gurevich and Podmoshenskii.⁸⁸ An estimate for the difference between electron temperature and gas temperature is obtained by considering the energy balance for the electrons under steady-state conditions; i.e., the energy gained by the electrons from the applied electric field is equated to the energy loss by elastic and inelastic collisions and the heat conduction losses.

In the earlier estimates (see Finkelnburg and Maecker¹) only the elastic collisions were considered. By inserting typical numerical values, differences of several thousand degrees Kelvin between the two temperatures are obtained. Gurevich and Podmoshenskii⁸⁸ included recently the inelastic collisions and the heat conduction losses as well. They concluded that especially energy exchange through the excitation of vibrational levels of molecules is quite effective for low-current arcs. By applying the energy balance equation to low-current arcs in air, argon, and mercury they arrived at differences between electron and gas temperatures which were of the order of a few percent or less. For high-current arcs with much higher degrees of atomic excitation and ionization, i.e. with a much higher frequency of the corresponding inelastic collisions, the differences should decrease further.

But even in this generalized energy balance equation not all dissipation mechanisms are considered, so that the derived temperature differences

⁸⁶ R. Mannkopff, *Z. Physik* **86**, 161 (1933).

⁸⁷ L. S. Ornstein and H. Brinkman, *Physica* **1**, 797 (1934).

⁸⁸ D. B. Gurevich and I. V. Podmoshenskii, *Opt. Spectry. (USSR)* (*English Transl.*) **15**, 319 (1963).

must be still regarded as upper limits. Indeed, in a parallel experiment based on a relaxation method, Gurevich and Podmoshenskii⁸⁸ found that the differences are <0.5% and 1.6% for atmospheric pressure low-current arcs in air and argon operated at 6000 and 7500°K, respectively, while they calculated differences of about 1% and 5%.

In view of their experimental and theoretical results one may conclude that for all practical situations (except perhaps for some low-current arcs in monatomic gases) the difference between electron and gas temperature is negligible. The earlier, too-restrictive criterion developed by Finkelnburg and Maecker¹ is therefore not cited here.

The second requirement for the existence of LTE, namely the predominance of collision processes, is a more general one and applies to any plasma, be it an arc, shock tube, or stellar source. Several authors^{1, 21, 89-91} developed criteria for this requirement, all based on the same following argument. First, it is recognized that the electrons, which have approximately the same cross sections but a much greater velocity than the heavy particles, are involved in most collision processes in arc plasmas with a significant degree of ionization, say above 1%. A general criterion may then be derived from the requirement that the electron collision rates should be much more frequent than the radiative decay rates. This criterion must apply for all excited atomic levels as well as the ground state, for which it is most restrictive. Griem,⁹¹ by requiring a ratio of 10 to 1 for the two rates, arrives at the following inequality if LTE is to hold down to the ground state (with deviations expected to be within 10%):

$$N_e \geq 9 \times 10^{17} \left(\frac{k_B T}{\chi_H} \right)^{1/2} \left(\frac{E_2}{\chi_H} \right)^3 [\text{cm}^{-3}]. \quad (10.32)$$

In this formula hydrogenic estimates are used for the relevant cross sections, χ_H is the ionization energy for hydrogen, and E_2 is the excitation energy of atomic level "2," i.e., the upper state of the principal resonance line. Although the above numerical relation was derived for a hydrogenic species, it may be expected to hold also for other chemical species of approximately hydrogenic level structure (most lighter elements), since the transition probabilities, which determine the radiative decay rate, canceled in the derivation.

Wilson⁸⁹ and McWhirter⁹⁰ have obtained similar expressions. Their results differ only by the magnitude of the numerical factors, which are slightly higher.

⁸⁹ R. Wilson, *J. Quant. Spectry. & Radiative Transfer* **2**, 477 (1962).

⁹⁰ R. W. P. McWhirter, in "Plasma Diagnostic Techniques" (R. H. Huddlestone and S. L. Leonard, eds.), Chapter 5. Academic Press, New York, 1963.

⁹¹ H. R. Griem, *Phys. Rev.* **131**, 1170 (1963).

Equation (10.32) applies to optically thin plasmas. However, arc plasmas are usually large and dense enough that the principal resonance lines are strongly self-absorbed. Consequently, the radiative decay rate of the first excited state is now balanced by the rate of radiative excitation of the ground state. For the ground state, radiative population from higher levels is then the only radiative mechanism not balanced by its inverse. This process, however, is estimated to be about one order of magnitude smaller than the decay through the first resonance line, as comparisons of the relevant transition probabilities show. Thus one may relax the criterion (10.32) to

$$N_e \geq 10^{17} \left(\frac{k_B T}{\chi_H} \right)^{1/2} \left(\frac{E_2}{\chi_H} \right)^3 [\text{cm}^{-3}]. \quad (10.33)$$

By inserting a typical arc temperature (10^4 °K) and typical values for E_2 (for lighter elements) one finds that this condition is usually fulfilled for electron densities above 10^{16} cm $^{-3}$.

The existence of partial LTE among moderately or highly excited states, e.g., for all states of principal quantum number n and above and the continuum, is achieved at much lower electron densities, since now the collision rates are much higher due to the higher cross sections. Griem^{21, 91} obtains for this case

$$N_e \geq 7 \times 10^{18} \frac{(z+1)^6}{n^{17/2}} \left(\frac{k_B T}{\chi_H} \right)^{1/2} [\text{cm}^{-3}]. \quad (10.34)$$

Again a similar criterion by McWhirter⁹⁰ leads to similar results. These criteria are consistent with the results of detailed calculations of Bates *et al.*,⁹² and McWhirter and Hearn,⁹³ who determined the steady-state populations of hydrogenic systems for various electron densities and temperatures.

In the inhomogeneous arc plasmas strong radial temperature gradients occur, which also represent a perturbation to the equilibrium. Thus an additional requirement must be fulfilled, namely that the heavy particles, atoms or ions, do not diffuse over regions of significantly different temperatures before they equilibrate. This additional criterion, which, of course, holds for any inhomogeneous plasma source, may be written as

$$\frac{T(r) - T(r+d)}{T(r)} \ll 1. \quad (10.35)$$

⁹² D. R. Bates, A. E. Kingston, and R. W. P. McWhirter, *Proc. Roy. Soc. A* **267**, 297 (1962); **A270**, 155 (1962).

⁹³ R. W. P. McWhirter and A. G. Hearn, *Proc. Phys. Soc. (London)* **82**, 641 (1963).

The diffusion length d has been quantitatively estimated for the important case, where neutral ($z = 0$) and singly ionized atoms ($z = 1$) of one element are present,⁹¹ as

$$d = \frac{7 \times 10^{14}}{\mu^{1/4}} \left(\frac{k_B T}{\chi_H} \right)^{1/2} \left(\frac{E_2}{f_{12} \chi_H} \right)^{1/2} \exp \left(\frac{E_2}{2k_B T} \right) \\ \times [(N_a^{(0)} + 10N_a^{(1)})(N_a^{(0)} + N_a^{(1)})]^{-1} [\text{cm}] \quad (10.36)$$

where μ is again the atomic weight and f_{12} is the oscillator strength of the principal resonance line (with lower state 1 and upper state 2). f_{12} is related to the transition probability by $f_{12} = 1.499 \times 10^{-16} \lambda^2 (g_2/g_1) A_{21}$ (λ in angstroms). Inserting numerical values one finds that d is of the order of 10^{-3} to 10^{-2} cm, which may be occasionally critical for narrow, constricted arcs, where temperature changes over this distance may be as large as a few percent. Griem⁹¹ notes, however, that this criterion is more critical for the point of highest temperature, i.e., the arc axis, than for the outer zones, where the absorption of radiation from the hotter axial region may effectively reduce the diffusion length.

The LTE validity criteria readily permit one to determine if in a given practical situation a state of LTE is achieved. However, one should not overlook the fact that the criteria have the character of estimates, and contain considerable uncertainties, since, for example, they are only derived for hydrogen-like systems. Furthermore, by considering only the principal energy transfer or exchange mechanisms, some criteria have the character of upper limits and may be overly restrictive. This applies especially to the existing criteria for the difference between electron and gas temperature, as the recent experimental work of Gurevich and Podmoshenskii⁸⁸ has shown. Also other experimental work, which shall now be briefly discussed, lends support to the notion that some validity criteria are too conservatively evaluated, since the existence of LTE is indicated for cases where the criteria are just marginally fulfilled. It appears that in these borderline situations only detailed experimental studies may conclusively show how closely LTE is approached.

Several recent experiments have contributed a great deal to determine accurately the extent of the regime of LTE in arcs. Krysmanski⁹⁴ has studied low-current arcs, at both atmospheric and reduced pressures, in air and hydrogen, to which he added traces of iron. He carried out intensity measurements for a number of Fe I and Fe II lines and found that at currents of 5, 2, and 0.3 A considerable deviations from LTE existed. The deviations for the 5-A arc were much smaller than for the lower currents,

⁹⁴ K. H. Krysmanski, *Ann. Physik* [7] 15, 207 (1965).

however. For the measured values of electron densities from 10^{12} to 10^{15} cm^{-3} this is completely consistent with the criteria. Kolesnikov and Sobolev⁹⁵ have measured arc temperatures for He and Ar arcs from absolute populations of excited atomic states as well as from relative line intensities. By doing this for a wide range of electron densities, they found that the two temperatures start to disagree for electron densities below 10^{16} cm^{-3} . For these densities the two temperatures also deviate from an "ionization" temperature, which is calculated directly from the Saha equation in conjunction with independent electron density measurements. The same gradual deviations from LTE with decreasing electron density have been observed by Richter⁶⁸ for an argon arc. The electron density where the deviations first become noticeable (10^{16} cm^{-3}) is somewhat lower than predicted by Eq. (10.33) ($N_e = 1.8 \times 10^{16} \text{ cm}^{-3}$). In another recent investigation with a 100 A wallstabilized helium arc, Bott^{95a} has found that complete equilibrium down to the ground state does not exist at electron densities below $2 \times 10^{15} \text{ cm}^{-3}$. A strong (but not sufficient) indication of LTE may be also obtained from the following test: The electron density is determined by two different methods, one of which depends sensitively on LTE (e.g., absolute line or continuum intensity measurements in conjunction with the equilibrium relations) while the other one does not (e.g., Stark broadening). This test has been applied to an argon arc,⁴⁷ and agreement between the two methods within 10% has been obtained for an electron density as low as $6 \times 10^{15} \text{ cm}^{-3}$.

Furthermore, indirect evidence for deviations from LTE may be derived from the dependence of measured transition probabilities on the region within the arc from which the measurements were made. For example, it has been observed in high-current oxygen⁹⁶ and argon⁵⁴ arcs that measured transition probabilities are essentially independent of position for the region around the arc axis, while at the outer arc zones with steeply decreasing electron densities the measured transition probabilities change significantly, probably due to deviations in the upper level populations from the equilibrium values. The constancy of the transition probabilities for the inner arc regions may also be interpreted as an indirect proof that the diffusion length [Eq. (10.36)] is very small.

In summary one may conclude that according to all validity criteria as well as experimental investigations LTE exists in the high-current atmospheric pressure arcs. However, for electron densities below 10^{16} cm^{-3} , as encountered in low-current arcs and at large radial distances of high-

⁹⁵ V. N. Kolesnikov and N. N. Sobolev, *Fiz. Probl. Spektroskopii* **1**, 119 (1962).

^{95a} J. F. Bott, *J. Quant. Spectry. and Radiative Transfer* **6**, 807 (1966).

⁹⁶ J. E. Solarski and W. L. Wiese, *Phys. Rev.* **135**, A1236 (1964).

current arcs, the deviations from LTE become significant. Thus for low-current arcs, say with currents smaller than 10 A, only partial LTE may be safely assumed to exist. One may then no longer speak of a single arc temperature, but rather of electron temperatures, kinetic gas temperatures, etc. Nevertheless, this regime may be still useful, e.g., for relative transition probability measurements of highly excited lines.

10.5. Applications

10.5.1. Atomic Transition Probabilities

By far the most frequent applications of arcs in atomic physics have been directed towards the determination of transition probabilities. The standard approach, based on Eq. (2.1.7), has been sufficiently discussed in Chapter 2.1 and needs no further comment.

Numerous applications of this method have been reported.[†] To name a few, there is the comprehensive piece of work by Corliss and Bozman⁹⁷ based on intensity measurements of Meggers *et al.*⁹⁸ These have been done with a 10-A arc operating in open air and with copper electrodes into which minute concentrations of the elements to be investigated have been admixed. These measurements have led to the determination of 25,000 transition probabilities for 70 elements, which are, however, of rather low accuracy (compare also Chapter 10.1). Many other measurements with low-current atmospheric arcs have been performed at Utrecht University (for a summary see Smit⁹⁹), and at London Observatory (for a summary see Foster¹⁰⁰). Stabilized arcs, i.e., water- and gas-stabilized arcs in the earlier work, and later wall-stabilized arc sources, have been applied to lines of many elements at Kiel University. Measurements have been reported on He, C, N, O, Ne, Si, Cl, Ar, Ti, Fe, and Cu. Similar work has been done

⁹⁷ C. H. Corliss and W. R. Bozman, Experimental transition probabilities for spectral lines of seventy elements. *Natl. Bur. Std. Monograph* No. 53 (1962).

⁹⁸ W. F. Meggers, C. H. Corliss, and B. F. Scribner, Tables of spectral line intensities. *Natl. Bur. Std. Monograph* No. 32 (1961).

⁹⁹ J. A. Smit, *Physica* 12, 683 (1946).

¹⁰⁰ E. W. Foster, *Rept. Progr. Phys.* 27, 469 (1964).

[†] Since a complete listing of all individual experiments would take up too much space here, we have to refer to the "Bibliography on Atomic Transition Probabilities," Ref. 43, where most of the references classified under emission ("emiss.") represent arc measurements. Some references, quoted earlier in this article in other connections, are representative for this type of work: For low-current arcs, see, for example, Refs. 41, 47, 97. For high-current arcs (mostly wall-stabilized), see Refs. 54, 61, 64, 84, 85, 96.

at London Observatory on the spectra of C, O, and Cl. Exclusively photoelectric measurements have been performed recently at the National Bureau of Standards on N, O, S, Ar, and Ni. With a modified wall-stabilized arc source adapted for vacuum-uv measurements, transition probability determinations of vacuum-uv lines of C and N have been carried out at the Max Planck Institute.

A different technique to determine absolute transition probabilities has been developed by Eberhagen.¹⁰¹ Relative transition probabilities are first determined as usual from intensity measurements. Then the current transport equation is combined with the relation for the line intensity to obtain the density in a rather indirect fashion, from which finally the absolute A_{kl} value is derived. This method may be applied either to one-element plasmas or to gaseous mixtures which contain an element of relatively low ionization potential in significant concentration so that this provides essentially all the electrons for the current transport. The accuracy of this method depends critically on some quantities in the current transport equation, of which the electron mean free path is normally rather uncertain. After Eberhagen's initial measurements on Sr,¹⁰¹ two further applications on Ba and Ca have been reported.¹⁰²

10.5.2. Continuum Emission Coefficients

Measurements of continuum radiation may be employed for the determination of continuum emission coefficients or the related absorption coefficients in a similar fashion as line radiation for the determination of transition probabilities. Experimental studies in this direction have received a stimulus since the development of the quantum defect method by Seaton⁷⁶ and Burgess and Seaton⁷⁷ for the calculation of these quantities. However, there is a principal difference between line and continuum radiation. Lines are generally separated by their different wavelength positions and are therefore easily identified so that their intensities may be individually measured. But the observed continuum radiation in a given frequency interval consists normally of many superimposed and practically inseparable contributions. The processes involved are the radiative recombination of electrons and ions, i.e., many different free-bound transitions, and transitions of free electrons in the field of ions, i.e., free-free transitions. In addition, for arc plasmas one has often to consider these same processes between electrons and atoms as well. These processes lead to the "negative-ion" continua (the free-bound process is often called radiative attachment).

¹⁰¹ A. Eberhagen, *Z. Physik* **143**, 392 (1954).

¹⁰² H. F. Eicke, *Z. Physik* **168**, 227 (1962); H. Köstlin, *ibid.* **178**, 200 (1964).

Measurements of free-free and free-bound argon continua with wall-stabilized arcs have been reported by Schlüter⁷⁵ and Wende.^{75a} The experimental results are only in fair agreement with the numerical calculations by Biberman *et al.*,⁷⁸ who applied the quantum defect method. The emission coefficients of negative-ion continua may be determined, if the contributions of the competing electron-ion recombination continua can be determined either through calculations or if the former may be separated from the other continua by virtue of their different temperature and density dependence. Arc measurements of the latter kind have been undertaken by Boldt¹⁰³ and Henning¹⁰⁴ for O⁻, N⁻, Cl⁻, and C⁻.

10.5.3. Line-Broadening Parameters

Arc experiments have also contributed a great deal to our understanding of line-broadening mechanisms. In the high-density arc sources pressure broadening is a pronounced effect. It is most strikingly observed for the hydrogen Balmer lines, which are strongly broadened by interatomic (linear) Stark effect in plasmas with significant degree of ionization. With recent advances in Stark-broadening theory (see also Section 10.3.3.1), a large number of calculated Stark-broadened parameters for hydrogen and hydrogenlike lines as well as lines of heavier elements became available.²¹ These data in turn have generated considerable interest in the acquisition of experimental comparison material, especially in measurements of half-widths and line shifts.

For the comparison with the corresponding theoretical values, the electron density and temperature in the arc plasma need to be determined first. In side-on observations, the Abel inversion process must be performed at a number of different positions over the wavelength range of the line, and the profile must then be graphically constructed from these discrete points (see the illustration in Fig. 10). Fortunately, many prominent Stark-broadened lines are rather broad, with half-widths of the order of angstroms at electron densities of 10^{17} cm^{-3} , so that precise width measurements may be performed even with medium-resolution spectrometers.

In the following, a number of recent representative arc experiments on line broadening are cited, which may be consulted for further details:

The most pronounced line broadening is exhibited by the hydrogen lines, which are subject to linear Stark effect. The first detailed measurement of the Balmer line H_{β} was performed by Jürgens⁴⁵ with a water-stabilized arc. Subsequent arc experiments^{15, 105} revealed significant discrepancies

¹⁰³ G. Boldt, *Z. Physik* **154**, 319, 330 (1959).

¹⁰⁴ H. Henning, *Z. Physik* **169**, 467 (1962); and *Z. Astrophys.* **62**, 109 (1965).

¹⁰⁵ H. R. Griem, *Z. Physik* **137**, 280 (1954).

with the then-available Holtsmark theory and stimulated new theoretical work in which as the principal new feature the hitherto neglected electron broadening was considered in addition to the ion broadening.²¹ Recent detailed arc experiments¹⁸ leave little doubt that for the Balmer line H_{β} , for which the most detailed and refined numerical calculations⁷⁰ have been

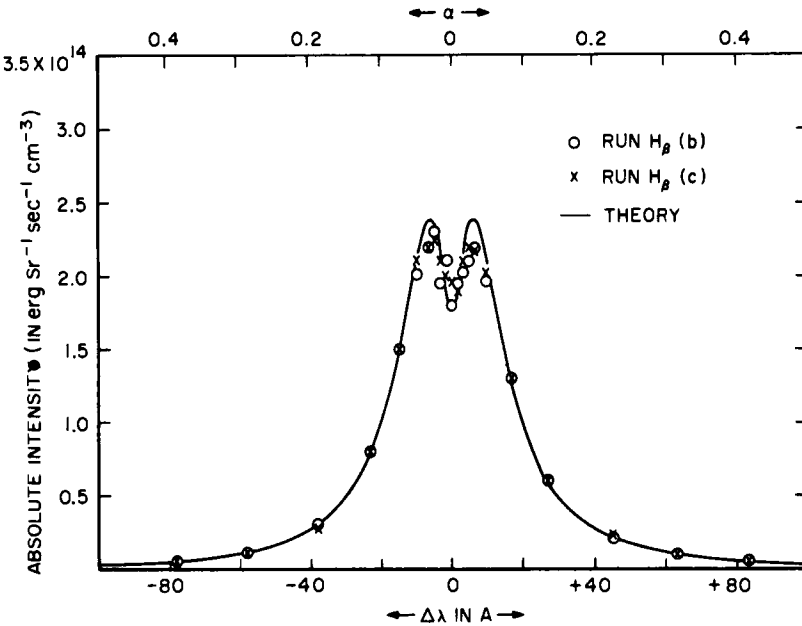


FIG. 10. Comparison of the calculated Stark-broadened H_{β} profile with arc measurements. The experimental conditions have been: run (b) $N_e = 6.40 \times 10^{16} \text{ cm}^{-3}$, $T = 12,210^\circ\text{K}$; run (c) $N_e = 6.43 \times 10^{16}$, $T = 12,220^\circ\text{K}$ [W. L. Wiese, D. R. Paquette, and J. E. Solarski, *Phys. Rev.* **129**, 1225 (1962).] The upper abscissa gives the wavelength intervals on a reduced scale as used in the calculations ($\alpha = \Delta\lambda/F_0$, with $F_0 = 1.25 \times 10^{-9} N_e^{2/3}$).

made, the theory is correct within a few percent. An illustration of the excellent agreement is provided in Fig. 10. For other Balmer lines, especially H_{α} and H_{γ} , where the calculations have not been brought to the same state of refinement, the comparison with arc data indicates a slight systematic deviation in the sense that the theoretical profiles appear to be too narrow.^{18, 108}

Two arc investigations have also been concerned with the intensity

¹⁰⁸ J. M. Bridges and W. L. Wiese, *Proc. Intern. Conf. Ionization Phenomena Gases 7th Conf., Belgrade, 1965*, Gradevinska Knjiga Publ., Belgrade 1966.

distribution in the far wings of hydrogen lines. While the agreement with theory is within the mutually estimated error limits for H_β ,¹⁸ the agreement is not satisfactory for the case of L_α .¹⁰⁷

A number of arc comparison measurements are also available for spectral lines of heavier elements which exhibit quadratic Stark effect. The experimental results on He, N, O, and Ar shifts and widths^{53, 54, 108} are in substantial agreement with the theoretical values.²¹ Some of these measurements have been performed over an extended range of electron densities and have confirmed the calculated linear dependence of shifts and widths with electron density. However, large discrepancies with the present theory exist for ionic Ar and S lines.^{54, 84†}

The conditions in the arc source may also be modified to such a degree that a different kind of pressure broadening, namely Van-der-Waals broadening by neutral atoms or molecules, becomes dominant. Stark broadening may be sufficiently suppressed if the degree of ionization, i.e., the electron density, is kept very low. At the same time, Van-der-Waals broadening may be enhanced, if the density of neutral atoms is very high. These conditions may be achieved by working at very high pressures, say, at about 100 atm, and at relatively low currents. Two experimental studies of Van-der-Waals broadening with high-pressure arc sources have been reported, namely Fe I lines broadened by H atoms and molecules, by Kusch,¹⁰⁹ and Ti I lines broadened by H atoms, by Meyer.¹¹⁰

10.5.4. Elastic Scattering Cross Sections

Cross sections for the elastic scattering of electrons by atoms may be determined in one element-plasmas by utilizing the current transport equation, given below. While this method does not approach the precision of

¹⁰⁷ G. Boldt and W. S. Cooper, *Z. Naturforsch.* **19a**, 968 (1964); H. R. Griem, *Phys. Rev.* **140**, A1140 (1965).

¹⁰⁸ W. Bötticher, O. Roder, and K. H. Wobig, *Z. Physik* **175**, 480 (1963); O. Roder and A. Stampf, *ibid.* **178**, 348 (1964); A. Stampf, *Z. Astrophys.* **58**, 82 (1963); M. Jung, *ibid.* **58**, 93 (1963).

¹⁰⁹ H. J. Kusch, *Z. Astrophys.* **45**, 1 (1958).

¹¹⁰ J. Meyer, *Z. Astrophys.* **60**, 94 (1964).

† These as well as other discrepancies, observed recently with shock tubes, have triggered much new theoretical work on line broadening. (See, e.g., H. R. Griem, *Phys. Rev. Letters* **17**, 509 (1966); D. E. Roberts, *Phys. Letters* **22**, 417 (1966) and **24A**, 694 (1967); J. Cooper and G. Oertel, *Phys. Rev. Letters* **18**, 985 (1967); J. Davis and D. E. Roberts, *Proc. Phys. Soc. (London)* **92**, 889 (1967); and D. E. Roberts and J. Davis, *ibid.*, January 1968; H. R. Griem, *Phys. Rev.* **165**, 258 (1968). However, none of the new theoretical approaches provides a fully satisfactory agreement with the experimental results as yet.

other more conventional experimental methods, like crossed-beam experiments, it is attractive because the scattered electrons possess very low energies, typically about 1 eV. This is a very interesting energy range, for which crossed-beam techniques encounter major technical difficulties.¹¹¹

The total current J in a radially symmetric arc column is given by

$$J = 2\pi E \int_0^{r_0} \sigma(r) dr, \quad (10.37)$$

where E is the field strength, r_0 the arc radius, and $\sigma(r)$ the local electrical conductivity. A simple expression for $\sigma(r)$ is obtained from the kinetic gas theory. Kolesnikov and Obukhov-Denisov,¹¹² applying the results of calculations by Ginzburg and Gurevich,¹¹³ refined the elementary formula by including explicitly the velocity dependence of the elastic scattering cross section (using a velocity distribution function rather than an average velocity) and by considering electron-electron collisions. Then one obtains (the element index is omitted)

$$\sigma(r) = \frac{e^2 N_e(r)}{(3m_e k_B T(r))^{1/2}} \frac{K_\sigma}{N^{(0)}(r) \langle Q_{\text{atom}} \rangle + \sum_{z=1} \dots N^{(z)}(r) \langle Q_{\text{ion}}^{(z)} \rangle}. \quad (10.38)$$

The "effective electrical conductivity" cross sections $\langle Q \rangle$ are closely related to the elastic scattering cross sections, and the factor K_σ is of order one. Further details and numerical values for K_σ are given by Kolesnikov and Obukhov-Denisov¹¹² and Ginzburg and Gurevich.¹¹³

The determination of the total scattering cross section for scattering of electrons by atoms, which is essentially represented by $\langle Q_{\text{atom}} \rangle$, requires thus: (a) the measurement of J and E ; (b) the measurement of particle densities and temperature as a function of radial position r , which is accomplished with side-on measurements and an Abel inversion; and (c) determination of $\langle Q_{\text{ion}}^{(z)} \rangle$, for which approximate theoretical expressions are available.^{1, 112} Normally, only singly charged ions ($z = 1$) need to be considered. $\langle Q_{\text{atom}} \rangle$ is most conveniently determined by solving Eq. (10.38) by trial and error, employing graphical integration. The measured value of $\langle Q_{\text{atom}} \rangle$ represents, strictly speaking, a mean value over all temperatures encountered in the arc. But since about 90% of the contribution to the integral [Eq. (10.38)] comes normally from the core of the column where the temperature changes by less than 10%, it may to a good approximation be considered as determined at a constant temperature.

¹¹¹ R. T. Brackmann, W. L. Fite, and R. H. Neynaber, *Phys. Rev.* **112**, 1157 (1958).

¹¹² V. N. Kolesnikov and V. V. Obukhov-Denisov, *Soviet Phys. JETP (English Transl.)* **15**, 692 (1962).

¹¹³ V. L. Ginzburg and A. V. Gurevich, *Soviet Phys. Usp. (English Transl.)* **3**, 147 (1960).

First cross-section measurements were performed by Schulz¹¹⁴ and Elenbaas¹¹⁵ on Ar and Hg. Maecker *et al.*¹⁴ and Drawin¹¹⁶ used water- and gas-stabilized arcs for cross-section measurements on H, He, C, N, O, Ar, and Fe atoms. Their cross sections for electron scattering by hydrogen atoms are much larger than those obtained from theoretical work or extrapolated from crossed-beam experiments. Instabilities in the arc column (see Section 10.1.3) are probably largely responsible for the discrepancies. Recent work with refined diagnostic techniques and wall-stabilized arc sources gives excellent agreement with all otherwise-obtained data.^{117, 118} (In the work of Kolesnikov and Obukhov-Denisov,¹¹² excellent agreement is obtained if the demixing effect is properly accounted for.)

¹¹⁴ P. Schulz, *Ann. Physik* [6] **1**, 318 (1947).

¹¹⁵ W. Elenbaas, "The High Pressure Mercury Vapour Discharge." North-Holland Publ., Amsterdam, 1951.

¹¹⁶ H. W. Drawin, *Z. Physik* **146**, 295 (1956).

¹¹⁷ W. L. Wiese, *Proc. Intern. Conf. Ionization Phenomena Gases, 6th Conf., Paris 1963*, **1**, 5. S.E.R.M.A. Publ., Paris, 1963.

¹¹⁸ V. Kühn and H. Motschmann, *Z. Naturforsch.* **19a**, 658 (1964).

AUTHOR INDEX

Numbers in parentheses are footnote reference numbers and indicate that an author's work is referred to although his name is not cited in the text.

- A**
- Abragam, A., 12
Ackerman, H., 4
Adrian, F. J., 28
Aisenberg, S., 286
Akhmedova, B. G., 262, 263
Akopyan, L. A., 210
Alam, M. N., 304
Albrecht, W. W., 305
Alford, W. P., 283
Alkemade, C. T. J., 194, 200, 211, 216, 218(86), 220
Allen, F. G., 299
Allen, J. S., 283
Alley, C. O., 13
Allis, W. P., 37, 39(21)
Alpher, R. A., 146, 151, 187
Alsofon, F. E., 182
Altshuler, S., 47, 48
Amelinckx, S., 276(9), 277, 304(9)
Andersen, H. H., 238
Anderson, D. E., 299, 301
Anderson, J. M., 99, 100, 123(19)
Anderson, L. W., 3, 21, 23(49), 25
Anderson, V. E., 288
Anderson, W. A., 15
Appleton, B. R., 252, 253
Appleton, J. P., 184
Appleyard, E. T. S., 1
Arditi, M., 24, 27
Armstrong, R. A., 304
Arndt, R., 241
Arrington, C. A., 228
Asbridge, I. R., 163
Ashkin, J., 276, 300(2)
Ashley, J. C., 298, 299(122)
Atkinson, W. R., 147
- B**
- Attix, F. H., 303
Avery, W. H., 196, 202, 203
Avramenko, L. I., 210
Azatyan, V. V., 210
- Bachmann, L., 286
Bailey, L. E., 241
Bailey, V. A., 45, 51, 54, 57
Bainbridge, K. T., 279
Baird, J. C., 3
Balakhnin, V. P., 210
Baldwin, G. C., 283
Ball, G. C., 244, 251
Balling, L. C., 20
Barker, P. H., 242
Barnes, C. W., 303
Barr, W. L., 317, 318
Barrat, J. P., 4, 5, 8, 11
Bartels, H., 326
Barton, G. W., 288
Bartsch, C. A., 169, 170(30)
Bascombe, K. N., 198(67), 199, 202(67), 221, 224(67), 225, 227(67)
Bassett, G. A., 303
Bates, D. R., 119, 120(42), 124, 344
Bauer, P. H., 274, 275
Bawn, C. E. H., 207
Beaty, E. C., 23, 27
Becker, A., 298
Becker, L., 318
Bednyakov, A. A., 262, 263
Behmenburg, W., 217
Behrndt, K. H., 285
Bekefi, G., 100, 102(22)
Belcher, H., 200

- Belewicz, E. M., 219
 Bell, F., 304
 Bell, G. D., 325, 346(47), 347(47)
 Bell, R. E., 284
 Bell, W. E., 16
 Bender, P. L., 21, 23, 27
 Berendsen, R., 227
 Berger, M. J., 300, 303(135)
 Berglund, C. N., 299
 Bergström, I., 242
 Bernheim, R. A., 25
 Bethe, H., 276, 289, 292(93), 300(2), 235
 Bethge, K., 240
 Beutler, H., 206
 Biberman, L. M., 337, 349
 Bingham, R. A., 284
 Biondi, M. A., 58, 59(45), 61(45), 80, 82,
 88, 106(25), 108, 109(27), 112(2), 113,
 116, 117(4), 118(4), 120(31), 122(31), 123
 Birkeland, J. W., 319
 Birkoff, R. D., 276, 280, 298, 299(112), 303
 Bishop, H. E., 301
 Bitter, F., 1
 Björqvist, K., 258
 Blackman, M., 304
 Blackman, V., 184
 Blackstock, A. W., 280
 Bleekrode, R., 211
 Bloch, F., 235
 Bloom, A. L., 16, 22
 Bockasten, K., 317, 318(28)
 Boers, A. L., 197, 200
 Boersch, H., 278
 Bogen, P., 312, 349(15)
 Bøgh, E., 257, 259
 Bohr, N., 233, 234
 Boldt, G., 315, 318, 335, 340, 341(85),
 347(85), 349, 351
 Borgers, A. J., 200, 229(88)
 Botha, J. P., 191, 193
 Bott, J. F., 346
 Bötticher, W., 318, 351
 Bouchiat, M. A., 24, 26
 Boyd, R. L. F., 111 112(32)
 Bozman, W. R., 347,
 Bracewell, R. N., 317
 Brackmann, R. T., 352, 272
 Bradbury, N. E., 34
 Bradley, J. N., 141, 145, 149(1), 156, 176,
 178, 179, 183(1)
 Bragg, J. K., 63
 Brandt, W., 260
 Branscomb, L. M., 337
 Brauer, W., 302
 Braun, W. H., 164
 Braunstein, A. I., 299
 Braunstein M., 299
 Bredov, M. M., 243
 Breit, G., 10
 Brennen, W., 228
 Brewer, J., 197
 Brewer, R. G., 16, 23, 25, 26
 Bridges, J. M., 340, 347(84), 350, 351(84)
 Brink, D. M., 5, 7
 Brinkman, H., 322, 342
 Broida, H. P., 195, 211
 Bromley, L. A., 204(126), 205
 Brossel, J., 1, 2, 3, 11, 24, 26
 Brown, D. B., 303
 Brown, F., 242, 244, 246, 248(29), 249, 250,
 251
 Brown, S. C., 38, 86, 88, 93, 94(10, 15),
 96(10), 100, 102(22), 123(10, 18), 124
 Brünger, W., 291
 Bryant, D. A., 283
 Bucka, H., 23
 Bulewicz, E. M., 198, 200(102, 103, 104, 105,
 106), 201, 211(49), 212, 214, 218(192),
 220, 229(102, 104, 105, 106)
 Burch, D. S., 210
 Burge, R. E., 290, 291
 Burgess, A., 337, 348
 Burgess, D. D., 326
 Burhop, E. H. S., 302
 Burhorn, F., 312, 325, 326, 333
 Burke, E., 202
 Burns, J., 299
 Busz, G., 309
 Bylander, E. G., 17
 Byron, S., 187
 Byron, S. R., 168, 185

C

- Calbick, C. J., 276(7), 277, 303(7)
 Calcote, H. F., 198(55, 70), 199(53), 200
 (53, 55, 76), 224, 225(54, 55), 227(70),
 228(53, 55, 75, 76), 229

- Caldwell, C. W., 304
 •Camac, M., 177, 182
 Cambel, A. B., 328, 329
 Camm, J. C., 146, 166
 Campbell, E. S., 205
 Campos, M., 241
 Carabetta, R. A., 220
 Carey, C., 180, 183(56)
 Carlson, R. C., 237
 Carnevale, E. H., 180, 183(56)
 Carrier, G., 186
 Carver, T. R., 24, 26, 27
 Castaing, R., 284, 305
 Cautin, M., 283
 Chabai, A. J., 163
 Chaikin, A. M., 210
 Chanin, L. M., 58, 59, 61
 Channing, D. A., 244, 251
 Charton, M., 220
 Chi, A. R., 23, 27
 Cholet, P. H., 17
 Christenhusz, R., 304
 Clouston, J. G., 179, 184
 Clyne, M. A. A., 224
 Cohen, N. B., 164
 Cohen-Tannoudji, C., 4, 5, 8, 11, 12(19)
 Colegrave, F. D., 3
 Collins, C. B., 118, 119(40)
 Compton, W. D., 147
 Connor, T. R., 120
 Cooke-Yarborough, F. H., 288
 Cooper, A., 198(62), 199
 Cooper, J., 326, 328, 329(57), 351
 Cooper, W. S., 351
 Coovert, R. E., 299
 Corliss, C. H., 321, 347(41)
 Corney, A., 4
 Cosslett, V. E., 290, 291(96), 301
 Cowan, J. A., 283
 Cowley, J. M., 304
 Craggs, J. D., 55, 72
 Creuzburg, M., 295, 303
 Crompton, R. W., 36, 37, 39(16), 41(16), 43,
 50(16)
 Crowe, R. W., 63
 Crowell, C. R., 299
 Cundy, S. L., 305
 Curtiss, C. W., 172
 Cutler, P. H., 297
 Cvetanovic, R. J., 207, 208
 Cyphers, J. A., 196, 202(39)
- D
- Dabbs, J. W. T., 237, 264(10)
 Dalgarno, A., 18, 19(45)
 Datz, S., 245, 254, 255, 256, 261, 265, 266,
 270, 272(82), 273
 Davidovits, P., 23
 Davidson, N., 184
 Davies, J., 351
 Davies, J. A., 242, 243, 244, 246, 248(29),
 249, 250, 258, 259
 Davis, J. C., 297
 Dearnaley, G., 252, 254, 262, 264
 de Boer, P. C. T., 164
 Deckers, J., 198(57, 58, 59, 60, 61), 199,
 224(57, 58, 59, 61), 227(60)
 Dedrick, K. G., 303
 de Haas, N., 204(119, 123, 124, 125), 205,
 210
 Dehmelt, H. G., 3, 8(10), 13(22), 19, 22,
 24
 De Jaegere, S., 198(61), 199, 224(61)
 Dekker, A. J., 302
 Del Greco, F. P., 211
 Delord, J. F., 299
 Demerdache, A., 214
 Denhartog, J., 258
 Deschizeaux, M. N., 4
 Dewey, F. C., Jr., 180
 Dicke, R. H., 2, 18, 27
 Dickinson, P. H. G., 125, 128, 129(4),
 138(4)
 Diederichsen, J., 205
 Diesen, R. W., 178
 Dietrich, W., 281
 Dietz, L. A., 283
 Dillon, J. A., 286
 Dirac, P. A. M., 5
 Dixon-Lewis, G., 193, 196, 204, 205(18),
 210, 216, 221, 222(20)
 Doebring, A., 58, 61
 Domeij, B., 242, 244, 248(29), 249, 258
 Drawin, H. W., 318, 353
 Droppleman, L. K., 229
 Drude, P., 85, 86(6)
 Druyvesteyn, M. J., 41, 72
 Duclos, D. P., 328, 329

Ducros, R., 283
 Duff, R. E., 165, 177
 Dufour, C., 108
 Duncumb, P., 304

E

Early, R. A., 182
 Eberhagen, A., 348
 Ecker, G., 328, 329
 Edels, H., 171, 317
 Edgecumbe, J., 286
 Egerton, A., 191
 Eicke, H. F., 348
 Elder, P., 319
 Elenbaas, W., 353
 El Hili, A., 305
 Ember, G., 204(122), 205
 Emeléus, K. G., 73
 Emmerson, J. McL., 288
 Emrich, R. J., 163, 172
 Emslie, A. G., 8
 Enge, H. A., 280
 Engelhardt, A. G., 49
 Engstrom, R. W., 109
 Ennos, A. E., 284, 303(50)
 Erginsoy, C., 245, 252, 253, 254, 261(55)
 Eriksson, L., 250, 258
 Ernst, R. R., 288
 Ertel, D., 241
 Euler, J., 308
 Evans, D. S., 283
 Evenson, K. M., 210
 Everhart, T. E., 278
 Evtuhov, V., 302
 Ewald, H., 280

F

Fabre, D., 276(12), 277
 Fahlman, A., 302
 Fain, D. L., 284
 Fairbairn, A. R., 179
 Fano, U., 234, 276(4), 277, 289, 292,
 293(92), 300(4)
 Farkas, G. Y., 109
 Farmery, B. W., 262
 Farnsworth, H. E., 299

Favin, S., 196, 202(24), 204(120), 205
 Fay, J. A., 182
 Fedoseev, E. P., 280
 Fehsenfeld, F. C., 118, 119(40), 131, 133,
 134, 136, 137, 138, 139, 229
 Feibelman, W. A., 108, 109(27)
 Feinberg, R. M., 182
 Feldman, S., 151
 Felmlee, X., 178
 Fenimore, C. P., 190, 196, 202(29), 205,
 221(32, 34), 222(30, 35, 37), 223(34, 36)
 Ference, M., 282
 Fergerson, E. E., 118, 119(40)
 Ferguson, E. E., 131, 133, 134, 136, 137,
 138, 139
 Ferrell, R. A., 292, 293(105) 294, 295,
 297(115)
 Ferron, J. R., 204(122), 205
 Feugier, A., 198(72), 199, 227(72)
 Field, G. B., 18
 Fink, M., 291
 Finkelnburg, W., 307, 309(1), 326, 329(1),
 336, 337, 342, 343, 352(1)
 Firsov, O. B., 250
 Fisher, L. H., 64, 70, 71(57), 72, 74
 Fite, W. L., 113, 125, 126, 130, 131, 136,
 139, 270, 272, 273, 274, 352
 Fliermans, L., 303
 Fluit, J. M., 265
 Flynn, C. P., 288
 Foner, S. N., 196, 197
 Fontana, P., 28
 Fontijn, A., 198(55, 71), 199, 224(56), 225,
 227(71)
 Formato, D., 100, 102(21)
 Forty, A. J., 303
 Foster, E. W., 347
 Fowler, H. A., 294, 299, 305
 Fowler, R. G., 147
 Fowler, R. H., 333
 Fraff, K., 285
 Francombe, M. H., 285
 Franken, P. A., 3, 4
 Frankl, D. R., 305
 Franz, F. A., 14, 23(36), 25
 Franzen, W., 8, 22
 Fraser, R. G. J., 270, 271
 Frazier, G., 204(118), 205
 Freely, J. B., 74
 Freeman, M. P., 317, 318(31), 319

- Frie, W., 317, 338
 Friedman, R., 196, 201, 202(39)
 Friedman, S. I., 283
 Friedman, W., 229
 Friedrich, J., 317
 Friesen, J., 243
 Fristrom, R. M., 190, 193, 196, 202(21, 24)
 203, 204, 205, 210(28), 222, 223
 Frommer, L., 208
 Frommhold, L., 61, 71, 75(62), 109, 116,
 120(31), 122(31)
 Frost, L. S., 34, 35(12), 36(12), 45(12), 46,
 47(12), 48(12), 51(12), 54
 Fukuhara, A., 304
 Fundingsland, O. T., 86, 94(10), 96(10),
 123(10)
- G**
- Garber, F. W., 298
 Garfinkel, A. F., 238
 Garvin, D., 208, 209
 Gatz, C. R., 228
 Gaydon, A. G., 179, 184, 185, 190, 191,
 192, 195, 211, 214, 220
 Geballe, R., 74
 Geets, J., 280
 Geiger, J., 100, 291
 Generalov, N. A., 179
 Gericke, W. E., 330, 347(64)
 Gerjuoy, E., 50
 Gerlach, R. L., 304
 Gershenson, Yu. M., 210
 Gevers, R., 276(8), 277, 304(8)
 Gibbs, B. G., 288
 Gibson, W. M., 252, 253, 254
 Giedt, R. R., 186
 Gilardini, A., 100, 102(21)
 Gilman, G. I., 138
 Ginzburg, V. L., 353
 Gjønnes, J., 304(163), 305
 Glaeser, W., 305
 Glass, G. P., 228
 Glass, I. I., 179, 184
 Glennon, B. M., 322, 331(43)
 Glick, A. J., 292, 293(105)
 Glick, H., 180
 Gobeli, G. W., 299
 Göing, W., 326
- Goldan, P. D., 133, 134, 136, 137
 Golden, D. E., 70, 71(57), 72
 Goldstein, L., 99, 100, 123(19)
 Gomer, R., 303
 Goodrich, G. W., 283
 Goringe, M. J., 304(163), 305
 Gosseries, A., 71
 Gould, L., 96, 100, 123(18)
 Gout, C., 276(12), 277
 Graham, R. L., 242, 284
 Gray, E. P., 116
 Greaves, C., 87
 Green, J. A., 198(67, 68), 199, 202(67, 68),
 224(67, 68), 225(67), 226, 227(67, 68)
 Green, M., 301
 Greene, E. F., 141, 148, 149(2), 151, 155,
 170, 173, 176, 179, 183(2)
 Greene, F. T., 196, 197
 Greybar, H. D., 151
 Griem, H. R., 317, 325, 326(21), 328,
 329(21), 334, 336, 343(21), 344(91), 345,
 349, 350(21), 351(21)
 Grissom, J. T., 288
 Grivet, P., 279
 Grossetete, F., 19, 21(46), 23(46)
 Grunfelder, C., 196, 202(21, 24), 203
 Gruszczynski, J. S., 176, 183(37)
 Guinn, V. P., 208
 Gunton, R. C., 84, 123
 Gurevich, A. V., 353
 Gurevich, D. B., 342, 343
 Gwyn, P. P., 209
- H**
- Hachenberg, O., 302
 Haines, R. L., 208
 Hall, C. R., 304(163), 305
 Hall, J. G., 143, 149(3), 186
 Hamilton, D. R., 283
 Hamm, R. N., 303
 Haneman, D., 298
 Hanke, C. C., 238
 Hansen, F. C., 182
 Hansen, N. R., 298
 Hansen-Schmidt, J., 305
 Hanson, R. J., 20
 Hardwick, E. R., 170
 Harrison, H., 170

- Harrison, M. A., 74
 Harrower, G. A., 302
 Hartman, T. E., 286
 Hartunian, R. A., 163, 164, 170, 182, 186
 Harwell, K., 187
 Hashimoto, H., 304
 Hass, G. 238
 Hasted, J. B., 55, 125
 Hawkins, W. B., 2, 8
 Heyhurst, A. N., 198(69), 199, 224(69), 227
 Hayne, G. S., 3
 Heald, M. A., 86, 93(9), 97(9), 98(9), 99, 102(9)
 Healey, R. H., 45, 50(30), 51
 Hearn, A. G., 344
 Hearne, K., 317
 Heath, D. F., 195
 Heavens, O. S., 285
 Heide, H. G., 284, 303(51)
 Heidenreich, R. D., 276(5), 277, 289, 304(5)
 Heierman, J. H., 217
 Heil, H., 299
 Heinen, H., 245
 Heller, W., 207
 Henneberg, W., 279
 Henning, H., 349
 Henry, L., 305
 Herlitz, S. I., 317, 318(32)
 Herman, R., 28
 Herman, R. M., 25, 26
 Herrmann, H., 245, 248(35)
 Herrmann, R., 194
 Herschbach, D. R., 208
 Hersey, M. D., 287, 289(83)
 Hertzberg, A., 180
 Herzfeld, K. F., 184
 Herzog, R., 280
 Hickmott, T. W., 299
 Hilgner, W., 291
 Hines, R. L., 241
 Hink, W., 303
 Hinnov, E., 216
 Hintenberger, H., 265
 Hirsch, P. B., 276(12), 277, 284(13), 304(13, 163), 305
 Hobart, J., 3
 Hobson, J. P., 304
 Hodges, A. J., 17
 Hodgins, J. W., 208
 Hofmann, F. W., 200(101), 201, 216, 218(84), 229(94, 101)
 Hogan, J. M., 198(55), 199, 224(56), 225(56)
 Holden, W. R., 147
 Holland, L., 285, 286(63)
 Holland, R. E., 260, 261
 Hollander, T., 200, 216, 218
 Holloway, D. F., 262
 Holloway, W. W., 3
 Hollweg, J. V., 299
 Hörlzl, J., 302
 Hooker, W. J., 166
 Hooymayers, H. P., 220
 Hörmann, H., 317
 Hornbeck, J. A., 35, 61
 Hörfeldt, O., 302
 Hornig, D. F., 170
 Horstmann, M., 305
 Horton, C. W., 280
 Howe, L. M., 244, 251
 Howie, A., 276(13), 277, 284(13), 304(13, 163), 305
 Hoyaux, M., 280
 Hubbard, J., 292
 Hubbell, H. H., 303
 Hudson, R. L., 196, 197
 Huldt, L., 216
 Hunt, W. W., 283
 Hurle, I. R., 185, 186
 Hurst, C. A., 43
 Huxley, L. G. H., 36, 37, 39(16), 41(16), 50(16)
- I
- Ibers, J. A., 291
 Ifarov, G. A., 259
 Inglis, D. R., 201
 Ioup, G. E., 288
 Ishida, K., 305
 Isles, G. L., 193
- J
- Jackson, J. M., 184
 Jacobs, T. A., 186
 Jacquinot, P., 108
 Jahn, R. G., 187

- James, C. G., 198, 211(49), 212, 214, 216, 217(207), 218(209), 219(207), 220(194)
 Jehanno, C., 283
 Jenkens, D. R., 220
 Jerrick, J., 319
 Jespersgaard, P., 248, 250
 Jessey, M. E., 169, 170(30)
 Johnson, D. C., 304
 Johnston, H. S., 170, 209
 Johnston, K. H., 299
 Johnstone, A. D., 283
 Jones, A. F., 288
 Jones, E., 70
 Jones, G. W., 196, 202(29), 205, 221(32, 34), 222(30, 35, 37), 223(34, 36)
 Jory, R. L., 36, 37
 Julliot, C., 283
 Jung, M., 351
 Jürgens, G., 311, 323, 349
- K**
- Kainuma, Y., 304
 Kalff, P. J., 200, 218(86)
 Kalibjian, R., 283
 Kaminsky, M., 264
 Kamiya, Y., 305
 Kane, E. O., 299, 301
 Kanter, H., 301
 Kantrowitz, A., 151
 Kaplan, D. E., 177
 Karpinski, J. Z., 283
 Kaskan, W. E., 198, 202, 211, 220, 222(109)
 Kasner, W. H., 82, 113, 117(4), 118(4)
 Kastler, A., 1, 2, 3
 Katz, M. J., 285
 Katz, S., 317, 318(31), 319
 Kaufman, E. D., 208,
 Kaufman, F., 211, 236
 Kay, D. H., 284
 Keck, J., 186
 Kelly, J. C., 303
 Kemp, N. H., 182
 Kennedy, M. J., 283
 Kerr, D. E., 116
 Kessler, J., 291
 Khan, I. H., 304
 Khan, J. M., 260
 Kiker, W. E., 238
- King, I. R., 199, 202(80), 224, 228
 Kingston, A. E., 119, 120(42), 344
 Kistemaker, J., 264, 265
 Kistiakowsky, G. B., 178, 208
 Klein, L., 28
 Klein, M. P., 288
 Klemperer, O., 277, 278(15), 280
 Knable, N., 23
 Knewstubb, P. F., 198(63, 64, 65, 66), 199, 200, 224(63, 65, 66), 227(66)
 Knight, H. T., 178
 Kobayashi, K., 303
 Koch, H. W., 290
 Koehler, D. R., 288
 Kohn, H., 200, 216, 217, 218(84)
 Kolb, A. C., 334, 350(70)
 Kolesnikov, V. N., 346, 352, 353
 Kolesnikova, R. V., 210
 Komareva, R. F., 243
 Kondratev, V. N., 210
 Kornelsen, E. V., 244, 248(29), 249
 Kostkowski, H. J., 211, 224
 Köstlin, H., 348
 Krasnow, M. E., 293
 Krause, M. O., 288
 Kröll, W., 328, 329
 Krysmanski, K. H., 345
 Kühn, V., 353
 Kunkel, W. B., 114
 Kurzius, S. C., 198(55), 199, 200(55), 225(55), 228(55)
 Kusch, H. J., 351
 Kuyatt, C. E., 278, 279, 280
 Kydd, P. H., 178
- L**
- Labuhn, F., 340
 Lamb, L., 187
 Lambert, R. H., 3
 Lampert, M. A., 100
 Land, E. H., 17
 Landau, L., 184
 Lander, J. J., 298, 304
 Lang, I. G., 243
 Langdorf, A., 289
 Langstroth, G. F. O., 125
 Larenz, R. W., 333
 Lassettre, E. N., 293

- LaVilla, R. E., 294
 Lawson, W. H., 285, 286(72)
 Leder, L. B., 277, 279
 Lee, R. D., 324
 Lee, R. J., 147
 Legler, W., 293
 Lehmann, C., 251
 Leibfried, G., 245, 251
 Leisegang, S., 278
 Lenz, F., 290, 300
 LeRoy, D. J., 207, 208
 Liley, B. S., 43
 Lin, S. C., 151, 187
 Lindhard, J., 233, 234, 235, 236, 258
 Lindsay, A. L., 204(126), 205
 Ling, J., 304
 Litovitz, T. A., 184
 Little, P. F., 74
 Littlewood, K., 198(62), 199
 Llewellyn Jones, F., 62, 70
 Lochte-Holtgreven, W., 322
 Loeb, L. B., 34, 50, 51, 55, 57, 59, 60, 61,
 62, 72, 73, 74, 75
 Lorentz, H. A., 85, 86(6)
 Losev, S. A., 177, 179
 Lowke, J. J., 35
 Lozier, W. W., 308
 Lucovsky, G., 17
 Lunt, R. W., 73
 Luscher, E., 3, 23, 25
 Lutz, H. O., 244, 245, 246, 248(35), 255,
 256, 261
 Lyddane, R. H., 282
 Lynch, J., 16
- M**
- MacCallum, S. P., 70
 MacRae, A. U., 304
 McCargo, M., 244, 246, 248, 249, 250
 McChesney, M., 328
 McConnell, W. J., 303
 McCoubrey, A. O., 102
 McDaniel, E. W., 59
 McEwan, M. J., 211
 MeFee, J. H., 274
 McGee, K. E., 283
 McGinnies, R. J., 303
 McIntosh, A. I., 43
- McIntyre, J. D., 243
 McKinley, J. D., 209
 McLean, E. A., 334
 McNeal, R. J., 23, 25
 McRae, E. G., 304
 McWhirter, R. W. P., 119, 120(42), 343,
 344
 Macek, A., 201
 Mack, J., 172
 Maecker, H., 307, 309(1), 311, 312, 313,
 317, 322, 326, 329(1), 333(12, 24), 336,
 337(24), 338, 342, 343, 352(1), 353
 Mahan, B. H., 84
 Mailander, M., 217
 Major, F. G., 4, 13(22)
 Majorana, E., 11
 Malov, A. F., 280
 Mannami, M., 305
 Mannkopff, R., 342
 Marcus, P. M., 274
 Margenau, H., 28, 85, 86
 Margerie, J., 3
 Mark, H. J., 168
 Markarious, R., 258
 Markstein, G. H., 209
 Marple, D. T. F., 284
 Marrone, P. V., 163, 170, 182, 186
 Marsh, O. J., 258
 Marshak, I. S., 77
 Marshall, T., 180, 183(56)
 Martin, E. D., 146
 Marton, L., 277, 280, 294, 305
 Mashkova, E. S., 265
 Massey, H. S. W., 55, 298, 302
 Mastrup, F., 338
 Matthews, J. W., 285
 Mattuck, A., 202
 Matzke, H., 258
 Mayer, J. W., 258
 Meek, C. A., 73
 Meggers, W. F., 347
 Megill, L. R., 229
 Mendlowitz, H., 277, 280, 294
 Menz, W., 291
 Menzel, D., 303
 Menzel, E., 286
 Metchnik, V., 303
 Metherell, A. J. F., 282, 304(163), 305
 Methfessel, S., 299
 Meyer, G., 305

- Meyer, J., 351
 Michael, J. V., 228
 Miller, W. J., 198(55, 70, 71), 199, 200(55),
 224(56), 225(55, 56), 226, 227(71), 228(55)
 Millikan, R. C., 184, 196
 Milne, E. A., 333
 Milne, T. A., 196, 197
 Mirrels, H., 161, 162, 164, 166
 Misell, D. L., 288
 Misso, C. E. F., 283
 Mitchell, A. C. G., 7, 16(27), 216
 Mitchell, I. V., 262
 Mitchell, J. W., 303
 Mittelstadt, V. R., 123
 Moak, C. D., 254, 255, 256, 261, 264
 Modica, A., 178
 Molchanov, V. A., 265
 Möllenstedt, G., 281
 Molnar, J. P., 118
 Monahan, J. E., 289
 Monchick, L., 204(120), 205
 Moore, A. J. W., 287
 Moore, C. E., 322, 328(42)
 Moore, G. E., 270, 273
 Morris, D., 111, 112, (32)
 Morrison, J., 298, 304
 Morrison, J. D., 288
 Moskowitz, J. W., 209
 Motschmann, H., 353
 Mott, N. F., 184, 298
 Motz, J. W., 290
 Muntz, E. P., 177, 178
 Murphy, P. W., 326, 336(53), 351(53)
- Nichols, L. K., 123
 Nicholson, R. B., 276(13), 277, 284(13),
 304(13)
 Niedrig, H., 305
 Nielsen, K. O., 233, 259
 Nielsen, R. A., 34
 Nieuwpoort, W. C., 211
 Niki, H., 228
 Niles, F. E., 118
 Noggle, T. S., 254, 255, 256, 261
 Nolan, J. F., 34
 Nonoyama, M., 304
 Norbeck, E., 237
 Nordling, C., 302
 Norman, G. E., 337, 349(78)
 Northcliffe, L. C., 255
 Novick, R., 3
 Null, M. R., 308

O

- Obukhov-Denisov, V. V., 352, 353
 Oen, O. S., 246
 Oertel, G., 351
 Ogilvie, R. E., 303
 Okuneva, N. M., 243
 Olsen, H., 290
 Olsen, H. N., 309, 310, 317, 329, 330, 333,
 337(62), 347(64)
 Ornstein, L. S., 322, 342
 Osanov, B. A., 283
 Oshchepkov, P. K., 283
 Oskam, H. J., 80, 88, 112(3), 123
 Otto, A., 297
 Ozherelev, B. V., 210

N

- Nagamatsu, H. T., 146
 Nakai, M. Y., 298, 299(122)
 Nakano, H., 70, 71(57)
 Nalbandyan, A. B., 210
 Nedelec, O., 4
 Neiler, J. H., 254
 Nelson, O. L., 299
 Nelson, R. S., 246, 251, 262
 Nemeth, E. M., 209
 Nestor, O. H., 317
 Neugebauer, C. A., 285, 296(69)
 Newkirk, J. B., 285, 286(64)
 Neynaber, R. H., 352

P

- Pack, J. L., 34, 35(12), 36, 43, 44, 45,
 47(12), 48, 51(12), 52, 61, 104, 106(24),
 118(24)
 Padley, P. J., 191, 193(10), 200(102, 104,
 105, 106), 201, 215, 216, 218(10), 220
 (201), 229(102, 104, 105, 106)
 Páschke, R., 302
 Page, F. M., 200
 Palmer, H. B., 170
 Pandya, T. P., 206
 Panfilov, V. N., 210
 Panin, B. V., 265

- Paquette, D. R., 314, 315, 318, 324, 325,
 334(18), 346(47), 347(47), 350(18), 351(18)
 Perez, J., 123
 Parker, J. H., Jr., 37, 41, 42, 51(18)
 Parker, W., 284
 Parrish, W., 288
 Pashley, D. W., 276(13), 277, 284(13),
 285, 286(65), 287(65), 304(13)
 Passel, T. O., 241
 Patch, R. W., 177
 Patrick, R. M., 148
 Paul, W., 111
 Payne, K. G., 228
 Peacock, F., 204(127), 205
 Pearce, W. J., 317
 Pebay-Peyroula, J. C., 4
 Pell, E. M., 286
 Penning, F. M., 72
 Pesic, D., 220
 Peters, H., 3
 Peters, M. F., 15
 Peters, Th., 312, 333(12), 337, 353(14)
 Petritz, R. L., 17
 Petschek, H. E., 187
 Pfender, E., 311
 Pfund, A. H., 308
 Phelps, A. V., 34, 35, 36, 43, 44, 45, 46,
 47(12), 48, 49, 51(12), 52, 54, 58, 59(45),
 61(45), 86, 94(10), 96, 104, 106(24),
 118(24), 123(10), 124
 Phillips, J. C., 292
 Phillips, L. F., 211, 212, 216, 218(196),
 220
 Phillips, W. R., 242
 Picus, G. S., 299
 Piercy, G. R., 244, 246, 248(29), 249, 250
 Pines, D., 292, 296
 Pipes, L. A., 317
 Pipkin, F. M., 3, 20
 Pistoulet, B., 299
 Pittaway, L. G., 304
 Plumb, R. C., 285, 287
 Podmoshenskii, I. V., 342, 343, 345
 Pöhlau, C., 245
 Pokhil, G. P., 259
 Polanyi, J. C., 209
 Polanyi, M., 206, 207, 208
 Poncelet, J., 227
 Popenoe, C. H., 326, 330(54), 336(54),
 346(54), 347(54, 64), 351(54)
 Porile, N., 241
 Porteus, J. O., 288
 Potter, D. L., 260
 Powell, C. F., 34
 Powell, C. J., 287, 294, 296, 297
 Powers, D., 242
 Powling, J., 191, 192
 Pradal, F., 276(12), 277
 Prasad, A. N., 55, 72
 Prescott, R., 196, 202(21)
 Pringle, J. P. S., 242, 244, 251
 Pruett, G. R., 17
 Purcell, E. M., 18
 Puzanov, A. A., 262, 263
- Q
- Quinn, J. J., 298, 299(123)
- R
- Rabi, I. I., 10
 Rabinovitch, B. S., 207, 208
 Rabinowicz, J., 169, 170(30)
 Raether, H., 35, 62(15), 66, 74, 77(15),
 276(11), 277, 292, 297(11), 304
 Ramsden, S. A., 334
 Ramsey, A. T., 21, 23(49), 25
 Ramsey, N. F., 13
 Rapp, D., 209
 Rauth, A. M., 301
 Read, F. H., 242
 Reed, J. F., 207, 208
 Reed, J. W., 45, 50(30), 51
 Rees, A. L. G., 304
 Rees, J. A., 37
 Regel, A. R., 243
 Reid, R. W., 197, 212, 214(193), 218(193)
 Reimer, L., 303, 304
 Reinhard, H. P., 111
 Repenning, K. J., 318
 Resler, E. L., 151
 Resler, E. L., Jr., 180
 Reuter, J. L., 198, 224(54), 225(54)
 Rhodin, T. N., 304
 Richter, J., 334, 338, 346
 Risk, C. G., 49
 Ritche, R. A., 295, 297(114)

- Ritchie, R. H., 288, 298, 299(122), 303
Roberts, D. E., 351
Roberts, J. A., 17
Roberts, R. W., 286
Robertson, W. W., 118, 119(40)
Robins, J. L., 304
Robinson, H. G., 3
Robinson, L. B., 28
Robinson, M. T., 246
Roder, O., 351
Rogers, D. A., 176, 183(37)
Rogers, F. T., 280
Rompe, R., 328
Rook, H. L., 285
Rose, D. J., 72, 88, 94(15)
Rose, M. E., 6
Rose, P. H., 146, 166
Rosenfeld, J. L. J., 192, 216
Roshko, A., 166
Rosser, W. A., 228
Rott, N., 168
Roustdard, C., 299
Rouzeyre, M., 299
Rowland, P. R., 284
Ruark, A. E., 15, 282
Rubin, S., 241
Rusin, L. Yu., 210
Russo, A. L., 163, 186
Rutherford, E., 34
Rutherford, J. A., 113, 125, 126(6), 130(6),
 131, 136(6), 139
- S**
- Sachyan, G. A., 210
Sadowski, C. M., 209
Sakaoku, K., 303
Salzberg, H., 272
Sandner, P., 240
Sands, R., 3
Sapp, W. W., 283
Sarkisyan, E. N., 210
Satchler, G. R., 5, 7
Sato, H., 285
Sattler, A. R., 254
Sauder, W. C., 288
Sauerbrey, G., 285, 286(72)
Savoye, E. D., 299, 301
Sayers, J., 125, 128, 129(4, 7), 131, 138
Schaetti, N., 283
Scharff, M., 233, 234, 235(3), 236(3)
Schenk, H., 312, 353(14)
Scheurich, J. T., 224
Schiff, H. I., 133, 134, 136, 137
Schiffer, J. P., 260, 261
Schiøtt, H. E., 233, 234, 235(3), 236(3)
Schlüter, D., 337, 349
Schlumbohm, H., 71, 75(63)
Schmeltekopf, A. L., 118, 119(40), 131,
 133, 134, 136, 137, 138, 139
Schmidt, H., 240
Schmitt, H. W., 238, 254
Schmitt, R. A., 241
Schmitz, G., 307, 337
Schnautz, H., 310
Schneider, J., 200(101), 201, 229(94, 101)
Schönherr, O., 310
Schofield, K., 200, 218, 221, 222(231), 230
Schott, O., 286
Schottky, W., 80
Schuckert, R. D., 245
Schulz, P., 353
Schumacher, B. W., 276(6), 277
Schwartz, R. N., 184
Scott, G. G., 15
Scott, P. B., 274, 275
Scott, W. T., 290, 300
Scribner, B. F., 347
Seaton, M. J., 337, 348
Seiwatz, R., 298
Selig, O., 244
Series, G. W., 1, 4
Shaw, A. E., 282
Shaw, T. M., 84, 123
Sharpe, J., 109
Sharpless, R. L., 228
Shearer, L. D., 4, 12
Shen, K. Y., 334, 350(70)
Shilov, A. E., 210
Shin, J. J., 286
Shoulders, K. R., 283
Shuler, K. E., 195, 200
Shumaker, J. B., Jr., 313, 317, 318, 326,
 329, 330(54), 336(54, 61), 346(54), 347(54,
 61, 64), 351(54)
Siegbahn, K., 279, 288(27)
Silverman, S. M., 293
Simpson, J. A., 278, 279, 280, 282, 294,
 301

- Sims, G., 243
 Siprikov, I. V., 283
 Sizmann, R., 244, 245, 246, 248(35), 304
 Skinner, G. T., 183
 Skinner, H. W. B., 1
 Skvortsov, B. N., 283
 Slater, J. C., 87
 Slater, M., 280
 Slatis, H., 284
 Slawsky, Z., 184
 Smiley, E. F., 182
 Smit, J. A., 197, 220, 347
 Smith, D., 125, 129(7), 131, 138(7)
 Smith, F. T., 207, 208, 228
 Smith, G. F., 302
 Smith, G. H., 290, 291
 Smith, H., 200, 211
 Smith, H. P., Jr., 260
 Smith, J. N., Jr., 272, 273, 274
 Smith, M. W., 322, 331(43)
 Smith, W., 180
 Snoek, C., 264, 265, 266, 267, 272(82)
 Snow, W. R., 125, 126(6), 130(6), 136(6)
 Sobolev, N. N., 346
 Sorensen, H., 238
 Softley, E. J., 178
 Solarksi, J. E., Jr., 314, 315, 324, 334(18),
 346, 347(96), 350(18), 351(18)
 Sonner, A. H., 283
 Soshea, R. W., 302
 Spalding, D. B., 191, 193
 Speidel, R., 285
 Spencer, L. V., 303
 Spicer, W. E., 299, 301
 Spindt, C. A., 283
 Squire, W., 180
 Stampa, A., 351
 Stark, J., 246
 Starr, L. H., 34
 Steacie, E. W. R., 207
 Steenbeck, M., 328
 Stein, S., 50
 Steinberg, M., 184
 Steinberger, S., 313
 Stephenson, R. J., 282
 Stern, E. A., 295, 297(115)
 Sternglass, E. J., 283, 301
 Sternheimer, R. M., 275
 Stickney, R. E., 270
 Stuart, R., 301
 Stuart, R. N., 301
 Süsskind, C., 278
 Suffredini, C. S., 241
 Sugarman, N., 241
 Sugden, T. M., 191, 192, 193, 197, 198(63),
 69, 73), 199, 200, 202(67, 68), 211(49),
 212, 214(193), 215, 216, 217(207),
 218(193, 196, 209), 219(14, 207), 220
 (194, 201), 224(63, 65, 67, 68), 225(67),
 226, 227(66, 67, 68)
 Sutton, M. M., 196, 204(19), 216, 221(19),
 20, 204), 222(20, 230)
 Swaine, J. W., 287
 Swan, J. B., 288, 297
 Swanson, N., 294, 296
 Sze, S. M., 299
- T
- Taelemans, G., 227
 Talbot, L., 156
 Tanaka, K., 305
 Taylor, E. H., 270, 273
 Taylor, R. L., 184
 Teller, E., 184, 201
 Thabet, S. K., 191
 Theimer, O., 328
 Thomas, B. S., 288
 Thomas, G., 284
 Thomas, H., 299
 Thomas, R. N., 290, 291(96), 301
 Thomas, V. G., 63
 Thompson, M. W., 246, 251, 259
 Thompson, W. P., 186
 Thrush, B. A., 200, 224
 Titchmarsh, E. C., 317
 Tizard, H. T., 34, 57
 Toennies, J. P., 141, 148, 149(2), 151, 155,
 170, 173, 176, 179, 183(2)
 Tolansky, S., 238, 244(14), 285, 286
 Tomboulian, D. H., 286
 Tomlin, S. G., 303
 Tonomura, A., 305
 Townsend, J. S., 34, 40, 41, 45, 51, 57, 70,
 72, 75
 Townsend, P. D., 303
 Travers, B. E. L., 199, 200(77), 228(77)
 Treanor, C. E., 186
 Trilling, L., 274, 275

- Trimpf, R. L., 164
 Tsvetkov, Yu. D., 210
 Tubbes, M. R., 303
 Tüxen, O., 124
 Tulinov, A. F., 259, 262, 263
 Turcotte, D. L., 229
 Turner, A. F., 238
 Turner, J. E., 300
 Tyndall, A. M., 34

U

- Uggerhøj, E., 257
 Uhlenbusch, J., 307
 Uhler, J., 242
 Ulyanov, K. N., 337, 349(78)
 Unsöld, A., 337
 Uyeda, R., 304, 305

V

- Vainshtein, B. K., 291
 Van de Graaff, R. J., 34
 Van der Held, E. F. M., 216, 217
 van Lint, V. A. J., 123 125, 126(6), 130(6),
 136(6), 241
 van Tiggelen, A., 198(57–61, 72), 199,
 224(61), 227(60, 72)
 van Trigt, C., 216
 Varga, P., 109
 Varney, R. N., 64
 Varnum, C. M., 26
 Vaughan, A., 177
 Venable, D., 177, 178
 Vennik, J., 303
 Vermilyea, D. A., 285, 286(64)
 Voevodskii, V. V., 210
 von Ardenne, M., 62
 von Engel, A., 62
 von Hartel, H., 207, 208
 von Zahn, U., 111
 Voshall, R. E., 34, 35(12), 36(12), 44,
 45(12), 47(12), 48(12), 51(12)
 Vriens, L., 197

W

- Wachman, H. Y., 274, 275
 Wahlin, H. B., 34

- Walker, F. J., 237, 254, 264(10)
 Walker, R. E., 204(119–121, 123), 205
 Walker, R. F., 285
 Walker, W. W., 264
 Walther, V., 265
 Ward, A. L., 72
 Warhurst, E., 207
 Warren, R. W., 37, 41, 42, 51(18)
 Warren, W. R., Jr., 176, 183(37)
 Watanabe, H., 305
 Waters, P. M., 285
 Watson, R., 177
 Webber, E. W., 4
 Weber, J., 200
 Wegner, H. E., 252, 253, 254
 Wehner, J. F., 205
 Weinberg, F. J., 195, 204(127), 205, 206,
 228
 Weller, C. S., 123
 Wells, G. F., 254
 Wende, B., 337, 349
 Wendt, G., 246
 Westenberg, A. A., 190, 196, 202, 203, 204
 (118, 119, 123, 124, 125), 222, 204(120),
 205, 210(28)
 Whaling, W., 242
 Wharton, C. B., 86, 93(9), 97(9), 98(9), 99,
 102(9)
 Wheeler, R. C., 200
 Whelan, M. J., 276(13), 277, 282, 284(13),
 304(13, 163), 305
 White, D. R., 146, 184, 187
 Whittaker, D., 171
 Whittle, J., 301
 Whitton, J. L., 244, 251
 Wiechmann, W., 241
 Wielgoz, K., 241
 Wiese, W. L., 314, 315, 318, 322, 324, 325,
 326(49), 329, 330(49), 331(43), 334(18),
 336(53, 61), 338, 340, 346(47), 347(47),
 61, 84, 96), 350(18), 351(18, 53, 84), 353
 Wijsman, R. J., 71
 Wilde, D. J., 289
 Wiley, W. C., 283
 Wilkins, R., 186
 Williams, A., 196, 204(19), 205(18), 216(18),
 221(19, 20, 204), 222(20, 230)
 Williams, C. W., 238
 Williams, H., 199, 200(77), 228(77)
 Williams, R., 208

- Wilson, J., 186
Wilson, J. H., 198(62), 199
Wilson, R., 343
Wilson, W. E., 210
Windsor, M. W., 184
Winter, J. 2, 11
Wise, H., 228
Witteborn, F. C., 182
Wittke, J. P., 18
Wobig, K. H., 351
Wohl, K., 204(122), 205
Wolfhard, H. G., 190, 195(2), 205, 211
Wollnik, H., 280
Wolter, A. R., 286
Wooten, F., 301
Worley, R. D., 260
Wray, K. L., 185, 186
Wyatt, M. E., 123
- Yaffie, L., 284
Yaggy, L. S., 302
Yankow, V. V., 329
Yokley, C. R., 317, 318(34)
Young, A., 317
Young, R. A., 228
- Zeegers, P. J. Th., 211
Zeitler, E., 290
Zemansky, M. W., 7, 16(27), 61, 216
Zeppenfeld, K., 304
Zimen, K. E., 241
Zörner, K. -H., 288
Zollweg, R. J., 299
zu Putlitz, G., 4

Y

Z

SUBJECT INDEX

A

- Abel inversion process, 315-319
"Accommodation coefficient," 269
Acoustic waves, speed, 179
Afterglows, atomic collision studies, 113-124
 electron-ion recombination, 113-118
 mechanism, 118-123
cavity methods for measurements, 87-96
definition of, 78-79
excitation methods for, 82-85
flowing, chemical aspects of, 133-139
 mass spectrometry of, 131-133
free space microwave propagation measurements, 96-99
guided wave propagation measurements, 99-100
mass spectrometric techniques for, 111-113
microwave radiation measurements, 100-102
observational methods for, 85-113
particle continuity equations, 79-82
reflected microwave signal measurements, 93
stationary, mass spectrometry of, 124-131
 apparatus, 124-127
 data analysis methods, 128-131
studies using, 78-79
Ambipolar diffusion coefficient, in afterglow studies, 80
Apparatus, for optical pumping, 13-18
Atomic beams, for optical pumping, 13
Atomic collisions of electrons, ions, and excited atoms, 78-124
 particle continuity equations, 79-82
Atomic transition probabilities, electric arc use in, 347-348
"Atomistic" description of solids, 289-304
Atoms, excited, collisions of, 78-124
Attachment coefficient, measurement of, 56

Auger electron emission, 202

Avalanche, electron, definition, 66-67

B

- Bethe-Bloch stopping formula, 235
Botha-Spalding burner, 192, 193
Breakdown, direct-current type, 75-77
 near atmospheric pressure, 77
Buffer gases, in flowing afterglows, 133-136
 in optical pumping, 13

C

- Cathode sputtering of thin-surface layers, 244-245
Cavity methods for afterglow measurements, 87-96
"Channeling" in penetration studies, 245-264
Chemical etching in thin surface removal, 243
Chemiluminescent method of flame study, 214-215
Chronointerferometer, 172-173
Collision cross section for attachment, 56
 measurement of, 57
Collision cross sections from swarm experiments, 45-48
 fractional energy loss per collision f , 50-54
 quantitative descriptions, 56
Collision deactivation measurement, 220
Complex conductivity of electrons, in afterglow studies, 85, 86
Continuum emission coefficients, electric arc use for, 348-349
Crossed beam technique for measurement of relaxation times, 24
CuH emission as a measure of relative [H], 212
Current density in afterglow studies, 79

D

- Dark discharge, 63
 Density measurements of shock waves, 171-177
 Diffusion measurement in electron swarms, 32-34
 Diffusion coefficient in afterglow studies, 79-80
 Diffusion flame technique, 207-208
 Diffusion flames, 206
 Dilute flame method, 206-207
 Double resonance technique, 1
 Drift velocity of electron swarms, 34
 Druyvesteyn distribution, 41, 50

E

- Egerton-Powling burner, 191-192
 Elastic scattering cross sections, electric-arc use in studies of, 351-353
 Electric arcs, 307-353
 Abel inversion process, 315-319
 applications of, 347-353
 in atomic transition probabilities, 347-348
 in continuum emission coefficients, 348-349
 in elastic scattering cross sections, 351-353
 in line-broadening parameters, 349-351
 arc sources, 307-315
 fluid-stabilized types, 309-312
 high-current, controlled atmospheric types, 309
 low-current atmospheric types, 308-309
 plasmas, local thermal equilibrium (LTE) in, 341-347
 temperature and density determinations in, 319-341
 absolute line intensities, 330-333
 Fowler-Milne method, 333-334
 in multielement arc plasmas, 338-341
 relative line intensities, 320-326
 stark widths and shifts, 334-337
 with density known, 327-334
 without density known, 320-326
 well-stabilized types, 312-314

- Electrolytic peeling of thin surfaces, 243-244
 Electromagnetic absorption methods, in flame studies, 229
 Electromagnetic shock tubes, 148
 Electron avalanche, definition of, 66-67
 Electron beam densitometers, in shock-wave studies, 177-178
 Electron collision frequency, derivation of, 86
 Electron detectors, 282-284
 Electron energy analyzers, 279-282
 Electron filter, 57-58
 Electron guns, 278-279
 Electron impact technique, 1
 Electron-ion recombination, afterglow studies of, 78
 Electron multiplier detector, 282-283
 Electron-solid interactions, 275-305
 analyzers for, 279-282
 detectors for, 282-284
 electron scattering in, 277-278
 experimental strategy, 287-289
 guns for, 278-279
 specimen preparation, 284-287
 Electron-spin resonance (ESR), in flame kinetic studies, 209-210
 Electron swarms, 29-77
 attachment and ionization occurring simultaneously, 74-75
 characteristic variables, 29-31
 collision cross sections by, 45
 cross sections for rotational excitation by, 48-49
 diffusion coefficient in, 38
 diffusion measurement in, 32-34
 coefficient of diffusion, 33-34
 mean free path for momentum transfer, 38
 direct-current breakdown, 75-77
 D/ μ measurement, 37
 experimental values, 41-44
 vs. E/ p , 41
 drift velocity in, 31-33
 experimental values of, 45
 electron attachment and electron affinity studies, 55-56
 measurement at low E/ p , 57-60
 electron detachment from negative ions, 60-61

electron drift speeds, measurement, 34–36
 electron shutter method, 35
 light source pulsing, 36
 voltage pulsing process, 36
 electron energies above room temperature, 48–49
 E/N , definition of, 31, 64
 E/p and pd , definitions, 30–31
 ionization by electron collisions, 61–69
 kinetic theory of diffusion in, 37–40
 kinetic theory of drift velocity and mobility, 39–40
 loss of kinetic energy of electrons in gases, 49–51
 mobility in, 32, 46
 observables of experiments on, 31
 Electrons, atomic collisions of, 78–124
 in flames, 198
 measurement, 227–229
 Emission intensity, in spectroscopy, 102
 Etalon, 106
 Excitation methods for afterglows, 82–85
 Excited atom ionizing collisions, afterglow studies of, 78

F

Fabry-Perot interferometer, 106
 measurements on dissociative recombination, 120
 Faraday cage, 282
 Flame intensity profiles, 218
 Flame kinetic studies, 189–230
 experimental techniques, 209–229
 optical studies, 209–220
 Flame photometry, [O] determination by, 214
 Flames, collisional deactivation measurement, 220
 composition of, 190–209
 definition of, 189
 diffusion type, 206
 electromagnetic absorption methods for, 229
 electrons in, measurement, 227–229
 equilibria and nonequilibria in, 194–195
 high-pressure types, 205
 in high-temperature studies, 189
 ions and electrons in, 198–201

isothermal type, 218–220
 life-period method, 208
 low-pressure type, 202–205
 microprobe sampling, 221–227
 scavenger methods, 223–227
 premixed type, 201–202
 radicals in, 196
 rate constants from, 230
 sources of, 191–194
 Flowing afterglows, chemical aspects of, 133–139
 mass spectrometry of, 131–133
 Fluid-stabilized arcs, 309–312
 Fowler-Milne method, modified, 333–334
 Free-space propagation methods, 96–99

G

Gases, loss of kinetic energy of electrons in, 49–51
 Gas-stabilized arcs, 309–312
 Gaydon-Wolfhard burner, 192
 Geiger counter, 282
 Guided wave propagation in afterglow studies, 99–100

H

Hanle effect, 4
 High-frequency electrodeless discharge lamp, 16
 Hot wires, in shock-wave studies, 180

I

Inelastic scattering of electrons, 292–297
 Interference filters, for optical pumping, 17
 Ionization, by electron collisions, 61–69
 Ionization gage, in shock-wave studies, 170
 Ions, atomic collisions of, 78–124
 in flames, 198
 Isothermal flames, 218–220

L

Langmuir probes, 199, 228–229
 Level-crossing technique, 4
 “Life-period” method, 208
 Line-broadening parameters, electric-arc use in studies of, 349–351

Local thermal equilibrium (LTE) in arc plasmas, 341-347
 Lorentz conductivity, derivation of, 86

M

Mach number, 144
 Mach-Zehnder interferometer, 171
 Magnetic fields, Helmholtz pair, 15
 for optical pumping, 14-16
 Mass spectrometry, of afterglows, 111-113,
 124-139
 in combustion studies, 190, 198, 221-227
 Metastable atom diffusion, afterglow studies of, 78
 Metastable atomic states, optical pumping of, 3-4
 Microprobe sampling, 203
 in flame studies, 221-227
 Microwave bridge, 98
 Microwave "noise" power, determination of, 101
 Microwave radiation measurements, in afterglow studies, 100-102
 Microwaves, use in afterglow studies, 78-79, 85-87
 Molecular beam, in shock wave studies, 183
 Multiple scattering of electrons in solids, 299-301

N

Negative ion-neutral reactions, 139

O

Optical absorption, measurements of, 104-106
 in spectroscopy, 102
 Optical pumping, 1-28
 apparatus for, 13-18
 containment, 13-14
 diagram, 18
 light sources, 16
 magnetic fields, 14-16
 photodetectors, 17-18
 definition of, 1-2
 hyperfine frequency shifts, 26-28
 interaction of the alkali spin with the nuclear moment, 26

level-crossing technique, 4
 light sources for, 16
 limitations of, 4
 of metastable atomic states, 3-4
 relaxation processes, 21-28
 crossed beam technique, 24
 hyperfine pumping, 23
 magnetic resonance line-shape, 22
 measurement of relaxation times, 22-24
 relaxation interactions, 24-26
 transient methods, 22-24
 spin exchange, 18-21, 23
 theoretical foundations, 4-12
 Optical pumping matrix, 7
 Optical studies on flames, 209-220

P

Particle continuity equations, 79-82
 Particle-solid interactions, 231-305
 "atomistic" description of solids, 289-304
 in crystalline solids, 304-305
 elastic scattering, 290-291
 electron-solid interactions, *see* Electron-solid interactions
 group velocity of reflected beams, 273
 heavy particles, 231-275
 penetration experiments, *see* Penetration experiments . . .
 at high-electron energies, 290-297
 inelastic scattering, 292-297
 at low electron energies, 297-299
 multiple scattering of electrons, 299-301
 secondary electron processes, 301-304
 Auger electron emission, 302
 electron slowing-down spectrum, 302-303
 radiation, 303
 secondary electron emission, 302
 structural and chemical change, 303
 "stagnation detector," 273
 "sticking probability," 271
 surface atom interactions, 264-274
 surfaces free of adsorbed gases, 271-272
 thermal energy collisions at surfaces, 268, 275
 time of flight techniques, 274
 Penetration experiments on particle-solid interactions, 232-264

backscattering from thick targets, 257-258
 "channeling" in, 245-264
 of fast heavy ions, 254-257
 ranges in axial types, 248-251
 crystal lattice effects, 245-264
 emergence patterns, 260-262
 emission from lattice sites, 258-259
 energy loss in thin layers of material, 237-240, 252-257
 interactions with surface atoms, 264-268
 ionic charges of heavy particles, 236-237
 ranges in, 240-245
 secondary particle yields, 258-260
 surface barrier detectors for, 262-264
 surfaces free of adsorbed gases, 271-272
 thin-surface-layer removal, 243-245
 transmission and reflection studies, 251-252
 Phosphor screen, 282
 Photographic plate, 282
 Photomultipliers, current mode pulse counting, 108
 noise in, 109
 Photon shot noise, 17
 Plasma frequency, definition, in afterglow studies, 86-87
 Plasmon excitation, 292
 $p\text{-}n$ junction photodiodes, 17
 Polarizers, for optical pumping, 17
 Probability of attachment per collision, measurement, 56

Q

Q of microwave cavity, determination of, 94

R

Radicals in flames, 196-198
 Ramsauer-Townsend effect, 48
 Random solid, general theory for, 232-236
 Rate constants, from flame studies, 230
 Reaction rate, in afterglow studies, 81
 Reflected microwave signal measurements, 93
 Resonance fluorescence, 16
 Retardation sheets, for optical pumping, 17

S

Scavenger methods, in flame combustion studies, 223-224
 Secondary electron processes in solids, 301-304
 Secondary ion reactions in flowing afterglows, 136-137
 Self-reversal of atomic lines, 16
 Shape factor for plasma containers, 89
 Shock tubes, 141-187
 description of, 141
 electromagnetic type, 148
 flows, deviations from ideal calculations, 157-167
 measurement techniques in, 169-171
 optical methods in measurements, 170
 reflected shock nonuniformities, 168-169
 shock strength, 145
 shock wave production in, 141-149
 strong shock generation, 146-148
 Shock-wave relations, 149-157
 Shock waves, boundary layer, 164
 density measurements of, 171-177
 optical methods, 171-173
 schlieren and shadowgraphs, 173-176
 dissociation relaxation studies, 185
 electron beam densitometry of, 177-178
 equilibrium gas studies of, 181-183
 equilibrium studies, 183-187
 ionization rates, 186-187
 in measurement of basic physical properties, 181
 optical absorption methods
 partial density of particular species, 178
 production in shock tubes, 141-149
 properties of, 149-157
 recombination of atoms in, 186
 shock curvature of, 164
 temperature measurement of, 179-180
 hot wires, 180
 optical methods, 179
 speed of acoustic waves, 180
 vibrational relaxation, 184
 visualization of, 173-174
 X-ray absorption studies, 178
 Sodium continuum as a measure of relative $[\text{OH}]$, 212-214
 Sodium-chlorine method for absolute $[\text{H}]$, 212

- Sodium-lithium method for absolute [H], 211-212
- Solids,
"atomistic" description of, 289-304
scattering of electrons in solids, 290-291
- Space charge, in afterglow studies, 80
- Spectral line-shape determinations at low intensity, 106-108
- Spectral line-shape studies, in spectroscopy, 102
- Spectrometry, in particle-solid studies, 241-242
- Spectroscopy, of afterglows, 102-110
line-shape determinations at low intensity, 106-108
low-intensity optical emission measurements, 103-104
photomultipliers for, 108
time-sampling techniques, 102-103
weak optical absorption measurements, 104-106
in combustion studies, 190
for measuring atomic and radical concentrations, 209-210
- Spin-exchange cross section, 19
- Spin exchange in optical pumping, 18-21
nuclear spins, 21
spin temperature, 21
- Spin-exchange process, 3
- "Stagnation detector," 273
- Stark effect in plasmas, 349
- Sugden burner, 192, 193-194
- Swarms, 29-139
atomic collisions of electrons, *see* Atomic collisions
electron type, *see* Electron swarms
- T**
- Thermal energy collision at surfaces, 268-275
- Thermal ion-neutral reactions, 124
- Thick-absorber technique in particle-solid studies, 241
- Thin films, for electron-solid interaction studies, 284
- Thin film thermometers, in shock-wave studies, 170
- Thin foils, 238
- Three-body reactions, in afterglow studies, 81
- Townsend discharge, 63
electrons, energy distribution, 64
- Townsend ionization coefficients, 64-66
first coefficient, 64, 70-72
experiment evaluation of, 72-73
second coefficient, 65-66
experimental evaluation of, 73-74
- Transient methods for measurement of relaxation times, 22-24
- Transmission and reflection of particles at solids, 251-252
- Two-body rate coefficient, in afterglow studies, 81
- U**
- Ultraviolet absorption spectroscopy, in flame kinetic studies, 210-211
- V**
- Vacuum evaporation, in thin-film preparation, 284-285
- Vacuum photocells, for optical pumping, 17
- "Van der Held" dilution curves, 216-217
- W**
- Wax-lined cells, in optical pumping, 14
- X**
- X-ray absorption, in shock-wave studies, 178